

GL03143

THE GEYSERS-CLEAR LAKE SEISMIC MODEL WORKSHOP

Pajaro Dunes, California

28-30 October 1979

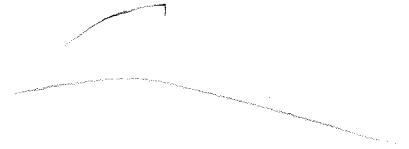


Table of Contents

	<u>Section</u>
"Field Trip Guide to The Geysers"	A
"Seismic Monitoring at The Geysers Geothermal Field, California" S. M. Marks, R. S. Ludwin, K. B. Louie, C. G. Bufe	B
"Seismic-Reflection Investigations at Castle Rock Springs, The Geysers Geothermal Area" Roger P. Denlinger and Robert L. Kovach	C
"Wave Equation Modeling of a Portable Heat Source, The Geysers, Northern California" Roger P. Denlinger	D
"Applications of Termal Water Chemistry in The Geysers-Clear Lake Geothermal Area, California" Fraser E. Goff and Julie M. Donnelly	E
"Geochronology and Evolution of the Clear Lake Volcanics, Northern California" Julie M. Donnelly and B. Carter Hearn	F
"Continental-Edge Volcanism at Clear Lake, California: Hot Spot, Leaky Transform, or Heated Oceanic Slab?" B. Carter Hearn, Julie M. Donnelly, and Fraser E. Goff	G
"The Clear Lake Volcanics and The Geysers Geothermal System, California" Julie M. Donnelly and B. Carter Hearn	H
"Geothermal Prospecting in The Geysers-Clear Lake Area, Northern California" Fraser E. Goff, Julie M. Donnelly, J. M. Thompson, and B. Carter Hearn, Jr.	I
"Geology and Geochronology of the Clear Lake Volcanics, California" B. Carter Hearn, Julie M. Donnelly, and Fraser E. Goff	J
"Gravity and Magnetic Studies of The Geysers-Clear Lake Geothermal Region, California, U.S.A." William F. Isherwood	K
"Geothermal Reservoir Interpretation from Change in Gravity" William Isherwood	L
"Abnormal P-wave Delays in The Geysers-Clear Lake Geothermal Area, California" H. M. Iyer, D. H. Oppenheimer, and T. Hitchcock	M
"Large Teleseismic P-Wave Delays in The Geysers-Clear Lake Geothermal Area" H. M. Iyer, David H. Oppenheimer, Tim Hitchcock, Jeffrey N. Roloff, and John M. Coakley	N

Section

"Seismological Investigations at The Geysers Geothermal Field" E. L. Majer and T. V. McEvilly	O
"Relation of the Tectonics of Pre-Tertiary Rocks to Geothermal Resources in The Geysers-Clear Lake Area of Northern California" Robert J. McLaughlin	P
"Significance of Age Relations Above and Below Upper Jurassic Ophiolite in The Geysers-Clear Lake Region, California" R. J. McLaughlin and E. A. Pessagno, Jr.	Q
"Pre-Tertiary Geology and Structural Control of Geothermal Resources, The Geysers Steam Field, California" Robert J. McLaughlin and William P. Stanley	R
"Compressional and Shear Waves in Saturated Rock During Water-Steam Transition" Hisao Ito, John DeVilbiss, and Amos Nur	S
"Pore Fluids and Seismic Attenuation in Rocks" Kenneth Winkler and Amos Nur	T
"Attenuation of Teleseismic P-Waves in The Geysers-Clear Lake Region" Chi Yuh Young and Ron Ward	U
"2-D Linear Inversion of Inaccurate δt^* Data" Ronald W. Ward and Chi-Yuh Young	V

FIELD TRIP GUIDE TO THE GEYSERS-CLEAR LAKE AREA

FOR THE CORDILLERAN SECTION OF
THE GEOLOGICAL SOCIETY OF AMERICA

APRIL, 1977

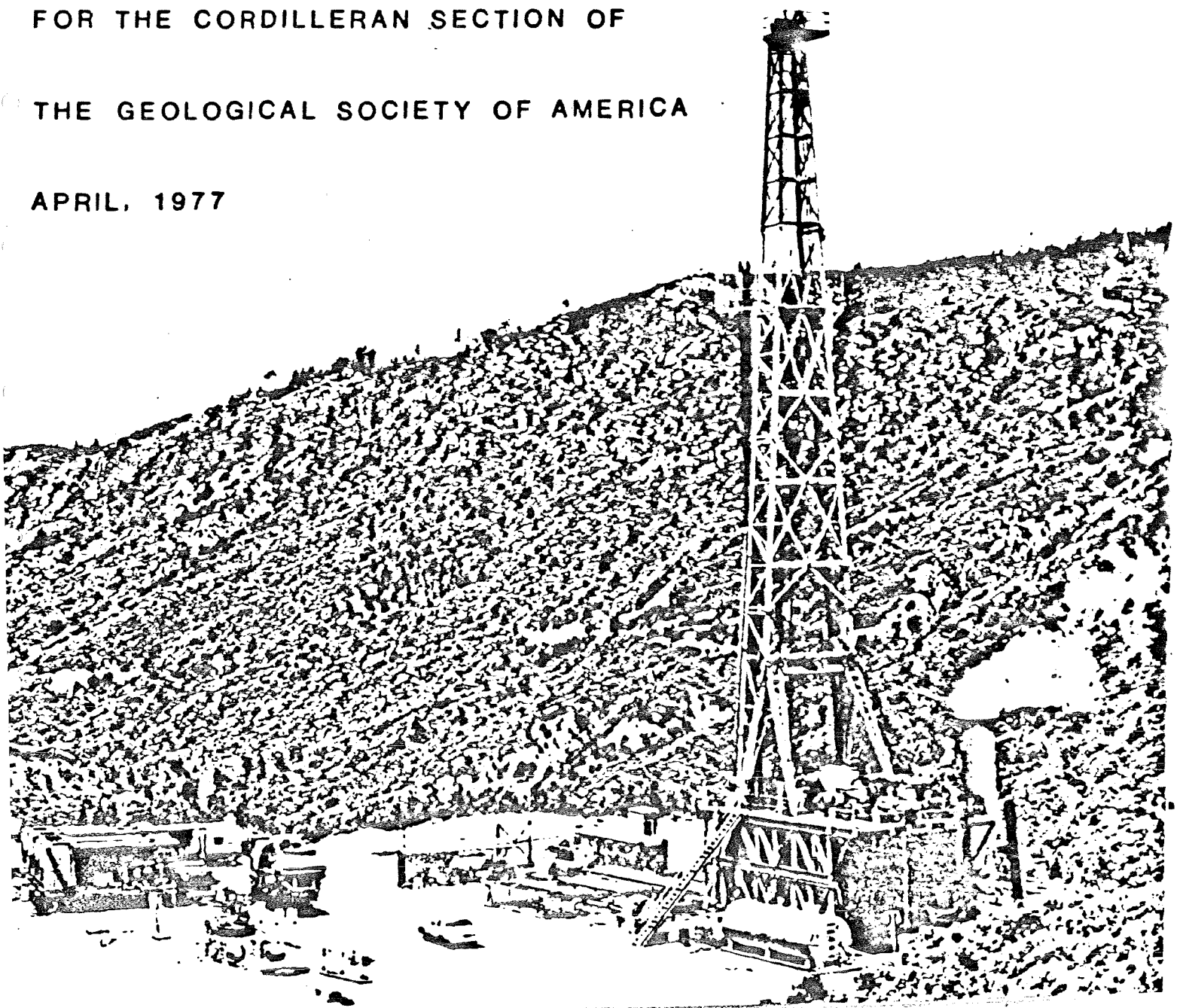


TABLE OF CONTENTS

	<u>Page</u>
Introduction and acknowledgements -----	1
Road Map -----	2
The Franciscan assemblage and Great Valley sequence in The Geysers- Clear Lake region of northern California, by R. J. McLaughlin -----	3
The Clear Lake Volcanics, California: geology and field trip guide, by J. M. Donnelly, B. C. Hearn, Jr., and F. E. Goff -----	25

FIELD TRIP GUIDE TO
THE GEYSERS-CLEAR LAKE AREA

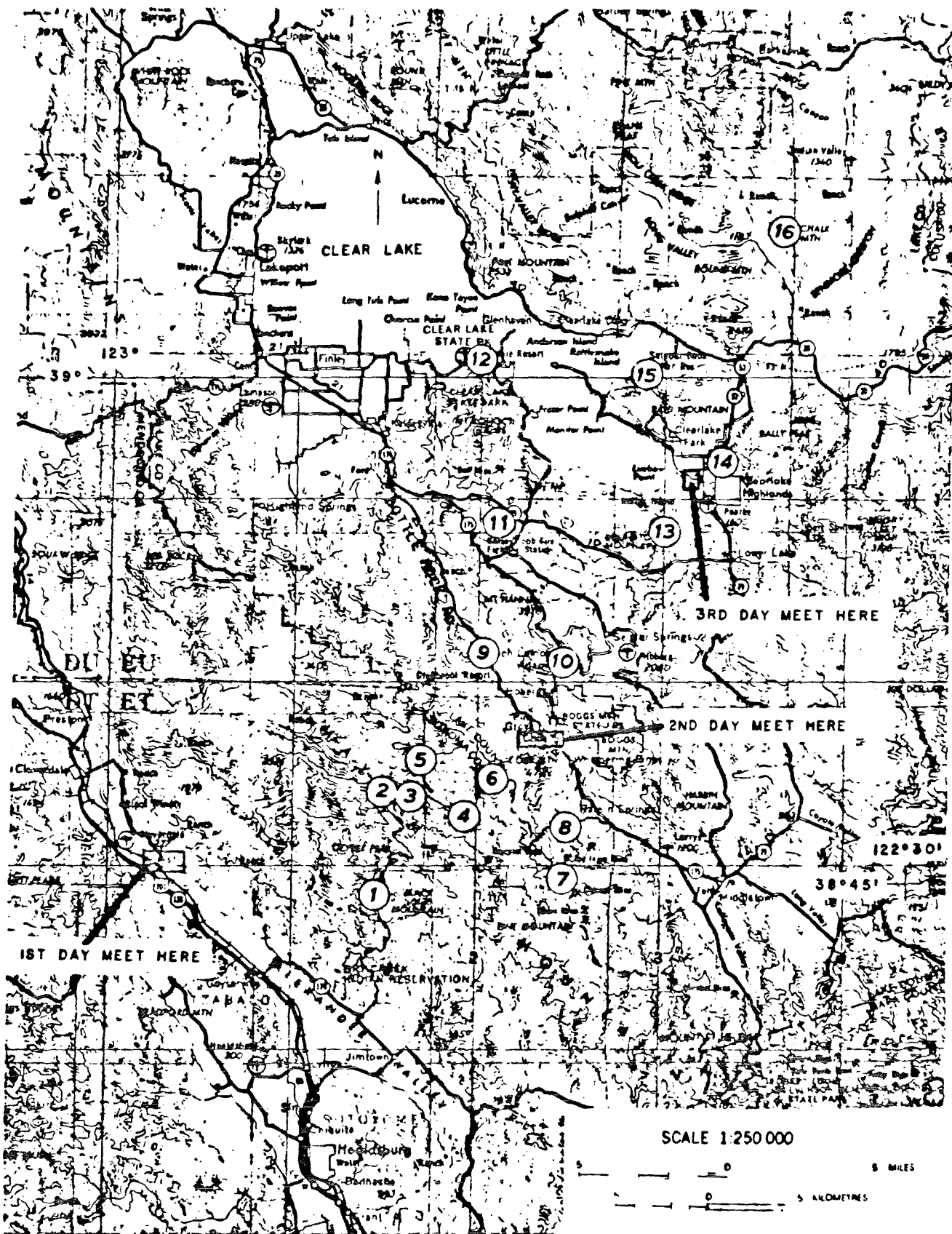
For the Cordilleran Section of
The Geological Society of America
April, 1977

Cover photograph: Montgomery Drilling Company rig (Aminoil, USA - Federal #1) successfully reached steam in this producing well three kilometers southeast of The Geysers. Cobb Mountain, a 1.1 million year old composite silicic dome of the Clear Lake Volcanics, overlies Franciscan rocks in background.

INTRODUCTION AND ACKNOWLEDGEMENTS

The Geysers - Clear Lake area was chosen in 1971 as one of the major areas for investigation in the USGS Geothermal Research Program. Studies under that program have been designed to determine the origin and structural setting of the geothermal resources in the area, to test methods of finding such resources, and to provide background data for monitoring of the effects of exploration and possible development of geothermal resources. This continuing program involves geologic mapping, petrologic studies, isotopic dating and paleomagnetism, geochemical studies of thermal waters, interpretation of drill-hole data, land-based and airborne geophysical surveys, study of heat flow, and monitoring of seismicity and geodetic changes. Such data are useful for assessment of geothermal resources and geothermally-related environmental effects and additionally will provide valuable knowledge of the water resources, slope stability, seismic safety, volcanic hazards, and mineral deposits of the area. Preliminary results of many studies (see bibliography) have been published or released as open-file reports in order to make the data available to the public, to local counties and other governmental agencies, and to private companies.

We wish to thank all property owners who have allowed us access to their land during our field investigations and for the field trip stops in this guidebook. We also wish to thank Union Oil Company for its participation in this field trip and for granting access to its lease holdings. The cooperation of Aminoil, USA, Shell Oil Company, and Thermogenics Corp. is also gratefully acknowledged. Technical reviews by colleagues at the U.S. Geological Survey substantially improved our manuscripts: McLaughlin thanks A. M. Sarna-Wojcicki and V. M. Seiders; Donnelly, Hearn, and Goff thank D. A. Swanson and P. C. Bateman.



ROAD MAP--Map of The Geysers-Clear Lake region showing locations of field trip stops.

THE FRANCISCAN ASSEMBLAGE AND GREAT VALLEY SEQUENCE
IN THE GEYSERS-CLEAR LAKE REGION OF NORTHERN CALIFORNIA

by

Robert J. McLaughlin
U.S. Geological Survey
345 Middlefield Road
Menlo Park, California 94025

Franciscan Assemblage

The Franciscan assemblage of The Geysers-Clear Lake region consists largely of mildly to moderately metamorphosed sandstone, conglomerate, and argillite, subordinate basaltic volcanic rocks (greenstone) and chert, and minor limestone, blueschist, antigoritic serpentinite, amphibolite, and eclogite. These rocks are preserved in imbricate thrust slices varying in degree of deformation from coherent interbedded sequences to chaotic melanges (Hsu, 1968). Blocks of blueschist, amphibolite, and eclogite are generally confined to zones of melange.

The Franciscan assemblage in The Geysers-Clear Lake region ranges from Late Jurassic (lower Tithonian) to early Late Cretaceous (post-lower Cenomanian) age (McLaughlin and Pessagno, in press, 1977), although rocks assigned to the Franciscan coastal belt to the northwest of The Geysers region are considered to be of Late Cretaceous to early Tertiary (Eocene) age (Evitt and Pierce, 1975).

Great Valley Sequence

Within the region of The Geysers steam field, only a few residual patches of basal Great Valley strata are present, positionally above thick masses of ophiolite. These strata consist of mafic breccias of probable early to middle Tithonian age, overlain by mudstone and minor basaltic sandstone of probable Late Jurassic (mid-Tithonian) to Early Cretaceous age. The stratigraphy of the Great Valley sequence northeast of The Geysers steam field was described by Swe and Dickinson (1970).

Within the Coast Ranges, strata of the Great Valley sequence range from Late Jurassic (upper Kimmeridgian and/or lower Tithonian) to Late Cretaceous age, and are separated from structurally underlying rocks of the Franciscan assemblage by a deformed regional thrust (Coast Range thrust of Bailey and others, 1970).

Depositional and Tectonic Framework of the
Franciscan Assemblage and the Great Valley Sequence

The deformed ophiolite sheet found below the base of the Great Valley sequence occupies the upper plate of the Coast Range thrust throughout the California Coast Ranges (Bailey and others, 1970). This ophiolite is thought to represent Jurassic oceanic crust that formed the floor of an arc-trench gap, upon which strata of the Great Valley sequence were deposited (Dickinson, 1970). A trench above an east-dipping subduction zone was situated to the west of the

site of Great Valley sedimentation, and some workers also have suggested that this trench was separated from the Great Valley sequence by an island arc; although others dispute this suggestion. Far to the west of the trench was a spreading ocean ridge, where new basaltic ocean floor was upwelling.

Both terrigenous and pelagic sediments, together with associated basalts of the Franciscan assemblage were deposited in the trench, while pelagic oozes accumulated to the west, between the trench and the spreading ridge. As spreading at the ridge progressed, the Franciscan rocks were thrust as a series of imbricate wedges eastward, beneath oceanic crust and the positionally overlying Great Valley sequence.

The easternmost parts of the Franciscan assemblage were carried down to the deepest levels in the subduction zone, and consequently metamorphosed to high pressure lawsonite-bearing rocks. Less deeply subducted rocks, which were situated further to the west, were metamorphosed respectively to pumpellyite-, prehnite-pumpellyite-, or laumontite-bearing rocks with decreasing depth.

Previously subducted, older Franciscan rocks were accreted to the hanging wall of the subduction zone, and locally uplifted and reworked into the younger Franciscan sediments as successively more westward sediment wedges were underthrust. As the locus of subduction stepped westward between Late Jurassic and early Tertiary time, Franciscan wedges compressed beneath the over-riding upper plate of the Coast Range thrust were faulted upward into the lower part of the ophiolite sheet in the upper plate, and some of these wedges were faulted through the ophiolite and exposed to erosion during early Tertiary time.

Within the past 3-6 million years, passage of the Mendocino triple junction northwest of The Geysers-Clear Lake region initiated a change in relative motion between the Pacific and North American plates, terminating subduction beneath The Geysers-Clear Lake region, and initiating strike-slip motion. At this time, some older thrust faults were reactivated as strike-slip features, reflecting the transition from subduction to strike-slip tectonics.

Structure of The Geysers Geothermal Area

The Geysers steam field occupies the northeast limb of a southeast plunging antiform whose core is composed of Franciscan rocks (Fig. 1). The southeast plunge of this antiform is inferred from regional dip and from the surface and subsurface distribution of ophiolitic rocks in the upper plate of the Coast Range thrust. Cutting this antiform are northwest-trending faults along which numerous narrow serpentinite belts extend from the main ophiolite mass out into the underlying Franciscan terrane. These narrow serpentinites that are sheared into the Franciscan assemblage may have formed by downward drag of the serpentinite along steep-dipping faults during vertical and horizontal movement of wedges of Franciscan rock beneath ophiolite in the upper plate of the Coast Range thrust.

Franciscan rocks in the Mayacmas Mountains form the core of an antiform, the Mayacmas antiform, which is divisible into at least three roughly stratiform, fault-bounded structural units that reflect the northeast dipping imbricate structure imposed on the Franciscan during subduction. The positions of these structural units relative to adjacent units are substantially different from their original positions in the subduction zone, due to the differential movement between thrust wedges following subduction and metamorphism, that was

responsible for shearing of ophiolite from the upper plate of the Coast Range thrust, downward into the Franciscan assemblage.

The three structural units in The Geysers area (Fig. 1) were differentiated on the basis of 1) gross lithology, and 2) degree of textural reconstitution of graywacke sandstones. The structurally lowest rocks exposed in the Mayacmas Mountains are well-bedded, weakly reconstituted graywacke sandstones and minor interbedded argillite, assigned to metamorphic textural zone 1 of Blake and others (1967). This unit is in part distinguished by a lack of associated greenstone and chert. The weakly metamorphosed sandstones of unit 1 commonly contain albite + phengite ± pumpellyite.

Structural unit 2 above unit 1 consists of slabs of: 1) well bedded to massive graywacke that locally contains thick lenses of conglomerate and chert; 2) massive lenticular zones of shaly melange containing sporadic masses of blueschist and amphibolite, 3) prominent slabs of cherty basaltic greenstone, and 4) minor ultramafic rocks containing antigorite or actinolite. Presence of conglomerate in this unit suggests a more proximal source for the sediments of unit 2 as compared to the structurally lower graywackes of unit 1. Rocks of unit 2 were probably more deeply subducted than the graywackes of unit 1, since unit 2 graywackes have metamorphic textures ranging from textural zone 1 to 2 of Blake and others (1967), and locally are lawsonitic. Unit 2 graywackes contain albite + quartz + pumpellyite + phengite ± lawsonite ± glaucophane.

The structurally highest Franciscan rocks, unit 3, are highly reconstituted, locally conglomeratic metasandstones with minor interbedded metacherts and meta-greenstones, assigned to textural zones 2 and 3 of Blake and others (1967). The metagraywacke of this unit generally contains quartz + phengite + lawsonite ± albite ± jadeite ± glaucophane ± pumpellyite. Unit 3 metagraywacke is present beneath the Coast Range thrust in the southeast central part of The Geysers steam field, in the axial area of the Mayacmas antiform. However, in Cobb Valley, north of The Geysers, unit 3 is overthrust by rocks of structural unit 2, which intervenes between unit 3 and the Coast Range thrust in that area. Melange zones are also present within unit 3, but these melanges have a matrix of lawsonitic metagraywacke and locally contain very large sheared blocks ("knockers") of blueschist and amphibolite or greenschist.

The Mayacmas antiform is bounded by and in part broken by major strike-slip and extensional faults, probably produced since the San Andreas fault system was initiated in the late Tertiary. Two major northwest-trending strike-slip fault systems bound the Mayacmas Mountains on the northeast and southwest, and these systems apparently have also sustained major late Tertiary to Quaternary vertical movement, as evidenced by the uplifted mass of the central Mayacmas Mountains.

The Collayomi fault zone bounds the range on the northeast, in part coinciding closely with a segment of the Coast Range thrust along the north side of the Cobb and Collayomi Valleys. Evidence for Quaternary vertical and right-lateral offsets along the Collayomi fault zone has been found in the faulted older terrace gravels and Quaternary volcanic rocks of the Cobb Valley.

The Maacama fault zone, present in the southwest corner of the geologic map (Fig. 1), bounds the Mayacmas Mountains on the southwest. This fault zone has been active in late Quaternary time, as inferred from the presence of numerous sag ponds, entrenched topography, undissected scarps, and offset and

captured drainages along its trace. A long history of uplift and lateral offset along fault slices adjacent to the Maacama fault zone is also suggested by the presence of isolated graben-like structural basins containing late Tertiary non-marine deposits, and by several hanging valleys that have been uplifted during Quaternary time. Other important faults within The Geysers steam field are the Mercuryville fault zone, and faults along Big Sulphur Creek.

Structural Model for The Geysers Vapor-Dominated System

A structural model of The Geysers geothermal system can be constructed by integrating structural data from the Franciscan assemblage with geophysical and geochemical studies. This model provides a reasonable explanation of the observed aspects of the geothermal system.

The most important regional control to the geothermal system, the distribution of heat and(or) magma at depth, may be indicated in part by a large-scale 30 milligal negative gravity anomaly. Isherwood (1976), and Chapman (1975) suggested that the negative gravity anomaly over The Geysers-Clear Lake area delineates a magma body above its Curie temperature, centered more than 10 km below the Clear Lake region (Fig. 2). Given that over the closure of this gravity low there is adequate heat at depth, regional structure of the Franciscan and Great Valley rocks above this heat source appears to be the next most significant factor. Heat from the magma body is transmitted upward and to the west-northwest along channel ways in fractured rocks between northeast to southeast-dipping imbricate thrusts on the northeast flank of the Mayacmas antiform (Fig. 3).

Ultramafic rocks belonging to the ophiolite in the upper plate of the Coast Range thrust, structurally overlie Franciscan rocks over much of this region; and in addition, another structurally lower thrust slice of actinolitic serpentinite is present within The Geysers steam field. These thick sheared ultramafic sheets, along with sheet-like, sheared shaly melange units have very low permeabilities, and as such, they also have poorer thermal conductivities than interlayered slabs of fractured graywacke carrying water in the liquid and vapor phases. The serpentinites and shaly melange units are thus important both in retaining heat and water in the geothermal system, and in directing heat to the southwest. The westward directed heat convection may also in part explain why the vapor-dominated part of The Geysers-Clear Lake geothermal system is on the southwest (up-dip) edge of the negative gravity anomaly.

The main area of hydrothermal venting and alteration for The Geysers geothermal system is presently along the en-echelon fault system of Big Sulphur Creek, notably near The Geysers Resort at the southwest edge of the steam field (Fig. 3). Evidence of a former vent area is present further to the southwest, where prominently altered Franciscan rocks are present along the trend of the Mercuryville fault zone. Coincidentally, the Mercuryville fault zone bounds the closure on the southwest lobe of the regional negative gravity anomaly (Fig. 2), and it also appears to be the southwestern limit of hydrothermal alteration on the northeast flank of the Mayacmas antiform. No steam production is known southwest of the Mercuryville trend, and at least two unsuccessful steam wells are known to have been drilled near the fault zone. The fault zone dips at a moderate angle (45° - 60°) to the northeast, roughly coincident with the structural dip of the Franciscan (Fig. 3). This data may indicate: 1) that the regional heat source for The Geysers geothermal system does not extend any significant distance southwest of the Mercuryville fault zone; and 2) that

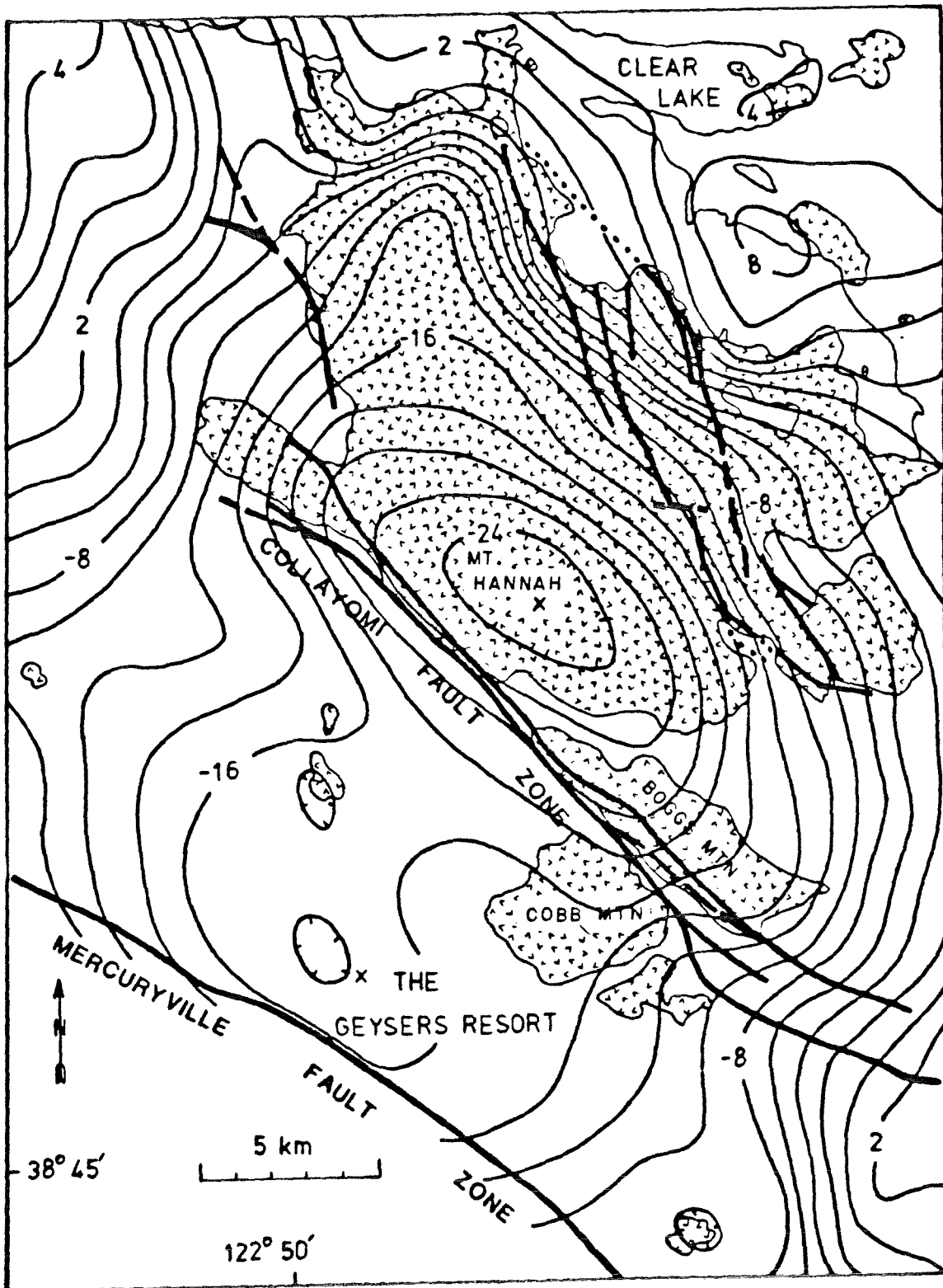
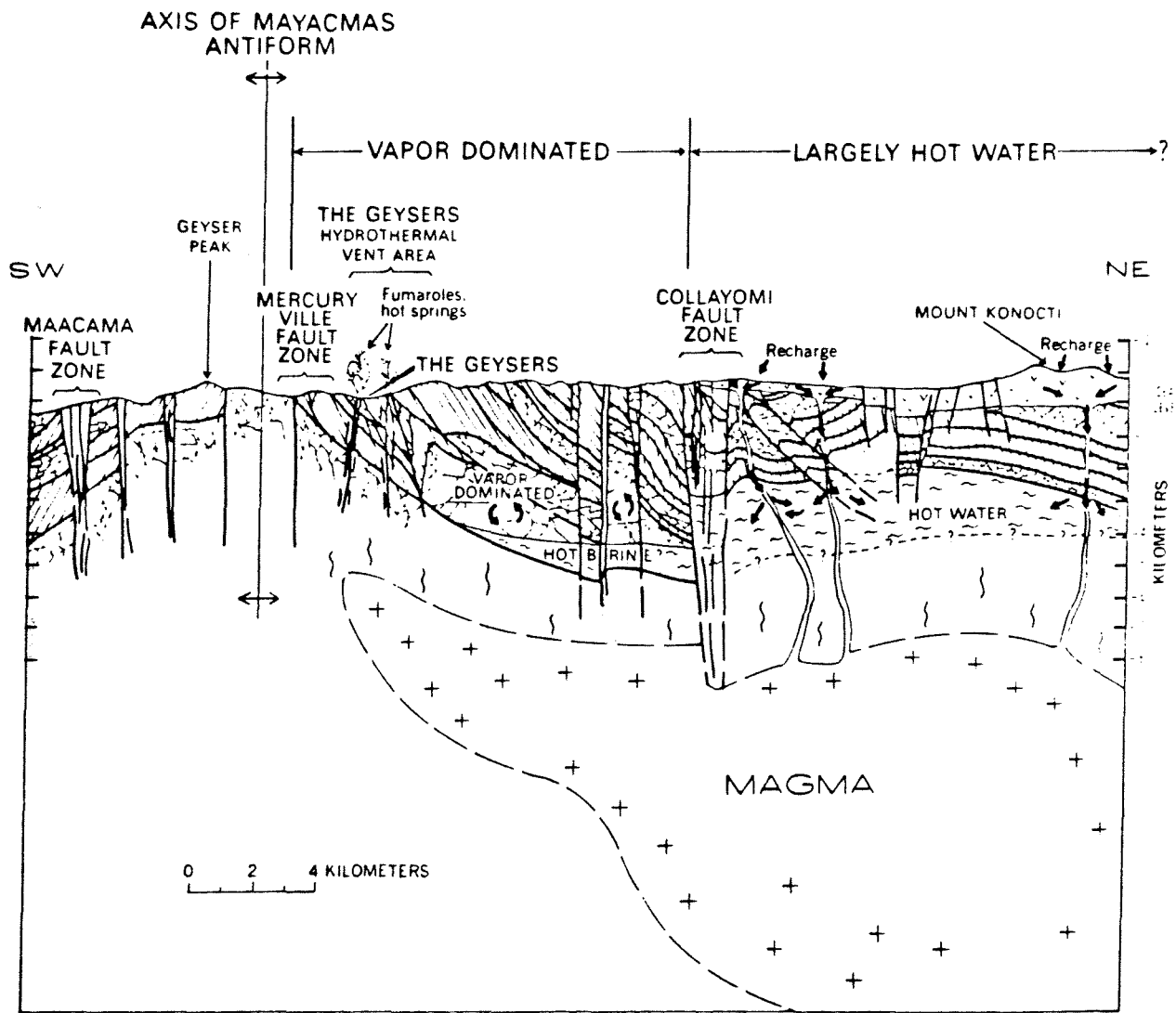


Figure 2. Residual Bouguer gravity of The Geysers-Clear Lake area, from Isherwood (1976), reduced at 2.67 gm/cm^3 ; 2 milligal contour interval. The Clear Lake Volcanics is shown with a V-pattern. The Collayomi fault zone divides the major gravity low into northeast and southwest lobes, and the Mercuryville fault zone bounds the gravity anomaly on the southwest side of The Geysers steam field.




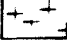
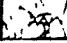

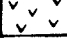
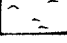
- | | |
|---|---|
|  Impermeable cap rocks (Serpentine, greenstone, melange, metagraywacke) |  Partially crystallized magma body inferred to be at depth with center below 10 kilometers |
|  Fracture networks in graywacke reservoir rocks |  Water vapor in steam reservoir above boiling water table |
|  Clear Lake Volcanics and associated vents providing recharge to geothermal system |  Hot water |

Figure 3. Structural model for The Geysers geothermal system. Cross-section through The Geysers-Clear Lake region, from the Maacama fault zone on the southwest, to Mount Konocti on the northeast, depicting structural elements of The Geysers-Clear Lake geothermal system.

the footwall of the northeast-dipping Mercuryville fault zone forms the floor to the steam reservoir in The Geysers Resort area.

According to White and others (1971), a vapor-dominated geothermal system may begin as a hot water system, but if natural hydrothermal leakage through surface venting of hot springs and fumarolic activity exceed the natural recharge of meteoric water to the system, the hot water reservoir will diminish and become increasingly more saline due to higher concentrations of dissolved solids. Eventually the diminishing water table in the reservoir falls to a point where the vapor phase dominates a large region of the reservoir above the water table, thus establishing a vapor dominated hydrothermal system. The vapor phase is retained as long as steam withdrawal exceeds recharge and the reservoir is not completely depleted (White and others, 1971). The alteration trend along the Mercuryville fault zone, if related to The Geysers geothermal system, may thus represent a former vent area on the southwest edge of The Geysers system. The northeast-dipping regional structure would require that as the reservoir shrank, the vent area would shift northeastward (down-dip) to where it now vents in Big Sulphur Creek (Fig. 3).

Within the steam reservoir the distribution of vapor is governed largely by fracture networks in slabs of graywacke that have had access to an adequate but not excessive charge of meteoric water. These fractures may connect at depth (perhaps 4-5 km) to a water table of boiling brine (White and others, 1971). Recharge of meteoric water to the geothermal system is highly restricted, since although the reservoir is underpressured with respect to hydrostatic head, the fracture networks are largely within rocks that are otherwise impermeable. The fractured reservoir rocks are also sealed above and below by such impermeable Franciscan rock types as shaly melange, sheared greenstone, serpentinite, and foliate metagraywacke. Some recharge to the system probably occurs along steep-dipping extensional faults that cut the various thrust plates. However, the principal means of recharge to The Geysers steam field may be through volcanic vent areas beneath Cobb Mountain associated with permeable flows and domes of rhyolite and dacite (Goff and others, in press). These volcanic rocks and their vents may act as funnel-like collecting areas for meteoric water that cut across several thrusts and thus provide recharge to considerable depth at several structural levels. The large volume of meteoric water carried in these recharge areas may also locally flood the steam system around volcanic vent areas. Northeast of the steam field, young volcanic rocks cover a much larger area, and there are also many more volcanic vents to provide extensive recharge, thus preventing the development of conditions necessary for maintaining a vapor dominated system.

The Collayomi fault zone east of The Geysers steam field apparently marks a major change in the character of the geothermal reservoir, since evidence from the geology (Donnelly and others, 1976) and from geochemical (Goff and others, in press) and geoelectrical studies (Stanley and others, 1973) indicate that to the east of this fault zone the geothermal system may be dominated by hot water. An electrical resistivity study by Stanley and others (1973), showed that an extensive area beneath the Clear Lake volcanic field, approximately bounded on the southwest by the Collayomi fault zone, is underlain by rocks of relatively low electrical resistivity (Fig. 4). Most of the region of low resistivity is over ophiolitic rocks overlain by a thick section of Great Valley sequence in the upper plate of the Coast Range thrust (Brice, 1953; Swe and Dickinson, 1970). Goff and others (in press) found that the thermal waters in this area of low resistivity have higher ionic strengths and consequently

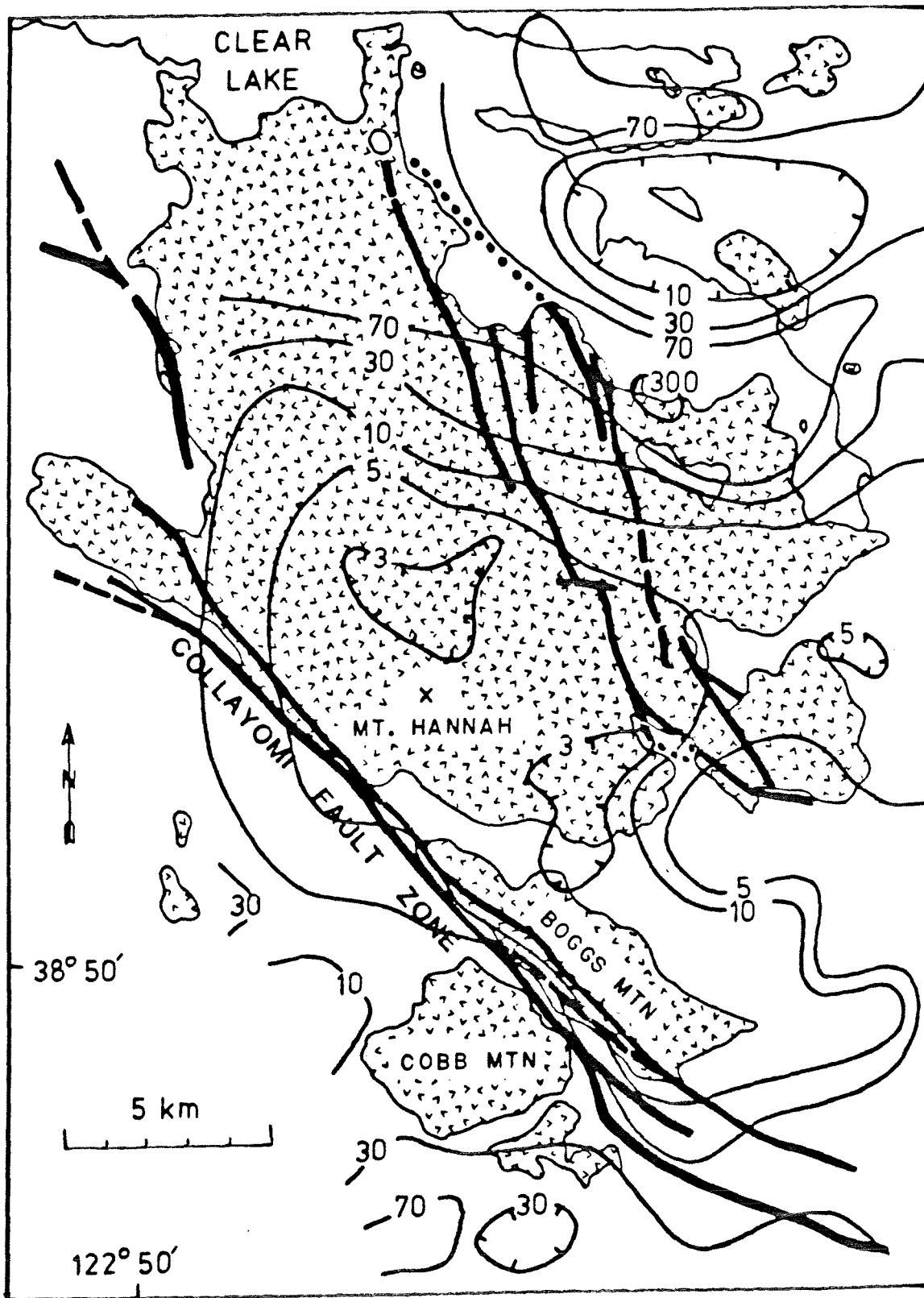


Figure 4. Electrical resistivity of The Geysers-Clear Lake area, from Stanley and others (1973). Contours are in ohm-meters. V-pattern indicates the Clear Lake Volcanics and heavy lines are major faults. The regional resistivity low centered beneath Mount Hannah is approximately bounded on the southwest by the Collayomi fault zone.

greater electrical conductivities than thermal waters from the vapor dominated production area southwest of the Collayomi fault zone. According to Goff and others, this relatively high ionic strength, and temperatures inferred from geothermometry suggest that the area northeast of the Collayomi fault zone is underlain by a $>200^{\circ}$ C hot water system.

The inferred change in geothermal reservoir conditions across the Collayomi fault zone may be due in part to the absence of most of the upper plate of the Coast Range thrust over an extensive area on the southwest (uplifted) side of the Collayomi fault zone. The extensive area of impermeable ophiolite overlain by Great Valley sediments northeast of the Collayomi fault zone may significantly inhibit escape of heat and thermal waters from the geothermal system in that area, and also help direct convection of heat westward and updip toward The Geysers steam field. On the other hand, in the elevated Mayacmas Mountains fault block southwest of the Collayomi fault zone, escape of thermal fluid from the system has been greater and recharge volume is significantly smaller than over the central part of the Clear Lake volcanic field, northeast of the fault zone.

FIELD TRIP GUIDE FOR G.S.A. CORDILLERAN SECTION, GEYSERS-CLEAR LAKE TRIP

First Day

MILEAGE:

- 0.0 Assemble at Asti Winery parking lot, 8:00 A.M. Proceed from Asti, south on Highway 101 to Geyserville exit; exit freeway at Geyserville; travel south on old Highway 101, and turn east at intersection in center of town. Cross Russian River and follow Highway 128 through Alexander Valley toward Calistoga.
- 10.2 At intersection of The Geysers Road with Highway 128, turn left at stop sign.
- 10.6 Turn left at intersection of The Geysers Road with Red Winery Road, and begin climbing out of Alexander Valley. Along The Geysers-Healdsburg Road, cross the Maacama fault zone, which bounds the southwest side of the Mayacmas Mountains. Steeply tilted and folded nonmarine gravels exposed along the road are assigned to the Sonoma Volcanics, of middle and late Pliocene age. These gravels are overlain and interbedded with basalt and rhyolitic welded tuff, also assignable to the Sonoma Volcanics. Here, the Maacama fault zone cuts and bounds the northeast side of the Sonoma Volcanics. Some strands of the fault zone show evidence of late Quaternary activity and display youthful physiographic features.

After crossing the Maacama fault zone continue northeastward, passing into landslide-prone, pervasively sheared melange terrane of the Franciscan assemblage. Resistant masses standing above the grass covered slopes are sheared blocks in the melange. These blocks are composed of chert, greenstone, graywacke, blueschist, eclogite, amphibolite, and limestone. Many of the landslides in this area are enormous, and of the block-slide type. Uplift of the Mayacmas Mountains, coupled with general incompetency and steepness of the melange terrane are major contributing factors to landslides in this area.

15.6

STOP 1. Ophiolite sequence of Geysers Peak and Black Mountain

At this locality (see Fig. 5) the upper part of a fragmented ophiolite is present structurally above rocks of the Franciscan assemblage. A remnant of basal strata of the Great Valley sequence is also present, in depositional contact with the underlying ophiolite.

The basal contact of the ophiolite upon the Franciscan assemblage is a deformed thrust fault considered to be an outlier of the Coast Range thrust of Bailey and others, 1970. Among the features to observe at this locality are

1. Basal strata of the Great Valley sequence. These strata vary in attitude from steeply tilted to nearly horizontal, and are cut by at least two steep-dipping faults. The basal strata consist of thin-bedded, flysch-like sandstone and mudstone composed of basaltic detritus, with sporadic carbonate concretions, and thick sedimentary lenses of coarse diabase breccia in the lowermost part. The age of the strata at this locality is unknown, but similar strata above ophiolite elsewhere in the region contain mollusks of Late Jurassic (Tithonian) age.
2. Basaltic pillows, pillow breccia, and tuff are exposed along The Geysers road on Black Mountain. This unit appears to be the structurally highest part of the ophiolite succession in this area. Southeast of The Geysers road, on Black Mountain, a tuffaceous chert lens interbedded with these volcanic rocks contains radiolaria of late Kimmeridgean or early Tithonian (Late Jurassic) age.
3. Diabase and microgabbro compose a sill or concordant dike complex that underlies the pillow flows. Some of this diabase is exposed along the road just southeast of Cold Creek, where it is in fault contact with the basalt flows; here the diabase appears to be overlain depositionally by mafic breccia at the base of the Great Valley sequence. The diabase and microgabbro sills are thickest beneath Geysers Peak, to the northwest of the road, where they form a 1500 foot-thick southwest dipping slab. Pyroxenes in this diabase have been extensively replaced by brown and green hornblende, and epidote is an abundant replacement mineral in the intrusive and extrusive rocks, presumably due to low grade greenschist-facies metamorphism.

Although elsewhere in the region cumulate pyroxene gabbro is present in ophiolitic rocks, such gabbro is present only locally in the Geysers Peak-Black Mountain area, beneath the basaltic flows and diabase sills, and is not exposed along The Geysers-Healdsburg Road. Serpentinized and sheared harzburgite peridotite is present as a thin sheet from a few feet up to 500 feet thick along the base of the ophiolite complex in this area.

Resume driving northeast and down Black Mountain through basaltic rocks. Cross serpentinized peridotite in the Geysers Peak fault zone,

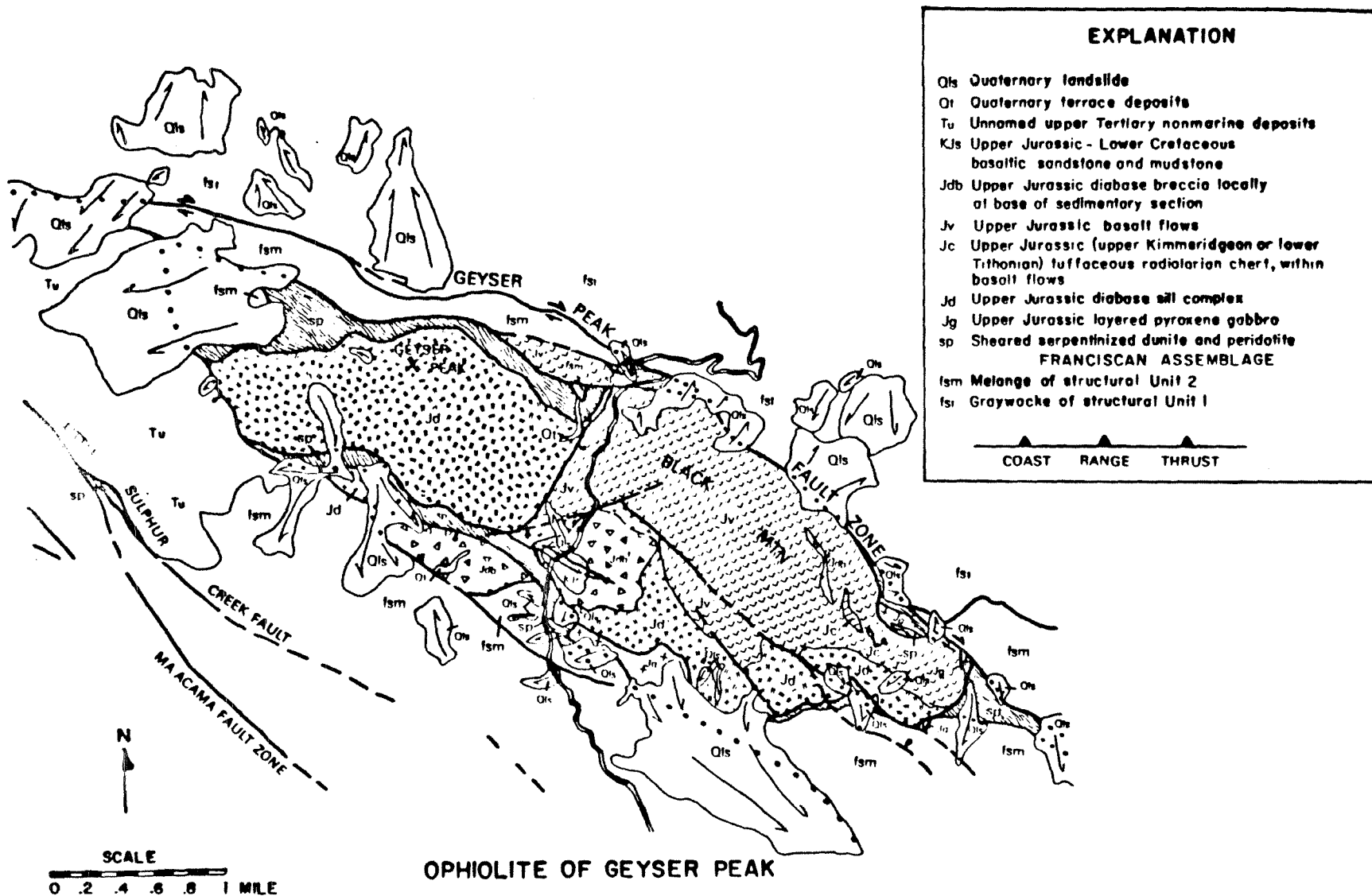


Figure 5. Ophiolite of Geyser Peak. Geologic map depicting ophiolite complex at Stop 1, from McLaughlin and Pessagno, 1977, in press, and McLaughlin unpublished data.

pass through landslide covered Franciscan graywacke, and cross Little Sulphur Creek drainage. Well bedded Franciscan graywacke of structural unit 1 is exposed in Little Sulphur Creek. As you climb out of Little Sulphur Creek, more of this graywacke is exposed in the road cuts, where it is pervasively broken and faulted. This graywacke is believed to be the structurally lowest unit in The Geysers region. It is characterized by a lack of associated chert and volcanic rocks, and by its relatively un-reconstituted sedimentary fabric. As you climb higher on the north side of Little Sulphur Creek canyon, note the prominent northwest-trending belt of serpentinite that follows the Mercuryville fault zone.

- 19.6 Mercuryville fault zone: Continue up Mercuryville grade and cross the Mercuryville fault zone at the Culver Baer mine, where mercury deposits are associated with silica carbonate rock, a product of hydrothermally altered serpentinite. In this area the hydrothermal alteration and mercury mineralization largely follow an elongate ultramafic body sheared out along the Mercuryville fault zone, although alteration also extends into the rocks adjacent to the fault zone. This prominent zone of alteration is the approximate southern limit of significant hydrothermal alteration in The Geysers region. Closure on the south side of a 30 milligal negative gravity anomaly that presumably indicates subsurface distribution of a regional heat source, also coincides roughly with the Mercuryville fault zone, which is consistent with the interpretation that the fault zone is near or at the southwest limit of the steam field (see Figs. 2 and 3).

Surface and subsurface structural data indicate that the Mercuryville fault zone dips at 40° - 60° to the northeast, and separates well bedded Franciscan sandstone of the lower structural unit (unit 1) in the footwall, from pervasively sheared melange with abundant blocks of graywacke, chert, greenstone, amphibolite, and glaucophane schist in the hanging wall (unit 2). After crossing the Mercuryville fault zone continue driving toward The Geysers, and drop down northeastward into Big Sulphur Creek canyon. This area is covered by many large and complex landslides, in part related to the pervasively sheared, jumbled character of structural unit 2.

At the junction of The Geysers-Healdsburg Road with the Cloverdale-Geysers Road, turn southeast along Big Sulphur Creek canyon. At this point you will pass from melange into a coherent Franciscan terrane consisting of interbedded greenstone, chert, and graywacke.

- 22.6 STOP 2. Vista point view of production area north of Big Sulphur Creek; Discussion of steam production by D. S. McMurdie, Union Oil Company; Observe relationships between Franciscan greenstone and chert;

At this locality, the following features are noteworthy:

1. The north side of Big Sulphur Creek Canyon is covered by very large block-type landslides in this area, and several wells drilled early in the development of the steam field were sited on some of these landslides. Two such wells in this area have had blow-out failures.

2. A zone of intensely acid-leached, hydrothermally altered Franciscan rocks (largely graywacke) can be seen on the north side of Big Sulphur Creek. This area is part of the principal vent zone for The Geysers hydrothermal system. The alteration zone consists of fumaroles and sporadic hot springs that vent along steep-dipping $N30^{\circ}-40^{\circ}W$ trending en echelon faults that diagonally transect Big Sulphur Creek. Venting of steam and hot water to the southeast of this area also occurs beneath the base of a major northeast-dipping sheet of ultramafic rock. Most near surface hydrothermal alteration appears to result from hydrothermal fluids that have migrated upward along steep-dipping faults and fractures, and spread laterally beneath the impermeable lower contact of the north-dipping ultramafic sheet on the northeast side of Big Sulphur Creek.

This area is also the epicentral region for innumerable small earthquakes and microearthquakes. Current topics of research involve the questions of how much of this seismic activity is tectonic, how much may be related to subsidence due to withdrawal of geothermal fluids, and (or) how much might be related to reinjection of fluids.

3. In the road cuts at this locality, observe the following relationships: (a) Slightly pillowed basaltic flows of the Franciscan assemblage that dip steeply to the east, locally with red cherty shale between the flows; (b) Overlying the basalt flows is a prominent 221 foot-thick lens of radiolarian chert. Radiolaria extracted from this chert have been studied in considerable detail by E. A. Pessagno, of the University of Texas at Dallas, and found to range in age from Late Jurassic (early Tithonian) at the base, to Late Cretaceous (early Cenomanian) at the top. Two zones of recrystallized chert separate major radiolarian age assemblages. Overlying the chert is steep-dipping medium grained Franciscan graywacke, locally with prominent carbonaceous debris.

Continue down road about 0.6 miles to the southeast from Stop 2, to near The Geysers Resort. Turn off paved road to left and park along gravel road near trailer.

23.2 STOP 3. Hydrothermal area along Big Sulphur Creek

Walk down road to where numerous fumaroles can be observed along Big Sulphur Creek. The creek has excavated below the toes of several large landslides, and on-going hydrothermal activity has acid-leached landslide and stream terrace materials, in addition to the bedrock. Several fumarolic vents can be observed to issue from altered, locally well-bedded Franciscan graywacke, along small open fractures that are visible in the scoured creek bottom. This venting of steam along fractures is an excellent illustration of the mode of occurrence of steam in Franciscan reservoir rocks in the subsurface.

****NOTE--STEAM ISSUING FROM THESE FUMAROLAS IS SUPERHEATED, AND MAY NOT BE READILY DETECTABLE ON A DRY DAY. KEEP FACES, HANDS, AND FEET AWAY**

FROM FUMARoles AND AVOID CRUSTY GROUND THAT MIGHT BE UNDERLAIN BY HOT GROUND WATER.

Return to cars, drive back to paved road and proceed southeast past The Geysers Resort. This now run-down hot spring resort was a spa of world renown between the 1860's and early 1900's, visited by such dignitaries as Ulysses S. Grant, William Jennings Bryan, and Theodore Roosevelt.

After passing southeast of The Geysers Resort, the road enters Union Oil Company geothermal lease holdings. Permission to travel any of these roads must be secured from Union Oil Company. At about 0.3 miles from the resort, where the paved road crosses Big Sulphur Creek, leave the paved road and proceed along a dirt road, through a gate, and up Big Sulphur Creek. Note the prominent northwest-trending, hydrothermally altered shear zone at the intersection with the dirt road. Follow the dirt road upstream through a sequence of southeast-dipping, dust-coated Franciscan conglomeratic graywacke, chert, basalt, and thin zones of shaly melange. Several narrow shear zones of hydrothermally altered rock observable in road cuts delineate a northwest-trending fault zone continuous with the fumarolic vent area near The Geysers Resort.

At about 1.5 miles from The Geysers Resort (24.8 mi) the road traverses Dianna Rock, a resistant, sheared mass of basaltic greenstone. Beyond Dianna Rock pass through an area of well-bedded metagraywacke (textural zone 2) with a prominent flaggy cleavage nearly parallel to bedding. This metagraywacke contains the metamorphic assemblage quartz + pumpellyite + phengite ± lawsonite ± glaucophane ± albite. At about 25.0 miles pass into a narrow zone of actinolitic serpentinite with inclusions of sheared greenstone and blueschist. Cross Big Sulphur Creek and park off road.

25.0 STOP 4. Lunch stop and view of Franciscan rocks in Big Sulphur Creek

After lunch gather at cement bridge for a short walk down Big Sulphur Creek. During this traverse, we will view metasedimentary rocks that appear to have pierced the prominent sheet of ultramafic rock that locally caps the steam reservoir. The ultramafic sheet dips to the north-northeast, but it also is tilted gently to the southeast, conformable to the regional plunge of Franciscan structures. Exposed in the piercement feature, along the base of the ultramafic sheet, is a discontinuous zone of blueschist, which is seen in water-scoured exposures upstream (southeast) from the cement bridge. In the core of the piercement structure, below the blueschist zone, and downstream from the bridge, is an interesting sequence of textural zone 2 metaconglomerate and interbedded metagraywacke. Walking downstream from the cement bridge, observe the following features:

1. Hot, gaseous springs bubbling through terrace deposits along the contact between metasediments and structurally overlying blueschist.
2. Stretched-pebble metaconglomerate along Big Sulphur Creek. The metaconglomerate texture becomes increasingly more

reconstituted and the abundance of quartz veining increases near contact margins. The conglomerate clasts include black chert, diorite, diabase, argillite, and abundant silicic volcanic porphyry.

3. Adjacent to and interbedded with the stretched-pebble conglomerate is thin bedded, fine-grained textural zone 2 metagraywacke with interbedded metashale. Although this thin-bedded sequence of metagraywacke and metashale has a prominent foliation subparallel to bedding, sedimentary structures are locally well preserved. This apparently little-disturbed sedimentary texture, however, is misleading, since these rocks have been subjected to very tight isoclinal folding and the folds are commonly transposed by shearing parallel to the fold axes. Further downstream are excellent exposures of highly contorted metagraywacke and metashale. Isoclinal folds, transposition structures, small-scale faulting, and complex folding at several scales can be observed here. The presence of complexly deformed quartz-carbonate veinlets cutting these beds suggests that most of this deformation occurred plastically under considerable pressure, at much deeper crustal levels. The presence of sparse amounts of lawsonite in these metagraywackes is compatible with this interpretation.

A few relatively thick metashale partings up to several feet thick can also be observed in this area. Associated with these shaly zones are boudinaged masses of green basaltic metatuff. Return to vehicles, turn around, and back track downstream to paved road (mileage-26.6). Recross Big Sulphur Creek on paved road and drive up hill into the Union Oil Company--P.G.&E. development area. Travel up through intensely altered fumarolic area on north side of Big Sulphur Creek below prominent serpentinitized and hydrothermally altered ultramafic cap rock. Pass through several gigantic landslides that cover parts of the ultramafic sheet with graywacke and greenstone debris.

At about 2 miles from the last crossing of Big Sulphur Creek, turn off paved road to right, and drive past P.G.&E. offices. Note the prominent closed depression to the right, marking the upper end of a large rotational landslide block. Proceed on the steam field road approximately 1.5 miles to well pad GDC-88 overlooking Big Sulphur Creek Canyon.

33.0

STOP 5. Ultramafic sheet on the north side of Big Sulphur Creek

The purpose of this stop is to look more closely at the major northeast-dipping slab of serpentinite forming part of the caprock to the steam reservoir. Most serpentinite in this part of the Coast Ranges consists of lizardite and chrysotile serpentine mineral assemblages, in most instances relatable to ultramafic rocks in the upper plate of the Coast Range thrust. However, the mineralogy of the serpentinite sheet exposed for more than 6 miles along the northeast side of Big Sulphur Creek is unusual in that its mineral assemblage is largely actinolite \pm talc \pm antigorite \pm chlorite, suggesting temperatures $>300^{\circ}\text{C}$ during serpentinitization. This evidence thus suggests that serpentinitization occurred deeper in the crust and (or) at more elevated temperatures than the lizardite-chrysotile serpentinitization present in ultramafic rocks elsewhere in the area. This ultramafic body is a distinctive lithologic

marker in the subsurface, and is traceable to the north for a considerable distance at depth in the steam field. The base of this actinolitic serpentinite is a thrust fault. The serpentinite is overlain, probably along another thrust, by a thick unit of Franciscan pillow lava, pillow breccia, tuff, minor conglomerate, and chert. Return to the paved road and continue up hill through the steam field, passing through landslide debris from the basaltic unit overlying the serpentinite of the last stop, and pass into in-place basaltic flows.

- 33.6 Along ridge line look to the north across Squaw Creek Canyon toward pine-topped ridge (Caldwell Pines). This ridge is capped by an olivine basalt dated by K-Ar methods at 1.64 ± 0.11 m.y. (Hearn and others, 1976).

Beyond Caldwell Pines, Mount Konocti and Clear Lake basin are visible. Continue along paved road, cross sheared upper contact of basalt flows and pass through an area of interbedded graywacke, pebbly to bouldery shale, and basaltic rocks.

- 35.1 Cross narrow, elongate lizardite-chrysotile serpentinite unit. This serpentinite delineates the base of a warped thrust slice dipping 35° - 60° to the northeast beneath Cobb Mountain.

- 35.2 Turn right at the road intersection, and drive southeast below base of Quaternary volcanic rocks, approximately parallel to the serpentinite-lined fault zone dipping beneath Cobb Mountain.

- 36.0 STOP 6. Quaternary volcanic rocks of Cobb Mountain--presentation by F. E. Goff

The large white boulders in the top of this landslide and draping the slopes of Cobb Mountain are crystal-rich biotite rhyolite of the Clear Lake Volcanics. Cobb Mountain was built in a rather quick and voluminous episode of silicic eruptions which started with extrusion of roughly 5 km^3 of rhyolite about 1.1 m.y. ago. This was followed at 1.05 m.y. by a summit eruption of porphyritic dacite and a final flank eruption of crystal-poor dacite. The last two units are out of sight on the summit and northeast side of the mountain and consist of perhaps another 1.5 km^3 of flows.

The rock is rhyolite flow, not tuff or welded tuff, as can be seen from the lack of fragmental or welded textures. It is generally vesicular with abundant phenocrysts of biotite, plagioclase, sanidine, and quartz. The vesicles sometimes contain dark needles of edenite, a sodic amphibole (R. Erd, 1975, oral commun.). Where well exposed, the rhyolite grades upward from basal breccia to frothy and spherulitic rhyolite to over 300 m of devitrified rhyolite. The pumiceous carapace of the rhyolite flow is locally preserved beneath the summit dacite. Preliminary paleomagnetic studies show that the rhyolite has a unique magnetic direction. The overlying dacite is magnetically reversed.

Major faults bound the west edge of Cobb Mountain and offset volcanic units by about 100 meters near the mountain's center, but there is no evidence to suggest these faults are active. The close spatial association of young volcanic rocks with The Geysers steam field implies that

they are both manifestations of the same deep-seated heat source. At present, no steam wells have been drilled through volcanic rocks on Cobb Mountain, but Union Oil Company plans to drill at least one deep exploratory hole in the future.

Resume driving southeast below Cobb Mountain through structural unit 2 Franciscan graywacke.

37.2 Pass P.G.&E. power plants 9 and 10, and continue along the road on the north side of Big Sulphur Creek canyon, roughly parallel to the strike of Franciscan structure. Cross and recross the sheared contact of greenstone and graywacke.

38.2 While driving along strike, road crosses a thin melange zone with a gouged pebbly shale matrix, containing blocks of greenstone, graywacke, to chert, and minor blueschist. The road crosses this thin melange zone 39.7 several times.

The general tendency of bedding and shear fabric of Franciscan sedimentary rocks in this area is to dip steeply or at a low angle north-northeastward, beneath Cobb Mountain.

40.0 To the right, view of Little Geysers fumarolic area in the lower part of a large landslide complex. The landslide involves rocks of the serpentinite unit viewed at stop 5. The faulted upper contact of this serpentinite with overlying graywacke is at an abrupt break in slope nearly coincident with the top of the landslide. The percolation pond and benched-off area at the top of this landslide is the site of a spectacular blow-out that occurred in March 1975, that was described in detail recently by C. F. Bacon (1976).

Continue down road, cross the lower contact of graywacke into serpentinite, and drive past the blowout site toward Big Sulphur Creek.

41.6 At the road intersection, turn left, drive past steam wells, and leave Union Oil Company steam field by the Socrates Mine Road. Turn left at Socrates Mine Road and proceed up hill through hydrothermally altered serpentinite, graywacke, and greenstone, to alluvial flat. Bear to right at the first major road intersection, and follow Socrates Mine Road northeast, to the next major road intersection.

42.9 Intersection with road to Aminoil and Shell Oil Company federal leases-- turn right and drive southeast, through poorly exposed textural zone 2 metagraywacke of structural unit 2.

43.5 Cross upper contact of metagraywacke, pass through a thin zone of glaucophane schist, and into sheared serpentinitized peridotite. This extensive serpentinite sheet is continuous with an ophiolite sequence that is overlain by strata of the Great Valley sequence 5 miles (8 km) to the southeast, beneath the Sonoma Volcanics of Mount St. Helena. The faulted base of this ultramafic sheet is interpreted to be the deformed Coast Range thrust of Bailey and others, 1970. Drive along the ridge southeastward through serpentinitized peridotite. To the left of the ridge note a huge mass of Franciscan melange that is apparently surrounded by serpentinite. This mass of melange may be interpreted either as intrusive into, thrust over, or as a tectonic inclusion

within, the ultramafic rocks.

- 44.5 Note several small isolated masses of Franciscan conglomerate surrounded by serpentinite along the road. Cross out of serpentinite and into textural zone 1 conglomeratic graywacke thrust over serpentinite. These relationships just observed suggest that the concept of emplacement of Franciscan rocks beneath the Coast Range ophiolite along a single thrust fault is too simplified a model. In this area emplacement must have occurred along a thick zone involving Franciscan rocks intersheared with the lower part of the overriding sheet of oceanic crust.

Alternatively, the complex relationships we see between the basal Coast Range ophiolite and Franciscan rocks may result from deformation post-dating initial emplacement of the Franciscan beneath the Coast Range thrust.

- 45.2 STOP 7. View of Mount St. Helena and southeast extension of the geothermal area--presentation by B. C. Hearn, Jr., and J. M. Donnelly.

From here, you can see Mt. St. Helena, about 7 miles to the southeast. Mt. St. Helena, according to K. F. Fox, Jr. (written communication), is a thick pile of tuff breccia, rhyolite breccia, lithoidal rhyolite, and welded tuff. Rhyolite is the chief component of the upper 800-2000 ft. of the mountain. This rock is locally columnar jointed, and on the western and northern slopes the jointing is well enough developed to define perhaps a half dozen or more stratiform layers, suggesting that the mass is a pile of subhorizontal to steeply tilted flows. Relic eutaxitic fabrics and shard textures are locally present within the rhyolite near interflow contacts and are particularly well developed in the upper most part of the pile, suggesting that much of the rhyolite originated as a welded tuff. A specimen of this rock from the crest of the mountain was dated at 2.9 ± 0.2 m.y. (Mankinen, 1972). A similar unit, but generally less than 100 ft. thick, scabs pyroclastic rocks along ridges to the south.

There are small patches of volcanic rocks along the ridge between here and Mt. St. Helena, including Pine Mountain about 1.5 miles south. Pine Mountain itself is rhyolitic in composition and gives a K-Ar date of 2.04 ± 0.04 m.y. It is crystal rich, containing abundant quartz, sanidine, and biotite and we have included it within the Clear Lake volcanic field. It is the oldest dated rock in the Clear Lake field, but older rocks may occur to the southeast among largely unmapped remnants of basalt and andesite flows which lie between mapped Sonoma and Clear Lake Volcanics. One such mafic lava at Table Mountain, has been dated at 1.94 ± 0.06 m.y. Sonoma and Clear Lake volcanism appear to be distinct temporally, spatially, and petrologically. The northern 2.9-5.3 m.y. old Sonoma volcanic field is 80 percent pyroclastic, 15 percent rhyolite, and 5% andesite and basalt, and the flow rocks contain little, if any phenocrystic quartz (K. Fox, Jr., 1975, oral commun.). The Clear Lake Volcanics, by contrast, are 5 percent or less pyroclastic, and nearly all lavas of all compositions contain quartz. K-Ar dating shows that volcanism has, in general, been moving to the north through time, both in the Coast Ranges in general, and within the Clear Lake volcanic field.

Turn around and back track to Socrates Mine Road. Turn right and follow the main road northeast, and downhill approximately 3.5 miles to the intersection with Highway 175. A left turn takes you toward the Clear Lake resort area.

(END OF ROAD LOG FOR THE FIRST DAY)

References Cited

- Bacon, C. F., 1976, Blow out of a Geothermal Well, The Geysers Steam Field, Sonoma County, California: California Geology, January 1976.
- Bailey, E. H., Blake, M. C., Jr., and Jones, D. L., 1970, On-land Mesozoic Oceanic Crust in California Coast Ranges, in Geological Survey Res., 1970: U.S. Geol. Survey Prof. Paper 700C, p. 70-81.
- Blake, M. C., Jr., Irwin, W. P., and Coleman, R. G., 1967, Upside-down metamorphic zonation, blueschist facies, along a regional thrust in California and Oregon, in U.S. Geological Survey Research, 1967: U.S. Geol. Survey Prof. Paper 575C, p. 1-9.
- Brice, J. C., 1953, Geology of Lower Lake Quadrangle, California: California Div. of Mines and Geology Bull. 166, 72 pp.
- Chapman, R. H., 1975, Geophysical Study of the Clear Lake Region, California: California Div. of Mines and Geology Special Rept. 116, 23 pp.
- Dickinson, W. R., 1970, Clastic sedimentary sequences deposited in shelf, slope, and trough settings between magmatic arcs and associated trenches: Pacific Geology, v. 3, p. 15-30.
- Donnelly, J. M., 1976, Active faulting in The Geysers-Clear Lake area, northern California: Abstract, Geol. Soc. of America 72nd Ann. Cordilleran Sec. Mtg.
- Evitt, W. R., and Pierce, S. T., 1975, Early Tertiary ages from the coastal belt of the Franciscan Complex, northern California: Geology, v. 3, p. 433-437.
- Goff, F. E., and McLaughlin, R. J., 1976, Geology of the Cobb Mountain-Ford Flat geothermal area, Lake County, California: U.S. Geol. Survey open file map 76-221, 1:24,000, 1 sheet.
- Goff, F. E., Donnelly, J. M., Thompson, J. M., and Hearn, B. C., Jr., in press, Geothermal prospecting in The Geysers-Clear Lake area, northern California: Geology, v. 5, 26 p.
- Hearn, B. C., Jr., 1976, Preliminary geologic map and cross-section of the Clear Lake Volcanic field, Lake County, California: U.S. Geol. Survey open file map 76-751, 1:24,000.
- Hsu, K. J., 1968, Principles of Melanges and their Bearing on the Franciscan-Knoxville paradox: Geol. Soc. of America Bull., v. 79, p. 1063-1074.
- Mankinen, E. A., 1972, Paleomagnetism and potassium-argon ages of the Sonoma Volcanics, California: Geol. Soc. America Bull., v. 83, p. 2063-2072.
- McLaughlin, R. J., 1975, Preliminary compilation of in-progress geologic mapping in The Geysers geothermal area, California: U.S. Geol. Survey open file map 75-198, 1:24,000.
- _____, 1974, Preliminary geologic map of The Geysers steam field and vicinity, Sonoma County, California: U.S. Geol. Survey open file map 74-238, 1:24,000.

McLaughlin, R. J., and Pessagno, E. A., in press, Significance of age relationships above and below Upper Jurassic ophiolite in The Geysers-Clear Lake region, California: Geol. Soc. of America Bull., 22 pp.

McLaughlin, R. J., and Stanley, W. D., 1976, Pre-Tertiary geology and structural control of geothermal resources, The Geysers steam field, California: Proceedings Second U.N. Symposium on Dev. and Use of Geothermal Res., San Francisco, May 1975, p. 475-485.

Stanley, W. D., Jackson, D. B., and Hearn, C. B., Jr., 1973, Preliminary results of geoelectrical investigations near Clear Lake, California: U.S. Geol. Survey open file report.

Swe, W., and Dickinson, W. R., 1970, Sedimentation and thrusting of late Mesozoic rocks in the Coast Ranges near Clear Lake, California: Geol. Soc. America Bull., v. 81, no. 1, p. 165-188.

White, D. E., Muffler, L. J. P., and Truesdell, A. H., 1971, Vapor-dominated hydrothermal systems compared with hot water systems: Econ. Geology, v. 66, no. 1, p. 75-97.

THE CLEAR LAKE VOLCANICS, CALIFORNIA: GEOLOGY AND FIELD TRIP GUIDE

Julie M. Donnelly, U.S. Geological Survey, Menlo Park, CA 94025,
B. Carter Hearn Jr., U.S. Geological Survey, Reston, VA 22092,
and Fraser E. Goff, U.S. Geological Survey, Menlo Park, CA 94025

Introduction

The Clear Lake Volcanics, of late Pliocene to Holocene age, cover an area of about 400 km², 150 km north of San Francisco in the California Coast Ranges. Among Quaternary volcanic fields of the western United States, the Clear Lake Volcanics is unique in that it rests on both the Franciscan assemblage and the Great Valley sequence and is considerably west of the projection of the Cascade trend of young volcanic fields. The Clear Lake volcanic field is the youngest and most northerly of a series of volcanic centers which increase in age southward.

The Sonoma Volcanics, of Pliocene age (published potassium-argon ages 5.3 to 2.9 m.y., Mankinen, 1972), extend north from the San Francisco Bay area to the vicinity of Mt. St. Helena, 10 km southeast of The Geysers steam field. The youngest date, 2.9 ± 0.2 m.y., is on a welded ash-flow tuff at the summit of Mt. St. Helena, near the northern limit of the Sonoma Volcanics and close to the Clear Lake Volcanics. Most volcanic rocks of the Clear Lake field are geographically separate from and lie north of the Sonoma Volcanics. The oldest K-Ar date for the Clear Lake Volcanics is 2.04 ± 0.04 m.y. (Hearn and others, 1976a), from the rhyolite of Pine Mountain (10 km northwest of Mt. St. Helena). This date suggests a gap of 0.8 m.y. or less between Sonoma and Clear Lake volcanism.

The main part of the Clear Lake volcanic field occupies the southern part of the Clear Lake topographic basin and extends southward toward the crest of the Mayacmas Range (fig. 1). Outliers of Clear Lake Volcanics are (1) quartz-bearing olivine basalt flows and vents which extend southeastward for 35 km to Lake Berryessa and have not been mapped by us, (2) isolated small areas of extrusive and intrusive rocks which occur within 10 km of the main volcanic field.

Current studies

Many important earlier studies have contributed to knowledge of the Clear Lake area. Previous field trip guides which cover part of the Clear Lake Volcanics are by Emerson and Rich (1966) and Hauge and others, (1972).

Detailed geologic mapping of the Clear Lake Volcanics by personnel of the U.S. Geological Survey (Hearn and others, 1975b, 1976b; Goff and McLaughlin, 1976) is nearly complete. Some outliers of the volcanic field are shown on geologic maps of The Geysers area (McLaughlin, 1974, 1975). Gravity and aeromagnetic data (U.S. Geological Survey, 1973; Isherwood and Chapman, 1975) have been interpreted by Chapman (1966, 1975) and Isherwood (1975, 1976). Electrical resistivity data have been evaluated by Stanley and others (1973). Preliminary results of seismic

monitoring are given by Bufe and Lester (1975), Bufe and others (1976), Iyer and Hitchcock (1975), and Steeples and Iyer (1976), extending the limited study of micro-earthquakes of The Geysers area by Hamilton and Muffler (1972) and Lange and Westphal (1969). Donnelly and others (1976) reported on some possibly active fault zones. Repeated surveys of triangulation and levelling networks, and monitoring of lake level (Lofgren, 1973) will determine whether there is current deformation related to regional tectonics or to geothermal production. C. S. Gromme and E. A. Mankinen are studying the paleomagnetism of volcanic rocks erupted during or close to the Jaramillo normal magnetic event. Urban and others (1976) presented limited data on heat flow in the vicinity of the potential geothermal area.

Data from cores of sediments beneath Clear Lake have been reported by Sims and Rymer (1975a-g, 1976a), Casteel and others (1975); Adam and Sims (1976), and Adam (1976) in connection with a drilling program initiated to assess the frequency of earthquakes near the Clear Lake area (Sims, 1974). Sims and Rymer (1974, 1976b) have studied the distribution of gaseous springs in Clear Lake and the structural control of the Clear Lake basin. M. J. Rymer is studying the Cache Formation in the Clear Lake basin. Casteel and Rymer (1975) have reported on fossil fishes of the Cache Formation.

Preliminary data and interpretation of the geochemistry of thermal waters by Goff and others (1976, 1977 in press) and Donnelly and others (1976) provide more comprehensive coverage of the Clear Lake volcanic field and add to the data reported by Waring (1915), Berkstresser (1968), and Barnes and others (1973a, b), and White and others (1973).

Geologic setting

The Clear Lake Volcanics overlies the Franciscan assemblage of Late Jurassic to Eocene age, the Great Valley sequence of Late Jurassic to Late Cretaceous age, and sedimentary rocks of Paleocene and Eocene age, and is in part interbedded with the youngest part of the Pliocene and Pleistocene Cache Formation of Anderson (1936). Serpentinized mafic and ultramafic rocks (ophiolite) form the base of the Great Valley sequence, which has moved across the structurally complex Franciscan assemblage along the Coast Range thrust. The Great Valley sequence is preserved in a broad northwest-trending zone of complexly folded thrust sheets (Swe and Dickinson, 1970; Berkland, 1973). The Paleocene and Eocene rocks may have been involved in the thrusting (Swe and Dickinson, 1970; Berkland, 1973). The northwestward extent of the allochthonous Great Valley sequence concealed beneath the volcanic field can be approximately delineated by high chloride content of well and spring waters, characteristic of the Great Valley sequence (Goff and others, 1977 in press; Donnelly and others 1976). The closest occurrence of Great Valley sequence in the area north of Clear Lake is in the Middle Mountain block (Berkland, 1973) a klippe surrounded by the Franciscan assemblage.

The type Cache Formation, most of which predates the Clear Lake Volcanics, consists of fresh-water, dominantly fluvial but locally lacustrine deposits which filled an irregular fault-bounded basin largely east of the present Clear Lake Basin. Problems persist in the usage of

the term Cache Formation. Clastic and volcanoclastic deposits which occur beneath, within and geographically near the Clear Lake Volcanics have been assigned to the upper part of the Cache Formation by previous workers (Brice, 1953; McNitt, 1968a; Hodges, 1966; Swe and Dickinson, 1970; Casteel and Rymer, 1975), but have a range of age from about 1.6 m.y. to probably less than 0.05 m.y., distinctly younger and differing texturally from most of the Cache Formation in its type area 4-15 km east of Clear Lake. In that area the formation contains only a few clasts derived from the Clear Lake Volcanics and those are from the early basalts (>1.6 m.y.). Because many of the clastic and volcanoclastic deposits within and on the west border of the Clear Lake volcanic field are younger than the type Cache, isolated from it, and of different lithology, subdivision of the Cache Formation or revision of its usage is in order.

Sedimentary deposits cored from beneath Clear Lake (Sims and Rymer, 1975a-g, 1976a) represent a continuous record of sedimentation for about the last 135,000 years (core 4, Sims and Rymer, 1975c; Adam, 1976), and provide a unique record of faunal, floral and climatic conditions in the Clear Lake basin (Casteel, Adam and Sims, 1975; Adam and Sims, 1976; Adam, 1976). The cored sediments beneath Clear Lake probably overlie older fluvial and lacustrine deposits (lake deposits of Kelseyville, as used by Hearn and others 1976a) at unknown depth below the deepest hole. Whether any part of the type Cache Formation occurs at even greater depth beneath Clear Lake is unknown; lakeshore exposures of Cache Formation are limited to the extreme southeast end of Clear Lake.

Lithology of Clear Lake Volcanics

The Clear Lake Volcanics consists of basalt, andesite, dacite, and rhyolite, which occur as domes, flows, and relatively few pyroclastic deposits in a structurally and chronologically complex sequence. Rock names are based in part on field identifications and are tentative until more complete chemical data are available. The term basalt includes basaltic andesites with up to 58 percent silica. The term dacite includes rhyodacites, which are difficult to distinguish from dacite in the field.

The Clear Lake Volcanics, in contrast to the generally quartz-free Sonoma Volcanics (K. F. Fox, Jr., personal communication), characteristically contains quartz as phenocrysts in the more silicic types and as 1 mm - 15 cm rounded to subangular, commonly resorbed grains of controversial origin in mafic rock types. All the basalts contain olivine, from less than 1% to 10%. The andesites typically contain phenocrysts of plagioclase and orthopyroxene, clinopyroxene, and rarely olivine, and vary widely in amount of pyroxene.

The many dacites range from highly porphyritic to sparsely porphyritic, containing phenocrysts of plagioclase, clinopyroxene, orthopyroxene, and quartz. Most varieties also possess small amounts of biotite, hornblende, or both. Olivine is rare. Many highly porphyritic varieties contain sanidine phenocrysts and are probably of rhyodacitic composition. Some sparsely porphyritic varieties have widespread glassy chilled facies.

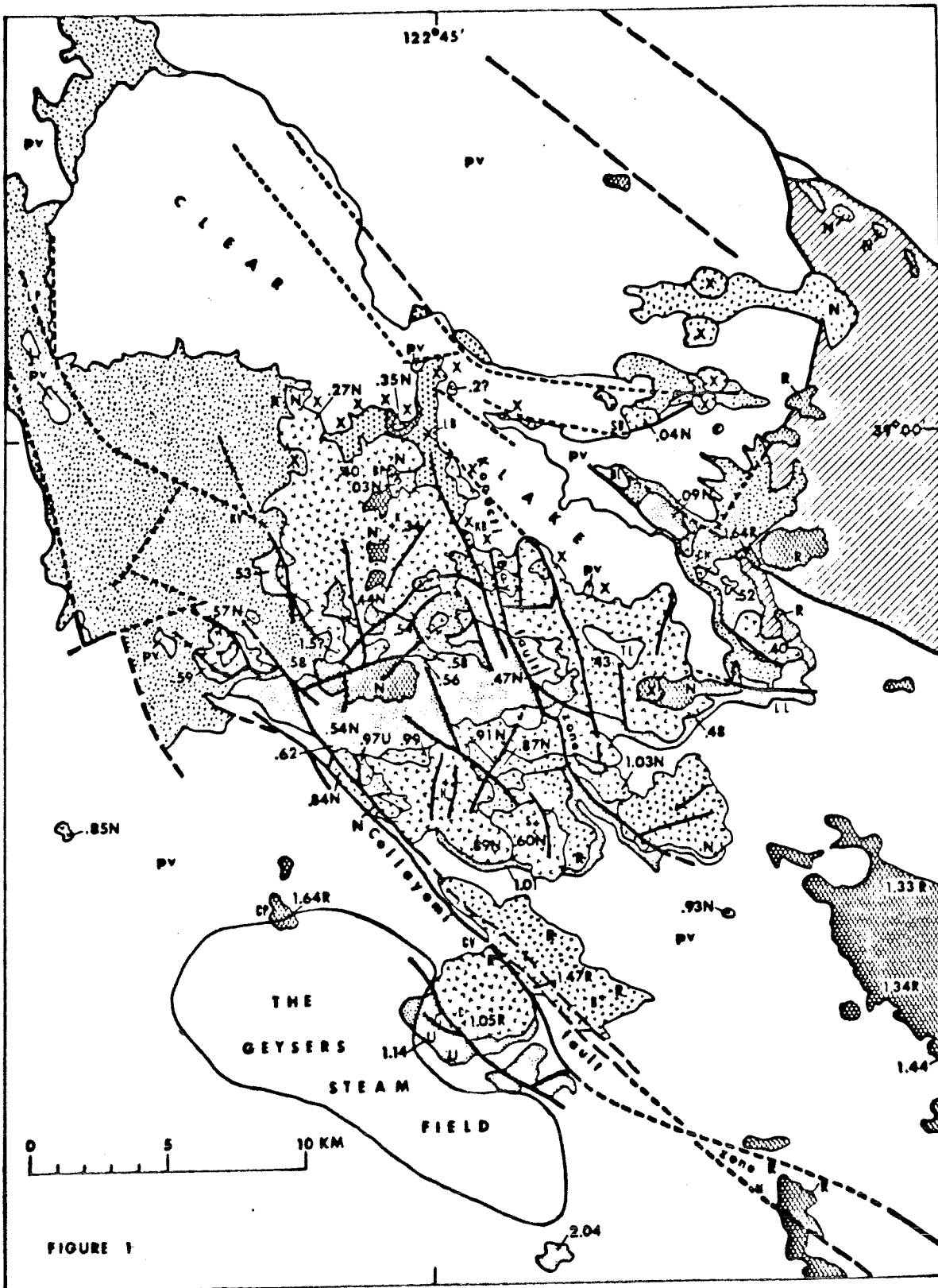


FIGURE 1

EXPLANATION FOR FIGURE 1

Generalized geologic map of Clear Lake volcanic field, showing K-Ar ages and magnetic polarities. Lake and alluvial deposits are shown only near Clear Lake. Outcrop pattern of the Cache Formation is modified from Brice (1953). Order of volcanic units in explanation is not sequence of eruption. X denotes only young vents, less than about 0.1 m.y. old; older vents are not shown. Lateral extent of cinder cones shown where associated with flows. Numerous contacts between units within the patterned areas of single rock types have been omitted for clarity. A few contacts between flows of different age and/or magnetic polarity are shown within a single rock type. Faults dashed where inferred, dotted where concealed. Geology in part modified from Brice (1953), Lake County Flood Control and Water Conservation District (1967), McNitt (1968a,b,c), and Sims and Rymer (1976b). Abbreviations of geographic names (+ denotes location): B-Boggs Mountain, C-Cobb Mountain, H-Mount Hannah, K Mount Konocti, S-Seigler Mountain, BP-Buckingham Peak, KB-Konocti Bay, CP-Caldwell Pines, CV-Cobb Valley, SB-Sulphur Bank, BL-Borax Lake, LB-Little Borax Lake, TL-Thurston Lake, CH-Clearlake Highlands, KV-Kelseville, LL-Lower Lake, LP-Lakeport, M-Middletown.

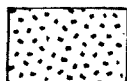
CLEAR LAKE VOLCANICS (Pleistocene and Upper Pliocene):



Young
pyroclastic
deposits



Basalt



Andesite



Dacite



Rhyolite

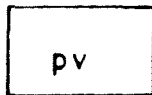
OTHER UNITS:



Lake and alluvial deposits (mostly Holocene)

Syn-volcanic clastic deposits (Pleistocene)

Cache Formation (Pliocene and Pleistocene)



Pre-volcanic rocks (Lower Tertiary, Cretaceous, and Jurassic)

K-Ar dates of units are shown by numbers, e.g. .48; magnetic polarities are shown by the symbols N (normal), R (reverse), and U (unique, low-angle).

The rhyolite is of two types, biotite-bearing and nearly biotite-free. Biotite rhyolite is typically crystal-rich (15-30 percent quartz and feldspar phenocrysts), and its glassy facies tend to be perlitic. Biotite-free rhyolite is typically crystal poor (3 percent or less of plagioclase and orthopyroxene phenocrysts) and has widespread obsidian along flow borders. Only one biotite-free rhyolite (rhyolite of Bonanza Springs) forms a large volume of pyroclastic material. No rhyolitic ash-flow deposits are present in the Clear Lake Volcanics, whereas they are common in the Sonoma Volcanics.

The preserved volume of volcanic rocks that are more silicic than andesite is about 35 km³ if the Mt. Konocti pile bottoms at lake level, and 50 km³ if it extends 300 m below lake level. The preserved volume of basalt and andesite is about 10 to 15 km³, but the original volume before erosion may have been twice that.

Eruptive sequence

In general, the volcanic rocks are progressively younger northward through the field. K/Ar dates range from 2.04 to 0.03 m.y. and most are in good agreement with magnetic-polarity determinations and known stratigraphic relations. The main part of the field is younger than 1.0 m.y., and much of the central part is younger than 0.6 m.y. The volcanic sequence is complex, however, and is best understood by referring to Hearn and others (1976a).

The oldest dated unit is the 2.04 ± 0.04 m.y. rhyolite of Pine Mountain, 10 km northwest of Mt. St. Helena (see road map at beginning of guidebook). The oldest dated basalt, 1.94 ± 0.04 m.y., is the Table Mountain flow 10 km southeast of Middletown, close to the present northeastern limit of preserved Sonoma Volcanics. The widespread quartz-bearing olivine basalts east and southeast of the main part of the Clear Lake field give ages of 1.33 ± 0.52, 1.34 ± 0.27, 1.44 ± 0.10, and 1.64 ± 0.09 m.y. Some of these basalts marginally overlap the Sonoma Volcanics southeast of Middletown. Although the absolute range of age of these olivine basalts is uncertain, their K/Ar ages and consistent reverse magnetic polarity (Hearn and others, 1976a) suggest that they are between about 1.3 and 1.6 m.y. old, within the Matuyama magnetic epoch (Cox, 1969). Three other units may belong to the same eruptive episode: olivine basalt of Caldwell Pines, within The Geysers steam field (1.64 ± 11 m.y.); olivine andesite of Ford Flat, beneath Cobb Mountain (1.69 ± 0.20 m.y.); and andesite of Boggs Mountain (1.47 ± 0.04 m.y.).

A possible hiatus from about 1.3 to 1.15 m.y. was ended by the eruptive sequence of biotite rhyolite (1.14 ± 0.02 m.y.) to crystal-rich dacite (1.05 ± 0.02 m.y.) to crystal-poor dacite (undated) at Cobb Mountain, the composite silicic dome closest to the steam field. A widespread obsidian-bearing rhyolitic tuff and tuff breccia (rhyolite of Bonanza Springs, 1.01 ± 0.03 m.y.), which was erupted from a source northeast of Seigler Mountain, underlies much of the southern edge of the volcanic field. This tuff was assigned to the Cache Formation by Brice (1953), but its equivalent has not been found in the type Cache Formation.

Subsequent eruptions from vents in the south-central part of the field between about 1.0 and 0.8 m.y. produced a variety of andesites and dacites, including the dacite of Tyler Valley northwest of the steam field. Several units show normal or unique low-angle magnetic polarity probably acquired during the Jaramillo normal polarity event. The currently accepted limits of the Jaramillo, 0.89 ± 0.95 m.y. (Cox, 1969), are not well defined and may be more accurately determined by recent detailed magnetic sampling of the Clear Lake Volcanics.

No volcanic activity occurred between about 0.8 and 0.6 m.y., after which a major period of silicic volcanism began in the central part of the field. After the eruption of some dacite, about 4 km^3 of sparsely porphyritic rhyolite of Thurston Creek erupted from vents along an arcuate trend concave to the north (fig. 1). The rhyolite gives a range of dates from 0.466 ± 0.014 m.y. near its eastern limit to 0.63 ± 0.03 m.y. in its western part, but its age of 0.56 ± 0.01 m.y. at Sulphur Mound Mine (stop 11) is most closely bracketed by underlying biotite dacite 0.58 ± 0.01 m.y. old and overlying biotite rhyolites 0.54 ± 0.01 m.y. and 0.50 ± 0.01 m.y. old. The domal accumulation of dacite at Seigler Mountain (fig. 1 and road map), 0.60 ± 0.01 m.y., is an exception to the generally older ages in the southern part of the field.

From about 0.55 to 0.40 m.y., eruption of small volumes of biotite rhyolite (in part pyroclastic) alternated at different vents with eruptions of small volumes of basalt in the central part of the field. These local basalts and biotite rhyolites, and the earlier widespread biotite-free rhyolite, were partly covered by the ten or more voluminous flows and domes of dacite which built 1,000 m high Mt. Konocti between about 0.40 and 0.25 m.y. Two cinder cones of olivine basalt high on Mt. Konocti are partially buried by flows of dacite 0.34 ± 0.01 m.y. old. Dacites within a band of flows and domes aligned from Mt. Konocti east-southeast to the vicinity of Clearlake Highlands give ages of 0.40 ± 0.04 to 0.52 ± 0.06 m.y. and thus could be coeval with the early dacite of Mt. Konocti.

The youngest silicic eruption produced the rhyolitic obsidian of Borax Lake, at 0.088 ± 0.013 m.y. The rhyolite of Borax Lake may be chemically related to an underlying olivine dacite flow (Bowman and others, 1973). Adjacent olivine basalt, erupted from an underlying subdued cinder cone, could be an even older member of the variation series.

The most recent eruptive activity, basaltic to andesitic in composition, was in part phreatomagmatic, producing pyroclastic maar deposits near the lake. The cinder cone and flow at Buckingham Peak, and the cinder cones and flows along a N. 10° E. trend across the east arm of Clear Lake, also date from this period. The andesite flow at Sulphur Bank (White and Roberson, 1962) overlies sediments from which a carbonized log yielded a ^{14}C date of $44,500 \pm 800$ years (M. Stuiver, written communication). Phreatomagmatic eruptions along the lake shore have left a widespread blanket of pyroclastics, some of which are base-surge deposits (stop 12).

The series of young basaltic to andesitic eruptions is probably represented by the many beds of mafic ash reported in cores of sediments beneath Clear Lake (Sims and Rymer, 1975a-g, 1976a). The youngest ash recognized in these cores is about 10,000 years old.

Structure

The youngest faults in The Geysers-Clear Lake area trend northwest or north-northwest, parallel and subparallel to the general structure grain of the Coast Ranges and the San Andreas fault system. Two prominent fault zones, the Collayomi and the Konocti Bay, follow these trends. Faults also trend east and northeast, but are dominated by the other directions. The overall pattern may fit a model of conjugate northwest and northeast faulting within the San Andreas system. Most are normal faults but several of the northwesterly-trending faults show geomorphic features suggestive of right-lateral strike slip movement, such as offset drainages. In the Collayomi fault zone, a young age of right-lateral strike-slip movement is suggested by linear topographic features, drainage offsets, and serpentinite that is squeezed up between volcanic units as young as 1.1 m.y. Along one fault in the zone, offset of volcanic units 0.5-0.6 m.y. old suggests an average movement of about 1 mm/yr for the past half million years.

The Clear Lake topographic basin is delineated in part by faults of north, north-northwest, and west trend (Sims and Rymer, 1974, 1976b). Northward tilting of lake and fluvial deposits less than 0.6 m.y. old south of Kelseyville, and the presence of deep water and steep slopes near the northeast shores of Clear Lake, suggest that northward or northeastward tilting of the lake basin has continued to recent time, as a result of relative uplift to the south.

The possibility of active deformation is indicated by earthquakes within the volcanic field and the Clear Lake structural basin. Earthquake epicenters are located (Hamilton and Muffler, 1972; Chapman 1975; Bufe and others, 1976) close to the Collayomi and Konocti Bay fault zones, and residents living close to both zones report felt earthquakes. Earthquakes also may be associated with the faults that bound parts of the Clear Lake basin. Ongoing seismic studies (Bufe and Lester, 1975; Bufe and others, 1976) will help locate active faults and will generate fault-plane solutions to determine source mechanisms. Monitoring changes in elevation and horizontal distances (Lofgren, 1973) has the potential of characterizing current deformation and tilting in The Geysers-Clear Lake area.

Although parts of the volcanic field show local subsidence and the Clear Lake structural basin is probably continuing to subside, evidence for large-scale caldera collapse is lacking. The largest circular collapse feature is a 1.6 km diameter basin southeast of Mt. Konocti (fig. 1). The shape of the northern part of Clear Lake and some adjacent faults suggest partial control by circular collapse, but this pattern could be fortuitous. Young volcanic rocks do not occur around the northern part of the lake.

Geophysical studies

Gravity surveys (Chapman, 1966; Isherwood and Chapman, 1975) show a circular 25 mgal gravity low about 20 km in diameter, centered over Mt. Hannah in the south-central part of the volcanic field (McLaughlin, this guidebook, fig. 2). The gravity anomaly and aeromagnetic data (U.S. Geological Survey, 1973) have been interpreted as expressions of a magma chamber about 6 to 8 km in diameter whose top is within 10 km of the surface (Chapman, 1966, 1975; Isherwood, 1975, 1976).

Electrical resistivity data show a well-defined resistivity low, bilobate toward the east, which is nearly coincident with the gravity low (Stanley, Jackson, and Hearn, 1973). Deep electrical soundings show that low resistivity persists to at least 5 km depth. Either geothermal fluids, normally saline, or a thick section of Great Valley sequence which typically contains saline fluids, could contribute to the resistivity low. Normal resistivity of Great Valley marine shale is low enough to explain the resistivity low. However, the occurrence of predominantly Franciscan lithology in a drill hole (Kettenhofen 1) on the north edge of the resistivity low, and the structural complexity of Great Valley sequence next to the volcanic field, imply that a several-thousand meter section of marine shale beneath the volcanic field is unlikely. Thus the resistivity low possibly has a dominant contribution from fluids at elevated temperature and salinity above a heat source at depth.

Preliminary data on teleseismic P-waves arriving within the area of the gravity low show delays of 0.5 to 1.5 seconds, which are consistent with the presence of a volume of hot rock and magma of about 10 km diameter (Steeple and Iyer, 1976; Iyer and Hitchcock, 1975).

Thermal waters

Application of Na-K-Ca and silica geothermometry to the chemistry of thermal springs and wells, and drill-hole data indicate that a hot water system at about 200°C underlies the Clear Lake volcanic field northeast of the Collayomi faultzone, which probably forms the northeast limit of The Geysers steam field (Donnelly and others, 1976; Goff and others, in press). Most thermal waters emerge along fault zones and have high magnesium contents owing to the presence of serpentinite at the surface or inferred at depth. Small vapor-dominated (steam) systems could be present in local structures with low porosity and permeability beneath the volcanic field, but their waters, which would be chemically distinctive, have not been found in the wells and springs sampled so far. The 80 or more volcanic vents may provide access for recharge water of volume sufficient to prevent the formation of a widespread vapor-dominated system beneath the volcanic field.

Relatively chloride-rich water and low resistivity (Goff and others, 1977 in press) outline the concealed extent of the Great Valley sequence beneath the volcanic field. Northeast of Clear Lake, where existing maps show only Franciscan assemblage, high chloride waters suggest that the Franciscan is misidentified or that the Great Valley sequence occurs at depth beneath Franciscan rocks (Goff and others, 1977 in press).

Magma chamber and future volcanic activity

Geophysical data indicate that there is a significant volume of hot and molten rock, i.e. a magma chamber or magma reservoir, at about 10 km depth beneath the Clear Lake volcanic field. Presence of a high-level magma chamber is also suggested by the large volume of silicic, relative to mafic, volcanic rocks (Smith and Shaw, 1975). In addition, the numerous warm springs and areas of alteration and gas emission indicate a major heat source at depth. The central magma chamber is most likely the ultimate heat source for The Geysers steam field. The area above the inferred magma chamber also is a "shadow zone" (Smith and Shaw, 1975) in which no young mafic vents occur, presumably because dense mafic magma from greater depth could not penetrate the lower density, silicic magma in the shallow magma chamber.

What is the likelihood of future eruptions in or near this young volcanic field? The lack of ash-flow tuffs and the complex eruptive history over the past 2 m.y., with intensive activity in the past 1 m.y. and the youngest eruption only 10,000 years ago, suggest that the field could be in an early evolutionary stage leading to major ash-flow eruptions and large-scale caldera collapse, as shown by other silicic magma systems such as at Long Valley caldera, California, Valles caldera, New Mexico, and the Yellowstone Park caldera complex. Such an eruption would be a volcanic hazard of major importance. However, because the Clear Lake field lies in a different tectonic setting, its volcanic system may not follow the same evolutionary course. If the walls and roof of the magma chamber are being constantly fractured by stress along branches of the San Andreas fault system, frequent leakage of magma may prevent the accumulation of volatiles necessary for a voluminous ash-flow eruption.

The northward progression of eruptions through time indicates that sites of future eruptions are more likely to be close to, beneath, or northeast of Clear Lake. Such eruptions would probably be of mafic composition, although the 90,000-year-old rhyolite of Borax Lake indicates that silicic eruptions could also occur. Mafic eruptions would produce cinder cones and flows of relatively small to moderate volume. Near the lake, such eruptions might be phreatomagmatic, producing explosive maar-type deposits and causing a significant hazard to the area of the lake shore and within a few kilometers of the eruption site. The frequency of mafic eruptions is difficult to predict. Spacing of reported ash beds in cores from sediments beneath Clear Lake suggests that mafic volcanic activity was frequent from about 55,000 to 10,000 years ago, but quiescent for the past 10,000 years (Sims and Rymer, 1975a-g, 1976a).

The succession of younger volcanic centers northward through the Coast Ranges could fit a model of a fixed heat source beneath the North American plate, with the plate having a resultant apparent motion to the southeast or south-southeast. The inferred high-level magma chamber beneath the Clear Lake Volcanics may have been left behind to cool and crystallize, while the deep heat source now may be warming up the area to the northeast of Clear Lake, in preparation for a new focus of igneous activity. That area contains numerous thermal springs (Waring, 1915; Berkstresser, 1968; White and others, 1973; Barnes and others, 1973a, b; and Goff and others, 1977 in press) and some of the youngest volcanic rocks in the Clear Lake field are located immediately to the northeast of Clear Lake.

FIELD TRIP GUIDE*

Second Day

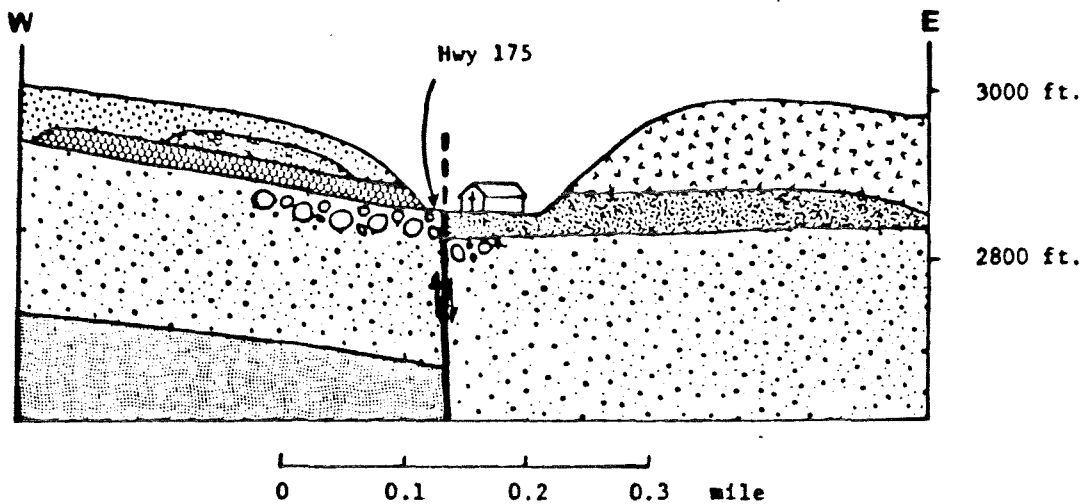
Cumulative Mileage

- 0.0 Cobb Village parking lot. Turn left and follow Highway 175 south.
- 1.9 The drainage of Putah Creek on the left follows the Collayomi Fault zone.
- 2.2 Shear zone of serpentine and young gravel containing cobbles of the andesite of Boggs Mountain (about 1.5 m.y.) and rhyolite of Alder Creek (about 1.1 m.y.).
- 4.1 Junction with Socrates Mine Road. Turn right and begin driving through Franciscan melange.
- 6.0 Gunning Creek.
- 6.6 Anderson Creek.
- 7.0 STOP 8. Lincoln Rock, view stop. (This stop is on private land and permission is required for access.)

Lincoln Rock is an exotic block of blueschist in Franciscan melange. Park next to McKinley steam wells of Aminoil USA (formerly Burmah Oil Co., and before that, Signal Oil Co.) and climb up on Lincoln Rock for a view stop. Don't fall in chasm. From here, you can see the rhyolite (1.1 m.y. rhyolite of Alder Creek) cliffs of Cobb Mountain to the north and the down-faulted complex of the same rhyolite (Goff and McLaughlin, 1976), which looks rather like a huge landslide, in front of you. The ridge to the east is made up of the Harbin Springs ophiolite capped by tree-bearing andesite of Boggs Mountain. The valley between here and the ophiolite contains Putah Creek, which approximately follows one trace of the Collayomi Fault Zone. This fault zone is a major northwest-trending feature which may act as the north-eastern boundary of the vapor-dominated geothermal area (Goff and others, 1977, in press). Our next stop will take a closer look at the Collayomi fault zone.

Return along Socrates Mine Road to

- 9.9 Junction with Highway 175. Turn left.
- 14.0 Intersection with Bottle Rock Road in Cobb. Turn left and notice on your left behind the laundromat an outcrop of sheeted dacite of Cobb Valley. The contorted sheeting probably indicates that this outcrop was near the end of the flow. Continue on Bottle Rock Road to
- 17.4 STOP 9. Collayomi fault zone.




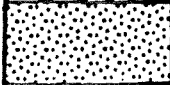

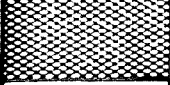



UNITS	K-Ar Age in m.y.	Magnetic Polarity
	0.60 \pm 0.01	N
	0.89 \pm 0.03	N
	0.87 \pm 0.02	N
	0.91 \pm 0.02	N
		R
	1.01 \pm 0.03	unknown
UNCONFORMITY		
		
Great Valley sequence		

FIGURE 2: Schematic cross-section through Highway 175 and church at Loch Lomond; facing directly north (relief exaggerated). K-Ar ages in millions of years.

This roadcut shows serpentinite, partly altered to silica-carbonate rock, faulted over Quaternary gravel. The exposed fault plane strikes N 70° W, dips about 50°N, and is part of the Collayomi fault zone, a possibly active fault zone related to the San Andreas system, which trends about N 45°-50°W along Cobb Valley. Most faults in the zone are high-angle with a component of right-lateral strike slip movement.

The Quaternary gravels contain abundant well-rounded pebbles of the andesite of Boggs Mountain (about 1.5 m.y.) and Cobb Mountain silicic lavas (about 1 m.y.) along with Franciscan and Great Valley rock types. Other uplifted and faulted gravels containing Clear Lake volcanic pebbles are present in High Valley and Rabbit Valley to the west.

From Stop 2, return south on Bottle Rock Road to

- 18.2 Junction with Sulphur Creek Road. Turn left.
- 18.5 As we cross the Collayomi fault zone, note the Sargent cypress trees growing on serpentinite to your left. Note also the Digger pines ahead, another tree which does well in impoverished serpentine soils.
- 19.5 Bear right on Harrington Flat Road.
- 19.7 Rocks of the Great Valley sequence of Late Cretaceous age (Unit IV, Swe and Dickinson, 1970) are exposed on the left, and andesite of Boggs Mountain is up hill on the right.
- 20.5 Junction with Highway 175. Turn left. Road drops into gully, and as it begins to rise again, the Great Valley sequence crops out on the left, overlain by bedded rhyolite tuff.
- 21.2 STOP 10. Loch Lomond Church; volcanic stratigraphy.

At the top of the hill, park on the right in the Loch Lomond church parking lot.

This stop displays what is probably the best stratigraphic section in the volcanic field. It shows several different rock types along with a complete section through the rhyolite of Bonanza Springs, an air-fall tuff which was erupted about 1 m.y. ago near Seigler Springs, two miles to the northeast. This tuff underlies the southern edge of the central volcanic field. The tuff has been locally tilted, faulted, folded, and water-worked. Here the top of the tuff contains rounded boulders of the andesite of Salmina Flat, a unit which is found in place to the north and east.

LUNCH

After lunch, continue north on Highway 175.

- 22.6 Ahead, beyond Salmina's Resort, is the composite dacite dome of Mt. Hannah, which lies at the center of the negative gravity anomaly associated with the Clear Lake volcanic field.

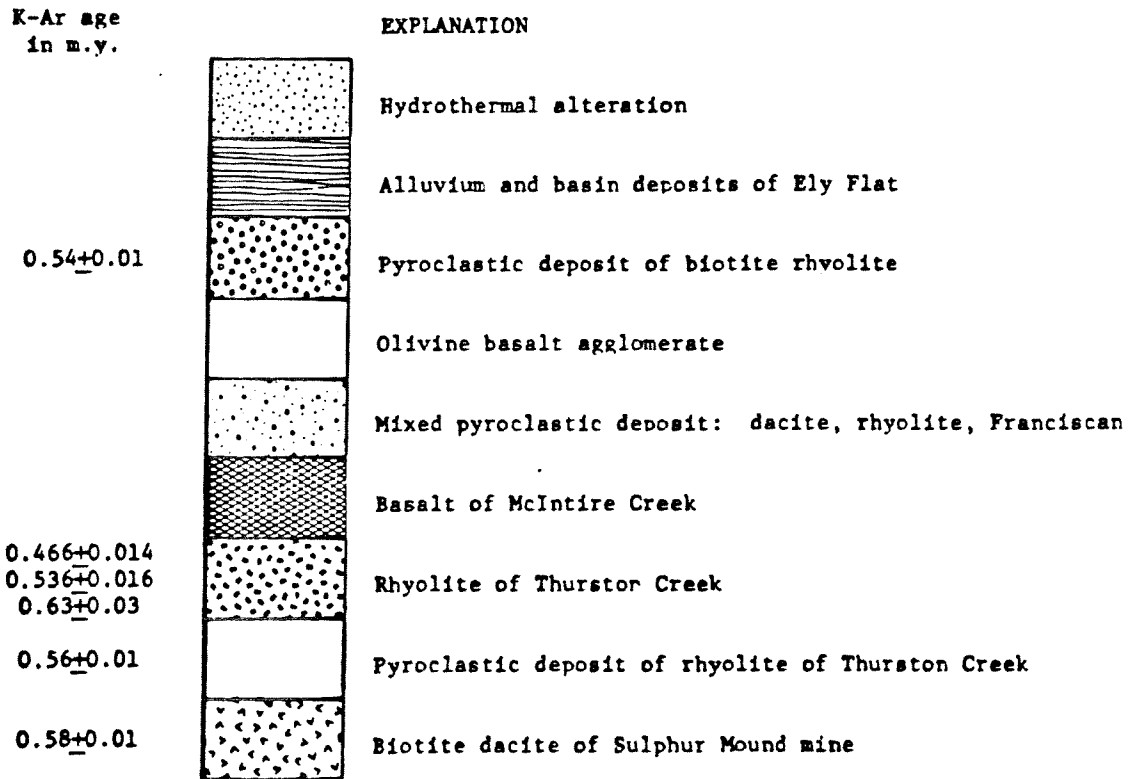
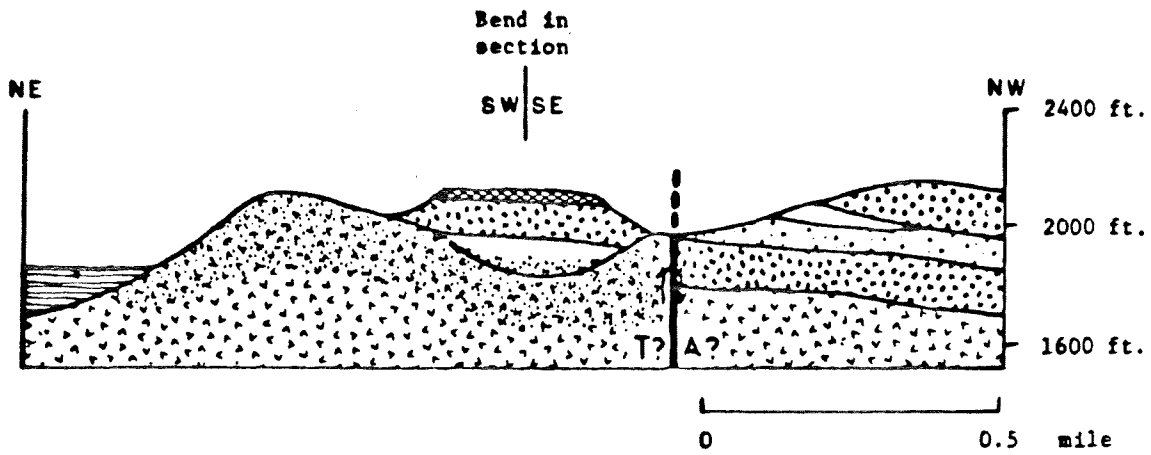


FIGURE 3: Schematic cross-section of Sulphur Mound area (relief exaggerated). K-Ar ages in millions of years.

- 26.5 Junction with Red Hill Road. Turn right and drive through walnut orchards planted on half-million year old rhyolitic obsidian and pyroclastic deposits of biotite rhyolite.
- 27.5 The small ridge directly ahead is the expression of a fault in pyroclastic deposits of biotite rhyolite.
- 28.7 Junction with Highway 29, facing Soda Bay Road. Turn left. Mt. Konocti is on right.
- 29.6 Junction with road into Sulphur Mound Mine. Turn left and drive about 1/4 mile in to the mine.

STOP 11. Sulphur Mound mine. (This stop is on private land and permission is required for access.)

This hydrothermally altered area is the site of active sulfur deposition by fumaroles and has been mined in recent years for agricultural sulfur. Cinnabar was prospected for and mined in this valley, probably near the turn of the century.

Stratigraphic relations within this valley and to the west show a complex sequence of flows and pyroclastic deposits (Figure 3), all of which pre-date the 0.3-0.4 m.y. Mt. Konocti edifice, and are younger than about 0.6 m.y. The opalized, bleached biotite dacite of Sulphur Mound Mine (dsm, 0.58 ± 0.01 m.y.) is overlain by air-fall pyroclastic deposits (rp, which includes pumiceous tuff breccia and lapilli tuff) of rhyolite of Thurston Creek, which are in turn overlain by an obsidian flow of rhyolite of Thurston Creek (r). The obsidian flow is overlain to the south by basalt of McIntire Creek (bm). The pyroclastic deposits (rp) were a precursor of the obsidian flow and contain blocks of biotite dacite of Sulphur Mound Mine and obsidian typical of rhyolite of Thurston Creek. Northeast-erly dips and size of blocks suggest that the pyroclastic rocks were erupted nearby to the south or southeast from a vent now concealed beneath the slightly younger obsidian flow. An obsidian block from the pyroclastic deposits gives a K-Ar date of 0.56 ± 0.01 m.y.; at other locations several km to the west and east in the arcuate, concave-northward outcrop area of rhyolite of Thurston Creek, obsidian gives dates of 0.466 ± 0.014 , 0.536 ± 0.016 , and 0.63 ± 0.03 m.y.

A prominent northeast-southwest fault crosses the west side of the valley, has dropped the northwest block down, and may show limited left-lateral displacement. Northwest of that fault, rhyolite of Thurston Creek is successively overlain by a mixed pyroclastic deposit (drp, containing fragments of dacite, rhyolite and Franciscan rocks), olivine basalt agglomerate (bo), and pyroclastic deposits of biotite rhyolite (rps). The biotite rhyolite pyroclastics cap the hill to the northwest, had a source vent to the north or northwest, and give 0.54 ± 0.01 m.y. on sanidine.

Hydrothermal alteration has destroyed the biotite, plagioclase, and sanidine phenocrysts in much of the dacite, leaving cavities net-veined with silica. Cinnabar occurs as thin veins and disseminated pink and orange areas in the altered dacite and rhyolitic pyroclastic deposits.

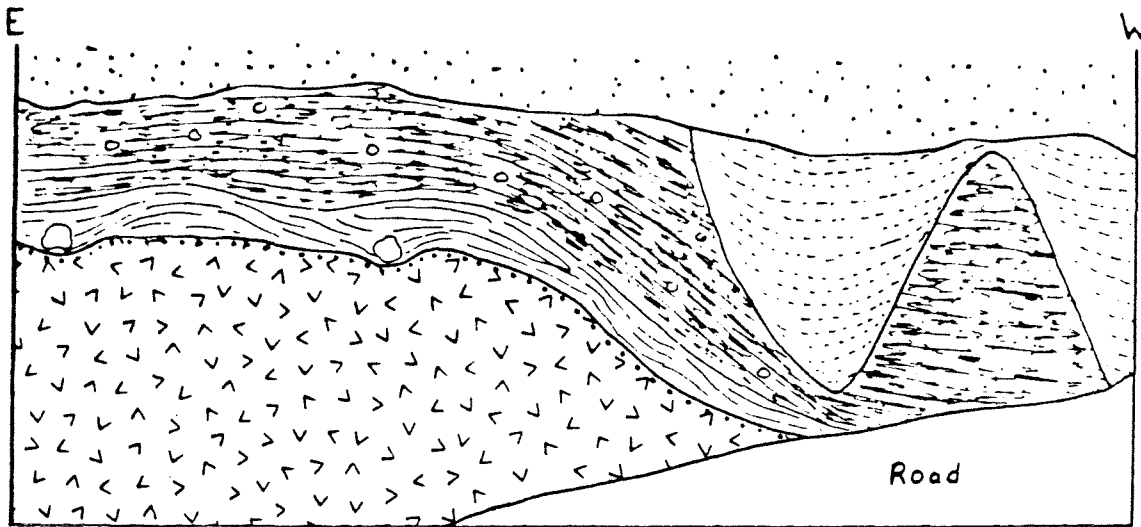
The white area 3.5 km to the north, on the south slope of Mt. Konocti, is the Bell mine, formerly mined for cinnabar and meta-cinnabar and now mined for decorative rock. The mine is mainly in altered and opalized, phenocryst-poor dacite of Bell mine, which had source vents close to the mine and at the low knobs about two-thirds of the way up the mountain. The Bell mine is an extinct alteration area; no hot springs or fumaroles are present.

The composite Mt. Konocti volcano is made up of about ten units of dacite, two partly buried mafic cinder cones, and a young olivine andesite flow and cinder cone at Buckingham Peak. Dacite from the eastern summit, Wright Peak, is 0.34 ± 0.01 m.y. old and overlies mafic cinders and colluvium which produce the smooth brush-covered slope below South Peak, the summit on the left.

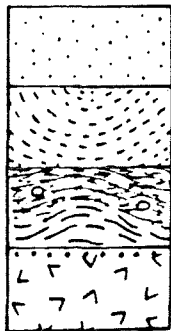
Return to Highway 29. Turn right.

Begin cumulative mileage again

- 0.9 Junction with Soda Bay Road. Turn left.
- 1.3 Drive through obsidian flow. Most of the pumiceous carapace has been eroded away but the rhyolite core is not exposed here.
- 1.7 Roadcut exposing a young reverse fault which is related to movement on the possibly active Konocti Bay Fault Zone. The dacite exposed in the roadcut was covered by lake beds and mafic pyroclastic deposits prior to faulting.
- 2.5 We are crossing one trace of the Konocti Bay Fault Zone; another trace forms the step in topography on the side of the hill high on the right.
- 2.9 Pt. Lakeview Road on the right. Continue straight ahead. On your left, notice an outcrop of dacite draped by pyroclastic deposits.
- 3.3 Konocti Bay is on your right; the "lava rings" of Mt. Konocti are straight ahead. These rings are arcuate ridges formed on the surface of viscous dacite lava during flowage.
- 4.3 The road turns west and drops abruptly over one trace of the Konocti Bay fault zone, which can be followed to the north as a topographic step low on the mountain slope.
- 7.0 Turn right on Crystal Drive and follow the sign to Buckingham Golf Course.



UNITS



Soil and colluvium

Mafic scoria

Maar deposits

Dacite of Mt. Konocti
(soil concretions at top)

FIGURE 4: Sketch of outcrop at Riviera Heights Marina
(about 40 feet high, 100 feet wide)

- 7.2 On the left is Little Borax Lake, maar volcano perhaps as young as 10,000 years old. It formed by eruption of magma through water or water-saturated rocks, producing the tuff ring which we will drive on as we bear left past the clubhouse. The lake is alkaline (pH 9.5) and was mined for borax about 1870. The explosive eruption at Little Borax Lake maar scoured much of the debris derived by landslide and/or previous eruptions from the prominent cliffs of Buckingham Bluffs, high on the mountain.
- 7.9 Join Soda Bay Road on the left and drive past dacite cliffs (0.35 ± 0.01 m.y.) on the left and Horseshoe Bend explosion crater on the right.
- 8.9 Entrance to Riviera Heights Marina. Turn right. Drive down steep hill to
- 9.3 parking lot at marina

STOP 12. PLEASE DON'T CLIMB ON THE OUTCROP. Riviera Heights marina.

(This stop is on private land and permission is required for access.)

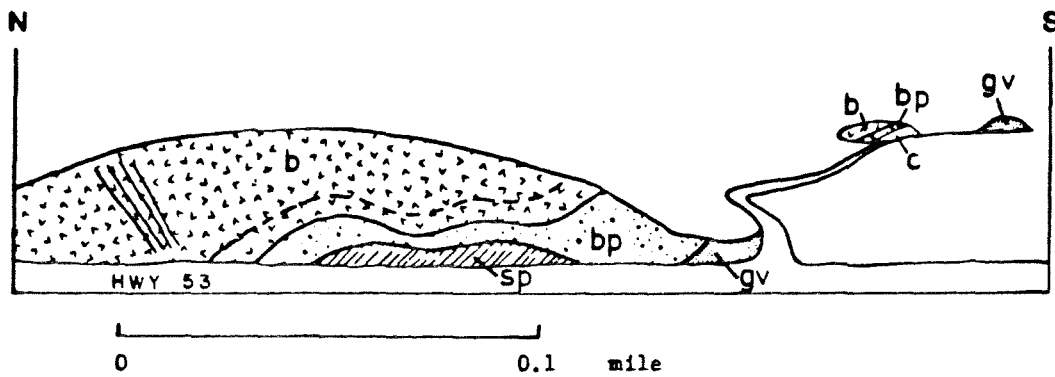
Here is an excellent exposure of maar deposits lying on a rather typical dacite of Mt. Konocti and overlain by scoria from a dry-land eruption, which formed a small mafic cinder cone. The maar deposits resulted from eruption of mafic lava through Clear Lake, probably 10,000-55,000 years ago (Sims and Rymer, 1975c). The initial phase of the eruption formed undulating base-surge beds, followed by air-fall beds, both showing mud-armored lapilli characteristic of maar-type eruptions. The base-surge beds show bedding sags, and inferred trajectories of elongate blocks and bombs suggest a source in the lake.

The dacite flow shows a typical brecciated appearance. Close examination reveals patches of fused breccia in the outcrop. This dacite is probably about 0.3-0.4 m.y. old, and a soil had begun to develop on its surface prior to the maar eruption as demonstrated by the pea-sized soil concretions found in the pale orange zone just below the overlying maar beds.

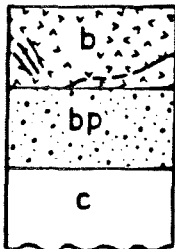
Return to

- 9.7 Soda Bay Road. Turn left.
- 10.7 Keep right on Soda Bay Road and drive under Buckingham Bluffs. Note the large blocks of dacite that have fallen off the bluffs, evidence of a conspicuous geologic hazard. Developers would like to build condominiums here south of the road.
- 11.6 Crystal Drive on left. Keep right and retrace route to
- 15.7 Junction with Pt. Lakeview Road. Turn left.

- 17.5 Ahead on your left is Baylis Point, a small peninsula composed of Franciscan graywacke, greenstone, and chert. It is unclear whether it has been upfaulted or whether it was simply an erosional high which was not completely covered by the dacites to the south.
- 19.0 Keep to the right and go up hill on Pt. Lakeview Road.
- 19.5 Below on your left is an explosion crater; on your right, dacite.
- 20.6 Roundtop Mountain cinder cone and quarry ahead.
- 21.1 STOP 13. Thurston Lake.
- On a clear day, Mt. Konocti is reflected on the surface of Thurston Lake, which is 100 feet higher than Clear Lake and lies in a 400-foot deep closed depression which was built by non-coalescing dacite domes and flows. Three types of dacite are found around the lake, the oldest of which overlies obsidian dated at 0.466 ± 0.014 m.y. and the youngest of which has been dated at 0.43 ± 0.02 m.y. The lake contains fresh, drinkable water which was once clear. The turbidity of the lake is caused by clay that has been eroding from lake beds in Manning Flat (1.5 miles to the southwest) since the topographic barrier between the flat and Thurston Lake basin was dynamited away, more than 40 years ago. Methane in gassy springs bubbles up through the lake in quantities large enough to have been used for heat by early residents. Union Oil Company plans to drill a geothermal exploratory well at the far end of the lake basin in the near future. Local residents report that a subterranean outlet is visible on the north shore of Thurston Lake in extremely dry years.
- 21.7 Continuing south, the crudely-bedded internal structure of a cinder cone is exposed in road cut on right.
- 22.5 Walnut trees (non-irrigated) grow beautifully on the young quartz-bearing olivine basalt flow erupted from Roundtop Mountain.
- 22.9 Highway 29. Turn left.
- 23.8 Great Valley sequence rocks exposed in road cut.
- 24.8 Highway 53. Turn left.
- 25.0 Tilted sequence of lake beds and volcanoclastic deposits on left. These sedimentary deposits were included in the Cache Formation by Anderson (1936), Brice (1953), and Casteel and Rymer (1975).
- 25.9 Cache Creek. Present outlet of Clear Lake, which is kept at an artificially high level by a dam 3 miles downstream.
- 27.9 Flashing yellow light; turn left into Clearlake Highlands.



UNITS

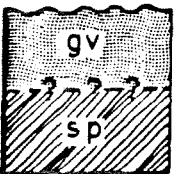


Massive basalt with sheeting near edge of flow;
basal breccia

Basaltic pyroclastic deposit

Fluvial deposits of the Cache Formation

UNCONFORMITY



Great Valley sequence

FAULT(?)

Serpentinite

FIGURE 5: Sketch of Highway 53 roadcut, facing east toward Schoolteacher Hill and Quackenbush Mountain (roadcut about 30 feet high).

- 28.6 The Lodge (restaurant) on the left.
- 28.7 Kathie's Inn on the left, which serves dinners and is the site of tomorrow morning's breakfast.

Continue on Lakeshore Drive to motels.

THIRD DAY

Begin cumulative mileage again

- 0.0 Rebud Park, behind Kathie's Inn. Leave parking lot and turn right on Lakeshore Drive.
- 0.4 Outcrop behind Shell station on right displays interbedded maar and lake beds which are older than the dacite of Cache Creek (0.40 \pm 0.04 m.y.).
- 0.9 Flashing red light at Highway 53. Turn left.
- 1.5 STOP 14. Schoolteacher Hill.

The basalt (a field term for a rock which contains both quartz and olivine and about 57% silica) at Schoolteacher Hill gives a K-Ar date of 1.64 \pm 0.09 m.y. (reverse polarity) and overlies maar-type pyroclastic deposits. These pyroclastic deposits in turn overlie gravels of the Cache Formation, rocks of the Great Valley sequence, and serpentinite. The pyroclastic material is mafic in composition and may represent the initial phase of the basalt eruption. The maar deposits are beautifully exposed in the quarry up hill from the Highway 53 roadcut, where, if you search, you can find fresh, black, olivine-bearing pumice. In the highway roadcut, the basalt flow is well exposed and displays a basal breccia overlain by massive lava; toward the edge of the flow, it becomes sheeted, a characteristic of many lavas (basalt through rhyodacite) in the Clear Lake field. The basalt here can be traced up and to the east into the mesa of Quackenbush Mountain. It is possible that this flow was erupted from a cinder cone half a mile to the west, which is nearly buried by lake sediments. If so, later tilting, which involved at least 700 feet of uplift to the east, occurred over a lateral distance of 2 miles since the lava was erupted about 1.6 m.y. ago.

Quackenbush Mountain is covered with a sprinkling of chert, as are most older basalt remnants showing reverse magnetic polarity, suggesting that these older basalts were erupted during a late stage of Cache deposition. The dominantly fluvial sediments of the main, older portion of the Cache Formation were deposited to the east in a basin covering at least 50 square miles, to a maximum depth of 6500 feet (Brice, 1953). Little is known about the detailed provenance of this Pliocene and Pleistocene deposit. Whether the isolated clastic and volcanic deposits within and west of the Clear Lake Volcanics should be included in the Cache Formation is questionable.

Continue north on Highway 53 to

- 1.9 Olympic Drive. Turn left toward Clearlake Park.
- 3.7 Junction with Lakeshore Drive. Turn right.
- 4.3 Where Lakeshore Drive turns west, go straight ahead to Arrowhead Road and follow it for a short distance to
- 4.9 Sulphur Bank Drive. On the right is obsidian of the rhyolite of Borax Lake (0.088 ± 0.13 m.y.), representing the youngest rhyolitic event in the Clear Lake volcanic field. The flow retains much of its pumiceous carapace and is partially mantled by human-chipped fragments. The obsidian was a major source for Indian tools found in the Coast Ranges.
- 5.6 Borax Lake is ahead on the right. This alkaline lake was probably formed when it was separated from Clear Lake either about 90,000 years ago by eruption of the rhyolite of Borax Lake or earlier by eruption of olivine basalt and olivine dacite. Borax Lake probably conceals a sedimentary record of at least the past 90,000 years. About 1865, borax was mined from this lake prior to discovery of the Death Valley deposits. To the east, on the edge of the rhyolite flow, is an area of active sulfur fuming, and just over the ridge to the north is Sulphur Bank mine, our next stop. Phillips Petroleum Company plans to drill a geothermal exploratory well at the far end of the lake.
- 8.1 Crest of Sulphur Bank Ridge. Below on the left is Sulphur Bank mine, and on the right is a view of Borax Lake. Rattlesnake Island to the left is a separate basaltic or andesitic center.
- 9.7 Turn sharply left into Sulphur Bank mine. Park and walk toward pit.

STOP 15. Sulphur Bank mine. (This stop is on private land and permission is required for access. We have been asked by the Bradley Mining Company to sign release forms.)

Sulphur Bank mine has produced the fourth largest volume of quicksilver in the United States, and according to White and Roberson (1962) "is the most productive mineral deposit in the world that is clearly related to hot springs." The mine is no longer producing mercury, and the open pit has filled with water since operations ceased in 1957. The pH of the "lake" in Herman Pit is 3.5, and it actively bubbles with carbon dioxide. On the north side of the pit is an active sulfur-fuming area which releases considerable H₂S, but no hot springs can be found above water near the mine today. They issued from the bottom of Herman Pit before flooding (Everhart, 1946).

The mercury was deposited in an andesite flow and underlying sedimentary rocks. Shallow ore bodies are localized along faults that cut the andesite. Deposition was apparently controlled

by the old ground water table (White and Roberson, 1962; see also earlier studies by Anderson, 1936; Ross, 1940; Everhart, 1946; Becker, 1888; LeConte and Rising, 1882; Whitney, 1865), below which the mercury was concentrated. Above that level, native sulfur was abundant and two million tons of sulfur were mined before the pink "contamination" from cinnabar brought recognition of the mercury deposit. Most of the production from the mine took place before 1900. Early mining was done underground by Chinese miners on 20-minute shifts. Noxious fumes and temperatures up to about 175°F eventually led to open-pit mining.

The andesite of Sulphur Bank mine overlies sediments in which datable carbonaceous material was found. A recent ¹⁴C age determination by M. Stuiver, University of Washington, gives 44,500 ± 800 years for a carbonized log, which is a maximum age for the andesite. No vent for the andesite has been found in the area of the mine, but the flow is traceable in sporadic outcrops for about half a mile to the northeast, to South Cone. At least six cinder cones are aligned north-south within 1 to 3 miles of the mine. Round Mountain which still retains a 40-foot summit depression, is the source of the andesite of High Valley, which we will pass on our way to the next stop.

LUNCH

- 9.9 Follow Sulphur Bank Drive northeast.
- 11.1 Highway 20. Turn right and head straight toward the gap between two young cinder cones. South Cone, on the right, is the source of the andesite of Sulphur Bank.
- 14.5 Highway 53 on right. Continue straight ahead on Highway 20. Mesa of Clear Lake quartz-bearing basalt (reverse polarity) overlies Cache Formation gravels and Franciscan rocks on right.
- 17.2 New Long Valley Road. Turn left.
- 17.4 Across the North Fork of Cache Creek are terrace-mantled Cache beds dipping to northwest.
- 19.7 Float of the andesite of High Valley caps Cache Formation gravels on the left. The andesite probably dammed the North Fork of Cache Creek. No datable material has been found in or under the flow, but both Anderson (1936) and Becker (1888) thought that it was very young. Becker thought the youthful appearance of the cinder cone (Round Mountain) associated with the flow suggested an age of about 10,000 years.
- 20.1 View of Chalk Mountain, ahead on right.
- 20.4 Spring Valley Road. Turn right.
- 21.4 Wolf Creek Road. Turn right.

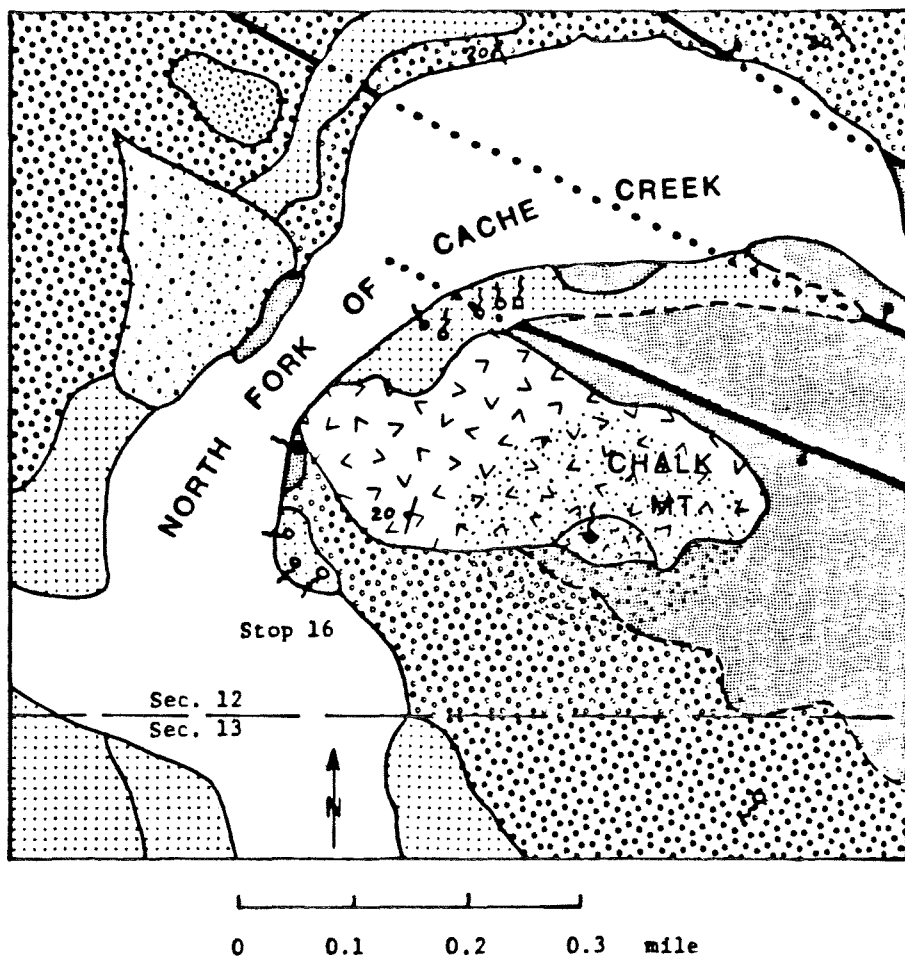
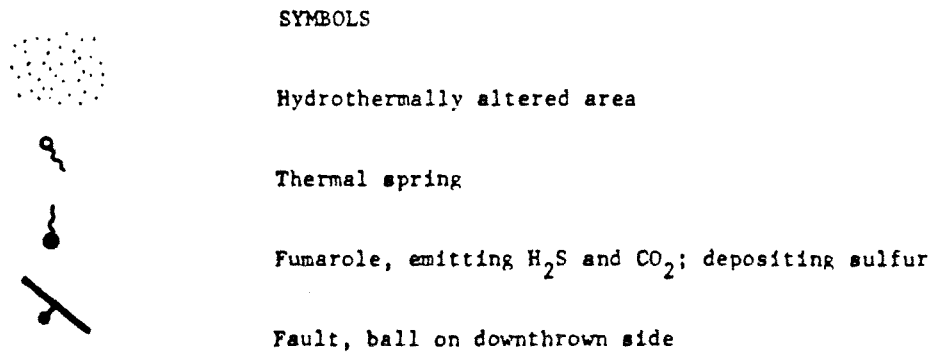
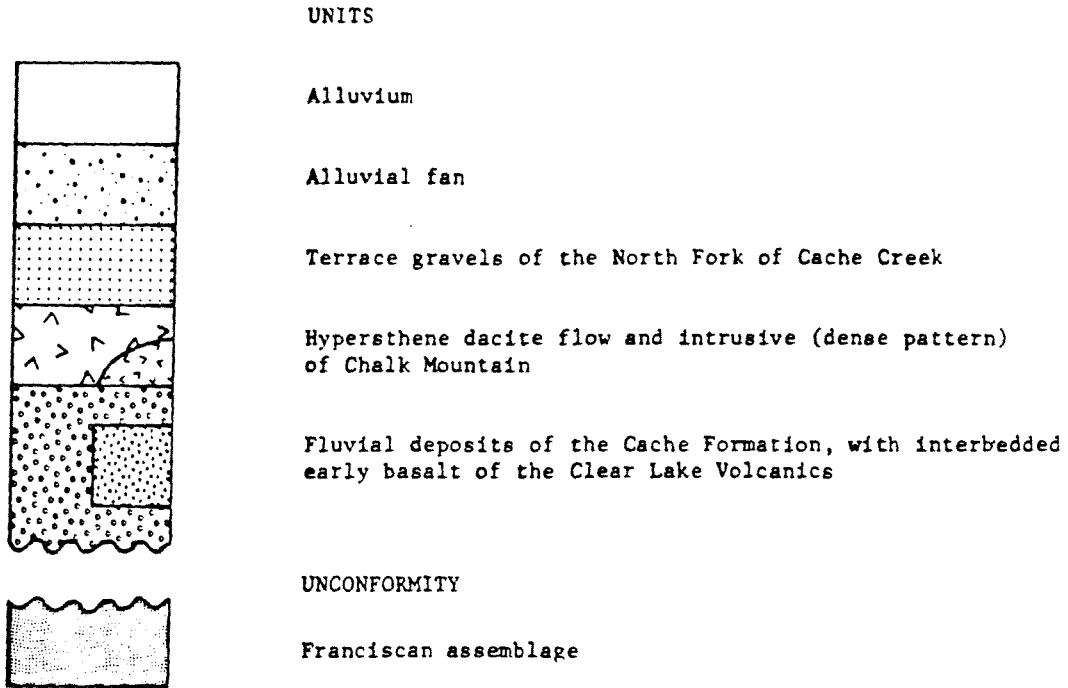


FIGURE 6: Geologic map of the Chalk Mountain area,
T. 14 N., R. 7 W.

See following page for explanation.

EXPLANATION FOR FIGURE 6



21.5

Turn left onto bridge, then right onto second bridge to cross the North Fork of Cache Creek to Chalk Mountain. Park on left.

STOP 16. Chalk Mountain. (This stop is on private land and permission is required for access.)

Chalk Mountain is located at a sharp bend in the North Fork of Cache Creek where the river empties out of a steep canyon into a broad, alluviated valley. The mountain itself consists of a dacite intrusive body and flow of the Clear Lake Volcanics. The flow overlies Cache Formation gravels and the Franciscan assemblage(?). To the south, the dacite is deeply eroded; nevertheless, the mountain is the site of active sulfur fuming and several thermal springs which are strongly mineralized (try tasting them!). This activity is concentrated here by a series of well defined faults which form part of the boundary between the Cache Formation and the Franciscan assemblage. These faults are also the locus of several thermal springs and silica-carbonate and serpentinite stringers, and one cuts off basaltic dikes that intrude the Cache Formation.

Of particular interest is the well-exposed though hydrothermally altered intrusive contact of dacite with Franciscan rocks in a quarry on the south side of the mountain. Also of interest are the salty springs found low on the north and northwest sides of the mountain. The springs have deposited extensive travertine terraces which locally cement coarse terrace gravels; at least one spring is depositing sulfur at its orifice.

Retrace route to Highway 20 and turn left toward Sacramento. Turn right at Highway 16 (toward Rumsey) and proceed through the Great Valley sequence to Interstate 5 where you can follow signs to Sacramento.

Bibliography

- Adam, D. P., 1976, Climatic fluctuations during the transition from the last interglacial to the last glacial: pollen evidence from Clear Lake, California: Geol. Soc. America, Abs. with Programs, v. 8, no. 6, p. 749.
- Adam, D. P., and Sims, John, 1976, A long, continuous pollen record from Clear Lake, California: Geol. Soc. America, Abs. with Programs, v. 8, no. 3, p. 349.
- Anderson, C. A., 1936, Volcanic history of the Clear Lake area, California: Geol. Soc. America Bull., v. 47, no. 3, p. 629-664.
- Barnes, I., Hinkle, M. E., Rapp, J. B., Heropoulos, C., and Vaughn, W. W., 1973a, Chemical composition of naturally occurring fluids in relation to mercury deposits in part of north-central California: U.S. Geol. Survey Bull. 1382A, 19 p.
- Barnes, I., O'Neil, J. R., Rapp, J. B., and White, D. E., 1973b, Silica-carbonate alteration of serpentine: wall rock alteration in mercury deposits of the California Coast Ranges: Econ. Geol., v. 68, no. 3, p. 388-398.
- Becker, G. F., 1888, Geology of the quicksilver deposits of the Pacific Slope: U.S. Geol. Survey Mon. 13, 486 p.
- Berkland, J. O., 1972, Clear Lake basin--a deformed Quaternary caldera (?): in Moores, E. M., and Matthew, R. A., eds., Geologic guide to the northern Coast Ranges--Lake, Mendocino and Sonoma Counties, California, Annual Field Trip Guidebook Geol. Soc. Sacramento, p. 6-25.
- Berkland, J. O., 1973, Rice Valley outlier--new sequence of Cretaceous-Paleocene strata in northern Coast Ranges, California: Geol. Soc. America Bull., v. 84, no. 7, p. 2389-2406.
- Berkstresser, C. F., Jr., 1968, Data for springs in the northern Coast Ranges and Klamath Mountains of California: U.S. Geol. Survey open-file report, 49 p.
- Bowman, H. R., Asaro, F., and Perlman, I., 1973, On the uniformity of composition in obsidians and evidence for magmatic mixing: Jour. Geology, v. 81, no. 3, p. 312-327.
- Brice, J. C., 1953, Geology of Lower Lake quadrangle, California: California Division of Mines, Bull. 166, 72 p.
- Bufe, C. G., and Lester, F. W., 1975, Seismicity of The Geysers-Clear Lake region, California: Trans. Am. Geophys. Union (EOS), v. 56, no. 12, p. 1020.
- Bufe, C. G., Pfluke, J. H., Lester, F. W., and Marks, S. M., 1976, Map showing preliminary hypocenters of earthquakes in the Healdsburg (1:100,000) quadrangle, Lake Berryessa to Clear Lake, California, January 1969-June 1976: U.S. Geol. Survey open-file report. 76-802.

- California Department of Water Resources, 1962, Reconnaissance report on upper Putah Creek basin investigation: Calif. Dept. Water Resources, Bull. 99, 254 p.
- Casteel, R. W., Adam, D. P., and Sims, J. D., 1975, Fish remains from Core 7, Clear Lake, Lake County, California: U.S. Geol. Survey open-file report 75-173, 67 p.
- Casteel, R. W., and Rymer, M. J., 1975, Fossil fishes from the Pliocene or Pleistocene Cache Formation, Lake County, California: U.S. Geol. Survey Jour. Research, v. 3, no. 5, p. 619-622.
- Chapman, R. H., 1966, Gravity map of Geysers area: California Division of Mines and Geology, Mineral Information Service, v. 19, no. 9, p. 148-149.
- Chapman, R. H., 1975, Geophysical study of the Clear Lake region, California: Calif. Div. Mines and Geology, Spec. Report 116, 23 p.
- Chesterman, C. W., 1956, Pumice, pumicite, and volcanic cinders in California: Calif. Div. Mines and Geology, Bull. 174, 119 p.
- Cox, A., 1969, Geomagnetic reversals: Science, v. 163, p. 237-245.
- Donnelly, J. M., Goff, F. E., Thompson, J. M., and Hearn, B. C., Jr., 1976, Implications of thermal water chemistry in The Geysers-Clear Lake area: Proc. Lake County (California) Geothermal Environmental Seminar-76, (in press).
- Donnelly, J. M., McLaughlin, R. J., Goff, F. E., and Hearn, B. C., Jr., 1976, Active faulting in The Geysers-Clear Lake area, northern California: Geol. Soc. America, Abs. with Programs, v. 8, no. 3, p. 369-370.
- Emerson, D. O., and Rich, E. I., 1966, Field trip, Sacramento Valley and northern Coast Ranges, in Geology of Northern California: Calif. Div. Mines and Geology, Bull. 190, p. 473-485.
- Everhart, D. L., 1946, Quicksilver deposits at the Sulphur Bank mine, Lake County, California: Calif. Jour. Mines and Geology, v. 42, p. 125-153.
- Franks, A. L., 1972, Geology and wastewater management, Lake County sanitation district no. 1: in Moores, E. M., and Matthews, R. A., eds., Geologic guide to the northern Coast Ranges--Lake, Mendocino, and Sonoma Counties, California, Annual Field Trip Guidebook Geol. Soc. Sacramento, p. 27-32.
- Frizzell, V. A., Jr., 1975, New evidence for activity on the Green Valley fault, Napa and Solano Counties, California: Geol. Soc. America, Abs. with Programs, v. 7, no. 3, p. 319.
- Garrison, L. E., 1972, Geothermal steam in The Geysers-Clear Lake region, California: Geol. Soc. America Bull., v. 83, no. 5, p. 1449-1468.

- Goff, F. E., Donnelly, J. M., Thompson, J. M., and Hearn, B. C., Jr., 1976, The Konocti Bay fault zone, California: Potential area for geothermal exploration: Geol. Soc. America, Abs. with Programs, v. 8, no. 3, p. 375-376.
- Goff, F. E., Donnelly, J. M., Thompson, J. M., and Hearn, B. C., Jr., 1977 (in press), Geothermal prospecting in The Geysers-Clear Lake area northern California: Geology.
- Goff, F. E. and McLaughlin, R. J., 1976, Geology of the Cobb Mountain-Ford Flat geothermal area, Lake County, California: U.S. Geol. Survey open-file map 76-221.
- Hamilton, R. M., and Muffler, L. J. P., 1972, Microearthquakes at The Geysers geothermal area, California: Jour. Geophys. Research, v. 77, no. 11, p. 2081-2086.
- Hauge, C., Kramer, J. C., Berkland, J. O., and Matthews, R. A., 1972, Field trip log: in Moores, E. M., and Matthews, R. A., eds., Geologic guide to the northern Coast Ranges - Lake, Mendocino and Sonoma Counties, California, Annual Field Trip Guidebook Geol. Soc. Sacramento, p. 111-132.
- Hearn, B. C., Jr., Donnelly, J. M., and Goff, F. E., 1975a, Geology and geochronology of the Clear Lake volcanic field, Lake County, California: U.S. Geol. Survey open-file report 75-296, 18 p.
- Hearn, B. C., Jr., Donnelly, J. M., and Goff, F. E., 1975b, Preliminary geologic map of the Clear Lake volcanic field, Lake County, California: U.S. Geol. Survey open-file report 75-391.
- Hearn, B. C., Jr., Donnelly, J. M., and Goff, F. E., 1976a, Preliminary geologic map and cross-section of the Clear Lake volcanic field, Lake County, California: U.S. Geol. Survey open-file map 76-751.
- Hearn, B. C., Jr., Donnelly, J. M., and Goff, F. E., 1976b, Geology and geochronology of the Clear Lake Volcanics, California: Proc. Second United Nations Symposium on the Development and Use of Geothermal Resources, v.1, p. 423-428.
- Hodges, C. A., 1966, Geomorphic history of Clear Lake, California: Ph.D. Dissertation, Stanford University, 210 p.
- Isherwood, W. F., 1975, Gravity and magnetic studies of The Geysers-Clear Lake geothermal region, California, U.S.A.: U.S. Geol. Survey open-file report 75-368, 37 p.
- Isherwood, W. F., 1976, Gravity and magnetic studies of The Geysers-Clear Lake region, California: Proc. Second United Nations Symposium on the Development and Use of Geothermal Resources, v. 2, p. 1065-1073.
- Isherwood, W. F., and Chapman, R. H., 1975, Principal facts for gravity stations in The Geysers, Clear Lake region, California: U.S. Geol. Survey open-file map 75-107.

- Iyer, H. M., and Hitchcock, T., 1975, Teleseismic residuals at The Geysers geothermal area: Trans. Am. Geophys. Union, (EOS), v. 56, no. 12, p. 1020.
- Lake County Flood Control and Water Conservation District, 1967, Big Valley ground-water recharge investigation, 63 p.
- Lange, A. L., and Westphal, W. H., 1969, Microearthquakes near The Geysers, Sonoma County, California: Jour. Geophys. Research, v. 74, no. 17, p. 4377-4378.
- LeConte, J., and Rising, W. B., 1882, The phenomena of metalliferous vein formation now in progress at Sulphur Bank, California: Am. Jour. Sci., 3rd ser., v. 24, p. 23-33.
- Lofgren, B. E., 1973, Monitoring ground movement in geothermal areas: Hydraulic Engineering and the Environment, Proceedings of the Hydraulic Division Specialty Conference, Bozeman, Montana, August 15-17, 1973, p. 437-447.
- Mankinen, E. A., 1972, Paleomagnetism and potassium-argon ages of the Sonoma Volcanics, California: Geol. Soc. America Bull., v. 83, p. 2063-2072.
- McLaughlin, R. J., 1974, Preliminary geologic map of The Geysers steam field and vicinity, Sonoma County, California: U.S. Geol. Survey open-file map 74-238.
- McLaughlin, R. J., 1975, Preliminary field compilation of in-progress geologic mapping in The Geysers geothermal area, California: U.S. Geol. Survey open-file map 75-198.
- McNitt, J. R., 1968a, Geologic map of the Kelseyville quadrangle, Sonoma, Lake and Mendocino Counties, California: California Division of Mines and Geology, Map Sheet 9.
- McNitt, J. R., 1968b, Geologic map of the Lakeport quadrangle, Lake County, California: California Division of Mines and Geology, Map Sheet 10.
- McNitt, J. R., 1968c, Geology of the Clearlake Oaks 15-minute quadrangle, Lake County, California: California Division of Mines and Geology, open-file release 68-12.
- Raymond, L. A., and Berkland, J. O., 1973, Geothermal steam in The Geysers, Clear Lake region, California: Discussion: Geol. Soc. America Bull., v. 84, no. 9, p. 3131-3134.
- Ross, C. P., 1940, Quicksilver deposits of the Mayacmas and Sulphur Bank districts, California: U.S. Geol. Survey Bull. 922-L, p. 327-353.
- Sims, John, 1974, Searching for prehistoric earthquakes in lake sediments: Earthquake Information Bull., v. 6, no. 1, p. 3-9.

- Sims, J. D., and Rymer, M. J., 1974, Gaseous springs in Clear Lake, California, and the structural control of the lake basin: Geol. Soc. America, Abs. with Programs, v. 6, no. 3, p. 254.
- Sims, J. D., and Rymer, M. J., 1975a, Preliminary description and interpretation of cores and radiographs from Clear Lake, Lake County, California: Core 1: U.S. Geol. Survey open-file report 75-665, 19 p.
- Sims, J. D., and Rymer, M. J., 1975b, Preliminary description and interpretation of cores and radiographs from Clear Lake, Lake County, California: Core 2: U.S. Geol. Survey open-file report, 75-266, 13 p.
- Sims, J. D., and Rymer, M. J., 1975c, Preliminary description and interpretation of cores and radiographs from Clear Lake, Lake County, California: Core 4: U.S. Geol. Survey open-file report 75-666, 19 p.
- Sims, J. D., and Rymer, M. J., 1975d, Preliminary description and interpretation of cores and radiographs from Clear Lake, Lake County, California: Core 5: U.S. Geol. Survey open-file report 75-381, 15 p.
- Sims, J. D., and Rymer, M. J., 1975e, Preliminary description and interpretation of cores and radiographs from Clear Lake, Lake County, California: Core 6: U.S. Geol. Survey open-file report 75-569, 18 p.
- Sims, J. D., and Rymer, M. J., 1975f, Preliminary description and interpretation of cores and radiographs from Clear Lake, Lake County, California: Core 7: U.S. Geol. Survey open-file report 75-144, 21 p.
- Sims, J. D., and Rymer, M. J., 1975g, Preliminary description and interpretation of cores and radiographs from Clear Lake, Lake County, California: Core 8: U.S. Geol. Survey open-file report 75-306, 15 p.
- Sims, J. D., and Rymer, M. J., 1976a, Preliminary description and interpretation of cores and radiographs from Clear Lake, Lake County, California, Core 3: U.S. Geol. Survey open-file report 76-208, 18 p.
- Sims, J. D., and Rymer, M. J., 1976b, Map of gaseous springs and associated faults in Clear Lake, California: U.S. Geol. Survey, Misc. Field Inv. Map MF-721.
- Smith, R. L., and Shaw, H. R., 1975, Igneous-related geothermal systems: in White, D. E., and Williams, D. L., eds., Assessment of Geothermal Resources of the United States--1975, U.S. Geol. Survey Circular 726, p. 58-83.
- Stanley, W. D., Jackson, D. B., and Hearn, B. C., Jr., 1973, Preliminary results of geoelectrical investigations near Clear Lake, California: U.S. Geol. Survey open-file report. 1828, 20 p.
- Steeple, D. W., and Iyer, H. M., 1976, Teleseismic P-wave delays in geothermal exploration: Proc. Second United Nations Symposium on the Development and Use of Geothermal Resources, v. 2, p. 1199-1206.

- Swe, W., and Dickinson, W. R., 1970, Sedimentation and thrusting of Late Mesozoic rocks in the Coast Ranges near Clear Lake, California: Geol. Soc. America Bull., v. 81, no. 1, p. 165-189.
- Urban, T. C., Diment, W. H., Sass, J. H., and Jamieson, I. M., 1976, Heat flow at The Geysers, California, USA: Proc. Second United Nations Symposium on the Development and Use of Geothermal Resources, v. 2, p. 1241-1245.
- U.S. Geological Survey, 1973, Aeromagnetic map of the Clear Lake area, Lake, Sonoma, Napa and Mendocino Counties, California: U.S. Geol. Survey, open-file map.
- Vantine, J. V., 1970, Engineering geology of the High Valley-Bear Valley conveyance system: Memorandum Report, State of California, The Resources Agency, Dept. Water Resources, Northern District, 35 p.
- Wagner, D. L., 1975, Mesozoic geology of the Walter Springs area, Napa County, California: M.S. Dissertation: San Jose State Univ., 68 p.
- Waring, G. A., 1915, Springs of California: U.S. Geol. Survey Water-Supply Paper 338, 409 p.
- White, D. E., and Roberson, C. E., 1962, Sulphur Bank, California, a major hot-spring quicksilver deposit: in Engel, A. E. J., James, H. L., and Leonard, B. F., eds., Petrologic Studies: A volume in honor of A. F. Buddington, p. 397-428.
- White, D. E., Barnes, Ivan, and O'Neil, J. R., 1973, Thermal and mineral waters of non-meteoritic origin, California Coast Ranges: Geol. Soc. America Bull., v. 84, no. 2, p. 547-560.
- Whitney, J. D., 1865, Geology: Calif. Geol. Survey, v. 1, 483 p.

SEISMIC MONITORING AT THE GEYSERS
GEOHERMAL FIELD, CALIFORNIA

by

S. M. Marks
R. S. Ludwin
K. B. Louie
C. G. Bufe

Principal Contributors:

P. W. Harsh
F. W. Lester
S. M. Briscoe
B. C. Hearn
R. J. McLaughlin

U.S. Geological Survey
345 Middlefield Road
Menlo Park, California 94025

Open-File Report 78-798

Prepared on behalf of the Division of Geothermal Energy,
U. S. Department of Energy

This is a preliminary and has not been edited or reviewed for
conformity with Geological Survey standards and nomenclature.

CONTENTS

	<u>Page</u>
Abstract	3
Introduction	3
Seismicity	5
Seismographic Coverage	5
Temporal Variations in Seismicity	7
Spatial Distribution of Hypocenters	15
Seismicity of Subregions	16
Magnitude-Frequency Relations	18
Seismic Deformation	18
Focal Plane Solutions and Stress Orientation	20
Synthesis	20
Further Studies	22
Acknowledgements	23
References	24

Tables

1 Comparison of pre-production and current seismicity in a large region including The Geysers	15
2 Earthquake frequency and cumulative moment data	19

Figures

1 Recent earthquakes (Jan 1975-Sept 1977) at The Geysers and along the Maacama and Rodgers Creek faults	6
2 U.S. Geological Survey seismographic stations, 1977. The stations immediately around The Geysers are shown in more detail in Figure 3..	8
3 History of the seismographic coverage of The Geysers area. Approximate traces of a few of the local faults are indicated by dashed lines. New telemetered stations went on line in late 1977 and early 1978	9
4 Zones searched in comparison of present (1975-1977, outlined by square) and pre-production (1962-1963, outlined by circle) seismicity levels. Circle represents a 60 km radius from CLS	11
5 Cumulative distribution of number of earthquakes as a function of coda duration at the Calistoga station, January 1962 through June 1963 ...	12
6 Relation between coda duration and magnitude at the Calistoga stations, based on events ($M \geq 2.5$) for which Richter magnitudes were determined (for circled area shown in Figure 3, and a b slope of 1.2). Average coda (dashed circle) length at $M = 3.0 \pm 0.1$ was 68 seconds	13
7 Index map of subregions for which moment-time histories and b slopes have been determined	18
8 Representative focal plane solutions for earthquakes at The Geysers and in the surrounding region. Preliminary faults are from McLaughlin and Hearn (unpublished data, 1978)	21

Plate

Steam production and cross section, The Geysers geothermal area, California.

Abstract

Two distinct clusters of microearthquakes have been identified at The Geysers, possibly relating to two independent pressure sinks resulting from steam production described by Lipman, and others (1977). Unlike earthquakes in the Maacama-Rodgers Creek fault zone to the south and west, earthquakes at The Geysers are confined to depths of less than 5 km. The present level of seismicity at The Geysers appears to be higher than the preproduction level and is higher and more continuous than the seismicity in the surrounding region. Earthquakes in the steam production zone at The Geysers resemble earthquakes in the surrounding region with regard to focal plane solutions, source characteristics and magnitude distribution (b slope). Subtle differences in earthquake characteristics may be resolved by analysis of more extensive data now being gathered in the region.

Introduction

The Geysers is the only geothermal area in the United States where electric power is being generated from underground steam. It lies adjacent to the Clear Lake volcanic system in which eruptions date from 2.04 million years ago to almost the present (.03 million years ago) (Donnelly, and others, 1977). The recent volcanic activity (Hearn, and others, 1976), the presence of a large negative gravity anomaly (Ishewood, 1976), the delay of P-wave traveltimes from distant earthquakes (Iyer, and others, 1978), and the extreme shallowness of the seismogenic zone (Bufe and Lester, 1975; Bufe, and others, 1978) suggest the presence of an intensive heat source in the form of a molten or near-molten

magmatic body beneath the area. The Franciscan assemblage and Great Valley sequence in which The Geysers development lies have been mapped by McLaughlin (1977).

Commercial power generation began at The Geysers in September 1960 with an 11 megawatt plant, but extensive development did not occur until 1967-68, when power production rose to 78 megawatts. Current production is 502 megawatts, with projections to exceed 900 megawatts in the near future. The region around the production area is under active investigation by several geothermal companies for future development. Currently, at full production, steam is being removed at a rate of 3.97×10^6 kg per hour, (Reed and Campbell, 1976) with 20 to 40 percent being reinjected.

This report describes preliminary results of an ongoing investigation of earthquake activity at The Geysers. The objectives of this study are:

1. To determine attenuation characteristics of the undersaturated (dry steam) region and source characteristics (from spectra and fault-plane solutions) of earthquakes occurring at The Geysers and to compare them with the characteristics of earthquakes outside the region.
2. To identify the degree of differentiation that is possible between microearthquakes natural to the geothermal area and those induced by production activities and to examine the relation of seismicity to rates of steam withdrawal, water injection, and subsidence.
3. To define in three dimensions the seismogenic zone at The Geysers, estimate deformation rate, and predict cumulative deformation in 5 to 10 years if microearthquake activity continues at the present level.

Seismicity

The Geysers geothermal development (see inset, Figure 1) is located 50 km northeast of the San Andreas fault within the broad zone of transform faulting between the Pacific and North American plates, and it thus lies in a tectonically active region. The segment of the San Andreas system opposite The Geysers last ruptured in the great earthquake of 1906. In October 1969 the largest earthquakes (M = 5.6 and M = 5.7) since 1906 in the Coast Ranges between San Francisco Bay and Cape Mendocino occurred on the Rodgers Creek fault at Santa Rosa, 40 km south of The Geysers.

Current (1975-1977) microseismicity in the vicinity of The Geysers is shown in Figure 1. Events in or near The Geysers cluster are also shown in map view and cross section on an expanded scale of 1:24,000 in Plate 1.

Seismographic Coverage

From 1911-1972 the only continuous network coverage of The Geysers was the regional network of seismographs of the University of California at Berkeley (UCB). The nearest station in continuous operation was Berkeley, 100 km southeast of The Geysers. During this period only two earthquakes (M = 3.1, 1963; M = 2.9, 1970) are listed in the UCB earthquake catalog (Bolt and Miller, 1975) as occurring within the boundaries of the area of Plate 1. In contrast, during 1973-74 Berkeley located two $M \geq 3$ events in this zone.

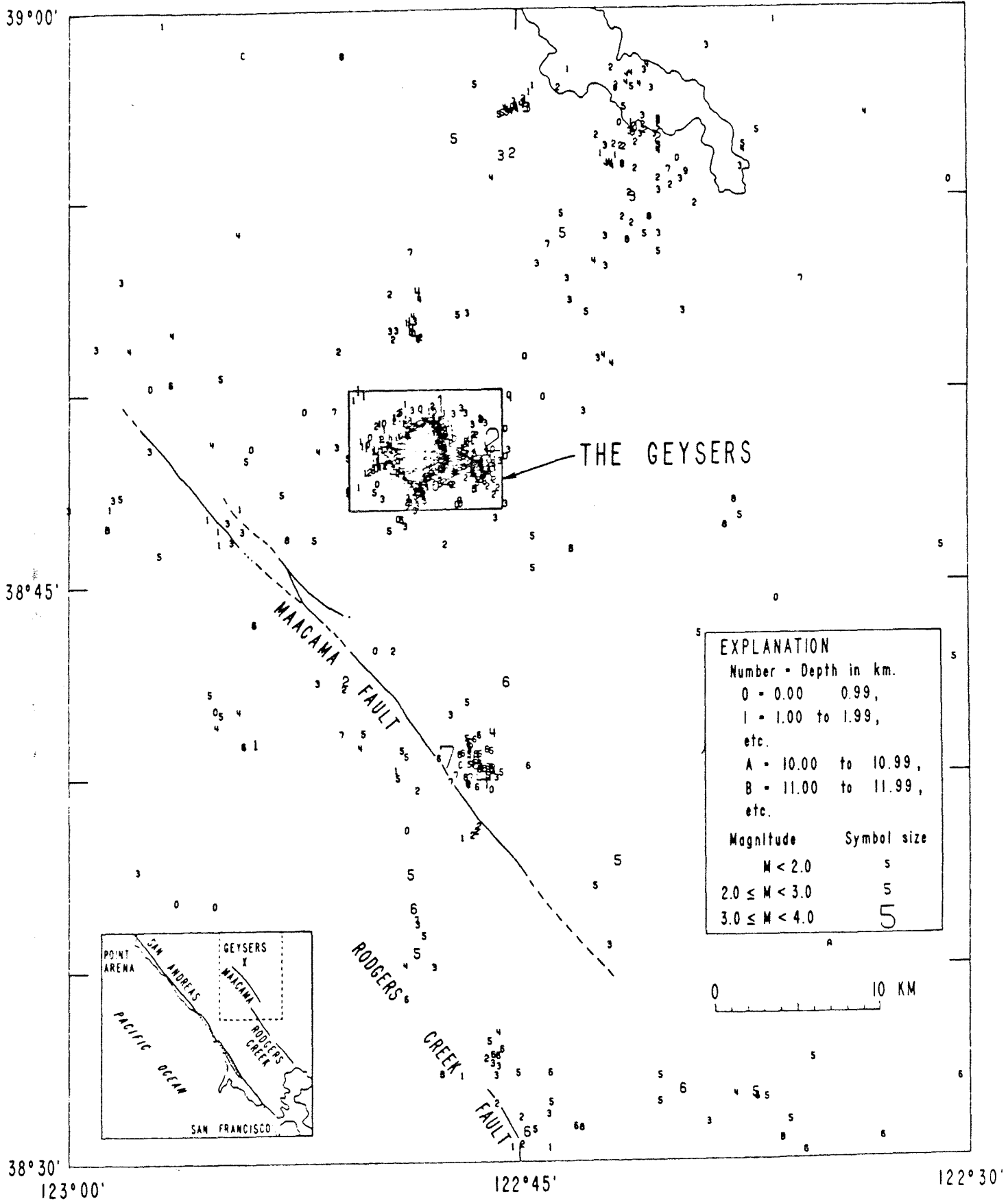


Fig. 1. Recent earthquakes (June 1975–Sept 1977) at The Geysers and along the Maacama and Rodgers Creek faults.

In the early 1960's, before extensive steam production had begun, UCB operated a seismographic station at Calistoga (CLS), 30 km southeast of The Geysers. CLS was a high-gain, short-period station that recorded many local earthquakes too small to be located by the Berkeley network. Thus it is not possible to ascertain whether these events originated at The Geysers. During March and April 1971, Hamilton and Muffler (1972) operated an 8-station seismic array for three weeks in The Geysers production area to monitor seismic activity. They located 53 small earthquakes within 10 km of the heavily exploited geothermal area.

In response to the interest generated by this work and reports of frequently felt earthquakes in the production area, the U.S. Geological Survey began upgrading its northern California network by adding more seismic stations to encompass The Geysers area (Fig. 2). In September 1973, the USGS network was extended into the vicinity of The Geysers, with stations installed at Alexander Valley and Pine Mountain. Although The Geysers was outside the network, earthquakes of $M \geq 2$ were routinely located there. At the beginning of 1975, the network was extended to surround The Geysers (Fig. 2). The distribution of stations presently operating in and around the steam production area at The Geysers is shown in Figure 3.

Temporal Variation in Seismicity

Since July 1975, seismographic coverage has been relatively complete, with location threshold approximately $M = 1.2$. Most of the micro-earthquakes located by Hamilton and Muffler (1972) were much smaller.

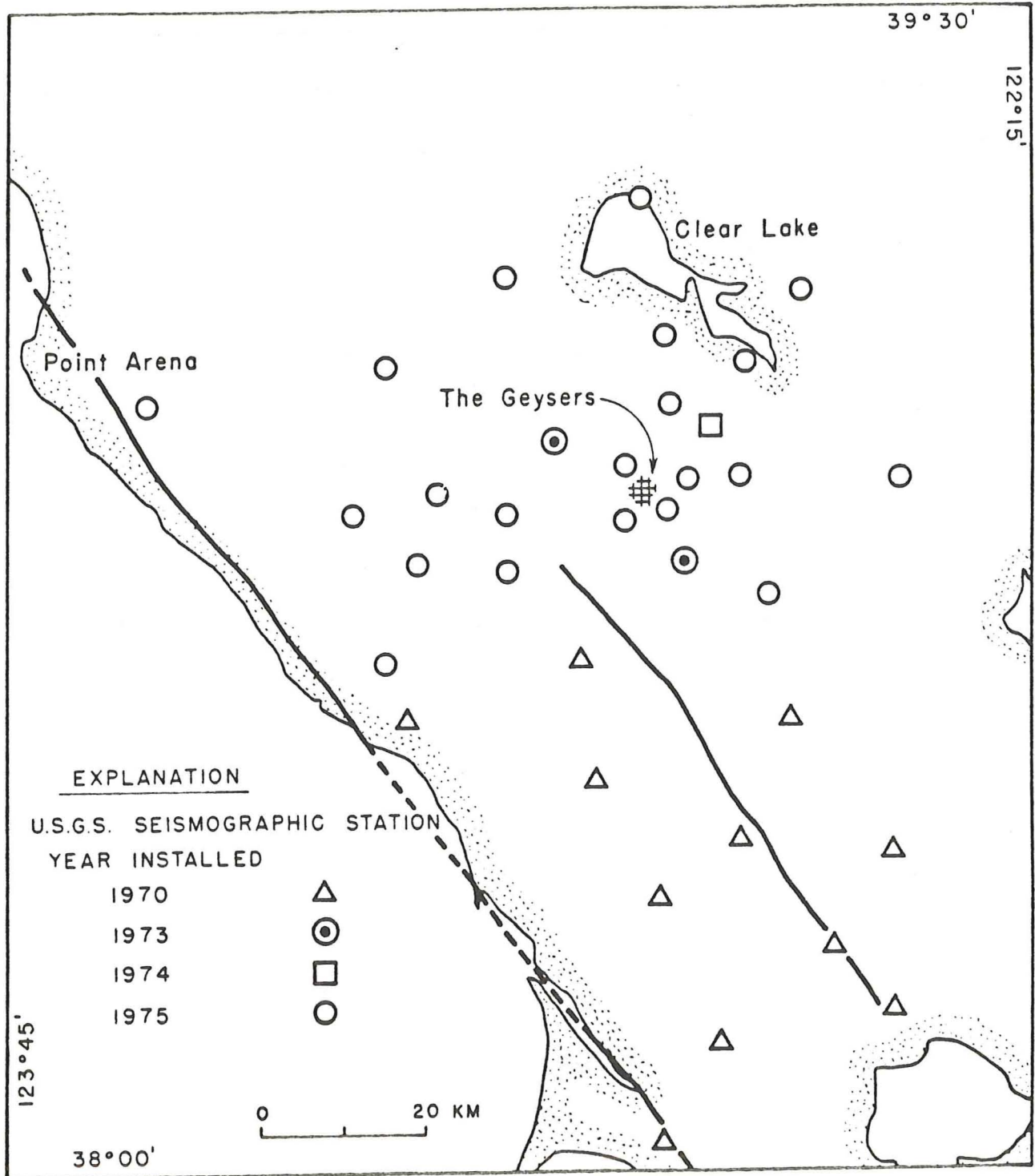


Fig. 2. U.S. Geological Survey seismographic stations, 1977. The stations immediately around The Geysers are shown in more detail in Figure 3.

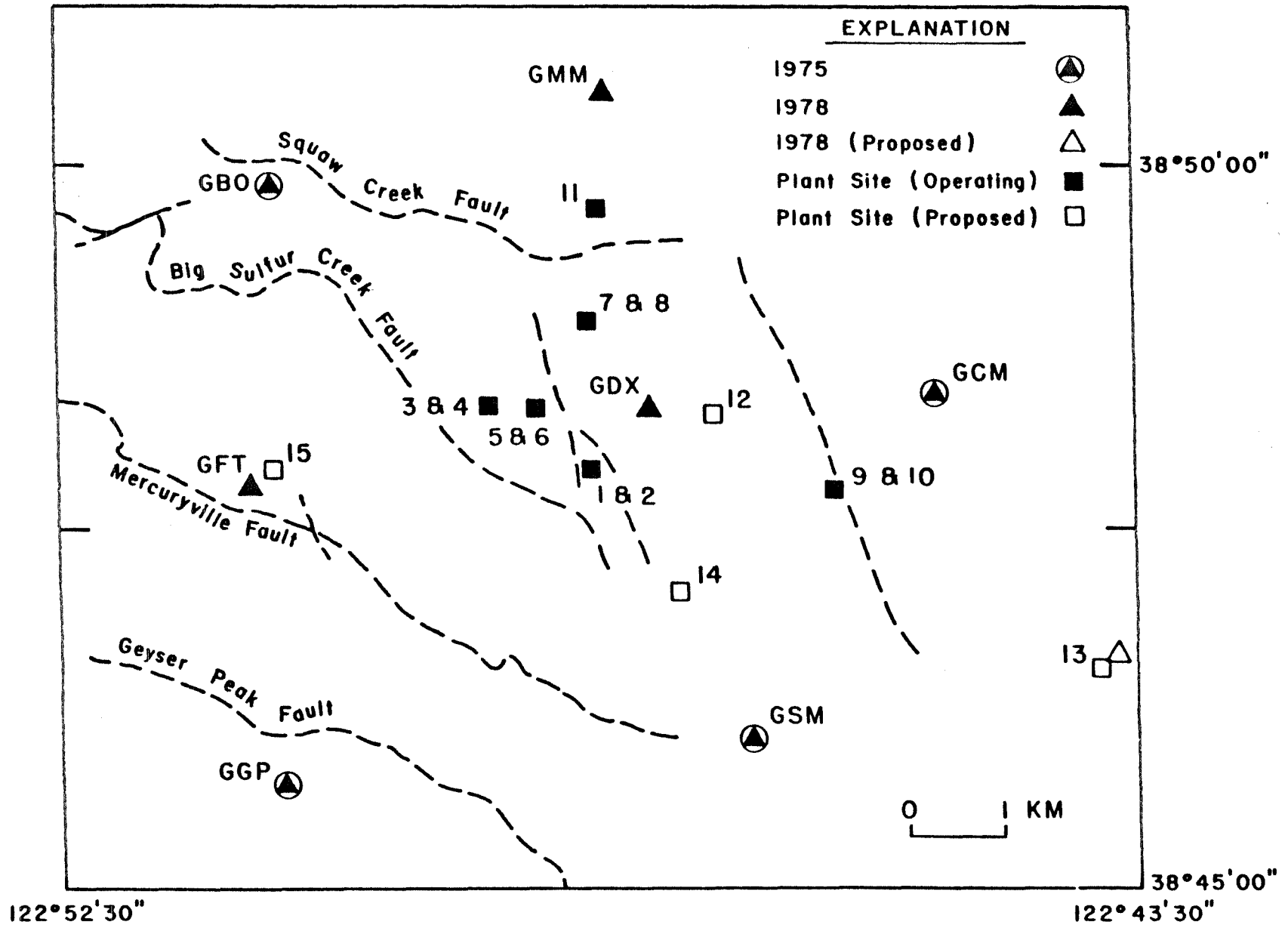


Fig. 3. History of the seismographic coverage of The Geysers area. Approximate traces of a few of the local faults are indicated by dashed lines. New telemetered stations went on line in late 1977 and early 1978.

Their largest event in three weeks of recording was of estimated magnitude 1.5. Since 1975 events of this magnitude occurred, on the average, every 2 or 3 days.

In an attempt to determine whether the level of activity in the region including The Geysers has changed significantly since the early 1960's, we have analyzed data from the UCB station at Calistoga (CLS). Magnitudes of events within a 60-km radius of CLS have been estimated from signal durations (coda lengths) assuming a linear relation between log duration and magnitude. The region examined can be approximated by the circular area with radius = 60 km (Fig. 4) corresponding to an S-P time of about 7 seconds. The Geysers lies well within this region. A log-log plot of cumulative number of events as a function of duration (D) was prepared (Fig. 5), and a linear relation ($\log N = -2.78 \log D + 5.46$) determined. This relation breaks down for coda lengths less than about 25 seconds; thus some events of shorter coda length are not being detected within the circle.

In order to convert the Calistoga coda information to magnitude estimates, it was necessary to tie duration to Richter magnitude. This was done at $M = 3$, for which Richter magnitudes are available from the UCB earthquake catalog (Bolt and Miller, 1975). Average coda length at $M = 3.0 \pm 0.1$ was 68 seconds, (see dashed circle in Fig. 6). The range of Richter magnitudes was not adequate, however, to determine the slope of the M vs. $\log D$ line. This was done by assuming the b slope for the region to be constant through time. A regional b value of 1.2, determined from USGS network 1975-77 data for the rectangular zone shown in

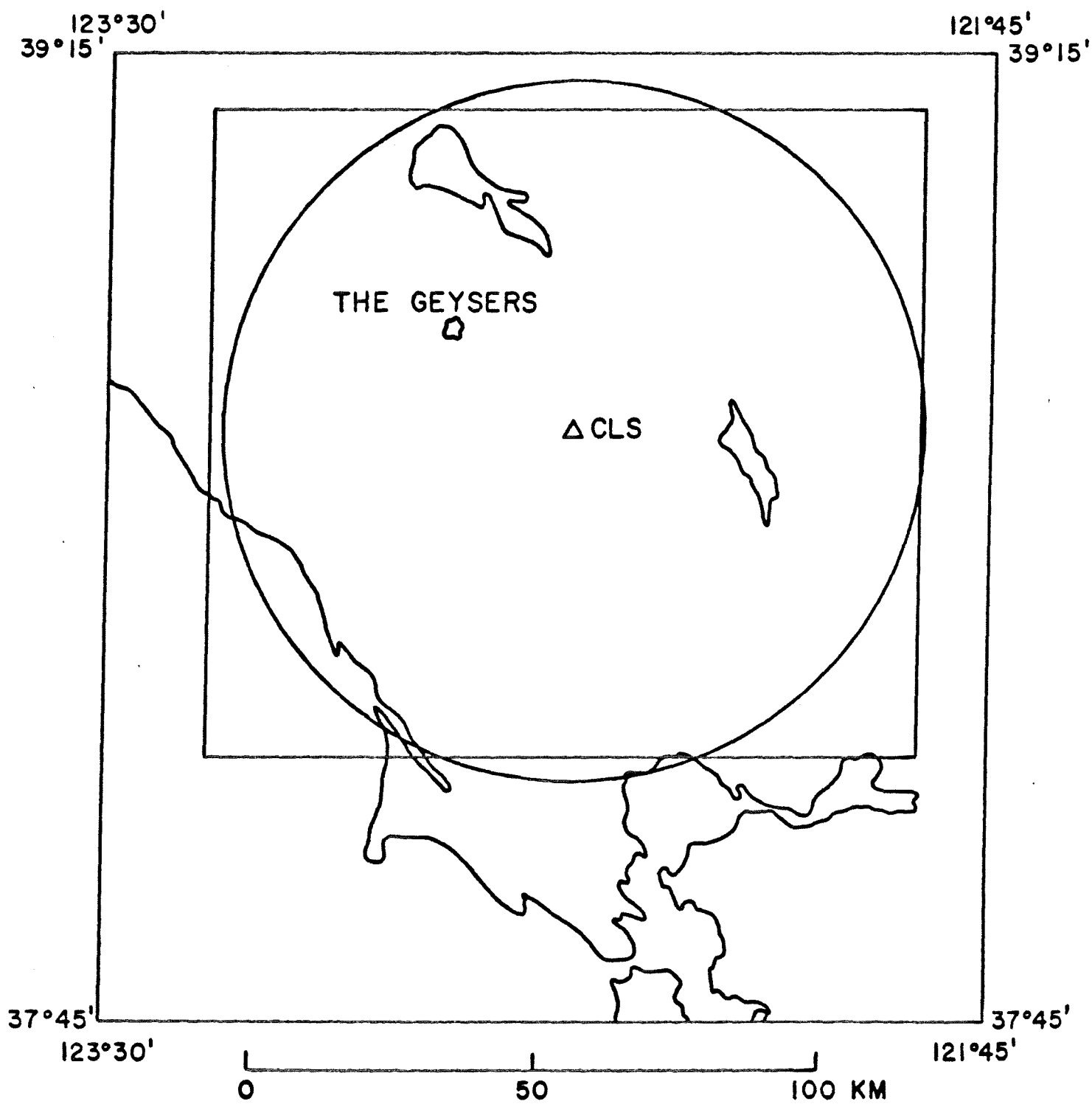


Fig. 4. Zones searched in comparison of present (1975-1977, outlined by square) and preproduction (1962-1963, outlined by circle) seismicity levels. Circle represents a 60 km radius from CLS.

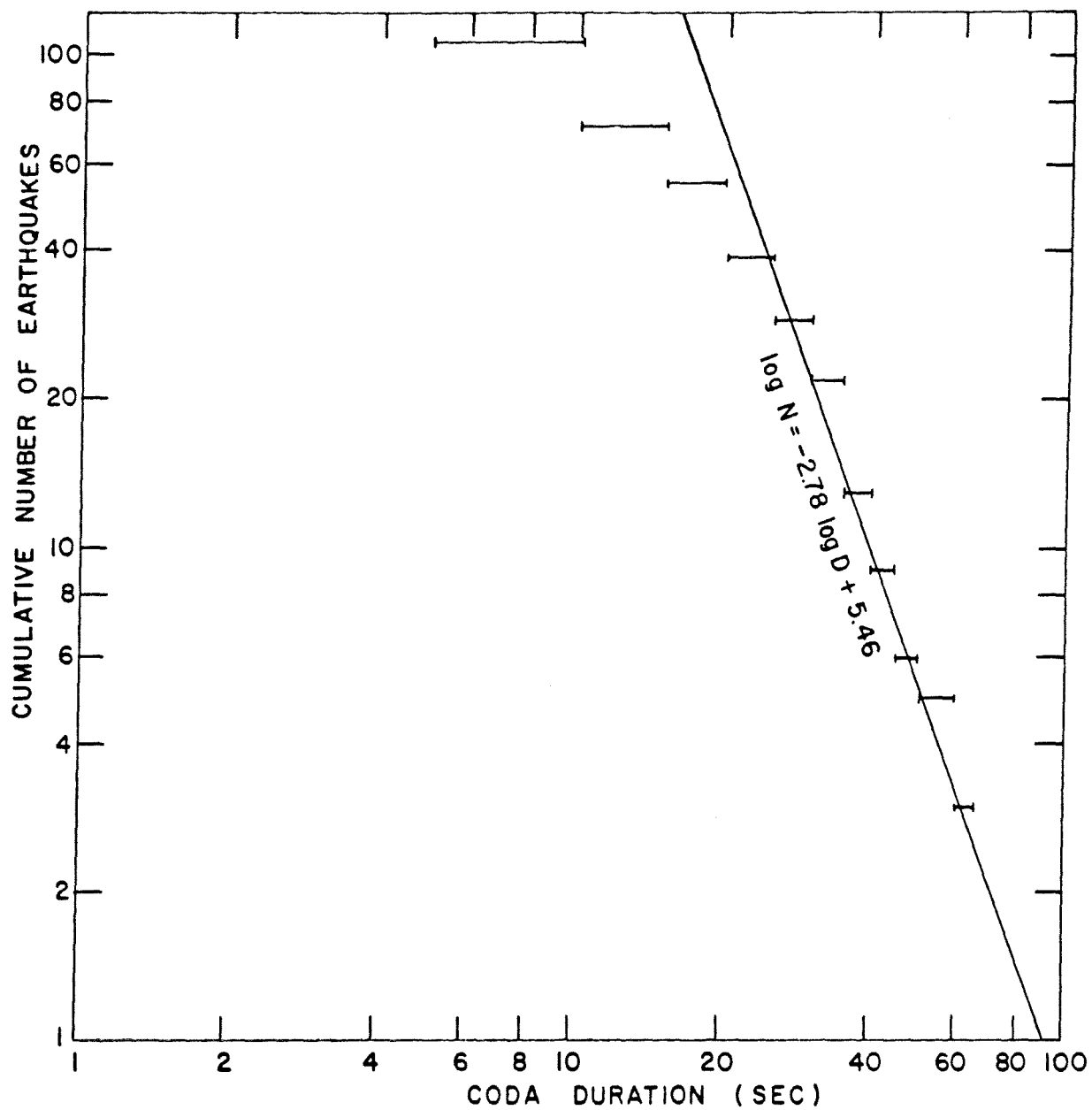


Fig. 5. Cumulative distribution of number of earthquakes as a function of coda duration at the Calistoga station, January 1962 through June 1963.

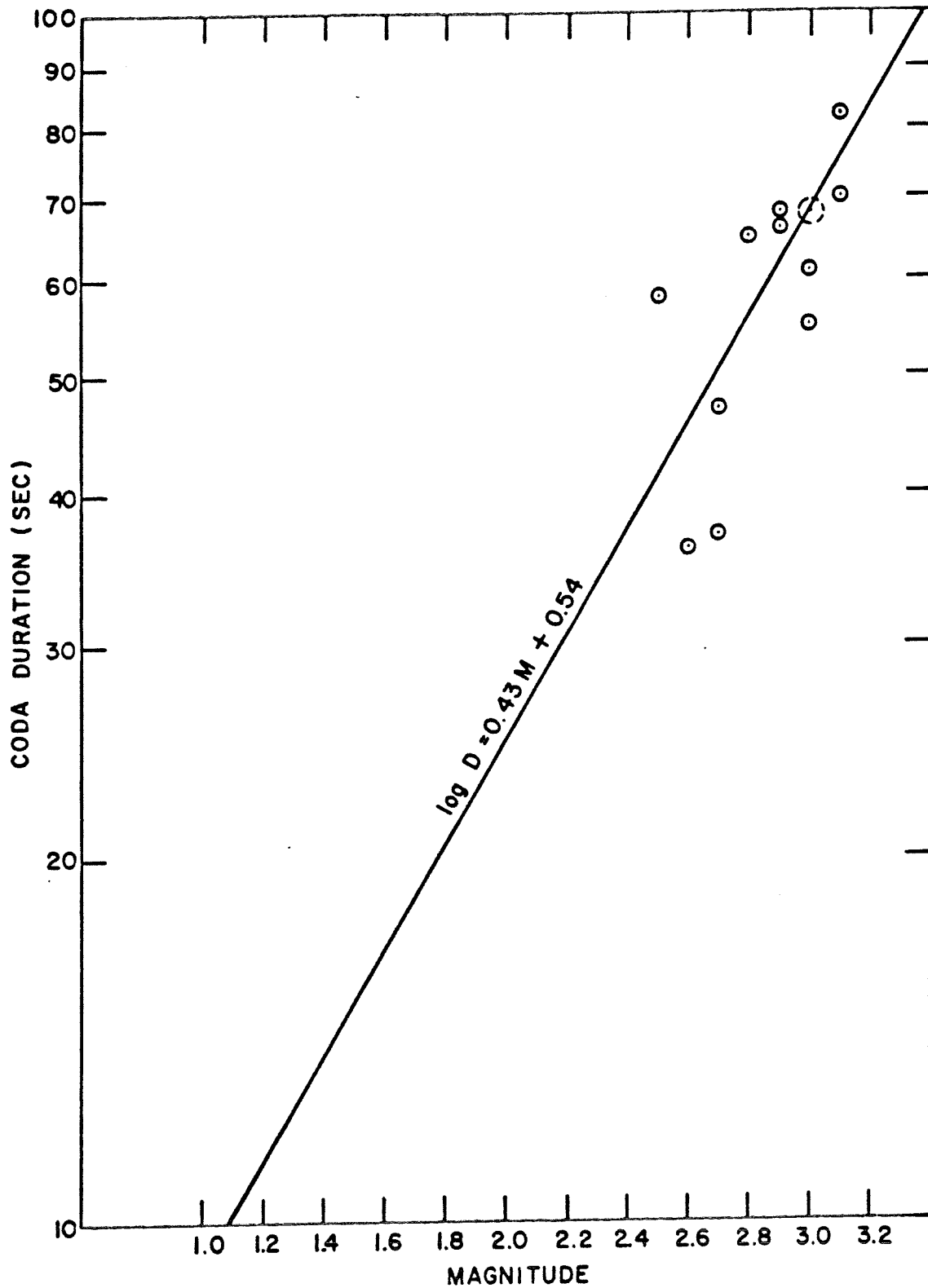


Fig. 6. Relation between coda duration and magnitude at the Calistoga station, based on events ($M \geq 2.5$) for which Richter magnitudes were determined (for circled area shown in Figure 3, and a b slope of 1.2). Average coda (dashed circle) length at $M = 3.0 \pm 0.1$ was 68 seconds.

Figure 4, was adopted. This b value is the same as that determined for The Geysers 1975-1977 earthquakes. Thus, since

$$\log N = a - 1.2 M \text{ and}$$
$$\log N = -2.78 \log D + 5.46,$$

the slope of the log D vs. M line is .43, and the duration-magnitude relation, constrained by the 68 second coda for magnitude 3, is

$$\log D = .43 M + .54$$

The data set is complete down to 25 seconds duration, which is $M = 2.0$ (Fig. 5). Thus, 37 earthquakes of $M \geq 2$ occurred in the circular region during the 18 month period January 1962-June 1963. Table 1 compares the preproduction (1962-63) rate of occurrence of $M \geq 2$ events with the present (April 1975-August 1977) rate of activity in the rectangular region of Figure 4. Magnitudes of 1975-1977 earthquakes were determined from durations at USGS stations after Lee, and others (1972).

Table 1: Comparison of pre-production and current seismicity at The Geysers and surrounding region, normalized for a 12-month period.

<u>Period</u>	<u>No. of events/yr (M \geq 2) in region</u>	<u>No. of events/yr (M \geq 2) Geysers only</u>
1962-63 (pre-production)	25	unknown
1975-77 (current)	47	24

From Table 1, we might conclude that the regional seismicity has increased and infer that the increase is attributable to increased seismicity within The Geysers 7.5' quadrangle.

Spatial distribution of hypocenters

Earthquakes located since 1975 (Plate 1) using the standard USGS central California crustal model (see, for example, Lester, and others, 1976) appear to define two distinct clusters of microearthquakes at The Geysers. The zone of greatest concentration of microearthquakes surrounds plants number 1 & 2, 3 & 4, 5 & 6, and 7 & 8. Plant 11 lies on the north edge of this zone. A secondary cluster of activity occurs in the vicinity of plants 9 & 10. Plants 12 and 14, which are not yet in production, lie along a seismic gap between the clusters. The location error for a blast fired south of plant #12 is only 200 meters

horizontally, and less than 1 km vertically; thus the earthquake locations are reasonably accurate and no large bias is present.

The shapes of the earthquake clusters overlap fairly well two pressure sinks in the steam field described by Lipman, and others (1977) and outlined on Plate 1. One sink developed as a result of steam withdrawals for Plants 1-8 and 11 and is reflected in high rates of subsidence described by Lofgren (1978). The other is a result of production for Plants 9 & 10. The sinks are apparently distinct from each other with no detectable pressure communication. The westward-dipping seismic gap between the earthquake clusters in Plate 1 may be the expression of a relatively unfractured, impermeable zone forming a barrier between reservoirs.

An east-west cross section through The Geysers on which hypocenters and injection wells have been projected is shown at the bottom of Plate 1. Earthquakes at The Geysers with reliable locations occur only at shallow depths ($h \leq 5$ km). However, shallow seismicity appears to be the rule for the entire region overlying the presumed magma body extending at depth from The Geysers to Clear Lake. In contrast, most earthquakes along the Rodgers Creek and Maacama faults south and west of The Geysers occur at depths greater than 5 km (Bufe, and others, 1978).

Seismicity of subregions

In order to identify differences in seismic characteristics of geothermal (steam or hot water) and regional tectonic regimes, subregions

(Fig. 7) were determined on the basis of the distribution of steam-producing wells and analysis of geothermal waters (Goff, and others, 1977, Julie Donnelly, oral communication, 1977). The "steam" subregion is complex, as The Geysers (Plants 1-8 and 11) and Geysers East (Plants 9 & 10) subregions have been removed from it.

Magnitude-frequency relations

Magnitude distribution [$\log N(m) = a - bM$] of earthquakes in The Geysers region shows a relatively high "b" value, which indicates an unusually rapid decrease in number of earthquakes with increasing magnitude. Such a high value may result from the structural heterogeneity of a geothermal region, but could also be characteristic of induced seismicity (Gupta and Rastogi, 1976). Table 2 summarizes b values and occurrence rates. Comparison of the b slope of earthquakes in the production zone with that of earthquakes elsewhere in the geothermal area suggests that the high b value is natural and not related to production. The "tectonic" subregion to the southwest has a somewhat lower b slope, but the difference is not statistically significant.

Seismic Deformation

Seismic moment (M_0) rates by subregion were estimated from earthquake magnitudes (M) by the empirical relation $\log M_0 = 1.5 M + 16$ (Bakun and Bufe, 1975). The moment is the product of slip along the fault, area of the fault surface, and rigidity of the rocks and is thus a measure of strain release. Moment rate per unit map area (Table 2) is highest in

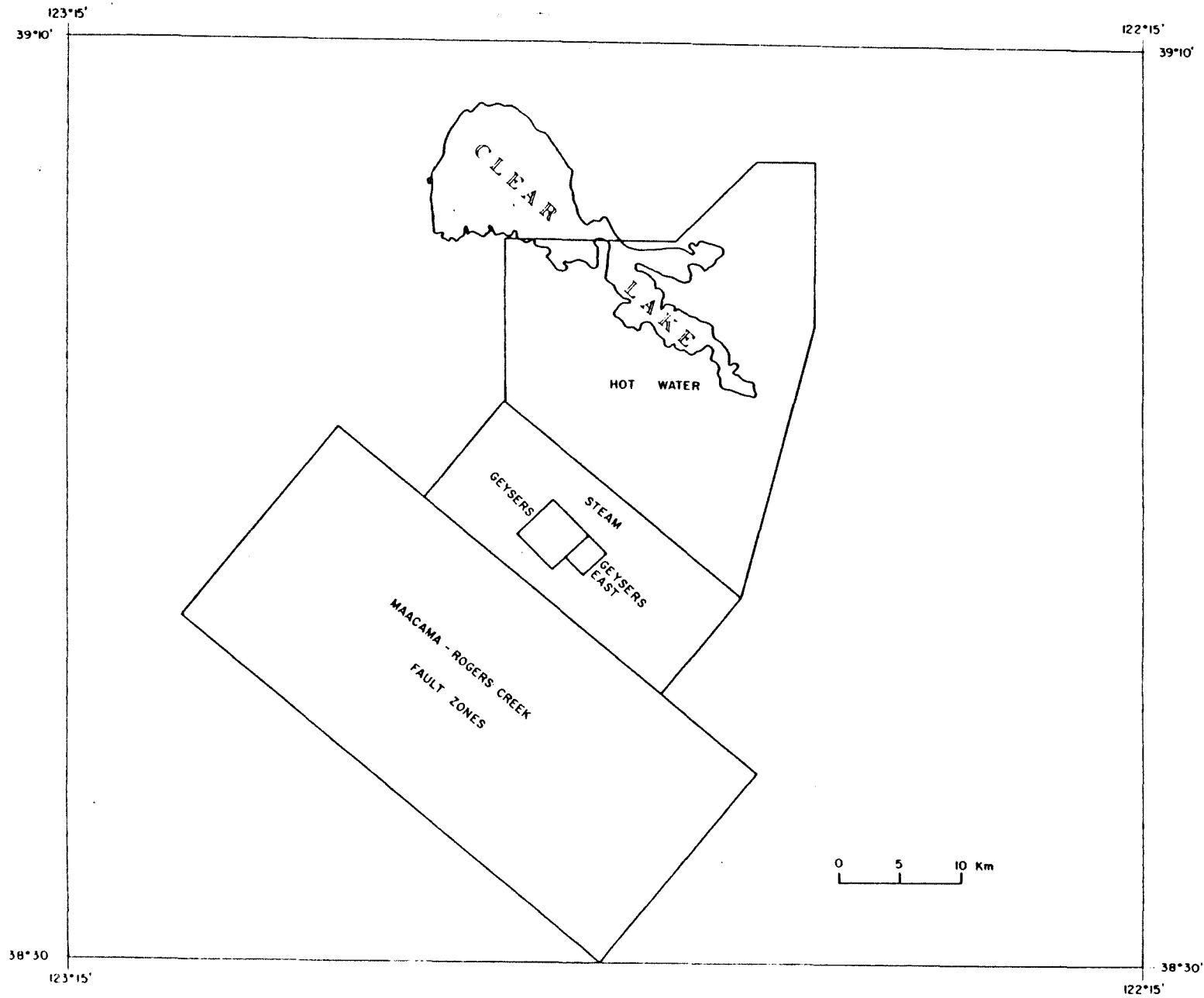


Fig. 7. Index map of subregions for which moment-time histories and b slopes have been determined.

Table 2. April 1975-August 1977. Earthquake frequency and cumulative moment data

		N	N/yr	Moment Rate	
	b	(M \geq 1.2)	M \geq 1.2)	N/yr/km ²	dyne-cm \times 10 ¹⁷ / km ² /yr
Geysers.....	1.2	498	206	12.41	928.
Geysers East....	1.3	57	24	4.53	396.
Undeveloped Steam.....	1.5	55	23	.10	6.74
Hot Water.....	1.2	95	39	.07	4.94
Maacama- Rodgers Creek...	1.1	64	26	.03*	1.74*

*Swarm activity along the Maacama fault since August 1977 indicates that these numbers do not accurately reflect the Maacama-Rodgers Creek seismicity which is episodic, in contrast to the more constant seismicity level presently observed at The Geysers.

the production zones. This result is consistent with surface deformation rates published by Lofgren (1978) showing horizontal (2 cm/yr convergence) and vertical (3 cm/yr subsidence) changes which suggest that the deep geothermal reservoir is being compressed both vertically and horizontally as fluid pressures within it are drawn down by production.

Focal plane solutions and stress orientation

Selected focal mechanisms of earthquakes are superimposed on a preliminary fault map of The Geysers and surrounding area in Figure 8. The lower hemisphere stereographic projections of P-wave first motions at the earthquake focus are interpreted in terms of double-couple earthquake mechanisms. Darkened quadrants are compressional, white quadrants dilatational. Tectonic stress orientation, deduced from P-wave first motions for events between June 1975 and September 1977, indicates maximum compression at N 30° E and minimum compression at N 60°W over most of the region north of 38° 35' (Bufe and others, 1978). This stress orientation is rotated 30° clockwise from that producing maximum right-lateral shear on faults subparallel to the San Andreas and Rodgers Creek systems, including the Maacama fault, and is consistent with north-westerly crustal extension. Stress orientation at The Geysers appears to be much the same as in the surrounding region. The dominant earthquake mechanism at The Geysers during this period was strike slip; fewer events indicated normal faulting.

Synthesis

Microearthquakes at The Geysers are strongly clustered around the regions of steam production and fluid injection. The present level of seismicity at The Geysers appears to be higher than the pre-production level and is higher and more constant than the seismicity in the surrounding region. Geodetic measurements described by Lofgren (1978) suggest that the deep geothermal reservoir is being compressed both

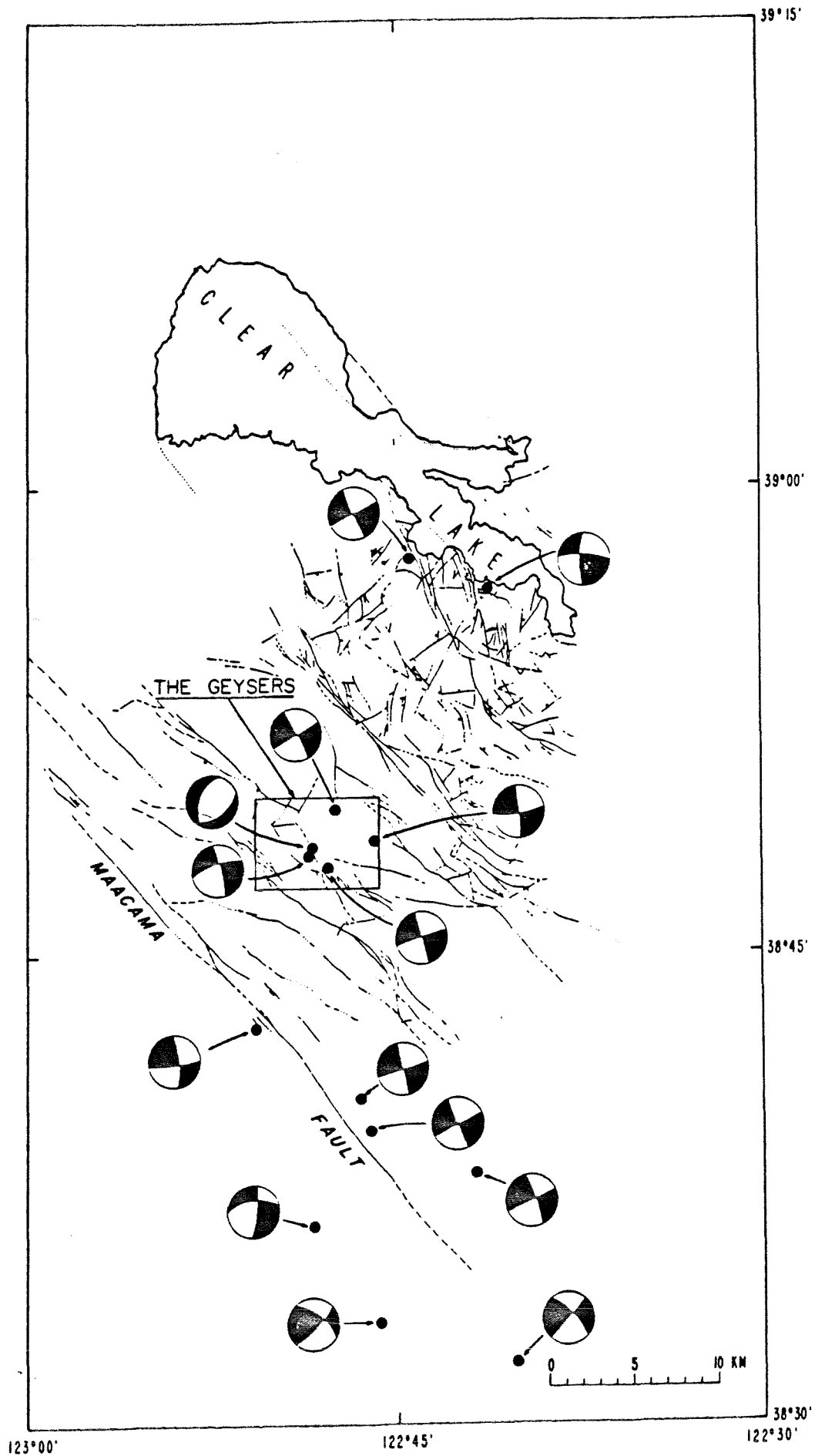


Fig. 8. Representative focal plane solutions for earthquakes at The Geysers and in the surrounding region. Preliminary faults are from McLaughlin and Hearn (unpublished data, 1978).

vertically and horizontally at rates of several centimeters per year as fluid pressures within it are lowered by production. It appears likely that much of the present seismicity at The Geysers is induced by steam withdrawal and/or injection of condensate. The mechanism by which this occurs warrants further study.

Further Studies

Majer and McEvilly (1978) and Peppin and Bufe (1978) have examined spectral characteristics of earthquakes at The Geysers. These earthquakes do not appear to be obviously anomalous in their characteristics, but analysis of data presently being gathered will determine whether there are subtle differences between source characteristics of earthquakes at The Geysers and those in the undeveloped geothermal regions nearby.

The current 502 MW capacity at The Geysers will be increased to 908 MW as soon as the four plants being constructed come on line in 1978 and 1979. Thus it is important to continue monitoring microearthquakes in The Geysers-Clear Lake geothermal field. The study of seismicity during development can be expected to give more definitive information on the effect of production on earthquake activity. The Geysers is the only producing geothermal area in the world where precise seismic monitoring is being done and for which data from a large dense regional network is available to complement the study. The data collected here may provide clues to answer the critical question as to how the seismicity of a geothermal area is altered by intensive exploitation.

Acknowledgements

The research for this manuscript was done for the Environmental Studies Branch, Division of Geothermal Energy, Department of Energy. We gratefully acknowledge Dr. Allan Jelacic of the Department of Energy for his valued suggestions. A special thanks to the staff of the California network for the processing of the data from which the earthquake hypocenters were obtained.

Dr. H. M. Iyer reviewed the manuscript and we are appreciative of his time and comments.

REFERENCES

- Bakun, W., and Bufe, C., 1975, Shear wave attenuation along the San Andreas Fault Zone in central California, Bulletin of the Seismological Society of America, 65, p. 439-459.
- Bolt, B., and Miller, R., 1975, Catalogue of earthquakes in northern California and adjoining areas, 1 January 1910-31 December 1972. University of California, Bulletin of the Seismographic Stations, 567 p.
- Bufe, C., and Lester, F., 1975, Seismicity of The Geysers-Clear Lake region, California, EOS, 56, p. 1020.
- Bufe, C. G., Marks, S. M., Lester, F. W., Louie, K., and Briscoe, S., 1978, Seismicity of The Geysers-Clear Lake geothermal area, California, Earthquake Notes, 49, no. 1, p. 32.
- Bufe, C., Pfluke, J., Lester, F., and Marks, S., 1976, Preliminary hypocenters of earthquakes in the Healdsburg (1:100,000) Quadrangle, Lake Berryessa to Clear Lake, California, U.S. Geological Survey Open-file Report 76-802.
- Donnelly, J. M., Hearn, B. C., Goff, F. E., 1977, The Clear Lake Volcanics, California: Geology and Field Trip Guide, in Field Trip Guide to The Geysers-Clear Lake Area, Cordilleran Section of The Geological Society of America, p. 25-56.
- Goff, F. E., Donnelly, J. M., Thompson, J. M., and Hearn B. C., 1977, Geothermal prospecting in The Geysers-Clear Lake area, northern California, Geology (in press).

- Gupta, H., and Rastogi, B., 1976, Dams and Earthquakes, Elsevier Publishing Company, Amsterdam.
- Hamilton, R., and Muffler, L., 1972, Microearthquakes at The Geysers geothermal area, California, Journal of Geophysical Research, 77, p. 2081-2086.
- Hearn, B. C., Donnelly, J. M., and Goff, F. E., 1976, Geology and geochronology of the Clear Lake volcanics, California, in Proceedings, Second United Nations Symposium on the Development and Use of Geothermal Resources, p. 423-428.
- Isherwood, W., 1976, Gravity and magnetic studies of The Geysers-Clear Lake geothermal region, ibid., p. 1065-1073.
- Iyer, H. M., Oppenheimer, D., Hitchcock, T., Roloff, J., Coakley, J., 1978, Large teleseismic P-wave delays in the Geysers-Clear Lake geothermal area, California, USGS Professional Paper, (in press).
- Lee, W. H. K., R. E. Bennett, and K. L. Meagher, (1972). A method of estimating magnitude of local earthquakes from signal duration, U. S. Geological Survey, Open-File Report, 28 p.
- Lester, F. W., S. L. Kirkman, K. M. Meagher, (1976). Catalog of earthquakes along the San Andreas fault system in central California, October - December 1973; U. S. Geological Survey, Open-File Report, 37 p.
- Lipman, S. C., Strobel, C. J., and Gulati, M. S., (1977), Reservoir performance at The Geysers field, in Proceedings of Lardarello, Italy, Workshop and Geothermal Resource Assessment and Reservoir Engineering Conference, (in press).

- Lofgren, B., 1978, Monitoring crustal deformation in The Geysers geothermal area, California, USGS Open-file Report 78-597, 19 pp.
- Majer, E., and McEvilly, T. V., 1978, Seismological investigations at The Geysers geothermal field, Geophysics, (in press).
- McLaughlin, R. J., 1977, The Franciscan Assemblage and Great Valley sequence in The Geysers-Clear Lake region of northern California, in Field Trip Guide to The Geysers-Clear Lake area, Cordilleran Section of the Geological Society of America, p. 3-24.
- Peppin, W., and Bufe, C. G., 1978, Induced (?) versus natural earthquakes: search for a seismic discriminant, Earthquake Notes, 49, no. 1, p. 65.
- Reed, M. J., and Campbell, G. E., 1976, Environmental impact of development in The Geysers geothermal field, U.S.A., in Proceedings, Second United Nations Symposium on the Development and Use of Geothermal Resources, p. 1399-1410.

SEISMIC-REFLECTION INVESTIGATIONS AT
CASTLE ROCK SPRINGS,
THE GEYSERS GEOTHERMAL AREA

by

Roger P. Denlinger and Robert L. Kovach
Department of Geophysics
Stanford University
Stanford, California 94305

ILLUSTRATIONS

	Page
Figure 1. Map showing regional geology and structure of the Geysers-Castle Rock Springs geothermal area.	36
2. Map showing regional geology and structure of study area.	4a
3. Map showing location of seismic stations and producing steam wells in study area.	4b
4. Stacked seismic section along line two showing reflection profile and two-way travel time.	5a
5. Geologic section along reflection line two.	5b
6. Interval velocity section calculated for seismic line two.	5c
7. Stacked seismic section along line one showing reflection profile and two-way traveltime.	5d
8. Geologic section along reflection line one.	5e
9. Interval velocity section calculated for seismic line one.	5f

ABSTRACT

Seismic-reflection profiling verifies the presence of an anticlinal trap in the vicinity of the Castle Rock Springs steam field. Strong reflection amplitudes recorded near the crest of the anticline correlate in depth with an observed fracture zone in a nearby well, and strong reflections within the core of the anticline may also be due to the fracture zone from which steam is produced in this area. Southwest of the anticline, a band of seismic energy may indicate the contact between fractured graywacke reservoir rock and its mafic caprock. The seismic sections also indicate southeast and northeast extensions of the cap which could not be inferred on the basis of previous information.

A strong deep reflection which we believe represented a tectonic boundary in the Franciscan assemblage was recorded below 4 km. This boundary dips northeastward, toward a possible heat source, and occurs at depths between the heat source and the steam system.

INTRODUCTION

The Geysers steam field produces more power than any other steam field in the world. Although numerous studies have been conducted in the field, little detailed information has been obtained that indicates the spatial distribution of the steam-filled fracture zones. The principal means of exploring in the area at present is explorational drilling until good steam zones are located.

The Castle Rock Springs steam system is near the periphery of the major steam field at The Geysers, as both by explorational drilling and the residual Bouguer gravity field of the area (Denlinger, 1979). The Castle Rock Spring steam field is of interest here because it is an example of an anticlinal warp within the predominantly east dipping geologic section. McLaughlin and Stanley (1975) hypothesized that fracturing induced by folding in the crest of these anticlines increases permeability. Therefore such anticlines could act as structural traps, concentrating upward-convecting geothermal fluid.

According to this model, some of the fracture zones would tend to be subhorizontal near the crest of the anticline. This raises the possibility that the fractures may be mapped by seismic-reflection profiling, given sufficient lateral continuity in both the fracture zones and the subsurface velocity structure.

In the spring of 1976, we conducted a seismic reflection survey over two profiles in the Castle Rock Springs area. The data obtained represent the first reflection survey undertaken in a Franciscan terrance, and we hope that the success of this project will prompt further seismic-reflection work in the Geysers area.

McLaughlin (1978) describes the regional structure of The Geysers and vicinity in terms of a southeast-plunging antiform. The major part of the area studied here occupies the northeast flank of this antiform, whose axis is close to the Mercuryville fault zone. In describing the local structure of the steam fields and the pattern of steam occurrences, McLaughlin and Stanley (1975) noted (1) the occurrence of impermeable mafic rocks overlying steam-filled graywacke that may serve as a caprock, and (2) the existence of anticlinal warps in the predominantly eastward dipping metagraywacke and shale. These may locally enhance fracturing and act as local structural traps in a convecting geothermal system.

ACKNOWLEDGEMENTS

This research was supported by the U.S. Geological Survey under contract number 14-08-0001-15329. Special thanks are due to Western Geophysical Company and the survey manager Stewart Mitchell for conducting the survey in difficult terrain. Ron Chambers, Ted Clee, and Chang-sheng Wu of Western's Research Division were most helpful during data processing. We also thank Aminoil and Shell Oil Companies for permission to enter their leaseholdings in the Castle Rock Springs area.

Figure 1. Regional geology and structure of the Geysers-Castle Rock Springs geothermal area, modified from McLaughlin (1978).

DATA ACQUISITION AND PROCESSING

Two lines were laid out along gravel roads in the Castle Rock Springs area (figs. 2 and 3). The survey was carried out by Western Geophysical, using standard field procedures. Four Vibroseis trucks spaced 3 m apart were used

Figures 2 & 3

near here

as a source, with a 16-s downsweep applied four times from each truck. The lines were laid out split spread, 12 fold, with a 33 m group interval and a cable length of 880 m (Sheriff, 1973). It was determined at the site that a 58-to 12-Hz downsweep gave the best signal-to-noise ratio. Data were recorded in floating-point form 250 times a second.

Processing was standard except for Western Geophysical automatic statics routine (Wiggins and others, 1976). Velocity spectra (Taner and Koehler, 1968) were used to pick preliminary velocities before statics determination. To reduce the possibility of introducing artificial coherence, the static time shifts were limited to one-half the dominant period of the data (20ms). After static corrections were determined, they were applied to the original cross-correlated data, and the velocity spectra, correlating the spectra with events observed on the records. Both floating-point (relative amplitude) and fixed-point (normalized amplitude) sections for lines one and two were produced. These are shown for comparison in figures 4 and 7.

The sections are unmigrated. The wavelengths observed range from 100 to 300 m, and ten points per wavelength are needed to migrate effectively. Because the station spacing used was 33 m, all but the longest wavelengths are too undersampled for migration processing.

Figure 2. Regional geology and structure of stude area, modified from McLaughlin (1978).

Figure 3. Location of seismic stations and producing steam wells in the study area.

INTERPRETATION

The velocity time curves that produce the most coherent sum of the data may be used to calculate an interval velocity structure for the lines (Dix, 1955). Assuming that plane interfaces separate regions of constant velocity, we used Dix's formula to calculate the velocity structure shown in figures 6 and 9. The interval velocity so obtained forms the basis for our interpretation of the seismic sections. In addition, we had lithologic logs for wells C5 (courtesy of Shell Oil Co.). Our velocities are in good agreement with the sonic log data for well C5, at the intersection of lines one and two.

The velocities structure found along line two is roughly consistent with the geologic structure shown in figure 5. Since the predominant wavelengths were averaging over distances of 100 m, much of the lithologic details cannot be seen. Strong reflections are also needed to pick velocities out of the noise during processing, and thus the strongest reflections control where the velocity horizons are placed.

A better correlation may be made between the two reflections sections (figs. 4 and 7) and the respective geologic sections. The anticlinal structural beneath shot-points 139 to 104 is evident as well as the gently dipping layered structured to the southeast. Reflected energy from the southeast flanks of the anticlinal can be seen below 1

Figures 4 - 9
near here

Figure 4. Stacked seismic section along line two showing reflection profile and two-way traveltime. V's mark position of velocity analyses. Southwest end of line one intersects at section location 8. A, Amplitudes mormalized to mear-surface rms amplitude. B, Structures accentuated for comparison with geologic section of figures 5. C, Relative amplitudes preserved.

Figure 6. Interval velocity section calculated for seismic line two. V's mark position of velocity analyses.

Figure 7. Stacked seismic section along line one showing reflection profile and two-way traveltime. V's mark the position of velocity analyses. Intersection of line two is at section location 8. Deep reflector near 2.1 seconds dipping northeast may represent a major tectonic boundary in the Franciscan assemblage. A, Amplitudes normalized to near-surface rms amplitude. B, Structures accentuated for comparison with geologic section of figure B. C, Relative amplitudes preserved.

Figure 8. Geologic section along reflection line one, (from McLaughlin, 1978).

Figure 9. Interval velocity section calculated for seismic line one. Major fault near shot-point 139 is a tectonic boundary evident from reflection data, surface geology, and lithologic data at Borrows well (see fig. 3).

second on section two. A thick fracture zone near the crest of the anticline in a nearby well correlates in depth with a strong reflection evident on seismic section two just below 0.3 seconds near shot-points 127 - 104. Other high-amplitude reflections associated with the anticline seen in section two may also indicate the presence of fracture zones, which would substantiate the anticlinal trap hypothesis of McLaughlin and Stanley (1975). Many reflections are highlighted within the anticlinal structure. Velocity information is lacking below 1.0 seconds (fig. 6) due to a lack of strong continuous events below this level. Thus the depths of events visible below this level cannot be determined.

Southeast of the anticline, the velocity and seismic sections (fig. 4 & 6) both verify the gently dipping layered structure McLaughlin (1978) determined on the basis of surface geology and well data. The base of the 2.38 km/s layer is interpreted on the basis of depth to be the base of the serpentinite. The melange section above greenstone shown in the geologic section is interpreted to be the 4.07 and 4.36 km/s layers. The contact between greenstone and graywacke (McLaughlin, 1978) could not be extended on the basis of available data. On the reflection section, however, a band of seismic energy at 1.1 seconds may indicate the extension of this contact and possible fracturing associated with this tectonic boundary. Based on the velocity above it, the depth of this boundary is about 1.7 km, which is the depth that producing steam zones begin to occur (from well information along the profile). It is possible here that the greenstone acts as an impermeable mafic cap for the fractured graywacke, which acts as the reservoir. The existence of a mafic or ultramafic cap over fractured graywacke fits the pattern of steam occurrences in other areas of the Geysers steam field (McLaughlin and Stanley, 1975).

Line one meets line two at the marked intersection on both the reflection and geologic sections. The velocities found for both sections are consistent with the sonic log for well C5, near the line intersection. The velocities and reflected events match between the lines, thus line one indicates how the geology near the intersection changes northeast of line two. Both the melange units and the seismic energy band just below 1.1 seconds on line two dip gently to the northeast. Much deeper, at about 2.1 seconds, a much stronger reflection dips toward the northeast. Assuming a average velocity of 4.23 km/s below the last reflector, this reflector is at least 3.1 km deep. Given the observed increase of velocity with depth, 4 km may be more likely. This reflector may indicate a major tectonic boundary in the Franciscan assemblage, and seismic energy reflected from it may be enhanced by increased fracturing along the boundary or by the presence of imbricate layers due to shearing. It occurs at a depth between the heat source (Isherwood, 1976) and the steam system observed in the wells. Thus if permeable, such a boundary could act as a conduit for convection of the geothermal fluid from the heat source into the geothermal system.

CONCLUSIONS

We have shown that seismic-reflection techniques applied to the steam system at Castle Rock Springs may be useful in detecting fracture systems within the steam reservoir and deep geologic structure beneath the reservoir. This survey was an experiment to determine whether or not standard reflection techniques, if modified with state-of-the-art processing schemes, would be useful in geothermal prospecting. Basically we succeeded in obtaining interpretable data in a difficult area, but significant improvement in survey design and processing can be made from what we learned from this project.

In designing this survey, a line length of 1.6 km (1 mile) was chosen as a compromise. If long line lengths are used, good control on velocity is obtained by convolving the records with some best-fit hyperbola, as the tail of the hyperbola which best fits a single velocity to a reflector is then well defined. In areas of strong lateral variations in velocity, however, the travel time - offset curve deviates significantly from a hyperbola. Thus, short lines are needed to improve the signal-to-noise ratio during the sum/convolution of the records with a best-fit hyperbola (an approximation). The price to be paid, with short lines, is decreased resolution in velocity and hence depth to a reflecting horizon.

Because we wanted to maximize our signal-to-noise ratio at depths between 1 and 3 km, we chose short lines, knowing that we would lose our depth resolution in doing so. A better, more expensive compromise would have been to run the survey 48-fold on lines two to three times longer than we used. Better still, and necessary if seismic reflection methods are to become a useful tool in geothermal exploration, will be good velocity control from outside sources such as reflection profiles or ^{ra}microearthquakes. Once

velocity is known, it is possible to construct the actual curve (other than assumed some hyperbola) along which the common midpoint data should be summed, and this will produce a dramatic improvement in the signal-to-noise ratio. In this way seismic-reflection methods will provide the most detailed information on the structure of geothermal systems.

REFERENCES CITED

- Denlinger, R. P., 1979, Geophysical constraints on The Geysers geothermal system, northern California [Ph. D. thesis]: Stanford, California, Stanford University, p.
- Dix, C. H., 1955, Seismic velocities from surface measurements: Geophysics, v. 20, no. 1, p. 68-86.
- Isherwood, W. F., 1976, Gravity and magnetic studies of the Geysers-Clear Lake region, California: United Nations Symposium on the Development and use of Geothermal Resources, 2d, San Francisco, 1975, Proceedings, v. 2, p. 1965-1073.
- McLaughlin, R. J., and Stanley, W. D., 1975, Pre-Tertiary geology and structural control of geothermal resources, the Geysers steam field, California: U.N. Symposium on Development and Use of Geothermal Resources, 2d, San Francisco, 1975, Proceedings, p. 475.
- McLaughlin, R. J., 1978, Preliminary geologic map and structural sections of the central Mayacmas Mountains and The Geysers Steam Field, Sonoma, Lake, and Mendocino Counties, California: U.S. Geological Survey Open-File Report 78-389.
- Sheriff, R.E., 1973, Encyclopedia dictionary of exploration geophysics: Tulsa, Oklahoma, Society of Economic Geologists, 1st edition.
- Taner, M. T., and Koehler, R., 1969, Velocity spectra-digital computer derivation and applications of velocity functions: Geophysics, v. 34 p. 859-881.
- Wiggins, R. A., Lamer, K. A., and Wisecup, R. D., 1976, Residual static analysis as a general linear inverse problem: Geophysics, v. 41, no. 5 p. 922.

FIGURE CAPTIONS

Figure 1 Regional geology and structure of the Geysers-Castle Rock Springs geothermal area, modified from McLaughlin (1978).

Figure 2 Regional geology and structure of study area, modified from McLaughlin (1978).

Figure 3 Location of seismic stations and producing steam wells in study area.

Figure 4 Stacked seismic section along line two showing reflection profile and two-way traveltime. V's mark position of velocity analyses. A, Amplitudes normalized to near-surface rms amplitude. B, Structures accentuated for comparison with geologic section of figure 5. C, Relative amplitudes preserved.

Figure 5 Geologic section along reflection line two (from McLaughlin, 1978). Vertical scale not the same as in Figure 4.

Figure 6 Interval velocity calculated for seismic line two.

Figure 7 Stacked seismic section line one showing reflection profile and two-way traveltime. V's mark position of velocity analyses. Deep reflector may represent a major tectonic boundary in the Franciscan assemblage. A, Amplitudes Normalized to near-surface rms amplitude. B, Structures accentuated for comparison with geologic section of figure 8. C, Relative amplitudes preserved.

Figure 8 Geologic section along reflection line one (from McLaughlin, 1978).

Figure 9 Interval velocity section calculated for seismic line one. Major fault near shotpoint 139 is a tectonic boundary evident from reflection data, surface geology, and lithologic data at Barrows well (see fig. 3).

WAVE EQUATION MODELING OF A PROBABLE HEAT SOURCE, THE GEYSERS, NORTHERN CALIFORNIA.

A previous analysis of the gravity, magnetic, and deep drill hole data from The Geysers area, Northern California placed size and density constraints on a probable heat source. The above data may be fit to a spherical source centered at a 13.5 km depth beneath Mt. Hannah, in which a density contrast of -0.27g/cc results in radius of 6.9 km. With these constraints, we investigate here whether or not this low density source may, with a reasonable velocity and attenuation contrast, be used to model the observed pattern of teleseismic P wave time delays and amplitudes found in The Geysers area.

In constructing a velocity structure velocities found from several refraction surveys were used. An approximation to the low density spherical shape was then mapped onto this and velocity and attenuation within the body were varied arbitrarily. Near vertical plane waves were propagated using a 45 degree approximation to the scalar wave equation on a 2-D grid with absorbing side boundaries. Attenuation was introduced naturally by allowing the velocity to be a complex function of frequency.

The results indicate that diffraction effects are minimized since the low velocity body occurs within one wavelength of the free surface (app. 5-6 km). In certain areas, discrepancies occur between the model and actual data in waveform and amplitude, and suggest that critical refraction and reflection as well as diffraction around the edges of the lens shaped body may be important. To first order, however, reasonably good agreement between model results and observations constrain velocity and attenuation values for the anomalous volume. Using values for velocity and attenuation, complex moduli for the anomalous volume may be calculated. Then, by assuming (1) that the volume is composed of rock and partial melt, and (2) a specific composition for the rock and partial melt, it is possible to set limits upon the percentage of partial melt within the anomalous volume.

APPLICATIONS OF THERMAL WATER CHEMISTRY IN THE GEYSERS-CLEAR LAKE GEOTHERMAL AREA, CALIFORNIA

GOFF, Fraser E., and DONNELLY, Julie M., U.S. Geological Survey, 345 Middlefield Road., Menlo Park, CA 94025

Geochemistry of thermal waters, geologic mapping, and geophysics have been used to delimit the Geysers steam field, estimate the possible temperature of the hot water system beneath the Pliocene and Quaternary Clear Lake Volcanics, and predict the unrecognized presence of Great Valley sequence rocks. Steam condensate waters are confined to an area southwest of the main Clear Lake volcanic field and the Collayomi fault zone. To the northeast, thermal waters of deep origin rise along fault zones, and estimated Na-K-Ca and adiabatic (quartz) reservoir temperatures indicate that a 200°C hot water system underlies the young volcanics. These estimates agree with measured temperatures from the few deep drill holes. Although thermal waters emerging northeast of the Collayomi fault zone are commonly rich in HCO_3^- , estimated Na-K-Ca temperatures are independent of ^{14}C . Thermal waters emerging from mapped Great Valley sequence rocks are consistently higher in chloride than similar waters from undisputed Franciscan rocks. Our data suggest that thermal waters containing greater than 300 mg/l chloride have passed through at least some rocks of the Great Valley sequence. The chloride concentrations of non-steam-condensate thermal waters can thereby be used to predict the concealed extent of Great Valley sequence rocks beneath the Clear Lake Volcanics. High chloride waters emerging northeast of the Collayomi fault zone suggest unrecognized areas or under-thrust slabs of Great Valley sequence rocks, e.g., along the east side of the Bartlett Springs fault zone, underlying the Cache Formation of Brice (1953), and thrust under the ophiolite sheet north of Wilbur Springs.

GEOCHRONOLOGY AND EVOLUTION OF THE CLEAR LAKE VOLCANICS, NORTHERN CALIFORNIA

DONNELLY, Julie M., U.S. Geological Survey, Menlo Park, CA 94025; and HEARN, B. Carter, Jr., U.S. Geological Survey, Reston, VA 22092

The Clear Lake Volcanics range in age from 2 million years to 10,000 years b.p., on the basis of K-Ar and ^{14}C dating. K-Ar dates indicate that volcanism was distinctly episodic with few or no eruptions during the periods 1.3-1.1, 0.8-0.6, and 0.3-0.1 m.y.b.p. Eruptive centers are generally younger from south to north. The volcanic field consists of a complex sequence of more than 100 mappable units ranging from basalt to rhyolite in composition. The youngest and oldest episodes of volcanism are dominantly basaltic, but the intermediate periods are characterized by dacite and rhyolite. During the period 0.6-0.3 m.y. ago, at least 35 km³ of dacite erupted, representing about a third of the total volume of the volcanic field. Andesites constitute only 5% of the total erupted volume and are largely confined to the intermediate period from 1.1-0.8 m.y.b.p. Virtually all of the lava was erupted as flows and domes. Seismic and gravity data have been interpreted to indicate the presence of a silicic magma chamber beneath the volcanic field. The geophysical data together with the temporal pattern of volcanism and the youthfulness of the most recent eruptions suggest that volcanic activity in the region has not ceased. The spatial pattern of volcanism implies that the next eruptions would occur near the north or northeast edge of the present volcanic field.

CONTINENTAL-EDGE VOLCANISM AT CLEAR LAKE, CALIFORNIA: HOT SPOT, LEAKY TRANSFORM, OR HEATED OCEANIC SLAB?

HEARN, B.C., Jr., U.S. Geological Survey, Reston, Virginia 22092
DONNELLY, J.M., U.S. Geological Survey, Menlo Park, California 94025
GOFF, F.E., Los Alamos Scientific Laboratory, Los Alamos, NM 87545

The 2.1-0.01 m.y. Clear Lake and older (3-10 m.y.) volcanic centers in the northern California Coast Ranges demonstrate a northward migration of volcanism with time. The volcanic centers are anomalously close (100-130 km) to the postulated position of the subduction zone between the Farallon and North American plates and are within the San Andreas transform fault system, which propagated northward as subduction ceased and the Mendocino triple junction migrated northward. The newly detached oceanic crustal slab was probably too cool and too shallow to be a source of partial melts. Major-, trace-element, and Sr 87/86 data suggest that the complex, northward-younging Clear Lake basalt-andesite-dacite-rhyolite sequence is the result of the combined effects of repeated ascent of mafic magmas from several chemically different mantle sources, storage in shallow magma chambers (now totalling 1400 km³), assimilation of Great Valley sequence, Franciscan assemblage and underlying crustal rocks, crystal fractionation, and magma mixing. Rare-earth element (REE) patterns suggest that the parental magmas originated by substantial partial melting of a light REE-enriched peridotite or eclogite mantle source rather than by partial melting of subducted ocean-floor basalt. The volcanic centers are postulated to be the surface manifestations of a mantle hot spot, perhaps a segment of the overridden East Pacific Rise, across which the North American plate, or a separate sliver of it, has apparently moved relatively southward. Pressure release during initiation or intensification of transform faulting may have accelerated the partial melting process and facilitated the ascent of deep-source magmas.

THE CLEAR LAKE VOLCANICS AND THE GEYSERS GEOTHERMAL SYSTEM, CALIFORNIA

DONNELLY, J. M., U.S. Geological Survey, Menlo Park, CA 94025

HEARN, B. C., Jr., U.S. Geological Survey, Reston, VA 22092

The Geysers steam field is the largest power-producing geothermal field in the world, presently yielding enough electricity to serve a city the size of San Francisco. It lies about 120 km north of San Francisco, adjacent to the 2.1- to 0.01-m.y.-old Clear Lake Volcanics, the youngest of a northward-younging set of Cenozoic volcanic fields in the California Coast Ranges. The Clear Lake Volcanics covers about 450 km² and is dominantly silicic: half of the total 100 km³ volume is dacite; 5% is andesite; no ash flows have been found. A source of both volcanism and geothermal heat appears to be a mid-crustal magma reservoir thought to contain perhaps 1400 km³ of silicic partial melt. A circular 25-milligal gravity anomaly, large teleseismic P-wave delays, and the absence of earthquake hypocenters deeper than 5 km together define a magma reservoir whose top is about 7 km beneath the volcanic field. Many thermal and mineralized springs are associated with the volcanic field, and geochemical studies indicate the existence of a hot-water geothermal system northeast of the steam field. Limits of both systems have been predicted from geochemical indicators. The volcanic field and the geothermal system lie within a tectonically active region cut by branches of the right-lateral strike-slip San Andreas fault system. Extension between branches of the San Andreas may facilitate invasion of the crust by basaltic melts from the upper mantle, followed by heating of the crust and formation of silicic melts. A complex petrogenetic history of the volcanism is implied by isotopic data, trace elements, and whole-rock chemistry.

Geothermal prospecting in The Geysers–Clear Lake area, northern California

Fraser E. Goff
Julie M. Donnelly
J. M. Thompson
U.S. Geological Survey
Menlo Park, California 94025
B. Carter Hearn, Jr.
U.S. Geological Survey
Reston, Virginia 22092

ABSTRACT

The geochemistry of thermal waters combined with mapping and geophysical studies have been used to define boundaries of the geothermal steam field in The Geysers–Clear Lake area, California. Chemical geothermometry and drill hole data imply that a 200 °C hot-water geothermal system underlies much of the 2.0 to 0.01-m.y.-old Clear Lake Volcanics. Chloride concentrations and electrical resistivity define the concealed extent of Great Valley sedimentary rocks underlying the young volcanic cover. We suggest that the 80 or more vents in the volcanic field act as permeable conduits for water recharge and thus prevent creation of a widespread vapor-dominated system northeast of the Collayomi fault zone.

INTRODUCTION

The Geysers–Clear Lake area in northern California has been renowned for over 100 years for the abundance of its thermal waters. The Sulphur Bank quicksilver mine on the shore of Clear Lake has been the most productive mineral deposit in the world directly resulting from hot-spring activity (White and Roberson, 1962).

Since the first producing steam well was drilled in 1955, The Geysers steam field has grown steadily to become the world's largest producer of geothermal power, yielding more than 500 MW·h/yr. Expansion of this steam field continues primarily to the south and east (Fig. 1). This paper combines geologic and geophysical information with new geochemical data to (1) predict deep reservoir temperatures, (2) interpret geologic structure, and (3) establish some probable boundaries of the steam field and adjacent hot-water zones.

GEOLOGIC SETTING

The Geysers–Clear Lake thermal region contains the Clear Lake volcanic field (Hearn and others, 1976a), which ranges in age from 2 m.y. to 10,000 yr (Hearn and others, 1976b; Sims and Rymer, 1975). The

Clear Lake Volcanics overlie Jurassic and Cretaceous rocks of the Franciscan assemblage and the Great Valley sequence (Brice, 1953; Swe and Dickinson, 1970; McLaughlin, 1975). A deformed sheet of ophiolitic rocks consisting mostly of serpentinite separates sheared and generally metamorphosed igneous and sedimentary rocks of the Franciscan assemblage from overlying, less-deformed marine deposits of the Great Valley sequence. The serpentinites are interpreted as oceanic crust that was thrust over Franciscan rocks along an eastward-dipping subduction zone (Bailey and others, 1970).

The regional structure is dominated by northwest-trending faults that include major Quaternary right-lateral strike-slip faults related to the San Andreas system (Donnelly and others, 1976). Many warm springs emerge along fault zones and contain high concentrations of magnesium (Fig. 2, Table 1) owing to the presence of serpentinite (Waring, 1915). Along the Konocti Bay fault zone, magnesium values as high as 238 mg/l suggest that the thermal waters pass through serpentinite before issuing from young volcanic rocks (Goff and others, 1976).

The region is seismically active but most earthquakes are small (magnitude 0 to 3).

The activity is shallow, with focal depths less than 5 km (Hamilton and Muffler, 1972; Bufe and others, 1976); epicenters commonly lie along mapped fault zones (Bufe and others, 1976).

Teleseismic *P*-wave delays of as much as 1 s in the area of the 25-mgal gravity low (Fig. 1) strongly suggest the presence of partially molten rock at depth (Iyer and Hitchcock, 1975). Modeling of the gravity anomaly suggests that a magma chamber containing silicic lava lies at perhaps 10-km depth beneath the southwestern part of the main volcanic field (Chapman, 1975; Isherwood, 1976). Since no corresponding magnetic high is associated with the gravity low, Isherwood theorized that the magma may still be above its Curie point approximately 550 °C. This relatively shallow magma body is probably the heat source for The Geysers–Clear Lake thermal anomaly.

GEOCHEMISTRY OF MINERAL WATERS

Sources of Data. During the past two years, U.S. Geological Survey personnel have sampled the existing springs and wells. The procedures are discussed in Presser and Barnes (1974) and in Thomp-

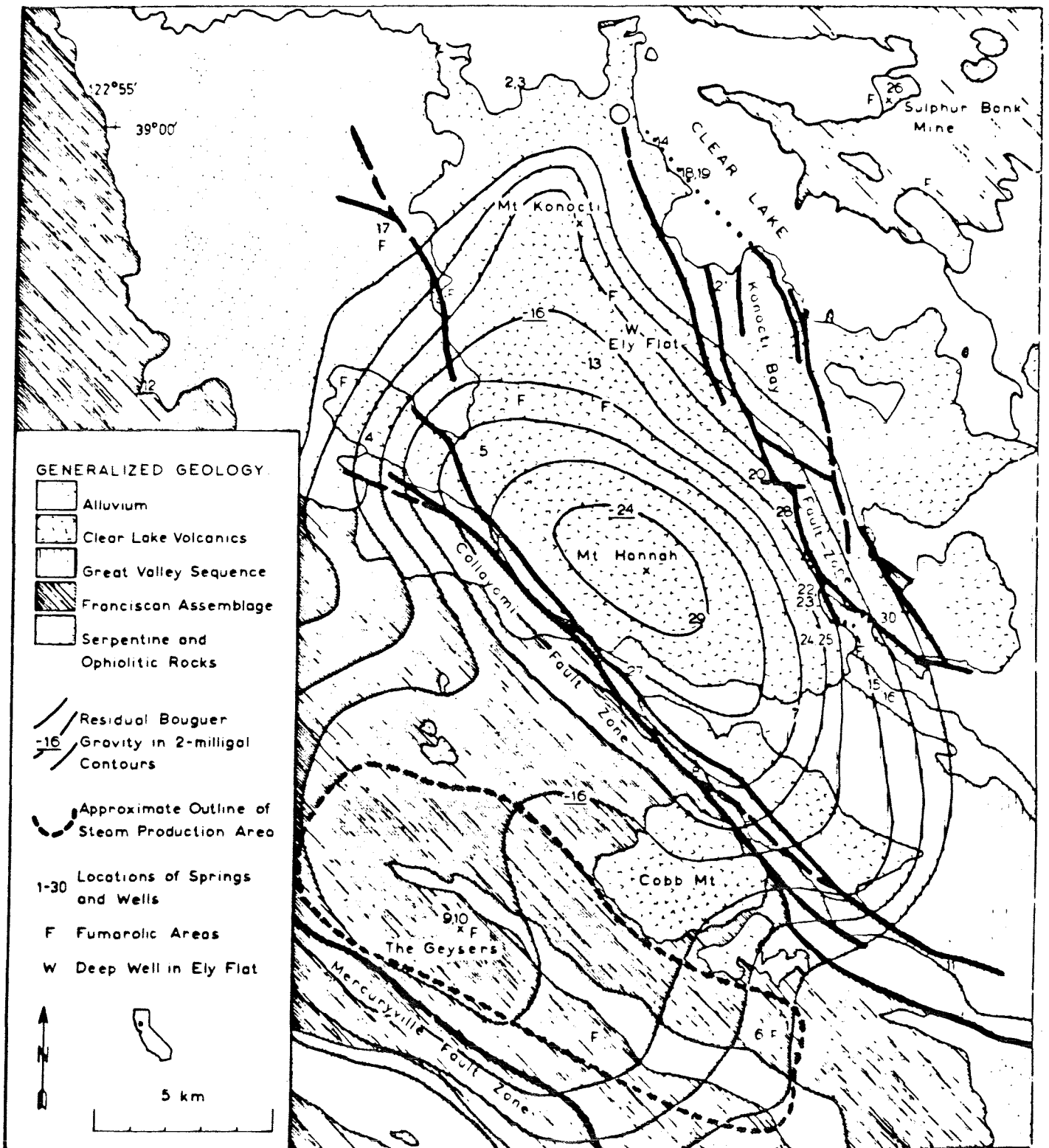


Figure 1. Generalized geologic map of The Geysers–Clear Lake area, northern California; major fault zones shown with heavy lines; gravity contours from Isherwood (1976).

TABLE 1. PARTIAL CHEMICAL ANALYSES, FLOW RATES, BEDROCK, AND GEOTHERMOMETRY FOR THERMAL AND SELECTED METEORIC WATERS IN THE GEYSERS - CLEAR LAKE AREA, CALIFORNIA

No.	Name	Thermal type	Measured Temp. (°C)	SiO ₂	Ca ²⁺	Mg ²⁺	Na ⁺	K ⁺	HCO ₃ ⁻	SO ₄ ²⁻	Cl ⁻	Field pH	Flow rate (litres/min)	Bedrock ^a	A.M.M.I. (°C)	Na-K-Ca p = 0.2; (°C)	Na-K-Ca p = 1.0; (°C)	Source ^b
1	Anderson Spring	1	52	60	94	42	36	7.3	292	320	2.4	6.11	10	F	---	---	---	r
2	Big Soda Spring #1	2	32	140	92	130	100	12	1180	1	63	5.86	>500	V;(F)	213	72	167	r
3	Big Soda Spring #2	2	30.5	136	93	130	100	13	1190	<1	66	5.81	---	V;(F)	210	74	171	r
4	Camelback Spring	2	25	95	21	58	16	4.1	380	8	4.7	6.33	30	Sp & V	194	51	189	r
5	Carlsbad Spring	2	25.5	104	12	95	140	15	547	<1	220	5.62	12	V;(GV)	202	135	187	r
6	Castle Rock Spring	1	73	113	<62	---	<62	---	---	24	6	---	30	F	---	---	---	w
7	Ettawa Spring	2	27	120	28	210	600	12	2560	4	150	6.48	4	GV & Sp	213	121	122	r
8	Gordon Spring	2	31	126	5.5	21	54	5.0	275	0.5	41	7.0	6	F & Sp	207	99	168	t
9	Geysers Spring #1	1	100	66	58	108	18	6	176	766	1.5	~7	---	F	---	---	---	wh
10	Geysers Spring #2	1	100	225	47	281	12	5	0	5710	0.5	1.8	---	F	---	---	---	wh
11	Harbir Spring	1	46	53	2.7	1.8	130	0.7	260	10	31	8.93	30	G & GV	---	---	---	r
12	Highland Spring	2	28	123	295	231	134	12	---	---	19	---	15	F	212	51	147	w
13	Honeycutt Well	2	20	81	6.5	7.1	10.8	8.3	43	22.3	4.8	6.0	0	V;(F)	196	95	260	t
14	Horseshoe Spring	2	41.5	163	155	144	125	21.5	1310	0.9	77.6	6.65	80	V;(F)	205	81	186	t
15	Howard Spring #1	2	42	160	32	320	240	23	1660	2	460	6.58	250	GV & Sp	202	132	180	r
16	Howard Spring #2	2	39	158	46	324	556	177	---	---	481	---	<4	GV & Sp	212	169	249	w
17	Kelseyville Well	2	24	110	93	111	484	36	---	639	164	---	>5	A1;(GV)	215	174	225	w
18	Konocti Spring #1	2	35	138	100	82	84	13.2	775	<0.2	47.6	6.70	80	V;(F)	205	71	178	t
19	Konocti Spring #2	2	34	139	105	85	87	13.4	699	1.0	50.0	7.0	4	V;(F)	207	71	177	t
20	Konocti CC Well	2	25	103	7.0	11	17.5	4.8	172	5.3	10	6.0	0-200	V;(F)	205	79	205	t
21	Riviera Well	2	29.5	120	42	42	43	6.9	447	0.4	42	6.5	0	V;(F)	205	62	175	t
22	Seigler Well #1	2	29	106	10.3	18.5	31.3	6.5	204	0.9	24.3	6.4	2	V;(F)	194	87	196	t
23	Seigler Well #2	2	31	106	10.7	20	35.5	7.1	208	1.3	24	6.4	150	V;(F)	189	90	196	t
24	Seigler Spring #3	2	52	170	30	238	162	20	1258	6.3	272	~6.2	28	GV & Sp	194	122	187	ba
25	Seigler Spring #4	2	42	160	21	140	212	40	875	7.2	297	~4.9	12	GV & Sp	203	186	222	ba
26	Sulphur Bank Well	2	99	203	26	23	1340	44	2600	680	900	8.1	geysers	F	170	196	155	b
27	Sulphur Crk Spring	2	26	119	30	220	260	25	1210	42	420	6.23	8	GV & Sp	213	139	180	r
<i>Depleted Background Cold Springs Issuing From Clear Lake Volcanics</i>																		
28	Diener Spring	---	9	64	3.2	4.2	9.0	4.3	67	5.5	4.8	6.0	20	V	---	---	---	t
29	Salmina's Spring	---	14	52	6.2	3.2	6.1	3.7	67	2.0	3.4	7.2	40	V	---	---	---	t
30	Joe's Spring	---	18	74	13.0	9.0	7.7	4.1	114	1.3	3.6	7.5	50	V	---	---	---	t

*1, steam-condensate or derivative type; 2, hot-water type; see text.

^aA1, alluvium; V, Clear Lake Volcanics; F, Franciscan assemblage; GV, Great Valley sequence; Sp, serpentinite; G, gabbro; (), bedrock inferred at depth.

^bAdiabatic mixing model. Background silica = 60 mg/litre; background temperature = 13 °C.

^c(Chemical) geothermometry inapplicable to steam condensate waters.

**Analyses from the following sources:

- ba = Barnes and others (1973)
- b = Berkstresser and others (1968)
- r = R. Mariner and others (unpub. data)
- t = J. M. Thompson and others (unpub. data)
- w = Waring (1915)
- wh = White and others (1971).

Analyses from Berkstresser, Waring, and White and others in parts per million. Other analyses in milligrams per litre.

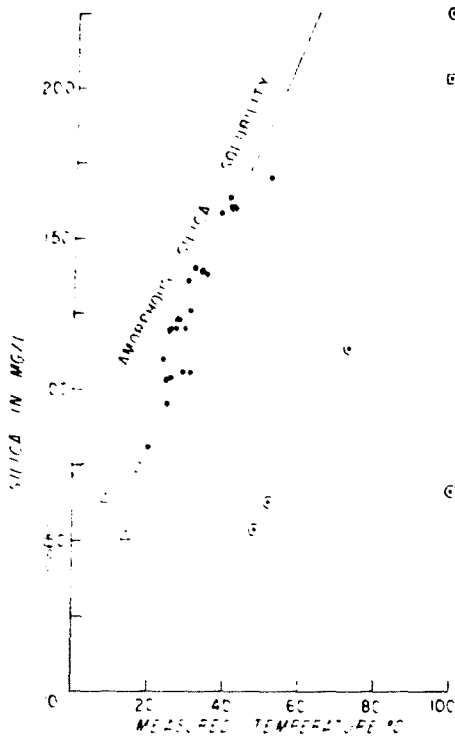


Figure 2. Analyzed silica versus measured temperature in thermal waters of The Geysers-Clear Lake area: dots enclosed by circles = type-1 steam-condensate waters; dots = type-2 thermal waters northeast of the Collayomi fault zone; dot enclosed by square = water at Sulphur Bank mine; triangles = background silica values from cold springs in Clear Lake Volcanics.

son (1975). Partial chemical analyses appear in Table 1.

The ambient air temperature for the Clear Lake region is about 13 °C (Brice, 1953). As a conservative estimate, we consider thermal waters to be those with temperatures greater than or equal to 20 °C.

Water Types. Two types of thermal water discharge in The Geysers-Clear Lake area. They can be distinguished on the basis of dissolved silica and chloride (Figs. 2, 3). Waters of type 1 (Table 1) are all undersaturated relative to amorphous silica at the measured spring temperature, and their chloride contents are lower than all of the other thermal waters of equivalent temperature. Most type-1 waters contain appreciable sulfate, and their pH may be as acidic as 1.8. These steam condensate waters and their derivatives occur in The Geysers steam field but are characteristic of other vapor-dominated geothermal systems such as Larderello (Italy) and Mud Volcano in Yellowstone National Park (White and others, 1971). Such waters are composed of steam condensate ± surface cold water ± oxidized H₂S gas that have reacted primarily with near-surface rocks

at temperatures of 100 °C or less (White and others, 1971). Ignoring the sulfate values of Table 1, type-1 thermal waters have a lower total of dissolved solids than type-2 thermal waters of equivalent temperature.

Thermal waters of type 2 discharge outside the steam field, are usually saturated with amorphous silica, and may contain hundreds of milligrams per litre of chloride. Bicarbonate concentrations may reach thousands of milligrams per litre and free CO₂ is usually present, but sulfate is generally less than 25 milligrams per litre. Type-2 water emerges throughout the Jurassic and Cretaceous rocks of the northern California Coast Ranges (Waring, 1915) and is probably responsible for the widespread alteration of serpentinite to silica-carbonate rock (Barnes and others, 1973).

Three surficial cold springs issuing from the Clear Lake Volcanics are listed in Table 1. In spite of their low content of dissolved species, they possess rather high silica concentrations that are derived from flow through glassy, mostly siliceous, volcanic rocks.

APPLICATIONS OF THERMAL WATER CHEMISTRY

Geothermometry. Chemical geothermometry based on the concentrations of temperature-dependent species (SiO₂; Na⁺, K⁺, Ca²⁺) has been used to predict subsurface reservoir temperatures in several geothermal systems (Fournier and Rowe, 1966; Fournier and Truesdell, 1973). The basic assumptions governing the use of these geothermometers are summarized in Fournier and others (1974) and Renner and others (1975). Subsurface temperature estimates cannot be made from type-1 steam condensate waters because these waters do not reflect equilibrium at depth. The known temperature in The Geysers steam field is 240 °C.

We estimated subsurface temperatures from type-2 waters by first using the empirical Na-K-Ca geothermometer of Fournier and Truesdell (1973). Their equation contains a factor, β , the value of which is dependent on whether or not the water equilibrated above 100 °C ($\beta = 1/3$) or below 100 °C ($\beta = 4/3$). Calculations with $\beta = 4/3$ yield estimated temperatures that are more than 25 °C above the measured temperature (except analysis 12—Highland Springs), which implies that all but one of these waters are not close to chemical equilibrium at the measured temperature. Thus, type-2 waters may be mix-

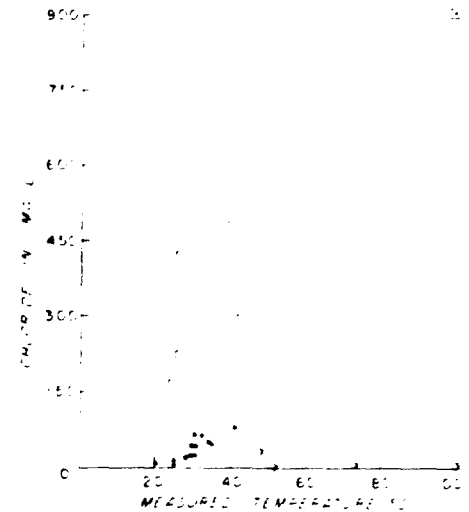


Figure 3. Analyzed chloride versus measured temperature: X = type-1 steam-condensate waters; circles = type-2 thermal waters issuing from areas with Great Valley sequence bedrock; dots = type-2 thermal waters issuing from areas with Franciscan and ophiolite bedrock; dot enclosed by square = Sulphur Bank mine water.

tures of deep hot water and surface cold water (Fournier and Truesdell, 1973). Within the limits of Na-K-Ca geothermometry as presently known, the estimates of deep reservoir temperature, using $\beta = 1/3$, are generally over 180 °C for type-2 waters. However, this geothermometer may be inapplicable for the $\beta = 1/3$ case if the $\log(\text{Ca}^{1/2}/\text{Na})$ is positive (all analyses except 26), if the $\beta = 4/3$ temperature is less than 100 °C, or if high concentrations of magnesium are present in the water (R. O. Fournier, 1976, written commun.). Pačes (1975) has suggested that high P_{CO₂} waters yield erroneous calculated temperatures with the Na-K-Ca geothermometer.

Because mixing of hot reservoir water with cold surficial water is indicated, the silica values of type-2 thermal waters were used to estimate subsurface temperatures using the adiabatic mixing model of Fournier and Truesdell (1974). The deep hot-water fraction is assumed to have equilibrated with quartz and to have separated steam adiabatically as it rose toward the surface and cooled before mixing. On this basis the calculated subsurface temperatures are consistently about 195 to 210 °C (Table 1). However, it is possible that an unknown proportion of the silica in the carbonated thermal waters has entered solution by dissolution of serpentinite at or near the observed spring temperature, as suggested by Barnes and others (1973). Waters high in free CO₂ are considered by Renner and others (1975) to be unreliable

indicators of subsurface temperatures. Thus the estimates of deep reservoir temperature may be subject to change in the future by further refinements in geothermometry.

Geochemistry as Indicator of Bedrock.

Table 1 reveals that all thermal waters emerging from Franciscan rocks (except Sulphur Bank mine water) have temperatures $< 100^{\circ}\text{C}$ when $\beta = 4/3$ is used, whereas all thermal waters from the Great Valley sequence have temperatures $> 120^{\circ}\text{C}$ when $\beta = 4/3$ is used. The concentrations of Na^+ , K^+ , and Ca^{2+} are apparently controlled in part by the rock through which the water flows as well as by the temperature at depth.

The two formations are also distinguished by their chloride values. Except for Sulphur Bank mine, type-2 thermal waters issuing from Franciscan rocks contain distinctly less chloride than waters of the same temperature issuing from the Great Valley sequence (Fig. 3). The latter trend is more diffuse, perhaps owing to the variable thickness of the overthrust Great Valley sequence in the area.

We can say definitely that the chloride contents of these thermal waters do not simply reflect a deep thermal origin as they do in Yellowstone National Park (Fournier and Truesdell, 1974) and other geothermal areas (Truesdell, 1976) where chloride values and ratios of chloride to other species have been used to predict deep reservoir temperatures. Rather, the bedrock in The Geysers-Clear Lake area is heterogeneous in chloride content, and the magnitude of this effect masks the deep thermal chloride component where the Great Valley sequence is present. This conclusion, in combination with the observed high sodium content of Great Valley waters, lends support to the idea that the Great Valley sequence contains considerable quantities of connate water (White and Roberson, 1962; White and others, 1973). The ion-rich connate water causes the predicted temperatures (with $\beta = 4/3$) to be higher in thermal waters issuing from Great Valley rocks than those flowing from Franciscan rocks.

The correlation of high-chloride waters with the Great Valley sequence is supported by the electrical resistivity data of Stanley and others (1973). The $10\text{-}\Omega\cdot\text{m}$ resistivity contour tends to enclose the area in which rocks of the Great Valley sequence are estimated to be thickest, where they are exposed south and east of the young volcanic rocks (Figs. 1, 4). The narrow resistivity high that follows the belt of serpentinite near Howard Springs

(Figs. 1, 4) corresponds to the core of a northwest-trending antiform where Franciscan rocks may lie at shallow depth (Brice, 1953; Swe and Dickinson, 1970). Franciscan bedrock beneath the Clear Lake Volcanics is indicated by low-chloride waters emerging along the north and central part of the Konocti Bay fault zone. To the west, in Ely Flat, the Kettenhofen 1 geothermal well (W in Fig. 1) was drilled through young volcanic rock into rocks that, from the cuttings, have been identi-

fied as Franciscan lithologies and serpentinite (R. McLaughlin, oral commun., 1976). The nearest exposed bedrock is Franciscan at Baylis Point where there is an associated $300\text{-}\Omega\cdot\text{m}$ resistivity high (Fig. 4).

We have used the resistivity and spring chemistry data to estimate the approximate boundaries between Great Valley and Franciscan rocks beneath the Clear Lake Volcanics (Fig. 4).

The resistivity low cannot be explained

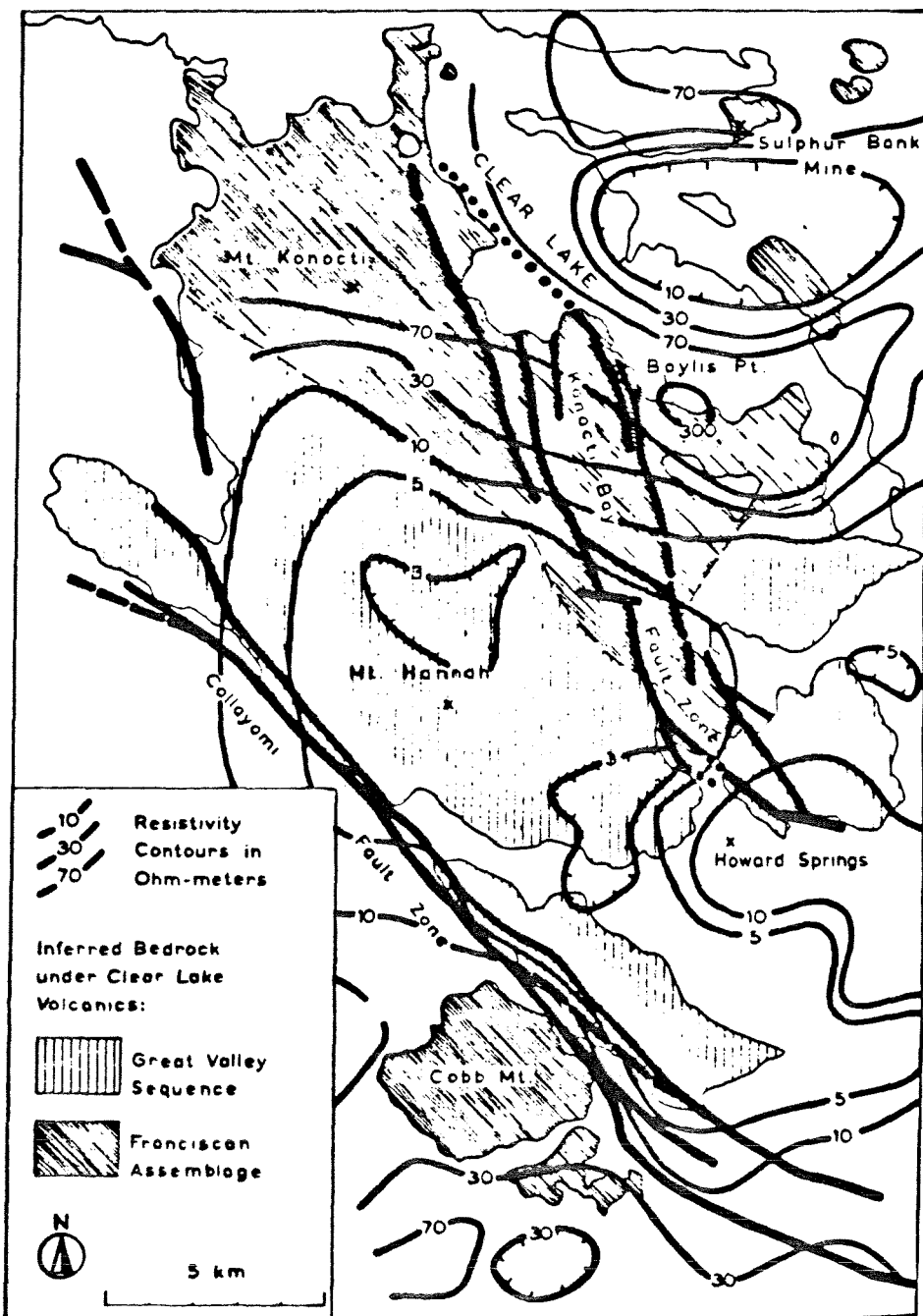


Figure 4. Outline of Clear Lake volcanic field with resistivity contours (Stanley and others, 1973) and two patterns indicating the two major types of bedrock under the volcanic field. Heavy lines are major fault traces.

entirely by the presence of the Great Valley sequence, whose thickness increases to the southeast away from the area of lowest resistivity. The high conductivity indicated near Mount Hannah must result from dual causes: the presence of relatively concentrated Great Valley connate waters and the presence at depth of hot water with relatively high ionic strength.

By extrapolation of these data, the high chloride content of Sulphur Bank water and the $10 \cdot \Omega \cdot m$ resistivity low south of the mine suggest that these waters issue from the Great Valley sequence (Figs. 3, 4). However, on geologic maps the sedimentary rocks and greenstones in and near the mine have been assigned to the Franciscan assemblage (Brice, 1953). If the high chloride content is not derived from the Great Valley sequence, then it must be controlled by some mechanism that does not operate in thermal waters beneath the main Clear Lake volcanic field. If the high chloride content is derived from the Great Valley sequence, then the Sulphur Bank graywackes have been assigned to the wrong formation, or Great Valley sequence rocks have been thrust beneath Franciscan rocks.

HIGH TEMPERATURES AND HOT WATER

The known extent of The Geysers steam field lies entirely southwest of the Collayomi fault zone. Northeast of this zone no steam condensate springs or their derivative waters are found, which implies that any drillable geothermal system beneath the main Clear Lake volcanic field is probably a hot-water type. The implication was verified at Sulphur Bank mine where deep wells encountered hot water. A temperature of $185^\circ C$ was reported in one well at about 440 m (White and others, 1973).

High temperatures were also found in the Kettenhofen 1 geothermal well. Although the actual temperature is not public information, an estimate was made (R. Potter, 1976, oral commun.) using the mud log of the well (courtesy of Pacific Energy Corp.). At 2,000 m the well was air drilled with mist and encountered a surge of steam when the inlet and outlet air pressure of the drill string were about 290 and 0 psi, respectively. From steam tables (Keenan and others, 1969), the temperature needed to flash water to steam at 290 psi (20 bars) is about $210^\circ C$. This falls within the range of temperatures predicted by the geothermometers (Table 1).

We have shown above that large areas

of the volcanic field are probably underlain by Franciscan rocks, which commonly have low permeability (R. McLaughlin, 1976, oral commun.). Economic quantities of hot water at drillable depths (presently less than 3,500 m) may not be easily extracted unless the wells are drilled close to fault zones where fractured rocks allow thermal waters to move freely upward.

RECHARGE

In the model of White and others (1971), a necessary condition for the existence of a vapor-dominated system is that water

recharge into the geothermal reservoir be less than discharge. If, as we postulate, there is no vapor-dominated system to the northeast of the Collayomi fault zone, it is possible that the vent pipes of the volcanic field act as permeable conduits for meteoric water, causing recharge of the geothermal reservoir to balance discharge. There are at least 80 such vents in the Clear Lake volcanic field, most of which probably consist of fractured lava or breccia (Hearn and others, 1976a). If this is true, steam could not exist in areas with a high density of such permeable vents. Only two volcanic vent areas lie adjacent

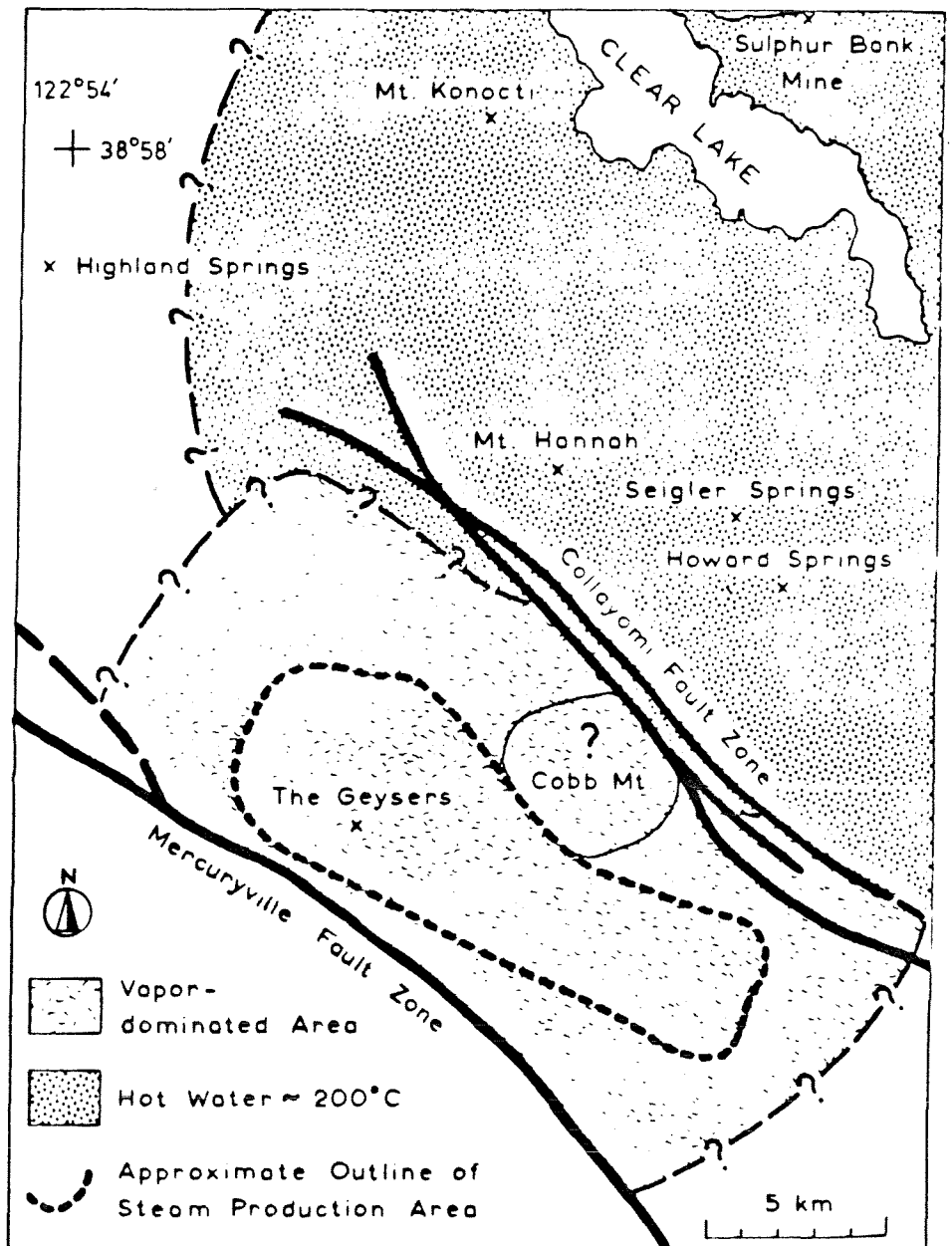


Figure 5. Approximate inferred limits of vapor-dominated and hot-water-dominated areas; heavy lines are major fault traces.

to the present steam field southwest of the Collayomi fault zone. Cobb Mountain (Fig. 5) may act as a recharge area for the steam field, perhaps even locally drowning out the steam.

LIMITS OF VAPOR-DOMINATED SYSTEM

Figure 5 shows the probable limits of the vapor-dominated zone. All type-1 springs of steam-condensate origin are found within the present steam production area except Harbin Springs (analysis 11), which issues at the contact between ophiolite and sedimentary rocks of the Great Valley sequence and thus has a relatively higher chloride content than other type-1 waters.

The southwestern limit is the Mercuryville fault zone, which forms the westernmost boundary of hydrothermal alteration (R. McLaughlin, 1976, oral commun.). To the northwest, no steam or deep hot water is indicated by the water chemistry at Highland Springs. The southeastern limit of the vapor-dominated zone is uncertain owing to a lack of water chemistry or drill hole data.

The northeastern limit corresponds to the Collayomi fault zone, which parallels distinct boundaries on the gravity and electrical resistivity maps (Figs. 1, 4). However, small vapor-dominated systems could exist at depth where local geologic conditions are favorable. If such small systems do exist, they are not tapped by emerging thermal waters northeast of the Collayomi fault zone.

REFERENCES CITED

- Bailey, F. H., Blake, M. C., Jr., and Jones, D. L., 1970. On-land Mesozoic oceanic crust in California Coast Ranges, in Geological Survey research 1970 U.S. Geol. Survey Prof. Paper 700-C, p. C70-C81.
- Barnes, Ivan, O'Neil, J. R., Rapp, J. B., and White, D. E., 1973. Silica-carbonate alteration of serpentinite: Wall rock alteration in mercury deposits of the California Coast Ranges: *Econ. Geology*, v. 68, no. 3, p. 388-398.
- Berkstresser, C. F., Jr., 1968. Data for springs in the northern Coast Ranges and Klamath Mountains of California: U.S. Geol. Survey Open-File Rept., 49 p.
- Brice, J. C., 1953. Geology of Lower Lake quadrangle, California: California Div. Mines and Geology Bull. 166, 72 p.
- Bufe, C. G., Pfluke, J. H., Lester, F. W., and Marks, S. M., 1976. Map showing preliminary hypocenters of earthquakes in the Healdsburg (1:100,000) quadrangle, Lake Berryessa to Clear Lake, California: U.S. Geol. Survey, Open-File Map 76-802.
- Chapman, R. H., 1975. Geophysical study of the Clear Lake region, California: California Div. Mines and Geology Spec. Rept. 116, 23 p.
- Donnelly, J. M., McLaughlin, R. J., Goff, F. E., and Hearn, B. C., Jr., 1976. Active faulting in The Geysers-Clear Lake area, northern California: *Geol. Soc. America Abs. with Programs*, v. 8, no. 3, p. 369-370.
- Fournier, R. O., and Rowe, J. J., 1966. Estimation of underground temperatures from the silica content of water from hot springs and wet-steam wells: *Am. Jour. Sci.*, v. 264, p. 685-697.
- Fournier, R. O., and Truesdell, A. H., 1973. An empirical Na-K-Ca geothermometer for natural waters: *Geochim. et Cosmochim. Acta*, v. 37, p. 1255-1275.
- 1974. Geochemical indicators of subsurface temperature—Pt. 2. Estimation of temperature and fraction of hot water mixed with cold water: *U.S. Geol. Survey Jour. Research*, v. 2, no. 3, p. 263-270.
- Fournier, R. O., White, D. E., and Truesdell, A. H., 1974. Geochemical indicators of subsurface temperature—Pt. 1. Basic assumptions: *U.S. Geol. Survey Jour. Research*, v. 2, no. 3, p. 259-262.
- Goff, F. E., Donnelly, J. M., Thompson, J. M., and Hearn, B. C., Jr., 1976. The Konociti Bay fault zone, California: Potential area for geothermal exploration: *Geol. Soc. America Abs. with Programs*, v. 8, no. 3, p. 375-376.
- Hamilton, R. M., and Muffler, L.J.P., 1972. Microearthquakes at The Geysers geothermal area, California: *Jour. Geophys. Research*, v. 77, no. 11, p. 2081-2086.
- Hearn, B. C., Jr., Donnelly, J. M., and Goff, F. E., 1976a. Preliminary geologic map and cross-section of the Clear Lake volcanic field, Lake County, California: U.S. Geol. Survey Open-File Map 76-751.
- 1976b. Geology and geochronology of the Clear Lake Volcanics, California, in *Proc. Second United Nations symposium on the development and use of geothermal resources*, San Francisco, California, May 20-29, 1975, Vol. 1: Berkeley, California, Lawrence Berkeley Laboratory, Univ. California, p. 423-428.
- Isherwood, W. F., 1976. Gravity and magnetic studies of The Geysers-Clear Lake geothermal region, California, U.S.A., in *Proc. Second United Nations symposium on the development and use of geothermal resources*, San Francisco, California, May 20-29, 1975, Vol. 2: Berkeley, California, Lawrence Berkeley Laboratory, Univ. California, p. 1065-1074.
- Iyer, H. M., and Hitchcock, T., 1975. Teleseismic residuals at The Geysers geothermal area. *Am. Geophys. Union Trans.*, v. 56, no. 12, p. 1020.
- Keenan, J. H., Keyes, J. G., Hill, P. G., and Moore, J. G., 1969. Steam tables. Thermodynamic properties of water including vapor, liquid, and solid phases. New York, John Wiley, 162 p.
- McLaughlin, R. J., 1975. Preliminary field compilation of in-progress geologic mapping in The Geysers geothermal area, California: U.S. Geol. Survey Open-File Map 75-198.
- Pačes, T., 1975. A systematic deviation from Na-K-Ca geothermometer below 75 °C and above 10⁻⁴ atm P_{CO₂}: *Geochim. et Cosmochim. Acta*, v. 39, p. 541.
- Presser, T. S., and Barnes, Ivan, 1974. Special techniques for determining chemical properties of geothermal water: U.S. Geol. Survey Water Resources Inv. 22-74, 15 p.
- Renner, J. L., White, D. E., and Williams, D. L., 1975. Hydrothermal convection systems, in *Assessment of geothermal resources of the United States—1975*: U.S. Geol. Survey Circ. 726, p. 5-57.
- Sims, J. D., and Rymer, M. J., 1975. Preliminary description and interpretation of cores and radiographs from Clear Lake, Lake County, California: Core 7: U.S. Geol. Survey Open-File Rept. 75-144, 21 p.
- Stanley, W. D., Jackson, D. B., and Hearn, B. C., Jr., 1973. Preliminary results of geoelectrical investigations near Clear Lake, California: U.S. Geol. Survey Open-File Rept., 20 p.
- Swe, W., and Dickinson, W. R., 1970. Sedimentation and thrusting of late Mesozoic rocks in the Coast Ranges near Clear Lake, California: *Geol. Soc. America Bull.*, v. 81, p. 165-188.
- Thompson, J. M., 1975. Selecting and collecting from thermal springs for chemical analysis: A method for field personnel: U.S. Geol. Survey Open-File Rept. 75-68, 11 p.
- Truesdell, A. H., 1976. Summary of section III, geochemical techniques in exploration, in *Proc. Second United Nations symposium on the development and use of geothermal resources*, San Francisco, California, May 20-29, 1975, Vol. 1: Berkeley, California, Lawrence Berkeley Laboratory, Univ. California, p. liii-lixix.
- Waring, G. A., 1915. Springs of California: U.S. Geol. Survey Water-Supply Paper 336, 409 p.
- White, D. E., and Roberson, C. E., 1962. Sulphur Bank, a major hot-spring quicksilver deposit, in Engel, A.E.J., James, H. L., and Leonard, B. R., eds., *Petrologic studies (Buddington volume)*: Boulder, Colo., Geol. Soc. America, p. 397-428.
- White, D. E., Muffler, L.J.P., and Truesdell, A. H., 1971. Vapor-dominated hydrothermal systems compared with hot-water systems: *Econ. Geology*, v. 66, p. 75-97.
- White, D. E., Barnes, Ivan, and O'Neil, J. R., 1973. Thermal and mineral waters of non-meteoritic origin, California Coast Ranges: *Geol. Soc. America Bull.*, v. 84, p. 547-560.

ACKNOWLEDGMENTS

Reviewed by R. O. Fournier, who along with I. Barnes offered many helpful comments. We thank P. Russell and R. Mariner for providing many of the unpublished chemical analyses. D. E. White, R. McLaughlin, and other colleagues at the U.S. Geological Survey made valuable suggestions.

MANUSCRIPT RECEIVED NOV. 19, 1976

MANUSCRIPT ACCEPTED MAY 9, 1977

Geology and Geochronology of the Clear Lake Volcanics, California

B. CARTER HEARN

U.S. Geological Survey, Reston, Virginia 22092, USA

JULIE M. DONNELLY

University of California and U.S. Geological Survey, Berkeley, California 94720, USA

FRASER E. GOFF

U.S. Geological Survey, Menlo Park, California 94025, USA

ABSTRACT

The 400-km² Clear Lake Volcanics, of late Pliocene(?) to Holocene age, unconformably overlies rocks of mainly the Franciscan assemblage and Great Valley sequence. The nearby Geysers geothermal production area is southwest of the volcanic field.

Stratigraphic relations, magnetic polarities, and K/Ar dates have established a complex volcanic series that ranges from less than 2.5 million years (m.y.) to less than 0.03 m.y. in age and in general is progressively younger from south to north. The oldest lavas are quartz-bearing olivine basalts which extend southeast of the main field and marginally overlap Sonoma Volcanics. The main part of the field is younger than 1.0 m.y., and the central part is younger than 0.5 m.y. The youngest rhyolite is 0.088 ± 0.013 m.y. The most recent activity, as young as about 0.010 m.y., produced basaltic to andesitic cinder cones and maar-type pyroclastic deposits. The sequences suggest changes in magma composition from basalt or andesite through dacite to rhyolite, although dacites are missing from some sequences.

The many normal faults in the field trend northeast, northwest, and north-northwest. The youngest faults trend north-northwest or northwest, approximately parallel to the San Andreas system. Inferred strike-slip offset on one northwest-trending fault suggests movement, if continuous, at an average rate of 1 mm/yr for the past 0.5 m.y. Earthquakes within the volcanic field and Clear Lake basin are suggestive of current deformation.

Gravity and resistivity lows over the volcanic field can be interpreted as being related to an underlying partially fluid magma chamber. Repeated silicic volcanism, lack of ash-flow tuffs, and lack of large-scale caldera collapse suggest that the volcanic system is in an early evolutionary stage. The size and youth of the volcanic system and the distribution of thermal springs and wells imply that the

volcanic field and its surroundings have considerable geothermal potential.

INTRODUCTION

The Clear Lake Volcanics of late Pliocene(?) to Holocene age covers 400 sq km about 150 km north of San Francisco in the Coast Ranges of California. (The Clear Lake Volcanic series of Brice [1953] is herein adopted for U.S. Geological Survey usage as Clear Lake Volcanics as used by California Department of Water Resources [1962].) The Geysers geothermal production area is beyond the southwest border of the field. This report presents preliminary results of a continuing program of detailed geologic mapping, geochronology, geochemistry, and geophysics. About two-thirds of the field has been mapped in detail at 1:24 000 scale (Hearn, Donnelly, and Goff, unpub. data); the remainder has been mapped by reconnaissance and photogeology.

Several previous investigators have contributed to the knowledge of this volcanic area and its surroundings, beginning particularly with Anderson's (1936) perceptive study. More recent studies were done by Brice (1953), California Department of Water Resources (1962), Hodges (1966), McNitt (1968a, b, c), Swe and Dickinson (1970), and Berkland (1972). McLaughlin (1974) has thoroughly mapped the Franciscan terrane in the vicinity of The Geysers geothermal field. Sims and Rymer (1974, 1975a and b) are studying the lake-bottom sediments and structural control of the Clear Lake basin.

Considerable geophysical information available for the Geysers-Clear Lake area consists of aeromagnetic data (U.S. Geological Survey, 1973), gravity and magnetic data (Chapman, 1966, 1975; Isherwood, 1975), and electrical data (Stanley, Jackson, and Hearn, 1973).

Hamilton and Muffler (1972) discussed earthquakes of local origin in The Geysers geothermal field. Investigation of deep and shallow thermal fluids (White and Roberson, 1962; Barnes et al., 1973) are continuing. Garrison (1972)

published a recent summary of geology and reservoir characteristics of the geothermal production area.

GEOLOGIC SETTING

The Clear Lake Volcanics overlie rocks of the assemblage of the Franciscan Formation of Late Jurassic to Eocene age, the Great Valley sequence of Late Jurassic to Late Cretaceous age, sedimentary rocks of Paleocene and Eocene age, and the Cache Formation as used by Brice (1953) of Pliocene and Pleistocene age. The main part of the Clear Lake volcanic field occupies the southern part of the Clear Lake topographic basin and extends southward toward the crest of the Mayacmas Range. Outliers of the field include: an area of quartz-bearing olivine basalt flows which extends southeastward 35-40 km from the east edge, isolated small areas of extrusive and intrusive rocks of probable Clear Lake volcanic affinity which occur as far as 16 km to the northeast, and several isolated small areas of volcanic rocks of undetermined affinity to the south and southwest.

The Sonoma Volcanics of Pliocene age extend from the San Francisco Bay area to the vicinity of Mt. St. Helena, 20 km southeast of The Geysers geothermal production area. Published ages on the Sonoma volcanics are 5.3 m.y. to 2.9 m.y. The youngest date is on a welded tuff at Mt. St. Helena at the northern end of the field (Mankinen, 1972), closest to the Clear Lake Volcanics. The Clear Lake Volcanics, with the exception of the early quartz-bearing olivine basalts, are geographically separate from the Sonoma Volcanics, and present data show no significant overlap in ages. However, the ages of isolated patches of volcanic rocks between Mt. St. Helena and Cobb Mountain are unknown.

The Clear Lake topographic basin is superimposed on a broad northwest-trending zone of complexly folded thrust sheets of Great Valley sequence and serpentinized mafic and ultramafic rocks which have been thrust across the structurally complex Franciscan assemblage (Swe and Dickinson, 1970; Berkland, 1973). The basal faults have been interpreted by those authors as equivalent to the Coast Range thrust which is the major boundary between Great Valley sequence the Franciscan assemblage. The basal faults have been interpreted by others (Maxwell, 1974) as relatively minor displacements on the border of nearly in situ local basins of deposition of Great Valley-type sediments. The southeastern part of the volcanic field unconformably overlies thrust sheets of Great Valley sequence and Paleocene and Eocene sedimentary rocks. The northwest limit of the allochthonous Great Valley sequence is concealed beneath the volcanic field or beneath lake sediments. The next occurrence of Great Valley sequence to the northwest, the Middle Mountain block (Berkland, 1973), is isolated north of Clear Lake.

The Cache Formation, most of which predates the Clear Lake Volcanics, consists of fresh-water sedimentary deposits which filled an irregular fault-bounded basin largely east of, and not coincident with, the present Clear Lake basin. Clastic and volcanoclastic deposits that occur beneath, within, and near to the Clear Lake Volcanics have been correlated with the upper part of the Cache Formation by previous workers (Brice, 1953; McNitt, 1968a; Hodges, 1966; Swe and Dickinson, 1970). However, many of those clastic deposits are isolated from the type Cache Formation and are dissimilar to it in lithology (M. J. Rymer, personal commun.). Also, many of those deposits are probably

younger than any part of the type Cache Formation.

The Clear Lake topographic basin is in part a structural basin, partially delineated by faults of north, north-northwest, northwest, and west trend (Sims and Rymer, 1974, 1975b). The basin has been partially filled by lake and flood plain deposits which are interbedded at depth with flows and pyroclastic deposits of the Clear Lake Volcanics. Sedimentary deposits beneath the present Clear Lake represent a probably continuous record of sedimentation for at least the last 150 000 years (core 4, Sims and Rymer, 1975).

CLEAR LAKE VOLCANICS

The Clear Lake Volcanics consist of basalt, andesite, dacite, and rhyolite, which occur as domes, flows, and pyroclastic deposits in a structurally and chronologically complex sequence (Figure 1). Rock names in this report are based mainly on field identifications and a small number of chemical analyses and are thus tentative until more chemical data are available. Rocks termed basalt may actually be basaltic andesite or andesite, chemically. The term rhyodacite has been difficult to apply in the field; many rocks that may be of rhyodacite composition are grouped with the dacites.

The Clear Lake Volcanics characteristically contain quartz not only as phenocrysts in the more silicic types but as 1 mm-15 cm rounded to subangular commonly resorbed grains of uncertain origin in mafic rock types. All the basalts contain olivine, in amounts ranging from a trace to about 10%. Andesites typically contain phenocrysts of plagioclase and orthopyroxene, with or without clinopyroxene, and vary widely in pyroxene content. The many dacites range from highly porphyritic to sparsely porphyritic varieties and contain phenocrysts of plagioclase, clinopyroxene, orthopyroxene, and quartz; many contain sanidine. Most varieties also possess small amounts of biotite or hornblende or both. Some sparsely porphyritic varieties have widespread glassy chilled facies. Two types of rhyolites are present, biotite-bearing and nearly biotite-free. Biotite rhyolites are typically crystal rich (15-30% quartz and feldspar phenocrysts), tend to be perlitic, and have formed significant pyroclastic deposits. Biotite-free rhyolites are typically crystal poor (3% or less phenocrysts) and show widespread glassy obsidian facies on flow borders. Only one biotite-free rhyolite formed a large volume of pyroclastic material. No rhyolitic ash-flow deposits are present in the Clear Lake field. The preserved volume of volcanic rocks that have compositions more silicic than andesite is about 35 cubic km if the Mt. Konocti pile bottoms at lake level, and 50 cubic km if it extends 300 m below lake level. The preserved volume of basalt and andesite is about 10 to 15 cubic kilometers.

GEOCHRONOLOGY

K/Ar dates range from about 2.5 m.y. to 0.03 m.y. or less and are in good agreement with magnetic-polarity determinations and known stratigraphic relations (Table 1). The main part of the field is younger than 1.0 m.y., and much of the central part is younger than 0.5 m.y. In general, the volcanic rocks are progressively younger northward through the field.

The oldest dated unit is the 2.46 ± 0.69 m.y. isolated olivine basalt at Caldwell Pines (Figure 1). Its affinity with

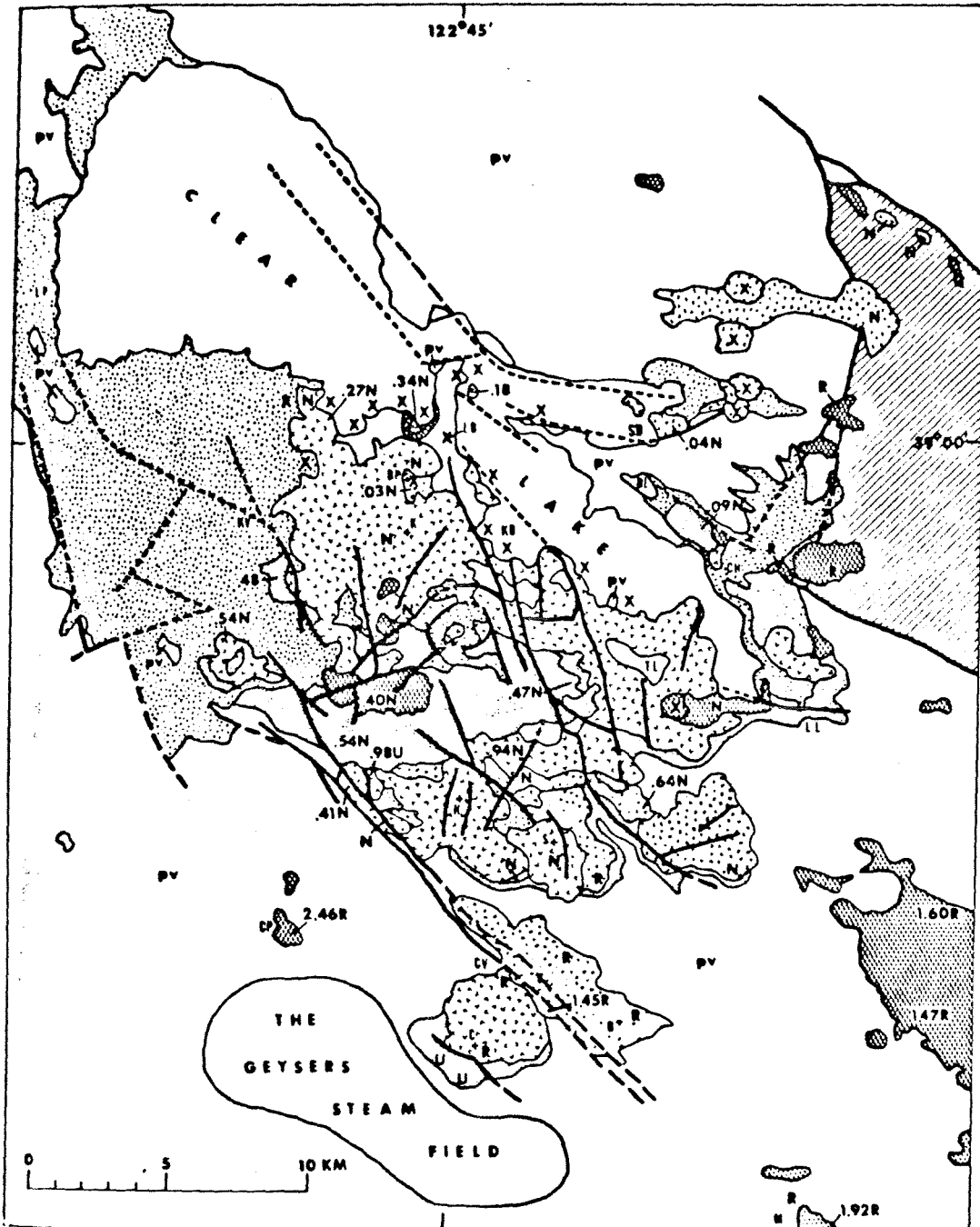


Figure 1. Generalized geologic map of Clear Lake volcanic field showing K/Ar ages and magnetic polarities. Lake and alluvial deposits are shown only near Clear Lake. Order of volcanic units in explanation is not sequence of eruption. Actual extent of cinder cones shown where associated with faults. Contacts shown within a single rock type are between units of different age and/or magnetic polarity. Faults dashed where inferred, dotted where concealed. Geology in part modified from Brice (1953), Lake County Flood Control and Water Conservation District (1967), McNitt (1968a, b, c), and Rymer and Rymer (in press). Abbreviations of geographic names (• denotes location): B = Boggs Mountain, C = Cobb Mountain, H = Mount Hannah, K = Mount Konocti, S = Sulphur Mountain, BP = Buckingham Peak, KB = Konocti Butte, CP = Caldwell Pines, CV = Cobb Valley, SB = Sulphur Butte, BL = Borax Lake, LB = Little Borax Lake, TL = Thurston Lake, CH = Clearlake Highlands, KV = Kelseyville, LL = Lower Lake, LP = Lakeport, M = Middletown (modified from Brice, 1952).

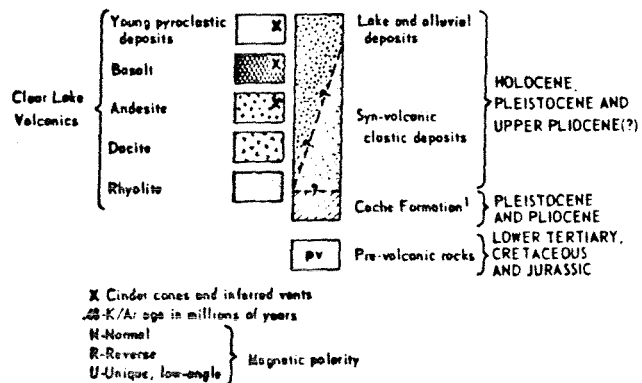


Table 1. Eruptive sequence, K/Ar ages, magnetic polarities and SiO₂ compositions of Clear Lake volcanics.

SiO ₂ as % of weight	Rock type				K/Ar age (m.y.) W-Whole rock B-Biotite S-Sanidine	Remanent magnetic polarity N-Normal R-Reverse U-Unique, low angle	Polarity event	Polarity epoch
	Basalt	Andesite	Dacite	Rhyolite				
55-62	○	○						
[55-57	○	○			0.30 ± .03W	N		
57	○	○				N		
56-57	○	○			0.04 ± .04W	N		
76-77			○		0.088 ± .013W*	N		
66			○					
55			○					
[68			○		0.18 ± .02S	N		
68			○			N		
57			○		0.27 ± .04S	N		
			○			N		
			○		0.34 ± .01S**	N		
			○			N		
71			○			N		
73			○			N		
			○					
			○					
56-59			○		0.40 ± .18W	N		
60			○		0.41 ± .04W	N		
72-74			○		0.48 ± .04S			
			○		0.48 ± .11B			
72-74			○		0.466 ± .015W*	N		
74-75			○		0.536 ± .016W*	N		
			○		0.54 ± .03S	N		
			○					
			○					
61-62			○		0.64 ± .04W	N		
67-70			○		0.94 ± .17W	N	Jaramillo	
67			○		0.98 ± .22W	U		
62			○			R		
			○			R		
			○					
			○		1.1?*	R		
[72			○			U		
60			○		1.45 ± .04W	R		
57			○		1.47 ± .29W	R		
			○		1.60 ± .53W	R		
			○		1.92 ± .77W	R		

*K/Ar by J. Von Essen and A. Atkinson, K analysis by L. Schlocker, U.S. Geological Survey. Other K/Ar ages by J. M. Donnelly, K analyses by J. Hampel.

**C. Wahrhaftig and G. H. Curtis, unpublished data.

Note: Lines connect units which have close spatial relations. Brackets designate groups of units of unknown relative age.

the Clear Lake Volcanics is uncertain; it may be a northern outlier of the older Sonoma Volcanics. The widespread quartz-bearing olivine basalts southeast of the main part of the Clear Lake field give ages of 1.47 ± 0.29 , 1.60 ± 0.53 , and 1.92 ± 0.77 m.y., and marginally overlap Sonoma Volcanics southeast of Middletown. Although the absolute range of age of these olivine basalts is uncertain, their consistent reverse magnetic polarity suggests that they are about 2.4 m.y. to 1.8 m.y. old or 1.6 m.y. to 0.7 m.y. old. To the west of the basalts, eruptions of andesite flows of Boggs Mountain at 1.45 ± 0.04 m.y. were followed by more silicic eruptions of dacite and rhyolite at about 1.1 m.y. at Cobb Mountain.

A widespread obsidian-bearing rhyolitic tuff and tuff breccia underlies much of the southern edge of the volcanic field, and was erupted from a source northeast of Seigler Mountain. This tuff was assigned to the Cache Formation by Brice (1953), but its equivalent is not known in the type Cache Formation. Subsequent eruptions produced a variety of andesites and dacites from vents in the southern and central parts of the field. Two petrographically similar silicic dacites, which have been dated at 0.94 ± 0.17 m.y. and 0.98 ± 0.22 m.y. and show normal and unique low-angle magnetic polarity respectively, probably record the 0.89 m.y.-0.95 m.y. Jaramillo normal magnetic event.

About 0.5 m.y. ago, a major period of silicic volcanism began in the central part of the field with the eruption of about 4 cubic km of sparsely porphyritic rhyolite, dated at 0.48 ± 0.04 m.y. In the interval 0.48 m.y. to about 0.3 m.y., eruption of small volumes of biotite rhyolite (dominantly pyroclastic) alternated with eruptions of small volumes of basalt and olivine basalt. These local basalts and biotite rhyolites, and the earlier widespread biotite-free rhyolite, were partially covered by the voluminous eruptions of dacite which built 1000 m high Mt. Konocti and created a ridge of coalesced dacite domes and flows aligned east-southeast from Mt. Konocti. On the southwest edge of Mt. Konocti, dacite overlies biotite rhyolite of 0.48 m.y. age. On the north side, a dacite dated at 0.34 m.y. is successively overlain by olivine basalt and by several hundred meters of younger dacite.

The domal dacitic accumulations of Mt. Hannah and Seigler Mountain seem to be exceptions to the generally older ages in the southern part of the field. Their topographic expression and presence of vesicular glassy facies indicate that both were probably built less than 0.5 m.y. ago.

The youngest silicic eruptions dated so far are a biotite dacite at about 0.18 ± 0.02 m.y., at lake level northeast of Mt. Konocti, and a rhyolitic obsidian southeast of Borax Lake, at 0.088 ± 0.013 m.y. The rhyolite of Borax Lake is chemically related to an adjacent earlier olivine dacite flow (Bowman, Asaro, and Perlman, 1973). An adjacent, and presumably underlying, subdued cinder cone of olivine-bearing basalt may represent an even older, parental basaltic magma which forms part of the variation series.

The most recent eruptive activity was basaltic to andesitic in composition and was in part phreatic. This activity produced the cinder cone and flow at Buckingham Peak, dated at 0.03 ± 0.03 m.y., and produced cinder cones and flows along a N.10°E. trend across the east arms of Clear Lake. The andesite flow at Sulphur Bank (White and Roberson, 1962) yielded a K/Ar date of 0.04 ± 0.04 m.y. Phreatic eruptions along the lake shore have left a widespread blanket of pyroclastic deposits and localized base-surge deposits, for example in the tuff ring surrounding the Little Borax Lake maar. This maar is younger than about 0.03 m.y., as its final eruption removed most of a large landslide which cut away about half of the cinder cone at Buckingham Peak.

The series of young basaltic to andesitic eruptions is probably represented by the many mafic ash beds in cores of sediments beneath Clear Lake (Sims and Rymer, 1975). The youngest ash recognized in a core from the southeastern arm of Clear Lake is about 10 (XX) years old (core 7, Sims and Rymer, 1975). Continuation of volcanic activity to such recent time indicates that there is potential for future eruptions.

The tentative eruptive sequence suggests that the composition of erupted magma changed from basalt or andesite through dacite to rhyolite, and from basalt or andesite to rhyolite without apparent intermediate rock types (Table 1). From the limited present data, such changes in composition show both extended and compressed time spans. Changes in magma compositions, and the large volume of silicic rocks, indicate that major differentiation or melting has occurred, which in turn implies a large magma chamber source for the volcanic system.

STRUCTURE

Faults in the Clear Lake Volcanic field trend from northeast to northwest, the northwest trend being dominant. The youngest faults trend northwest which is also parallel to the general structure grain of the Coast Ranges and parallel to the San Andreas fault system. Two prominent fault zones follow this trend—the Konocti Bay fault zone which extends east of Seigler Mountain to the northeast side of Mt. Konocti, and the Cobb Valley fault zone along the southwest side of Boggs Mountain. Although most faults are normal faults, several northwest- to north-northwest-trending faults show features suggestive of right-lateral strike slip displacement, for example, in the fault zone southeast of Kelseyville, locally within the Konocti Bay fault zone, and along much of the Cobb Valley fault zone. In the last zone, a young age of strike-slip movement is suggested by offset topographic features. Offset of contacts of volcanic units of 0.5 m.y. and younger age suggests that movement, if continuous, has been at a rate of about 1 mm/year for the past 0.5 m.y.

Active deformation within the volcanic field and within the Clear Lake structural basin is indicated by felt earthquakes, of magnitude as great as 4.6. Approximate locations of epicenters (Hamilton and Muffler, 1972; Chapman, 1975) suggest that some of the earthquakes are occurring close to the Cobb Valley fault zone. Some locally felt earthquakes are most intense south of Konocti Bay and are possibly associated with the Konocti Bay fault zone. Local earthquakes also may be associated with the faults that bound the Clear Lake Basin. McLaughlin and Stanley (1975) have found that microearthquakes are associated with a north-northwest-trending fault zone in The Geysers steam field. Ongoing seismic studies hopefully will enable more precise location of sources and mechanisms of local earthquakes; the monitoring of changes in level and horizontal distances (Lofgren, 1973) will characterize current deformation and tilting in the Clear Lake/Geysers area.

Although parts of the volcanic field show local subsidence and the Clear Lake structural basin is probably continuing to subside, evidence for large-scale caldera collapse is lacking. The largest local circular collapse feature is the 1.6 km diameter basin southeast of Mt. Konocti. Although the shape of the northern part of Clear Lake and some adjacent faults are suggestive of partial control by circular collapse, data are not sufficient to determine the validity of such a subsidence pattern.

GEOPHYSICAL STUDIES

Gravity data delineate a circular 25-30 mgal low, 30 km in diameter, centered at Mt. Hannah. The circular shape of the gravity low, superimposed upon the structural trend

of the Coast Ranges, indicates that the low is not related to density contrasts of structural blocks having northwest-southeast elongation. This gravity low has been interpreted as the expression of a magma chamber at a depth of 10 km or less (Chapman, 1966, 1975; Isherwood, 1975).

The occurrences of thermal springs and wells in and within about 20 km of the Clear Lake volcanic field imply that there is an anomalously hot mass at depth. Electrical surveys show a well-defined resistivity low which is beneath the south-central part of the volcanic field, is in part coincident with the gravity low, and extends to at least 5 km depth (Stanley, Jackson and Hearn, 1973). The resistivity low can be interpreted as being due to a thick section of marine shale or to the presence of hot saline fluids, or a combination of the two; however, limited drill hole data and the structural complexity of Great Valley and Franciscan rocks beneath and southeast of the volcanic field preclude the presence of a marine shale several thousand meters thick. Thus, the resistivity low is probably produced by combined effects of elevated temperature and salinity of water above a heat source at depth—a large mass of hot rock or magma.

CONCLUSIONS

The possible existence of a magma chamber beneath the Clear Lake volcanic field is supported by the volume of silicic volcanic rocks, by evidence of differentiation, and by the geophysical anomalies. The age, inferred depth, and volume of such a magma chamber indicate that the volcanic field and surrounding area have geothermal potential (Smith and Shaw, 1973). Confirmation of a magma chamber will depend on future data from drilling and from indirect deep-sensing methods.

By comparison with other silicic volcanic fields, the Clear Lake field is believed to be in an early stage of evolution. It has erupted a significant volume of silicic magma, has been active within the last 10 000-20 000 years, and has not yet reached a stage of voluminous ash-flow eruption and large-scale caldera collapse. However, if a regional strike-slip deformation parallel to the San Andreas system is being superimposed on localized deformation related to a magma chamber, the magmatic system may not be able to proceed through the stages of growth shown by other systems, but instead may be tapped more frequently by smaller eruptions. That some such process is operating in the Clear Lake field is suggested by the complex repetitive cycles of mafic-silicic eruptions. If the geometry of the magma chamber is continually changing and its roof is fracturing as a result of regional stresses, a progressive accumulation of gas-rich silicic differentiate, necessary for voluminous ash-flow eruption, may not occur.

The apparent northward decrease in age in both the Sonoma and Clear Lake volcanic fields suggests the possibility that both are surface manifestations of deep magma generation by the same thermal anomaly or hot spot in the mantle. The direction of migration of volcanic activity implies that, relative to the hot spot, the North American plate has moved south-southeast or southeast. The actual direction of migration of volcanic activity may have been modified by successive movement on right-lateral strike-slip faults, which would have produced an apparent clockwise rotation, from a northwest direction to a more northerly direction.

The geothermal potential of the Clear Lake volcanic field

and its surroundings is strongly indicated by the size and youth of the field, the presence of The Geysers production area, the inferred presence of a shallow subjacent magma chamber, and the distribution of thermal springs and wells. Further exploration for geothermal resources will better define the hydrology, heat flow, and vertical dimensions of the volcanic system.

ACKNOWLEDGEMENTS

We thank K. R. Taylor, J. E. Knight, and F. A. Wilson for assistance in field work, and S. Grommé, E. A. Mankinen, and W. F. Isherwood for laboratory confirmation of magnetic polarities. The second author thanks R. E. Drake and G. H. Curtis for assistance with K/Ar dating and thanks J. Hampel for potassium analyses, and has been supported in part by NSF Grant GA 40805. This paper has benefitted from reviews by R. L. Smith, R. G. Luedke, and F. A. Wilson.

REFERENCES CITED

- Anderson, C. A., 1936, Volcanic history of the Clear Lake area, California: *Geol. Soc. America Bull.*, v. 47, p. 629-664.
- Barnes, I., Hinkle, M. E., Rapp, J. B., Heropoulos, C., and Vaughn, W. W., 1973, Chemical composition of naturally occurring fluids in relation to mercury deposits in part of north-central California: *U.S. Geol. Survey Bull.* 1382A, 19 p.
- Berkland, J. O., 1972, Clear Lake basin—a deformed Quaternary caldera (?), in Moores, E. M., and Matthews, R. A., eds., *Geologic guide to the northern Coast Ranges—Lake, Mendocino and Sonoma Counties*, California: *Geol. Society of Sacramento, Annual Field Trip Guidebook*, p. 6-25.
- , 1973, Rice Valley outlier—new sequence of Cretaceous-Paleocene strata in northern Coast Ranges, California: *Geol. Soc. America Bull.*, v. 84, p. 2389-2406.
- Bowman, H. R., Asaro, F., and Perlman, I., 1973, On the uniformity of composition in obsidians and evidence for magmatic mixing: *Jour. Geology*, v. 81, p. 312-327.
- Brice, James C., 1953, *Geology of Lower Lake quadrangle*, California: California Div. Mines Bull. 166, 72 p.
- California Department of Water Resources, 1962, *Reconnaissance report on upper Putah Creek basin investigation*: California Dept. Water Resources Bull. 99, 254 p.
- Chapman, R. H., 1966, *Gravity map of Geysers area*: California Div. Mines and Geology Mineral Inf. Service, v. 19, p. 148-149.
- , 1975, *Geophysical study of the Clear Lake region*, California: California Div. Mines and Geology Spec. Rept. 116, 23 p.
- Garrison, L. E., 1972, *Geothermal steam in The Geysers-Clear Lake region*, California: *Geol. Soc. America Bull.*, v. 83, p. 1449-1468.
- Hamilton, R. M., and Muffler, L. J. P., 1972, *Microearthquakes at The Geysers geothermal area*, California: *Jour. Geophys. Research*, v. 77, p. 2081-2086.
- Hodges, C. A., 1966, *Geomorphic history of Clear Lake*, California [Ph.D. dissertation]: Stanford University, 210 p.
- Isherwood, W. F., 1975, *Gravity and magnetic studies of The Geysers-Clear Lake region, California: Second UN Symposium on the Development and Use of Geothermal Resources*, San Francisco, Proceedings, Lawrence Berkeley Lab., Univ. of California.
- Lake County Flood Control and Water Conservation District, 1967, *Big Valley ground-water recharge investigation* 63 p.
- Lofgren, B. E., 1973, *Monitoring ground movement in geothermal areas: Hydraulic Division Specialty Conference*, Bozeman, Montana, Proceedings—Hydraulic Engineering and the Environment, p. 437-447.
- Mankinen, E. A., 1972, *Paleomagnetism and potassium-argon ages of the Sonoma Volcanics*, California: *Geol. Soc. America Bull.*, v. 83, p. 2063-2072.
- Maxwell, John C., 1974, *Anatomy of an orogen*: *Geol. Soc. America Bull.*, v. 85, p. 1195-1204.
- McLaughlin, R. J., 1974, *Preliminary geologic map of The Geysers steam field and vicinity*, Sonoma County, California: U.S. Geol. Survey, open-file map 74-238.
- McLaughlin, R. J., and Stanley, W. D., 1975, *Pre-Tertiary geology and structural control of geothermal resources. The Geysers steam field*, California: Second UN Symposium on the Development and Use of Geothermal Resources, San Francisco, Proceedings, Lawrence Berkeley Lab., Univ. of California.
- McNitt, J. R., 1968a, *Geologic map of the Kelseyville quadrangle*, Sonoma, Lake and Mendocino Counties, California: California Div. Mines and Geology Map Sheet 9.
- , 1968b, *Geologic map of the Lakeport quadrangle*, Lake County, California: California Div. Mines and Geology Map Sheet 10.
- , 1968c, *Geology of the Clearlake Oaks 15-minute quadrangle*, Lake County, California: California Div. Mines and Geology, Open-file Release 68-12.
- Sims, J. D., and Rymer, M. J., 1974, *Gaseous springs in Clear Lake, California, and the structural control of the lake basin*: *Geol. Soc. America Abs. with Programs*, v. 6, p. 254.
- , 1975a, *Preliminary description and interpretation of cores and radiographs from Clear Lake*, California: *Core 7: U.S. Geol. Survey, open-file report 75-144*, 21 p.
- , 1975b, *Map of gaseous springs and associated faults in Clear Lake, California*: U.S. Geol. Survey, Misc. Field Inv. Map.
- Smith, R. L., and Shaw, H. R., 1973, *Volcanic rocks as geologic guides to geothermal exploration and evaluation [abs.]*: *EOS (Am. Geophys. Union Trans.)*, v. 54, p. 1213.
- Stanley, W. D., Jackson, D. B., and Hearn, B. C. Jr., 1973, *Preliminary results of geolectrical investigations near Clear Lake, California*: U.S. Geol. Survey, open-file report, 20 p.
- Swe, W., and Dickinson, W. R., 1970, *Sedimentation and thrusting of Late Mesozoic rocks in the Coast Ranges near Clear Lake, California*: *Geol. Soc. America Bull.*, v. 81, p. 165-189.
- U.S. Geological Survey, 1973, *Aeromagnetic map of the Clear Lake area, Lake, Sonoma, Napa and Mendocino Counties*, California: U.S. Geol. Survey, open-file map.
- White, D. E., and Roberson, C. E., 1962, *Sulphur Bank, California, a major hot-spring quicksilver deposit*, in Engel, A. E. J., James, H. L., and Leonard, B. F., eds., *Petrologic studies: A volume in honor of A. F. Buddington*: *Geol. Soc. of America*, p. 397-428.

Gravity and Magnetic Studies of The Geysers–Clear Lake Geothermal Region, California, USA

WILLIAM F. ISHERWOOD

U.S. Geological Survey, Denver, Colorado 80225, USA

ABSTRACT

Gravity and magnetic fields in The Geysers–Clear Lake region are interpreted in relation to the known geology and other available geophysical data. New gravity data provide additional detail within the area of geothermal steam production. Computer techniques were used for removal of the regional gravity field, anomaly enhancement, and modeling subsurface structures. The gravity field was separated into three components: (1) a regional field presumed to be due to deep crustal structure related to the continental margin; (2) a residual gravity low of approximately 30 mgal centered over Mount Hannah and having an approximate diameter of 20 km, which is caused, according to our model, by a magma chamber whose top lies within 10 km of the surface; and (3) a closed residual low over the original steam production field. This low is probably related to effects within 1.5 km of the surface and was modeled as a steam-saturated reservoir structure. Local magnetic highs correlate with surface outcrops of serpentinite and relief on the volcanic rocks. Upward continuation of the aeromagnetic data suggests that the serpentinite body along the Collayomi fault may extend to a depth of more than 3 km near Boggs Mountain, but that other serpentinite bodies are probably more shallow. A long-wavelength magnetic high (centered at $\sim 39^{\circ}03'N$ $122^{\circ}33'W$) and a magnetic low (centered at $\sim 38^{\circ}43'N$ $122^{\circ}47'W$) give half-width depth estimates of about 10 km. The center of the Mount Hannah gravity low lies in an area between these features and appears devoid of deep magnetic expression.

INTRODUCTION

In order to explore for economic steam reservoirs, it is important to know the complete, three-dimensional geology which governs such a system. The Geysers–Clear Lake region, California (Fig. 1), has the world's largest production of commercial power from a dry-steam geothermal reservoir. This paper describes gravity and magnetic field analysis at The Geysers which defines a possible deep geologic structure and heat source.

A small area from the recently published Santa Rosa gravity map (Fig. 2) illustrates the previous gravity coverage. The major gravity low centered over Mount Hannah, approximately 11 km northeast of The Geysers, drew the attention of several workers. Rodger Chapman (1966) first suggested a magma chamber at depth as a possible source

of the anomaly, the volcanic activity, and the geothermal reservoir. Although several other models have been investigated, the present study supports the presence of a magma chamber whose center is deeper than 10 km.

During the summer of 1974, I added 150 gravity stations with special attention to improving control in the region of steam production and the Mount Hannah low. These data were merged with the previous data and reduced to complete Bouguer gravity values with Bouguer reduction densities of 2.67 g/cm^3 and 2.45 g/cm^3 (Isherwood and Chapman, 1975). These two density values minimize terrain

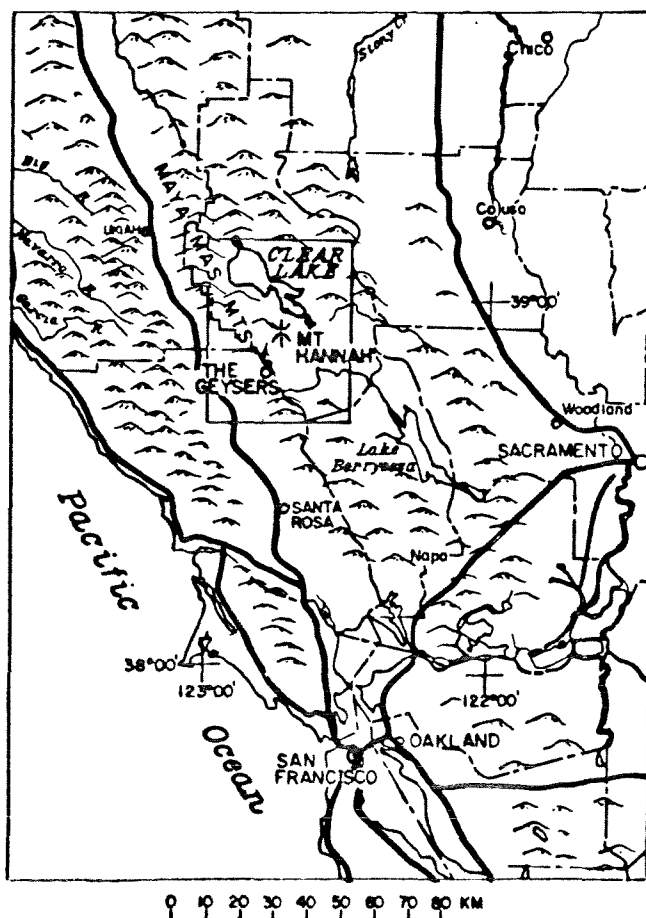


Figure 1. Index map, showing the region of discussion in this paper.

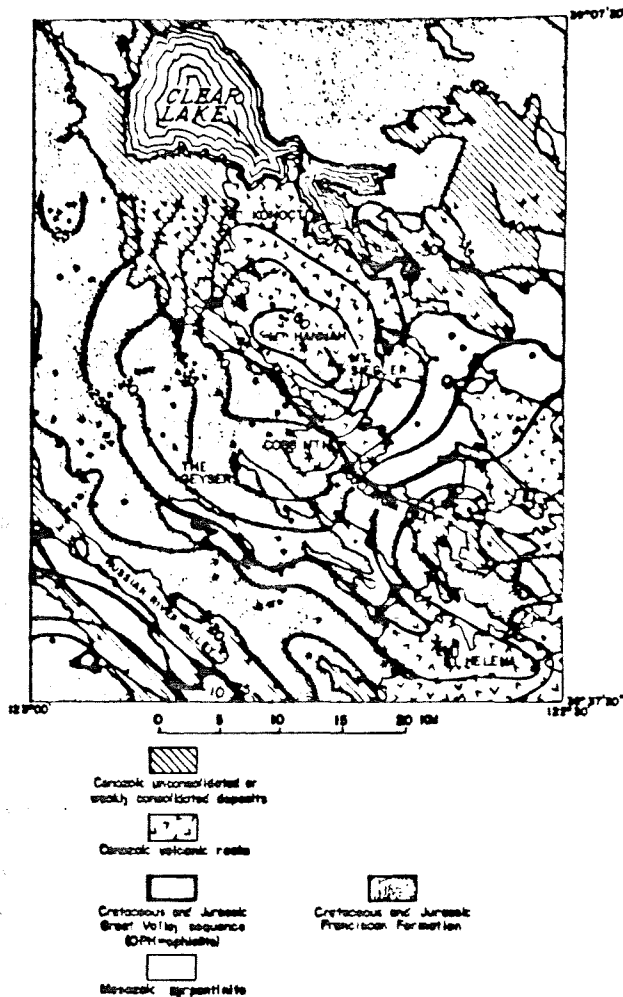


Figure 2. Generalized geology with gravity from Santa Rosa Gravity Map, (Chapman and Bishop, 1974).

effects within the Franciscan and Cenozoic volcanic terranes respectively. Consequently, the gravity field reduced at 2.67 g/cm^3 probably better represents the subsurface structure in the area southwest of the Collayomi fault zone which separates these terranes; and gravity at 2.45 g/cm^3 does similarly to the northeast.

The study of rock samples and well density logs yields a general notion of the physical distinction between rock units in the region (Table 1). Because sampling is usually biased in favor of rock units having conspicuous outcrops, weak (low-density) rocks have possibly been underestimated. In particular, weak shaly rocks in the Franciscan formation—referred to as melange—rarely appear as substantial exposures, but may form a matrix around many of the harder “knockers” which are well exposed. More well-log information is needed to determine the full effect of such units. Figures shown in Table 1 are based on small, not necessarily representative, sample sets of data with considerable scatter and are only intended to represent possible anomaly sources.

The field shown in the Santa Rosa and Ukiah 1:250 000-scale gravity maps (R. H. Chapman, unpub. data) provides the basis for removal of a regional gravity field. These two maps were hand digitized on a 5-km grid. The digital computer fitted polynomial surfaces of order 1 through 7 to the data. The sixth-order surface shown in Figure 3 was chosen as a good representation of the regional field without

Table 1. Rock properties.

Rock type ^a	Density (g/cm ³)	Susceptibility (emu/cm ³)
Franciscan formation		
Greenstone	2.9	1.0×10^{-4}
Graywacke	2.6	2.0×10^{-4}
Melange	2.4	5.0×10^{-5}
Blueschist	3.1	8.0×10^{-5}
Serpentinites	2.5	3.8×10^{-3}
Assumed average	2.67	5.0×10^{-4}
Clear Lake volcanics (upper Tertiary and Quaternary)*		
Olivine basalts	2.8	3.2×10^{-4}
Rhyolites and dacites	2.45	1.5×10^{-4}
Assumed average	2.5	1.7×10^{-4}
Hot silicic magma	2.2 [†] -2.4 [‡]	
Great Valley sequence		
Sediments	2.5	1.0×10^{-4}
Ophiolite	2.9	1.9×10^{-3}

* From Bruce (1953).

† From Murase and McBirney (1973).

‡ Average Franciscan material reduced by 10%.

perturbation by local anomalies. Note that this surface is nearly planar over the more restricted region of this study. This component of the total gravity field is attributed to deep crustal and upper mantle structure related to the continental margin. The values of the regional surface were subtracted from the complete Bouguer values at each station and the residuals were machine gridded and contoured.

The maps of residual gravity presented in Figures 4 and 5 show the following:

1. The major gravity feature (referred to as the Mount Hannah low) is a roughly circular depression of about 25

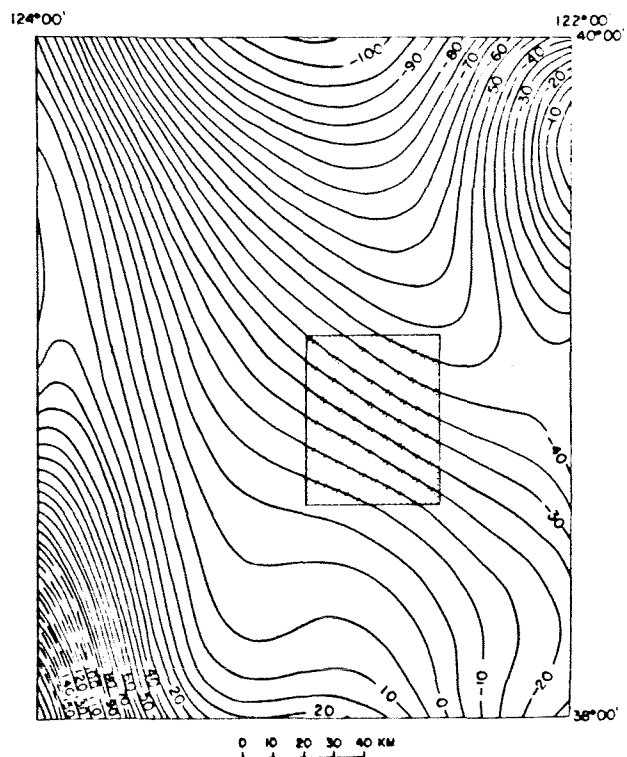


Figure 3. Sixth-order surface fit to regional gravity; 5-mgal contour interval. Shaded rectangle is the portion used to adjust complete Bouguer gravity values in this survey.

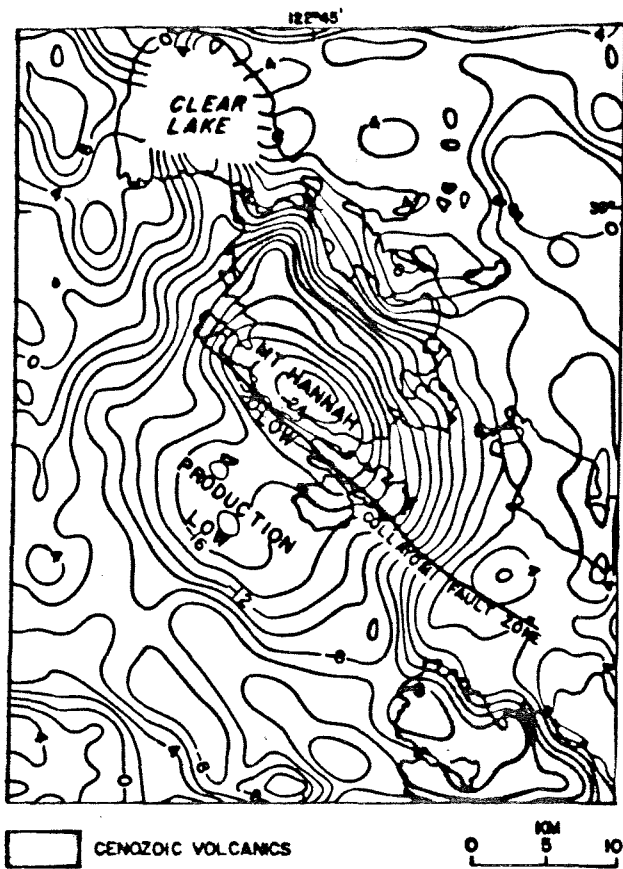


Figure 4. Residual gravity reduced at 2.67 g/cm^3 ; 2-mgal contour interval.

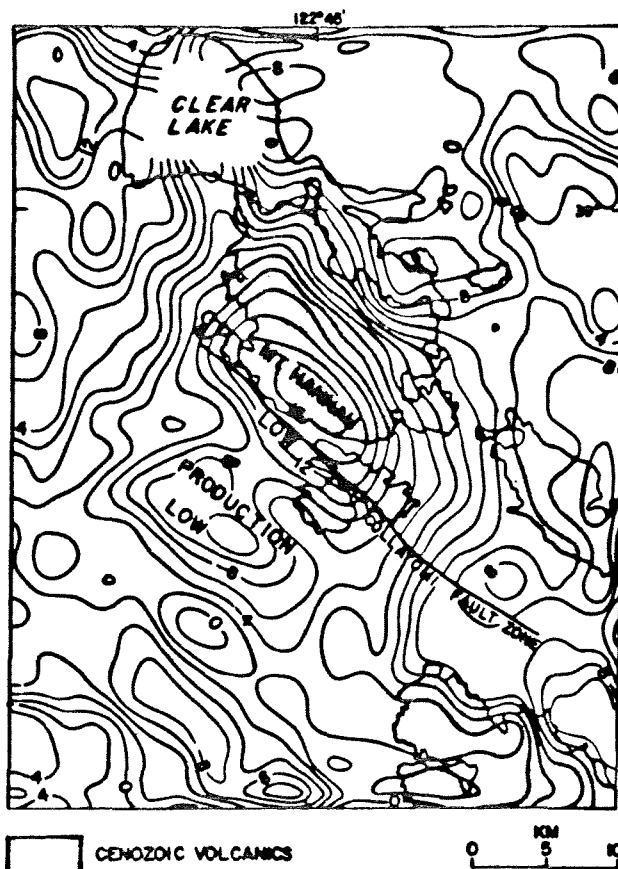


Figure 5. Residual gravity reduced at 2.45 g/cm^3 ; 2-mgal contour interval.

mgal and 30-km diameter. The steep gradients to the northwest and southeast of the center notably cross the structural grain of the region.

2. The Mount Hannah gravity low is centered near the southwest edge of the Quaternary volcanic field, and its gravity gradient extends more than 12 km into the Franciscan terrane.

3. Each of the recognized volcanic vents south of Clear Lake correlates with a residual gravity low. Such correspondence suggests a genetic relation.

4. There is now apparent a secondary closed low in the region of steam production at The Geysers. This closure (referred to as the production low) is separated from the closure near the summit of Mount Hannah by a ridge of higher gravity.

5. A noteworthy gravity high of at least 6 mgal lies northeast of the Mount Hannah low and is centered over the southeast arm of Clear Lake. Correlation with surface geology is not clear.

Table 2. Depth estimates from gravity anomalies.

Anomaly	Half-width estimate to center (km)	Gradient estimate to top (km)
Mt. Hannah low	11.5 (sphere)	7.5
Production low	2.2 (cylinder)	1.9
Southeast Clear Lake high	4.5 (sphere)	2.3

Rough approximations of the source depths are made in Table 2 using the half-width method (Nettleton, 1940) and the ratio of maximum anomaly to maximum gradient (Bott and Smith, 1958).

The depths estimated for the source of the production low have been penetrated by drilling of the producers: at least some of the anomaly, then, may be caused by reservoir structure.

AEROMAGNETICS

The results of an aeromagnetic (total field) survey flown in 1972 were compiled by the U.S. Geological Survey in an open-file report (1973). The flight elevation was 4500 feet (1372 m) barometric, with east-west flight lines at approximately 1.6 km spacing. Superimposing this map on available geologic and topographic reference maps enables the following observations:

1. The overall pattern is complex with high magnetic relief (for example, greater than 700 gamma within 10 km of Mount Hannah).
2. A major magnetic high in the northeast corner of the study area has recognizable expression over greater than 400 km^2 . Although there is no recognized surface exposure in this region which is likely to account for this anomaly, it lies on the trend of major serpentinite bodies (and magnetic highs) which bound the west side of the Great Valley.
3. Several local magnetic highs and lows clearly correspond to volcanic peaks close to the flight line. The signs of the

anomalies would indicate Mount Konocti to be normally magnetized, Cobb Mountain reversed, Mount Siegler normal, and Mount Hannah mixed or weak (see Fig. 2 for location). These findings agree with measured directions determined from rock cores with standard paleomagnetic methods for determining natural remanent magnetizations.

4. Other magnetic highs correlate well with mapped ultrabasic bodies. Such a relation has been noted throughout the California Coast Ranges (Saad, 1969; Byerly, 1966; Chapman, 1975).

A major component in observed aeromagnetic data is the local gradient of the earth's main field. In order to facilitate further processing, the open-file aeromagnetic map was digitized on a 1-km grid, making an array 57 rows by 45 columns. The main field component was then removed on the basis of the eight-order 1965 International Geomagnetic Reference Field (IGRF) updated to 1972, and adjusted by a constant to approximately a zero mean. The resultant residual magnetic field, Figure 6, shows no major differences in the anomaly pattern from the original map (U.S. Geological Survey, 1973).

UPWARD CONTINUATION

The field shown in Figure 6 contains contributions from topographic effects and changes of magnetization of small near-surface bodies primarily in the short-wavelength end of the spectrum. Upward continuation, which acts as a type

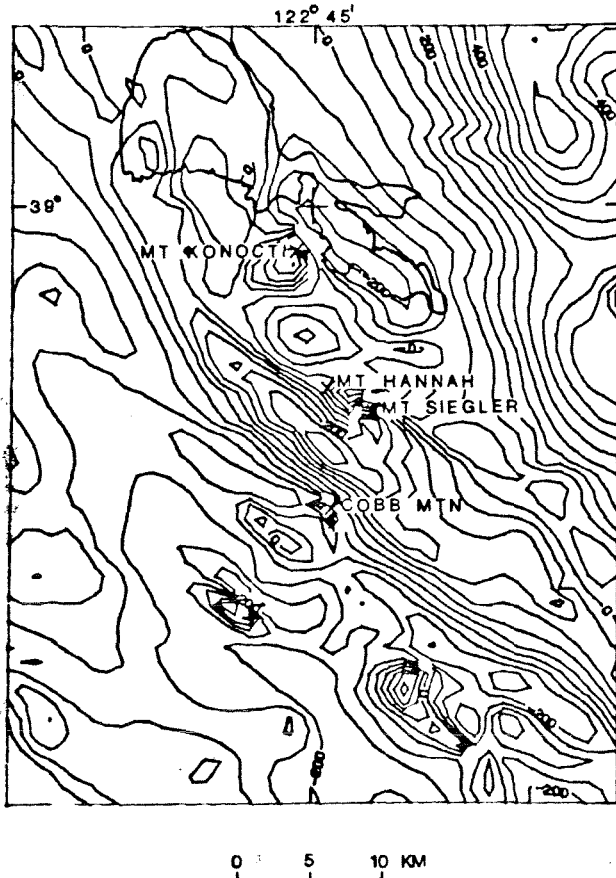


Figure 6. Total field magnetics of The Geysers; 50-gamma contour interval. Digitized on 1-km grid, IGRF removed.

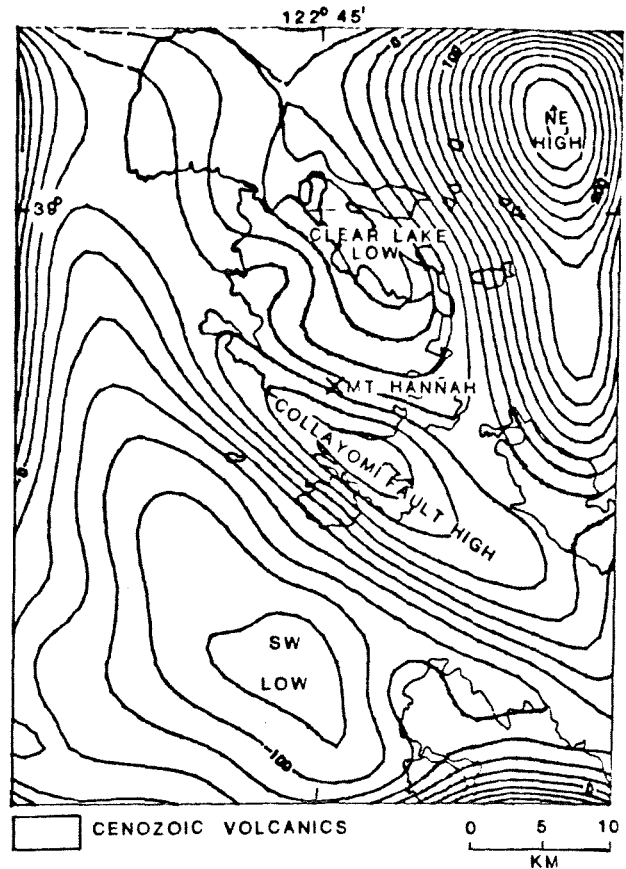


Figure 7. Magnetics continued upward 3 km; 20-gamma contour interval.

of wavelength filter, was used to de-emphasize these features. Figures 7, 8, and 9 show the residual aeromagnetic field continued upward 3 km, 5 km, and 7 km respectively. On the assumption that more superficial effects disappear first with the upward continuation, the following interpretations are made:

1. The most obvious topographic effects are quite subdued by 3-km upward continuation and are no longer recognized at 5 km.
2. With the exception of the serpentinite zone along the Collayomi fault, the magnetic highs associated with surface exposures of ultrabasics disappear by 3-km continuation. This is evidence that serpentinite along the Collayomi fault zone may have considerable depth south of Mount Hannah where the fault zone is buried by volcanics, whereas other ultrabasic bodies may be more shallow.
3. The magnetic low over the southeast arm of Clear Lake and north of the Collayomi fault high has the correct relation for a dipole low, at this magnetic latitude, associated with the high. Alternatively, it may be only a relative low between two magnetic highs. The fact that these two features disappear with the same upward continuation supports the suggestion that they are associated with roughly the same depth.
4. Although the source of these central anomalies may extend several kilometers deep, no sources in the central region are as deep as those apparently causing the magnetic high to the northeast or the magnetic low to the southwest.

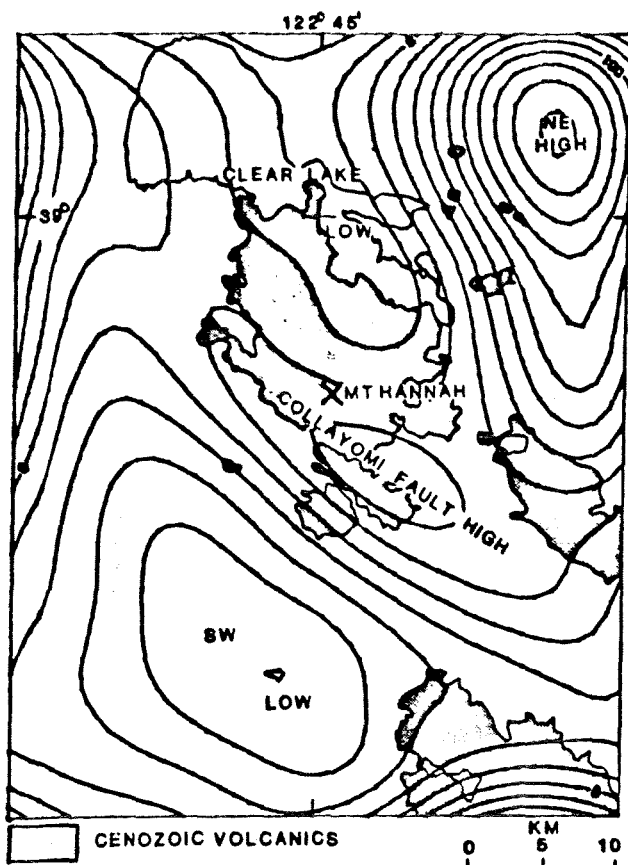


Figure 8. Magnetics continued upward 5 km; 20-gamma contour interval.

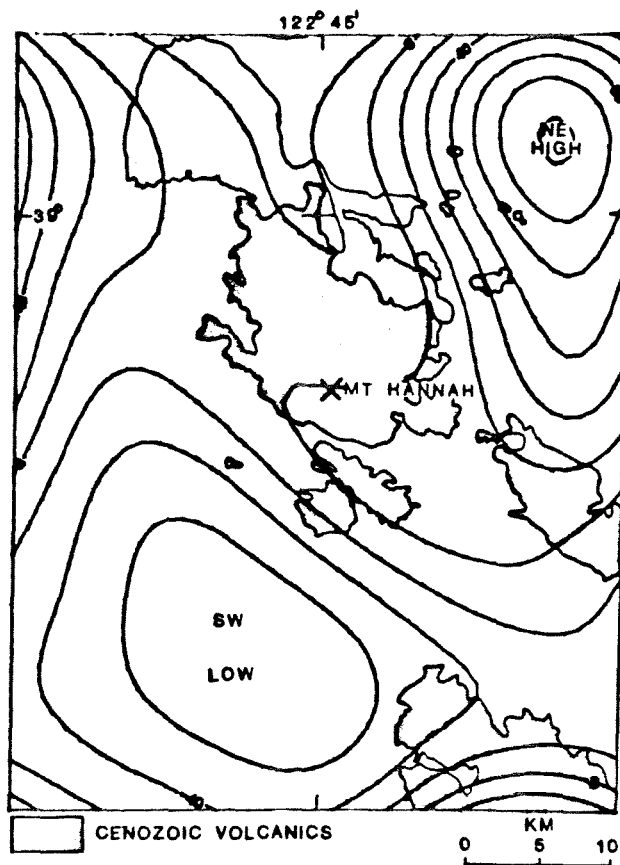


Figure 9. Magnetics continued upward 7 km; 20-gamma contour interval.

Choosing the four major anomalies brought to attention by upward continuation, depth estimates were made similar to those made for the gravity anomalies (Table 3).

PSEUDOGRAVITY

If magnetic and gravity anomalies are caused by the same body of uniform density and magnetization, then Poisson's theorem describes the relation between anomalies (for example, Garland, 1951). These assumptions are tested by computing pseudogravity from the magnetic field and comparing it with the observed gravity. Because of the low Koenigsberger Q ratio (natural remanent magnetism, NRM , divided by induced magnetization) found for serpentinites from the area, NRM has been discounted as a source of the major anomalies (Saad, 1969). Figure 10 shows the pseudogravity field using test values of apparent susceptibility, $k = 0.003$ emu and density contrast, $\Delta\rho = 0.15$ g/cm³ prepared from a filtered version of the aeromagnetics. Wavelengths shorter than about 6 km were removed to suppress terrain and other superficial effects. Although different choices of k and $\Delta\rho$ will change the magnitude and even the sign of the pseudogravity anomalies, their positions and shapes will remain unchanged. This map shows a pronounced gradient approximately at the Collayomi fault, but the overall pattern differs considerably from the observed gravity. Even allowing for different signs of $k/\Delta\rho$ on opposite sides of the Collayomi fault zone, the anomalies do not match the gravity, apparently because of the difference in wavelength components and an offset in their centers. This

Table 3. Depth estimates from magnetic anomalies.

Anomaly	Half-width estimate to center (km)		Gradient estimate to top (km)
	pole	sphere	
Collayomi high	1.9	3.2	1.3
Clear Lake low	1.6	3.1	1.8
Northeast high	6.8	10.8	6.8
Southwest low	6.8	10.8	5.8

is further evidence that the same bodies do not produce both the gravity and magnetic anomalies. One possible explanation, which will be examined more fully in the next section, is that the source body of the Mount Hannah low is above its Curie point, at which temperature remanent magnetization would disappear and susceptibility magnetization would also be exceedingly small. Consequently this body would have no magnetic expression.

SPECTRA

Bhattacharyya and Morley (1965) and Spector and Grant (1970) have popularized the idea of using the spectra of potential fields to estimate the depth to the causative bodies. Spectral methods appear particularly useful in such cases where near-surface sources tend to mask the effects of the deeper bodies of interest. As shown by the above workers and Odegard and Berg (1965), the slope of the gravity spectrum, plotted as the log of the amplitude versus wave

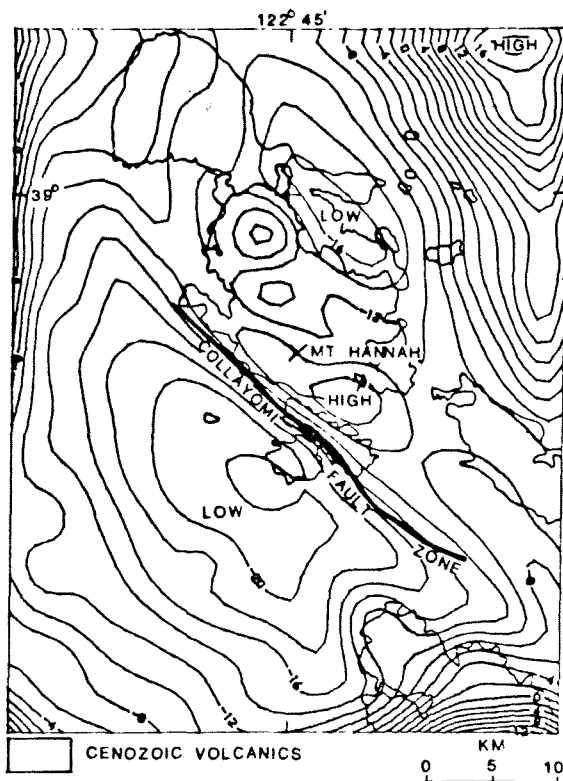


Figure 10. Pseudogravity derived from filtered magnetics (5-km cutoff) $\rho = +0.15$, $k = +0.003$; 2-mgal contour interval.

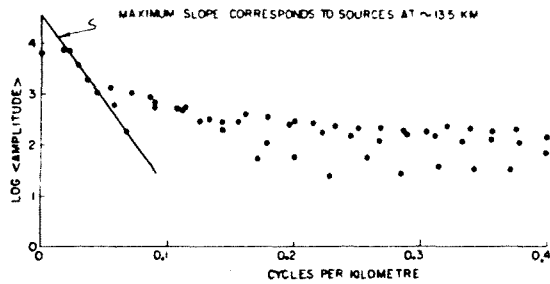


Figure 11. Frequency spectrum of gravity field at The Geysers; from 56-km by 45-km grid (radial averages).

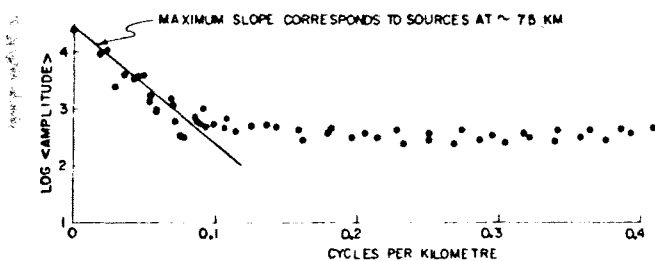


Figure 12. Frequency spectrum of pseudogravity derived from aeromagnetic data, The Geysers; 56-km by 44-km grid.

number, is proportional to the depth of an equivalent point source. Figure 11 shows such a plot obtained from the gridded residual gravity, and Figure 12 shows the same for the pseudogravity grid produced from the magnetics. (Using pseudogravity rather than magnetics assures comparability.) Both graphs show steep slopes at low wave numbers and

more gentle slopes at higher wave numbers. Interpretation of these slopes was made after comparisons with spectra derived from synthetic models of spheres at different depths. According to the slopes shown here, the gravity could result in part from a deep source whose depth (center of sphere) is approximately 13.5 km. The deepest component recognized as a magnetic source, reflected in the pseudogravity spectrum, is only about 7.5 km deep; and as we saw from the previous discussions, the deepest sources appear spatially related to the high northeast of Clear Lake and the low 10 km south of The Geysers. It has been reasoned (Bhattacharyya and Morley, 1965; Bhattacharyya and Leu, unpub. data, 1975) that a lack of deep magnetic sources in a region may be due to a rise in the level of the Curie isotherm.

LOW-PASS FILTERING AND DEEP MODEL

On the basis of the spectra, low-pass filters were designed to investigate the long-wavelength anomalies. Figure 13 shows the gravity field (at 2.67 g/cm³ reduction) filtered to eliminate wavelengths shorter than about 18 km (0.056 cycles/km). From the spectra, we would expect the remaining wavelengths to be dominated by the postulated deep source. This map looks as we might expect from a centrobaric mass centered under the bottom of the low. To test the 13.5-km depth estimation from the previous section, several representative profiles were drawn across the long-wavelength anomaly on the axes indicated in Figure 13. These profiles are compared in Figure 14 with that calculated

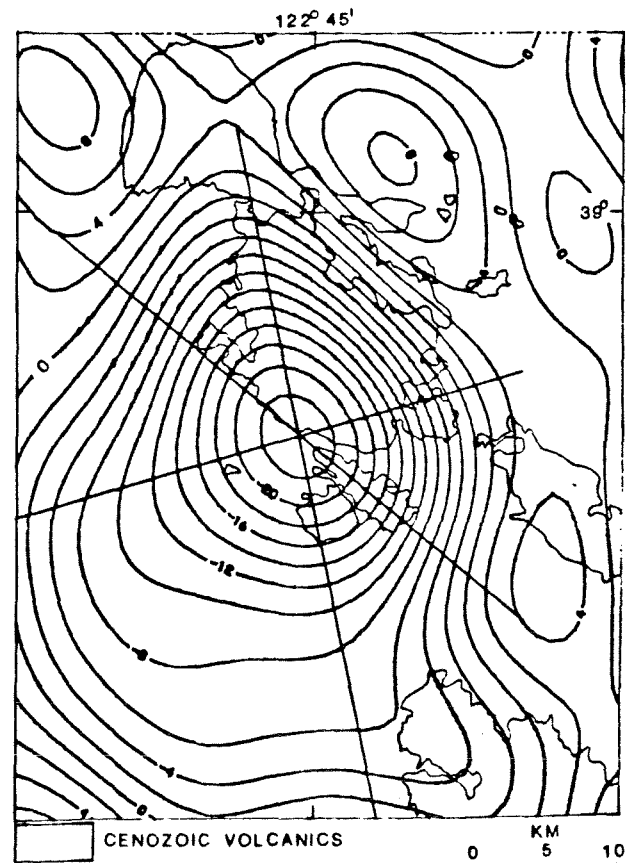


Figure 13. Gravity (at 2.67 g/cm³) low-pass filtered with approximately 18-km cutoff; 2-mgal contour interval. Lines are representative profiles used in Figure 14.

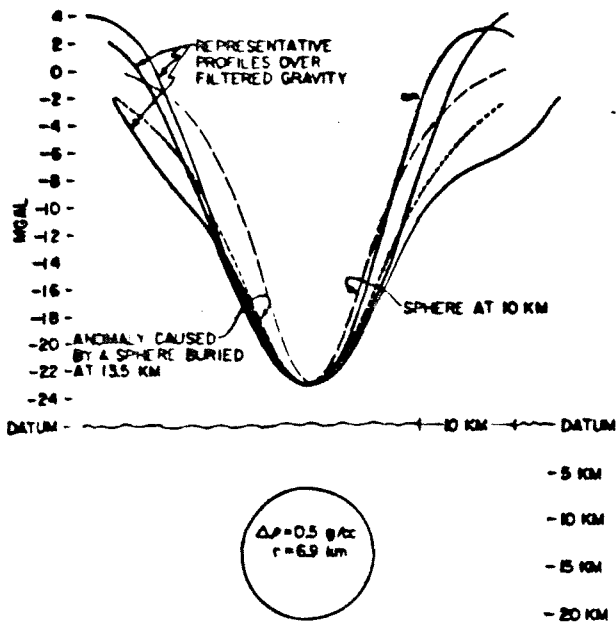


Figure 14. Representative profiles from Figure 13 compared with curves calculated for spheres buried at 13.5 km and 10 km. One possible limiting sphere for the 13.5-km source profile is shown below.

for a sphere with center at 13.5-km depth. Also shown is the calculated curve for a sphere at 10 km to illustrate the sensitivity of the anomaly shape to depth.

Although this anomaly is well-modeled by the field of a sphere at 13.5-km depth, this must be considered a limiting case. A more lenticular body or a body with a gradational density boundary could cause the same anomaly but be less deep.

Calculation can now be made for the mass deficiency, both from the curve for the postulated deep sphere and by Gauss' theorem. Table 4 shows the relation of density contrast, radius, and depth to the top of a sphere at 13.5-km depth (the curve in Fig. 14) and mass deficiency of 6.8×10^{14} kg. In practice, the calculation of mass deficiency by Gauss' theorem requires an assumption about the depth to the source (Grant and West, 1965, p. 270). Provided the regional field yields a reasonable gravity datum, the slightly different values of Table 5 are calculated.

Certain implications are now clear. If the density contrast is small, the source material must extend nearly to the surface. The volcanic rocks at the surface may indeed provide some small density contrast (0.1 to 0.2 g/cm³) with

Table 4. Limiting sphere with center at 13.5 km depth and 25-mgal anomaly above center (requiring a mass deficiency of 6.8×10^{14} kg).

$\Delta\rho$ (g/cm ³)	Radius (km)	Depth to top (km)
0.1	11.8	1.7
0.2	9.3	4.2
0.3	8.2	5.3
0.4	7.4	6.1
0.5	6.9	6.6
0.6	6.5	7.0
0.7	6.2	7.3
0.8	5.9	7.6

Table 5. Mass from Gauss' theorem.

$\Delta\rho$ (g/cm ³)	Depth of 13.5 km 5.3×10^{14} kg		Depth of 12 km 4.9×10^{14} kg		Depth of 10 km 4.2×10^{14} kg	
	Radius (km)	Top (km)	Radius (km)	Top (km)	Radius (km)	Top (km)
0.1	10.8	2.7	10.5	1.5	10.0	0
0.2	8.6	4.9	8.4	3.6	7.9	2.1
0.3	7.5	6.0	7.3	4.7	6.9	3.1
0.4	6.8	6.7	6.6	5.4	6.3	3.7
0.5	6.3	7.2	6.2	5.8	5.9	4.1
0.6	6.0	7.5	5.8	6.2	5.5	4.5
0.7	5.7	7.8	5.5	6.5	5.2	4.8
0.8	5.4	8.1	5.3	6.7	5.0	5.0

the Franciscan terrane to the south, west, and possibly north; but to the east this contrast is not apparent in surface rocks. Moreover, it is impossible to match the gravity gradients over the Franciscan terrane with low-density units limited to the northeast side of the Collayomi fault, which might be considered to be a vertical or northeast-dipping local boundary between Franciscan and Great Valley rocks (Garrison, 1972). This does not rule out the possibility of a complex low-density source made up in part by volcanics, Great Valley sediments, serpentinites, and low-density Franciscan melange; however, the required low-density units apparently have not been found in drill holes over 2-km deep south of the Collayomi fault zone.

The Santa Rosa gravity sheet (Chapman and Bishop, 1974) shows several outliers of Great Valley sequence rocks on the Franciscan terrane, none of which produce gravity anomalies comparable to the Mount Hannah low. This anomaly absence suggests that either the Great Valley outliers are generally shallow or that the true bulk-density contrast with Franciscan rocks is small.

On the other hand, if the body primarily responsible for the Mount Hannah gravity low does not come within about 5 km of the surface, it must be less dense than any unit listed in Table 1 except hot silicic magma. The circular appearance of the residual anomaly favors this interpretation as a magma chamber.

At least one hole has been drilled within a few kilometers of the center of the Mount Hannah low (Fig. 15). The well, Sullivan 1, in sec. 18, T. 12 N., R. 8 W., started in the serpentinite associated with the Collayomi fault and has penetrated almost 1900 m without leaving serpentinite (E. B. Towne, written commun.). Another well, about 6.5 km north of Mount Hannah, was drilled through the volcanic surface rocks for about 750 m and continued to about 2380 m depth in a complex sequence containing considerable greenstone and serpentinite. A density log for the hole indicates a range of densities for the volcanics between 2.3 and 2.5 g/cm³ with an average of about 2.4 g/cm³ and below the volcanics to the bottom of the available log (1800 m), a range of densities from 2.4 to 2.8 g/cm³ with an average of about 2.65 g/cm³. These suggest that the preferred model should include some near-surface contribution from the volcanics, but still requires a deep source to produce gravity expression well into the Franciscan terrane.

Additional subsurface information is available from interpretation of microearthquake surveys (Lange and Westphal, 1969; Hamilton and Muffler, 1972). Hypocenters shown on published maps lie mainly outside the region of the possible

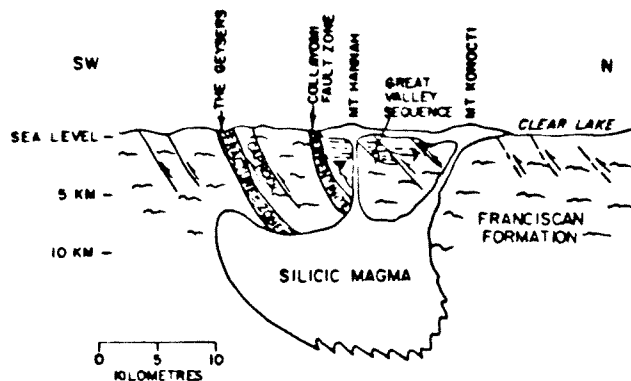


Figure 17. Generalized cross section through The Geysers-Clear Lake geothermal region.

1. A magma chamber which is hot enough to be above its Curie temperature, and is centered more than 10 km below the southwest edge of the volcanic field.
2. An apparent roof pendant and/or caprock which is important in directing hydrothermal activity to the southwest toward the producing steam field.
3. A fracture zone with steam-filled pore space acting as a reservoir capped by less fractured greenstones and, locally, ultrabasics.

Figure 17 combines these features schematically in a southwest-northeast section across the field.

Even simple modeling of the deep source, then, allows easy study of the remaining gravity features in terms of near-surface geology.

ACKNOWLEDGEMENTS

I thank Rodger Chapman, Julie Donnelly, Gordon Eaton, Carter Hearn, Ben Lofgren, Robert McLaughlin, and Dal Stanley for extensive discussions and early information from their own research. I also thank Carlos Bernal for able assistance in the field and all of the lease holders, land owners, and operators at The Geysers area for their cooperation.

REFERENCES CITED

- Bhattacharyya, B. K., and Morley, L. W., 1965, The delineation of deep crustal magnetic bodies from total field aeromagnetic anomalies: *Jour. Geomagnetism and Geoelectricity*, v. 16, p. 237-252.
- Bott, M. H. P., and Smith, R. A., 1958, The estimation of the limiting depth of gravitating bodies: *Geophys. Prosp. [Netherlands]*, v. 6, p. 1-10.
- Brice, J. C., 1953, *Geology of the Lower Lake quadrangle*, California: California Div. Mines Bull. 166.
- Byerly, P. E., 1966, Interpretation of gravity data from the Central Coast Ranges and San Joaquin Valley, California: *Geol. Soc. America Bull.*, v. 77, p. 83-94.
- Chapman, R. H., 1966, Gravity map of Geysers area: California Div. Mines and Geology Mineral Inf. Service, v. 19, p. 148-149.
- , 1975, Geophysical study of the Clear Lake region, California: California Div. Mines and Geology Bull.
- Chapman, R. H. and Bishop, C. C., 1974, Bouguer gravity map of California—Santa Rosa sheet: California Division of Mines and Geology, compiled in 1970.
- Eaton, G. P., Christiansen, R. L., Iyer, H. M., Pitt, A. M., Mabey, D. R., Blank, H. R., Jr., Zietz, I., and Gettings, M. E., 1975, Magma beneath Yellowstone National Park: *Science*, v. 188, no. 4190, p. 787.
- Garland, G. D., 1951, Combined analysis of gravity and magnetic anomalies: *Geophysics*, v. 16, p. 51-62.
- Garrison, L. E., 1972, Geothermal steam in The Geysers-Clear Lake region, California: *Geol. Soc. America Bull.*, v. 83, p. 1449-1468.
- Grant, F. S., and West, G. F., 1965, *Interpretation theory in applied geophysics*: New York, McGraw-Hill, 583 p.
- Hamilton, R. M., and Muffler, L. J. P., 1972, Microearthquakes at The Geysers geothermal area, California: *Jour. Geophys. Research*, v. 77, p. 2081-2086.
- Isherwood, W. F., and Chapman, R. H., 1975, Principal facts for gravity stations in The Geysers-Clear Lake region, California: U.S. Geol. Survey open-file report 75-106, 15 p.
- Lange, A. L., and Westphal, W. H., 1969, Microearthquakes near The Geysers, Sonoma County, California: *Jour. Geophys. Research*, v. 74, p. 4377-4378.
- Murase, T., and McBirney, A. R., 1973, Properties of some common igneous rocks and their melts at high temperatures: *Geol. Soc. America Bull.*, v. 83, p. 3563-3592.
- Nettleton, L. L., 1940, *Geophysical prospecting for oil*: New York, McGraw-Hill, 444 p.
- Odegard, M. E., and Berg, J. W., Jr., 1965, Gravity interpretation using the Fourier integral: *Geophysics*, v. 30, p. 424-438.
- Saad, A. H., 1969, Magnetic properties of ultramafic rocks from Red Mountain, California: *Geophysics*, v. 34, p. 974-987.
- Spector, A., and Grant, F. S., 1970, Statistical models for interpreting aeromagnetic data: *Geophysics*, v. 35, p. 293-302.
- U.S. Geological Survey, 1973, Aeromagnetic map of the Clear Lake area, Lake, Sonoma, Napa, and Mendocino Counties, California: U.S. Geol. Survey open-file report.

GEOTHERMAL RESERVOIR INTERPRETATION FROM CHANGE IN GRAVITY

William Isherwood
U.S. Geological Survey
Menlo Park, California 94025

Precision gravity methods provide new information regarding geothermal reservoir mechanisms and depletion. This paper discusses the principles of present interpretations and early conclusions from two producing geothermal fields, Wairakei, in New Zealand, and The Geysers, California.

The acceleration of gravity at any point on the earth's surface is a function of numerous factors including the mass distribution beneath the point and its absolute elevation. A change in the observed gravity at a fixed location in a geothermal field therefore can be interpreted in terms of change in elevation and fluid movement in nearby reservoir rocks, other factors being either corrected for or held constant. Modern gravity meters have sensitivities sufficient to reliably measure differences in gravitational acceleration of between 5 and 10 μgal (10^{-8} m/sec/sec), although changes in gravity measured to date, because they are dependent on baselines established with older equipment, are probably accurate to only about 30 μgal . A 5-10 μgal change can be caused either by several centimeters of elevation change or by the draining of liquid water from a layer about 1 meter thick from an infinite aquifer with 20 percent porosity. Careful repeat measurements of gravity provide the potential for detecting mass loss (depletion) from geothermal reservoirs, which can be used for determining the percentage recharge occurring, for detecting areas of drainage, and to test various reservoir models, provided that elevation change is measured independently and corrected for and production data are available. In practice this requires coordination with a first-order leveling program.

Despite theoretical expectations, it must be demonstrated that changes in gravity observed are in fact related to removal of geothermal fluid--especially when so many other effects could contribute to any one measurement. Trevor Hunt of New Zealand established the first practical test of precision gravimetry in geothermal studies at the Wairakei field (Hunt, 1970, 1977). After correcting for elevation changes and showing that other effects such as changes in local topography and differential changes in ground-water level could be neglected, Hunt's demonstration of the method came largely from the observations of gravity decreases correlating spatially with the limits of the exploited field. The resultant pattern was one of maximum gravity decrease centered on the main production borefield and tapering smoothly toward zero changes at several kilometers distance. This same part of the field showed moderate subsidence, a further suggestion of net loss of fluid from the system.

A program patterned on the New Zealand study was set up at The Geysers, California (Isherwood, 1977). But the situation is, for various reasons, much more complicated. Landsliding and active tectonics could be producing vertical ground motions unrelated to fluid withdrawal. As an underpressured, "vapor-dominated" system, The Geysers may have only slight subsidence potential because internal pore pressure is apparently not contributing much support to the rock matrix. Also, if the reservoir contained only vapor in the pore space (including, of course, fractures), then the mass loss conceivably is distributed over a large volume or is occurring at some distance from the well bores. Finally, California's present severe drought could change local ground-water levels. Despite these complications, areas of gravity decreases (with respect to a reference station outside the field) closely match areas of production (fig. 1). Thirty-six of the gravity stations coincide with remeasured elevation points. Figure 2 shows the correlation between subsidence and gravity decrease. The resultant correlation of +0.72 is particularly significant, inasmuch as changes of gravity caused by landslides or block tectonic elevation changes would produce a correlation coefficient of -1.

Both Wairakei and The Geysers clearly show a net mass loss in the reservoir region. Determining the actual mechanism of loss is prerequisite to understanding the reservoir dynamics. For both reservoirs, the most likely mechanism is the replacement of hot liquid water ($\rho_{\text{water}} @ 240^{\circ}\text{C} = 0.8 \text{ g/cm}^3$) in the pore space by water vapor ($\rho_{\text{steam}} @ 240^{\circ}\text{C} = 0.02 \text{ g/cm}^3$) and removal of excess fluid. Where this flashing takes place can be further constrained (as will be explained later). Alternate mechanisms of mass loss seem unlikely or inadequate to explain observed changes. For example, evacuating steam of density 0.02 g/cm^3 from the pores of a vapor-dominated system could cause only about 0.001 g/cm^3 bulk density change (using the 5 percent porosity suggested for vapor-dominated systems); to change gravity by the amounts observed at The Geysers in just 2 1/2 years would require depletion to a depth of at least 9 km for a 40 km^2 field. Changes in density of the liquid or rock, though possible, would presumably be toward greater density, due to reservoir cooling. Similarly, any change in porosity (presumably due to subsidence) would tend to increase bulk density and consequently not contribute to a gravity decrease.

If gravity measurements are made with sufficient coverage and precision to permit accurately contouring the change in gravity over an area, then Gauss' potential theorem can be used to determine the total change of mass (in this case the net fluid loss) without assuming a shape or depth of the source. Hunt used this approach in studying mass loss from the Wairakei field over a 16-year period. Comparison of the mass loss calculated from gravity with the measured mass of produced fluid showed as much as 90 percent net loss during the early years of exploitation but an apparent increase in natural recharge percentage with prolonged production. If a true steady-state situation is eventually attained, the initial unfavorable

trends in lowered pressure, flow rate, etc., may be temporary, at least for some hot water systems. Continued monitoring will be required to confirm whether an equilibrium recharge rate has indeed been reached at Wairakei.

Preliminary calculations of the mass balance at The Geysers by Gauss' theorem show the mass loss to be essentially the same as the calculated mass of produced steam during the same time. Because of the limited areal coverage and duration of the study, this estimate of 0 percent recharge could be in error by as much as 20 percent. This uncertainty should be reduced in a few years as instrumentation is upgraded and the net is expanded to more gravity stations and more than 150 km additional first-order leveling lines. Still unresolved are (1) whether lack of recharge is related to the drought, and (2) barring eventual recharge, how large a volume can be tapped by the present wells.

Interpretations regarding the distribution of mass loss are not unique, although the "forward calculations" are. That is, if we know the net mass removed and its distribution (shape and depth) the gravity effect at all surface points can be calculated. Through such calculations more substantial conclusions about The Geysers geothermal reservoir have been made. The work at The Geysers typifies the additional information that can be derived. Certain assumptions are useful in simplifying computations. Recognizing that the distribution of mass loss may be complicated in detail, the first assumption is that we may treat the loss as a body or small number of bodies with some uniform density change. Due to the normally smooth character of the gravity field and distance from source to observation, this bulk characterization is considered reasonable. That the bulk density change is not exactly known scarcely affects the results. Representative parameters are established using reservoir properties considered reasonable on the basis of geologic and reservoir engineering studies.

For convenience of calculation, the shape of the mass loss is assumed to be that of a cylinder with its axis vertical (fig. 3). Using the mass of the net produced fluid (estimated at 7.5×10^{10} kg over 2 1/2 years) as a maximum loss, the gravity effect at the surface can be calculated for various combinations of cylinder radius and depth. Figure 4 shows such a matrix for a bulk density change of 0.04 g/cm^3 . (This density change would result from the flashing of hot water of density 0.82 g/cm^3 to steam of density 0.02 g/cm^3 if the liquid initially saturated a uniform 5 percent porosity or filled half the pore volume at 10 percent porosity.) For instance, a cylinder of 1 km radius, which would have a thickness of about 600 m (density contrast and mass given), would have a gravity effect directly above it of $129 \mu\text{gal}$ if the top were 1500 m deep and bottom about 2100 m deep and an effect of only $84 \mu\text{gal}$ if the top were 2000 m deep and bottom at about 2600 m. Because a change in the radius changes the thickness, an optimum radius produces the maximum effect--in all cases decreasing with depth. The shaded zone on figure 4 represents the observations at The Geysers, where a

maximum observed change is about 120 ± 30 μgal . Within this shading, the observed changes could be accounted for by this set of parameters and zero recharge. If the true parameters fall to the left (shallower) side of the shading where the calculated effect is too large, the observed change could have been caused by less mass loss--indicating partial recharge. To the right of the shaded zone the calculated effect is less than observed, showing (1) that there is additional mass loss by some unknown mechanism or (2) that such a shape-depth combination would be impossible. A change in the density contrast by a factor of 2 changes the depth to the center of the cylinder only a few percent at the depth range of interest, although the top and bottom will vary more to accommodate the appropriate change in cylinder thickness. Similarly, the maximum depth to the mass loss can not be increased greatly by considerations of shape (e.g. sphere versus cylinder) and it actually decreases if the regions around individual production sites are considered separately. Consequently, if we assume no additional mass loss beyond what has been produced, we can rule out the possibility of steam boiling solely off a water table deeper than about 2500 m. Some contribution from this depth is not precluded, but the major loss must be shallower, probably near the 1-2 km depth of most well completions. This supports the model of Truesdell and White (1973) which proposes liquid water throughout the reservoir, such water flashing to steam as a direct result of pressure decrease caused by exploitation.

Regions of drainage may be recognized by comparing a map of elevation-corrected changes in gravity to areas of known production. Asymmetry to the pattern of gravity change at Wairakei (Hunt, 1977) suggests greatest depletion to the west of the main production borefield. At The Geysers, some of the critical stations surrounding the present field have not yet been leveled to provide elevation correction. Consequently, although measurements from the stations to the southwest (around power plant 15, fig. 1) are suspect because of their apparent large decreases in gravity, we must await the leveling data for interpretation.

Projections of reservoir longevity at The Geysers and elsewhere will be reliable only when we have a longer period of observation and our interpretation techniques are refined. Gravity changes reflect what has happened between measurements, and, in conjunction with other reservoir data, can eventually allow for projections which will lead to informed management of reservoirs.

REFERENCES

- Hunt, T. M., 1970, Gravity Changes at Wairakei Geothermal Field, New Zealand: Geol. Soc. America Bull. v. 81, p. 529-536.
- Hunt, T. M., 1977, Recharge of Water in Wairakei Geothermal Field Determined from Repeat Gravity Measurements: New Zealand Jour. Geology and Geophysics, v. 20, p. 303-317.
- Isherwood, W. F., 1977, Reservoir Depletion at The Geysers, California: Geothermal Resources Council, Transactions, v. 1, p. 149 (summary).
- Truesdell, A. H. and White, D. E., 1973, Production of Superheated Steam from Vapor-Dominated Geothermal Reservoirs: Geothermics, v. 2, p. 154-173.

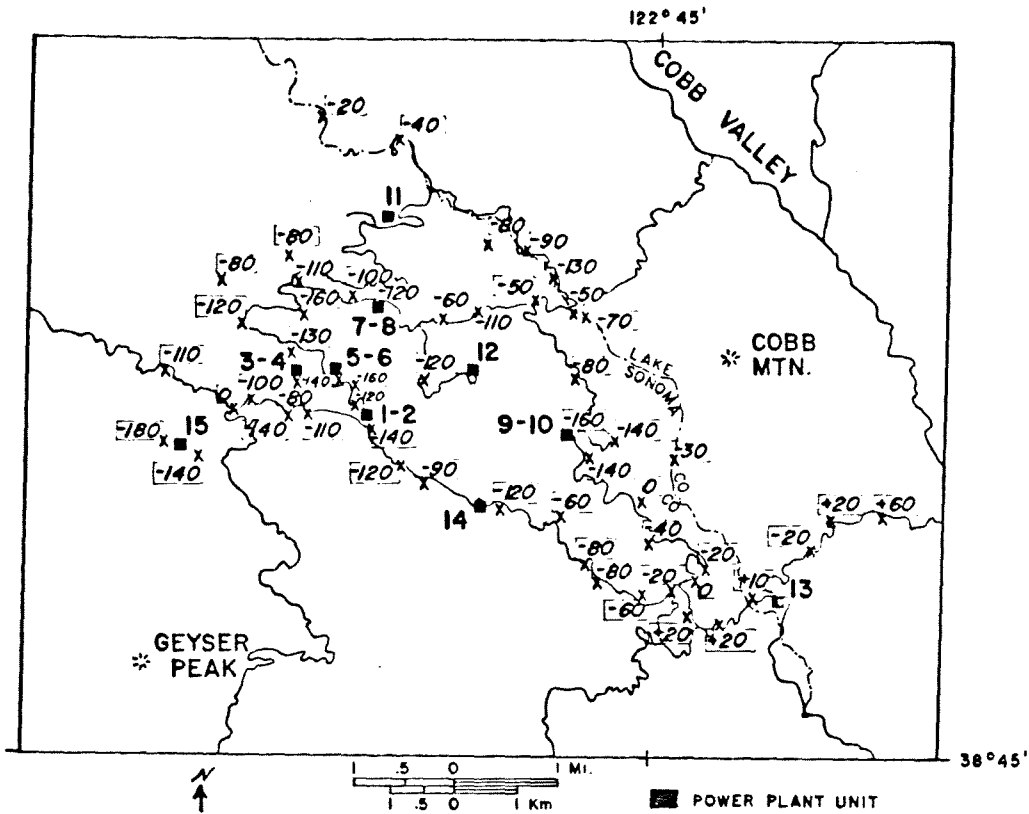


Figure 1. GRAVITY CHANGES, IN μGAL , BETWEEN JULY 1974 AND FEB. 1977, THE GEYSERS GEOTHERMAL AREA, CALIFORNIA.

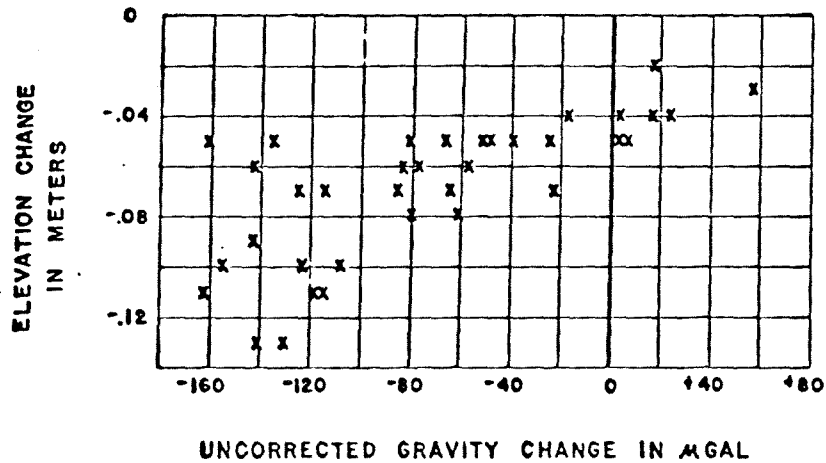


Figure 2. Relation between gravity change (July 1974 to Feb. 1977) and elevation change (late 1973 to late 1975), at The Geysers, California.

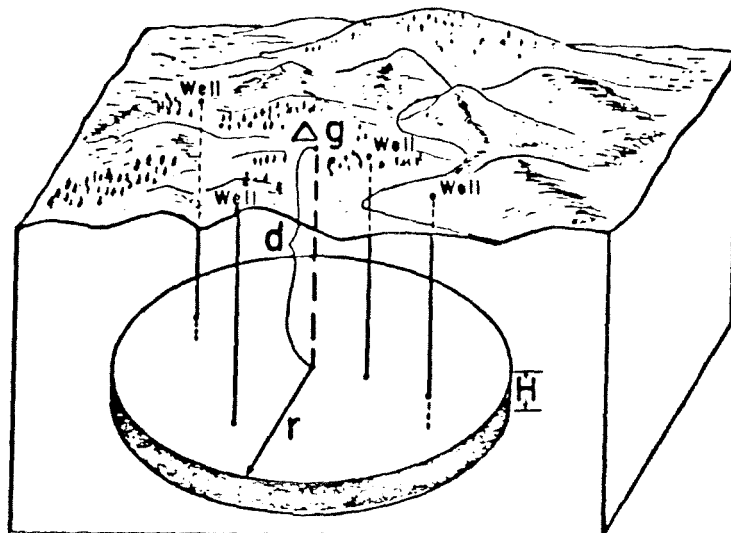


Figure 3. CYLINDRICAL APPROXIMATION TO MASS LOSS

$$\Delta g \text{ (in } \mu\text{gal)} = 41.85 \rho \left[H - \left(\sqrt{(d+H)^2 + r^2} - \sqrt{d^2 + r^2} \right) \right]$$

(in meters)

Radius (km)	Depth to top (meters)						
	0	500	1000	1500	2000	2500	3000
.1---	167	16	8	5	4	3	3
.5---	750	275	136	62	55	40	31
1.0---	726	387	213	129	84	59	43
1.5---	405	272	177	117	81	58	44
2.0---	242	182	132	96	70	53	41
2.5---	156	125	98	75	58	46	36
3.0---	110	87	75	60	49	39	32
3.5---	81	69	59	49	41	34	28
4.0---	62	55	47	40	34	29	25

Figure 4. GRAVITY EFFECT OF CYLINDER WITH $\Delta\rho = 0.04 \text{ g/cm}^3$
(in μgal) FOR MASS OF TOTAL PRODUCING FIELD

Abnormal P-Wave Delays in The Geysers—Clear Lake Geothermal Area, California

H. M. Iyer, D. H. Oppenheimer, and T. Hitchcock

Abnormal P-Wave Delays in The Geysers–Clear Lake Geothermal Area, California

Abstract. *Large teleseismic delays, exceeding 1 second, are found near Mount Hannah in the Clear Lake volcanic field and in the steam-production area at The Geysers. The delays are superimposed on a general delay field of about 0.5 second extending over the volcanic rocks and the steam reservoir. It is postulated that a magma chamber under the surface volcanic rocks with a core of severely molten rock beneath Mount Hannah and a highly fractured steam reservoir probably underlain by partially molten rock at The Geysers are responsible for the observed delays. Both zones extend to depths of 20 kilometers or more.*

The Geysers geothermal power facility, 130 km north of San Francisco, California, is located in part of one of the few known dry-steam geothermal systems in the world. It is situated southwest of the Clear Lake volcanic field in which rocks range in age from 2×10^6 to 10,000 years (1). Geologic and geophysical evidence suggests that a crustal magma chamber is present under the volcanic field and is probably the heat source responsible for the observed geothermal phenomena in the area (2–5). A complex system of faults and fractures is thought to provide paths for deepwater circulation, and the resulting hydrothermal system furnishes the superheated steam that drives The Geysers turbines to produce electricity.

Seismic wave velocities are sensitive to the presence of both magma, hypothesized to be present under the Clear Lake volcanic field, and fractured rock, indicated by the high permeability in the steam reservoir under The Geysers. It is possible to delineate the shape of low-ve-

locity magmatic bodies and to estimate the velocity contrast with respect to the surrounding regional velocity by using seismic waves from distant earthquakes (teleseisms) (6–8). We examined teleseismic P waves recorded in The Geysers–Clear Lake geothermal area at 26 stations of the telemetered seismic network operated by the U.S. Geological Survey and at 12 portable stations in the area (9). The results are quite unexpected. The seismic waves are delayed over a large area encompassing the geothermal production zone and the volcanic field. Relative delays as large as 1 to 1.5 seconds found at some of the stations indicate a subsurface velocity decrease of 25 percent extending to a depth of 20 km or more. Although a reduction in the velocities of upper crustal material in volcanic and geothermal areas is not surprising, the possibility of an exceptionally large velocity decrease in The Geysers–Clear Lake geothermal area suggests extreme variations in the properties of the underlying material. The implications of such extreme variations, although not clearly understood, are important in assessing the degree of partial melt in the Clear Lake magma system and the characteristics of The Geysers dry-steam reservoir.

Severe changes in wave form occurred in the teleseismic signals recorded at the permanent stations GMK (Mount Konocti), GGL (Glenview), and GSG (Seigler Mountain) located in the Clear Lake volcanic field, station GBO (Black Oaks) located in the steam-production zone (Fig. 1a), and at the portable stations CL05 (located adjacent to GSG in Fig. 1a), CL06, and CL07 (5). The signal distortion made it difficult to determine the

onset of teleseisms. Our study, therefore, is based on 48 teleseisms for which P-wave arrival times could be read with confidence (10). Following standard procedures, we computed (6) residuals with respect to Herrin's travel time tables (11). In order to correct for source and path errors, we obtained relative residuals by subtracting from each value the residual at a reference station located well outside the anomalous area under investigation. We have used NMW (Mark West Springs) and CL02 as reference stations for the telemetered and portable networks, respectively (Fig. 1a). The teleseisms used are mainly from the northwest, southeast, and southwest azimuths. Taken together, these events provide a cone of seismic rays with an angle to the vertical of about 20° , sampling the crust and upper mantle under each station.

The average relative residuals for each of the three azimuth groups are contoured in Fig. 1, b to d. Because of the variation in data quality from station to station, the averages are based on a maximum of 11 and a minimum of two readings per station per azimuth group. The results for the southwest azimuth (Fig. 1b) show that the delay field is dominated by values greater than 1.5 seconds in the vicinity of GGL in the volcanic field, and greater than 1 second in the vicinity of GBO in the steam-production area. This field is superimposed on a wide zone comprising the volcanic field and production area where the delays are greater than 0.5 second. These results suggest that a broad low-velocity zone may underlie not only the region of Quaternary volcanism but also the Mesozoic Franciscan complex to the west, and that abnormally low velocities may underlie Mount Hannah and the steam-production zone. The lateral extent of the anomalous structure is clearly constrained on the south and west sides as shown by the abrupt change of the residuals to near zero values in these directions. However, owing to inadequate station coverage, the definition of the anomaly to the north and east of Clear Lake is quite uncertain. An examination of azimuthal variations in the delay patterns shows the northwest delays to be less than the southwest delays by 0.7 second at GGL and 0.5 second at GBO (Fig. 1, b and c). Similarly, significant changes in the spatial variation of delays are also observed between the northwest and southeast azimuths (Fig. 1, c and d).

The first step in interpreting the observed delays is to estimate the effect of near-surface structure. Using data from calibration explosions detonated by the

Length Limit for Reports: The average length of individual Reports in *Science* has been steadily increasing. At the same time, the number of pages allotted to Reports has remained constant and cannot be increased. The net result has been that fewer Reports on fewer subjects are being published, many that receive excellent reviews must be rejected for lack of space. The overall rejection rate is more than 80 percent. In order to increase the acceptance rate we will enforce the length requirements: one to seven double-spaced manuscript pages of text, including the references and notes, and two displayed items which together will occupy no more than half of a published page. Long Reports are subject to delays in reviewing and editorial consideration. After Reports are reviewed, those that exceed the length limit will be returned to authors for shortening before a final decision is made. Reports that are short will not be subject to these delays.

Statistical Review of Papers: As part of our continuing effort to improve the quality of papers published in *Science*, Reports and Articles that depend on statistical inference for their conclusions will be sent to statisticians (in addition to other referees) for review.

U.S. Geological Survey, Major and McEvilly (12) and Warren (13) have modeled the top 3 km of the crust in The Geysers-Clear Lake area. Their results show that the velocities in the upper layers under the volcanic field and the steam-production zone are not abnor-

mally lower than those in the surrounding rock and hence cannot account for the large teleseismic delays. Moreover, at most stations used in this study, the deviations of the P-wave arrival times from the explosions with respect to travel times predicted by the crustal models

are, in general, negligible and indicate that no localized anomalous structures are present immediately under the stations. The exceptions are stations GGL and GSG where the refraction data (according to Warren's model) imply that surface corrections as high as 0.4 second due to shallow low velocities may be required. However, these stations show maximum teleseismic delays of 1.5 and 0.9 second, respectively; these results require the postulation of deeper low-velocity structure to explain a large portion of the teleseismic delays.

Assuming that the delays are caused by a deep low-velocity body in the crust, we have attempted a simple inversion of the teleseismic data to estimate the dimensions of the body and the velocity contrast inside it relative to the surrounding regional velocity. The procedure used is to compute the length of the anomalous ray path required to cause the observed delays for a given velocity contrast (6, 8). Knowing the anomalous path length, the angle of emergence of the seismic ray, the azimuth of the seismic source, and the depth to the top of the low-velocity region, we can compute the *x*, *y*, and *z* coordinates of the lower surface of the anomalous body.

We have assumed that the top of the body is flat and located at a depth of 4 km. We assume a flat top, although it may not be physically realistic, purely for mathematical convenience. This assumption does not introduce serious errors in the delineation of the anomalous body. In the absence of data from detailed seismic reflection and refraction surveys, we have only indirect evidence to place any constraint on the depth to the top of the body. The assumed depth of 4 km is therefore tentative and based on the paucity of earthquakes below this depth (14). The reduction in seismicity can be attributed to several mechanisms, including elevated temperatures causing stable sliding rather than stick slip (15), high pore pressures which reduce the effective stress across fault planes, and aseismic slip (creep). However, the simultaneous occurrence of low velocity and low seismicity may also be due to the presence of partially molten or fractured rock incapable of supporting shear stress at shallow depths greater than 4 km in The Geysers-Clear Lake geothermal area. Results of the inversion satisfying the above criteria are shown in Fig. 2, a and b. This model is nonunique and serves only as a conceptual point of view. The model shows a large triangular region comprising the Clear Lake volcanic field and the steam-production zone in which there is an average veloc-

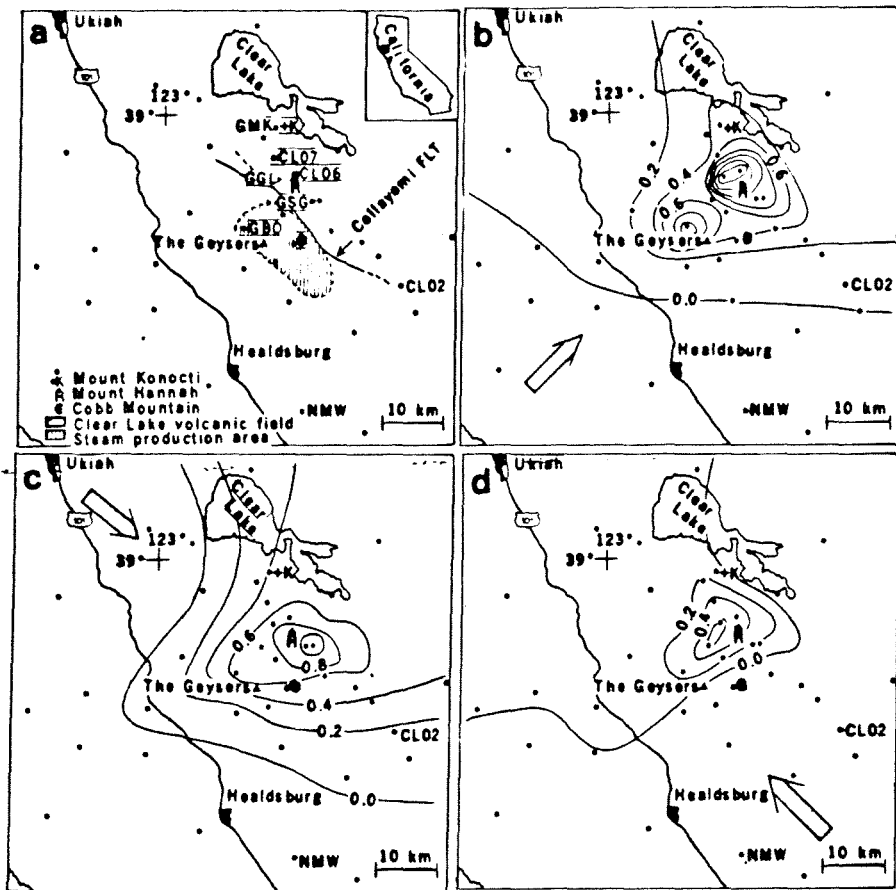


Fig. 1. (a) Station locations (dots) in The Geysers-Clear Lake region. The inferred approximate outlines of the Clear Lake volcanic field (dotted) and the dry-steam (hachured) areas are shown. Relative teleseismic P-wave residual contour maps for (b) southwest events, (c) northwest events, and (d) southeast events are shown. The contour interval is 0.2 second. The arrows in (b) to (d) represent the direction of approach of teleseismic signals.

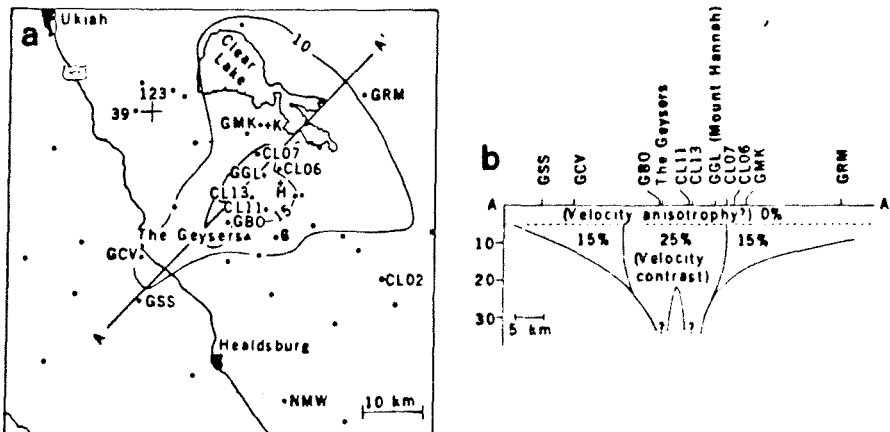


Fig. 2. (a) Calculated depth to the bottom of the anomalous body required to account for the observed delays. The top of the body is assumed to be flat and at a depth of 4 km. The velocity decrease between the 10- and 15-km contours is assumed to be 15 percent and within the 15-km contour (shaded area) to be 25 percent. (b) Conceptual model of the subsurface structure and the percentage of decrease in velocity along the line A-A' of (a) passing through the production and volcanic zones.

ity decrease of about 15 percent with respect to regional velocity. An important feature of the model is a core region beneath Mount Hannah and the steam-production zone where a 25 percent decrease in velocity is required to satisfy the data (shaded area in Fig. 2a). The low-velocity body extends to an average depth of 10 to 15 km, with the core regions extending to 20 km or more. The shape of the low-velocity body is not well defined, and there are thus deficiencies in our modeling procedure.

A reduction of the compressional seismic wave velocity within the earth can be due to a variety of factors (7). However, geologic and other geophysical data support our observations and indicate the presence of a magma body under the Clear Lake volcanic field. Chapman (3) has suggested the possibility of a magma chamber under Mount Hannah to explain the large gravity low in the region. Isherwood (4) inverted gravity and aeromagnetic data to model a magma chamber 10 to 15 km in diameter under Mount Hannah. Hearn *et al.* (2) have also shown that geologic and geochronological evidence strongly support the hypothesis that an active magma chamber may be present under the Clear Lake volcanic field. The attenuation of teleseismic body waves (5) and the shallow seismicity (14) are other geophysical observations that lend support to the magma chamber hypothesis. We propose, therefore, that the low-velocity body under Mount Hannah represents rock in a state of partial melting. Unfortunately, few laboratory data exist to make possible an estimation of the degree of partial melting from seismic data. Even a theoretical model, such as that proposed by Walsh (16) in which partial melting occurs in randomly oriented penny-shaped cracks, requires knowledge of both P- and S-wave velocity and attenuation to obtain this estimate.

It is possible that the dry-steam reservoir associated with The Geysers may be responsible for some of the P-wave delays observed in that zone. Laboratory data by Nur and Simmons (17) show that the compressional velocity in dry, porous rocks is significantly lower than in the fluid-saturated condition. However, the seismic refraction survey of Majer and McEvilly (12) at The Geysers does not show a sufficient velocity anomaly in the top 3 km to account for the observed teleseismic delays. Thus, any delay attributed to the dry-steam field must be occurring at depths greater than 3 km, necessitating that the fracture system extend to about 20 km. Alternatively, the magma chamber postulated to be

beneath Mount Hannah may extend beneath The Geysers and together with an overlying fracture system may be responsible for the observed delays. The strong azimuthal variation of delays at stations near The Geysers (Fig. 1) also suggests that an anisotropic velocity distribution in either the fractured dry-steam system or within the magma body may be present. Walsh (18) has shown that the compressibility of rocks with cracks is anisotropic. However, since the maximum velocity decrease occurs along a plane perpendicular to the direction of crack orientation and since the teleseismic waves travel at an angle to the vertical of about 20°, a complex fracture model will be required.

A significant feature of our model is a core region in which the velocity decrease may be as high as 25 percent. Data from other areas of Quaternary volcanism such as Yellowstone National Park, Wyoming, and Long Valley, California, show the existence of magma chambers requiring 10 to 15 percent velocity contrast (7, 8). Whether the higher velocity decrease postulated at Mount Hannah means that the magma chamber in this locality is in a higher state of partial melt than that under Yellowstone or Long Valley cannot be determined until shear wave velocity and attenuation data are collected.

H. M. IYER
D. H. OPPENHEIMER
T. HITCHCOCK

*Office of Earthquake Studies,
U.S. Geological Survey,
Menlo Park, California 94025*

References and Notes

1. B. C. Hearn, J. M. Donnelly, F. E. Goff, in *Proceedings of the Second U.N. Symposium on the Development and Use of Geothermal Resources* (Government Printing Office, Washington, D.C., 1976), vol. 1, pp. 423-428.
2. ———, *U.S. Geol. Surv. Prof. Pap.*, in press.
3. R. H. Chapman, *California Division of Mines and Geology, Special Report 116* (1975), 23 pp.
4. W. F. Isherwood, in *Proceedings of the Second U.N. Symposium on the Development and Use of Geothermal Resources* (Government Printing Office, Washington D.C., 1976), vol. 2, pp. 1065-1073.
5. C. Y. Young and R. M. Ward, *U.S. Geol. Surv. Prof. Pap.*, in press.
6. H. M. Iyer, *Nature (London)* **253**, 425 (1975).
7. ——— and R. M. Stewart, in *Proceedings of the Chapman Conference on Partial Melting in Upper Mantle* (State of Oregon Department of Geology and Mineral Industries, Portland, 1977), pp. 281-299.
8. D. W. Steeples and H. M. Iyer, *J. Geophys. Res.* **81**, 849 (1976).
9. D. W. Steeples and H. M. Iyer were the first to observe the large teleseismic delays at The Geysers, using data from six seismic stations [see *Proceedings of the Second U.N. Symposium on the Development and Use of Geothermal Resources* (Government Printing Office, Washington, D.C., 1976), vol. 2, pp. 1202-1203]. More detailed but preliminary results were presented by H. M. Iyer and T. Hitchcock at the fall annual meeting of the American Geophysical Union, San Francisco, 1975 [*Eos (Trans. Am. Geophys. Union)* **56**, 1020 (1975)] and by H. M. Iyer, D. H. Oppenheimer, and T. Hitchcock at the Geothermal Resources Council annual meeting, Hilo, 1978.
10. We used a computer capable of displaying several traces simultaneously to scale and time-shift traces for visual correlation of the P phases. This ensured an estimated accuracy of 0.1 second for the arrival time readings.
11. E. Herrin, *Bull. Seismol. Soc. Am.* **58**, 1196 (1968).
12. E. Majer and T. V. McEvilly, *Geophysics*, in press.
13. D. H. Warren, *U.S. Geol. Surv. Prof. Pap.*, in press.
14. C. G. Bufe, S. M. Marks, F. W. Lester, R. S. Ludwin, M. C. Stickney, *U.S. Geol. Surv. Prof. Pap.*, in press.
15. W. F. Brace and J. D. Byerlee, *Science* **168**, 1573 (1970).
16. J. B. Walsh, *J. Geophys. Res.* **74**, 4333 (1969).
17. A. Nur and G. Simmons, *Earth Planet. Sci. Lett.* **7**, 183 (1969).
18. J. B. Walsh, *J. Geophys. Res.* **70**, 381 (1965).

23 October 1978, revised 22 February 1979

LARGE TELESEISMIC P-WAVE DELAYS IN
THE GEYSERS-CLEAR LAKE GEOTHERMAL AREA

by

H. M. Iyer

David H. Oppenheimer

Tim Hitchcock

Jeffrey N. Holoff

John M. Coakley

U.S. Geological Survey

Menlo Park, California

Contents

	Page
Abstract.....	3
Introduction.....	4
Data analysis and results	6
Reading of teleseisms.....	7
Computation of residuals.....	8
Distribution of teleseisms.....	10
Spatial distribution of relative residuals.....	10
Discussion	14
Effect of local geologic structure.....	16
Deep delay sources.....	19
Magma chamber under Mount Hannah.....	21
Low-velocity body associated with the dry-steam reservoir.....	23
Conclusions.....	25
References cited.....	26

Illustrations

	Page
Figure 1. Generalized geologic map of the Geysers-Clear Lake region.	6a
Figure 2. Residual gravity map of the Geysers-Clear Lake region.	6b
Figure 3. Map showing inferred approximate outlines of vapor-dominated and steam-production zones in the Geysers-Clear Lake region.	6c
Figure 4. Two typical teleseisms recorded by the seismic network in the Geysers-Clear Lake region.	7a
Figure 5. Illustrations showing computer manipulation of seismograms.	8a
Figure 6. Graphs showing variation of relative residuals as a function of distance.	11a
Figure 7. Relative residual contour maps.	11b
Figure 8. Profile of northwest, southeast residual values and gravity along line AA' of figure 7 <u>B</u> , <u>C</u> .	15a
Figure 9. Maps showing calculated depth to bottom of anomalous body required to account for observed delays.	20a
Figure 10. Map showing composite of figure 9 <u>A</u> , <u>B</u> .	21a
Figure 11. Conceptual model of subsurface structure and percent decrease in velocity in The Geysers-Clear Lake region.	25a

ABSTRACT

It has long been postulated that the Clear Lake volcanic field is underlain by a magma chamber. In order to see if a magma chamber is present and, if so, to delineate its shape and physical properties, teleseisms recorded by 26 telemetered and 12 portable seismic stations were examined. Severe signal shape changes and large teleseismic delays were observed at stations located on the volcanic field centered at Mount Hannah and at the geothermal production zone at The Geysers. For teleseisms in the southwest azimuth, the average delays were 1.5 seconds at Mount Hannah, 0.9 s at Siegler Mountain, and 1.0 s at Black Oaks in the steam production zone. For events in the other azimuths the delays were less by as much as 0.5 s though still considered quite significant. The spatial distribution outlines a broad region of 0.5-s delay centered at Mount Hannah and extending into the production zone to the southwest, with large delays exceeding 1 s near The Geysers and at Mount Hannah. Results of a seismic refraction survey in the region show that the delays cannot be attributed to anomalous velocities associated with the complex geologic structure near the surface, and hence a deep low-velocity body in the upper crust is required to explain their presence. A simple modeling technique involving computation of the length of anomalous ray paths is used to determine the size of the low-velocity body. The results show that a plausible model is one in which the low-velocity body about 10 km thick with compressional velocity lower than normal by 15 percent and extends under the young Clear Lake volcanic field and the

steam production zone. The body also has a deep core underlying Mount Hannah and part of the production zone in which the velocity decrease is about 25 percent. We believe that the low-velocity body under the volcanic zone is composed of partially molten rock, and that under the production area is composed of fractured rock filled with dry steam with or without an underlying magmatic body.

INTRODUCTION

It has long been postulated that a reduction in P- and S-wave velocities and strong S-wave attenuation can be expected in regions of Cenozoic volcanism, but few actual data were available to substantiate these claims. Kubota and Berg (1967) and Matumoto (1971) used the observed strong attenuation of S waves from nearby earthquakes to postulate the presence of several magma pockets under the Mount Katmai volcanic region, Alaska. Only during the last few years have teleseismic P waves been used to probe the structure of the crust and upper mantle under volcanic areas. Iyer (1975) found teleseismic delays in excess of .4 s in Yellowstone National Park, Wyo., and interpreted them in terms of a deep crustal and upper mantle magma chamber. Subsequent work has shown that the magma body, which extends to depth of 150-250 km, has a horizontal extent almost as large as the Yellowstone caldera at the surface but increases with depth (Iyer, 1979). Steeples and Iyer (1976a, 1976b) found nearly 0.5 s relative teleseismic delays in Long Valley, Calif., another potential geothermal area with surface volcanic and

thermal expressions. The spatial pattern of the delays and their magnitude are thought to be caused by a magma body approximately 10 km in diameter beneath the central part of the caldera. The compressional-wave velocity inside the body was estimated to be 10 to 15 percent less than in the surrounding rock. In another active geothermal region, the Imperial Valley, Calif., preliminary study of teleseisms gave inconclusive results (Steeple and Iyer, 1976a). Recently, however, Savino and others (1977), using a technique of combined inversion of teleseismic and gravity data, showed that in the Imperial Valley, the crust under the geothermal areas outlined by high heat flow is thinner than elsewhere. Teleseismic delays of about 0.2 s, observed in another geothermal area in the Coso Range of southern California, have been shown to be caused by a low-velocity body at a depth of 10 km beneath the area where recent rhyolitic volcanism, high heat flow, and hydrothermal activity are present (Reasenber and others, 1979).

Steeple and Iyer (1976a) first presented preliminary observations of large delays in the vicinity of The Geysers geothermal area. In this paper and a summary paper (Iyer and others, 1979), we present evidence that large teleseismic delays are indeed present in the volcanic field and the geothermal production zone of The Geysers-Clear Lake region. We show that the probable cause of the delays is a body of low-velocity material in the upper crust.

The Geysers is one of the very few dry-steam systems known in the world. It is located southwest of the Clear Lake volcanic field (fig.), which ranges in age from 2 m.y. to 10,000 years (Donnelly and others, his volume). A strong gravity low with amplitude of approximately -25 gal in the region (fig. 2) has been interpreted as representing the

presence of a shallow magma chamber (Isherwood, this volume). Goff and others (1977), analyzing the geochemistry of thermal waters and available geophysical data, postulated a dual hydrothermal system for the Geysers-Clear Lake region, composed of a hot water system located under the volcanic zone between Clear Lake and the Collayomi fault zone and a vapor-dominated system southwest of Clear Lake under The Geysers (fig. 3; Goff and others, 1977, fig. 5). These studies suggest that the teleseismic residual (P-delay) technique would be useful in the Geysers-Clear Lake area to delineate the magmatic heat source in the volcanic zone and the steam reservoir under the production zone.

Figs. 1, 2, 3 near here

DATA ANALYSIS AND RESULTS

The U.S. Geological Survey has been monitoring the seismicity of the Geysers-Clear Lake region since May 1975, using part of the extensive telemetered seismic network in northern California. In this study we analyzed teleseisms recorded during 1976 and 1977 by 26 stations of this network located between Santa Rosa and Clear Lake (fig. 2, 3). The region south of Clear Lake, the area of study, includes the locations of current geothermal steam production, recent volcanic flows, and the gravity anomaly cited above. In addition to the permanent network, a northwesterly profile of 12 closely spaced portable seismic stations passing through the center of the Mount Lassen gravity anomaly was in

operation during July to September 1976. Information regarding the temporary and permanent stations is given in table 1.

Reading of teleseisms

Severe signal-shape changes were observed at stations GMK (Mount Konocti), GGL (Glen View), GSG (Siegler Mountain), and GBO (Black Oaks), in comparison to other recording stations. Stations GMK, GGL, and GSG are located on the Clear Lake Volcanics, and GBO is located on the steam-production zone (fig. 1, 3). These changes in signal shape made it difficult to pick the onset of teleseisms recorded by the network; hence, it was necessary to reject a large number of events. Our present study is, therefore, based on only a small fraction of recorded events for which the P-wave arrival times could be read with a reasonable degree of confidence. Figure 4 shows two typical teleseisms recorded by the telemetered network. The event originating near the Bonin Islands shows a drastic signal shape change at GGL and less severe, though noticeable changes, at GBO and GMK. The northern Chile event shows strong alternation of signal at GMK. Where extreme variation in signal shapes resulted in ambiguous picks, those stations were rejected for that event.

Fig. 4 near here

Stations CL05, CL06, and CL07 of the portable network also showed very severe signal-shape changes, and, hence, few readings from these stations were used in this study. Young and Ward (this volume) have examined in detail the signal shape changes and attenuation in the Geysers - Clear Lake area using our data from the portable network.

An Eclipse computer was used to analyze the teleseisms recorded by the permanent network. Data telemetered into Menlo Park, Calif. were multiplexed with IRIGE time code from a digital chronometer and WWVB radio time code and recorded on 1 inch magnetic tape. The computer was used to search the time code, demultiplex and digitize the signals, and display the data on a cathode ray tube for interactive manipulation. A digitizing rate of 100 samples per second was used for all events in this study. An interactive picking algorithm allows the user to scale and time-shift individual traces for visual correlation and to determine the consistency of phases by lining up the waveform of all traces (fig. 5A, B). Typically, two picks were made per event and were chosen within the first two cycles of the teleseism. The precision of the picks by this method is ± 0.1 s.

Fig. 5 near here

As the 1/2 inch tapes from the portable stations could not be manipulated by the Eclipse system, playbacks of teleseisms were manually picked for first breaks using a criterion similar to that of the permanent stations. Correct picks for stations CL05, CL06, CL07, CL11, and CL13 were quite difficult to make. Again, ambiguous picks were rejected in the analysis.

Computation of residuals

The traveltime from the source of the earthquake to the recording station is calculated by subtracting from the arrival time the earthquake origin time reported in the U.S. Geological Survey's Preliminary Determination of Epicenters (PDE). The theoretical traveltime is calculated from the standard Herrin traveltime tables using the epicentral distance and depth of the event (Herrin, 1968). From the epicenter location, also reported in the PDE, and the station coordinates, the distance and azimuth of the epicenter from the station is computed. Traveltime residuals are then obtained by subtracting from the observed traveltime the theoretical traveltime. Accordingly, a negative residual indicates an arrival earlier than predicted, and a positive residual (delay) indicates an arrival later than that predicted. Such raw residuals contain the contributions from structures in the crust and upper mantle under the recording station, effects associated with differences in station elevations, contributions due to errors in earthquake location (approximately ± 25 km), origin-time errors, and the effects due to earth structure under the earthquake source and along the propagation path of the waves. Together these effects and resulting errors could be, on an average, as high as ± 0.5 second. In addition to these errors, the timing of anything other than first arrivals adds a component to the residuals which is constant for all the stations, neglecting any distortion in signal shape across the seismic array. To correct for these effects, it is common practice to use relative residuals, calculated for each event by subtracting from all raw residuals the raw residual at a reference station. The reference station is normally located well outside the area under investigation. Stations NMS

(Mark West Springs) and CL02 were established as the reference stations for the permanent and temporary networks respectively.

Distribution of teleseisms

The 48 teleseisms analyzed in this study were recorded by both the temporary and permanent networks (table 2). They originate mainly in the northwest, southeast, and southwest azimuths. Normally, the events along the southeast and northwest azimuths have a good distance distribution ranging from 40 to 90 degrees (1 degree = 111 km). These events provide a reverse profile along the northwest-southeast direction and enable the study of crustal and upper mantle structure. The events in the southwest azimuth occur in a narrow distance range of 70 to 90 degrees. Occasionally, events are recorded from other azimuths (for example, Russian nuclear events occur to the north). The angle measured from the vertical at which the seismic rays reach the surface ranges from 16° to 26° for distances 40° to 90° . An optimum use of the total possible distribution of events in distance and azimuth was not achieved because in this study only selected events of superior quality were analyzed. A more detailed study, including a three-dimensional mathematical inversion of teleseismic residual data, is anticipated.

Spatial distribution of relative residuals.

The relative residuals with respect to stations NMW and CL02 have been averaged for each of the three main azimuth groups (table 3). The unaveraged residuals for events along the three prime azimuths as a function of distance

Figs. 6 and 7 near here

at stations GGL, GSG, GMK, and GBO are shown in figures 6A, B, C, and D, respectively. The data have been corrected for elevation differences by assuming a normal surface velocity of 6.0 km/s along the ray path. Results for events from the southwest azimuth exhibit the largest relative residuals (to be called residuals or delays hereafter). For this azimuth the residuals in seconds are shown near station locations in figure 7A. Delays greater than 0.5 s coincide with a region which exhibits a gravity low defined by values less than -15 mgal (fig. 2). The delay field is dominated by large values of 1.5 s at stations GGL and CLO6, 0.9s at station GSG in the vicinity of GGL, and 1.1 s at GBO in the steam production area. The few readings available at stations CL11 and CL13 indicate that the large delays at GBO and GGL represent two separate maxima within the general 0.5-s delay field. Note that the gravity low also exhibits dual minima (fig. 2). Isherwood (this volume) describes the -25 mgal low near the southwest edge of the Quaternary volcanic field as the "Mount Hannah low" and the secondary -15 mgal low in the region of steam production as the "production low". The correspondence between the teleseismic delays and gravity lows suggest that they are both caused by the same bodies composed of material of lower-than-normal compressional velocity and density. A broad, low-velocity zone underlies not only the region of Cenozoic volcanism bounded by Mount Kononkti, Mount Hannah, and Cobb Mountain but also the Mesozoic Franciscan complex to the west. Superimposed on this low-velocity zone are the very low velocities under Mt. Hannah and under the

steam production zone. Note the extremely small relative delays at all the stations to the west and south of the 0.2 s contour; these small values, which are within the noise level of our data, indicate that the crustal structure to the south and west of the anomalous region is fairly homogeneous. This homogeneity over a large area confirms the appropriateness of the choice of reference stations NMW and CLO2. Also, note that the small delays at stations GGP (Geysler Peak), GSM (Socrates Mine), GPM (Pine Mountain), and GCV (Cloverdale) constrain the possible extent of the production zone anomaly to a narrow zone a few kilometers southwest of GBO. In the absence of data in this region, the contours are drawn such that the larger delays lie within the extent of the production low. There is also considerable uncertainty in the definition of the low-velocity zone northeast of the main anomaly. Stations GRT (Round Top Mountain) and GRM (Round Mountain) both show about 0.3 s delay. It is not clear whether these delays are associated with the main anomalies or are due to station effects. Similarly, GHS to the north and NMI to the south show about 0.25 s delays. Because of these uncertainties, the 0.2-s contour is left open on the northeast.

Figure 7B depicts the spatial distribution of average delays for events from the northwest azimuth. Details of the data are given in table 3 and figure 6A - 6D. Figures 6A, 6D, 7A, 7B demonstrate that delays for the northwest azimuth in comparison with the southwest azimuth are lower by about 0.7 s at GGL and 0.5 s at GBO. GSG has roughly the same delay of about 0.9 s for both azimuths, and the residual anomaly is now centered at this station. Note that the dual peaks in delay contours seen for the southwest events do not appear at this azimuth, although the magnitude of the average delay field (0.5 s) and the spatial extent is quite similar for both data sets. As previously noted, the boundaries of the delay field are constrained on all

sides except northeast of the main anomaly. The delays at GHG, GMK, GRT, GRM, and NMT are approximately 0.4 s outlining a broad region northeast of Clear Lake.

As mentioned earlier, the data from the northwest and southeast azimuths, when analyzed together, provide reverse profile information. This reversal in azimuths allows one to determine whether the observed anomalies are associated with surface features or with a deeper structure, such as a magma body. In this context a comparison between the northwest delay pattern (fig 7B) with the southeast pattern (fig. 7C) demonstrates that delays greater than 0.5 s occur over a much narrower zone for events arriving from the southeast as opposed to the northwest. Several stations to the south and southeast of GGL, which showed large northwest delays (for example GSG, GCM, and GEG) show very

Fig. 8 near here

small southeast delays. A clear change in the pattern of delays is observed as the source direction is reversed; the change is most apparent south of the main anomaly. Figure 8, a profile of the northwest and southeast delays along a northwest line passing through GGL, clearly demonstrates this effect; the largest delays occur at different locations as the azimuth of travel of the seismic waves is reversed. For the southeast azimuth the largest delay, 0.6 s, occurs at GGL, whereas for the northwest azimuth the largest delay, 1 s, occurs at GSG. Note also that the two delay profiles are different in appearance; the southeast profile has a much narrower peak than the northwest

profile. The peak of the Bouguer gravity profile (fig. 8) coincides with the peak for delays from the southeast. Because of the complex delay patterns, interpretation of the Geysers - Clear Lake data in terms of a simple body at depth will be more complicated than in the case of Long Valley (Steeles and Iyer, 1976b).

DISCUSSION

The large teleseismic delays in the Geysers - Clear Lake region can be broadly divided into three components: (1) the general delay field of 0.5-s amplitude centered at Mount Hannah and extending into the steam production zone to the southwest, (2) the large delays of 1 s and greater observed in the vicinity of Mount Hannah, and (3) the large delay at station GBC in the steam production zone. It is not difficult to interpret these observations in terms of a crustal magma chamber under Mount Hannah and a magma chamber overlain by a dry-steam reservoir under the production zone. In fact, the recent volcanism in the Geysers - Clear Lake region, the availability of thermal energy, and the presence of gravity lows are all indications of the presence of a magmatic heat source. The presence of a magma chamber at depth under Mount Hannah was first suggested by Chapman (1966) to explain the large gravity low in the region. Isherwood (1976), analyzing recent gravity and aeromagnetic data, modeled a magma chamber 10 to 15 km in diameter with its center at a depth of 15 km under Mount Hannah and estimated the magma to be above the Curie temperature (550° C). If it is assumed that there is a velocity decrease of 15 percent inside a magma body of 15 km diameter, a maximum delay of about 0.5 s can be expected over the body. Such a velocity

contrast appears reasonable, based on observations at Long Valley (Steepler and Iyer, 1976a, b) and Yellowstone (Iyer and Stewart, 1977; Iyer 1979), for a crustal magma chamber. However, in order to explain the large delays in excess of 1 s at GBO (over the production zone) and at GGL and surroundings, it is necessary to postulate an unusually large velocity contrast within a body of realistic size or an unusually large body with reasonable contrast. Iyer (1979) found that a body approximately 150-250 km deep with velocity contrast of 5 to 15 percent was required to explain the 1.5 sec delay observed inside the Yellowstone caldera. The spatial distribution of delays for various azimuths in the Geysers - Clear Lake area excludes the deep-body hypothesis and suggests that unusually large velocity contrasts are necessary to explain the large delays.

Magma alone need not be the causative mechanism for low seismic velocities. Theoretical and laboratory results suggest that a large compressional velocity decrease can occur in rock containing an abundance of dry cracks (Birch, 1960; Walsh, 1965). Thus, a dry-steam system, such as that postulated under the production zone, may also be at least partly responsible for the observed delays in that region. A tentative interpretation of the delay field in the Geysers - Clear Lake area, therefore, is that it reflects the presence of a magmatic body in which the seismic velocity decreases by about 15 percent regionally but which has greater velocity decrease under Mount Hannah (due to a higher degree of partial melting than in the surrounding rock) and in the production zone (due to the presence of a dry-steam system over the partially molten rock). However, before pursuing this line of interpretation, it is necessary to examine the effect of local geologic structure on the delays.

Effect of local geologic structure

Seismic wave velocities are a function of local geologic structure near the seismic recording stations. The anomalous stations GGL and GSG are located on the Clear Lake Volcanics, a complex sequence of volcanic rocks overlying an unknown thickness of rocks of the Great Valley sequence and ophiolite on a Franciscan basement complex. Station GBO, showing a maximum delay of 1.0 s for the southwest azimuth, is located over the Franciscan metavolcanic rocks in a region of complex geology (McLaughlin, this volume) and is within the steam production zone (Goff and others, 1977). However, we shall show that results based on seismic-refraction surveys indicate that the delays associated with the top 5 km under these stations are only of the order of a few tenths of a second.

During September 1976 the U.S. Geological Survey fired five shots in the Geysers - Clear Lake area to study the regional crustal structure. In an attempt to evolve velocity and attenuation models for the Geysers steam production zone, Majer and McEvilly (1979) analyzed data from two of the shots (Skaggs Springs and The Geysers) recorded by the U.S. Geological Survey telemetered network and an array of 13, closely spaced portable stations. Using data from a selected group of U.S. Geological Survey stations which are not located on the young volcanic rocks, they found best-fitting regional velocities of 4.49 and 4.98 km/s, respectively, for the top two layers in the upper 3 km of the crust. Station GMK showed the largest refraction delays, 0.2 to 0.45 s, with respect to this model. Stations GBO, GGL, and GSG, which show large teleseismic delays, were delayed by only 0.1 s for the shots, and

were similar to teleseismically non-anomalous station GPK and GGP. Thus, it appears that the contribution to the delays due to structure in the top 2 to 3 km of the crust at these stations is quite small. Using data from the closely spaced array of portable stations oriented in a northeasterly direction perpendicular to the regional geologic trends with the center of the array located about 2.5 km from GBO, Majer and McEvilly postulate a model for the top 3 km of the crust in its vicinity. This model shows a thin layer of high-velocity, high-Q (low attenuation) material underlain by a low-velocity zone of unknown thickness. The important finding from our point of view is that the top few kilometers of the crust contributed only about ± 0.1 s to the anomalous delay observed at station GBO in the production zone and at stations GGL and GSG in the volcanic zone.

Warren (1978, this volume), in an attempt to estimate the seismic velocity in the top few kilometers of the volcanic zone, also analyzed the data from the Skaggs Springs explosion recorded by the group of northeasterly stations including the anomalous stations GGL, GSG, and GBO. He fitted the data to a crustal model in which the top 3.7 km is made up of two layers with velocities 4.2 and 5.2 km/s, respectively. These velocities are somewhat different from those of Majer and McEvilly. However, Warren found more significant differences in the refraction residuals; the delays at stations GGL and GSG are 0.32 and 0.44 sec, respectively. According to Warren's model, GBO does not show any delays. We are unable to explain the discrepancy between the results of Majer and McEvilly (1979) and Warren (this volume). The same data set was used to construct both models, though Warren did not use all the data. The results of Majer and McEvilly suggest that the large

teleseismic delays observed cannot be attributed to local geology. However, Warren's results indicate that even with appropriate correction the largest teleseismic delay at GGL will still exceed 1.0 s, but the delay at GSG will be reduced to about 0.6 s.

The residual at station GMK, based on the refraction model of Majer and McEvilly, is of the same order as the teleseismic delays for the northwest and southwest azimuths (0.4 s). GMK is located on Mount Konocti which is near the region of youngest silicic eruptions in the Clear Lake volcanic field (Donnelly and others, this volume). Two drill holes near Mount Konocti reached a depth of about 1.5 km but did not locate the lower boundary of the Clear Lake Volcanics. The consistency between the magnitudes of delays obtained by refraction and teleseismic surveys indicates that the teleseismic delays at GMK may be due to purely surface effect of the volcanic rocks. The results at GBO, GGL, and GSG show that even with extreme corrections, large delays must still be explained by deeper phenomena. The effect of deeper rocks, such as those of the Great Valley sequence and ophiolite, is difficult to evaluate and may contribute to the large delays observed at GGL and GSG through some fortuitous combination of effects. However, a body 25 km thick in which the velocity is 25 percent less than that of the surrounding material is required to produce a relative delay of 1.0 s. It is quite unlikely that such thick, low-velocity material overlies the Franciscan basement under the Clear Lake Volcanics.

Further evidence that complex surface geology is not a critical factor in interpreting the Geysers - Clear Lake teleseismic delays is provided by the results of a reflection survey conducted by Derlinger and Kovach (this

volume) in the Castle Rock Springs area, about 5 km to the southeast of the present production area. This region is under intensive investigation for geothermal potential. The velocity structure in the top 2 km of the crust does not show any low-velocity features; near-surface velocities are in the range of 2.1 to 2.8 km/s, and a high velocity of 5.5 km/s is observed at a shallow depth of 2.5 km. Station GSM is located in this general region and does not show any large delays.

Deep delay sources

The previous discussion indicates that even after applying corrections for surface geology to the teleseismic delays, it is still necessary to interpret a regional delay field of 0.5 s extending over part of the Clear Lake volcanic field and the steam production field including large delays of 1 s at GGL, GBC, and GSG.

We have made the following assumptions regarding the interpretation of the anomaly: (1) the observed relative delay observed at a station is caused by the seismic ray traversing obliquely through a low-velocity body; (2) the velocity decrease inside the body relative to the surrounding rock is constant throughout the body by a specified amount; (3) the top of the low-velocity body is flat and at a depth of 4 km. (This value is close to the maximum depth of the seismogenic zone under the Geysers-Clear Lake region (Bufe and others, this volume). If the low-velocity body is magmatic it will be unable to sustain earthquake strains.)

The anomalous ray path length inside the body is calculated at each station from residuals at various azimuths according to the equation:

$$L = -VR (1 + 1/k)$$

where, L is the distance ray travels in anomalous body, V is the velocity for normal ray path, R is the average relative residual (positive for delays), and k = fraction by which velocity inside the body deviates from normal; k is positive for higher-than-normal velocities and negative for lower-than-normal velocities. Having calculated L, the average angle of ray emergence at the surface, and the average event azimuth, it is possible to calculate the position of a three-dimensional surface of a body at depth.

Fig. 9 near here

The results of this modeling are shown in figure 9A and B, corresponding to a 15 and 25 percent velocity decrease. The contours indicate depths to the bottom of the low-velocity body. (As defined earlier the top of the body is flat and constrained to a depth of 4 km.). For a 15 percent velocity decrease there is considerable scatter in the values, due to computed depths arising from large and small residuals at different stations being projected adjacent to each other. However, in spite of the discrepancies, we can define approximately a low-velocity body about 10 km deep and extending over a broad triangular region from the northeast shore of Clear Lake area comprising the steam-production zone and part of the Clear Lake volcanic field, the body appears to be deeper than 10 km. The 20-km contour approximately defines the deepest section of the body with considerable uncertainty in the northeast boundary.

As mentioned above, previous work suggest that a 15 percent velocity decrease may be appropriate for low-velocity bodies in geothermal areas. However, as shown in figure 9B, P-wave delays in the Geysers-Clear

Lake region can also be modeled assuming a 25 percent velocity decrease. The 10-km contour outlines a smaller area than for the 15 percent model, but, encompasses the steam-production zone and the volcanic field. This model also reveals core regions near The Geysers and Mount Hannah where the low-velocity body may be 20 km or deeper. No serious contradictions in depth values were found for this model suggesting a 25% decrease in velocity may be more appropriate, particularly for the central part of the anomalous body.

Figure 10 near here

In figure 10 we show a consolidated model by combining both the 15 and 25 percent contrast models of Figures 9_A, and 9_B. In the following discussion, we shall concentrate on the hypothesis that the low-velocity body under Mount Hannah is of volcanic origin and that the body under the Geysers steam production zone is associated with the steam reservoir, with or without an underlying magmatic body.

Magma chamber under Mt. Hannah

The presence of a magma chamber under Mount Hannah was first proposed by Chapman (1966) and later Isherwood (1976), analyzing recent gravity and aeromagnetic data, has modeled a magma chamber with its center at a depth of 15 km under Mount Hannah. Using geologic and geochronological data, Hearn and others (this volume) show that the central part of the Clear Lake volcanic field underlain by the postulated magma chamber is younger than 0.5 m.y. The

geophysically inferred magma chamber, however, does not correspond to the youngest rocks of the Clear Lake Volcanics which lie to the northeast (Hearn and others, this volume). A strong resistivity anomaly (Stanley and Jackson, 1973) centered slightly to the northwest of Mount Hannah may also be due to indirect effects of the magma chamber. Young and Ward (this volume) have analyzed the spectra of teleseisms recorded by our portable seismic array in the Geysers - Clear Lake area and have found a broad low Q-zone over the Clear Lake Volcanics and the production zone. They postulate that the low Q is associated with a zone of partial melting or magma chamber underlying the Geysers - Clear Lake area.

In spite of our modeling limitations and difficulty in assigning appropriate velocity contrasts, no serious differences exist between Isherwood's gravity model and our model. However, Isherwood's model, based on an expected mass deficiency, does not specify the extent of melting inside the magmatic body. In our model a decrease in compressional velocity of 21-31 percent is required. A P-wave velocity decrease greater than 10 percent, though possibly caused by several factors, is best attributed to partial melt, particularly when observed in young volcanic areas. The interpretation of P-wave delays in terms of partially molten bodies has been discussed in detail in the analysis of Long Valley data by Steeples (1975) and Steeples and Iyer (1976b), and for Yellowstone by Iyer and Stewart (1977). In the Geysers - Clear Lake region we believe that the most plausible explanation of the observed delays in the Mount Hannah area is the presence of partially molten rock in the crust. Whereas the increase of temperature alone is sufficient to cause a slow decrease in the velocity of compressional waves, a dramatic

decrease in velocity occurs at the onset of partial melting (Mizutani and Kanamori, 1964; Spetzler and Anderson, 1968; Murase and McBirney, 1973). P-wave velocity data alone are not sufficient to determine the degree of partial melting. The accepted model for partially molten rock is one in which the main body of the solid has a large number of fluid-filled cracks. The extent of velocity decrease depends not only on the number of cracks but also on their shape. Measurement of other seismologic variables such as shear-wave velocities, and compressional and shear-wave attenuation are necessary in estimating the degree of partial melt in a magmatic system. A joint interpretation of our results together with the attenuation data of Young and Ward (1978, this volume), may provide further constraints in estimating the composition of the magma body under the Geysers - Clear Lake area.

Low velocity body associated with the dry-steam reservoir.

Goff and others (1977) modeled the Geysers - Clear Lake geothermal region as a dry-steam system under The Geysers between the Mercuryville and Collayami fault zones and an extensive hot-water system to the northeast (see fig. 5 of their paper and fig. 1 and 3 of this paper). Nur and Simmons (1969) have shown that the presence of dry fractures, as would be found in the dry-steam system, lowers the compressional velocity of a medium. Hence, a significant velocity decrease can be expected in a vapor-dominated field such as The Geysers in contrast to a water-dominated field. However, it is again difficult to make an estimate of the expected velocity decrease and to interpret that estimate in terms of production-zone size. Our models show

that a 25 percent velocity decrease requires depths of 25 to 30 km. However, note that this value is derived solely from the southwest delays at station GBO. The delays for other azimuths indicate about half that depth. Our modeling has incorporated the azimuthal dependence of the residuals, which results in the width of the anomalous low-velocity zone being restricted along the northwesterly direction.

The strong azimuthal dependence of the observed delays at GBO may also be attributed to material which has an anisotropic velocity distribution beneath the production zone. It is not unreasonable to expect velocity anisotropy in fractured rock. Walsh (1965) found that anisotropy can be due to the effect of cracks on the compressibility of rocks; the maximum velocity decrease occurs along a plane perpendicular to the crack orientation. In a study of the seismicity of the Geysers - Clear Lake area, Bufe and others (this volume) estimated the axis of maximum compression to be $N.30^{\circ} E$ which indicates that cracks should form about an axis of minimum compression oriented $N.15^{\circ} W$. Therefore maximum velocity decrease should occur approximately along a southwesterly direction as observed.

It is not possible to determine from seismic data alone whether part of the delays observed in the production zone are due to the extension of the Mount Hannah magma chamber underneath a fractured, steam-filled reservoir. Isherwood's magma chamber extends (see fig. 17 of his 1976 paper) under the steam production zone. In the absence of any definitive evidence and since no estimates as to the size of the steam reservoir are available, we will not speculate on the relative sizes of the steam reservoir and magma body under the geothermal production zone.

A conceptual model for the subsurface structure of the Geysers - Clear Lake region is shown in three cross-sectional diagrams along AA' (northwest through the volcanic zone), BB' (northwest through the production zone), and CC' (northeast through the production zone and volcanic zone) in figures 11A, B, and C. The models are primarily constructed from teleseismic data, but other geologic and geophysical information is also used for completeness.

Figure 11 near here

CONCLUSIONS

A plausible interpretation of the large teleseismic delays observed in the Geysers - Clear Lake region is that they are due to the presence of a low-velocity body in the crust. The body, with an average thickness of about 10 km extends over a large area to the south of Clear Lake including the steam production zone at The Geysers. The average compressional velocity inside the body is less than normal by about 15 percent. In a core region exists under Mount Hannah and part of the steam production zone, the velocity decrease exceeds 25 percent. We interpret the low-velocity body to be composed of partially molten rock under the volcanic zone, and fractured rock, responsible for the dry-steam reservoir, under the production zone. Because it is not possible to distinguish between low velocities due to partially molten rock and dry fractures from teleseismic residuals alone, it is not possible to determine whether a magmatic intrusion is present under the dry steam.

reservoir. Our results are in basic agreement with Isnerwood's (1976) analysis of gravity and magnetic data which also indicate the presence of a magma chamber under the Geysers - Clear Lake area. If the high degree of partial melting indicated by our results is valid, it would appear that the Clear Lake volcanic system is by no means extinct.

REFERENCES

- Birch, F., 1960, The velocity of compressional waves in rocks to 10 kilobars, part 1: *Journal of Geophysical Research*, v. 65, p. 1083-1102.
- Chapman, R. H., 1966, Gravity map of Geysers area: California Division of Mines and Geology Mineral Information Service, v. 19, p. 148-149.
- Goff, F. E., Donnelly, J. M., Thompson, J. M., and Hearn, B. C., Jr., 1977, Geothermal prospecting in The Geysers-Clear Lake area, northern California: *Geology*, v. 5, p. 509-515.
- Herrin, E., 1965, Seismological tables for P: *Bulletin of the Seismological Society of America*, v. 58, p. 1196-1219.
- Isherwood, W. F., 1976, Gravity and magnetic studies of The Geysers-Clear Lake geothermal region, California: *United Nations Symposium on the Development and Use of Geothermal Resources*, 2d, San Francisco, Proceedings, v. 2, p. 1065-1073.
- Iyer, H. M., 1975, Anomalous delays of teleseismic P waves in Yellowstone National Park: *Nature*, v. 253, p. 425-427.
- Iyer, H. M., 1979, Deep structure under Yellowstone National Park, U.S.A.: A continental "hot spot": *Tectonophysics*, v. 56, p. 165-197.
- Iyer, H. M., and Stewart, R. M., 1977, Teleseismic technique to locate magma in the crust and upper mantle, in Dick, H. J. B., ed., *Magma genesis*, Proceedings of the American Geophysical Union Chapman Conference on Partial Melting in the earth's upper mantle, 1977: Oregon State Department of Geology and Mineral Industries, p. 281-299.
- Iyer, H. M., Oppenheimer, D. H., and Hitchcock, T., 1979, Abnormal P-wave delays in The Geysers-Clear Lake geothermal area, California: *Science*, v. 204, p. 495-697.

- Kubota, S., and Berg, E., 1967, Evidence for magma in the Katmai volcanic range: *Bulletin Volcanologique*, v. 31, p. 175-214.
- Majer, E., and McEvilly, T. V., 1979, Seismological investigations at The Geysers geothermal field: *Geophysics*, v. 44, p. 246-269.
- Matumoto, T., 1971, Seismic body waves observed in the vicinity of Mount Katmai, Alaska, and evidence for the existence of molten chambers: *Geological Society America Bulletin*, v. 82, p. 2905-2920.
- Mizutani, H., and Kanamori, H., 1964, Variation of elastic wave velocity and attenuative property near the melting temperature: *Journal of Physics of the Earth*, v. 12, p. 43-49.
- Murase, T., and McBirney, A. R., 1973, Properties of some common igneous rocks and their melts at high temperatures: *Geologic Society of America Bulletin*, v. 84, p. 3563-3592.
- Nur, A., and Simmons, G., 1969, The effect of saturation on velocity in low porosity rocks: *Earth and Planetary Science Letters*, v. 7, p. 183-193.
- Reasenberg, P., Ellsworth, W., and Walter, A., 1979, Teleseismic evidence for a low velocity body under the Coso geothermal area; (In press), *Journal of Geophysical Research*.
- Savino, J. M., Rodi, W. L., Goff, R. C., Jordan, T. H., Alexander, J. H., and Lambert, D. G., 1977, Inversion of combined geophysical data for determination of structure beneath the Imperial Valley geothermal region: *Systems, Science and Software*, Report SSS-R-76-3412 to U.S. Department of Energy, 82 p.
- Spetzler, H., and Anderson, D. L., 1968, The effect of temperature and partial melting on velocity and attenuation in a simple binary system: *Journal of Geophysical Research*, v. 73, p. 6051-6060.

Stanley, W. D., and Jackson, D. B., 1973, Geoelectric investigations near Clear Lake, California: U.S. Geological Survey open-file report, 20 p.

Steeple, D. W., 1975, Teleseismic P-delays in geothermal exploration with application to Long Valley, California (Ph.D. thesis): Stanford, California, Stanford University, 228 p.

Steeple, D. W., and Iyer, H. M., 1976a, Teleseismic P-wave delays in geothermal exploration: United Nations Symposium on the Development and Use of Geothermal Resources, 2nd, San Francisco, Proceedings, v. 2, p. 1199-1205.

-----1976b, Low-velocity zone under Long Valley as determined from teleseismic events: Journal of Geophysical Research, v. 81, p. 849-860.

Walsh, J. B., 1965, The effect of cracks on the compressibility of rock: Journal of Geophysical Research, v. 70, p. 351-359.

Figure Captions

Figure 1 Generalized geologic map of the Geysens-Clear Lake area. (8a)

Figure 2 Residual gravity map of The Geysers-Clear Lake region: (after Isnerwood, 1976).

Figure 3 Inferred approximate outlines of vapor-dominated and steam-
production areas in the Geysers-Clear Lake region.

(11)



Figure 5 Computer display of a teleseism from Norfolk Island, October 17, 1977, recorded by eight stations of the Geysers-Clear Lake seismic network.

A, Arranged according to actual arrival times.

B, Traces shifted by computer to pick time of first break.

Note the absence of a sharp first break at station GBC. (8a)

Figure 4 Two teleseisms recorded by telemetered network in the Geysers -
Clear Lake region. Only eight stations per events are shown.
Note change in signal shape at stations GGL, GBO, and GMI.
A, Northern Chile, November 30, 1976.
B, Bonin Islands, December 12, 1976. (7a)

Figure 7 Relative residual contour maps.

A, Southwest events: to adjust for differences due to reference station locations, 0.08 sec has been added to all temporary station residuals.

B, Northwest events: to adjust for differences due to reference station locations, 0.20 sec has been added to all temporary station residuals.

C, Southeast events.

(11b)

Figure 6 Variation of relative residuals as a function of distance and azimuth at stations.

A, GGL,

E, GSG,

C, GPK,

D, GBO.

(11a)

Figure 9 Calculated depth to bottom of anomalous body required to account for observed delays. Top of body is considered flat and assumed to be at a depth of 4 km. Numbers near station locations indicate depth in km below (+) or above (-) the top of the body. Normal seismic velocity outside body is 6 km/sec.

A, 15 percent velocity decrease. Contour interval is 10 km.

B, 25 percent velocity decrease. Contour interval is 5 km. (20a)

Figure 8 Profile of northwest, southeast residual values, and gravity
along a southeast-northwest line AA' (see figure 7C) from CL01
to GHL. (15a)

Figure 11 Conceptual model of subsurface structure and percent decrease in velocity in the Geysers - Clear Lake region.

A, Northwest cross-section along AA' of figure 10 passing through volcanic zone.

B, Northwest cross-section along BB' of figure 10 passing through production zone.

C, Northeast cross-section along CC' of figure 10 passing through production and volcanic zones.

(25a)

Figure 10 Composite of figure 9 indicating depth to the bottom surface of body responsible for observed delays. Velocity decrease with respect to normal is 25 percent within shaded "core" area, and 15 percent outside core and within 10 km contour. Contour interval is 5 km. Profile lines indicate position of cross-sections shown in figure 11. (21a)

Table 1. - Station names, coordinates, elevations, and dates of operation

Station	Latitude (Deg)(Min)		Longitude (Deg)(Min)		Elevation (m)	Period of operation
CL01	38	41.74	122	30.67	524	7/4/76-7/22/76, 8/14/76-9/9/76
CL02	38	44.07	122	32.38	323	7/3/76-7/22/76, 8/14/76-9/9/76
CL03	38	46.79	122	35.30	330	7/3/76-7/22/76, 8/14/76-9/9/76
CL04	38	48.30	122	36.95	347	7/3/76-7/22/76, 8/15/76-9/9/76
CL05	38	52.26	122	42.33	1049	7/4/76-7/22/76, 8/15/76-9/10/76
CL06	38	54.67	122	42.33	756	7/4/76-7/22/76, 8/16/76-9/9/76
CL07	38	55.70	122	47.33	622	7/5/76-7/22/76, 8/16/76-9/9/76
CL08	38	57.90	122	48.71	494	7/4/76-7/22/76, 8/15/76-9/9/76
CL09	38	56.68	122	54.75	543	7/5/76-7/22/76, 8/15/76-9/9/76
CL 10	39	00.70	122	55.75	463	7/7/76-7/22/76, 8/16/76-9/9/76
CL 11	38	50.84	122	47.15	805	8/19/76-9/5/76
CL 13	38	51.95	122	48.30	786	8/21/76-9/4/76
GAX	38	42.65	122	45.30	379	permanent
GBG	38	48.84	122	40.76	1125	permanent
GBO	38	49.46	122	50.57	879	permanent
GCM	38	48.35	122	45.31	1286	permanent
GCV	38	46.14	123	0.89	150	permanent
GDC	38	46.03	123	14.31	772	permanent
GGL	38	53.80	122	46.58	893	permanent
GGF	38	45.88	122	50.65	1054	permanent
GHC	38	36.36	123	11.81	518	permanent
GHG	39	7.70	122	49.47	902	permanent
GHL	39	2.43	123	1.12	956	permanent
GMC	38	47.56	123	7.08	426	permanent
GMK	38	58.17	122	47.22	906	permanent
GMO	38	42.61	123	8.59	802	permanent
GPM	38	50.85	122	56.72	763	permanent
GRM	39	1.23	122	35.06	469	permanent
GRT	38	56.32	122	40.18	619	permanent
GSG	38	52.00	122	42.60	1080	permanent
GSM	38	46.16	122	46.88	1017	permanent
GSN	38	56.43	123	11.50	870	permanent
GSS	38	42.12	123	0.81	282	permanent
NHB	38	35.36	122	54.54	165	permanent
NMH	38	40.22	122	38.03	1200	permanent
NMT	38	46.34	122	26.76	422	permanent
NMW	38	33.03	122	43.37	134	permanent
NSH	38	31.20	122	36.43	326	permanent

Table 2. List of teleseisms

Event location	Date	Origin time (G.m.t.)			Depth (km)	Lat N		Long W.		Distance/Azimuth to GCL (degrees)	Numbers of stations recording
		h	M	S		DEG	MIN	DEG	MIN		
Kermadec Islands	1/24/76	21	48	25.9	78	-28	38.10	177	35.60	84.5/226.2	19
Fiji Islands	2/03/76	12	27	30.1	477	-25	8.20	-179	41.60	83.4/230.3	24
Colombia	5/19/76	4	7	15.8	157	4	27.80	75	47.00	54.6/116.6	22
Kermadec Islands	6/29/76	18	30	9.1	48	-33	49.00	177	50.00	88.5/223.1	24
*Kamchatka	7/10/76	11	37	12.8	387	47	24.00	-145	42.00	63.8/310.8	8
*Panama	7/11/76	16	54	31.8	22	7	18.00	78	30.00	50.5/116.6	5
*Panama	7/11/76	20	41	47.5	3	7	24.00	78	6.00	50.7/116.2	9
*Panama	7/17/76	2	5	22.0	25	5	48.00	82	42.00	48.7/122.0	7
*New Britian	7/17/76	21	6	32.1	53	-4	12.00	-152	48.00	88.4/263.4	5
*Kermadec Islands	7/20/76	22	51	43.1	370	-31	12.00	180	0.00	87.7/226.3	6
*Kuril Islands	7/22/76	6	57	22.1	79	46	12.00	-151	30.00	60.9/307.5	8
*Fiji Islands	8/15/76	18	43	45.0	509	-25	7.80	-179	42.00	83.4/230.5	3
*Aleutians	8/16/76	5	11	38.9	65	51	30.00	178	24.00	40.5/307.1	5
*Kamchatka	8/16/76	12	28	32.4	50	51	55.20	-158	25.80	54.5/311.6	5
*China	8/16/76	14	6	45.9	16	32	48.00	-104	12.00	96.6/321.9	4
*Chile	8/20/76	6	54	11.3	81	-20	24.00	70	0.00	76.7/130.1	6
*Alaska	8/22/76	2	1	47.4	144	60	12.00	153	18.00	28.9/328.1	6
*New Hebrides	8/22/76	21	9	41.9	31	-14	0.00	-170	54.00	81.2/244.3	10
*China	8/23/76	3	30	7.6	33	32	30.00	-104	12.00	96.9/321.7	10
*Chile	8/24/76	21	26	12.2	8	-25	18.00	70	42.00	80.1/133.7	8
*Aleutians	8/28/76	2	30	9.2	145	52	36.00	175	18.00	38.5/308.8	10
*Kermadec Islands	8/31/76	9	6	50.4	55	-30	6.00	178	6.00	85.8/225.8	9
*Kermadec Islands	8/31/76	13	22	10.9	51	-28	18.00	176	36.00	83.6/225.9	10
*New Hebrides	9/01/76	13	25	29.8	75	-20	24.00	-169	24.00	86.7/240.6	10
*Guatemala	9/02/76	10	20	25.9	81	13	18.00	90	0.00	38.3/122.4	7
*Solomon Islands	9/04/76	11	41	59.7	83	-10	12.00	-161	6.00	85.9/253.6	8
Kuril Islands	9/22/76	0	16	8.2	64	44	52.80	-149	13.50	62.6/306.9	24
Fiji Islands	11/25/76	14	6	35.4	442	-19	29.90	177	42.30	77.6/232.2	23
Chile	11/30/76	0	40	57.8	88	-20	31.20	68	55.10	77.7/129.2	22
Kazakh SSR	12/07/76	4	56	57.4	1	49	53.00	-78	54.30	89.5/346.2	19
Bonin Islands	12/12/76	1	8	50.1	491	28	2.60	-139	34.50	78.4/296.6	20
Nyukyu Islands	12/14/76	16	6	44.4	41	28	17.60	-130	41.90	84.3/301.8	24
Argentina	2/04/77	7	46	33.8	549	-24	41.30	63	21.70	84.2/128.1	22
Honshu, Japan	2/18/77	20	51	29.8	42	33	4.30	-140	49.00	74.5/300.0	24
Korea	3/09/77	14	27	53.6	528	41	36.40	-130	52.70	75.6/312.0	22
Kuril Islands	3/19/77	10	56	25.1	70	44	12.00	-148	11.80	63.6/306.6	16
Peru	4/09/77	4	4	12.5	564	-10	0.90	71	10.90	68.3/123.8	24

Table 2 - continued

Event location	Date	Origin time (G.m.t.)			Depth (km)	Lat N		Long W.		Distance/Azimuth to GCL (degrees)	Numbers station recorded
		H	M	S		DEG	MIN	DEG	MIN		
Honshu, Japan	4/20/77	20:	4.	29.4	493	30	35.90	-137	29.00	78.3/299.8	24
Solomon Islands	4/21/77	4:	24.	9.6	33	-9	57.90	-160	43.90	85.9/253.8	21
Fiji Islands	6/17/77	2:	29.	9.8	690	-19	52.60	179	5.90	78.7/233.0	21
Tonga Islands	6/22/77	12:	8.	28.3	33	-23	11.40	175	55.20	79.3/228.5	17
Fiji Islands	7/06/77	11:	28.	31.5	594	-21	4.10	178	34.40	79.3/231.8	21
Rat Islands	9/04/77	15:	40.	57.4	33	51	24.00	-178	25.80	42.2/307.0	18
Rat Islands	9/04/77	23:	20.	44.3	33	51	24.60	-178	21.60	42.2/307.1	21
Peru	10/08/77	3:	3.	38.3	100	-10	37.20	73	39.00	67.2/126.3	18
Fiji Islands	10/10/77	11:	53.	56.3	33	-25	39.60	174	46.80	80.6/226.1	21
Tonga Islands	10/14/77	4:	55.	33.8	33	-15	44.40	173	19.20	72.0/231.4	22
Norfolk Islands	10/17/77	17:	26.	40.3	33	-27	52.80	-172	52.80	89.6/232.9	22

*Teleseisms recorded by the temporary net

Table 3. - Mean relative residuals and their standard deviations for three azimuth groups.

Station	Azimuth range (deg)	Distance range (deg)	Number of Events	Relative residual (s)	Standard deviation (s)	
CL01	116.2 - 133.7	48.7 - 80.0	5	0.13	0.05	
	225.8 - 263.4	81.2 - 88.5	8	0.12	0.08	
	307.2 - 328.1	28.9 - 96.9	8	0.12	0.05	
CL02	116.2 - 133.7	38.3 - 80.1	6	0.00	0.00	
	225.8 - 263.4	81.2 - 88.4	8	0.00	0.00	1
	307.1 - 328.1	28.9 - 96.9	8	0.00	0.00	2
CL03	116.2 - 133.7	38.4 - 80.1	5	0.08	0.07	
	225.7 - 263.4	81.2 - 88.4	8	0.01	0.11	1
	307.1 - 328.1	28.8 - 96.8	7	0.10	0.03	2
CL04	116.1 - 133.7	38.5 - 80.2	5	0.04	0.12	
	225.7 - 263.4	81.2 - 88.4	7	0.15	0.11	1
	307.1 - 328.1	28.8 - 96.8	8	0.35	0.05	2
CL05	116.1 - 122.4	38.5 - 50.9	3	0.19	0.12	
	225.8 - 263.3	81.2 - 88.3	3	0.68	0.41	3
	307.0 - 328.0	28.7 - 96.7	8	1.06	0.31	2
CL06	116.1 - 122.4	38.6 - 50.9	3	0.83	0.47	3
	225.8 - 244.1	81.2 - 86.6	3	1.46	0.23	1
	307.4 - 321.6	60.7 - 96.6	3	1.53	0.13	2
CL07	116.1 - 133.6	38.6 - 80.3	4	0.44	0.06	
	225.6 - 253.4	83.6 - 86.6	4	0.35	0.14	1
	308.6 - 310.7	38.2 - 63.6	2	0.16	0.03	2
CL08	116.1 - 122.4	38.6 - 51.0	3	0.23	0.09	
	225.6 - 253.4	83.6 - 86.6	4	0.24	0.07	1
	308.5 - 321.5	38.2 - 96.6	3	0.24	0.16	2
CL09	121.7 - 133.5	49.1 - 80.4	3	0.12	0.09	
	225.5 - 253.3	81.1 - 87.7	6	-0.01	0.13	1
	307.3 - 321.5	38.2 - 96.5	3	-0.28	0.07	2

¹ Adjustment of +0.08 seconds necessary to account for differences in reference station locations for southwest events.

² Adjustment of +0.02 seconds necessary to account for differences in reference station locations for northwest events.

³ Value rejected in depth computation.

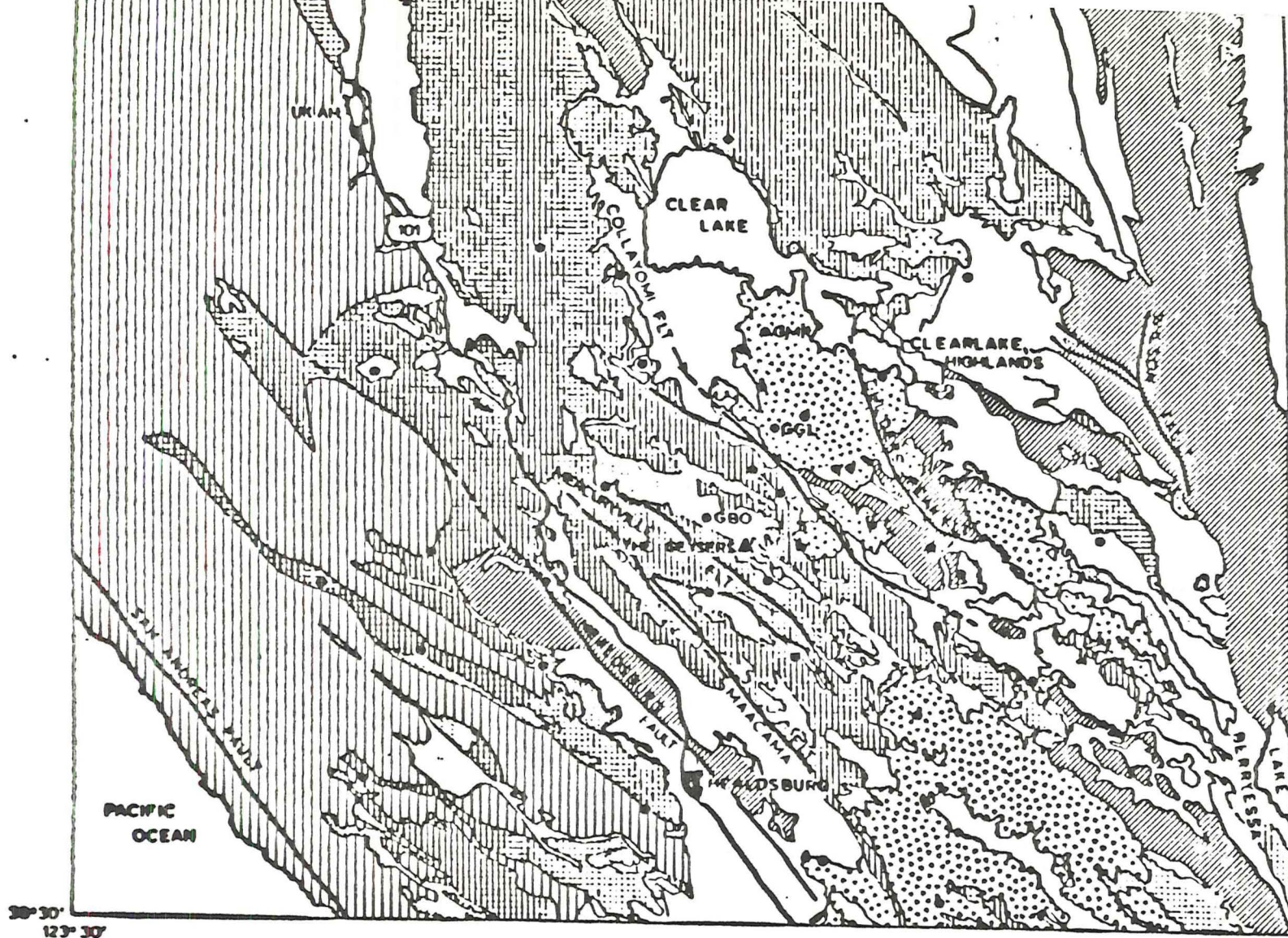
Table 3 - cont.

Station	Azimuth range (deg)	Distance range (deg)	Number of Events	Relative residual (s)	Standard deviation (s)
CL10	121.7 - 133.5	49.1 - 80.5	3	-0.03	0.11
	225.5 - 244.0	81.1 - 87.7	4	-0.12	0.11 1
	307.3 - 328.0	28.5 - 63.4	4	-0.19	0.06
CL11	240.5 - 253.4	81.1 - 86.6	3	0.47	0.13 1
	308.6 - 321.5	38.3 - 96.7	2	0.55	0.20
CL13	129.9 - 133.6	76.9 - 80.3	2	0.63	0.12
	225.6 - 244.1	81.1 - 86.5	3	0.46	0.14 1
	321.5 -	96.6	1	0.69	...
GAX	116.5 - 129.2	54.4 - 84.0	5	-0.15	0.03
	223.1 - 253.8	71.9 - 89.4	11	-0.01	0.07
	296.6 - 312.1	42.3 - 84.4	7	0.05	0.10
GBG	116.6 - 129.3	54.5 - 84.1	5	-0.01	0.06
	226.2 - 253.9	72.0 - 89.5	10	0.41	0.10
	299.9 - 312.1	42.3 - 84.4	7	0.56	0.12
GBO	116.5 - 129.2	54.6 - 84.2	5	0.30	0.04
	223.0 - 253.8	71.9 - 89.4	11	1.07	0.31
	296.6 - 312.0	42.2 - 84.3	9	0.66	0.21
GCM	116.6 - 129.2	54.6 - 84.1	4	-0.20	0.11
	223.1 - 253.1	72.0 - 89.5	11	0.38	0.09
	296.6 - 312.0	42.3 - 84.4	9	0.58	0.10
GCV	116.3 - 129.0	54.7 - 84.2	5	0.17	0.06
	222.9 - 232.8	71.8 - 89.3	8	0.17	0.04
	296.5 - 307.2	42.1 - 84.2	7	0.10	0.15
GDC	116.1 - 128.9	54.9 - 84.4	5	0.07	0.08
	222.8 - 253.5	71.6 - 88.2	9	0.06	0.08
	296.4 - 311.8	42.0 - 84.1	9	0.01	0.10
GGL	116.6 - 129.2	54.6 - 84.2	5	0.63	0.07
	223.1 - 233.0	72.0 - 88.5	6	1.50	0.21
	299.8 - 312.0	74.5 - 84.2	4	0.67	0.29
GGP	116.4 - 129.1	54.6 - 84.1	4	-0.07	0.08
	223.0 - 253.8	71.9 - 89.4	11	-0.01	0.07
	296.6 - 312.1	42.3 - 84.4	7	0.05	0.10

Table 3 - cont.

Station	Azimuth range (deg)	Distance range (deg)	Number of Events	Relative residual (s)	Standard deviation (s)
GHC	116.0 - 128.9	54.8 - 84.3	5	-0.02	0.05
	222.8 - 253.6	71.6 - 89.1	11	-0.05	0.06
	296.4 - 311.9	42.1 - 84.2	9	-0.05	0.11
GHC	123.9 - 129.2	68.5 - 84.3	3	0.18	0.10
	226.2 - 232.2	77.7 - 88.7	4	0.26	0.08
	296.5 - 311.9	42.1 - 84.2	6	0.26	0.15
GHL	116.5 - 129.1	54.9 - 84.4	5	-0.01	0.02
	222.9 - 253.6	71.9 - 89.5	11	0.08	0.06
	296.4 - 311.9	42.0 - 84.1	9	0.00	0.07
GMC	116.2 - 128.9	54.8 - 84.3	5	0.07	0.05
	222.8 - 253.6	71.7 - 89.3	11	-0.03	0.05
	296.4 - 311.9	42.1 - 84.1	9	-0.09	0.10
GMK	123.9 - 129.2	68.4 - 84.2	3	0.00	0.14
	223.0 - 253.6	72.0 - 89.6	11	0.41	0.15
	296.6 - 312.0	42.2 - 84.3	9	0.41	0.09
GMC	116.2 - 128.9	54.8 - 84.3	5	-0.17	0.04
	222.8 - 253.6	71.7 - 89.2	11	-0.14	0.06
	296.4 - 311.9	42.1 - 84.2	9	-0.19	0.09
GPM	116.4 - 129.1	54.6 - 84.2	4	0.02	0.06
	223.0 - 253.8	71.9 - 89.4	10	0.20	0.07
	296.6 - 312.0	42.2 - 84.3	9	0.15	0.07
GRM	116.8 - 129.4	54.5 - 84.1	5	-0.04	0.09
	223.3 - 253.9	72.2 - 89.7	6	0.35	0.08
	296.7 - 312.1	62.7 - 84.4	6	0.45	0.18
GRT	116.7 - 129.3	54.6 - 84.1	5	-0.26	0.08
	223.1 - 253.9	72.1 - 89.6	11	0.33	0.09
	299.8 - 312.1	42.3 - 84.4	6	0.32	0.14
GSG	123.9 - 126.3	67.1 - 68.3	2	-0.01	0.07
	231.5 - 253.9	72.0 - 89.6	4	0.92	0.10
	299.8 - 312.0	42.3 - 78.4	4	0.99	0.10
GSM	116.5 - 129.2	54.6 - 77.6	3	-0.18	0.04
	223.1 - 253.8	77.5 - 88.4	6	0.12	0.15
	296.6 - 306.9	62.7 - 84.4	6	0.40	0.11
GSN	123.5 - 128.9	67.5 - 84.5	4	0.17	0.05
	222.8 - 253.5	71.8 - 89.3	11	0.14	0.07
	299.6 - 311.8	41.9 - 84.0	9	0.05	0.10

Station	Azimuth range (deg)	Distance range (deg)	Number of Events	Relative residual (s)	Standard deviation (s)
GSS	116.3 - 129.0	54.7 - 84.2	5	0.00	0.03
	222.9 - 253.7	71.7 - 89.3	10	-0.09	0.07
	296.5 - 311.9	42.4 - 84.3	9	-0.04	0.10
NHE	116.3 - 129.1	54.6 - 77.6	2	-0.04	0.07
	223.0 - 233.0	71.7 - 89.3	8	-0.06	0.06
	296.6 - 307.4	42.3 - 84.4	6	-0.07	0.09
NMH	116.6 - 128.2	54.4 - 83.9	3	-0.18	0.04
	223.1 - 233.1	78.7 - 89.5	6	0.08	0.17
	299.9 - 307.0	62.9 - 78.5	4	0.09	0.03
NMT	116.8 - 124.1	54.3 - 68.1	2	-0.25	0.07
	223.3 - 233.1	77.7 - 89.7	5	0.21	0.06
	296.8 - 307.0	62.9 - 84.6	5	0.41	0.06
NMA	116.4 - 129.2	54.4 - 83.9	5	0.00	0.00
	223.1 - 253.9	71.8 - 89.4	5	0.00	0.00
	296.7 - 312.1	42.5 - 84.5	9	0.00	0.00
NSH	116.5 - 129.3	54.3 - 83.8	5	-0.13	0.05
	223.2 - 253.9	71.9 - 89.4	11	-0.04	0.04
	296.8 - 312.1	42.5 - 84.6	9	-0.02	0.06



38° 30'
123° 30'

0 30 KM

QUATERNARY, SEDIMENTARY AND METASEDIMENTARY ROCKS

UNDIVIDED CRETACEOUS MARINE

GREAT VALLEY SEQUENCE

FRANCISCAN FORMATION

MESOZOIC ULTRABASIC INTRUSIVE ROCKS

RECENT VOLCANIC

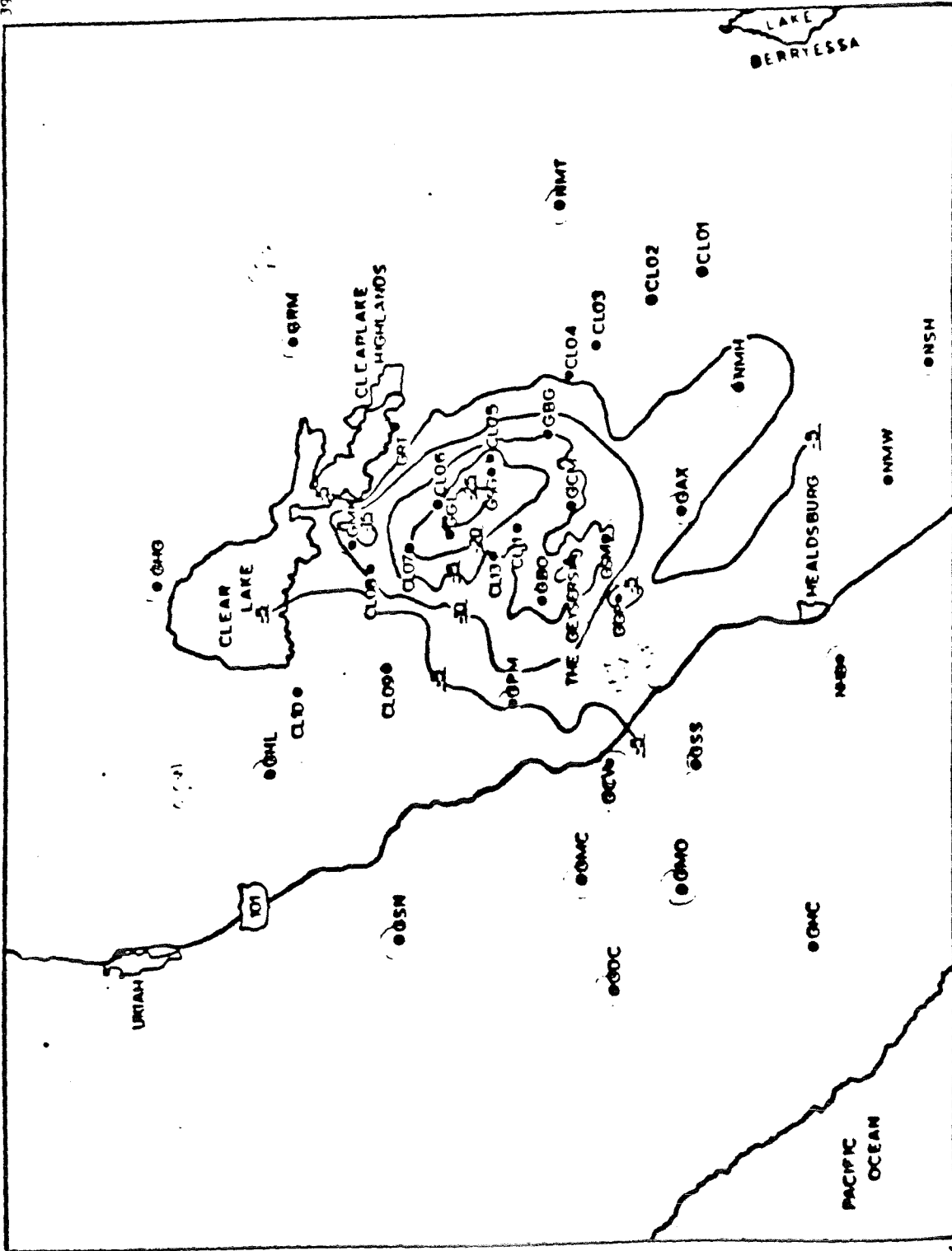
PLEISTOCENE VOLCANIC

PLIOCENE VOLCANIC

FRANCISCAN VOLCANIC AND METAVOLCANIC ROCKS

Fig. 1

122°15' 39°15'

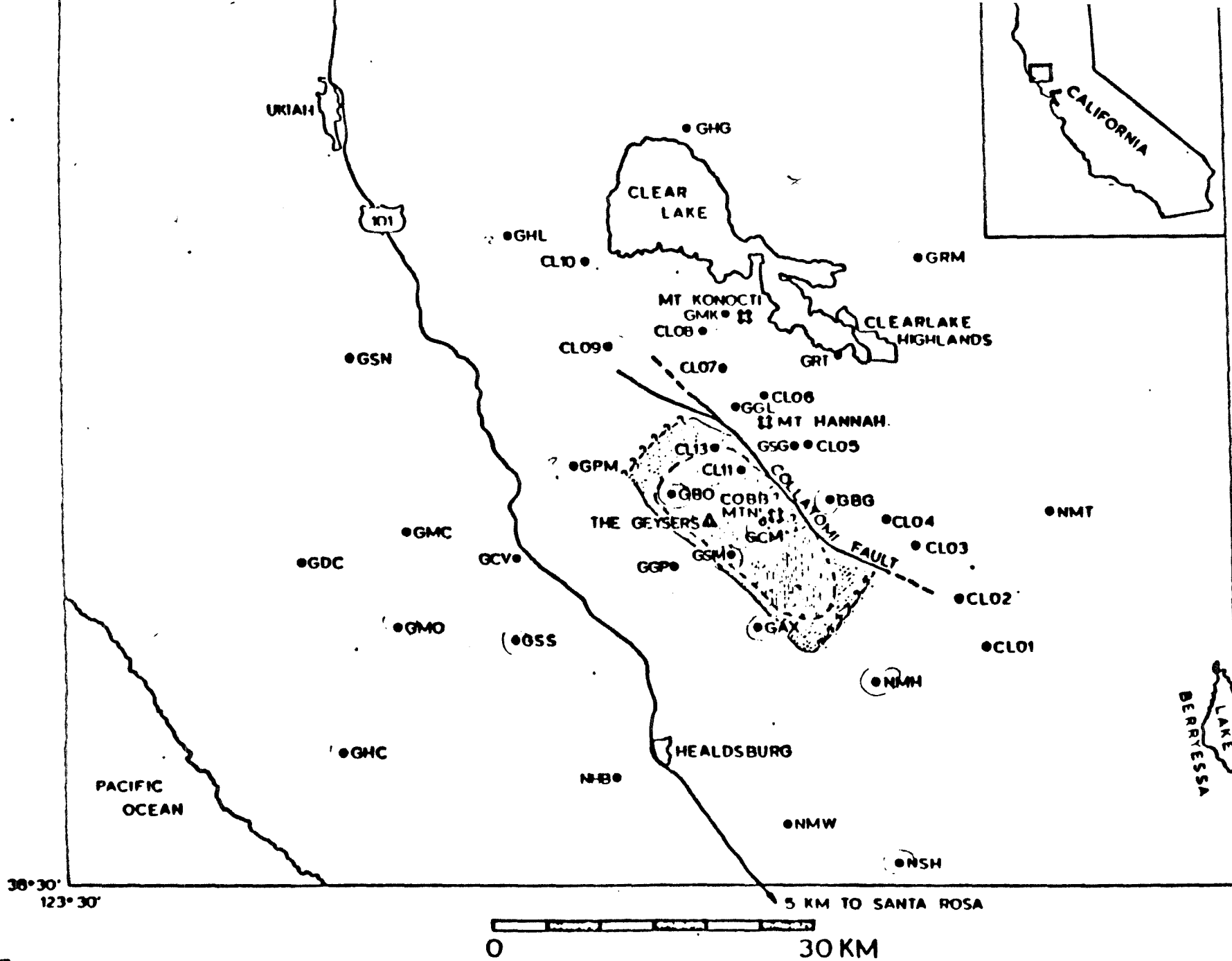


30°30' 123°30'



Residual Bouguer Gravity in 5-milligal Contours

Fig. 2





-  VAPOR-DOMINATED AREA
-  APPROXIMATE STEAM PRODUCTION AREA

Fig 3

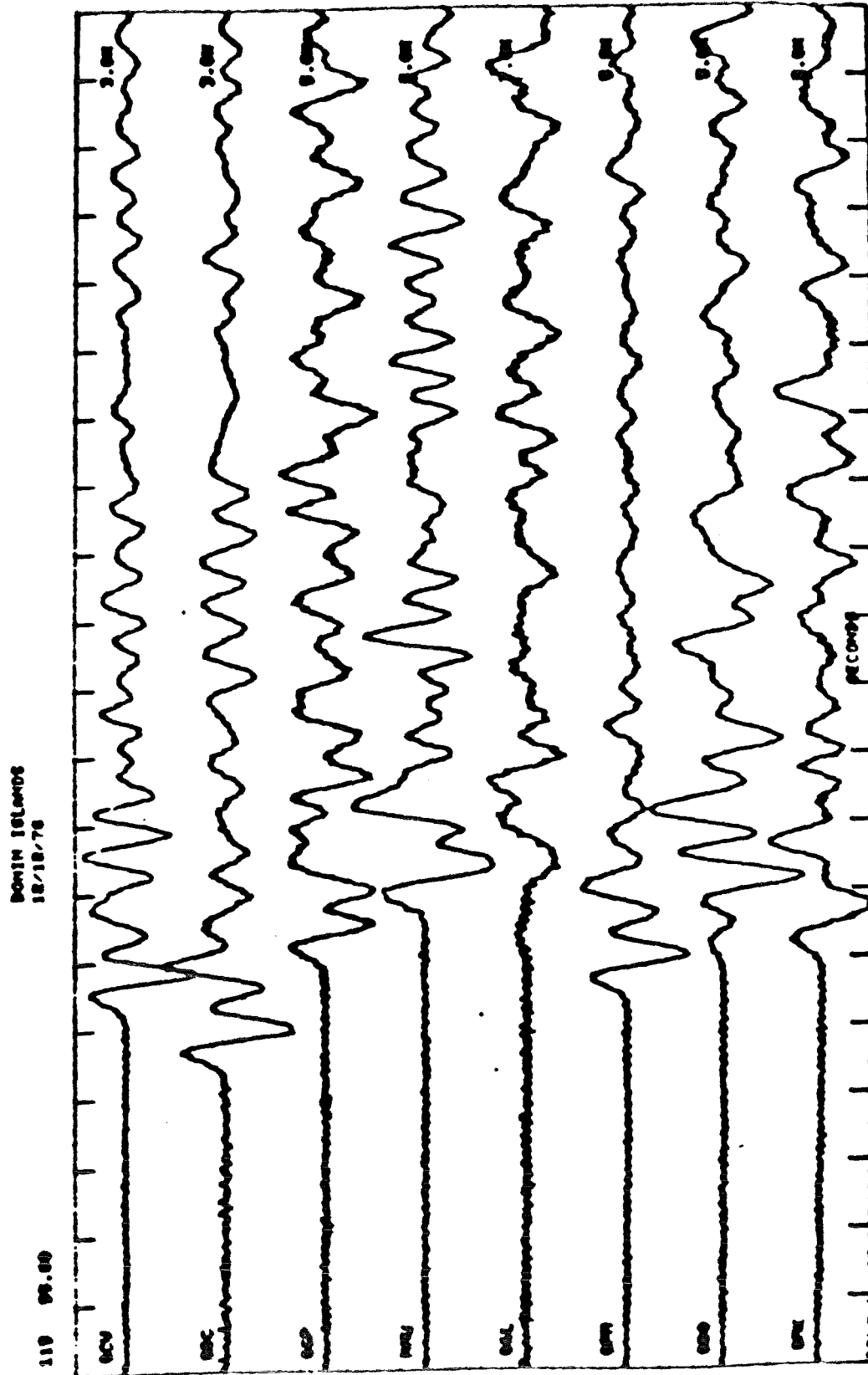


Fig. 4

NORTHERN CHILE
11/30/76

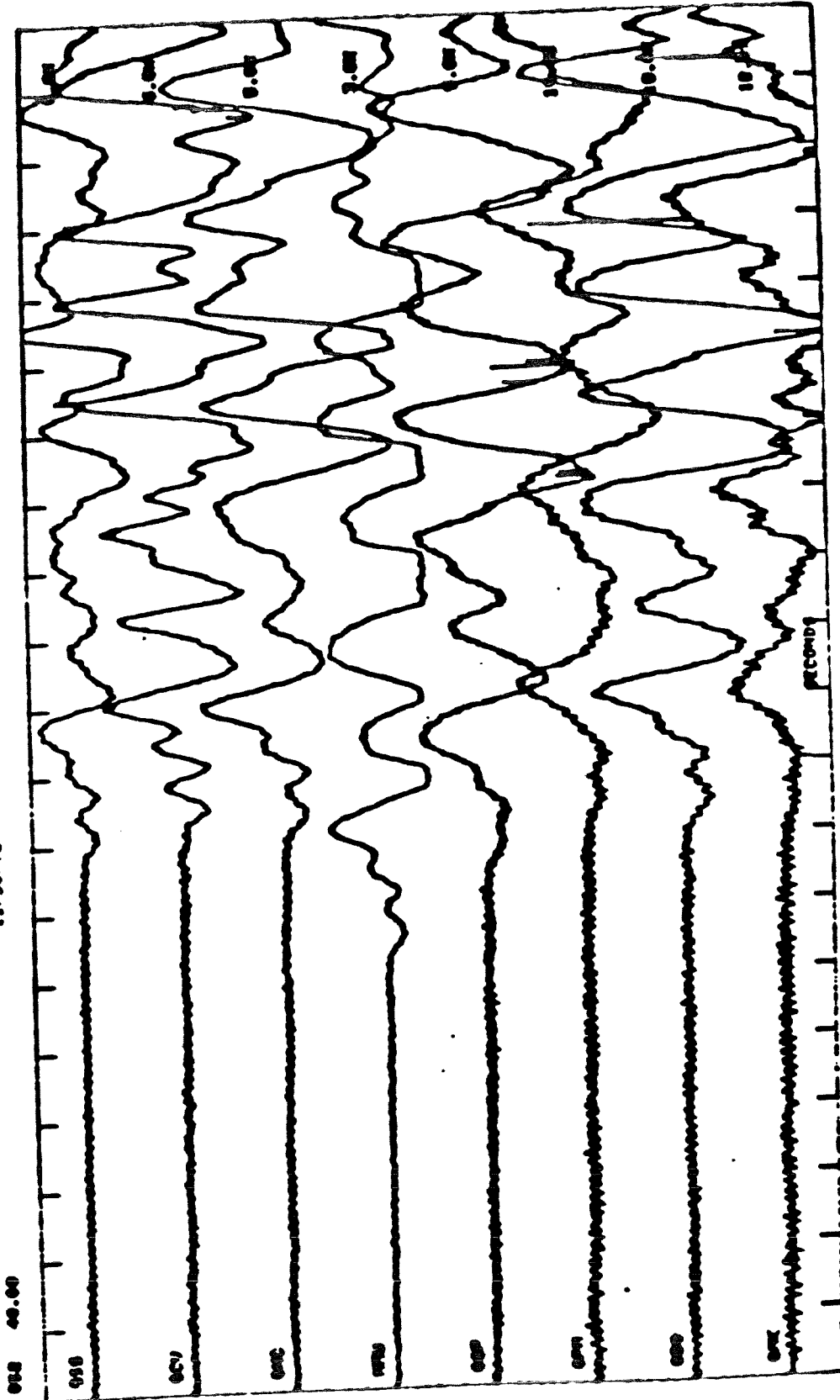


Fig. 4

00000000

NORFOLK ISLAND
77/10-17 17330

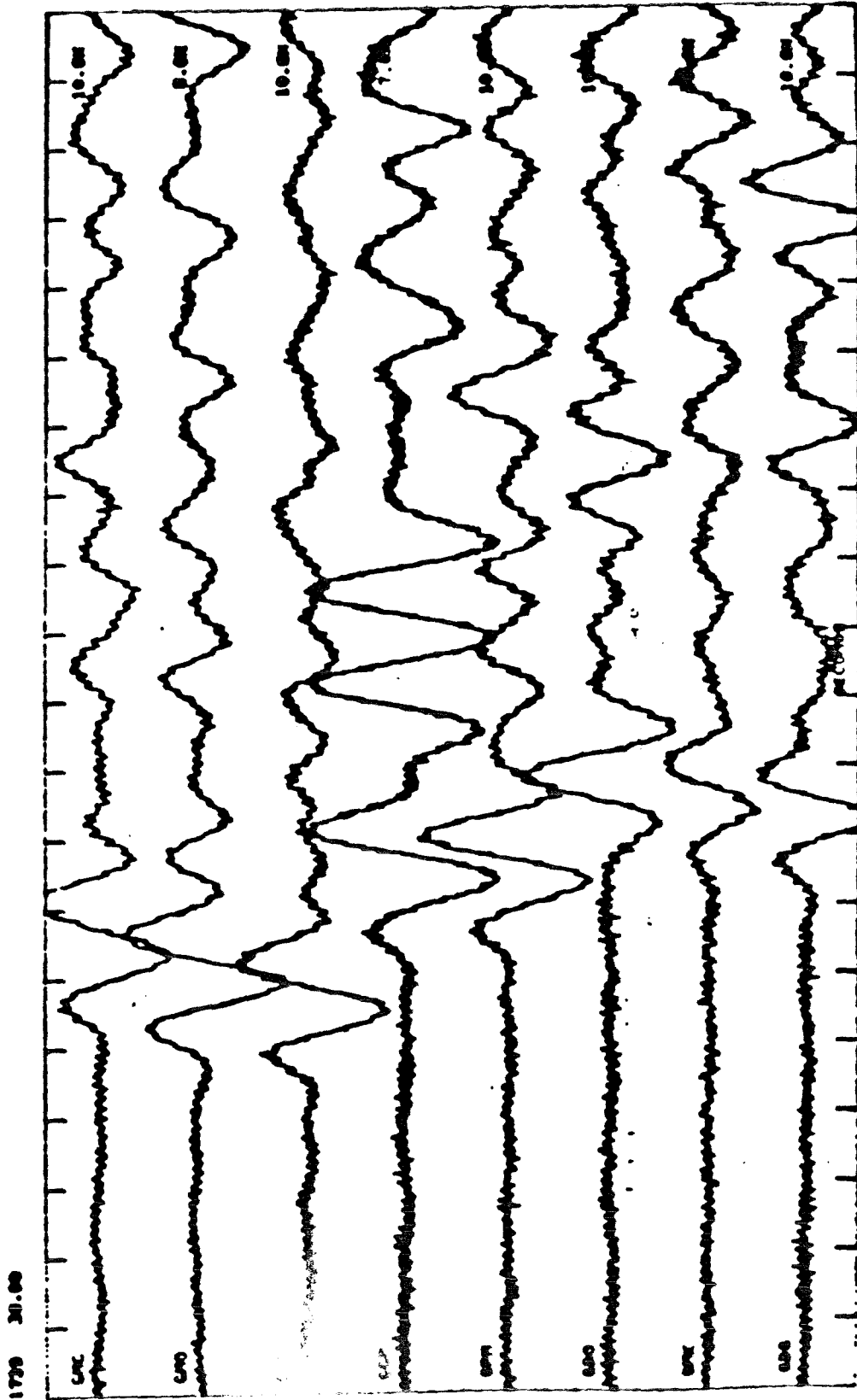


Fig. 5a

Continued
of

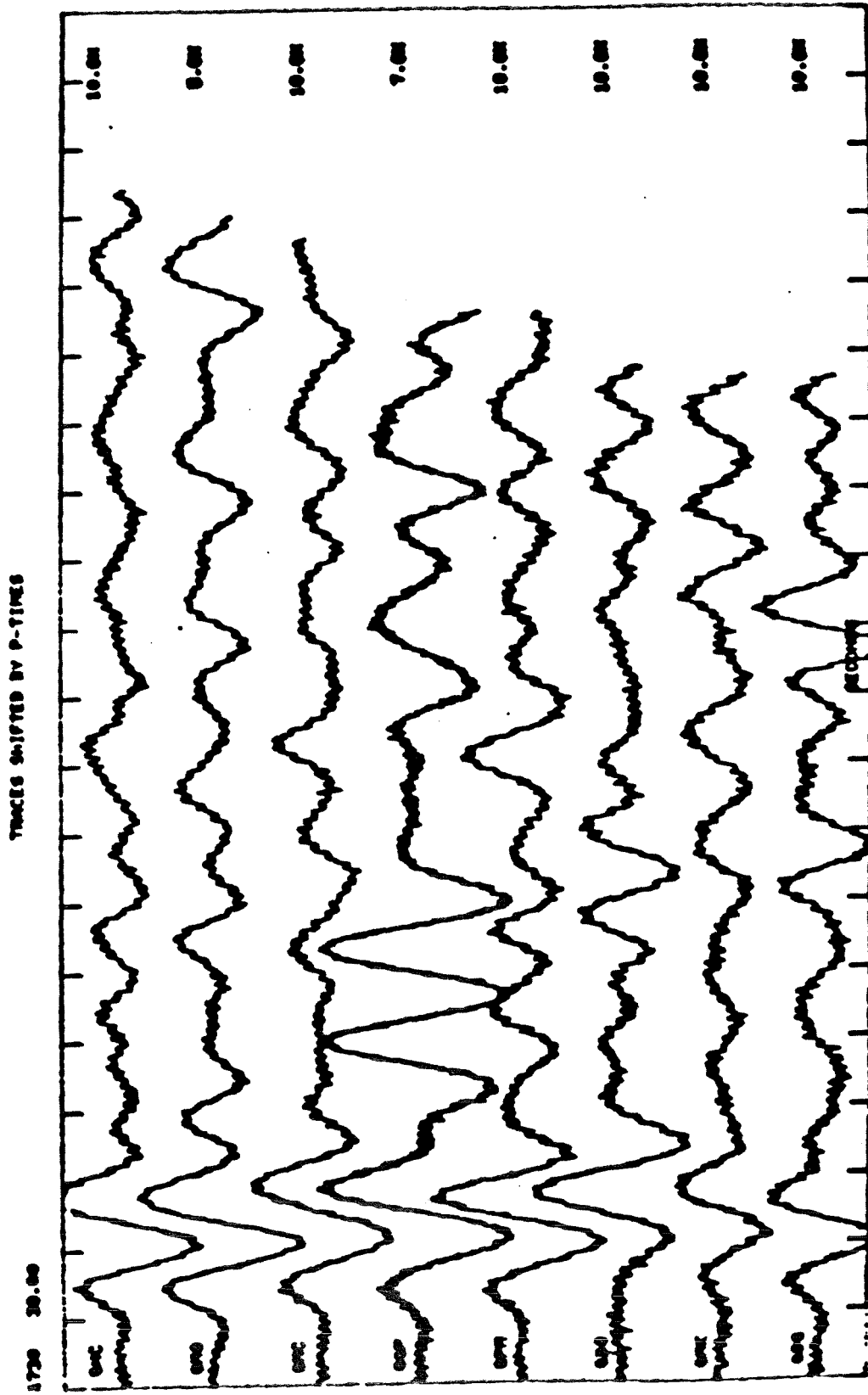


Fig. 5L

STATION: GBO

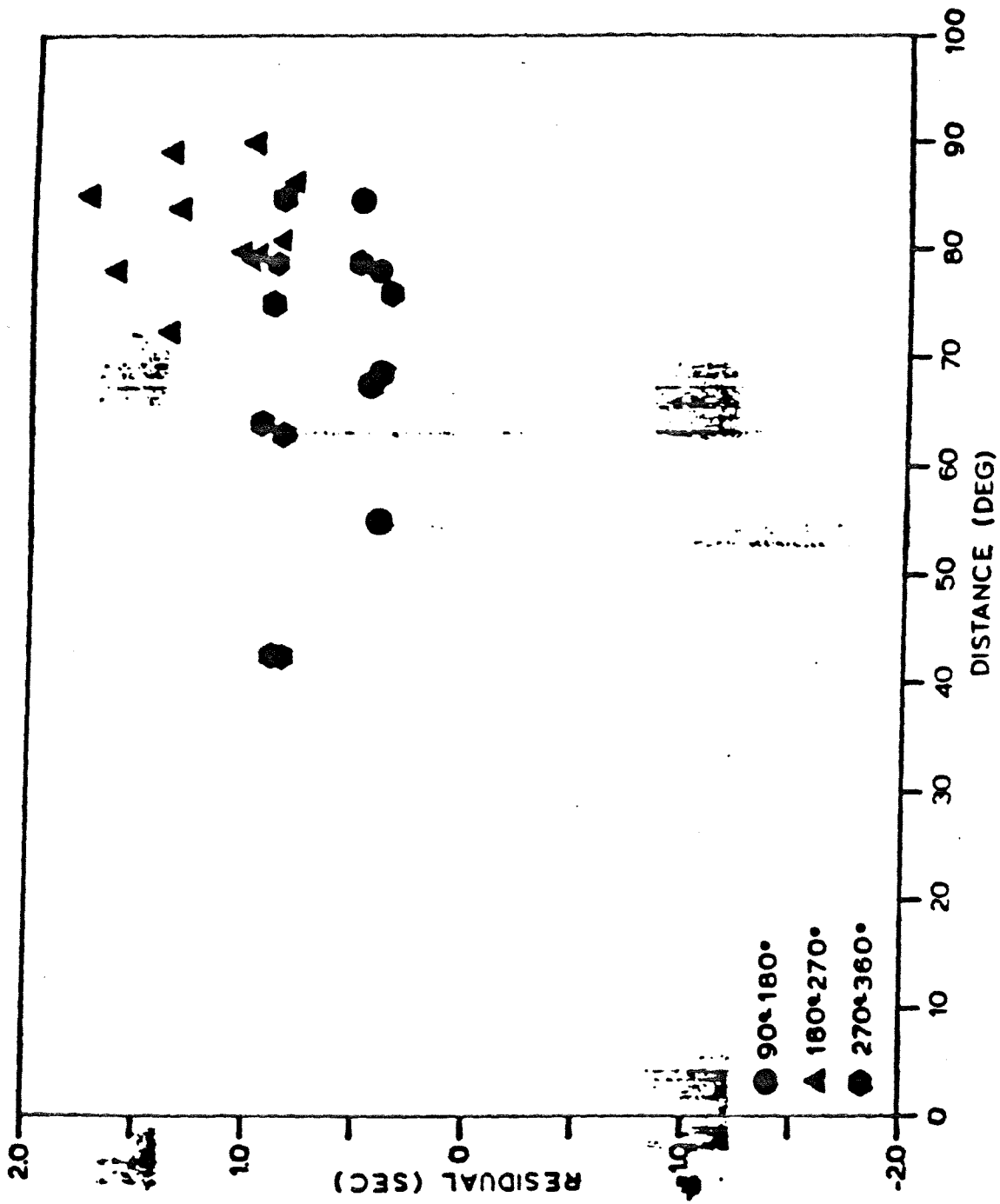
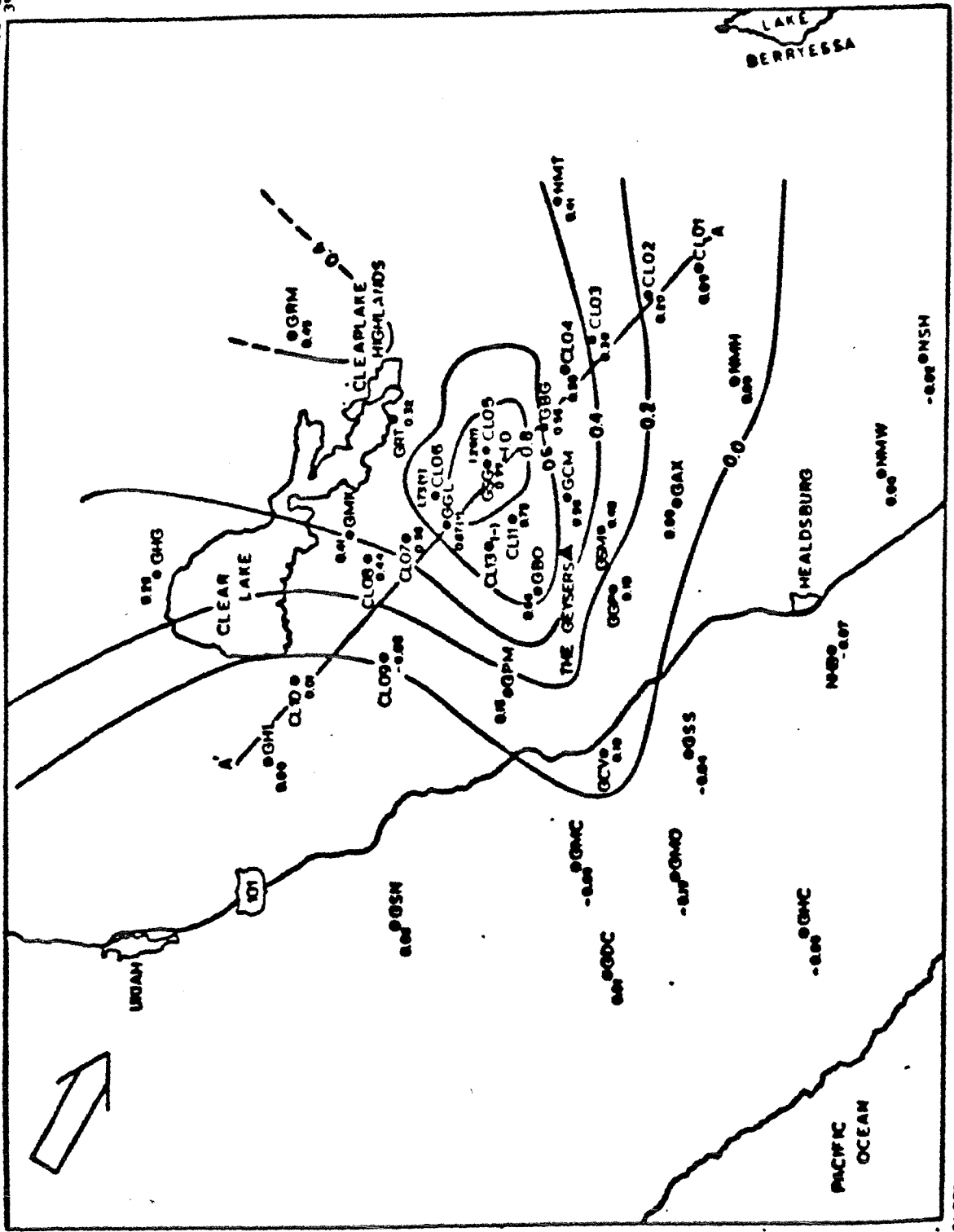


Fig. 6d

122-19
39-19



38°30'
123°30'

Fig. 76

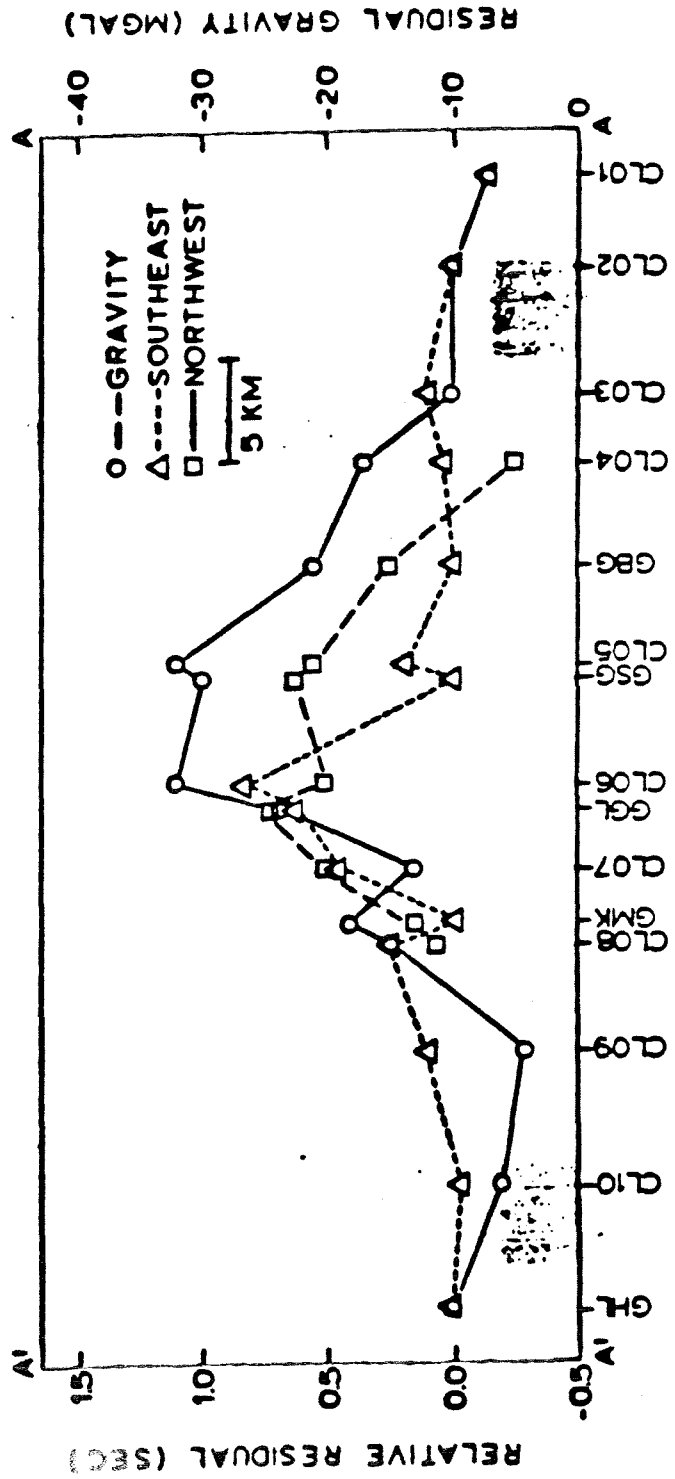


Fig. 8

122-19
39-19

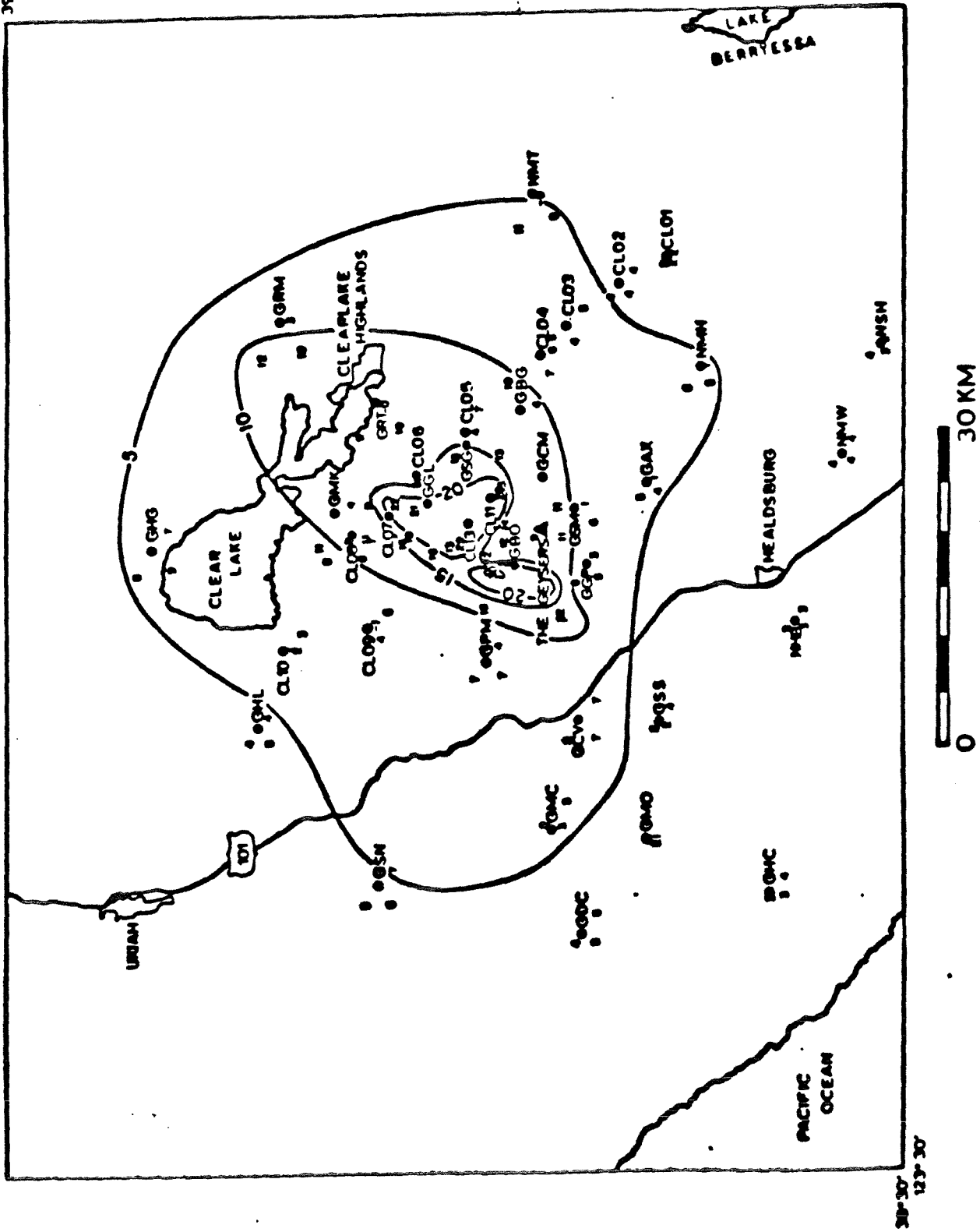


Fig. 96

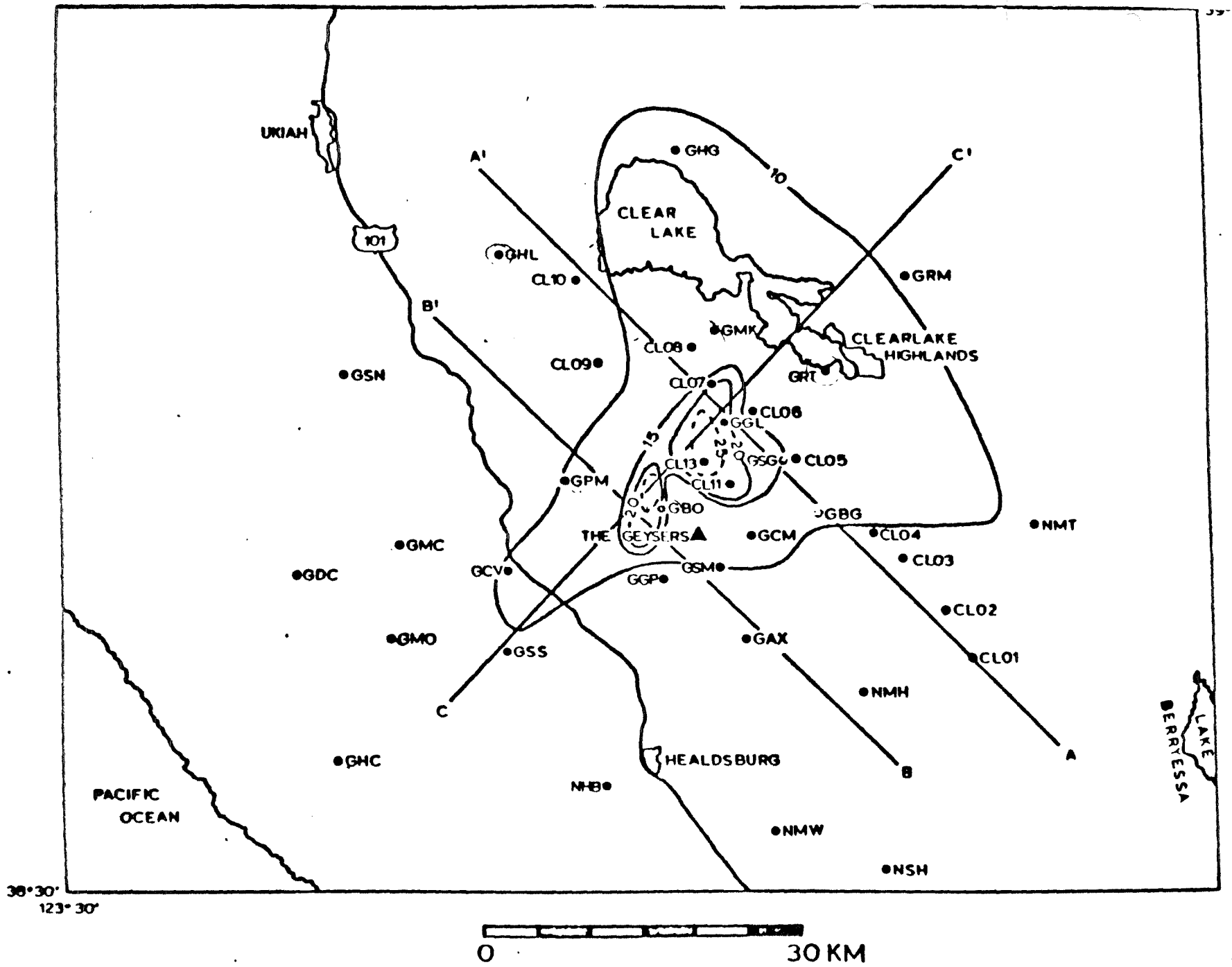


Fig. 10

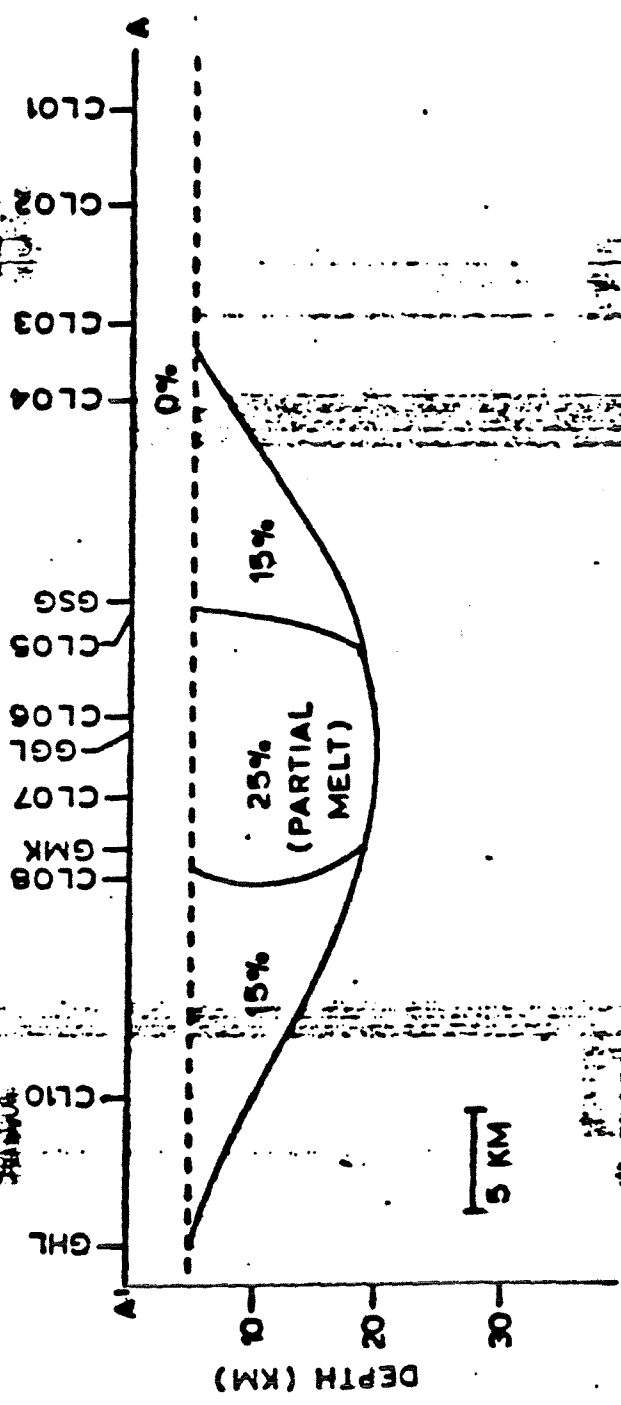


Fig. 11a

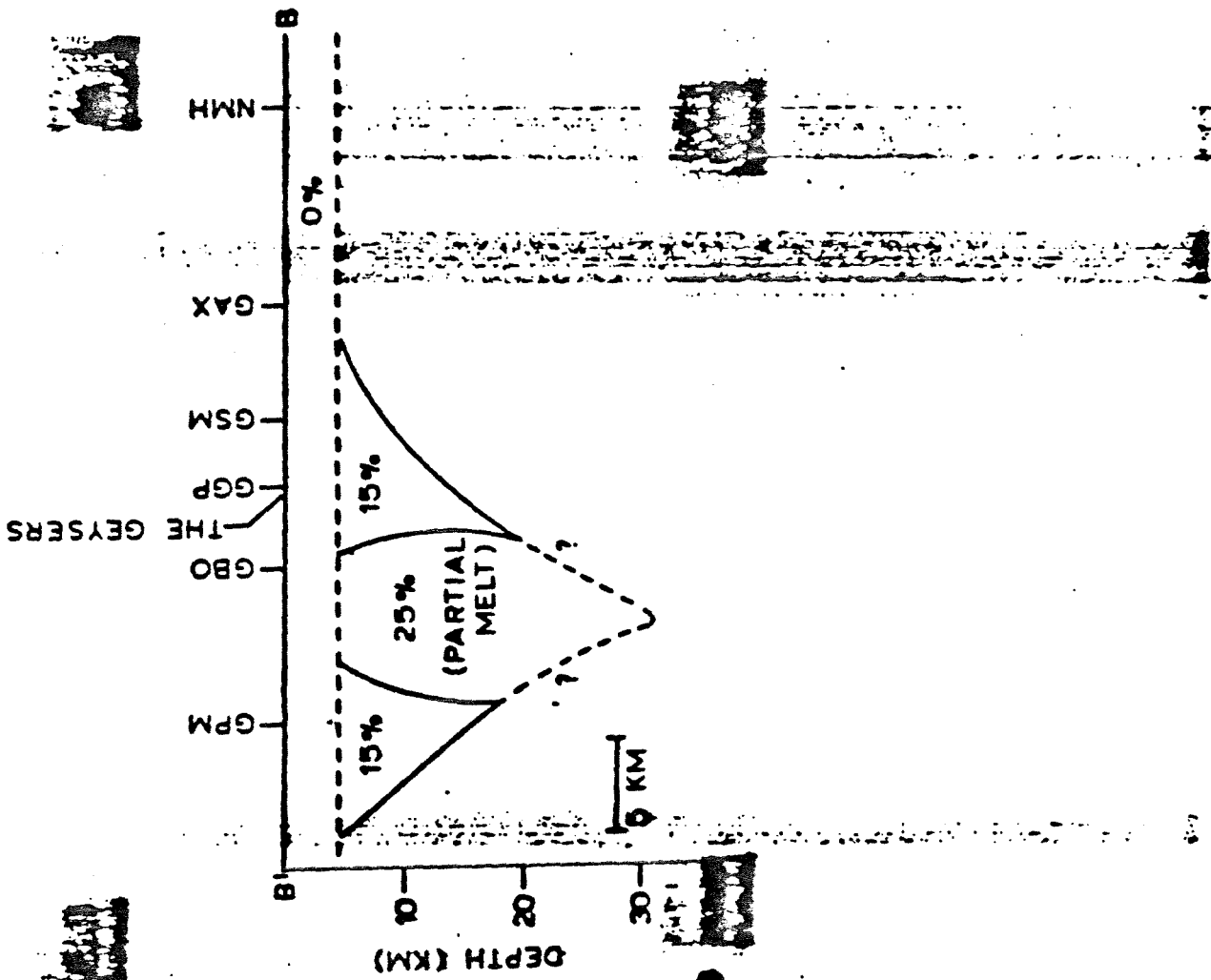


Fig. 11b

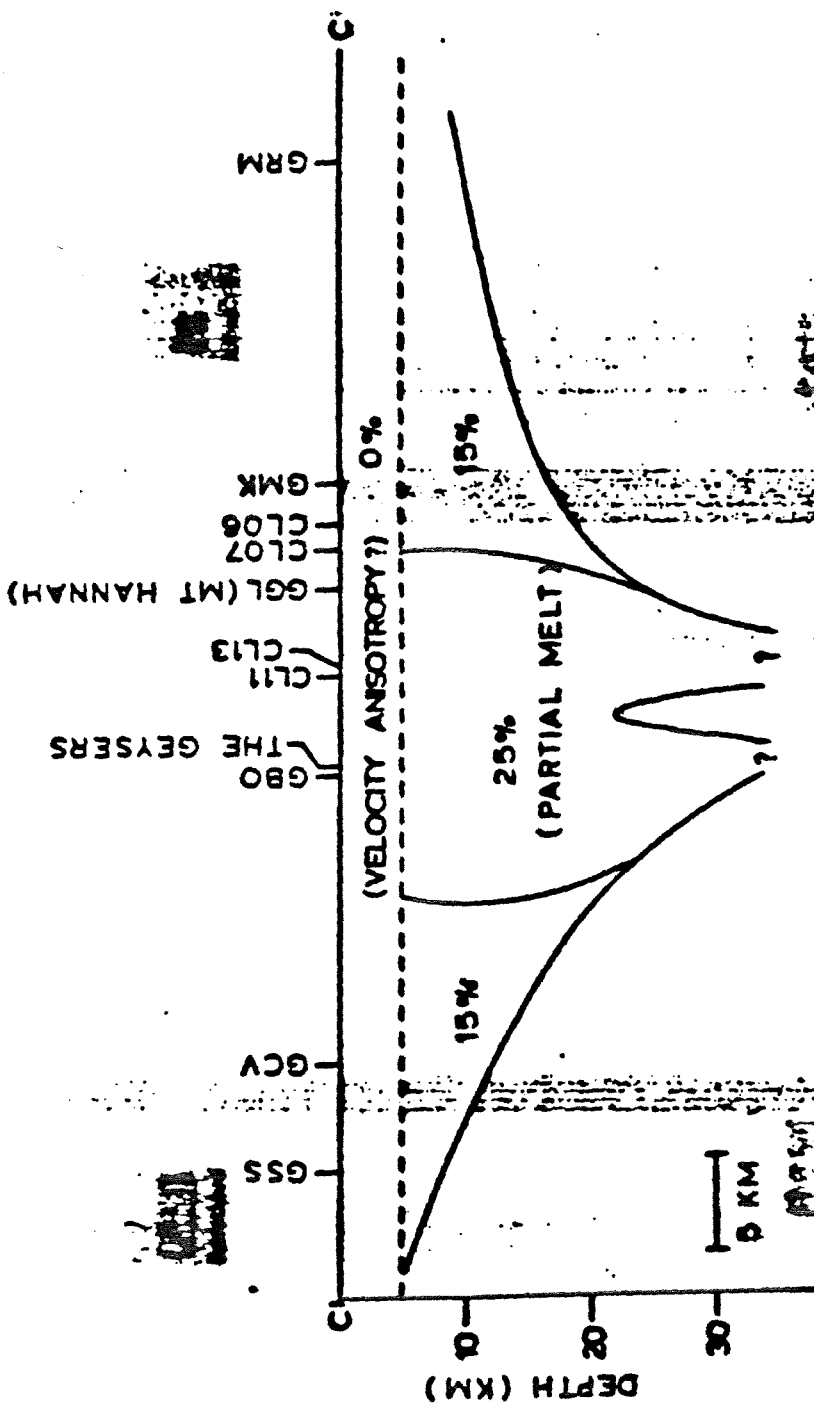


Fig. 11c

Seismological investigations at The Geysers geothermal field

E. L. Majer* and T. V. McEvilly*

Two short (4 and 6 day) recording periods at The Geysers geothermal field provided useful data on two large refraction explosions and numerous microearthquakes. The vapor-dominated reservoir appears to be characterized by regionally anomalous high *P*- and *S*-wave velocities and low attenuation, but the anomaly seems to decrease, possibly reversing, with depth. Microearthquakes occur in a diffuse pattern, with no indication of dominant throughgoing faults and an absence of activity in the main production zone. Mechanisms are generally consistent with northeast-southwest compression. Occurrence rates indicate a slightly high incidence of smaller magnitude shocks. It is possible that the microearthquake activity is related to an expanding steam zone. While the present anomalies appear to delineate the reservoir, it is not certain that they would have been detectable during exploration prior to large-scale exploitation of the field.

INTRODUCTION

In an investigation of the utility of seismological observations for geothermal reservoir evaluation, a 13-station approximately linear array of short-period vertical seismographs was set out across The Geysers geothermal field in northern California. The study was prompted by the planned detonations of two one-ton explosive sources, 8 and 18 km west of the field (Figure 1), for an unrelated U. S. Geological Survey (USGS) refraction study. In addition to the two explosions, 70 microearthquakes were recorded during the period September 20-24, 1976. The project was conducted under the Geothermal Exploration Technology Program at the University of California, Lawrence Berkeley Laboratory, which includes investigations of geophysical exploration techniques in different geothermal environments. A similar study of the type described here was conducted at Leach Hot Springs, Grass Valley, Nevada and revealed significant velocity and attenuation anomalies related to the hydrothermal system (Beyer et al, 1976). Fundamental data in such studies are velocity and attenuation of *P*- and *S*-waves relative to regional values, as well as source properties and spatial distribution of microearthquakes.

The linear array was placed through the producing steam field perpendicular to strike of the major geo-

logic trends in the region, as shown in Figure 1. Station 1 and the USGS Station SGM served as reference stations to the west and east, respectively, of the present production zone which extends from station 2 through station 12. The boundaries of the geothermal reservoir have not been defined. At the 12 temporary array stations, signals from 4.5-Hz vertical geophones were radio-telemetered to a central point and recorded, with time and tape speed compensation data, at 0.12 ips on a 14-channel FM tape recorder with 0-40 Hz bandwidth. The thirteenth station, east of the producing field, was a model MEQ-800 portable smoked-paper recorder. Conventional short-period USGS stations in the area provided additional arrival times and first motion data. The locations of the temporary University of California stations are given in Table 1. Based on the results of the 1976 study, to obtain additional wide dynamic range information on magnitudes and source properties of microearthquakes, a single channel 12-bit triggered digital cassette recorder and a smoked-paper recorder were set out near station 7 in the steam field July 22-25 and August 2-8, 1977. A total of 340 events were recorded on the smoked-paper recorder. The digital recorder malfunctioned during the July 22-25 period, but 101 events were recorded using a horizontal 4.5-Hz geophone and 54 events were recorded with a

Manuscript received by the Editor July 18, 1978.

* Seismographic Station, Department of Geology and Geophysics and Lawrence Berkeley Laboratory, University of California, Berkeley, CA 94720.

0016-8033/79/0201-503.00. © 1979 Society of Exploration Geophysicists. All rights reserved.

Table 1. Station and explosion data.

Station	Latitude (N)	Longitude (W)	Elev. (m)	Explosion #1 travelttime (sec) corrected/residual		Explosion #2 travelttime (sec) corrected/residual	
1	38° 47.124	122° 52.692	746	3.523	+.222	1.183	-.090
2	38° 47.847	122° 50.258	736	4.212	+.200	1.835	-.052
3	38° 48.100	122° 50.109	567	4.260	+.160	1.872	-.050
4	38° 48.210	122° 49.845	476	4.320	+.134	1.940	-.050
5	38° 48.483	122° 49.296	552	4.586	+.135	2.091	-.066
6	38° 48.653	122° 49.000	692	4.566	+.088	2.146	-.110
7	38° 48.669	122° 48.639	731	4.619	+.047	2.231	-.136
8	38° 48.840	122° 48.532	889	4.644	+.015	2.246	-.165
9	38° 48.891	122° 48.193	950	4.698	-.036	2.311	-.211
10	38° 48.788	122° 47.735	988	4.770	-.060	2.432	-.240
11	38° 49.045	122° 47.456	882	4.882	-.050	2.528	-.220
12	38° 49.474	122° 46.639	1050	5.159	-.075	2.826	-.203
13	38° 50.578	122° 45.662	721	—	—	3.21	-.21
*BKO	38° 49.46	122° 50.57	879	4.35	+.14	1.68	-.08
*PNM	38° 50.85	122° 56.78	783	3.62	+.14	1.07	-.06
*GYP	38° 45.88	123° 50.65	1054	3.77	+.05	2.05	-.03
*SKG	38° 42.12	122° 00.81	282	0.84	+.08	3.45	+.200
GLV	38° 53.80	122° 46.58	893	6.25	-.11	3.65	-.07
SGM	38° 52.03	122° 42.58	1080	6.85	+.17	4.29	-.08
BGG	38° 48.84	122° 40.76	1125	6.46	-.24	4.39	-.32
CMT	38° 48.35	122° 45.31	1284	5.14	-.26	3.01	-.42
SCR	38° 46.15	122° 46.87	1015	4.65	-.08	2.79	-.32
*MWS	38° 33.03	123° 43.37	144	7.15	+.01	7.05	+.16
*FTR	38° 31.36	122° 09.66	528	5.48	+.02	7.84	-.09
*HLB	38° 35.36	123° 54.54	165	4.05	+.02	5.34	+.03
*MOF	38° 42.61	123° 08.59	803	2.43	-.02	4.72	-.04
*MCL	38° 47.56	123° 07.80	428	2.83	+.06	3.93	-.01
*DRY	38° 46.03	123° 14.31	772	4.25	0.	5.92	+.03
*SNO	38° 56.43	122° 11.50	870	5.92	-.08	5.80	-.07
MKI	38° 58.17	123° 47.22	905	7.60	+.42	4.89	+.21
*HOC	38° 36.36	123° 11.81	518	4.40	0.0		

*Station used for velocity model

Explosion Locations and Origin Times:

	Time (UTC)	Day	Location
#1	1235 00.58	Day 266	38°43.50'N 123°01.44'W
#2	1235 00.64	Day 268	38°48.60'N 122°55.62'W

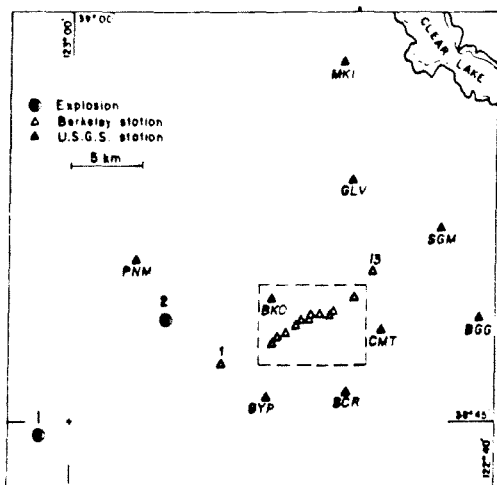


FIG. 1. Permanent (USGS) seismographic stations in the Geysers-Clear Lake area, and temporary (Berkeley) station array in the geothermal field. Box indicates area in subsequent maps. Refraction explosion locations are shown.

similar vertical geophone during the August 2-8 period.

The goal of this field experiment is an evaluation of the degree to which seismological data of the type considered can provide an indication of water state, porosity, permeability, and temperature within a geothermal reservoir, and thus offer a means of delineating field boundaries.

EXPLOSION DATA

P-wave velocities

A fundamental question in this study is whether the presence of the geothermal reservoir is evident in the velocity of propagation of *P*-waves. A regional reference traveltime curve shown in Figure 2, with velocities of 5.04 ± 0.10 km/sec and 4.57 ± 0.11 km/sec, was constructed from USGS station readings for both explosions omitting, however, stations in The Geysers and Clear Lake areas. Elevations and traveltimes are given in Table 1. Elevation corrections are made with respect to station 4 using 4.0 km/sec. Velocities determined for The Geysers and Clear Lake areas then can be compared for velocity anomalies to the re-

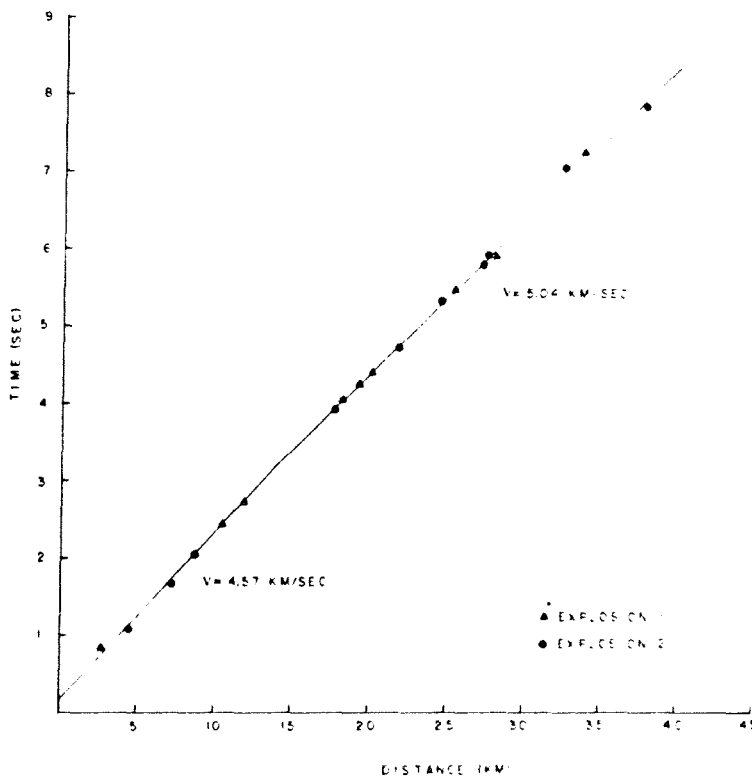


FIG. 2. Regional traveltimes versus distance graph for stations outside known geothermal area, based on the two explosions, corrected for elevations.

gional traveltime curve. The relatively low regional velocities in Figure 2 indicate that only the upper 2 to 3 km of the crust are sampled by the first arrivals from the explosions. It was hoped that by recording several regional earthquakes or teleseismic events the deep structure could also be studied. Unfortunately, no such events were recorded during the five-day field period (September 20–24, 1976).

Figure 3 is a graph of corrected traveltimes versus distance for the temporary stations, with respect to the regional data in Figure 2. The maximum elevation correction in the field is 128 msec at station 10, yielding a relative time advance of some 200 msec between stations 4 and 10. Slower correction velocities would increase the relative advances. Corrected traveltimes at stations 1 through 5 plus BKO, PNM, and GYP at 5–10 km distance, appear regionally slightly early for explosion 2, but some 150 to over 200 msec late for explosion 1. Along the temporary station array, early arrivals with relative *P*-wave advances of up to 200 msec are seen commencing around station 5 and continuing to the end of the temporary linear array at station 13. Corrected traveltime at station MGM to the northeast of the producing field appears regionally normal. Corrected traveltimes at USGS stations SCR, CMT, and BGG are also early, i.e., fast with respect to the regional reference (Figure 2). The corrected traveltime of station MK1, near Clear Lake, is especially late for both explosions. The general tendency seems to be that traveltimes in the production zone and southeast of it are early, and as one proceeds northeastward toward Clear Lake the times become regionally normal, then significantly delayed. This general pattern holds for both the near and far explosions. Close inspection of data from the far explosion reveals that, even though the shape of the curve is the same as that for the near source, the traveltimes from the far explosion have been delayed by up to 200 msec with respect to regional. The difference between residuals for the two explosions is a maximum at station 1, indicating the possibility of a low velocity region at intermediate depth (2–4 km) delaying arrivals from the far explosion in the area of this explosion. The postulated feature coincides with the Mercuryville fault zone and possibly with the western edge of the geothermal system.

Attenuation

In addition to the possibility of anomalous traveltime and velocity, we sought evidence for the production zone affecting the amplitude and waveform of the *P*-wave. Figure 4 is a seismogram section for explosion 1. It is evident from visual inspection of the first

two or three cycles of the *P*-wave that the waves are attenuated less within the production zone than at station 1, 5 km west of the production zone.

Two approaches were taken to estimate the attenuation effect at the different sites. The first approach is an adaption of a technique developed by Teng (1968) for analysis of teleseismic data. The ratio of the spectrum of the *P*-wave at each station to an arbitrary reference station is used to obtain the differential attenuation. It is assumed that *Q* is frequency-

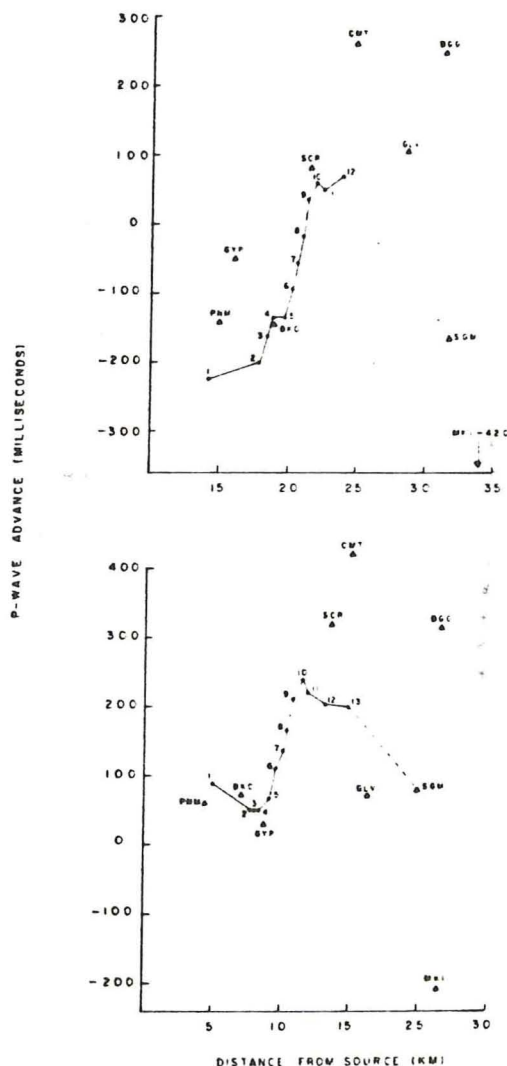


FIG. 3. Residual traveltimes, with respect to traveltimes shown in Figure 2, for stations within The Geysers-Clear Lake area and for explosions 1 (lower) and 2. Temporary stations are numbered, USGS stations are shown by name.

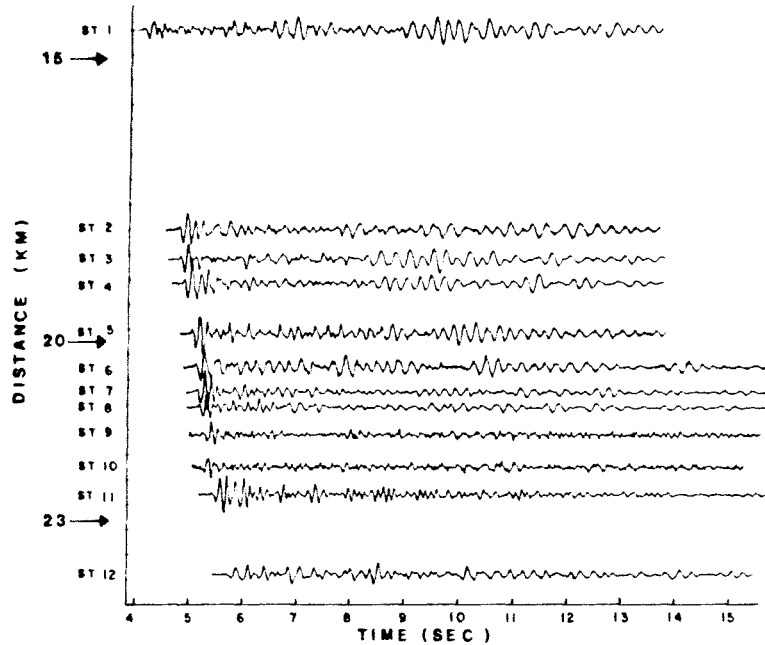


FIG. 4. Seismograms from the far explosion, plotted at equal gains and at relative distances.

independent over the particular frequency band used. The attenuation operator can be expressed as:

$$\exp \left[-\pi f \int_{\text{path}} \frac{ds}{QC} \right]$$

where

s = path length,

$$Q^{-1} = \text{intrinsic attenuation} = \frac{2\pi \Delta E}{E}$$

$\frac{\Delta E}{E}$ = fraction of strain energy dissipated per cycle,

C = P -wave velocity, and

f = frequency.

The path of integration is taken along the raypath. For constant Q , the log of the spectral ratio of the P -wave will be a linear function of frequency with slope, $-\pi \delta t / Q$, where δt is the travelt ime difference between the two stations. The resulting Q applies to the differential raypath. In practice, one corrects for differences in instrument response and radiation pattern or for any frequency dependent effects which differ at the two stations, and then fits a straight line to the resulting spectral ratio.

An assumption in this method is that the path to both points is the same except over the last fraction of

the total path. This results in a negative slope to the spectral ratio, with zero slope for infinite Q , i.e., no attenuation. In practice, positive slopes are obtained if the path to the first point contains a segment of low Q medium not common to the second path. Widely differing near-surface transfer functions at the two sites can also produce strange effects in the spectral ratio. To minimize such effects, it is necessary to use a smoothed average spectrum as reference in forming ratios. The seismograms from each site for the distant explosion were anti-alias filtered and digitized at 200 samples/sec. The digitized data were then plotted for comparison checks with the analog data to select the proper P -wave time intervals. P -wave 0.65-sec time windows were tapered with a 20 percent cosine taper, the average signal level was removed, and zeros were added to total 2^{10} sample points. The data were transformed with a fast Fourier transform and then was corrected for instrument response. Spectra were smoothed with a moving 10-point averaging window. The reduced spectral ratios then were computed and plotted.

The P -waveforms along with individual displacement amplitude spectra are shown in the first two columns of Figure 5. Signal-to-noise ratios are maximum in the 2–10 Hz range. The spectra are not corrected for geometrical spreading. The individual

spectra show generally less high frequency loss within the production zone. At stations 1 and 12, the spectra have no definite high frequency corner. However, most stations in the geothermal field, e.g., 7 and 8,

have well-developed corners at approximately 10 Hz, suggesting higher Q beneath the production zone.

The third column in Figure 5 shows reduced ratios with respect to an averaged spectrum, rather than with respect to the spectrum for station 1. (Initially, spectral ratios were obtained using the station 1 spectrum as reference. Examples are shown in Figure 6.) In an attempt to reduce the large variations in the ratios, an alternate reference spectrum was sought. The first cycle of the P -wave was analyzed, and its spectrum was smoothed and averaged using all the stations. The resulting average was used as the reference spectrum. Reduced spectral ratios with respect to this average spectrum are given in the third column of Figure 5. These reduced spectral ratios are nearly linear. A positive slope means a higher Q than average, a negative slope means a lower Q . Over the entire 1-10 Hz span, stations 1, 2, 6, and 12 exhibit negative slopes while all other sites have positive slopes, indicating a correlation between lower Q at the edges and outside the field, and higher Q within the production zone. Further attempts to use the slopes in Figure 5 for inversion to obtain Q structure are not warranted by the quality of the data.

To obtain a more reliable reference spectrum, more

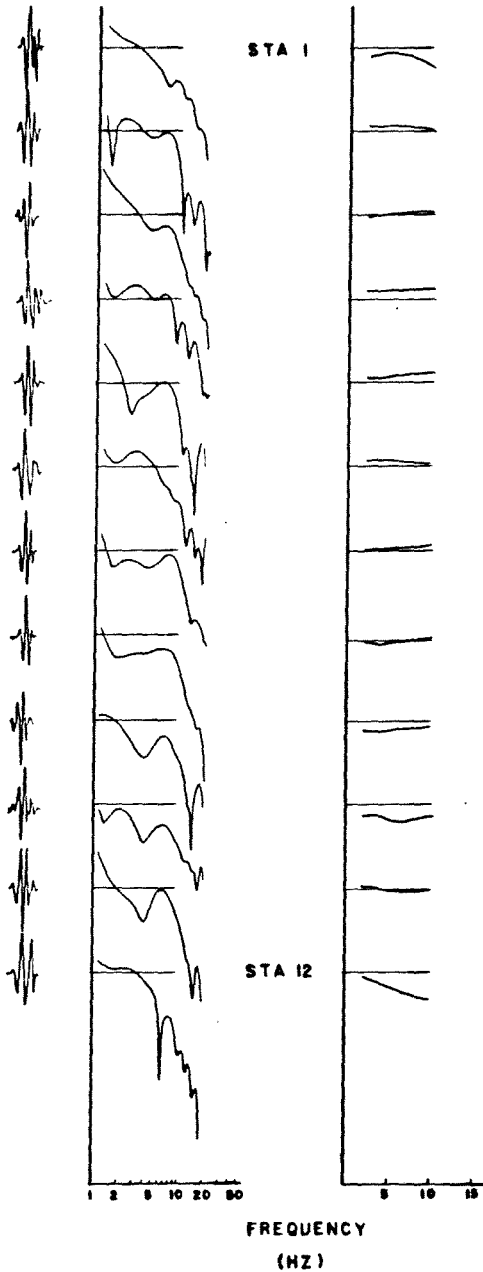


FIG. 5. P -wave signals (left), spectra (middle), and spectral ratios (right) with respect to smoothed reference spectrum (see text).

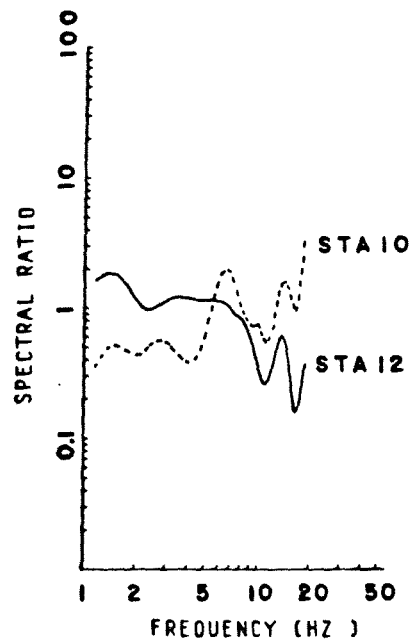


FIG. 6. Example spectral ratios with respect to station 1 spectrum, unsmoothed, as reference.

Table 2. Average attenuation values Q_i for various Q_r , for explosions 1 and 2 respectively.

Station	$Q_r = 30$	$Q_r = 45$	$Q_r = 60$
1	14.10	17.12	19.13
2	30.30	45.45	60.60
3	33.32	52.51	71.67
4	38.—	63.—	94.—
5	48.—	86.—	142.—
6	44.75	71.189	102.250
7	41.164	63.250	86.250
8	34.92	47.250	58.250
9	28.50	36.76	43.94
10	30.62	37.100	44.132
11	40.34	56.42	70.47
12	19.51	23.66	25.75

stations are needed outside the steam field, but this would have reduced the number of stations over the production zone. The frequency range 3–10 Hz is also susceptible to effects of very shallow structure, rendering difficult the estimation of meaningful spectra. In general, if the data are of sufficient bandwidth and dynamic range, if there are several reference stations outside the zone of interest, and if the target is large enough, then the method of reduced spectral averages probably can be used successfully to delineate anomalous Q zones. The effectiveness might also be increased if longer period P -waves are present in the signal, though the attenuation effects would become small on the scale of this experiment.

A second approach was used to localize the Q variation by considering only the amplitude of the first half cycle of the P -wave at each station, and by specifying more precisely the differential raypaths by using both explosions. The local velocity model shown in Figure 7 was assumed. We assign to a reference station with first half cycle amplitude A_r , a value Q_r for the vertical part of the path at the station. We can then calculate, based on the model raypath geometry, a value Q_i corresponding to the horizontal propagation path from the reference station to station i and the near-vertical propagation under i , according to

$$Q_i = \pi f \delta t_i / \left[\frac{\pi f \delta t_r}{Q_r} - \alpha \ln \frac{X_i}{X_r} - \ln \frac{A_i}{A_r} \right],$$

where

$\delta t_r, \delta t_i$ = difference in traveltimes to the reference station and to the surface sites from the source.

f = apparent frequency of the P -wave.

X_r, X_i = source to station distances, and

α = geometrical attenuation factor, assumed 1.5.

The resulting Q_i value will depend on the Q_r assumed, and it will contain information on the entire path from beneath the reference station to the surface at station i . As the Q values obtained are relative and

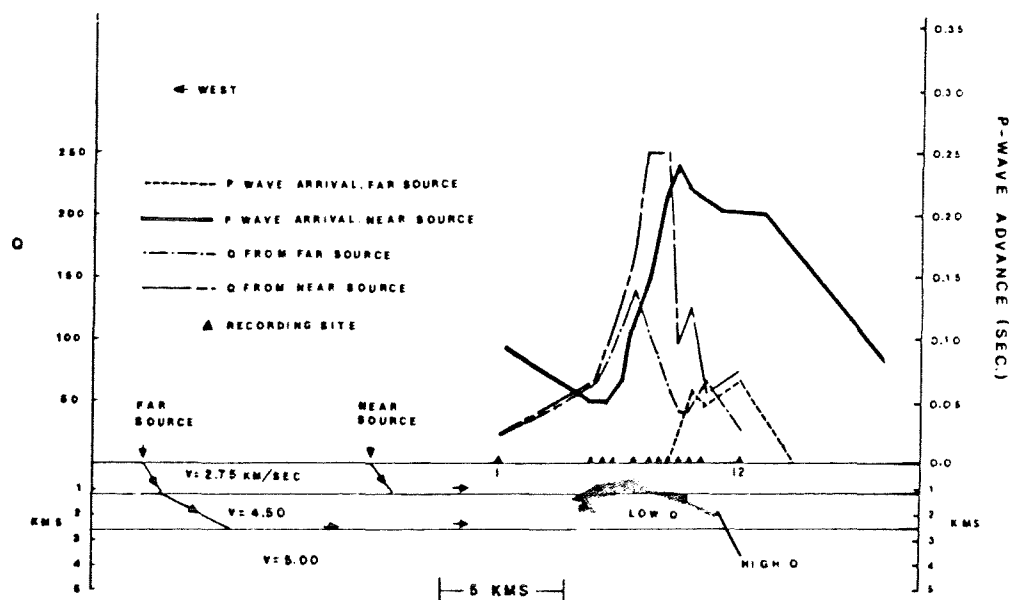


FIG. 7. Composite model for Q estimation, showing P -wave traveltimes residuals and Q_i through the production zone for both explosions. Zone of inferred high Q and high velocity is shaded. Q_r is assumed to be 60.

depend on the path assumptions, it is advisable to use a reference station near the region of interest. Results for Q_r values of 30, 45, and 60 for station 2, as reference, are given in Table 2 for both explosions. A maximum value of 250 was assigned to Q_i because the fractional change in amplitude of the wave for higher values of Q cannot be measured over the distance involved.

Resulting Q_i values for $Q_r = 60$, with traveltime data, are shown in Figure 7 across the field. For both explosions (and all values of Q_r) the apparent Q increases throughout the field then decreases again by station 12. This is the same general pattern seen for the spectral ratios. Q values obtained within the field are higher for the more shallow paths from the near source than for the deeper waves from the far source. Q within the steam field thus appears high with respect to regional values at shallow depths (<1 km), decreasing at greater depths. It is not clear whether the Q values decrease below regional values at depth. Data consistent with high Q in the field come also from the study of the corner frequencies of microearthquakes, discussed in the following section.

MICROEARTHQUAKES

Locations

During the five days of recording (September 20-24, 1976) 70 earthquakes were observed in the signals

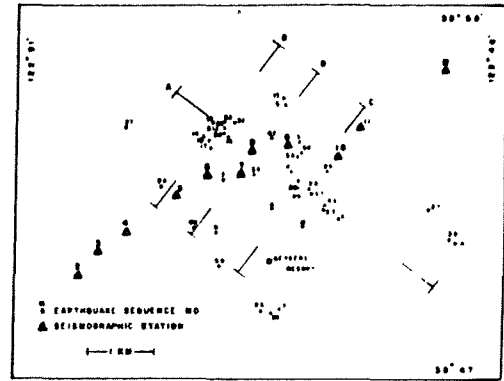


FIG. 8. Epicenters, with sequence numbers (see Table 3), for well-located microearthquakes recorded during the period September 20-24, 1976. Locations of sections in Figure 9 are indicated.

monitored at stations 1, 7, and 12. There were no local events recorded by the USGS stations PNM, BKO, SGM, CMT, SCR, BGG, and GYP that were not recorded by the temporary stations. However, there were 12 events recorded by the temporary stations that were recorded only by the two USGS stations closest to the production zone, BKO and CMT, indicating that the microearthquakes are confined to the general area of the steam field. The high rate of

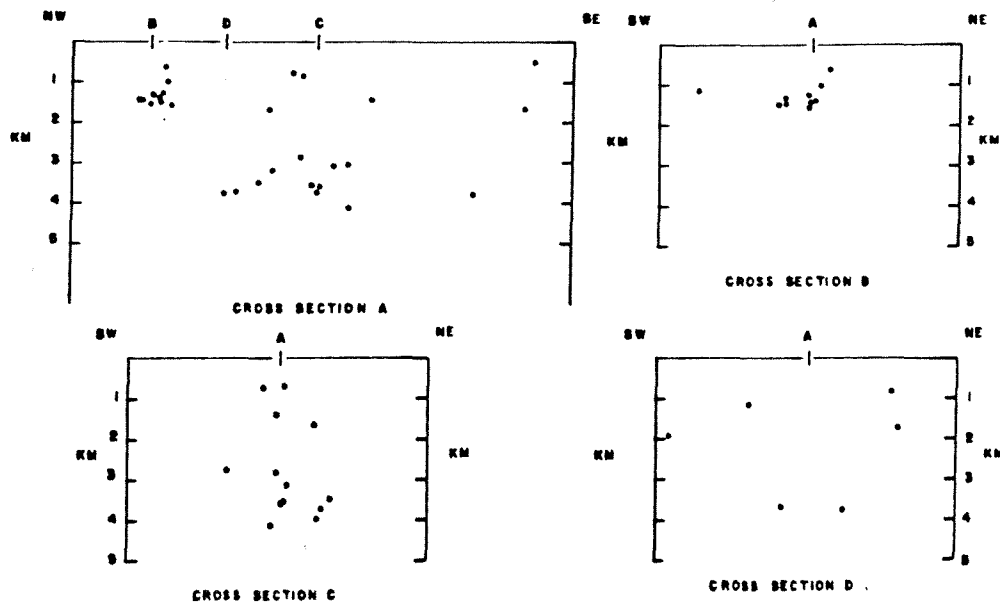


FIG. 9. Cross-sections of hypocenters through the steam production zone. Locations of section lines are shown in Figure 8.

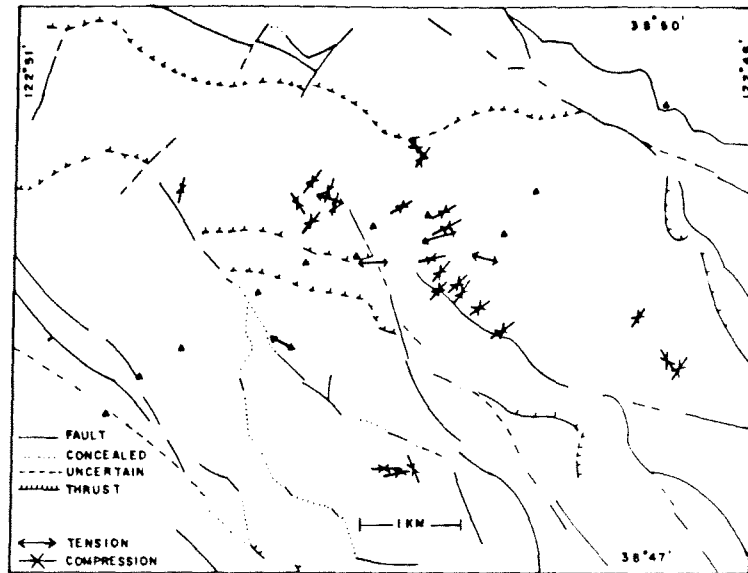


Fig. 10. Horizontal projections of principal stress axes from fault-plane solutions. Either compression or tension axis is given, whichever is near-horizontal. Faults shown are adapted from McLaughlin, 1974.

seismicity is apparently an ongoing phenomenon. Hamilton and Muffler (1972) recorded 53 events in three weeks with epicenters in the same general area. Lange and Westphal (1969) recorded 19 "small" earthquakes throughout the production zone during a four day observation period. In our later survey, July 22–25 and August 2–8, 1977, 340 events with *S-P* times less than 1 sec were recorded near station 7.

Hypocenters were estimated using a simple regional model of two layers over a half-space, velocities of 4, 5, and 6 km/sec and layer thickness of 1 and 5 km, respectively, obtained by minimizing the depth standard error in locating several large events at the center of the array using different velocities consistent with the explosion data. Events with clear arrivals on at least 5 temporary stations and 3 USGS stations were processed for locations. Forty of the 58 events processed could be located with standard errors less than 0.1 km, indicating fairly well constrained solutions. The epicenters plotted in Figure 8 and location data are listed in Table 3. Columns designated " M_{CB} " and " M_{CL} " in Table 3 are earthquake magnitudes discussed later. *S*-waves were not used in locating the events, but *S*-wave arrival times of events recorded at sites designated " σ_{group} " in Table 3, were used to estimate Poisson's ratio, discussed later.

Figure 9 shows microearthquake hypocenters pro-

jected onto vertical sections. Locations which are shown in Figure 8. The spatial distribution of foci is diffuse, showing no well-defined throughgoing faults. Focal depths are less than 5 km, with an apparent lack of foci in the depth range of 2 to 3 km. Seismicity is also low in the area first exploited for steam, less than 1 km north and northeast of The Geysers Resort (Figure 8). The wells in this area are shallow (less than 1 km) compared to more recent wells, which extend to nearly 3 km. In general, the production zone throughout the field is between 2 and 3 km in depth (Richard Dondanville, oral communication, 1977). Most of the larger events, e.g., 28, 29, 45, occurred in an area about 1 km northeast of the Geysers Resort. During the later field study, July 22–25, August 2–8, 1977, a magnitude 2.3 shock was recorded in this same general area.

The temporal distribution of events is also of interest. While clusters of events are seen, there is no indication of systematic migration through the field. For example, events 36 to 40 occurred within a two-hour period but in three separate areas. There were no apparent instances of foreshock activity followed by a main shock, nor of clear aftershock sequences. There were no long aseismic periods; the activity seems to progress at a more or less constant rate.

Mechanisms

P-wave polarities were used in focal mechanism

studies. Because complete azimuthal coverage was not obtained, there is ambiguity in the details of fault plane solutions. Only the better constrained solutions are shown on a regional fault map in Figure 10. Plotted are the horizontal components of the principal stress axes, mainly compressional in the northeast-southwest direction. This stress is consistent with strike-slip faulting on near-vertical, north-south trending faults, and is typical of regional Coast Range tectonics. Northeast-southwest reverse

faulting is also plausible. The northwest trending Collayami and north-northwest Konocti Bay fault zones in the Clear Lake volcanics to the northeast (Figure 1) are some 20 km long and show right-lateral and vertical movement. Donnelly (1977) states that the small (<1 km length) normal faults trending northeast and northwest at Clear Lake are probably the result of crustal adjustments from the extrusion of magma in the region. In The Geysers region, the northwest-southeast structural grain is

Table 3. Microearthquake locations.

Sequence number	M _{CB}	M _{CL}	Latitude	Longitude	Depth (km)	Standard error of epicenter (km)	σ group
1			38°48.54'N	122°48.06'W	0.71	.02	
2	0.6	-0.1					
3	0.4	-0.5	48.58'	48.86'	1.19	.07	5,12
4			48.35'	48.37'	2.79	.01	
5	0.2	-1.0	49.18'	48.26'	0.84	.05	5,12
6	0.4	-0.6	48.32'	47.70'	1.41	.03	
7	0.7	0.2	47.57'	48.25'	4.40	.07	1,5
8	0.2	-1.0	48.17'	48.93'	0.90	.10	
9	0.7	0.2	48.46'	48.16'	0.75	.07	
10	0.1	-1.3					
11	0.5	-0.4					
12	0.8	0.5					
13	0.4	-0.6					
14	0.1	-1.3	48.94'	49.06'	1.43	.07	7,12
15	0.4	-0.6	49.24'	48.25'	1.74	.03	5
16	0.4	-0.5	48.86'	48.82	1.58	.05	12
17	0.3	-0.7	48.84'	48.94'	1.49	.08	12
18	0.3	-0.9	48.89'	49.04'	1.30	.07	12
19	0.3	-0.9	49.06'	48.95'	1.41	.04	5
20	0.3	-0.7					
21	0.3	-0.8	48.98'	48.95'	1.54	.03	12
22	0.2	-1.2					12
23	0.3	-0.7	47.57'	48.34'	3.0	.05	5,12
24	0.3	-0.9	48.53'	49.50'	1.11	.01	5,7
25	0.6	0.1	48.36'	47.86'	4.14	.5	7
26	0.4	-0.5	47.56'	48.50'	3.0	.06	
27	0.4	-0.4	49.01'	49.84'	0.67	.09	1
28	0.7	0.3	48.51'	47.97'	3.55	.05	1
29	0.9	0.9	48.66'	47.80'	3.76	.05	1
30	0.8	0.8	48.97'	48.86'	1.25	.03	12
32	0.3	-0.8	49.05'	48.74'	0.60	.03	
33	0.4	-0.6					
34	0.7	0.1	48.78'	48.10'	1.64	.04	7
35	0.5	-0.2	48.63'	48.55'	3.70	.08	12
36			49.01'	48.84'	1.38	.04	12
37			48.37'	46.74'	3.77	.09	12
38	0.3	-0.8	48.50'	48.16'	2.86	.10	
39	0.4	-0.4	48.11'	46.54	1.64	.07	7,12
40	0.6	0	48.09'	46.49'	0.52	.10	7,12
41	0.3	-0.7	48.65	48.18'	3.18	.03	
42	0.7	0.2	48.93'	48.34'	3.75	.06	1
44	0.5	-0.3					
45	1.0	1.2	48.39'	47.81'	3.05	.05	5
46	0.5	-0.3					
47	0.2	-1.1					
48	0.3	-0.9					
49	0.4	-0.6	48.21'	49.17'	1.92	.04	1
50	0.7	0.3	47.90'	48.92'	0.40	.05	1,5
51	0.5	-0.1	48.88'	48.09'	3.50	.05	7
52	0.5	-0.1	49.01'	48.97'	0.98	.07	12
53	0.4	-0.5					
57			48.48'	47.95'	3.59	.04	
58	0.5	-0.3	48.80'	48.06'	4.01	.07	7

due to the prevailing fault pattern which consists of imbricate reverse faults cut by later strike-slip faults, reflecting the tectonic evolution of the area (McLaughlin and Stanley, 1975).

Magnitudes

Microearthquake magnitudes were obtained by averaging coda durations for events recorded at stations 5, 7, 9, and 12. These magnitudes (second and third columns in Table 3) are intended to be equivalent to the local Richter magnitude M_L , in order to compare Geysers earthquake occurrence rates to other central California seismicity. Two different formulas were used for magnitude determination. In the first, $M_{CL} = -0.87 + 2 \log_{10}(T)$ where T is the average coda length from the four stations. The amplitude threshold defining coda length was obtained by comparing measurements for the same events on records from this study with those for the USGS systems, with peak magnifications around 15 Hz used by Lee et al (1972) to develop the M_{CL} scale for central California earthquakes. The second formula $M_{CB} = 0.28 + 0.71 \log_{10}(T)$ was similarly obtained by Bakun and Lindh (1977) for earthquakes with coda lengths less than 30 sec in the 1975 Oroville, California sequence. If no magnitude is given in Table 3, at least one of the four stations did not have adequate data quality to obtain coda length.

Figure 11 shows the recurrence data fitted to $\log(N) = a - bM$ formulas where N is the total num-

ber of earthquakes assigned magnitudes. Values of b of 0.81 ± 0.3 and 2.3 ± 0.15 were found using the M_{CL} and M_{CB} formulas, respectively. A regional b -value of 0.83 ± 0.04 was calculated for 73 events, $2.8 < M_L < 4.8$, occurring within a 50 km radius of The Geysers between 1934 and 1973. C. Bufe (personal communication, 1977) has obtained a b -value of 1.2 for events in The Geysers area with M_{CL} magnitudes between 1 and 3. Extrapolation of the M_{CL} derived b -value of 0.8 to larger magnitudes implies the occurrence of two $M_{CL} = 3$ events per year, and a $M_{CL} = 4$ shocks every three years. However, this rate of occurrence of larger events at The Geysers has not been observed historically. This would indicate that some natural magnitude limiting process is in operation, that the local b -value is higher than the 0.8 regional value, or that the rate of seismicity is higher now than in recent decades. The M_{CB} recurrence predicts one $M_{CB} = 3$ events every 600 years, and 121,000 years between $M_{CB} = 4$ earthquakes. While $b = 2.3$ is anomalously high, a value somewhat greater than 1 is consistent with the absence of larger events in the area. The magnitude 3.7 earthquake near Cobb Mountain on September 22, 1977, indicates that the 2.3 b -value is too high, if this event is from the population of events in the production zone. The latter is not clear, but the shock did occur on the edge of the hypothesized steam zone (Geoff et al, 1977).

The application to The Geysers of coda magnitude

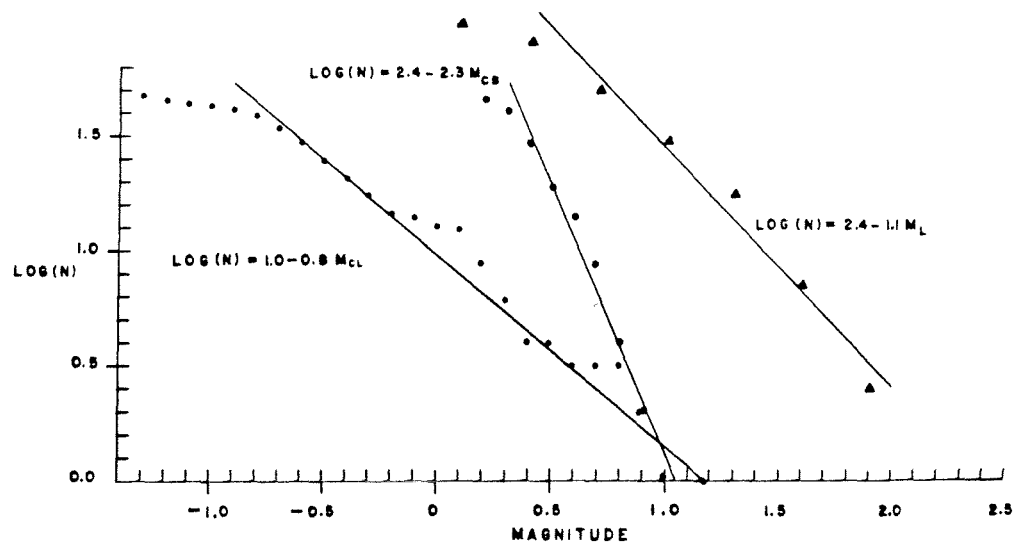


FIG. 11. Microearthquake occurrence data based on different magnitude formulas. M_{CL} and M_{CB} are coda-length magnitudes for the same 1976 data set (4 days). M_L is equivalent Wood-Anderson magnitude for the August 1977 data set (3 days).

formulas developed for other regions is a questionable step if occurrence data are compared to data for different regions. Coda lengths for several large events and the two explosions varied widely from one USGS station to the next, depending on distance and azimuth. Thus, although the same measurement used routinely by USGS was attempted, it suffered from the unusual variability of earthquake characteristics at The Geysers. The same near-station properties that affect the amplitude of the *P*-wave will affect the measured coda length. Attenuation appears anomalous in The Geysers, thus our magnitudes and resulting *b*-values may be meaningless for comparisons to other regions. It is important, but unfortunately difficult, to know if a unique geothermal earthquake exists with occurrence properties different from normal tectonic events.

Because the coda magnitudes are suspect for comparison purposes, we attempted to obtain Wood-Anderson magnitudes (M_L) using data from a single-component 12-bit triggered digital cassette recorder and a 4.5-Hz horizontal geophone set out near station 7 during August 5–8, 1977. One hundred and one events with *S*–*P* times less than 1 sec were recorded during the 3-day period. The events were recorded at a sample rate of 200/sec. The digitized time series were Fourier transformed, the instrument response removed, and the resulting spectra of the horizontal ground displacement were conditioned by the Wood-Anderson instrument response

$$\frac{-s^2}{s^2 + 2\delta\omega_n s + \omega_n^2},$$

where

$$\begin{aligned} s &= i\omega, \\ \delta &= \text{damping factor} = 0.8, \text{ and} \\ \omega_n &= \text{natural frequency of Wood-Anderson,} \\ &\quad \frac{2\pi}{0.8} \text{ rad/sec.} \end{aligned}$$

To avoid noise in the spectra at low and high frequencies, the data were band-limited between 3 and 40 Hz. The equivalent Wood-Anderson spectra were then inverted to the time domain, and the resulting synthetic Wood-Anderson seismograms were read for magnitude M_L in the conventional manner.

Ninety-eight events were processed for Wood-Anderson magnitudes (Figure 11), resulting in a magnitude range of 0 to 1.8, with a *b*-value of 1.1 ± 0.1 , between the two coda values of 0.8 and 2.3. The most reasonable estimated *b*-value for The Geysers field earthquakes, based on conventional M_L magnitude, is somewhat greater than unity, implying a

process producing a higher proportion of small magnitude events than is characteristic of the regional seismicity. As steam is produced and the hydrology altered, the *b*-values may change with time.

Velocities and Poisson's ratio

P- and *S*-wave velocity ratios (V_p/V_s) may be estimated using the Wadati diagram, where *S*–*P* interval time is plotted versus the *P*-wave arrival time at many different stations for a single event, assuming the same (V_p/V_s) along all propagation paths. The slope of the line through the points is $K - 1$ (where $K = V_p/V_s$). From K , Poisson's ratio σ may be calculated from

$$\sigma = \frac{(K^2 - 2)}{2(K^2 - 1)}.$$

This method, which gives an average σ along the paths between the stations and the event, does not require knowledge of the origin time of the earthquake. However, it does require a relatively large number of good *S*-wave arrivals to obtain a reliable slope. Because horizontal geophones were not used throughout this study, the number of sharp *S*-wave readings was limited for any particular event. Therefore, we elected to use multiple events at a single station as an alternative method for estimating $K - 1$. This method requires a knowledge of the origin time. However, because the events in this study were located using *P* times only, and the standard errors were small, it was felt that errors in the origin times would not obscure any significant lateral variation in σ . The method gives a value of Poisson's ratio along the path to the station for each source, relative to the *P*-wave velocity used in locating the earthquake. Stations 1, 5, 7, and 12 were selected for analysis using the events grouped as indicated in Table 3. The *S*–*P* interval time versus *P*-wave arrival time are plotted in Figure 12. $K - 1$ was determined by a least-squares fit to the data points constrained to pass through the origin for stations 1, 7, and 12, but through (0.0, 0.1) for station 5, where traveltime residuals were consistently between -0.1 and -0.2 sec, while the residuals averaged zero at the stations 1, 7, and 12. Resulting values of σ are 0.15, 0.21, and 0.24 at stations 5, 7, and 12, respectively. Two different values were obtained at station 1; namely, 0.32, using events that were outside of the field and travelpaths not passing through the production zone, and 0.27, for events in the center of the field with part of the path through the production zone. Although the data set is limited, this indicates lower values for σ within the production zone. Combs

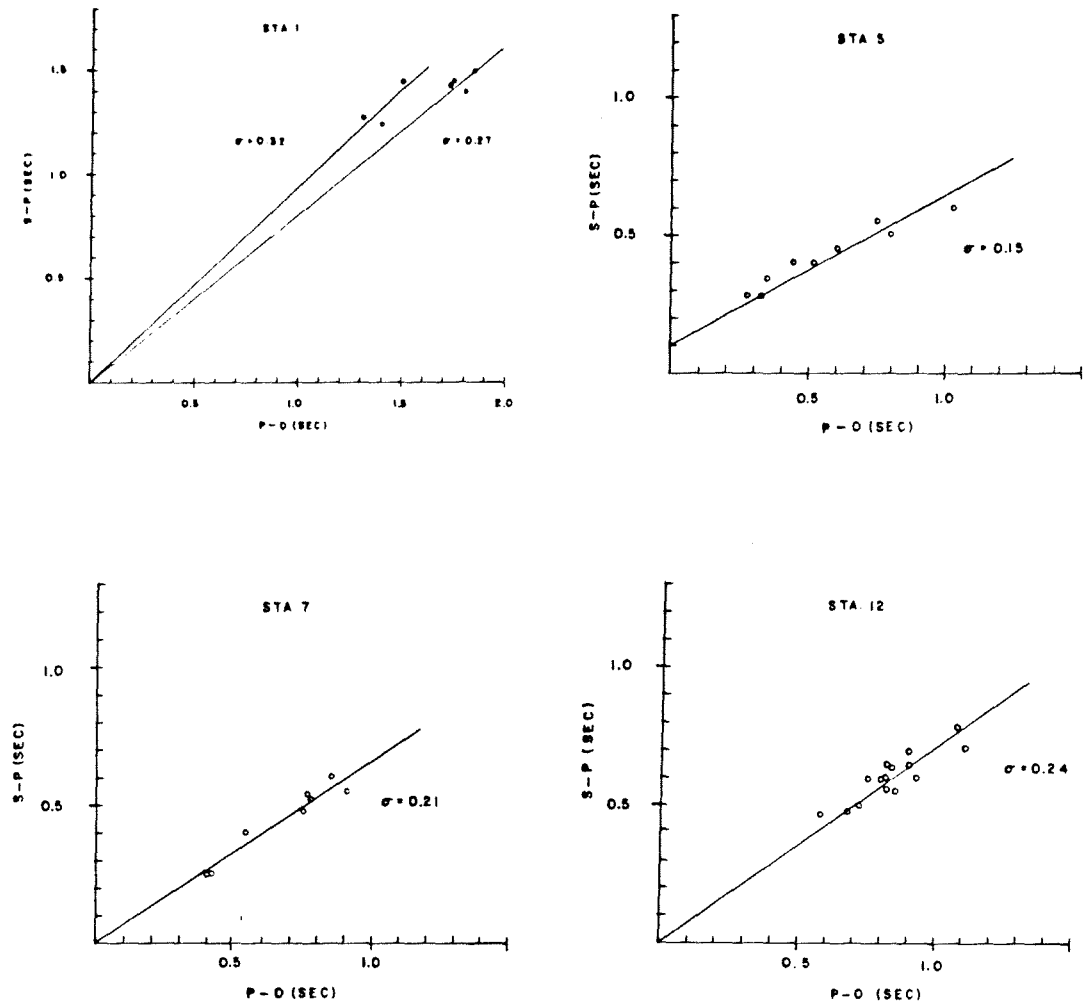


FIG. 12. Wadati diagrams for four stations, using multiple events and assumed origin times.

and Rotstein (1975) obtained a low Poisson's ratio of 0.15 at Coso Hot Springs using the same technique. In combination with evidence that the P -wave velocity is higher than regional within the field, the lower Poisson's ratio implies anomalously high values of the shear modulus within the reservoir. Such a characteristic if real may be related to vapor domination.

Source parameters

Spectral characteristics of selected events were examined in the search for anomalous features in The Geysers microearthquakes. A difficulty with this approach is the lack of comparative data on the spectral

characteristics of microearthquakes in other areas. Douglas et al (1970) and Douglas and Ryall (1972) have studied Basin and Range events and concluded that scaling laws accepted for large events seem to apply for earthquakes as small as magnitude 1. To allow comparison with other central California areas, Brune's (1970, 1971) widely used source model for S -waves, extended to P -waves, was applied. The parameters of interest are the seismic moment $M_0 = 4\pi R\rho V^3\Omega_0$, the stress drop $\Delta p = (7/16)M_0/r^3$, fault slip $u = M_0/\pi\rho V_s^2$, and source radius $r = 2.34 V/f_0 2\pi$, where R = distance from source to receiver, ρ = density (2.67 g/cm^3), Ω_0 = long period displacement spectral level, f_0 = corner frequency (f_p or f_s), and V = velocity.

of material (4.5 km/sec for V_p , 2.6 km/sec for V_s). In addition to source parameter effects such as attenuation, complex propagation path, site response and radiation patterns will affect the spectra. If spectra are averaged for many events or stations, these effects will tend to decrease. The approach is rough but does form a basis for comparing earthquakes. In this study the only correction made to the data was for instrument response, and source parameters were averaged over several stations.

Fourteen events were selected on the basis of magnitude and location within the field. Typical data are shown in Figure 13. Note the wide bandwidth (2-80 Hz) recoverable with the digital event recorder. Spectra are shown for the indicated data windows. Corner frequency f_0 was picked by using Q -corrected templates of the function

$$[1 + (f/f_0)^{2\delta}]^{-1/2} \exp(-\pi ft/Q)$$

for traveltimes $t = 0.5, 1.0, 1.5$ sec; $Q = 40, 80, 120, 250, 700$; $\delta = 3, 5, 7$; and $f_0 = 15, 20, 25, 30, 35, 40, 45, 50, 60$ Hz. First the long period level was defined, then each spectrum was fit for f_0, Q , and high-frequency roll-off δ . Results are listed in Table 4a for representative events recorded on the analog (FM) system. Tables 4b and 4c present results for P - and S -wave digital data, assuming an average hypocentral distance of 5 km to station 7. (These events were not located, as the entire network was not operating during the recording period.)

In Figure 14 plots of moment versus magnitude for M_{CL}, M_{CB} , and M_L are presented for the data sets in Table 4. As for b -values, the choice of magnitude alters the results significantly. The results obtained for this study are:

$$\begin{aligned} \text{Log}_{10}(M_0) &= (17.3 \pm 0.1) + (0.8 \pm 0.3)M_{CL}, \\ \text{Log}_{10}(M_0) &= (16.2 \pm 0.3) + (1.9 \pm 0.7)M_{CB}, \\ \text{Log}_{10}(M_0) &= (15.9 \pm 0.03) + (1.3 \pm 0.04)M_L. \end{aligned}$$

Results from other central California studies of M_0 versus M_L are:

(1) Bakun and Bufe (1975), San Andreas:

$$3.5 < M_L < 5,$$

$$1 < M_{CL} < 3.5,$$

$$\text{Log}_{10}(M_0) = (16.2 \pm 0.1) + (1.52 \pm 0.05)M_L.$$

(2) Bakun and Lindh (1977), Oroville, California

$$17 < \text{Log}_{10}(M_0) < 25,$$

$$\text{Log}_{10}(M_0) = (17.02 \pm 0.07) + (1.21 \pm 0.03)M_L.$$

(3) Johnson and McEvelly (1974), San Andreas

$$M_L > 2,$$

$$\text{Log}_{10}(M_0) = (17.60 \pm 0.28) + (1.16 \pm 0.06)M_L.$$

(4) Thatcher and Hanks (1973), Southern California

$$M_L > 3,$$

$$\text{Log}_{10}(M_0) = 16.0 + 1.5 M_L.$$

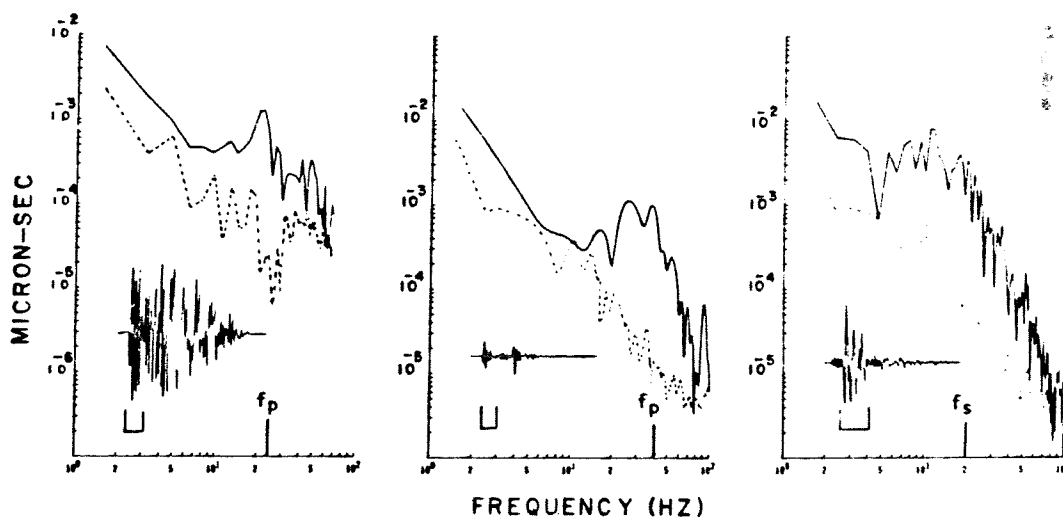


FIG. 13. Typical displacement spectra used in source studies. On left is P -wave recorded on FM tape system, center is P -wave recorded on digital system, and right is S -wave recorded digitally. FM signal is shown at higher gain than other two. Corner frequencies and data windows are indicated. Note the higher quality data obtained with the digital system.

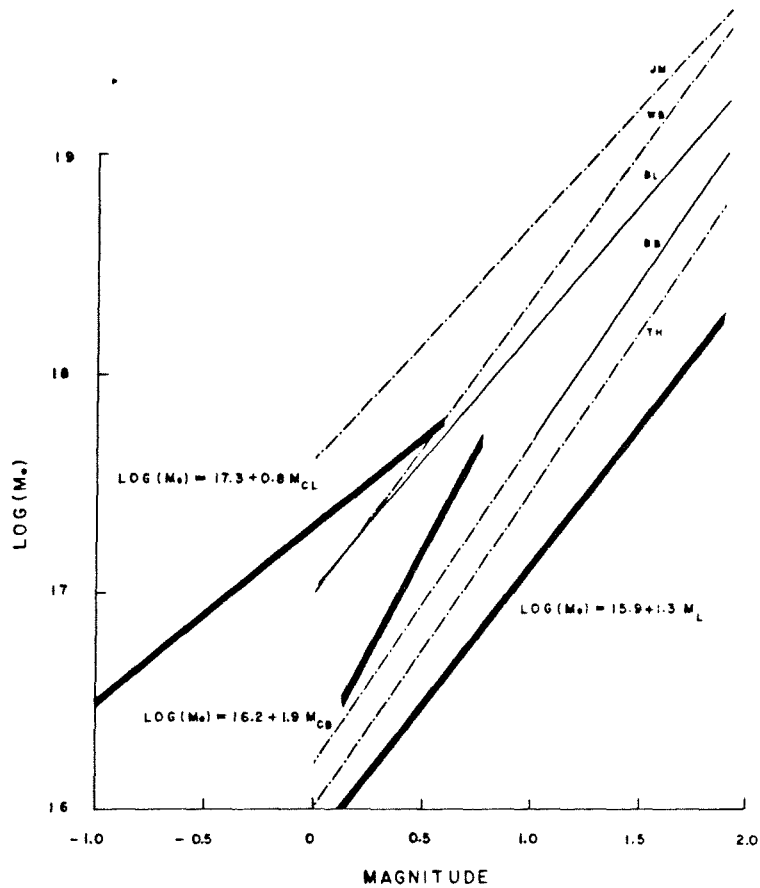


FIG. 14. Moment/magnitude relations for Geysers microearthquakes (heavy lines), using the three different magnitudes, compared with other such relations (*JM*, Johnson and McEvilly, 1974; *WB*, Wyss and Brune, 1968; *BL*, Bakun and Lindh, 1977; *TH*, Thatcher and Hanks, 1973; *BB*, Bakun and Bufe, 1975). Dashed line implies extrapolation from range of original data. M_{CL} and M_{CB} data from Tables 3 and 4a. M_L data from Table 4c.

(5) Wyss and Brune (1968), Parkfield, California

$$M_L > 3, \\ \text{Log}_{10}(M_0) = 17.0 + 1.4 M_L.$$

From these results, it appears that The Geysers events are slightly unusual if the M_L magnitude is used, i.e., for a given M_L , M_0 is smaller than for the other relations. In view of these results and the fact that normal b -values are indicated by the M_L magnitudes from equivalent Wood-Anderson seismograms, it seems that earthquakes at The Geysers are not markedly unusual compared to other central California events. The slightly higher M_L magnitudes may reflect locally low attenuation characteristics.

Corner frequencies are roughly independent of magnitude and moment, implying increasing stress drop with event size if corner frequency is not controlled by Q . Such a stress drop (ΔP)-magnitude (M_L) relation is evident in Table 4c where values of about 0.01 to 10 bars are seen for the magnitude range 0 to 2. However, when a particular event is examined at several different stations, we find that Q must be varied to maintain the same corner frequency. Implied Q values, relative to station 7, are given in Table 4a. It was thought that earthquakes beneath the production zone ($h > 3$ km) might exhibit lower corner frequencies (lower Q) than shallow events. Although the highest corner frequency obtained was for a shallow event ($h = 1.7$ km, $f_0 = 50$

Hz), there seems to be little correlation between source depth and corner frequency. The Q distribution implied by constraining f_0 to be constant at all stations for an event is generally the same as that indicated by the explosion data; i.e., high in the center of the field, decreasing towards the edges, and lowest outside the major production zone. No variation with depth can be established.

Because no events were recorded on both vertical and horizontal components, a comparison of Q_v and Q_h cannot be made. Only one station was used in the S -wave study. Thus, the S -wave data recorded on the horizontal geophones were used only for moment and magnitude determinations and not for a regional Q_h analysis as was done for P -waves.

The majority of events had high-frequency spectral

slopes δ of 3 to 5, and sometimes 7. The corner frequency and high-frequency slope depend on the source time-function as well as the source dimensions. The smoother the source function the greater the high-frequency roll-off. A source time-function that is relatively smooth in beginning (many continuous derivatives) and ending would produce a much more rapid roll-off than either a sharp explosion or a "chattering" or step-like rupture.

Source function rise-time information, if available in the spectrum, may be useful in determining the materials that are rupturing, the nature of rupture, and the state of stress as well as the source dimensions. Unfortunately, the effects of attenuation are extremely severe at the higher frequencies and almost impossible to remove accurately.

Table 4a. P -wave spectral parameters (analog FM system).

Event	STA	R (km)	M_0 (dyne-cm)	Q	f_0 (Hz)	δ	Depth (km)	ΔP (bar)	μ (cm)	r (m)
3	7	1.3	1.2×10^{17}	250						
3	11	2.5	1.7×10^{17}	120	25	5	1.2	0.23	2.02×10^{-3}	66
3	12	3.8	1.9×10^{17}	80						
37	7	4.7	1.3×10^{17}	250						
37	3	6.3	3.8×10^{17}	120	25	3	3.8	0.25	2.27×10^{-3}	66
37	11	4.1	1.5×10^{17}	250						
37	12	4.3	1.3×10^{16}	120						
39	7	3.6	6.4×10^{16}	250						
39	3	5.1	6.1×10^{16}	120	35	3	1.6	0.13	9.32×10^{-3}	47
39	11	2.7	1.6×10^{16}	80						
39	12	3.0	1.3×10^{16}	40						
42	7	3.8	3.4×10^{17}	250						
42	3	3.9	4.1×10^{17}	120						
42	11	4.0	3.5×10^{17}	120	25	5	3.8	0.48	4.32×10^{-3}	66
42	12	4.6	2.7×10^{17}	80						
42	1	8.0	2.6×10^{17}	60						
41	7	3.3	7.8×10^{16}	250						
41	3	4.1	4.8×10^{16}	120	30	3	3.2	0.14	1.01×10^{-3}	55
41	11	3.5	4.6×10^{16}	120						
41	12	4.2	3.7×10^{16}	40						
51	7	3.6	1.4×10^{17}	250						
51	3	4.5	1.7×10^{17}	120						
51	11	3.6	1.5×10^{17}	120	35	5	3.5	0.63	3.46×10^{-3}	47
51	12	4.2	1.3×10^{17}	40						
51	1	8.2	9.7×10^{16}	40						
7	7	4.8	2.0×10^{17}	250	30	7	4.4	0.52	3.89×10^{-3}	55
15	7	2.1	7.9×10^{16}	250	50	5	1.7	0.96	4.27×10^{-3}	33
17	7	1.6	1.0×10^{17}	250	30	7	1.5	0.26	1.94×10^{-3}	55
18	7	1.5	7.9×10^{16}	250	35	3	1.3	0.33	2.11×10^{-3}	47
28	7	3.7	4.0×10^{17}	250	25	5	3.6	0.61	5.41×10^{-3}	66
34	7	1.8	1.3×10^{17}	250	35	5	1.6	0.54	1.75×10^{-3}	47
38	7	3.0	1.0×10^{17}	250	25	7	2.9	0.15	1.35×10^{-3}	66
58	7	4.1	3.2×10^{17}	250	25	5	4.0	0.49	4.32×10^{-3}	66

Table 4b. P-wave spectral parameters (digital system).

M_0 (dyne-cm)	$\bar{R} = 5.0$ km		Station 7		r (m)
	f_0 (Hz)	ΔP (bar)	u (cm)		
1.6×10^{17}	40	1.02	5.6×10^{-3}	41	
3.7×10^{16}	40	0.23	1.3×10^{-3}	41	
2.1×10^{17}	20	0.17	1.8×10^{-3}	82	
2.1×10^{17}	20	0.17	1.8×10^{-3}	82	
1.6×10^{17}	25	0.24	2.2×10^{-3}	66	
2.6×10^{16}	35	0.19	6.9×10^{-4}	47	
8.5×10^{16}	40	0.54	2.9×10^{-3}	41	
6.3×10^{16}	40	0.40	2.2×10^{-3}	41	
8.5×10^{16}	35	0.36	2.3×10^{-3}	47	
2.4×10^{16}	40	0.15	8.4×10^{-4}	41	
5.3×10^{16}	40	0.33	1.9×10^{-3}	41	

Table 4c. (continued)

M_L	$\bar{R} = 5.0$ km		Station 7		r (m)
	M_0 (dyne-cm)	f_0 (Hz)	ΔP (bar)	u (cm)	
0.1	9.2×10^{15}	20	3.5×10^{-2}	6.9×10^{-4}	48
1.7	1.2×10^{16}	15	2.0×10^0	5.2×10^{-2}	64
0.4	3.0×10^{16}	25	2.3×10^{-1}	3.6×10^{-3}	38
0.6	4.1×10^{16}	30	5.3×10^{-1}	6.9×10^{-3}	32
1.4	2.4×10^{17}	20	9.4×10^{-1}	1.8×10^{-2}	48
0.5	4.1×10^{16}	25	3.0×10^{-1}	4.8×10^{-3}	38
0.6	4.1×10^{16}	20	1.5×10^{-1}	3.1×10^{-3}	48
0.2	1.6×10^{16}	30	2.1×10^{-1}	2.8×10^{-3}	32
0.3	1.8×10^{16}	25	1.3×10^{-1}	2.1×10^{-3}	38
0.5	3.0×10^{16}	25	2.3×10^{-1}	3.6×10^{-3}	38
0.5	1.6×10^{17}	20	6.3×10^{-1}	1.2×10^{-2}	48
0.4	1.8×10^{16}	25	1.3×10^{-1}	2.1×10^{-3}	38
0.1	1.4×10^{16}	25	1.0×10^{-1}	1.7×10^{-3}	38
0.8	6.1×10^{16}	25	4.6×10^{-1}	7.2×10^{-3}	38
1.0	1.4×10^{17}	20	5.5×10^{-1}	1.0×10^{-2}	48
0.8	1.2×10^{17}	15	2.0×10^{-1}	5.2×10^{-3}	64
0.1	8.1×10^{15}	30	1.0×10^{-1}	1.4×10^{-3}	32
0.8	1.2×10^{17}	20	3.9×10^{-1}	7.7×10^{-3}	48
1.3	3.0×10^{17}	25	2.3×10^0	3.6×10^{-2}	38
1.5	5.1×10^{17}	20	1.9×10^0	3.8×10^{-2}	48
0.9	1.2×10^{17}	20	4.7×10^{-1}	9.3×10^{-3}	48
1.3	2.0×10^{17}	15	3.3×10^{-1}	8.7×10^{-3}	64
0.7	1.0×10^{17}	20	3.9×10^{-1}	7.7×10^{-3}	48
1.2	3.0×10^{17}	20	1.1×10^0	2.3×10^{-2}	48
1.0	1.4×10^{17}	20	5.5×10^{-1}	1.0×10^{-2}	48
1.2	2.0×10^{17}	20	7.9×10^{-1}	1.5×10^{-2}	48
0.4	1.6×10^{16}	25	1.2×10^{-1}	1.9×10^{-3}	38
0.9	1.0×10^{17}	20	3.9×10^{-1}	7.7×10^{-3}	48
0.0	4.1×10^{15}	35	8.4×10^{-2}	9.5×10^{-4}	27
1.7	1.0×10^{16}	15	1.6×10^0	4.3×10^{-2}	64
0.8	8.1×10^{16}	25	6.1×10^{-1}	9.7×10^{-3}	38
0.7	8.1×10^{16}	26	6.1×10^{-1}	9.7×10^{-3}	38
0.6	5.1×10^{16}	15	8.3×10^{-2}	2.1×10^{-3}	64
0.2	7.1×10^{15}	20	2.7×10^{-2}	5.4×10^{-4}	48
0.1	5.1×10^{15}	25	3.8×10^{-2}	6.0×10^{-4}	38
0.5	4.1×10^{16}	10	1.9×10^{-2}	7.7×10^{-4}	96
0.4	3.0×10^{16}	15	5.0×10^{-2}	1.3×10^{-3}	64
0.2	1.2×10^{16}	25	9.2×10^{-2}	1.4×10^{-3}	38
0.5	5.1×10^{16}	25	3.8×10^{-1}	6.0×10^{-3}	38
0.6	7.1×10^{16}	25	5.4×10^{-1}	8.4×10^{-3}	38
1.0	1.8×10^{17}	20	7.1×10^{-1}	1.4×10^{-2}	48
0.3	5.1×10^{15}	35	1.0×10^{-1}	1.1×10^{-3}	27
0.8	8.1×10^{16}	25	6.1×10^{-1}	9.7×10^{-3}	38
0.7	8.1×10^{16}	25	6.1×10^{-1}	9.7×10^{-3}	38
0.3	1.5×10^{16}	30	2.0×10^{-1}	2.6×10^{-3}	32
1.2	2.0×10^{17}	15	3.3×10^{-1}	8.7×10^{-3}	64
0.4	1.6×10^{16}	25	1.2×10^{-1}	1.9×10^{-3}	38
0.4	1.4×10^{16}	30	1.8×10^{-1}	2.4×10^{-3}	32
1.8	1.6×10^{16}	10	7.9×10^{-1}	3.1×10^{-2}	96
0.3	1.4×10^{16}	25	1.0×10^{-1}	1.7×10^{-3}	38
0.3	1.4×10^{16}	25	1.0×10^{-1}	1.7×10^{-3}	38
0.7	7.1×10^{16}	25	5.4×10^{-1}	8.4×10^{-3}	38
0.7	1.0×10^{17}	15	1.6×10^{-1}	4.3×10^{-3}	64
0.3	1.8×10^{16}	25	1.3×10^{-1}	2.1×10^{-3}	38
0.7	5.1×10^{16}	25	3.8×10^{-1}	6.0×10^{-3}	38
0.5	3.0×10^{16}	30	4.0×10^{-1}	5.2×10^{-3}	32
0.2	1.0×10^{16}	25	7.7×10^{-2}	1.2×10^{-3}	38
0.5	3.0×10^{16}	15	5.0×10^{-2}	1.3×10^{-3}	64
0.6	3.0×10^{16}	25	2.3×10^{-1}	3.6×10^{-3}	38
0.5	5.1×10^{16}	15	8.3×10^{-2}	2.1×10^{-3}	64
0.4	3.2×10^{16}	30	4.2×10^{-1}	5.5×10^{-3}	32
0.9	1.8×10^{16}	15	3.0×10^{-1}	7.8×10^{-3}	64
1.8	1.2×10^{16}	25	9.2×10^0	1.4×10^{-1}	38
1.1	1.6×10^{17}	25	1.2×10^0	1.9×10^{-2}	38
0.2	8.1×10^{15}	25	6.1×10^{-2}	9.7×10^{-4}	38
0.2	1.2×10^{16}	25	9.2×10^{-2}	1.4×10^{-3}	38
0.6	5.1×10^{16}	25	3.8×10^{-1}	6.0×10^{-3}	38

Table 4c. S-wave spectral parameters (digital system).

M_L	$\bar{R} = 5.0$ km		Station 7		r (m)
	M_0 (dyne-cm)	f_0 (Hz)	ΔP (bar)	u (cm)	
0.6	4.1×10^{16}	25	3.0×10^{-1}	4.8×10^{-3}	38
0.3	1.2×10^{16}	25	9.2×10^{-2}	1.4×10^{-3}	38
0.9	7.1×10^{16}	25	5.4×10^{-1}	8.4×10^{-3}	38
0.5	2.0×10^{16}	25	1.5×10^{-1}	2.4×10^{-3}	38
0.4	1.6×10^{16}	25	1.2×10^{-1}	1.9×10^{-3}	38
1.6	1.2×10^{16}	35	2.5×10^1	2.8×10^{-1}	27
1.6	4.1×10^{17}	20	1.5×10^0	3.1×10^{-2}	48
0.9	6.1×10^{16}	25	4.6×10^{-1}	7.2×10^{-3}	38
0.4	2.0×10^{16}	25	1.5×10^{-1}	2.4×10^{-3}	38
0.5	2.0×10^{16}	30	2.6×10^{-1}	3.4×10^{-3}	32
1.4	3.0×10^{17}	25	2.3×10^0	3.6×10^{-2}	38
0.8	1.2×10^{17}	15	2.0×10^{-1}	5.2×10^{-3}	64
1.1	1.8×10^{17}	25	1.3×10^0	2.1×10^{-2}	38
0.4	3.0×10^{16}	25	2.3×10^{-1}	3.6×10^{-3}	38
0.3	1.4×10^{16}	20	5.5×10^{-2}	1.0×10^{-3}	48
0.2	1.8×10^{16}	25	1.3×10^{-1}	2.1×10^{-3}	38
0.6	6.1×10^{16}	20	2.3×10^{-1}	4.6×10^{-3}	48
1.1	1.2×10^{17}	25	9.2×10^{-1}	1.4×10^{-2}	38
0.3	2.0×10^{16}	25	1.5×10^{-1}	2.4×10^{-3}	38
0.0	2.4×10^{15}	15	4.0×10^{-3}	1.0×10^{-4}	64
0.3	1.8×10^{16}	20	7.1×10^{-2}	1.4×10^{-3}	48
1.4	3.0×10^{17}	20	1.1×10^0	2.3×10^{-2}	48
0.5	3.2×10^{16}	25	2.4×10^{-1}	3.8×10^{-3}	38
0.6	4.1×10^{16}	25	3.0×10^{-1}	4.8×10^{-3}	38
0.4	2.0×10^{16}	20	7.9×10^{-2}	1.5×10^{-3}	48
0.6	6.1×10^{16}	15	1.0×10^{-1}	2.6×10^{-3}	64
0.4	4.1×10^{16}	20	1.5×10^{-1}	3.1×10^{-3}	48
1.1	4.1×10^{17}	15	6.6×10^{-1}	1.7×10^{-2}	64
0.4	3.0×10^{16}	25	2.3×10^{-1}	3.6×10^{-3}	38
1.3	3.0×10^{17}	15	5.0×10^{-1}	1.3×10^{-2}	64
1.2	1.8×10^{17}	20	7.1×10^{-1}	1.4×10^{-2}	48
0.2	1.2×10^{16}	20	4.7×10^{-2}	9.3×10^{-4}	48

DISCUSSION

Summary of observations

The significant points observed are:

- I. Microearthquakes
 - (1) High level of activity $0 < M_L < 2$ at 25 to 30 events/day.
 - (2) Distribution in space and time
 - (a) Shallow foci, < 5 km.
 - (b) No dominant throughgoing faults defined.
 - (c) Low seismicity in known steam zones and in original production areas.
 - (d) Slightly higher than normal b -value, using M_L .
 - (e) No systematic pattern to occurrence.
 - (3) Spectral characteristics
 - (a) Slightly anomalous M_0 versus M_L relation (low M_0 for given M_L).
 - (b) High corner frequencies, no clear dependence on M_0 .
 - (c) f_0 for P -waves greater than for S -waves.
 - (d) No relation between f_0 and depth.
 - (e) Low (~ 1 bar) estimated stress drops.
 - (4) Fault plane solutions generally consistent with regional NE-SW compressive stress
- II. Velocity data
 - (1) Locally high velocity in production region.
 - (2) Broad regionally lower velocity zone extending lateral out of production zone at depth.
 - (3) Apparent low Poisson's ratio in production zone.
- III. Attenuation data
 - (1) Shallow high Q zone in production zone from explosions and microearthquakes.
 - (2) Deeper lower Q zone from explosions.

A discussion of these observations relative to the vapor-dominated reservoir at The Geysers follows. Implications are investigated, based on known field characteristics, as to possible reflection of reservoir dynamics in the seismological data.

Reservoir properties

A fundamental question in geothermal exploration is the role of microearthquake data in the detection and delineation of geothermal reservoirs, and in specifying the properties of a reservoir. Earthquake genesis may reflect the steam reservoir properties. The Geysers geothermal field is a vapor dominated reservoir, as opposed to a hot water or brine system characteristic of the Basin and Range or Imperial Valley regions. The temperature and pressure of the vapor region is fairly constant, ranging within a few degrees of 240°C at 30 to 40 bars (Weres et al, 1977).

An unusual characteristic of the reservoir is that the steam is much below expected hydrostatic pressures for the depths involved (2–3 km). Several hypotheses have been advanced to explain the pressure differential. In one, an "incrustation seal" has formed on the edge of the reservoir, inhibiting pressure equalization from surrounding groundwater (White et al, 1971). Minerals such as calcite and anhydrite, whose solubilities decrease with increasing temperature, may reduce permeability at the margins by precipitation from the cooler ground water upon entering the geothermal zone. A similar model proposes an expanding reservoir in which groundwater cannot flow rapidly enough into the low pressure steam zone to equalize pressure, by virtue of a high withdrawal rate and adequate heat source to convert pore water into steam. A third explanation calls upon "traps" of steam, similar to gas traps found in oil producing regions, sealed from surrounding waters.

The dominant rock type in The Geysers reservoir is Franciscan graywacke (McLaughlin and Stanley, 1975), which is initially impermeable and nonporous, but extensively sheared and fractured so that its porosity and permeability is sufficient to provide the existing reservoir. Drill cuttings have shown evidence of secondary porosity from hydrothermal dissolution of minerals (Weres et al, 1977). In successful steam wells "geothermal sand" (alteration products of the minerals) is often encountered above the steam zones (Joe Laffeur, personal communication, 1977). The steam-water interface is probably irregular, reflecting different porosities and capillary effects. The actual amount of economic steam in the reservoir will depend upon the rock type, porosity, permeability, water content, and available heat.

An important characteristic of The Geysers reservoir is that it seems to be a maximum enthalpy system. Saturated steam has a maximum enthalpy (heat content) of 2804 kJ/kg at 234°C and 30 bars. The enthalpies of steam entering boreholes from different units at The Geysers are very near this value (Weres et al, 1977). Why the steam enthalpy is at this particular value is not entirely clear. However, other steam reservoirs (Lardarello, Italy, and Kawah Kamojang, Indonesia) also exhibit to some degree the maximum enthalpy phenomenon (Weres et al, 1977; James, 1968).

Natural leakage, commercial production and inter-connected reservoirs are factors proposed to explain the maximum enthalpy phenomenon at The Geysers. Steam flowing toward the wells begins to be saturated at some temperature above 234°C and is expanded isoenthalpically to less than 30 bars under conditions

which allow the water to condense. For example, an initially water-saturated isolated reservoir, due to commercial production or surface leakage, would eventually boil dry at temperatures and pressures below 234°C and 30 bars, respectively, depending upon permeability and initial temperature. On the other hand, if there were an unlimited amount of wet steam available from an interconnected source, the temperature and pressure would stabilize at the maximum enthalpy point. As production continued, steam withdrawn from the 234°C zone would spread, and new wells would develop the maximum enthalpy condition. The actual case is doubtless between unlimited steam and zero steam, which may account for deviation from the maximum enthalpy point.

The state of the reservoir prior to commercial production is not clear. Weres et al (1977) hypothesizes that there was a shallow initial vapor zone, but, as production increased, the "deep water table" was boiled down by two or more km to the present 2.5 km. In this "cracked sponge" model water is boiled rapidly from interconnected cracks; however, there is still a large amount of water left behind in the body of the sponge or in the fine pore structure of the rock, which can serve as a water supply to the steam reservoir. White et al (1971) suggest a system initially water saturated, but evolving to convection with the introduction of a potent heat source. Eventually, near-surface temperatures and pressures allow the onset of boiling. Due to limited recharge and permeability, the hot water system becomes a vapor-dominated system. An important aspect of White's model is the recharge area. Because of limited permeability at the incrustation seal, there would be large pressure gradients near the field margins between the reservoir, which is much below hydrostatic pressure, and the exterior of the reservoir, possibly at or above hydrostatic pressure. With increased production the vapor front advances, exposing new regions to pressure differentials. The front would stop advancing when either the heat source was insufficient to cause boiling or the permeability increased so that the recharge and discharge rates balanced.

Seismologically, the significant aspects of these reservoir models are: (1) The system is at maximum enthalpy with limited recharge but with extensive fracture permeability. (2) It is low pressure and nearly constant temperature. (3) It may be expanding at a rate depending upon porosity, permeability, and net discharge.

From the concept of differential pressure, one would expect microearthquakes to occur where high pore pressures reduce the strength of the materials. The observed locations of microearthquakes appear to

concentrate on the margins of the production zone (above and below), where the models would predict the highest pore pressures. Activity is very low, however, above and below the older production zones, implying the steam source for the older production zone is mainly steam flow from the surrounding reservoir, rather than groundwater from above and below. The occurrence of microearthquakes randomly in time and space also suggests an interconnected geothermal system. The events do not seem to migrate through the field and their pattern suggests no dominant throughgoing faults. The area may be intensely fractured, with the pressure differential activating locally small faults.

Historical data are insufficient to show that microearthquakes are migrating with an expanding reservoir. However, the limited data available do suggest an increasing rate of seismicity. Lange and Westphal (1969) detected a rate of 4 events/day in the fall of 1968. Hamilton and Muffler (1972) recorded a rate of 2-3 events/day in the spring of 1971. At the time of the present study, the power generation rate was 550 MW or about seven times the 1971 rate. The microearthquake activity during this study was 25-30 events/day or about ten times the rate observed in previous studies. As this study was conducted in a different manner from previous studies, and because of the short sampling times, it would be difficult to conclude firmly that the microearthquake activity is related to steam withdrawal.

The slightly higher than regional *b*-value may indicate stress within the microearthquake region. Studies on microfracturing of rock (Scholz, 1968; Wyss, 1973) have shown that *b*-values depend primarily on the state of stress, and to a lesser extent on the physical properties of the rock. Scholz (1968) found that in a low-stress state, energy was released in small events, resulting in high *b*-values. This was particularly true of ductile and high porosity rocks. He also noted that small magnitude events occur in material where crack closing and sliding are important, with the larger events occurring in situations where new fractures are propagating. While the calculated stress drops are small, it should be realized that due to attenuation it is virtually impossible to obtain a high stress estimate for microearthquakes, i.e., corner frequencies of 100 Hz would be associated with stress drops of a few bars at $M_0 = 10^{16}$, and corner frequencies cannot be observed at such levels.

The Geysers events are not anomalous compared to regional stresses. Almost all events exhibited strike-slip or dip-slip faulting with the principal compressive stresses in the northeast-southwest direction.

It seems plausible that the direction of failure is controlled by regional stress while the rate of failure is controlled by local stress levels.

Thermally induced differential expansion between water in isolated voids and the rock matrix (Knapp and Knight, 1977) is an attractive microearthquake source mechanism from several points of view. Earthquakes would be expected to occur where the permeability is low and the temperature gradient is high, at the edges of the reservoir. In order to produce an event of detectable size, the fracture must coalesce simultaneously over an area of several m^2 . Knapp and Knight calculate that, if all the pores fracture at once in a cubic meter of rock with porosity 1 percent, a zero magnitude event would result. In reality only selected pores fracture, those with preferential orientation with respect to the maximum principal stress. Thermally induced differential expansion may act only as a triggering mechanism for formation of small faults, the maximum size of which would be limited by the scale of variations in rock permeability, porosity and available heat. This failure model would explain an apparent upper magnitude threshold and the higher than regional b -value. The differential expansion hypothesis is also consistent with the observed fault plane solutions since the model predicts fracture consistent with the direction of the regional stress field.

McGarr (1976) theorized that the volumetric moment, approximately $\mu|\Delta v|$, is a measure of the amount of seismic failure in response to shear stresses induced by volume change (where μ = shear modulus, $|\Delta v|$ = volume change). Several examples support his theory: volume changes in mining operations, volume changes due to fluid injection (Denver earthquakes), and volume changes associated with uplift (Matsushiro, Japan). An estimate of Δv at The Geysers involves the amount of fluid withdrawn, less groundwater recharge and fluid reinjection. This can be compared to the calculated Δv from the summed moments of the observed seismicity, 1.5×10^{21} to 10^{22} dyne-cm/year, depending on the occurrence used for magnitude 3 events. The larger value (10^{22}), implies Δv of 5×10^{10} cm^3 /year, the total volume change necessary to accomplish the observed seismicity, assuming McGarr's model of earthquake genesis. The volume of fluid withdrawn can be calculated from the power generation. At a capacity of 550,000 kW, using a steam rate of 10 kg/kWh and a specific volume of water of 1.2 cm^3 /g, the Δv for 1 year is 5×10^{13} cm^3 , some 10^3 times greater than the Δv calculated from the seismicity rate. In other words, McGarr's hypothesis would predict a much higher level of seismicity if the total

Δv were consumed by seismic failure. However, the actual Δv available for earthquake generation is much smaller due to groundwater recharge and reinjection. A recharge rate equal to discharge would imply no volume change or microearthquakes. This may explain why seismicity does not change with withdrawal rate in a hot water dominated reservoir that is in hydrostatic equilibrium (Helgeson, 1968; Combs, 1976). Recharge, however, is not instantaneous, nor would one expect the volume change from seismic failure to equal the net volume of water withdrawn. The seismicity may reflect volumetric change in the reservoir and, if so, the microearthquakes would indicate the regions of expansion of the vapor dominated zone. Temporal change in the spatial pattern of seismicity may occur too slowly to be of practical use. Cessation of events on the edge of the reservoir may indicate an equilibrium situation where the recharge rate is equal to the discharge or the reservoir has expanded to the point where it has been extended beyond a heat source that is sufficient to produce vaporization of available water.

It is not certain whether the steam withdrawal and associated volumetric change is a direct cause of microearthquakes at The Geysers. Because the environment is hydrologically active and because of the intimate relation between fluids and faulting (Hubbert and Ruby, 1959; Nur, 1973), it is probable that fluid withdrawal is a contributing factor. However, only as production increases and expands to areas that are now seismically inactive will we know whether fluid withdrawal is inducing the microearthquakes. Positive correlation would open a new methodology for reservoir modeling, and some consideration should be given to instrumentation of new production areas prior to development.

Another failure mechanism which may influence microearthquake activity is "stick-slip" (Brace and Byerlee, 1966) in which the motion occurs in a series of discrete rapid slips. In general, stick-slip is enhanced by high pressure or normal stresses, low temperature, the presence of strong brittle materials such as feldspars and quartz, the absence of gouge, and lower surface roughness. At higher confining pressures, the dominant factor controlling friction strength is effective pressure (Stesky, 1977). In The Geysers reservoir where the temperature is high, and pressure is low, stick-slip would not be expected to dominate. At the reservoir edges where pressures are higher and temperatures are lower, with possible embrittlement due to dehydration (Heard and Ruby, 1965; Raleigh and Paterson, 1965), one would more readily expect stick-slip behavior. The lack of deep events would, in the context of stick-slip earth-

quakes, imply elevated temperatures beneath the reservoir (4–5 km).

The moment versus magnitude relation for The Geysers, using M_L , results in a low zero-magnitude moment compared to other central California earthquakes. In terms of the seismic waves, for a given moment (low frequency relation), the amplitude used to determine the magnitude (higher frequency radiation) is larger than for other regions. This is consistent with the high Q observation, but it is difficult to separate source and path effects without dense station coverage.

An indication that source information may be masked by path effects is found in the differences between P - and S -wave corner frequencies. P -wave corner frequencies f_p are around 30 Hz, and the S -wave corner frequencies f_s are about 20 Hz. Assuming that fault propagation at a finite rupture velocity controls the observed corner frequencies, and that the rupture velocity is less than the S -wave velocity, then consistent observation of $f_p > f_s$ is incompatible with the faulting models. In fact, if the fault can be modeled as a long, narrow crack propagating unilaterally, we should observe $f_s > f_p$ over half the radiation pattern. A plausible explanation for the different observed results is the effect of attenuation along the propagation path. A value of Q_s one-third to one-half that of Q_p would be adequate to produce the observed corner frequencies. If we assume the actual value of f_s at 40 Hz, and that it has been reduced by attenuation to 20 Hz for a traveltime t of 1.5 sec for the S -wave, the Q required for the reduction in f_s can be computed from $Q = t/t^*$ where $t^* = 0.5/f_s$, a value approximately correct for a factor of two reduction in apparent corner frequency (Johnson and McEvilly, 1974, Figure 5). The resulting Q_s , 120, is consistent with the Q_p estimation within the field. This illustrates the extreme difficulty in recovering source parameters such as stress drop or dimensions from microearthquake spectra, even at a distance of 5 km or less.

From the S -wave corner frequencies, calculated stress drops were between 0.1 and 3.0 bar. Because a large number of events at varying azimuths were analyzed, these stress drops are probably representative estimates for the field. The relatively constant values of corner frequency may be indicative of path effects (Q controlled) rather than source effects (time function or dimensions). The larger moment events generally occurred deeper in the field than did smaller events. Assuming uniform detection capability with depth, the larger events would be occurring at depths where the largest pressure differences exist between hydrostatic and the reservoir fluid pressure. The

constant corner frequencies can be interpreted as a uniform source dimension of about 50 m. In a low pressure reservoir with constant permeability and porosity, one would expect uniform source dimensions. Elsewhere in central California, foci are distributed evenly without much correlation between depth and magnitude to depths of 10 to 12 km (McNally, 1976). The fact that earthquakes in The Geysers do not occur deeper than 4 or 5 km is strong evidence for their close association with the geothermal system.

Velocities

The low Poisson's ratio within the production zone suggested by the microearthquake data may indicate partial saturation of reservoir rocks. Toksöz et al (1976) found that even a small amount of gas as an immiscible mixture in a brine reduces the compressional wave velocity V_p , the net effect being a reduced Poisson's ratio. Nur and Simmons (1969) observed that V_p decreased with decreasing water saturation in low porosity rocks. Both studies would predict the observed low Poisson's ratio for a vapor dominated reservoir.

As can be seen in Figure 3, there is a P -wave advance (higher velocity) with respect to regional throughout the production zone for shallow propagating waves from the near explosion. For deeper waves from the far explosion, the P -wave velocity appear regionally low, as would be expected within a vapor zone. However, the reduced P -wave velocity is observed over a broad area, much broader than the present production zone. If the presence of steam is controlling the velocity, it would seem that the reservoir is more extensive than presently defined by drill holes. However, P -wave velocity variations in geothermal environments can occur because of structural or stratigraphic variations. For example a 0.3 sec P -wave advance, observed in a Nevada hot springs environment, was clearly due to silica deposition within valley sediments around the hot spring (Beyer et al, 1976). A similar explanation in terms of compositional differences may apply in The Geysers area. Iyer and Hitchcock (1975) observed P -wave delays throughout much of the Clear Lake-Geysers region, and attributed it to a heat source beneath the area. The P -waves from the distant explosion may have been affected by such deeper lower velocity material. Because of the low pressures involved, it is difficult to estimate the temperatures necessary to account for a 10 to 20 percent velocity decrease.

Lin (1977) from laboratory measurements found for central California rocks about -7×10^{-4} km/

sec °C velocity change for graywacke and quartz monzonite at pressures greater than 4 kbar, and about -10^{-3} km/sec °C for gabbros. He also found graywacke velocities at room temperature and pressure to vary from 4.8 to 5.7 km/sec with increasing metamorphism. Murase and McBimey (1973) found that for common igneous rocks at 1 bar and less than 600°C there is no change with temperature in seismic velocity. Assuming the dominant material underlying The Geysers to be Franciscan graywacke with a temperature coefficient for *P*-wave velocity of -10^{-3} , a decrease in velocity from 5.0 to 4.25 km/sec (15 percent) at 3 km depth implies an implausible temperature increase of 750°C. It is thus difficult to explain a broad low velocity zone beneath The Geysers by a temperature increase alone.

It appears that the effects of high temperature, degree of water saturation, geologic structure, and the compositional change within the hydrothermal region are combined in producing the observed velocity variations. Detailed studies utilizing distant sources and near vertical propagation through sections will shed light on the regional velocity structure. Results of the present study are clear, however, in the fact that the producing reservoir is characterized by detectably anomalous local seismic wave velocities.

Attenuation

The observed attenuation differences may reflect variations in shallow structure and topography throughout the geothermal field and at reference stations. In a finite-element simulation of a ridge with 20 degree slope, Smith (1975) found that the maximum spectral ratio enhancement was a factor of two at the peak. Data for The Geysers show a factor of 10–20 difference, with little correlation to topography. It is also well known that near-surface effects such as thick, low velocity alluvium can cause amplification, with the degree of enhancement proportional to the contrast in acoustic impedance, and frequencies of the spectral peaks correspond roughly to multiples of the travelttime through the superficial layer. There is no evidence for anomalously low velocity shallow materials. For a velocity of 2 km/sec, the thickness required for enhancement in the 5–10 Hz range would be 100–200 m. More restrictive, the underlying material would have to be unreasonably high velocity for significant enhancement. Further, the instrument locations were selected to avoid obvious alluvium or landslide surfaces. It is conceivable that bizarre geometrical effects in propagation paths could produce the observed amplitudes. If the actual struc-

ture deviates greatly from the model assumed for reducing the data, the observed amplitudes could reflect focusing. However, the uniformity and spatial extent of the high-*Q* regions argues against such mechanisms. In the formula used for *Q* estimation, the distance or velocity used in the model would need to be changed to unreasonable values to explain the variations. Therefore, the most plausible explanation for the observed amplitude variations is real differences in *Q* throughout the field.

Johnson et al (1977) have shown that *Q* is a function of confining pressure and saturation. They found that both Q_p and Q_s for dry rocks are initially higher and increase much more rapidly with confining pressure than for rocks containing pore water. The effect was attributed to friction and crack closure in the material. Gardner et al (1964) also showed that *Q*, as a function of water content alone, increased as the water content decreased. In a theoretical study, White (1975) computed compressional and shear wave velocity and attenuation for partially gas saturated porous rocks. He concluded that for compressional waves, the pressure gradients created by a wave traveling through a rock will cause flow of the fluid relative to the rock skeleton and result in attenuation. If the pore-rock matrix is homogeneous, the pressure gradients will be small and the attenuation due to fluid flow will also be small. However, if the rock has mixed saturation, such as pockets of gas or partial gas saturation, then the pressure gradients are higher near the inhomogeneities and the loss of energy due to fluid flow will be significant. These effects could explain the shallow high-*Q* zone and the deeper low-*Q* zone at The Geysers. As postulated earlier (Weres et al. 1977), the reservoir may be characterized by a relatively shallow region where the pores are vapor-dominated. In this region the behavior described by Johnson et al (1977) and Gardner et al (1964) may prevail to produce higher *Q*. Deeper within the reservoir there may be sufficient water for attenuation because of the fluid-flow mechanism of White (1975), thus resulting in the lower *Q* values. On the other hand, the degree of pore water saturation has opposite effects on *P*-wave velocity and attenuation. Our data indicate decreases with depth for both parameters within the reservoir, suggesting that water content cannot be the controlling factor for both velocity and attenuation. As for velocity, it would appear that low pressure, temperature, and compositional heterogeneity may contribute along with water content, to the anomalous attenuation. Temperature effects on attenuation at low pressures, however, can be nonlinear and unpredictable.

CONCLUSIONS

The utility of seismological data in the detection and delineation of a geothermal reservoir must depend upon the physical nature of the particular hydrothermal system. There are far too few case histories of geothermal fields to provide even general characteristics of reservoir properties in seismological terms. Nor has it been established unequivocally that there exists such a phenomenon as the "geothermal earthquake". Further, there is no compelling evidence that a geothermal reservoir acts as a deep radiator of seismic body waves. It is in such light that observations and conclusions of this study must be viewed, in the context of the low pressure vapor-dominated steam reservoir at The Geysers, as seen with a very limited data base in terms of spatial and temporal sampling.

In terms of regional conditions for central California, The Geysers area appears anomalous to some degree in earthquake occurrence and source parameters, seismic wave velocities, and attenuation properties of the reservoir rocks. Microearthquakes are distributed diffusely, generally absent within the production zone. Depths are less than 5 km. Mechanisms are consistent with northeast-southwest compressive stress, but no throughgoing faults are indicated. Earthquake occurrence rate suggests a slightly higher than normal *b*-value, or a seismicity rich in lower magnitude shocks relative to larger events. Both *P*- and *S*-wave velocities are higher than regional values in the shallow reservoir; the *S*-wave velocity, from the low Poisson's ratio, is even more anomalous than *P*. Attenuation is low where velocities appear high. There is indication that velocity and attenuation become less anomalous deeper in the field. The anomalous source parameters, low seismic moment for a given magnitude, may be merely a reflection of low attenuation.

It is unfortunate that in this case we cannot say whether these anomalies were present previous to production. The limited observations, along with proposed reservoir models, are consistent with a hypothesis in which the anomalous characteristics are closely related to reservoir depletion. It would be of great value to have such data for a potential geothermal field prior to exploitation.

The microearthquakes may relate to large pressure or temperature gradients, or to volume changes associated with fluid removal. If so, the distribution may delineate the boundary of the steam zone. In several reservoir models this boundary is dynamic, driven by exploitation of the field, and the resulting seismicity offers promise for monitoring the steam zone configuration.

Source parameters based on high frequency radiation of *P*- and *S*-waves, such as fault propagation and dimensions, source rise time, and stress drop, suffer in estimation from the high corner frequencies associated with these small events. Even at observation distances of only 5 km or less, and with the high *Q* values seen in the field, attenuation masks earthquake spectral details at frequencies above 20–30 Hz. Fault plane solutions, based on first motions, generally reflect response to northeast-southwest compression. More detailed studies may provide information on the fracture mechanisms involved at the field margins.

Anomalous high *P*- and *S*-wave velocities and low attenuation characterize the production zone. Extrapolation to in-situ reservoir properties from laboratory and theoretical studies on similar rock types is difficult, thus the mechanisms for the anomalies are not clear. Pressure, temperature, vapor-domination, and chemical alteration must be involved to various degrees.

Clearly our experiment shows that seismological data taken today are useful in delineating the present production zone of The Geysers. Further, the data may offer a means of monitoring the reservoir configuration and properties as these change during exploitation. It is not clear, however, that the same situation would have prevailed prior to major production of the field, and that the same seismological measurements would have been successful at The Geysers in an exploration context.

ACKNOWLEDGMENTS

This research was supported by the U.S. Department of Energy, through the Lawrence Berkeley Laboratory program in geothermal studies. Special thanks are due personnel of the operating companies at The Geysers field, particularly Richard Dondanville of Union Oil Co., who provided access to the area for data acquisition.

REFERENCES

- Bakun, W. H., and Bufe, C. G., 1975, Shear wave attenuation along the San Andreas fault zone in central California. *Bull. SSA*, v. 65, p. 439–459.
- Bakun, W. H., and Lindh, A. G., 1977, Local magnitudes, seismic moments, and coda durations for earthquakes near Oroville, California. *Bull. SSA*, v. 67, p. 615–629.
- Beyer, H., Dey, A., Liaw, A., Majer, E., McEvilly, T. V., Morrison, H. F., and Wollenberg, H., 1976, Preliminary open file report geological and geophysical studies in Grass Valley, Nevada. Lawrence Berkeley Lab. Rep., LBL-5262.
- Brace, W. F., and Byerlee, J. D., 1966, Stick-slip as a mechanism for earthquakes. *Science*, v. 153, p. 990.
- Brune, J. N., 1970, Tectonic stress and spectra of seismic shear waves from earthquakes. *J. Geophys. Res.*, v. 75, p. 4997–5009.

- 1971, Correction (to Brune 1970): *J. Geophys. Res.*, v. 76, p. 5002.
- Combs, J., 1976, Microearthquake studies before and during fluid withdrawal and reinjection test, East Mesa geothermal field, Imperial County, California. Contribution 7-77, Center for Energy Studies, University of Texas at Dallas.
- Combs, J. and Rostein, Y., 1975, Microearthquake studies at the Coso geothermal area, China Lake, California: 2nd U.N. Symp. on the Dev. and Use of Geothermal Resources, San Francisco, p. 909-916.
- Donnelly, J. M., 1977, Geochronology and evolution of the Clear Lake volcanic field: Ph. D. thesis, University of California, Berkeley.
- Douglas, B. M., and Ryall, A., 1972, Spectral characteristics and stress drop for microearthquakes near Fairview Peak, Nevada: *J. Geophys. Res.*, v. 77, p. 351-359.
- Douglas, B. M., Ryall, A., and Williams, R., 1970, Spectral characteristics of central Nevada microearthquakes: *Bull. SSA*, v. 60, p. 1547-1559.
- Gardner, G. H. F., Wyllie, M. R. J., and Droschak, D. M., 1964, Effects of pressure and fluid saturation on the attenuation of elastic waves in sands: *J. Petroleum Tech.*, v. 16, pp. 189-198.
- Goeff, F. E., Donnelly, J. M., and Hearn, B. C., 1977, Geothermal prospecting in The Geysers-Clear Lake Area, northern California: *Geology*, v. 5, 509-515.
- Hamilton, R. M., and Muffler, L. J. P., 1972, Microearthquakes at The Geysers geothermal area, California: *J. Geophys. Res.*, v. 77, p. 2081-2086.
- Heard, H. C., and Rubey, W. W., 1966, Tectonic implications of gypsum dehydration: *GSA Bull.*, v. 77, p. 741-760.
- Helgeson, H. C., 1968, Geologic and thermodynamic characteristics of the Salton Sea geothermal system: *Am. J. Science*, v. 2 (66), p. 129-166.
- Hubbert, M. K., and Rubey, W. W., Role of fluid pressure in mechanics of overthrust faultings: *Bull. GSA*, v. 70, p. 115-166.
- Iyer, H. M., and Hitchcock, T., 1975, Teleseismic residuals at The Geysers geothermal area: *AGU Trans.*, v. 56, p. 1020.
- James, R., 1968, Wairakei and Lardarello: Geothermal power systems compared: *New Zealand J. Science*, v. 11, p. 706-719.
- Johnson, L. R., and McEvilly, T. V., 1974, Near-field observations and source parameters of central California earthquakes. *Bull. SSA*, v. 64, p. 1855-1886.
- Johnson, D. H., Toksöz, M. N., and Timur, A., 1979, Attenuation of seismic waves in dry and saturated rocks. II: Mechanisms, *Geophysics*, v. 44.
- Knapp, R. B., and Knight, J. E., 1977, Differential thermal explosion of pore fluids: Fracture propagation and microearthquake production in hot pluton environments: *J. Geophys. Res.*, v. 82, p. 2515-2522.
- Lange, A. L., and Westphal, W. H., 1969, Microearthquakes near The Geysers, Sonoma County, California: *J. Geophys. Res.*, v. 74, p. 4377-4382.
- Lee, W. H. K., Bennett, R. E., and Meagher, K. L., 1972, A method of estimating magnitude of local earthquakes from signal duration: USGS open file rep.
- Lin, W., 1977, Velocities of compressional wave in rocks of central California at high pressure and high temperature and applications to the study of the crustal structure of California coast ranges: Ph.D. thesis, University of California, Berkeley.
- McGarr, A., 1976, Seismic moments and volume change: *J. Geophys. Res.*, v. 81, p. 1487-1494.
- McLaughlin, R. J., and Stanley, W. D., 1975, Pre-Tertiary geology and structural control of geothermal resources, The Geysers steam field, California: 2nd U.N. Sympos. on Dev. and Use of Geothermal Res., San Francisco, p. 475-485.
- McNally, K. C., 1976, Spatial, temporal, and mechanistic character in earthquake occurrence: A segment of the San Andreas fault in central California: Ph.D. thesis, University of California, Berkeley.
- Murase, T., and McBirney, A. R., 1973, Properties of some common igneous rocks and their melts at high temperature: *Bull. GSA*, v. 84, p. 3563-3592.
- Nur, A., 1973, Role of pure fluids in faulting: *Phil. Trans. R. Soc. Lond.*, v. 274, p. 297-304.
- Nur, A., and Simmons, G., 1969, The effect of saturation on velocity in low porosity rocks: *Earth Plan. Sci. Letters*, v. 7, p. 183-193.
- Raleigh, C. B., and Paterson, M. S., 1965, Experimental deformation of serpentinite and its tectonic implications: *J. Geophys. Res.*, v. 70, p. 3965-3985.
- Scholz, C. H., 1968, The frequency-magnitude relation of microfracturing in rock and its relation to earthquakes: *Bull. SSA*, v. 58, p. 399-415.
- Smith, W. D., 1975, A finite element study of the effects of structural irregularities on body wave propagation: Ph.D. thesis, University of California, Berkeley.
- Stesky, R. M., 1977, Rock friction—effect of confining pressure: Proc. Confer. II Experimental studies of rock friction with application to earthquake prediction. U.S.G.S., p. 331-353.
- Teng, T., 1968, Attenuation of body waves and the Q structure of the mantle: *J. Geophys. Res.*, v. 73, p. 2195-2216.
- Thatcher, W., and Hanks, T. C., 1973, Source parameters of southern California earthquakes: *J. Geophys. Res.*, v. 77, p. 1549-1565.
- Toksöz, M. N., Cheng, C. H., and Timur, A., 1976, Velocities of seismic waves in porous rocks: *Geophysics*, v. 41, p. 621-645.
- Weres, O., Tsao, K., and Wood, B., 1977, Resource technology and environment at The Geysers: Lawrence Berkeley Lab., LBL-5231.
- White, D. E., Muffler, L. J. P. and Truesdell, A. H., 1971, Vapor-dominated hydrothermal systems compared with hot-water systems: *Econ. Geol.*, v. 66, p. 75-97.
- White, J. E., 1975, Computed seismic speeds and attenuation in rocks with partial gas saturation: *Geophysics*, v. 40, p. 224-232.
- Wyss, M., 1973, Towards a physical understanding of the earthquake frequency distribution: *Geophys. J. R. Astr. Soc.*, v. 31, p. 341-359.
- Wyss, M., and Brune, J. N., 1968, Seismic moment, stress, and source dimensions for earthquakes in the California-Nevada region: *J. Geophys. Res.*, v. 73, p. 4681-4694.

Relation of the Tectonics of Pre-Tertiary Rocks
to Geothermal Resources in The Geysers-Clear Lake
area of Northern California

by

Robert J. McLaughlin
U.S. Geological Survey
Menlo Park, California

Contents

Abstract

Introduction

Tectonic setting of the Great Valley Sequence
and Franciscan Assemblage

Blueschist metamorphism and emplacement of the
Coast Range Thrust

Source Terranes for the Franciscan Assemblage

Tertiary and Quaternary Tectonics

The Geysers Steam Reservoir

Geologic Setting

Franciscan Rocks Associated with the Steam
Reservoir

Boundaries of the Steam Reservoir

Structure of the Steam Reservoir

Influence of Regional Stress Upon Reservoir
Structure

Insights into Reservoir Structure from Surface

Geology

Reservoir Recharge

Conclusions

References Cited

Illustrations

- Figure 1. Generalized regional geology of the northern Coast Ranges of California, showing location of The Geysers steam field.
- Figure 2. Plate tectonic reconstruction for the North American plate margin from 40 m.y.a. to present, using the reconstructions of Atwater from 40 to 20 m.y.a. (A), and those of Blake and others from 10 m.y.a. to present (B).
- Figure 3. Map of northern California showing northward progression of Tertiary and Quaternary volcanism with time, major northwest-trending faults of the San Andreas fault system and extrapolated positions of the Mendocino fracture zone between 3 and 5 million years ago.
- Figure 4. Major crustal features of northern California and their relation to emplacement of magma beneath The Geysers-Clear Lake area.
- Figure 5. Generalized geologic map and cross sections of The Geysers steam field.
- Figure 6. Structural model for The Geysers geothermal system.
- Figure 7A. Map showing pattern of faulting over The Geysers steam reservoir.
- Figure 7B. Diagram of principal horizontal vectors of the stress field for The Geysers area, suggested by Bufe and others, this publication, and predicted displacements for vertical faults of various

orientations.

- Figure 8. Block diagram illustrating relationship of open fault and fracture networks of The Geysers steam reservoir to the principal vectors of regional horizontal compression and extension.
- Figure 9. Complex structural high associated with the Castle Rock Springs area of The Geysers steam field, modified after McLaughlin and Stanley, 1976.
- Figure 10. Geology of The Geysers Resort area, illustrating folds in Franciscan chert and extensive hydrothermal activity along Big Sulphur Creek.
- Figure 11. Hypothetical relationship of open fractures to a downward-opening structural high produced by horizontal extension and a downward-pinching structural high produced by horizontal compression.
- Figure 12. Geologic map and cross section of a diapiric structure associated with unproductive exploratory wells in The Geysers steam field.

Abstract

The Geysers-Clear Lake geothermal area lies within the central Franciscan belt of northern California in a complex terrane of northeast-dipping imbricate thrust slices that have been warped and cut by steep-dipping strike-slip and normal faults. Introduction of magma into the crust beneath the Geysers-Clear Lake area can be related to east-southeast extension accompanying northward propagation of the San Andreas transform system between the Clear Lake region and Cape Mendocino within the last 3 million years. The initiation of strike-slip faulting during this time terminated subduction of elements of the Farallon plate beneath North America as strike-slip motion was taken up along the Pacific-North American plate boundary. The mechanism for magma generation appears to require a heat source in the mantle that mixed mantle derived melts with various crustal rocks. These crustal rocks may have included the Franciscan central and coastal belts, ophiolite, Great Valley sequence rocks, and possibly middle to late Tertiary rocks subducted prior to initiation of strike-slip faulting.

The Geysers steam reservoir is on the northeast limb of a major southeast-plunging antiform in Late Mesozoic rocks of the Franciscan assemblage. The reservoir is also located over the southwest side of a major negative gravity anomaly interpreted to delineate the presence of magma within the upper crust. The most significant parameters limiting the extent of the steam reservoir seem to be the distribution of heat and open fracture networks, the presence of cap rocks that retain fluid in the reservoir rocks, and the presence of areas of adequate hydrothermal leakage that allow the system to remain vapor dominated.

The orientation of regional stress determined from earthquake studies in The Geysers area predicts that north to northeast-oriented steep-dipping faults and fractures should produce maximum horizontal extension in the steam reservoir. Vertical extension may also be significant in low dipping or subhorizontal fractures in the axial regions of anticlinal warps and horst-like structures. Local structures of probable significance to steam production include a structural high associated with the Castle Rock Springs area, and southeast-plunging folds in Franciscan rocks overthrust by serpentinite near The Geysers Resort.

Specific areas and mechanisms of natural recharge to The Geysers steam reservoir are poorly known. However, the vent areas for rhyolites and dacites that cap Cobb Mountain may provide conduits that allow deep circulation into the reservoir rocks. Northeast of the steam field, the numerous vents underlying a thick cover of volcanic rocks may have promoted the development of a hot water dominated geothermal system due to an excess of recharge.

Introduction

The Geysers steam field of northern California is the world's largest commercial geothermal development exploited for the purpose of electrical production. The area of commercial development lies within a roughly circular 600 square km area over which young volcanism and active hydrothermal manifestations are apparent. The vapor-dominated Geysers steam reservoir occupies about 300 square km along the southwest side of the geothermal region, extending to unknown depths below about 3 km. The steam reservoir is entirely within an allochthonous basement of complexly deformed and metamorphosed marine sedimentary and igneous rocks assigned to the Franciscan assemblage and to the largely coeval Great Valley sequence.

The structure of these Late Mesozoic and early Tertiary rocks and present regional tectonics strongly influence the geothermal system. It is the purpose of this paper to describe these structural and tectonic relationships, with particular reference to the recent studies of the U.S. Geological Survey and to plate tectonic concepts.

Tectonic setting of the Great Valley Sequence

and Franciscan Assemblage

The northern California Coast Ranges east of the San Andreas fault (fig. 1) consist mainly of two approximately coeval units now separated by a great regional thrust referred to as the Coast Range thrust (Bailey and others, 1970). The upper plate of the Coast Range thrust consists of a fragmented ophiolite complex of Late Jurassic age (= the Coast Range ophiolite) considered to represent oceanic crust (Bailey and others, 1970; McLaughlin and Pessagno, 1978) overlain depositionally by moderately deformed marine sedimentary rocks referred to as the Great Valley sequence (Bailey and others, 1964). The Great Valley sequence ranges from Late Jurassic to Late Cretaceous in age, and consists of coarse ophiolite breccia or tuff near the base (McLaughlin and Pessagno, 1978), overlain by conglomerate, mudstone, and sandstone. The Great Valley sequence is interpreted to represent arc-trench gap or fore-arc basin deposits that were derived from a Klamath-Sierran island arc terrane as a series of coalescing submarine fans (Dickinson, 1970; Ingersoll and others, 1977). The basal part of the Great Valley sequence was largely derived from the depositionally underlying Coast Range ophiolite (McLaughlin and Pessagno, 1978).

Figure 1 near here

Rocks in the lower plate of the Coast Range thrust have been assigned to the Franciscan assemblage (or Franciscan Complex of Berkland and others, 1972) and consist of a heterogeneous assemblage of intensely deformed and mildly to moderately metamorphosed sandstone, shale, chert, and mafic igneous rocks. Serpentinite, limestone, amphibolite, eclogite, and high-grade blueschist are found as minor but significant constituents. Franciscan rocks and their equivalents are now known to extend along the Pacific coast of North America at least from Baja California, Mexico, to southern Alaska (Jones and others, in press). Initial deformation and metamorphism of these rocks apparently occurred in Cretaceous and early Tertiary time, as the result of oblique northeast-directed subduction and strike-slip. Popular plate tectonic models (Dickinson and others, 1970; Blake and Jones, 1974; Hamilton, 1969) interpreted rocks of the Franciscan assemblage to have been deposited in a trench over an east-dipping subduction zone located to the west of the fore arc basin of the Great Valley sequence. However, paleomagnetic evidence presented recently by Jones and others (in press), and arguments put forth by McLaughlin and Pessagno (1978), and Blake and Jones (1978), suggest that this model is overly simplistic. The paleomagnetic data indicate that as much as 30 degrees of northward translation of Mesozoic plate elements occurred along the Pacific margin in pre-Late Cretaceous time (Jones and others, in press). It is not clear what the relative importance of transform and oblique subduction were in these displacements, but

by implication, elements of the Franciscan assemblage and possibly even the Great Valley sequence may have sustained large-scale northward displacement from their original sites of deposition prior to, during, or following periods of pre-Late Cretaceous subduction.

In northern California, the Franciscan assemblage has been divided into broad northwest-trending thrust fault-bounded structural belts by Jones and others (1976), Berkland and others (1972), and Blake and Jones (1974) (fig. 1): (1) an eastern (Yolla Bolly) belt of Late Jurassic and Early Cretaceous age is composed of intact lawsonite-grade metasediments, with minor interbedded metachert and very minor interbedded meta-igneous rocks. (2) A somewhat younger central belt to the west, is composed of rocks of Late Jurassic to Late Cretaceous age, that were deformed into extensive melanges and broken formations in later Cretaceous time. The broken formations of the central belt consist of pumpellyite to lawsonite-grade metasediments and argillite, basaltic igneous rocks, and chert, and differ from the melanges in displaying local stratal continuity, in being significantly less penetratively sheared, in having lower argillite to sandstone ratios, and in generally not containing exotic blocks such as eclogite, amphibolite, high-grade blueschist, or serpentinite. (3) A still younger western (coastal) belt of Late Cretaceous to Eocene age consists mainly of broken formations of K-feldspar-bearing laumontite-grade arkosic sandstone and shale. Basaltic igneous rocks, blueschist, eclogite, amphibolite, limestone, and chert are rarely present in the coastal belt. These various belts of Franciscan rocks have probably sustained large components of strike-slip movement relative to one another and to the upper plate of the Coast Range thrust, in addition to major crustal shortening associated with

subduction.

Blueschist metamorphism and emplacement of the Coast Range thrust

Two principal occurrences of blueschist are recognized in the Franciscan assemblage: (1) displaced blocks of high-grade fine- to coarsely crystalline blueschist that were derived from metamorphosed basalt, eclogite, amphibolite, or rocks with more siliceous protoliths; and (2) extensive intact terranes of graywacke and minor interbedded chert and igneous rocks that have been metamorphosed to blueschist grade and contain lawsonite. The first type of blueschist occurrence is most common as blocks in melange terranes, especially along the west side of the central Franciscan belt. High-grade blueschist blocks are rarely found in the coastal belt, but are found sporadically in some melanges in the eastern Franciscan belt. The second type of blueschist occurrence includes most of the eastern Franciscan belt and several large slabs in the central Franciscan belt (fig. 1).

The unusual depressed temperature and high pressure gradients necessary to produce blueschist mineral assemblages (Bailey and others, 1964; Coleman and Lee, 1962) are widely regarded as indicative of conditions encountered in subduction zones (Bailey and others, 1970; Ernst, 1970; Ernst, 1971; Platt, 1975). The age of this blueschist metamorphism is thought to constrain the timing of subduction. Coleman and Lanphere (1971) have dated glaucophane and white mica from high-grade blueschist blocks in the Franciscan assemblage by K-Ar methods and demonstrated that the metamorphism took place in the Late Jurassic, about 150 m.y.a.. By contrast, dating of highly reconstituted blueschist-grade metagraywackes from the South Fork mountain schist terrane of the eastern Franciscan belt by conventional and ⁴⁰Ar-³⁹Ar methods (Lanphere and others, 1978) suggests a metamorphic age of 115-120 m.y. for these rocks. Suppe and Armstrong (1972) found a wide age range of 150 to 70 m.y. for blueschist metamorphism of eastern and central belt Franciscan rocks, and interpreted this wide age range to indicate that subduction occurred in the Late Jurassic and sporadically throughout most of the Cretaceous, simultaneously with sedimentation.

Blake and others (1967) have documented a regional increase in the degree of schistosity development in metagraywackes of the eastern Franciscan belt that corresponds to an increase in abundance of blueschist minerals such as lawsonite. It was found that both degree of schistosity and development of high pressure mineral assemblages increase structurally upward toward the Coast Range thrust. This inverted metamorphic zonation was related by them to emplacement of the Coast Range thrust. Bailey and others (1970) later interpreted the Coast Range thrust as the hanging wall of a subduction zone. By this interpretation the age of blueschist metamorphism gave a maximum age of 115-120 m.y. for emplacement of the Coast Range thrust above rocks of the eastern Franciscan belt (about Albian-Aptian time). However, in the Geysers-Clear Lake area inverted metamorphic zonation adjacent to the Coast Range thrust cannot be demonstrated except locally due to post-metamorphic imbrication of eastern belt Franciscan rocks with central belt rocks. Furthermore, paleontologic evidence from the Geysers area demonstrates that emplacement of the Coast Range ophiolite above the Franciscan central belt occurred no earlier than Cenomanian time, or less than about 96 m.y.a in that area (McLaughlin and Pessagno, 1978).

Source terranes for the Franciscan Assemblage

The source areas for Franciscan detritus have been eliminated by subduction, and/or transform faulting. The original location and composition of these source areas is unknown, although some insights can be obtained from study of the petrology and sedimentology of Franciscan sandstones and conglomerates.

In spite of the association of Franciscan sandstones with mafic igneous rocks and cherts of oceanic affinity, the sandstone compositions reflect island arc or continental sources. The petrology of these sandstones shows them to be arkosic to subarkosic in composition, although some are also volcanic-lithic (R. McLaughlin and H. Ohlin, unpublished data; Blake and Jones, 1978). The ages of radiolarians present in abundant chert detritus in conglomerates of the central Franciscan belt indicate the chert detritus is derived partly from older Franciscan cherts interbedded with graywacke and greenstone of the central belt (McLaughlin and Pessagno, ¹⁹⁷⁸ in press) and partly from older Mesozoic sources (Seiders and Pessagno, in press). More than 20 percent K-feldspar is typically found in sandstones of the coastal belt, 0 to 6 percent is typical of sandstones along the west side of the central Franciscan belt, and sandstones in the main part of the central and eastern belts usually contain only one percent or less. This eastward regional decrease in K-feldspar may be partly due to the presence of white mica at the expense of K-feldspar, with increasing metamorphism.

The presence of early Mesozoic hypabyssal silicic and intermediate plutonic rocks and of pelagic sedimentary clasts in several conglomerates in the central Franciscan belt and lower part of the Great Valley sequence has led Seiders and Pessagno (in press) to suggest the Calaveras formation and its equivalents in the Sierra Nevada and Klamath Mountains as possible sources for this detritus. An island arc active to the west in the early Tertiary has been proposed by Beutner (1977) to explain the bimodal compositions of andesitic and quartzo-feldspathic graywacke sequences in the Franciscan coastal belt. Other island arc terranes, including early Cretaceous arc-related rocks at Trinidad head in northern California and an arc thought to have been the source for the late Jurassic Otter Point formation in southwestern Oregon (Blake and Jones, 1978) are also possible sources of Franciscan sandstone detritus.

The provenance of the blocks of amphibolite and eclogite present in melange terranes of the central Franciscan belt is unknown. The high temperatures and pressures of formation of the mineral assemblages in these rocks indicated by experimental work suggests that they are displaced from lower crust and upper mantle levels. Many of the blocks have sheared and polished rinds of actinolite and serpentinite, and others contain retrograde blueschist mineral assemblages. Emplacement of these rocks into the melanges must have involved large vertical displacements, and at least partial transport within serpentinite, possibly accompanied by large-scale gravity or submarine sliding.

Tertiary and Quaternary tectonics

Plate tectonic reconstructions (figs. 2a and 2b) by Atwater (1970) and Blake and others (1978) trace the evolution of the San Andreas transform fault system from the time that the north American plate came into contact with the Pacific and Farallon oceanic plates about 40 m.y.a. This triple junction (= Mendocino triple junction) migrated northward along the North American plate margin from southern California to its present position at Cape Mendocino in northern California, terminating subduction that was occurring north of the triple junction, and initiating a broad right-lateral transform shear (the San Andreas fault system) southeast of the propagating transform front.

Figure 2 near here

The western North American plate now consists largely of elements of the Farallon plate that were accreted by subduction and strike-slip during the Late Cretaceous and Tertiary, prior to passage of the Mendocino triple junction. The Franciscan coastal belt and at least part of the central Franciscan belt probably consist of elements of the Farallon plate.

Data of E. A. Silver published by Blake and others (1978) show that the azimuth of shear between the Pacific and North American plates (fig. 2b) changed from a more northerly to a more westerly orientation between about 10 m.y.a. and the present, resulting in a slightly extensional regime along and within the San Andreas fault system. This change in motion facilitated creation of extensional basins within the San Andreas system and in the northern Coast Ranges. Prominent examples of these basins in northern California are Ukiah and Little Lake Valleys, Round Valley, and Clear Lake basin, all of which are typical of the types of extensional basins proposed by Crowell (1974a, b) to lie within a major strike-slip fault system.

Plate reconstructions by Silver further indicated that subduction terminated and that the San Andreas system was initiated in the northern Coast Ranges between Point Arena and Cape Mendocino within the last 10 m.y. (fig. 2b). The average rate of right-lateral motion for the last 4-6 m.y. between the Pacific and North American plates is estimated at about 5.5 cm/year (Atwater and Molnar, 1973). Extrapolation of the Mendocino triple junction backward in time along the present boundary between the North American and Pacific plates (= the San Andreas fault) at this rate suggests that the triple junction was opposite the latitude of The Geysers-Clear Lake area approximately 3 m.y.a. (fig. 3). Significant components of Pacific-North American plate motion apparently are also taken up by subsidiary fault members of the strike-slip system east of the main San Andreas fault (figs. 3 and 4, and Herd, 1978). This implies that Clear Lake basin and several other San Andreas-related extensional basins between Clear Lake and Cape Mendocino are less than 3 m.y. old. The orientation and position of the present Eel River basin north of Cape Mendocino suggests that it may be one of the basins suggested by Blake and others (1978) to have formed in front of the northward propagating Mendocino triple junction (figs. 2b, 3, and 4).

Figure 3 near here

The timing of Clear Lake volcanism indicates that it closely followed passage of the Mendocino triple junction and propagation of San Andreas-related extensional structures. Propagation of the triple junction past the Clear Lake area seems to have preceded the changeover from Sonoma to Clear Lake volcanism between 2.9 and 2.0 m.y.a. (Donnelly, 1977; Hearn and others; and Donnelly and Hearn, this volume). Hearn and others (1976b, and this volume) have pointed out that volcanism in the northern Coast Ranges shifted northward with time (fig. 3). They argued that this time-space progression resulted from passage of the North American plate over a stationary mantle plume or hot spot.

This author favors a model for emplacement of magma into the crust beneath the Geysers-Clear Lake area that is closely tied to passage of the Mendocino triple junction and crustal extension within the San Andreas fault system. Andreas shear system (McLaughlin, 1977a). Donnelly (1977) also related late Cenozoic volcanism and magma emplacement to propagation of the San Andreas fault system. Sonoma and Clear Lake volcanism might thus be characterized as magma leakage along a propagating land-bound transform fault system. North to northeast-oriented normal faults associated with right-lateral shear couples within the San Andreas system apparently acted as the conduits for venting of the Clear Lake magmas (Hearn and others, this volume).

Magma sources for the region are highly conjectural, but strontium isotope and trace element studies of the Clear Lake volcanics (Futa and others, and Hearn and others, this volume) suggest that the lavas are derived from primitive mantle material that underwent considerable mixing with various crustal rocks. A stationary hot spot or mantle plume might have provided the mechanism to produce these mantle derived melts as suggested by Hearn and others (this volume). However, absolute motion of North America derived from assuming the presence of a stationary hot spot is significantly more complex than suggested in the simplistic hot spot model of Morgan (1972) and crustal characteristics suggested to be associated with most hot spots by Morgan apparently cannot be applied to The Geysers-Clear Lake area.

Figure 4 attempts to relate regional tectonics and deep crustal conditions to the presence of magma beneath The Geysers-Clear Lake area. Clear Lake magmas have passed upward through the Franciscan central belt and rocks in the upper plate of the Coast Range thrust, and may also have passed through the Franciscan coastal belt and younger Tertiary rocks subducted with the Farallon plate prior to initiation of strike slip.

Figure 4 near here

The Geysers Steam Reservoir

Geologic Setting

The Geysers steam reservoir occupies the northeast limb of a complexly faulted southeast-plunging antiform that forms the core of the Mayacmas Mountains (McLaughlin, 1975). The southwest limb of this antiform is sheared right-laterally along several Tertiary and Quaternary faults. The Maacama fault zone--a prominent active right-lateral fault of the San Andreas system is the furthest southwest of the faults that bound the Mayacmas antiform. The northeast side of the Mayacmas uplift is bounded by yet another major northwest-trending en echelon member of the San Andreas fault system--the Collayomi fault zone. Major uplift of the Mayacmas Mountains has occurred between the Maacama and Collayomi fault zones due to north-northeast-oriented compression.

Broad, southeast-plunging folds in The Geysers region trend somewhat more westerly than the San Andreas-related strike-slip faults. These folds are in large part the result of late Tertiary and Quaternary north-south compression that either preceded or accompanied strike-slip faulting. Contemporaneous sets of subtle east-trending warps are locally present in uplifted areas between E-W trending normal and thrust faults (see structural section 1 between geothermal wells CA-1862 and CA 956-1 in Figure 5).

The southeast-plunging folded regional structure of the area is made apparent by distribution of ophiolite in the upper plate of the Coast Range thrust, and positionally overlying strata of the Great Valley sequence. A thick, folded and imbricated section of ophiolite and Great Valley sequence are present northeast of the Collayomi fault zone, covered to a large extent by Clear Lake volcanics (fig. 5). These rocks wrap over Franciscan rocks several kilometers southeast of the map area shown in fig. 5 (see McLaughlin and Stanley, 1975) and over the crest of the Mayacmas Mountains just northwest of the summit of Mount St. Helena. On the southwest side of Mount St. Helena the ophiolite is sheared and fragmented right-laterally along the broad Mercuryville-Geyser Peak-Maacama fault zones. One large mass of ophiolite which composes Geyser Peak and Black Mountain, is separated right-laterally along this fault system about 18 kilometers from the Mount St. Helena mass. A post-Pliocene right-lateral offset of about 20 kilometers along the Mercuryville-Geyser Peak-Maacama fault zones is also implied by offset of the Sonoma Volcanics along the Maacama fault zone, although at least part of the apparent offset may be due to uplift across fault zones.

Figure 5 near here

Franciscan Rocks Associated with the Steam Reservoir

Rocks of the central and eastern Franciscan belts compose the uplifted core of the Mayacmas antiform, and underlie the entire area of The Geysers steam field. These central and eastern belt Franciscan rocks are subdivided in The Geysers area into several fault-bounded slab-like units based on lithologic criteria and their degree of metamorphism (fig. 5). The structurally lowest unit in the area may merely be an intact sandstone slab within the central Franciscan belt. The unit is exposed in the core of the Mayacmas antiform and consists of well bedded fine- to coarse-grained graywacke and minor shale, with a very weak metamorphic fabric (textural zone 1 of Blake and others, 1967). The rocks of this unit are penetratively sheared and well fractured and constitute a broken formation. The unit is characterized by its weak metamorphism (pumpellyite grade) and an absence of chert, greenstone, polymict conglomerate, or exotic blocks. The lower unit extends at depth beneath the area of steam field development and probably constitutes part of the reservoir rocks.

The lower structural unit is overlain northeast of the Mercuryville fault zone and southwest of the Geyser Peak fault zone by an intermediate structural unit consisting in part of large slabs of conglomeratic and lithic graywacke interbedded with chert and basalt flows. These slabs are interleaved with melanges containing sporadic blocks of blueschist, amphibolite and eclogite, in addition to chert, basalt and graywacke. The graywacke of the intermediate structural unit is reconstituted to textural zones 1 and 2 of Blake and others (1967) and contains pumpellyite and local lawsonite. Also intercalated in this intermediate structural unit is a thick northeast-dipping slab of actinolitic serpentinite, having a mappable extent along strike of approximately 10 kilometers, and traceable northeastward in the subsurface for about 1.5 kilometers from its surface exposure along Big Sulphur Creek (fig. 5). The actinolitic ultramafic body, along with other highly sheared rocks of the intermediate structural unit comprise a series of thick, northeast-dipping impermeable cap rocks. The interleaved fractured slabs of graywacke in the intermediate structural unit apparently act as reservoir rocks at several different structural levels.

The structurally highest Franciscan rocks in the steam field locally consist of highly reconstituted lawsonitic metagraywacke (textural zone 2 to 3 of Blake and others, 1967) and minor metachert and metavolcanic rocks that may be correlative with the eastern (Yolla Bolly) belt. The metagraywacke of this upper structural unit is extensively recrystallized and may contain jadeite or glaucophane in addition to lawsonite. These upper structural unit rocks have a penetrative schistosity that makes them poorer reservoir rocks than structurally lower, less metamorphosed graywackes.

Prominent imbricate thrusts of Late Cretaceous and Tertiary age in the map area have juxtaposed rocks of the intermediate and upper Franciscan structural units with ophiolitic rocks in the upper plate of the Coast Range thrust. The lower ultramafic part of the ophiolite has in several places been downdropped along these thrusts, and sheared laterally along the thrust boundaries, so that the original base of the upper plate of the Coast Range thrust is difficult, or impossible to recognize in many places (fig. 5). These later thrusts may represent transitional structures produced during changes in plate motion from northeast-directed subduction to strike-slip fault movement. The late thrusts formed after initial emplacement of the Coast Range thrust and formation of melanges in the central Franciscan belt, and they include nearly all of the thrusts that now separate major structural units in The Geysers area.

Boundaries of the Steam Reservoir

A structural model for The Geysers steam reservoir introduced by McLaughlin (1977a), that incorporates elements of a model suggested by Isherwood based on gravity and magnetics, is shown in figure 6 in somewhat modified form. The Geysers steam reservoir is apparently confined to the northeast limb of the Mayacmas antiform (fig. 6). It is bounded on the southwest side by the northwest-trending Mercuryville fault zone, and on the northeast by the Collayomi fault zone. A hot water dominated reservoir whose extent is unknown in detail is present northeast of the Collayomi fault zone (Goff and others, 1977). On the northwest and southeast, the steam reservoir boundaries are less well determined. It is thought to extend no further to the northwest than Tyler Valley. On the southeast, the reservoir may extend to the vicinity of the Hellen-Wallstreet mercury mines of Dry Creek Canyon. Local inactive hydrothermal areas and several small rhyolite and dacite intrusives (including Pine Mountain and Pilot Knob are present near the crest of the Mayacmas Mountains southwest of the Helen-Wallstreet mines. These areas may either lie within or are somewhat beyond the southeast extension of the steam reservoir.

Figure 6 near here

The Geysers-Clear Lake geothermal area is believed to be heated by a silicic magma body centered below 10 kilometers, the top of which is within about 7 kilometers of the surface (Isherwood, 1976; Chapman, 1975). The distribution of this magma at depth is probably the most significant factor controlling the northwest, southeast, and southwest boundaries of the steam reservoir. Beyond the extent of potent heat conductance, the steam system presumably passes into a cold water-dominated system, except in areas where it is prevented from doing so by a lack of permeability. The presence and regional distribution of the magma is suggested geophysically by closure on a large-scale -30 milligal bouguer gravity anomaly centered beneath the Clear Lake Volcanics, and by large delays in the travel time of teleseismic p-waves (Iyer and Hitchcock, 1975; Iyer and others, this volume). The Geysers steam field lies along the southwest side of the gravity anomaly, within the confines of closure on the gravity low (fig. 1).

The northeast-dipping Mercuryville fault zone also appears to have considerable local influence on the southwest boundary of the steam reservoir. Near The Geysers Resort, there is a marked decrease in the number of successful steam wells drilled near the fault zone, and a lack of intense hydrothermal alteration southwest of the fault zone. In addition the fault zone coincides approximately with closure on the southwest side of the regional gravity low. Prominent hydrothermal alteration along the trend of the Mercuryville fault zone suggests that in the past it was a major thermal vent area for The Geysers hydrothermal system, perhaps when there was a larger volume of water in the reservoir and/or heat supply to the system was greater. The hydrothermal reservoir may since have boiled down and shrunk down-structure and northeastward along the Mercuryville fault zone to where it now vents along steep-dipping faults in Big Sulphur Creek (fig. 6).

The northeast extent of The Geysers steam field appears to be limited by the Collayomi fault zone, according to the interpretation of thermal water chemistry by Goff and others (1977) who suggest that hot water resources are present northeast of the Collayomi fault zone. Although reservoir rocks for the hot water system are poorly known due to their thick volcanic cover and a lack of deep drill hole data, they probably involve both Franciscan rocks and marine strata of the Great Valley sequence. The hot water system in this area has not yet been successfully developed but might include local vapor-dominated areas (Goff and others, 1977). Existence of a deep vapor-dominated system separated by impermeable rocks from the overlying hot water system has been suggested as a remote exploration possibility by some geothermal companies. Regional structure probably accounts at least in part for the change in character of geothermal resources northeast of the Collayomi fault zone. Much of this area to the northeast is underlain by a thick folded and imbricated section of Great Valley sequence and ophiolitic rocks in the upper plate of the Coast Range thrust. This cover of Great Valley sequence rocks and ophiolite, is on the down-thrown side of the Collayomi fault zone, and probably has acted as an impermeable cap to inhibit escape of thermal fluid from the underlying Franciscan reservoir rocks (McLaughlin, 1977). Goff and others (1977) further suggest that numerous lava vents beneath the Clear Lake volcanics provide conduits for recharge to deep structural levels. Although an extensive

volcanic cover is present to the northeast, the uplifted Mayacmas Mountains southwest of the Collayomi fault zone largely exposes only Franciscan rocks. In this uplifted area, maintenance of a hot water system is inhibited, because little if any recharge occurs, and several of the fractures and fault zones that are significant reservoir structures at depth are also conduits for leakage of the reservoir at the surface in the hydrothermal areas.

Structure of the Steam Reservoir .

The most difficult structural features to delineate in The Geysers-Clear Lake region are those that control the local distribution of steam within the production area. Confirmation of such structural control is best accomplished through interpretation of closely-spaced drillhole data in conjunction with the surface geology. Development of The Geysers steam field has not yet reached a stage where local structural features are known in detail. However by analogy with the longer production history of the Larderello steam field in central Italy, reservoir decline may soon bring about the necessity for more thorough evaluations of local structural features at The Geysers to determine the more economically productive areas.

The steam reservoir is in most instances within interconnected fracture networks in intact slabs of graywacke in the intermediate and possibly the lower Franciscan structural units (fig. 5 and 6). These reservoir rocks, along with intercalated melanges, greenstone, semi-schistose metagraywacke, and serpentinite that act as the cap rocks, compose a stack of northeast- to southeast-dipping imbricate thrust sheets (McLaughlin, 1977). Heat is convected in water and steam in the fracture networks of the reservoir rocks to the southwest and southeast, up-structure toward The Geysers steam field.

1

Of primary importance to the production of steam from the reservoir rocks is distribution, continuity, and density of the open fracture networks, since rocks in the steam reservoir are otherwise impermeable. Through-going fracture networks are statistically most abundant in the least reconstituted graywackes, although a few producing steam wells have in fact produced from Franciscan greenstone.

It is apparent from the surface geology that within graywacke units there are very large phacoid-shaped masses of more or less unfractured sandstone surrounded by more penetratively fractured and sheared sandstone. This characteristic strongly implies the presence in the subsurface of unproductive, unfractured regions within reservoir rocks. Thus boudinage and brittle shear fracture, in combination with original lenticularity of Franciscan sandstone units may be of great significance in determining distribution of the open fracture networks. Discontinuous communication of reservoir rock fractures in The Geysers steam field was described recently by Lipman and others (1977) in their evaluation of reservoir performance in the Sulphur Bank and Happy Jack areas. Early steam wells drilled in these areas tapped shallow reservoir fractures at depths above 640 meters that had static pressures much lower than the prevailing pressures in a separate, more extensive fracture system 183 meters deeper. This led to the early recognition of two separate discrete steam reservoirs at different structural levels. More recent studies of reservoir drainage by Lipman and his colleagues have demonstrated that while these fractured areas are separated locally by pendants of impermeable, unfractured rock, the shallow fracture network is connected with the deeper more regional fracture zone elsewhere in the area.

Influence of Regional Stress Upon Reservoir Structure

The large number of shallow earthquakes associated with The Geysers steam field indicate that the region is tectonically active and that stress is locally relieved along zones of weakness in rocks of the steam reservoir. The steam reservoir occupies a more or less rigid uplifted block between two major strike-slip fault zones (fig. 7A). This uplifted block is broken by numerous faults, fractures, and joints formed prior to, and during development of the San Andreas shear system.

McLaughlin and Stanley (1975) indicated that the steep dipping northwest-trending strike-slip and normal faults along which fumaroles and hot springs vent near The Geysers Resort may be major channelways from the steam reservoir. They further suggested that the hydrothermal lubrication of these fault zones (fig. 7A) may promote the release of regional stress and localization of shallow earthquakes.

Figure 7A near here

Recent seismic studies (Bufe and others, this publication; Bufe and Lester, 1976) coupled with investigations of vertical and horizontal surface changes over the area of steam production (Lofgren, this publication) suggest that much seismic activity at The Geysers may also be due to fluid withdrawal and reservoir subsidence, probably along pre-existing faults in the area of steam production.

Earthquake first motion studies by Bufe and others (this publication) indicate that the vectors of maximum regional compression in The Geysers area range from about N 30°E to more northerly orientations compatible with the right-lateral offsets observed on northwest-trending faults of the San Andreas system. An approximate north-south maximum compression vector agrees with the observed sense of offset on most of the major Quaternary faults in The Geysers area (fig. 7A). The 30° of eastward scatter in the vectors of compression may be due wholly or in part to local factors such as (1) variable amounts of strain accumulated within The Geysers-Clear Lake region; (2) the release of strain along fault segments of variable lengths and orientations; or (3) the effect of steam reservoir subsidence upon the distribution of regional stress.

Optimum horizontal extension predicted from the earthquake studies of Bufe and his colleagues is perpendicular to the vectors of principal compression (fig. 7B), indicating that fractures oriented north- to N 30° E are highly favorable geothermal targets. More northwest- or northeast-oriented fractures should exhibit lesser components of extension in addition to strike-slip and thrust faulting (fig. 7B).

Figure 7B near here

Insights into Reservoir Structure from Surface Geology

Cataldi and others (1963, 1977) have shown that wells producing high volumes of steam in the Larderello area of central Italy are associated with the crests of northwest-plunging horsts. Detailed well production data necessary to demonstrate such a relation at The Geysers are generally unavailable, but upwarps and other structural highs could be of considerable importance to reservoir permeability in the subsurface of The Geysers steam field. In the axial regions of structural highs significant vertical extension can occur along low-dipping or subhorizontal bedding planes, joints, fractures and thrust faults. These open subhorizontal features may be particularly significant where intersected by favorably oriented vertical fractures (fig. 8).

Figure 8 near here

Structural highs have been mapped over The Geysers steam reservoir by McLaughlin (1978), and a horst-like structure in the Castle Rock Springs area of the steam field was described by McLaughlin and Stanley (1975). Numerous producing wells are associated with this structural high, possibly due to localization of favorably oriented open fracture networks (fig. 9).

Figure 9 near here

The axial regions of folds similarly should be important in producing permeability in the subsurface. Folded Franciscan rocks of differing competency and permeability are present near The Geysers Resort, where interbedded graywacke, chert, greenstone, and melange are major constituents of the Franciscan assemblage (fig. 10). These rocks form a slab of relatively intact strata tightly folded into southeast-plunging anticlines and synclines. The graywacke, chert, greenstone, and melange involved in the folding are overthrust by a thick sheet of serpentinite which acts as a reservoir cap rock (fig. 10). In the subsurface, the chert, greenstone and melange are local impermeable barriers to hydrothermal circulation and the graywackes compose the permeable reservoir rocks. Hinge areas of the southeast plunging folds (fig. 10) should be the loci of tensional fractures and faults which probably provide important open fracture networks to the graywackes in the subsurface, where they project beneath the serpentinite cap rock.

Figure 10 near here

All fault bounded uplifts do not necessarily contribute to the permeability of The Geysers steam reservoir. Figure 11 illustrates that downward-pinching uplifts formed through horizontal compression are likely to develop fracture networks that close with depth. These compressional features may be less desirable exploration targets than the downward opening horst-like features resulting from extension, since extensional uplifts are more likely to contain fractures that open with depth. Shell Oil Company has extensively explored a diapir-like uplift in the southeast part of The Geysers steam field (fig. 12) and drilled three exploration wells. High temperature gradients were reported in these wells (Fehlberg, 1975), but no commercially significant open fracture networks were encountered. The failure of these wells to encounter appreciable open fractures may be related to the diapiric compressional uplift over which the wells were sited.

Figures 11 and 12 near here

Horizontal extension is also important along warps or irregularities in the trend of steep-dipping strike-slip faults (fig. 8). No specific examples of such a feature are known within The Geysers steam field, but significant extension is indicated southwest of The Geysers along the Maacama strike-slip fault zone, where late Tertiary fluvial and lacustrine sedimentary rocks are deposited in elongate fault bounded depressions that formed contemporaneously with sedimentation.

Reservoir Recharge

White and others (1971) have shown that steam in The Geysers hydrothermal system is derived for the most part from meteoric water. They further hypothesized that vapor dominated hydrothermal systems such as The Geysers may begin as hot water systems and ultimately boil down to the vapor dominated state. They argue that in such a system, the reservoir rocks must have a low recharge rate and hydrothermal leakage in the form of hot springs and fumaroles (and presently, steam wells), must exceed recharge, in order for the vapor state to be maintained. Some natural recharge is necessary in their model, however, to ensure that the system does not completely boil off. Vapor dominated hydrothermal systems do not maintain a perfect balance between reservoir leakage and recharge, and thereby eventually do get drowned or boil off. However, the time framework for this is unknown.

Natural recharge to The Geysers system is constrained by the largely impermeable character of the Franciscan reservoir rocks. However, since the steam reservoir is underpressured with respect to surrounding water dominated parts of the system (White and others, 1971) meteoric water is readily absorbed, provided that conduits into the reservoir are present.

Induced recharge of the reservoir may be demonstrated by the numerous re-injection wells in The Geysers steam field. These wells recycle approximately 25 percent of steam condensate collected from the cooling towers of geothermal power plants. This re-injected condensate represents only a small percentage of the total volume of fluid mined from the system, since a much larger volume is lost through evaporation. However, it is not known whether these re-injected fluids circulate into deep levels of the steam reservoir.

Specific areas of natural recharge in The Geysers region, if they exist, are subject to speculation. Goff and others (1977) suggested that Quaternary and late Tertiary volcanic vents are major sources of reservoir recharge. Within The Geysers steam field, Cobb Mountain, a funnel-shaped volcanic dome composed of a rhyolite and two dacites of early Pleistocene age, may be a major source of this recharge. The silicic rocks of Cobb Mountain have a high porosity and are capable of absorbing large volumes of meteoric water during the rainy season. At least three vents beneath Cobb Mountain presumably might act as conduits that allow meteoric water to percolate deep into the Franciscan basement. Other volcanic vents present within and adjacent to the vapor dominated part of the steam field include vents beneath small volumes of olivine basalt at Caldwell Pines, a small rhyolite dome southeast of Castle Rock Springs (Pine Mountain), and possibly the vents beneath small dacite and rhyolite intrusions (Pilot Knob) adjacent to Mount St. Helena. In the region northeast of the Collayoni fault zone, extensive Quaternary volcanic flows and domes are underlain by numerous vents, and thus significantly larger volumes of water may recharge this part of the hydrothermal system (Goff and others, 1977). This larger potential recharge area may be significant in limiting the extent of the vapor dominated geothermal system.

At least some recharge to the reservoir probably occurs along segments of steep-dipping extensional faults. Some additional downward percolation may occur along the Mercuryville and Collayomi fault zones, especially where the faults transect or coincide with major drainages or where large volumes of water are trapped along extensional warps or along contacts between different rock units.

Conclusions

Major vapor-dominated geothermal systems such as the one in The Geysers-Clear Lake area are rare, and this perhaps is due to the complex tectonics of the northern Coast Ranges.

The structural stacking of permeable and impermeable rocks in The Geysers steam reservoir and the penetrative shear deformation characteristic of Franciscan melanges and broken formations, are thought to be the consequence of deformation associated with the formation of melanges and subduction. The pattern of distribution and orientation of fracture networks within the steam reservoir are largely controlled by this early episode of penetrative deformation that preceded propagation of the San Andreas fault system.

Considerable evidence indicates that extension associated with the San Andreas fault system provided deep zones of weakness along which magma was emplaced into crust beneath the Geysers-Clear Lake area. Late Tertiary and Quaternary volcanism apparently closely followed the termination of subduction and initiation of strike-slip faulting. Furthermore, several of the present depositional basins in the northern Coast Ranges, including Clear Lake basin, appear to be the result of east-southeast extension within the broad zone of right-lateral shear created since passage of the Mendocino triple junction and initiation of the San Andreas fault system.

The present pattern of regional stress may be the principal factor determining which fracture networks control permeability in the steam reservoir. First-motion studies of earthquakes predict that maximum horizontal extension should occur along north- to northeast-oriented vertical fractures. Significant vertical extension may occur along upwarps in subhorizontal fractures and partings. Permeability provided by vertical extension may be particularly significant along the axes of anticlinal or horst-like structures, especially where subhorizontal fractures are intersected by the north- to northeast-oriented vertical fractures. Local bends or warps in northwest-oriented strike-slip faults may also produce significant horizontal extension.

Several specific structures described in this paper are of unproven importance to steam production at The Geysers. However, depletion of The Geysers steam reservoir is occurring at a growing rate due to increases in exploration and development activity. Geothermal developers may soon find it necessary to consider the economic advantages of preferential exploitation of specific structures in the older, more depleted areas of the steam field.

Figure 1. Generalized regional geology of the northern Coast
Ranges of California, showing location of The Geysers steam
field.

Figure 2. Plate tectonic reconstruction for the North American plate margin from 40 m.y.a. to present, using the reconstructions of Atwater from 40 to 20 m.y.a. (A), and those of Blake and others from 10 m.y.a. to present (B).

Figure 3. Map of northern California showing northward progression of Tertiary and Quaternary volcanism with time, major northwest-trending faults of the San Andreas fault system and extrapolated positions of the Mendocino fracture zone between 3 and 5 million years ago.

Figure 4. Major crustal features of northern California and their relation to emplacement of magma beneath The Geysers-Clear Lake area.

Figure 5. Generalized geologic map and cross sections of The Geysers steam field.

Figure 6. Structural model for The Geysers geothermal system.

Figure 7A. Map showing pattern of faulting over The Geysers
steam reservoir.

Figure 7B. Diagram of principal horizontal vectors of the stress field for The Geysers area, suggested by Bufe and others, this publication, and predicted displacements for vertical faults of various orientations.

Figure 8. Block diagram illustrating relationship of open fault and fracture networks of The Geysers steam reservoir to the principal vectors of regional horizontal compression and extension.

Figure 9. Complex structural high associated with the Castle Rock Springs area of The Geysers steam field, modified after McLaughlin and Stanley, 1976.

Figure 10. Geology of The Geysers Resort area, illustrating folds in Franciscan chert and extensive hydrothermal activity along Big Sulphur Creek.

Figure 11. Hypothetical relationship of open fractures to a downward-opening structural high produced by horizontal extension and a downward-pinching structural high produced high by horizontal compression.

Figure 12. Geologic map and cross section of a diapiric structure associated with unproductive exploratory wells in The Geysers steam field.

References Cited

- Atwater, T., 1970, Implications of plate tectonics for the Cenozoic tectonic evolution of western North America: Geol. Soc. of America Bull., vol. 81, p. 3513-3536.
- Atwater, T., and Molnar, P., 1973, Relative motion of the Pacific and North American plates deduced from sea floor spreading in the Atlantic, Indian, and south Pacific Oceans: in Kovach, R. L., and Nurk A., eds., Proc. of the conference on tectonic problems of the San Andreas fault system: Stanford Univ. Pubs. Geol. Sci., vol. 13, p. 136-148.
- Bailey, E. H., 1946, Quicksilver deposits of the western Mayacmas district, Sonoma County, California: California Jour. of Mines and Geology, State Mineralogist's Rept., vol. 42, no. 3.
- Bailey, E. H., Blake, M. C., Jr., and Jones, D. L., 1970, On-land Mesozoic Oceanic Crust in California Coast Ranges: U.S. Geol. Survey Prof. Paper 700-C, p. C70-C81.
- Bailey, E. H., Irwin, W. P., and Jones, D. L., 1964, Franciscan and related rocks and their significance in the geology of western California: Calif. Div. of Mines and Geology, Bull. 183, 177 p.
- Berkland, J. O., Raymond, L. A., Kramer, J. C., Moores, E. M., and O'Day, M., 1972, What is Franciscan?: Amer. Assoc. of Petrol. Geologists, Bull., vol. 56, no. 12, p. 2295-2302.
- Blake, M. C., Jr., and Jones, D. L., 1974, Origin of Franciscan melanges in northern California: Soc. Econ. Paleontologists

and Mineralogists Spec. Pub. 19,, p. 255-263.

- Blake, M. C., Jr., and Jones, D. L., 1978, Allochthonous Terranes in northern California?--A Reinterpretation : Mesozoic Paleogeography of the Western United States, Pacific Coast Paleogeography symposium 2, Pacific Section, Soc. of Econ. Paleontologists and Mineral., April 1978, 573 p.
- Blake, M. C., Jr., Campbell, R. H., Dibblee, T. W., Jr., Howell, D. G., Nilsen, T. H., Normark, W. R., Vedder, J. C., and Silver, E. A., 1978, Neogene Basin Formation in Relation to Plate-Tectonic Evolution of San Andreas fault system, California: Amer. Assoc. of Petrol. Geol. Bull., v. 62, p. 344-372.
- Blake, M. C. Jr., Irwin, W. P., and Coleman, R. G., 1967, Upside-down metamorphic zonation, blueschist facies, along a regional thrust in California and Oregon: U.S. Geol. Survey Prof. Paper 575-C, p. C1-C9.
- Brice, J. C., 1953, Geology of Lower Lake quadrangle, California: Calif. Div. of Mines and Geology Bull. 166, 72 p.
- Bufe, C. G., and Lester, F. W., 1975, Seismicity of The Geysers-Clear Lake region, California: E.O.S. Transactions of the Amer. Geophysical Union, vol. 56, no. 12, p. 1020.
- Cataldi, R., Lazzarotto, A., Muffler, ^{L.J.F.} P., Squarci, P., and Stefani, G., 1977, Assessment of geothermal potential of central and southern Tuscany: in Proceedings of the Larderello workshop on geothermal Resource Assessment and Reservoir Engineering, Sept. 12-16, 69 p.

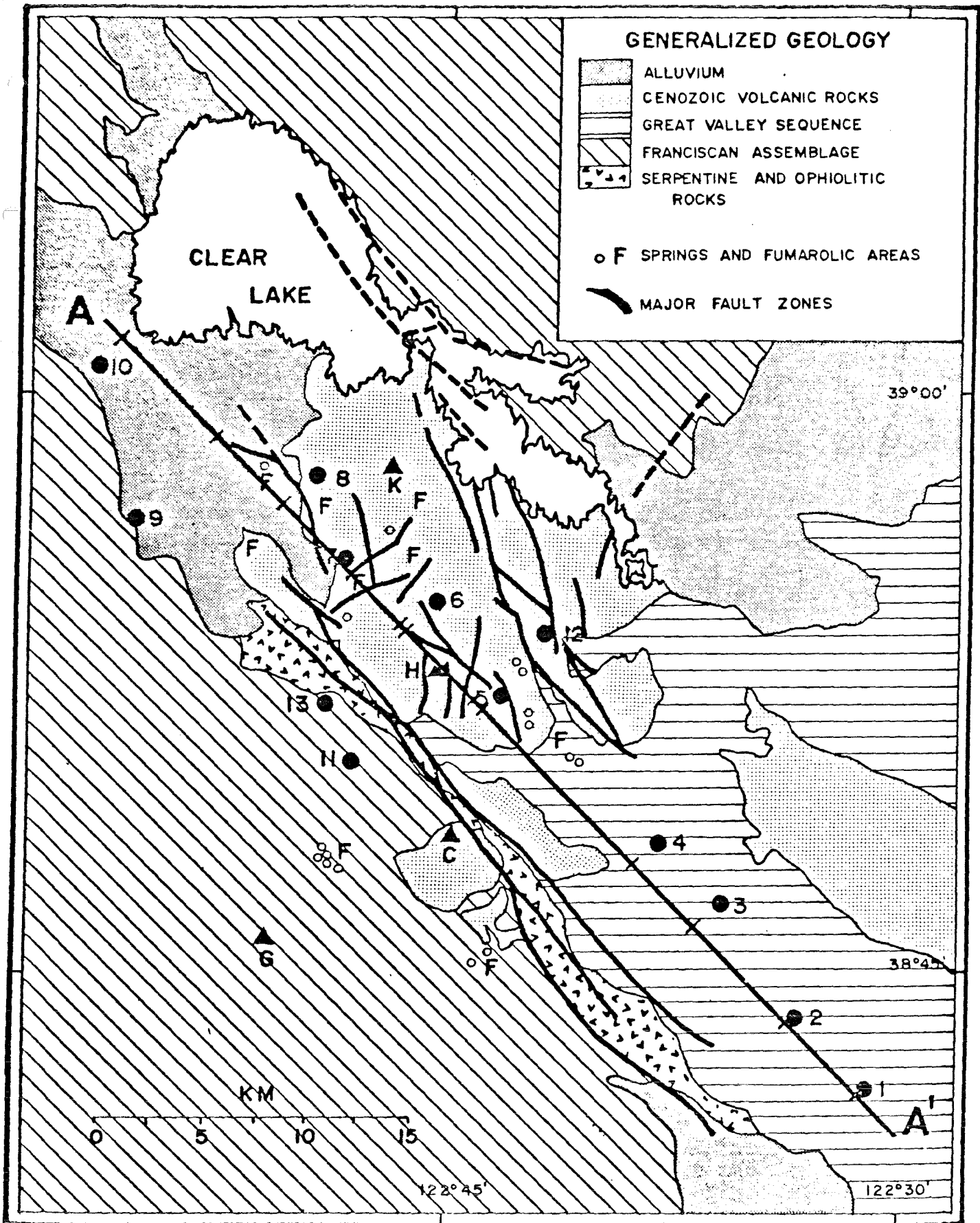
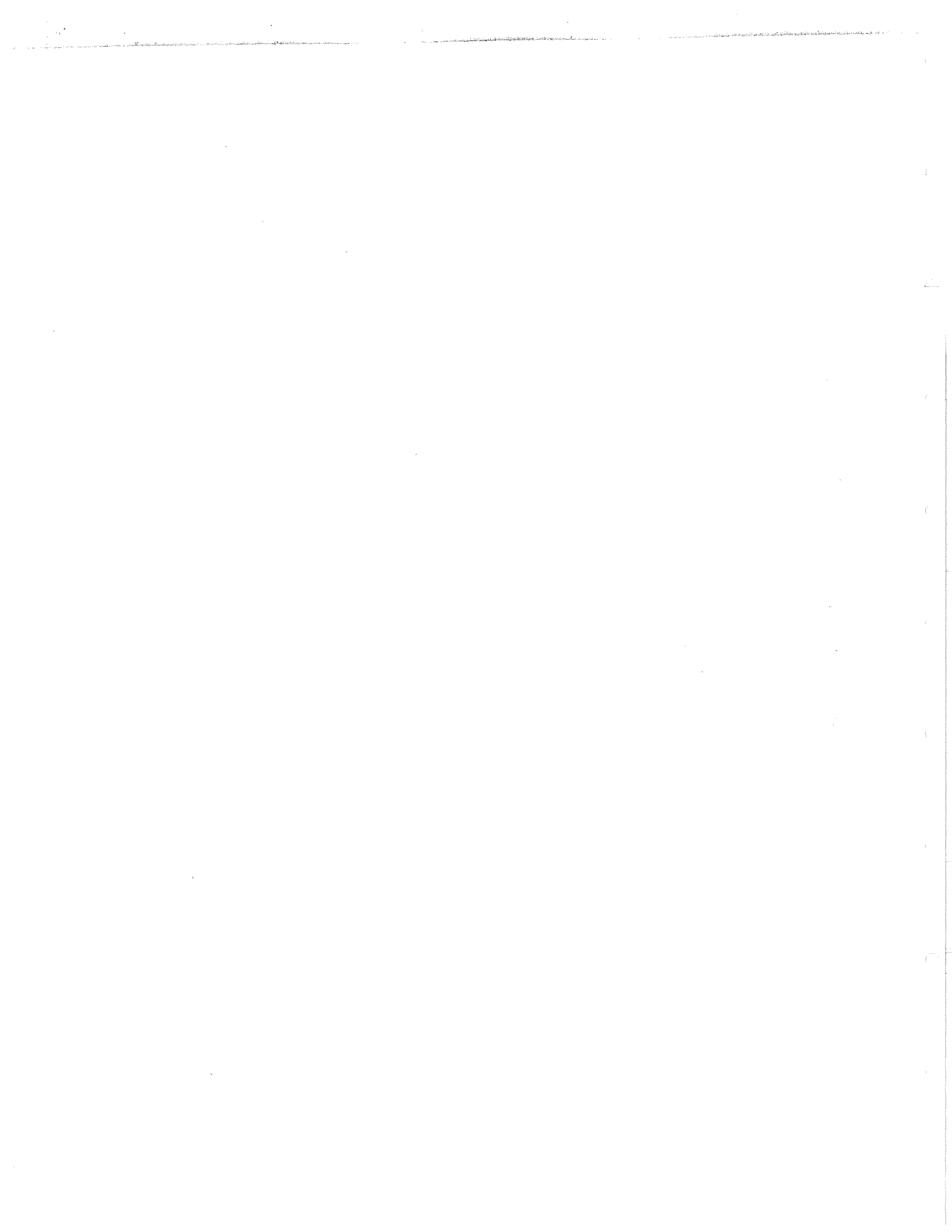


Figure 6



- Cataldi, R., Stefani, G., Tongiorgi, M., 1963, Geology of Larderello Region (Tuscany): contribution to the study of the geothermal basins: in Proc. of Spoleto meeting on Nuclear Geology of Geothermal Areas, C.N.R. Laboratorio di Geologia Nucleare-Pisa (E. Tongiorgi, ed.), p. 235-261.
- Chapman, R. H., 1975, Geophysical study of the Clear Lake Region, California: California Div. of Mines and Geol. Spec. Rept. 116, 23 p.
- Coleman, R. G., and Lanphere, M. A., 1971, Distribution and age of high-grade blueschists, associated eclogites, and amphibolites from Oregon and California: Geol. Soc. of Amer. Bull., v. 82, p. 2397-2412.
- Coleman, R. G., and Lee, D. E., 1963, Glaucophane-bearing metamorphic rocks of the Cazadero area, California: Jour. of Petrology, v. 4, p. 260-261.
- Crowell, J. C., 1974, Sedimentation along the San Andreas fault: in Modern and Ancient Geosynclinal Sedimentation, S.E.P.M. Special Public. No. 19, p. 292-303.
- Crowell, J. C., 1974, Origin of Late Cenozoic Basins in Southern California: in Tectonics and Sedimentation, S.E.P.M. Special Publ. No. 22, p. 190-203.
- Dickinson, W. R., 1970, Clastic sedimentary sequences deposited in shelf, slope, and trough settings between magmatic arcs and associated trenches: Pacific Geology, v. 3, p. 15-30.
- Donnelly, J. M., 1977, Geochronology of the Clear Lake volcanic field: Univ. California, Berkeley, PhD. thesis, 48 p.

- Donnelly, J. M., Hearn, B. C., Jr., and Goff, F. E., 1977, The Clear Lake Volcanics, California: Geology and Field Trip guide: in Field Trip guide to The Geysers-Clear Lake area for Cordill. Sect., Geol. Soc. of Amer., p. 25-56.
- Eaton, J. P., 1963, Crustal Structure from San Francisco, California, to Eureka, Nevada, from Seismic-Refraction Measurements: Jour. of Geophysical Res., v. 68, p. 5789-5806.
- Ernst, W. G., 1971, Do mineral parageneses reflect unusually high-pressure conditions of Franciscan metamorphism?: Amer. Jour. Sci., v. 270, p. 81-108.
- Ernst, W. G., 1970, Tectonic contact between the Franciscan melange and the Great Valley sequence-- crustal expression of a Late Mesozoic Benioff zone: Jour. Geophys. Research, v. 75, p. 886-902.
- Fehlberg, E. L., 1975, Shell's Activity in The Geysers Area: Proc. of workshop on geothermal Reservoir engineering, Rpt. 5GP-TR-20, Stanford Univ., Dec. 15-17, 7 p.
- Goff, F. E., Donnelly, J. M., Thompson, J. M., and Hearn, B. C., Jr., 1977, Geothermal prospecting in The Geysers-Clear Lake area, northern California: Geology, vol. 5, no. 8, p. 509-515.
- Goff, F. E., and McLaughlin, R. J., 1976, Geology of the Cobb Mountain-Ford flat geothermal area, Lake County, California: U.S. Geol. Survey open file map 76-221.

- Hamilton, W., 1969, Mesozoic California and the underflow of Pacific mantle: Geol. Soc. Amer. Bull., v. 80, no. 12, p. 2909-2429.
- Hearn, B. C., Jr., Donnelly, J. M., and Goff, F. E., 1976a, Preliminary geologic map and cross-section of The Clear Lake volcanic field, Lake County, California: U.S. Geol. Survey open file map 76-751.
- Hearn, B. C., Jr., Donnelly, J. M., and Goff, F. E., 1976b, Geology and geochronology of the Clear Lake volcanics, California: in Proc. of 2nd United Nations Sym. on Dev. and Use of Geothermal Res., May 20-29, San Francisco, vol. I, p. 423-428.
- Hearn, B. C., Jr., Donnelly, J. M., and Goff, F. E., 1975, Preliminary geologic map of the Clear Lake volcanic field, Lake County, California: U.S. Geol. Survey open-file map 75-391.
- Herd, D. G., in press, Neotectonic framework of coastal California and its implications to microzonation of the San Francisco Bay Region, in Proc. of 2nd International Conference on Microzonation, San Francisco, 1978.
- Ingersoll, R. V., Rich, E. I., and Dickinson, W. R., 1977, Field Trip Guide to the Great Valley Sequence: 73rd Ann. Cordilleran Section Meeting, Geol. Soc. of Amer., April, 1977.
- Isherwood, W. F., 1976, Gravity and magnetic studies of The Geysers-Clear Lake geothermal region, California: in Proc.

of 2nd United Nations Sym. on Dev. and Use of Geothermal
Resources, vol. II, p. 1065-1073.

Iyer, H. M., and Hitchcock, T., 1975, Teleseismic residuals of
The Geysers geothermal area: E.O.S. Transactions of the
Amer. Geophysical Union, vol. 56, no. 12, p. 1020.

- Jones, D. L., Blake, M. C., Jr., Bailey, E. H., and McLaughlin, R. J., 1978, Distribution and Character of upper Mesozoic subduction complexes along the west coast of North America: Proc. 25th Internat. Geological Congress, Sydney, Australia, in Tectonophysics, v. 47, p. 207-222 (in press).
- Jones, D. L., Silberling, N. J., and Hillhouse, J., 1978, Wrangellia--a displaced continental block in northwestern North America: Canadian Jour. of Earth Science (in press).
- Lanphere, M. A., Blake, M. C., Jr., and Irwin, W. P., 1975, Early Cretaceous Metamorphic age of the South Fork mountain schist in the northern Coast Ranges of California: Abst., 71 Ann. Cordilleran Sect. meeting, Geol. Soc. of Amer., California State Univ., Los Angeles, California, p. 340.
- Lipman, S. C., Strobel, C. J., and Gulati, M. S., 1977, Reservoir Performance of the Geysers field: in Proceedings of the Larderello workshop on geothermal Resource Assessment and Reservoir Engineering, sept. 12-16, 22 p.
- Mankinen, E. A., 1972, Paleomagnetism and Potassium-Argon Ages of the Sonoma Volcanics, California: Geol. Soc. of America Bull., v. 83, p. 2063-2072.
- McNitt, J. R., 1968, Geology of the Kelseyville quadrangle, Sonoma, Lake, and Mendocino Counties, California: California Div. of Mines and Geology Map Sheet 9.
- McNitt, J. R., 1963, Exploration and Development of geothermal power in California: California Div. of Mines and Geology, Spec. Rept. 75, 45 p.

- McLaughlin, R. J., 1978, Preliminary geologic map and structural sections of the central Mayacmas Mountains and The Geysers steam field, Sonoma, Lake, and Mendocino Counties, California: U.S. Geol. Survey Open file map 78-389, 2 sheets, 1 map 1:24,000, explanation, and structural sections.
- McLaughlin, R. J., 1977a, Late Mesozoic-Quaternary plate tectonics and The Geysers-Clear Lake geothermal anomaly, northern Coast Ranges, California: Geol. Soc. Amer., Abst. with Programs, vol. 9, no. 4, p. 464.
- McLaughlin, R. J., 1977b, The Franciscan assemblage and Great Valley sequence in The Geysers-Clear Lake region of northern California: in Field Trip guide to The Geysers-Clear Lake area for the Cordilleran Section of the Geol. Soc. of America, April 1977, p. 3-24.
- McLaughlin, R. J., 1976, Significance of age relationships above and below Upper Jurassic ophiolite: Abstract, 72nd Ann. Cordilleran Sect. meeting, Geol. Soc. of Amer., Abst. with Programs, p. 395.
- McLaughlin, R. J., 1975a, Structure of Franciscan Rocks in the central Mayacmas Mountains, Sonoma and Lake Counties, California: Abstract, Geol. Soc. of Amer. 71st Ann. Cordilleran Sect. meeting, p. 345-346.
- McLaughlin, R. J., 1975b, Preliminary compilation of in-progress geologic mapping in The Geysers geothermal area, California: U.S. Geol. Survey open file map 75-198, 2 sheets.

- McLaughlin, R. J., 1974, Preliminary geologic map of The Geysers steam field and vicinity, Sonoma County, California: U.S. Geol. Survey open-file map 74-238.
- McLaughlin, R. J., and Pessagno, E. A., Jr., (1978), Significance of age relations above and below upper Jurassic ophiolite in The Geysers-Clear Lake region, California: U.S. Geol. Survey Jour. of Res., vol. __, p. __.
- McLaughlin, R. J., and Stanley, W. D., 1976, Pre-Tertiary geology and structural control of geothermal resources, The Geysers steam field, California: in Proc. of the 2nd United Nations Sym. on Dev. and Use of Geoth. Res., 20-29 May, 1975, vol. I., p. 475-486.
- Morgan, W. J., 1972, Plate Motions and Deep Mantle Convection: Geol. Soc. of Amer. Mem. 132, 22 p.
- Ogle, B. A., 1953, Geology of Eel River Valley Area, Humboldt County, California: Calif. Div. of Mines and Geol. Bull. 164, 128 p.
- Platt, J. P., 1975, Metamorphic and deformational processes in the Franciscan Complex, California: Some insights from the Catalina Schist terrane: Geol. Soc. Amer. Bull., v. 86, p. 1337-1347.
- Seiders, V. M., Pessagno, E. A., Jr., and Harris, A. G., 1979(?), Fossiliferous pebbles in conglomerates in Franciscan and related rocks, California Coast Ranges: Geology, (in press).

- Seiders, V. M., and Pessagno, E. A., Jr., in press, Radiolarians and conodonts in the Franciscan assemblage and the Great Valley sequence of the California Coast Ranges: *Geology*, .14 p.
- Suppe, J., and Armstrong, R. L., 1972, Potassium-Argon dating of Franciscan metamorphic rocks: *Amer. Jour. Sci.*, v. 272, p. 217:233.
- Swe, W., and Dickinson, W. R., 1970, Sedimentation and thrusting of late Mesozoic rocks in the Coast Ranges near Clear Lake, California: *Geol. Soc. of Amer. Bull.*, vol. 81, no. 1, p. 165-189.
- White, D. E., Muffler, L. J. P., and Truesdell, A. H., 1971, Vapor-dominated hydrothermal systems compared with hot water systems: *Economic Geology*, vol. 66, p. 75-97.
- Yates, R. G., and Hilpert, L. S., 1946, Quicksilver deposits of the eastern Mayacmas District, Lake and Napa Counties, California: *California Jour. of Mines and Geology*, vol. 42, no. 3, p. 231-286.

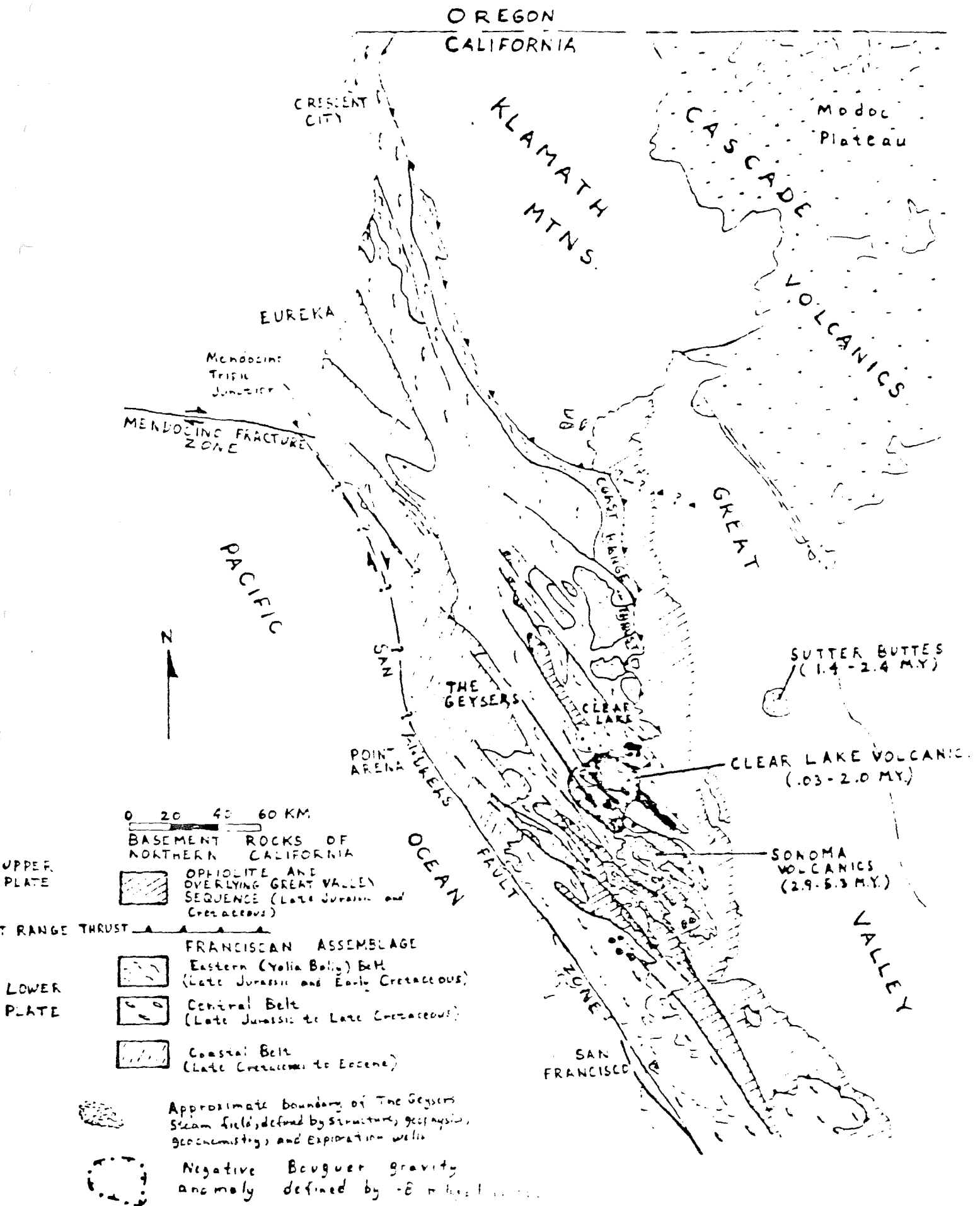
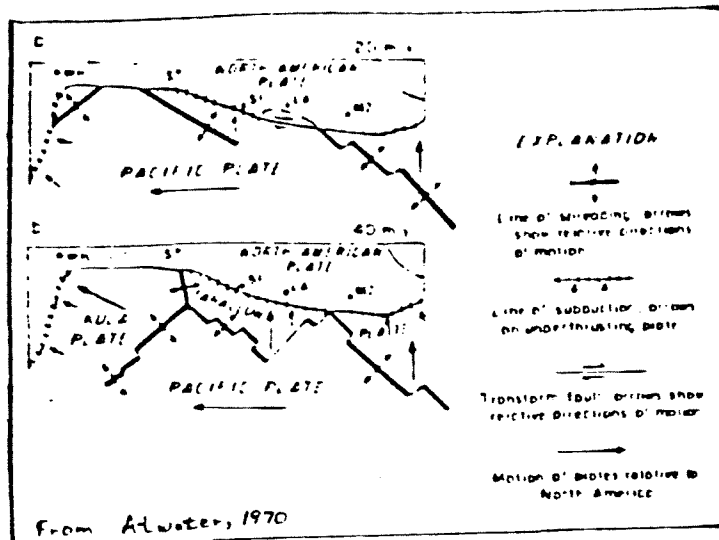
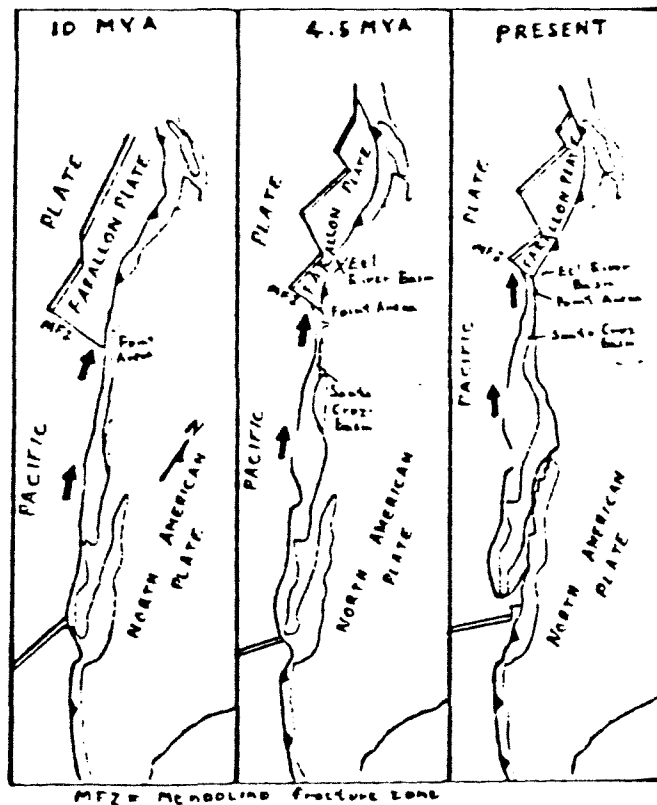


Figure 1. Generalized map of northern California, showing the northern Coast Ranges and the Geysers Steam field

the northern Coast Ranges and the Geysers Steam field



A.



from Blake and others, 1978

B.

Figure 2. Plate tectonic reconstruction for the North American plate margin from 40 million years ago to present, using the reconstructions of Atwater from 40 to 20 my.a. (A.), and those of Blake and others from 10 mya. to present (B.).

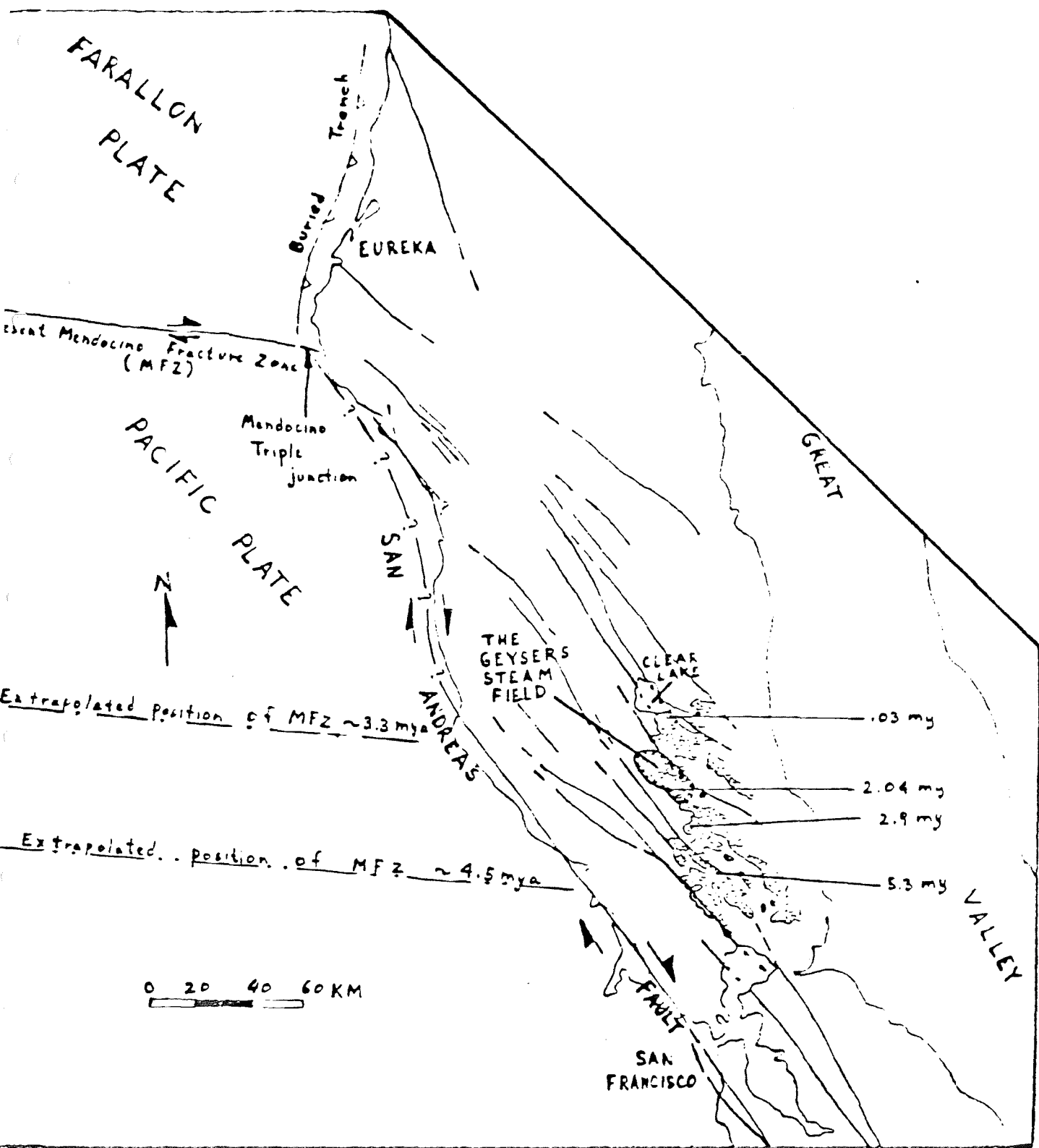
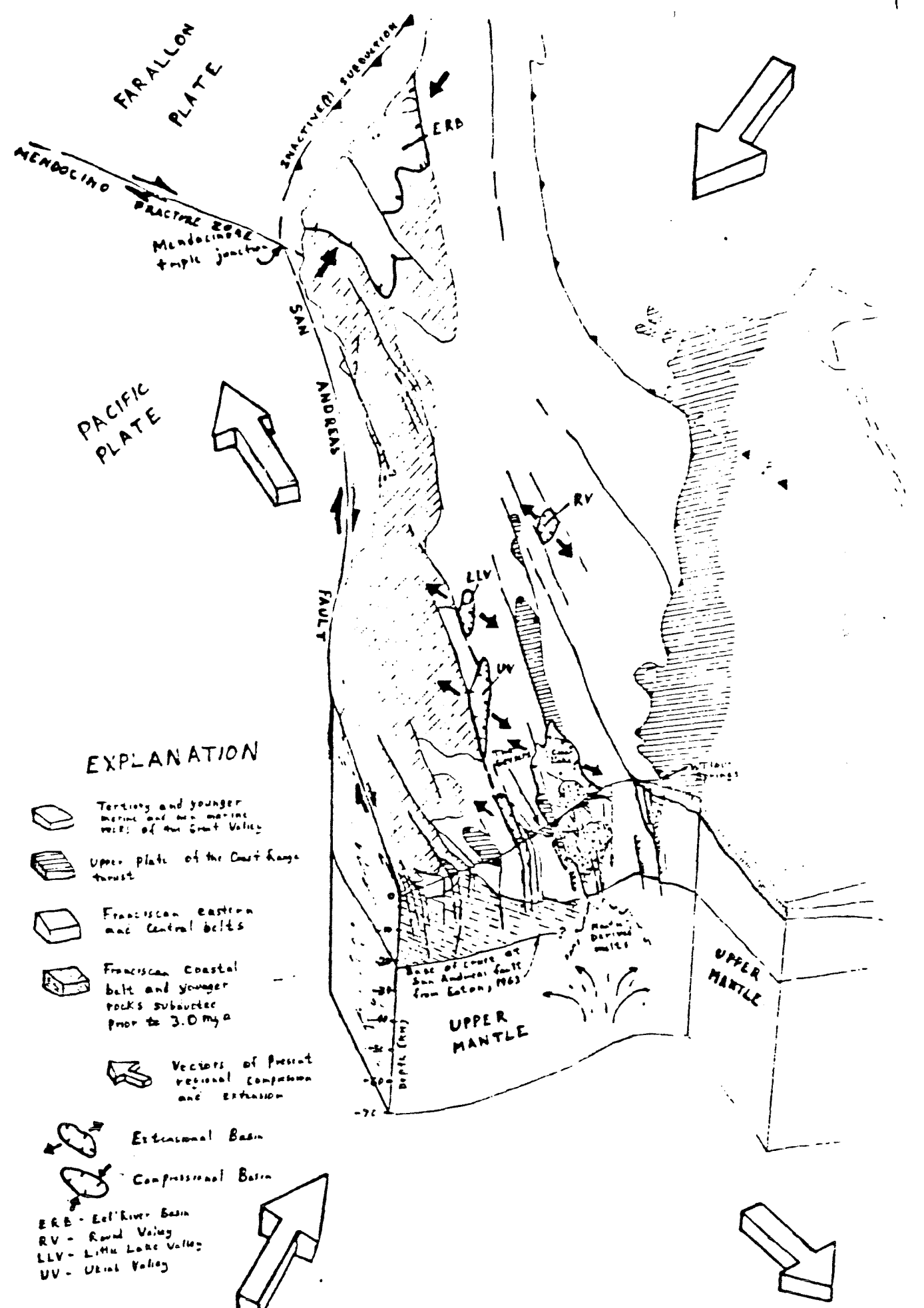
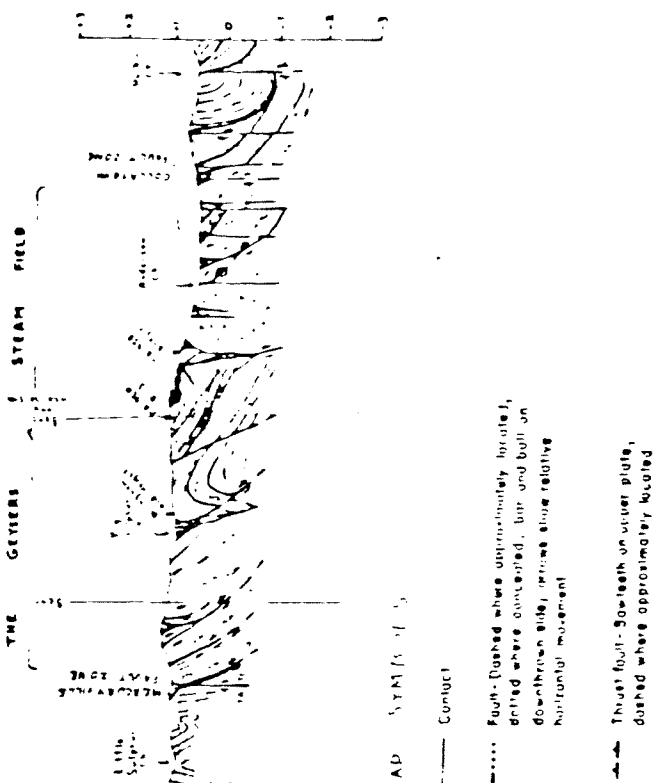
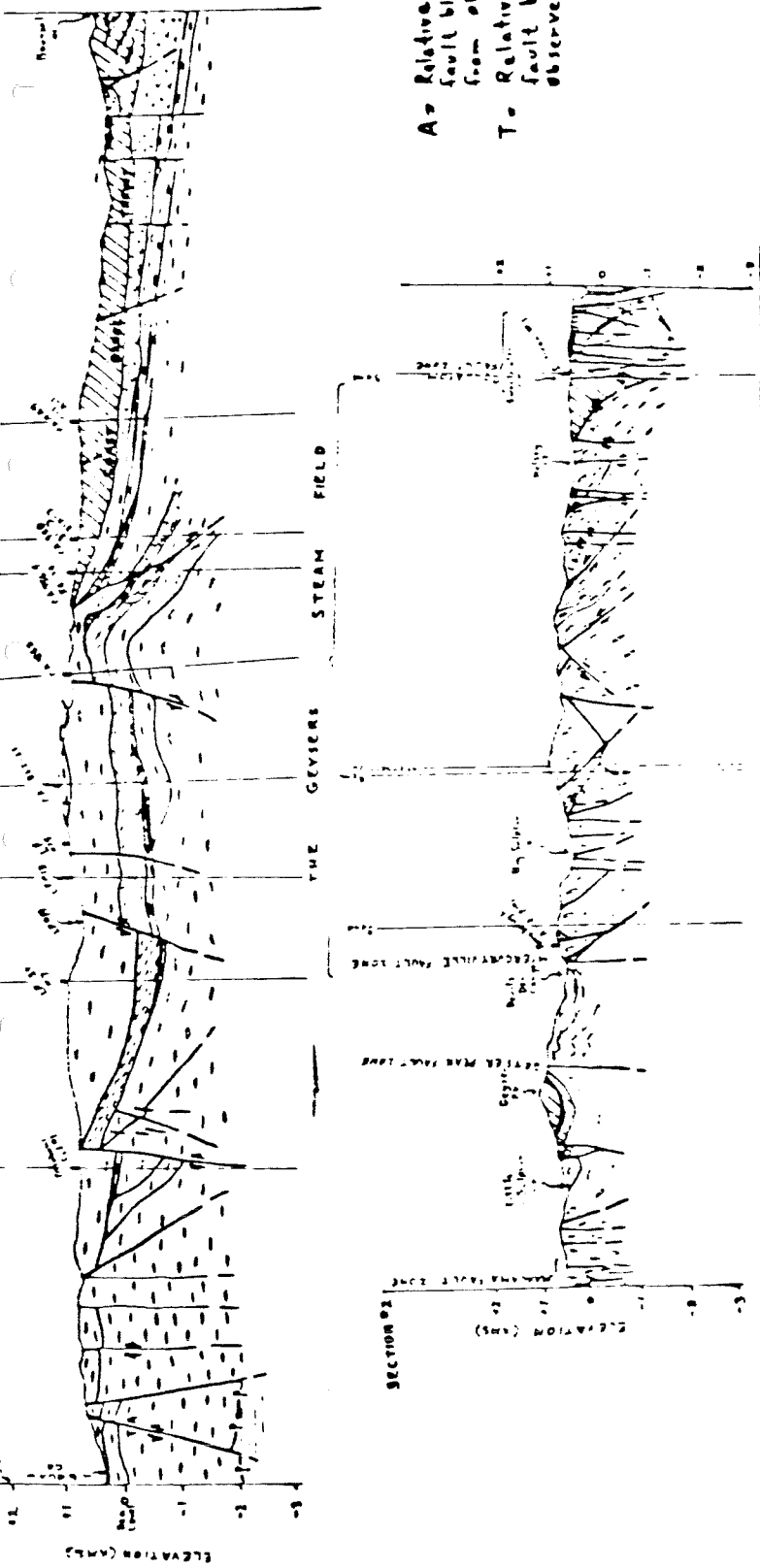


Figure 3. Map of northern California showing northward progression of Tertiary and Quaternary volcanism with time, major northwest-trending faults of the San Andreas fault system, and extrapolated positions of the Mendocino fracture zone between 3 and 5 million years ago. Ages of volcanic rocks in millions of years are from Dennelly, 1977, and Mankinen, 19



EXPLANATION

- Tertiary and younger marine and non-marine rocks of the Great Valley
- Upper plate of the Coast Range thrust
- Franciscan eastern and central belts
- Franciscan Coastal belt and younger rocks subducted prior to 3.0 mya
- Vectors of present regional compression and extension
- Extensional Basin
- Compressional Basin
- ERB - Eel River Basin
- RV - Rural Valley
- LLV - Little Lake Valley
- UV - Ukiah Valley



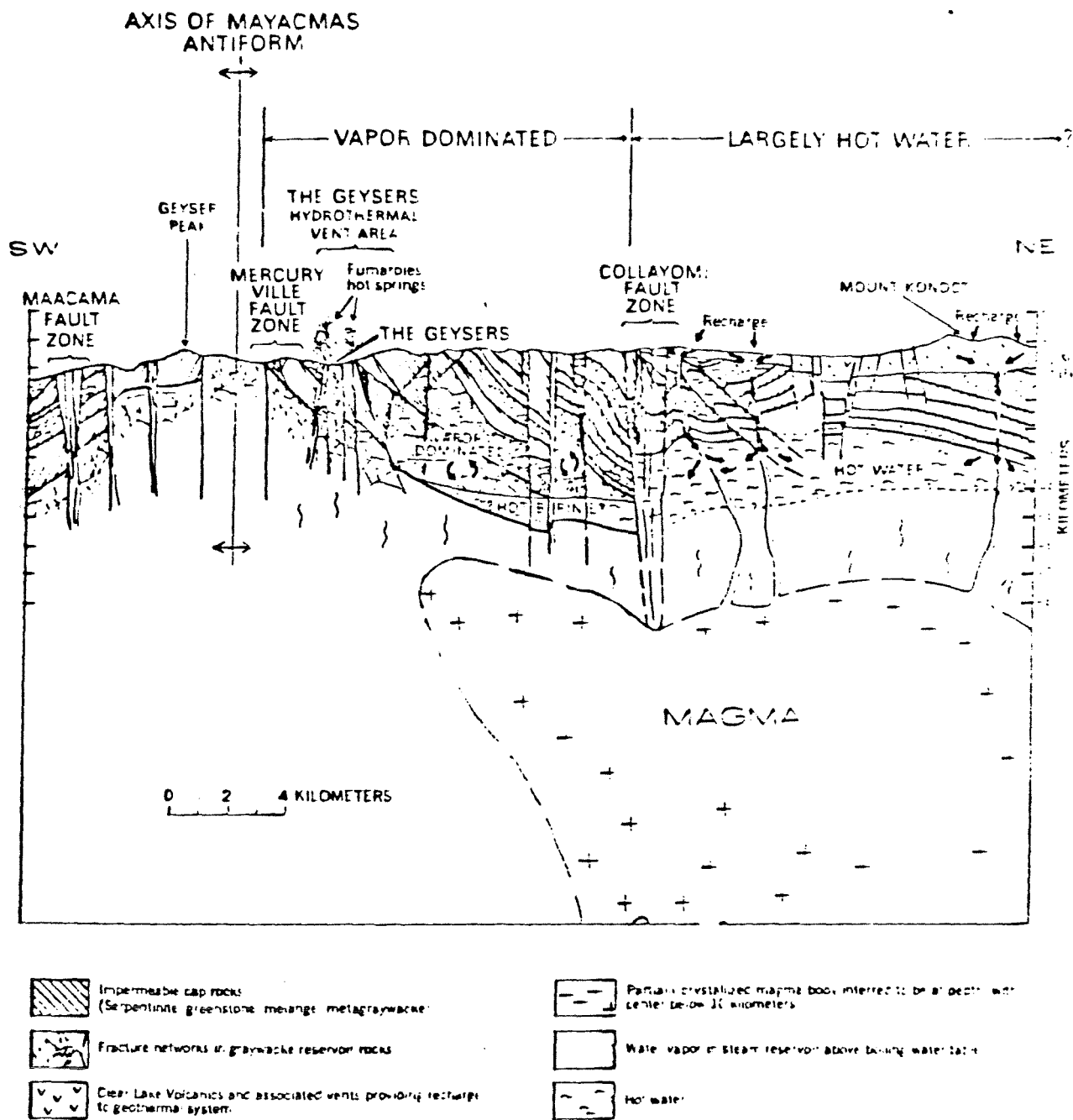
- EXPLANATION**
- Clear Lake Volcanics (Late Tertiary and Quaternary)
 - Sonoma Volcanics and associated alluvial deposits (Pliocene)
 - Fluvial and lacustrine deposits (Late Tertiary)
 - Great Valley Sequence (Late Jurassic and Cretaceous)
 - Ophiolite (Late Jurassic)
Composed of serpentinites, gabbro, diabase, basalt flows, mafic breccia, and minor chert
 - Franciscan Assemblage (Late Jurassic and Cretaceous)
Structural Unit 3 (Probably equivalent to Valle Berry belt - mostly) siliceous metasediments with minor metachert and metagranite
 - Structural Unit 2 (metamorphosed and broken formation of sandstone, shale, greenstone, chert, bluish amphibolite, eclogite) and minor hornblende sandstone
 - Structural Unit 1, sandstone and shale
 - Actinolite serpentinite

MAP SCALE 1:50,000

Contact

— — — — — Fault - Dashed where approximately located, solid where contoured, but und bolt on downthrown side, unless along relative horizontal movement

— — — — — Thrust fault - Solid on upper plate, dashed where approximately located



6
 Figure 8. Structural model for The Geysers geothermal system. Cross-section through The Geysers-Clear Lake region, from the Maacama fault zone on the southwest, to Mount Konocti on the northeast, depicting structural elements of The Geysers-Clear Lake geothermal system. Modified after McLaughlin, 1972b



Figure 7A. Map showing pattern of faulting over The Geysers steam reservoir. Areas of prominent hydrothermal alteration are designated by stippie pattern; Black arrows illustrate dip and sense of faulting along the Maccama and Collayomi fault zones. Large hollow arrows illustrate approximate orientation of vectors of regional extension, suggested by Bate and others, this publication; Heavy line indicates approximate boundary of the steam reservoir.

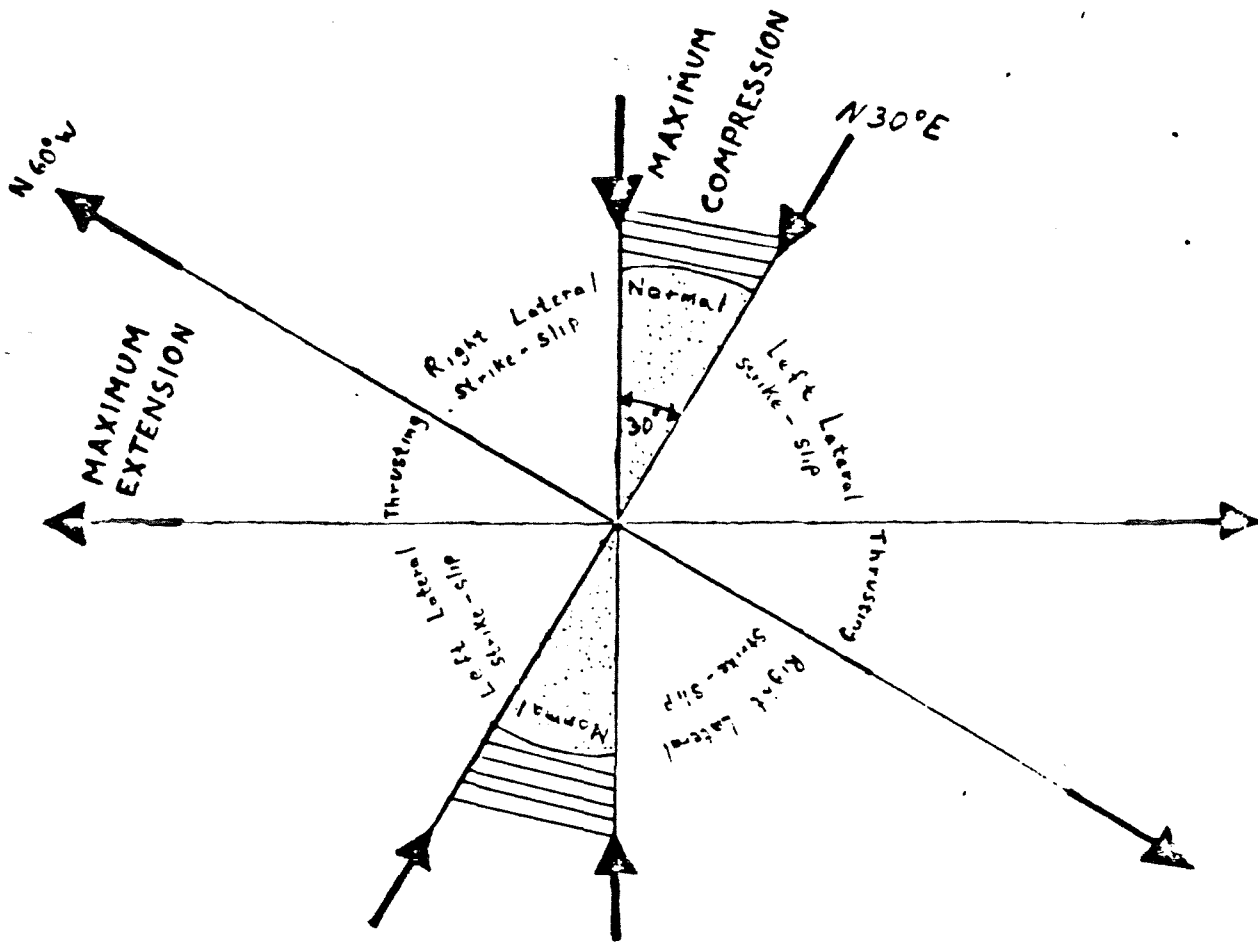


Figure 7B. Diagram of principal horizontal vectors of the stress field for the Geysers area suggested by Bufe and others, this publication, and predicted displacements for vertical faults of various orientations. Stippled sectors delineate the orientation range of faults and fractures producing optimum extension, that are significant to permeability of the steam reservoir.

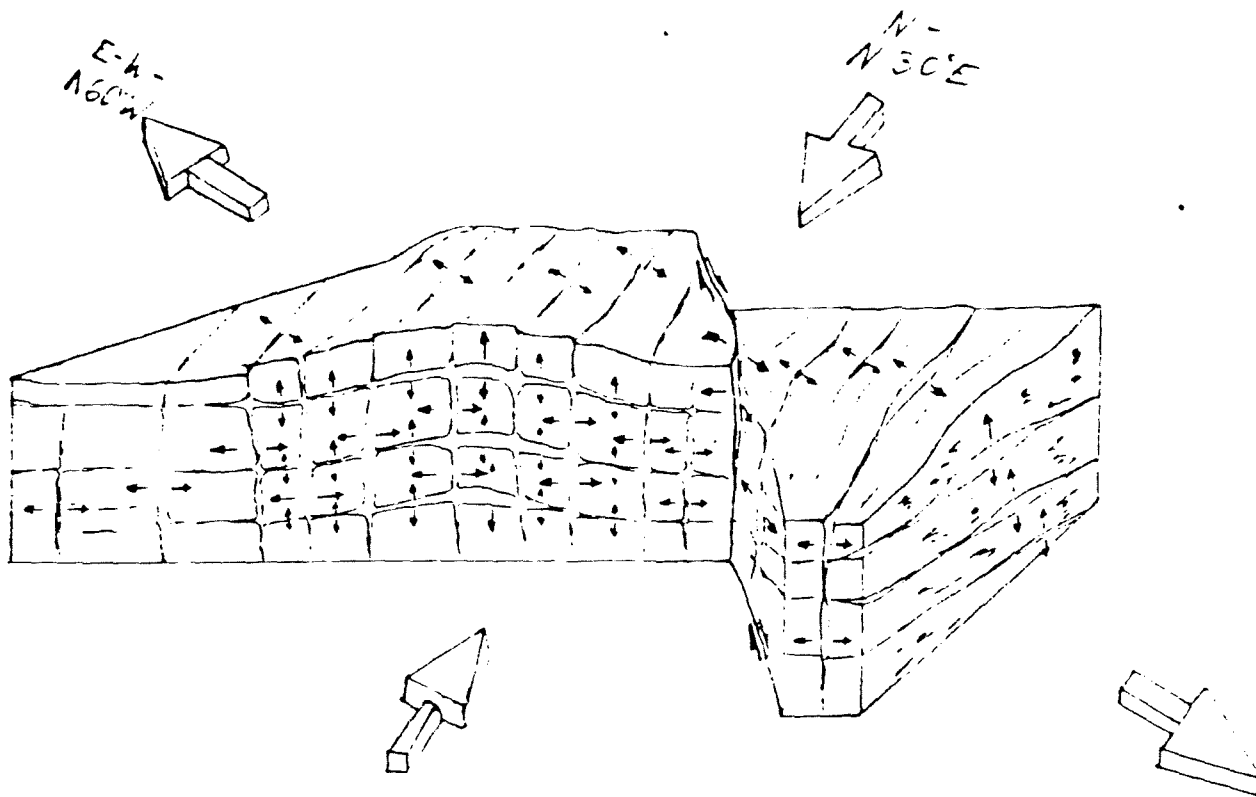


Fig. 8. Block diagram illustrating relationship of open fault and fracture networks to the flexure system relative to the principal vectors of regional horizontal compression and extension. Significant horizontal extension may occur along northeast-trending vertical faults and fractures, and locally along horizontal warps in strike-slip faults. Vertical extension may be associated with subhorizontal faults, fractures, or bedding planes where deformed into anticlinal warps or horst-like structures.

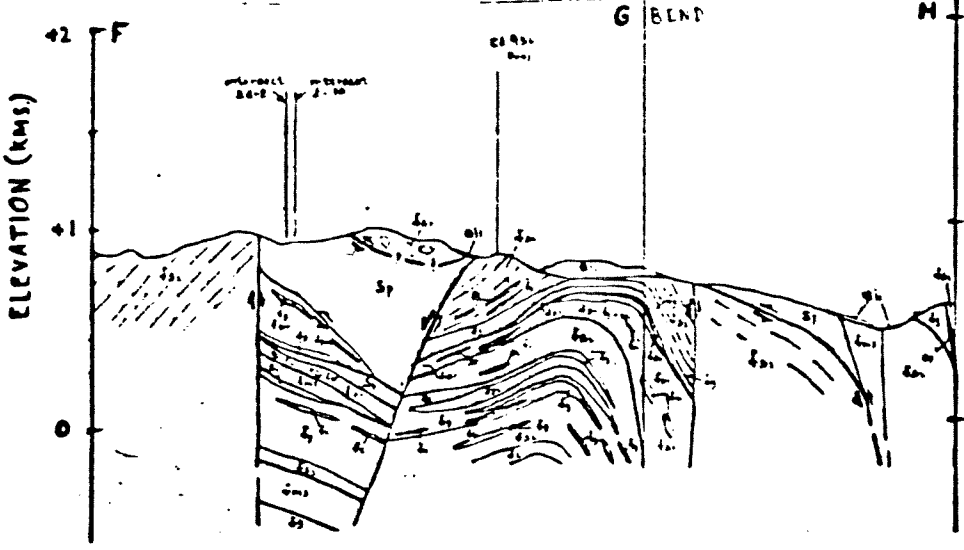
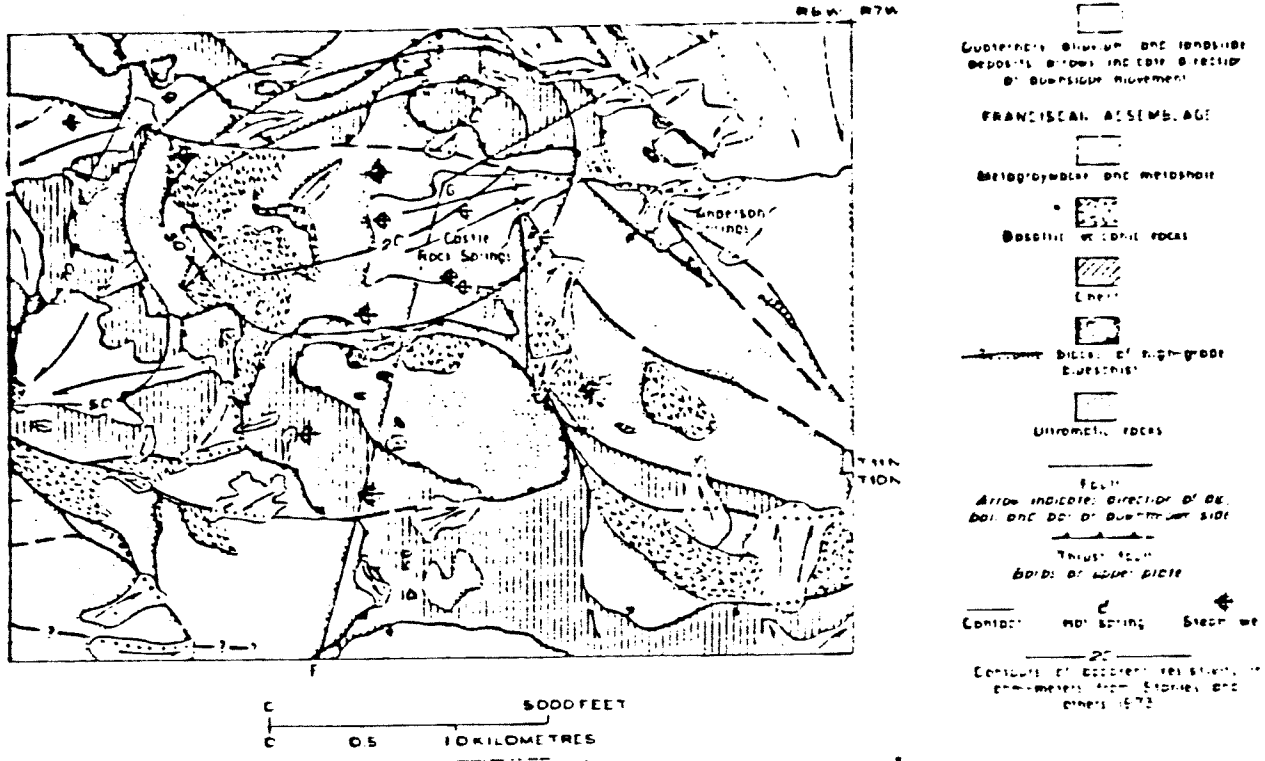
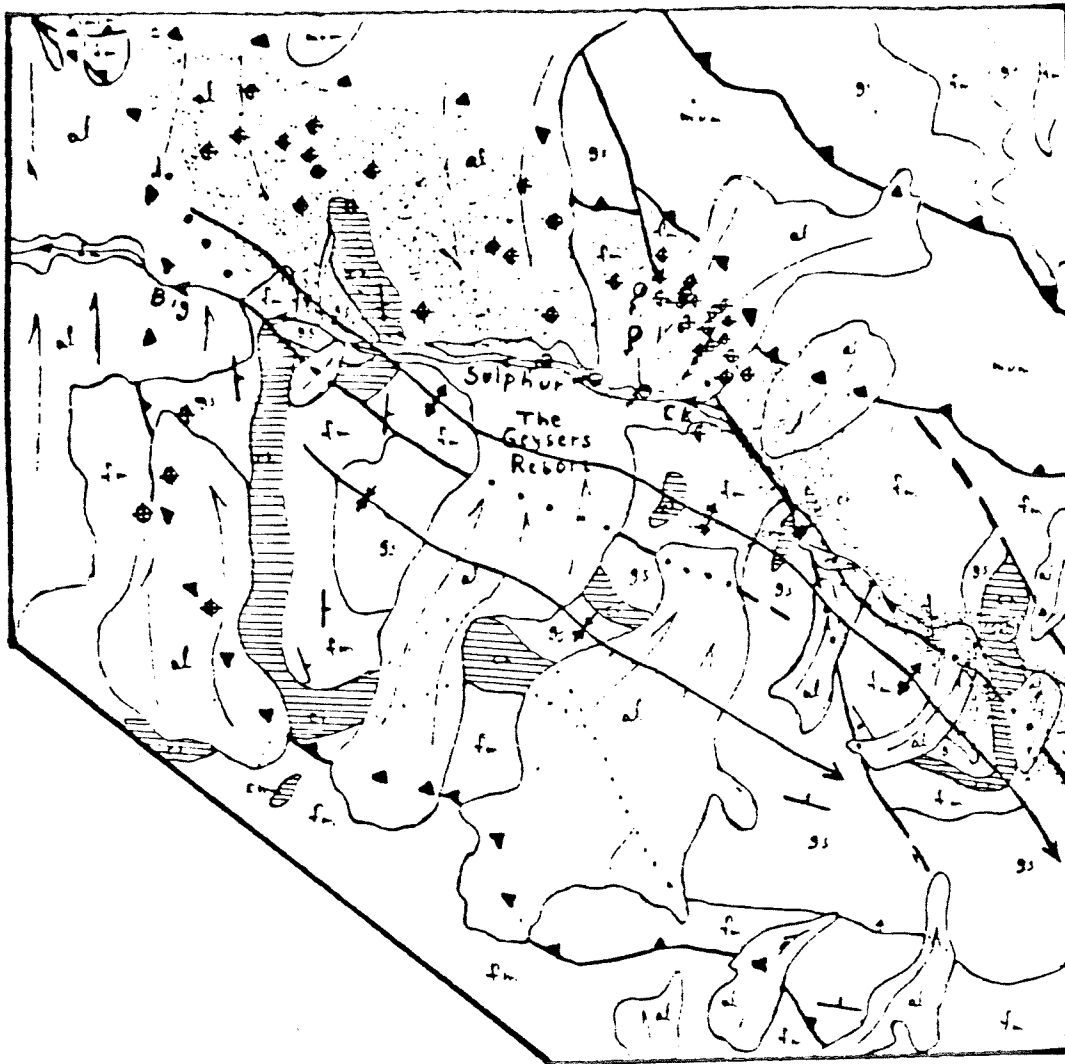


Figure 9 Complex structural high associated with the Castle Rock Springs area of The Geysers steam field, modified after McLaughlin and Stanley, 1976



EXPLANATION

al Alluvial deposits including talus

FRANCISCAN ASSEMBLAGE

- fm melange, undivided
- gs greenstone
- ch chert
- mun ophiolitic serpentinite

SYMBOLS

- hydrothermal alteration
- steam well
- hot spring or fumarolic area

Thrust fault

low-angle fault belt or disjunctive fault

Plunging anticline Plunging syncline

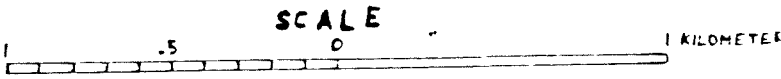
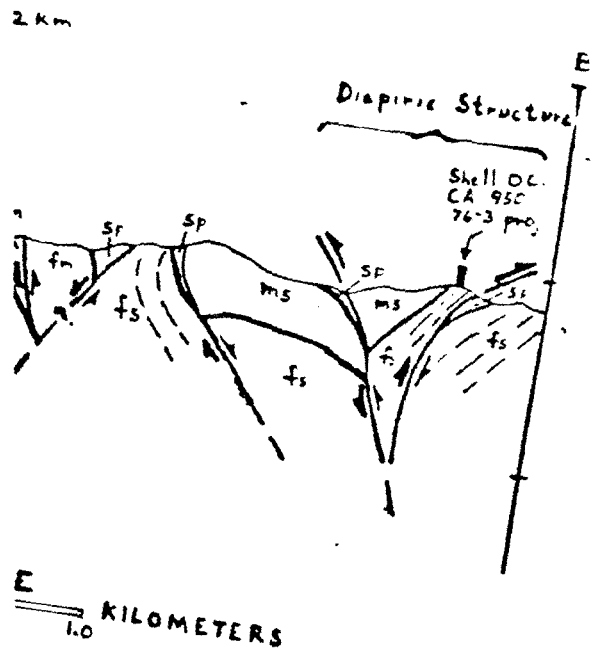
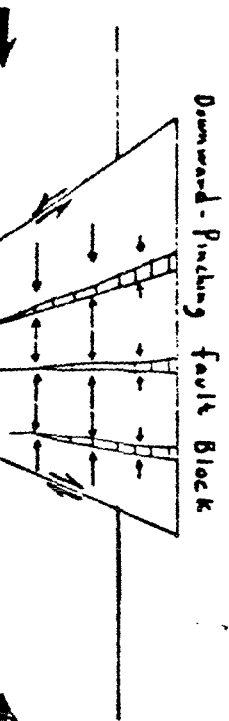
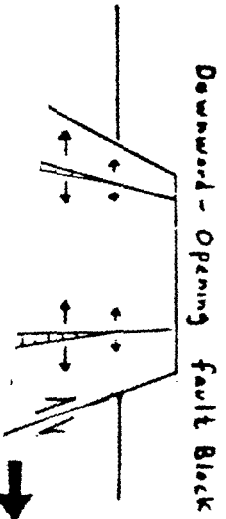


Figure 10. Geology of The Geysers Resort area, illustrating folds in Franciscan chert, and extensive hydrothermal activity along Big Sulphur Creek. Leakage from the steam reservoir is localized in melange beneath an overthrust cap of serpentinite



a diapiric structure
exists in The Geysers

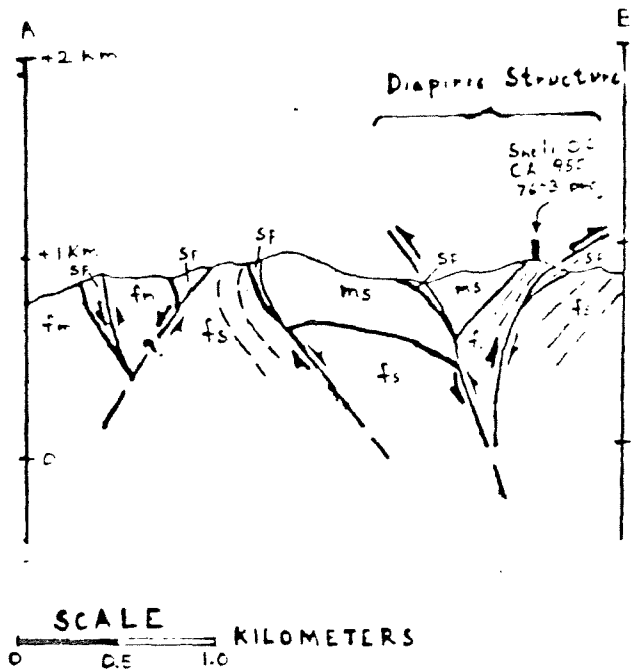
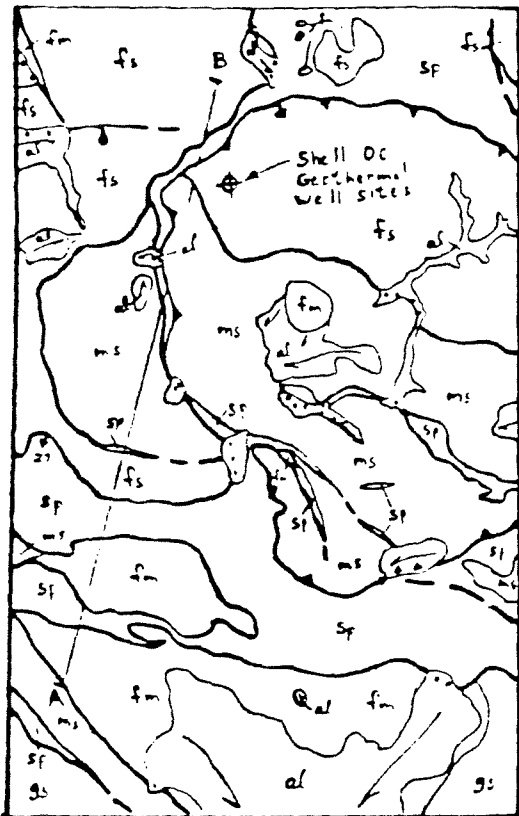


Figure 12. Geologic map and cross section of a diapiric structure associated with unproductive exploratory wells in The Geysers Steam field

SIGNIFICANCE OF AGE RELATIONS ABOVE AND BELOW UPPER JURASSIC OPHIOLITE IN THE GEYSERS-CLEAR LAKE REGION, CALIFORNIA

By R. J. McLAUGHLIN and E. A. PESSAGNO, Jr.,¹
Menlo Park, Calif., Dallas, Tex.

Abstract.—In The Geysers-Clear Lake area of northern California, a fragmented Upper Jurassic ophiolite overlain depositionally by the Great Valley sequence is juxtaposed over deformed and metamorphosed rocks of the Franciscan assemblage along the Coast Range thrust. The basal strata of the Great Valley sequence consist of thick breccias of mafic clasts, identical in composition to the upper part of the ophiolite. These breccias and their contact relations suggest that more than 1 km of the upper part of the ophiolite was locally eroded in early Tithonian time. On the basis of their radiolarian faunas, cherts in the Franciscan assemblage below the ophiolite range in age from Late Jurassic (early Tithonian) to Late Cretaceous (early Cenomanian). Of particular significance is an individual chert body (= The Geysers chert) of this age range. The early Cenomanian radiolarians, except for two occurrences associated with pelagic limestone, are significantly younger than those previously reported from the Franciscan assemblage. The existence of a sequence of Late Jurassic to Late Cretaceous radiolarian chert places critical constraints on subduction models for emplacement of the Franciscan assemblage beneath the Coast Range ophiolite and Great Valley sequence in The Geysers-Clear Lake area. From early Tithonian to post-early Cenomanian time, the Franciscan assemblage received pelagic sedimentation far from any site of subduction. By other data, blueschist metamorphism of subducted Franciscan strata also occurred during this time. The radiolarian data from The Geysers area permit a correlation with Upper Cretaceous pelagic limestones in the Laytonville area northwest of The Geysers and also imply that the Great Valley sequence was never depositionally in contact with the Franciscan assemblage.

A laboratory technique developed by Pessagno and Newport (1972) has made it possible to rapidly extract radiolarian assemblages from cherty pelagic sedimentary rocks for paleontologic dating. This extraction technique has been particularly useful in dating pelagic sediments above ophiolite sequences. In this report, we present new biostratigraphic data, based largely on radiolarian cherts dated by Pessagno, bear-

ing on the age of some Franciscan rocks and the Great Valley sequence of the northern California Coast Ranges. These data clarify the relation of Franciscan rocks to the overlying Upper Jurassic ophiolite at the base of the Great Valley sequence and have critical implications for plate tectonic models.

Acknowledgments.—Numerous scientists of the U.S. Geological Survey have provided support to this project. We should like to acknowledge D. L. Jones for collaboration of paleontologic data and molluscan fossil identifications; W. V. Sliter for his work on Late Cretaceous foraminifers; J. M. Donnelly and F. E. Goff for their collaboration of geologic mapping in the vicinity of Harbin Springs; H. N. Ohlin for his help in drafting, extraction of radiolarians from cherts, and assistance in the field; and D. H. Sorg for assistance in field mapping. W. R. Evitt of Stanford University, is gratefully acknowledged for his pollen study of several carbonate concretions. The work was in part supported by grants to E. A. Pessagno from the National Science Foundation (GA-35094 and DES-72-01528-A01). Finally, we thank C. A. Hopson, of the University of California at Santa Barbara, for his helpful insights into the ophiolite sequences at Harbin Springs and Geyser Peak.

REGIONAL RELATIONS

The Franciscan assemblage (Bailey and others, 1964), designated the "Franciscan Complex by Berkeley and others (1972), is composed of highly deformed and, in places, chaotically mixed sedimentary and igneous rocks. Present plate tectonic models imply that these rocks were deposited west of or over an east-dipping subduction zone along the western American continental margin in late Mesozoic time. Some workers (Bailey and others, 1964; Dickinson,

¹ University of Texas at Dallas.

1970) interpret the Great Valley sequence to have been deposited in an arc-trench gap, located to the east and upslope from the Franciscan trench. However, others (Blake and Jones, 1974) suggest that the trench was separated by an island arc from the basin in which sediments of the Great Valley sequence were deposited. Evidence for the existence of this hypothetical island arc has been controversial.

The complex depositional framework of the Franciscan assemblage is poorly understood. Most Franciscan strata are graywacke turbidites representing marine deposition on channelized parts of deep-sea fans or in associated submarine canyons. Pelagic limestones and cherts are present in small, but significant, amounts. These pelagic sedimentary rocks were deposited as siliceous and calcareous ooze on the tops and flanks of submarine volcanic highs or on distal abyssal plains in oceanic areas far from the influence of terrigenous sediment. Basaltic volcanic rocks of oceanic affinity are associated with the pelagic and terrigenous sedimentary rocks.

During late Mesozoic and early Tertiary time, Franciscan strata were deformed and metamorphosed along an east-dipping subduction zone formed at the continental margin (Blake and others, 1967; Ernst, 1970; Blake and Jones, 1974). During this eastward underthrusting, the Franciscan strata were concurrently overridden by oceanic crust depositionally overlain by strata of the Great Valley sequence. The more deeply subducted Franciscan rocks were metamorphosed to blueschist mineral assemblages and locally to greenschist and amphibolite assemblages (Platt, 1975). Rocks subducted to shallower depths were metamorphosed to pumpellyite, prehnite-pumpellyite, and laumontite assemblages (Blake and others, 1974; Blake and Jones, 1974). At the present time, Franciscan rocks are separated from the less deformed Great Valley sequence by serpentinitized ultramafic and related mafic rocks of the late Mesozoic ophiolitic ocean crust upon which Great Valley strata were originally deposited. The underthrust lower contact between the ophiolite and Franciscan assemblage was named the "Coast Range thrust" by Bailey, Blake, and Jones (1970).

OPHIOLITE AND GREAT VALLEY SEQUENCE OF THE GEYSERS-CLEAR LAKE AREA

The regional distribution of the ophiolite that underlies the Great Valley sequence in the northern Coast Ranges is shown on figure 1. Its distribution within The Geysers-Clear Lake region, where it is highly deformed as the result of early Tertiary to late Quaternary folding, thrusting, and strike-slip faulting, is

shown in more detail on the geologic map (fig. 2) and on the cross sections (fig. 3) of the area. In parts of the area, this deformation has made recognition of the sole of the Coast Range thrust extremely difficult.

As a result of deformation of the ophiolite sheet in the upper plate of the Coast Range thrust, serpentinite crops out in numerous narrow, discontinuous linear belts entirely bounded by Franciscan rocks.

Most of these linear belts of serpentinite can either be traced into the ophiolite sheet or along shear zones that cut major masses of the ophiolite. These relations strongly suggest that most of the serpentinite bodies in this area were derived from the ophiolite sheet at the base of the Great Valley sequence by local down faulting of the ultramafic lower part of the ophiolite into underlying Franciscan rocks. Exceptions are a few serpentinite bodies having serpentine mineral assemblages of antigorite, talc, and actinolite that have higher temperature-pressure stability fields than the lizardite and chrysotile assemblages characterizing serpentinites in the ophiolite. Such higher temperature-pressure serpentinite mineral assemblages may characterize ultramafic rocks underthrust with the Franciscan assemblage beneath the Great Valley sequence. Dropping of the ophiolite into underlying Franciscan rocks possibly resulted from folding together with lateral and vertical adjustment of subducted Franciscan slabs beneath the overlying ophiolite during the Cenozoic (fig. 3). Subsequent removal of the upper part of the ophiolite would then result in the linear pattern of serpentinite shown on the geologic map of The Geysers area (fig. 2).

Thick sections of mafic igneous rocks overlie the serpentinitized ultramafic part of the Coast Range ophiolite at the following three localities in The Geysers area: Harbin Springs, Mount St. Helena, and Geyser Peak. At each locality, the ophiolite sections are overlain by strata of the Great Valley sequence (fig. 2). The chemistry and petrology of the ophiolite sections at Harbin Springs and Mount St. Helena were previously studied by Bezore (1969); the section at Geyser Peak has not previously been described in detail. The main ophiolite sections at all three localities are schematically summarized by figure 4; for comparison, a composite of these sections is shown with a standard section of modern oceanic crust, as suggested by Ludwig, Nafe, and Drake (1970), on figure 4B.

The ophiolites of Harbin Springs and Mount St. Helena are nearly equivalent, although some difference in thickness of gabbro units is evident (fig. 4A). The Geyser Peak section differs significantly from the others in that it contains only a thin unit of ultramafic rock, a small amount of unaltered gabbro, and a thick unit

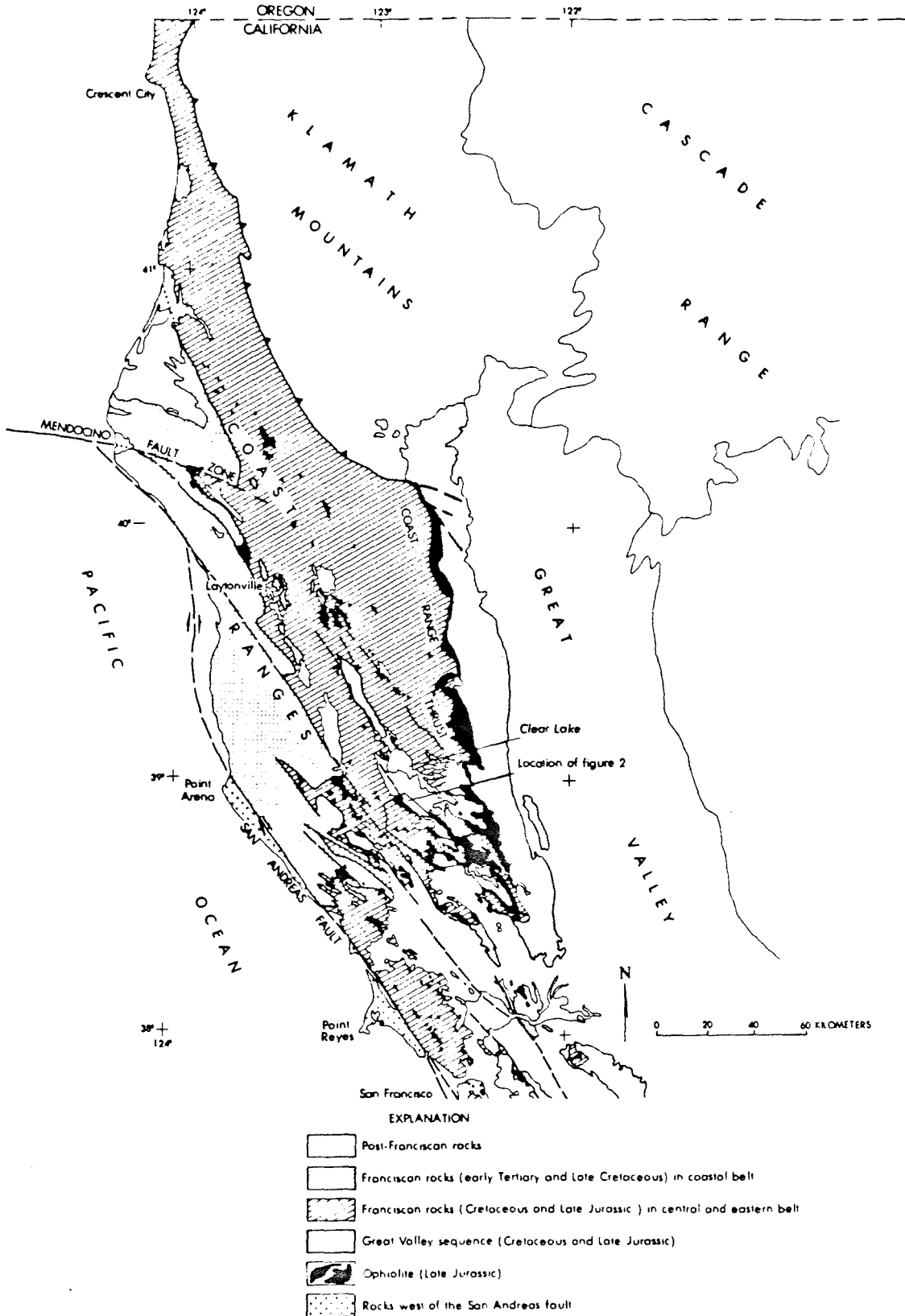


FIGURE 1.—Location of The Geyser–Clear Lake region in the northern California Coast Ranges, showing distribution of ophiolite at the base of the Great Valley sequence.

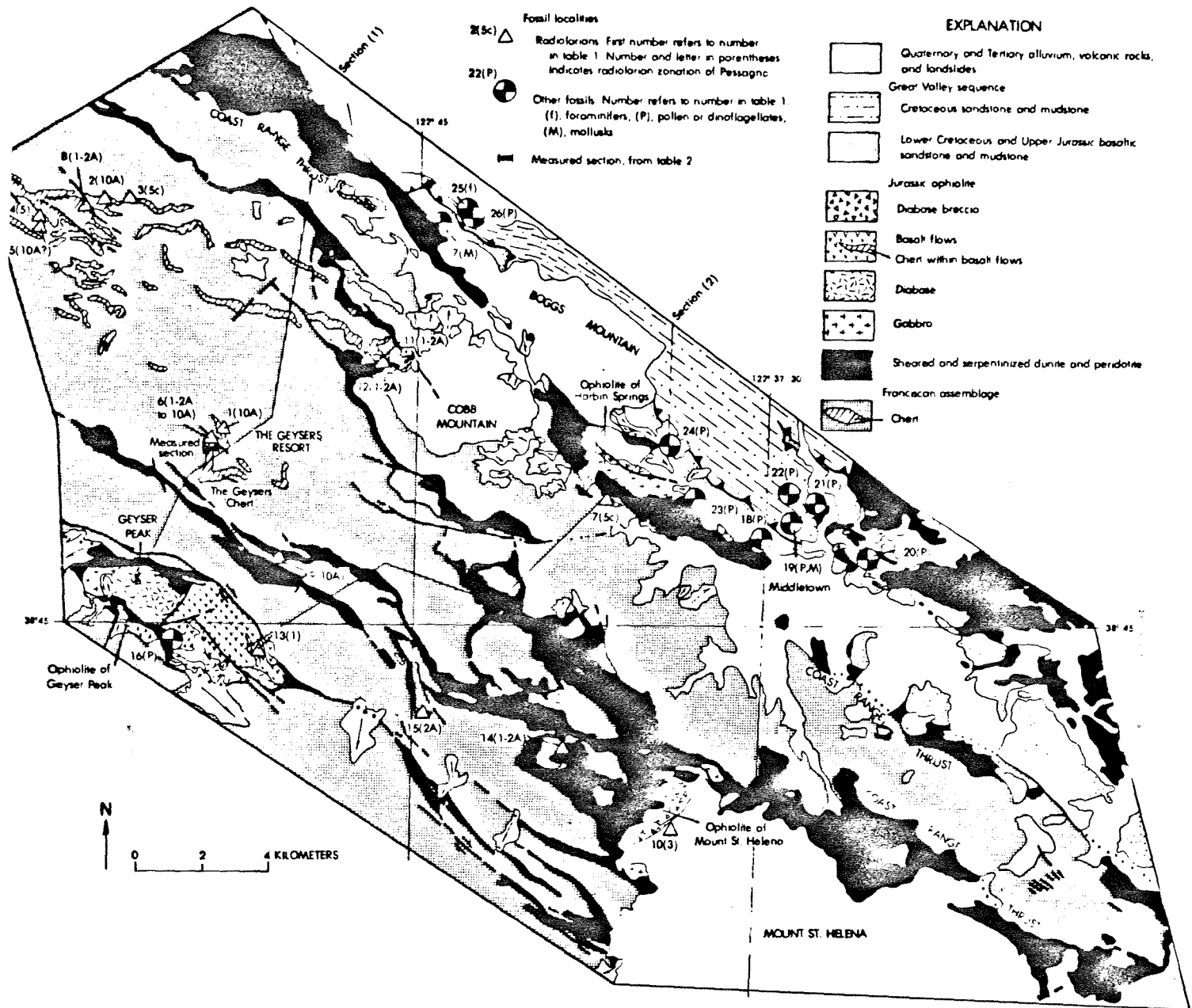


FIGURE 2.—Generalized geologic map of The Geysers area showing distribution of ophiolite and fossil localities.

of composite diabase sills overlain by basalt pillows and pillow breccia not present at the other two ophiolite localities.

Of particular significance is the presence at the top of the ophiolite at all three localities, and at a number of other localities in the Coast Ranges as far north as Paskenta, of a distinctive breccia composed largely of angular fragments of diabase, locally abundant glassy basalt, and, rarely, chert. The close association of the breccia locally with basaltic sandstone at the base of the Great Valley sequence, together with its persistence at the top of the ophiolite, resting locally upon dif-

ferent units, strongly suggests that this breccia is a sedimentary deposit (perhaps a talus accumulation) eroded from the top of the ophiolite. The comparative sections for Harbin Springs, Mount St. Helena, and Geyser Peak (fig. 4) suggest that at least the upper 1 km of ophiolite was eroded locally. Wagner (1975), in studying a similar breccia unit in the Pope Valley area about 20 km southeast of Middletown, came to similar conclusions as to its origin.

Differential erosion cannot account for all differences between the ophiolite section at Geyser Peak and those at Mount St. Helena and Harbin Springs. Cer-

RADIOIOLARIAN ZONATION FROM PESSAGNO (1977)

SERIES	STAGE	RADIOIOLARIAN ZONATION			
		Zone	Subzone	Number	
Upper Cretaceous	Maestrichtian	<i>Orbiculiforma renillaeformis</i>		16	
	Companian	<i>Patulibracchium dickinsoni</i>		15	
		<i>Crucella espartoensis</i>	<i>Phaseliforma carinata</i>	14C	
			<i>Patulibracchium lawsoni</i>	14B	
	<i>Protoxyphotractus perplexus</i>		14A		
	Santonian	<i>Alievium gallowayi</i>		13	
	Coniacian	<i>Alievium praegallowayi</i>	<i>Orbiculiforma vacaensis</i>	12B	
			<i>Archaeospongoprimum triplum</i>	12A	
	Turonian	<i>Alievium superbum</i>	<i>Archaeospongoprimum venadoensis</i>	11B	
			<i>Halesium sexangulum</i>	11A	
Cenomanian	<i>Rotaforma hessi</i>	<i>Quinquecapsularia spinosa</i>	10B		
		<i>Cassideus riedeli</i>	10A		
	<i>Archaeospongoprimum tehamaensis</i>		9		
Lower Cretaceous	Albian	U	<i>Petasiforma foremanae</i>	8	
		L	<i>Kozurium zingulai</i>	7	
	Aptian	U	<i>Parvicingula</i>		6
		L			
	Barremian Hauterivian		<i>Thanarla conica</i>		
	Valanginian	U	<i>Obesacapsula rotunda</i>	<i>Cecrops septemporatus</i>	5C
M		<i>Pseudoeucyrtis paskentaensis</i>		5B	
L		<i>Parvicingula jonesi</i>		5A	
Berriasian					
Upper Jurassic	Upper and Middle Tithonian	<i>Parvicingula altissima</i>		4	
	Lower Tithonian	<i>Trilonche ordinaria</i>		3	
		<i>Parvicingula hsui</i>			
	Lower Tithonian	<i>Emiluvia hopsoni</i>	<i>Mirifusus baileyi</i>	2B	
			<i>Mirifusus guadalupensis</i>	2A	
	Upper Kimmeridgian	<i>Parvicingula s.s.</i>		1	
<i>Emiluvia hopsoni</i>					
	<i>Eucyrtidium(?) pycnum</i>		0		
	<i>Parvicingula s.s.</i>				

FIGURE 2.—Continued

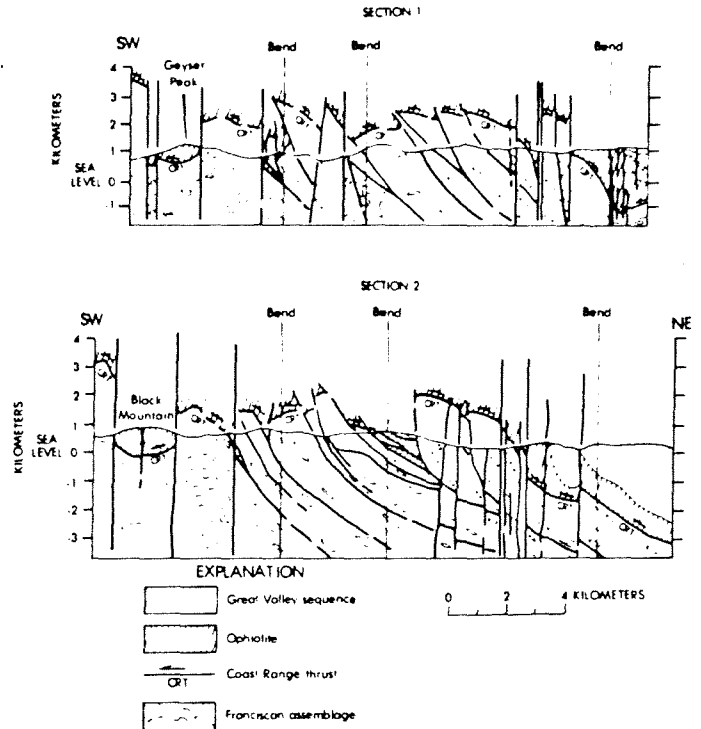


FIGURE 3.—Cross sections through The Geysers area, showing Cenozoic deformation of the Coast Range thrust of Bailey, Blake, and Jones (1970). Section lines are as indicated on fig. 2.

tainly much of the ultramafic section was cut out by faulting, and differences in thicknesses of gabbroic and basaltic rocks may be partly or wholly accounted for by faulting. Saleeby (1975) described an ophiolite in the western Sierra Nevada foothills of California that he interpreted to have been deformed by tectonic transport and progressive serpentinization. Serpentinization was thought to increase the mobility of the ultramafic lower part of the ophiolite, which then intruded and fragmented the overlying less mobile basaltic and gabbroic rocks, thereby distending the ophiolite section. A similar process may partly explain differences in composition and thickness of ophiolite sections in the northern Coast Ranges.

The Coast Range ophiolite has been dated in the northern Coast Ranges by potassium-argon methods (Lanphere, 1971) and to the south at Point Sal, Calif., by the uranium-lead method (Hopson and others, 1975). The potassium-argon dates on amphiboles associated with gabbro and peridotite and the uranium-lead dates on zircons in gabbroic parts of the ophiolite both indicate an age range of 150 to 160 million years.

Within the area of this study at Geyser Peak (fig. 2, loc. 11; table 1), a thin, discontinuous tuffaceous chert zone is present within basalt flows in the upper part of the ophiolite (fig. 4.4). Well-preserved radiolarians

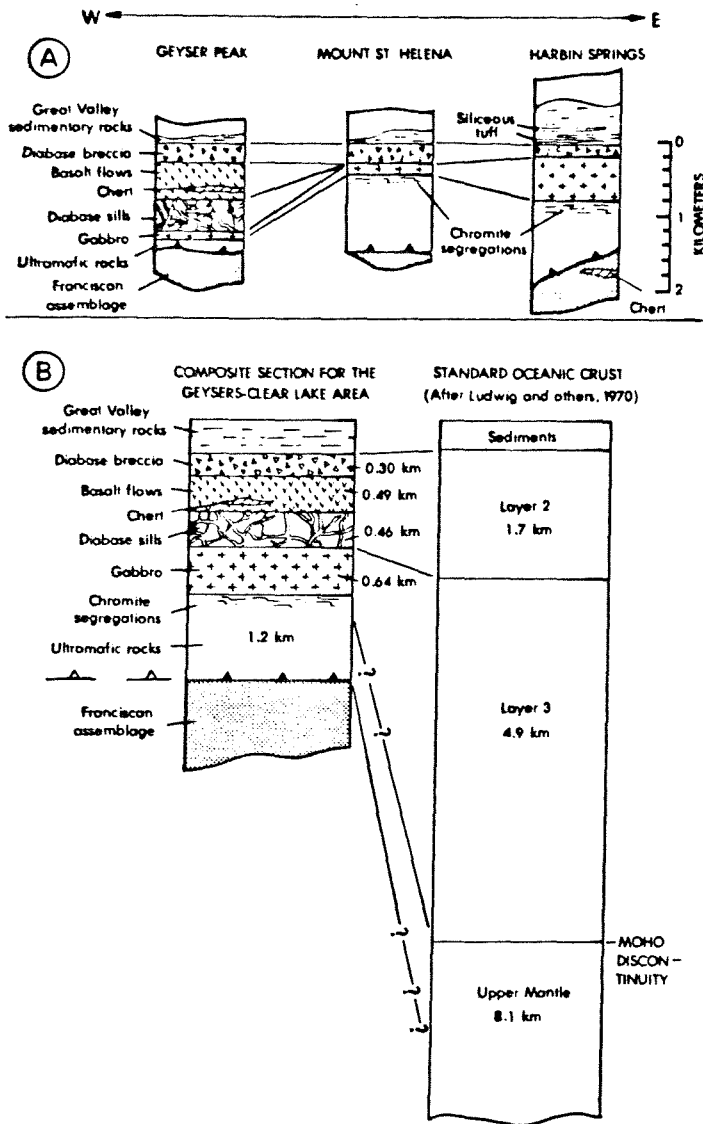


FIGURE 4.—Major ophiolite sections in The Geysers area compared with a standard section of oceanic crust. *A*, Ophiolite sections at Geyser Peak, Mount St. Helena, and Harbin Springs (localities shown on fig. 2). *B*, Composite of ophiolite sections on figure 4A compared with a standard section of oceanic crust. Modified from Ludwig, Nafe, and Drake (1970).

present in the thickest part of this chert are of late Kimmeridgian or early Tithonian age (Zone 1 of Pessagno, 1977). (The data of Van Hinte (1976, p. 493) and Pessagno (1977) indicate that the upper Kimmeridgian should now be included in the lower Tithonian. The Tithonian as defined in this fashion would be equivalent to the Russian Volgian.) There are no reliable absolute ages for the Kimmeridgian and Tithonian Stages of the Jurassic (see, for instance, Van Hinte, 1976; Van Eysinga, 1975). From the available data, we can say only that the middle and

upper parts of the Coast Range ophiolite (excluding structurally lower sheared ultramafic rocks) formed some time between 160 m.y. ago and early Tithonian time.

Strata of the Great Valley sequence depositionally above the ophiolite contain *Buchia piochii* (Swe and Dickinson, 1970; fig. 2, loc. 17, and table 2) and are, therefore, assignable, in part, to the middle and upper Tithonian (Zone 4 of Pessagno, 1977). At Mount St. Helena, radiolarians (fig. 2, loc. 10) in calcareous mudstone approximately 76 m stratigraphically above the diabase breccia are of early Tithonian age (Zone 3 of Pessagno, 1977). The age of the breccia at the top of the ophiolite must therefore be early Tithonian (Zones 1–3).

These age relations indicate that, briefly during the late Kimmeridgian or early Tithonian, pelagic sediments and volcanic tephra were deposited between extrusions of submarine basalt, perhaps along the crest of a submarine ridge, to form tuffaceous radiolarian chert. Somewhat later in early Tithonian time, the ophiolite underwent submarine erosion that locally removed as much as 1 km of the upper part of the section. The material now present as diabase and basalt breccia may represent talus or rubble accumulations around eroded submarine highs. The presence of this coarse ophiolite detritus at the base of the Great Valley sequence implies the existence of a major western source for Great Valley sediment during Late Jurassic time.

FRANCISCAN ROCKS STRUCTURALLY BELOW OPHIOLITE

Subducted Franciscan rocks structurally below the Great Valley sequence and Coast Range thrust in this area consist of a series of northeast- to southeast-dipping slabs of graywacke, basaltic volcanic rock, and chert separated by units of melange and (or) sheared serpentinite (McLaughlin and Stanley, 1976; McLaughlin, 1974, 1975). These rocks are largely unfossiliferous, except for abundant radiolarians in cherts. The age of the radiolarian assemblage occurring in the various chert bodies varies considerably (fig. 2, table 1). Most localities contain radiolarians assignable to the late Kimmeridgian or early Tithonian (subzone 1–2A). At some localities, including one where a prominent chert lens lies structurally below the ophiolite of Harbin Springs (loc. 7), the radiolarians are of Early Cretaceous (late Valanginian, subzone 5C) age. At several localities, Late Cretaceous (early Cenomanian, subzone 10A) radiolarian faunas are present. These early Cenomanian faunas were earlier considered to be Early Cretaceous (Hauterivian) by McLaughlin

TABLE 1.—List of Radiolaria localities

Map No. on figure 2	Formation	Location ¹	Age
1	Franciscan assemblage.	457.5 m E, 366 m S, NW cor. sec. 23 T. 11 N., R. 9 W.	Late Cretaceous (early Cenomanian, subzone 10A).
2	-- do --	793 m S, 762.5 m W, NE cor. sec. 28 T. 12 N., R. 9 W.	Do.
3	-- do --	732 m S, 152.5 m W, NE cor. sec. 28 T. 12 N., R. 9 W.	Early Cretaceous (late Valanginian, subzone 5C).
4	-- do --	533.8 m N, 152.5 m W, SE cor. sec. 30 T. 12 N., R. 9 W.	Early Cretaceous (Berriasian and Valanginian, zone 5).
5	-- do --	518.5 m N, 152.5 m W, SE cor. sec. 30 T. 12 N., R. 9 W.	Questionably Late Cretaceous (early Cenomanian, subzone 10A?).
6	-- do --	610 m S, 137.3 m E, NW cor. sec. 13 T. 11 n., R. 9 W.	Late Jurassic (late Kimmeridgian and early Tithonian, subzone 1-2A) to Late Cretaceous (early Cenomanian subzone 10A).
7	-- do --	274.5 m E, 213.5 m S, NW cor. sec. 30 T. 11 N., R. 9 W.	Early Cretaceous (late Valanginian, subzone 5C).
8	-- do --	579.5 m S, 152.5 m W, NE cor. sec. 29 T. 12 N., R. 9 W.	Late Jurassic (late Kimmeridgian and early Tithonian, subzone 1-2A).
9	-- do --	289.8 m S, 640.5 m E, NW cor. sec. 31 T. 11 N., R. 8 W.	Late Cretaceous (early Cenomanian, subzone 10A).
10	Great Valley sequence.	701.5 m N, 793 m W, SE cor. sec. 20 T. 10 N., R. 7 W.	Late Jurassic (early Tithonian, zone 3).
11	Franciscan assemblage.	579.5 m N, 690.5 m E, SW cor. sec. 8 T. 11 N., R. 8 W.	Late Jurassic (late Kimmeridgian and early Tithonian, subzone 1-2A).
12	-- do --	579.5 m N, 503.3 m E, SW cor. sec. 8 T. 11 N., R. 8 W.	Do.
13	Ophiolite of Geysers Peak.	732 m S, 457.5 m W, NE cor. sec. 1 T. 10 N., R. 9 W.	Late Jurassic (late Kimmeridgian or early Tithonian, zone 1).
14	Franciscan assemblage.	762.5 m E, 579.5 m S, NW cor. sec. 13 T. 10 N., R. 8 W.	Late Jurassic (late Kimmeridgian and early Tithonian, subzone 1-2A).
15	-- do --	671 m N, 335.5 m W, SE cor. sec. 9 T. 10 N., R. 8 W.	Late Jurassic (late Kimmeridgian and early Tithonian, subzone 2A).

¹ Location data originally given in feet and miles, are converted to metric units in accordance with the system adopted by the U.S. Geological Survey.

(1976) and McLaughlin and Stanley (1976); samples from a detailed measured section near The Geysers Resort now indicate a Late Cretaceous (Cenomanian) age. An early Cenomanian fauna was extracted from a chert clast enclosed in locally conglomeratic graywacke (loc. 9), indicating that these cherty graywacke units are early Cenomanian or younger in age and that

detritus in these graywackes was probably, in part, locally derived from older Franciscan cherts.

The Geysers chert

The most completely studied Franciscan chert in the area (loc. 6) forms a lens, 67.4 m thick, that crops out in a roadcut 1.1 km northwest of The Geysers Resort

AGE RELATIONS, UPPER JURASSIC OPHIOLITE, CALIFORNIA

TABLE 2.—List of other fossil localities

Map No. on figure 2	Formation	Location ¹	Fossils	Age	Identified by	Reference
16	Great Valley sequence.	1373 m W, 1190 m N, SE cor. sec. 2 T. 10 N., R. 9 W.	Dinoflagellate fragments.	Early Cretaceous?	W.R. Evitt	Written commun., 1973.
17	— do —	915 m N, 640.5 m E, SE cor. sec. 28 T. 12 N., R. 8 W.	Mollusks (<i>Buohia piochit</i>).	Late Jurassic (middle Tithonian).	D.L. Jones	Oral commun., 1976.
18	— do —	0.3 km slightly west of N from Harbin Springs-Big Canyon road junction	Dinoflagellates	Early Cretaceous or Late Jurassic.	W.R. Evitt	Swe, 1968.
19	— do —	1.01 km N from Harbin Springs-Big Canyon road junction	Pollen, mollusks	Late Cretaceous	W.R. Evitt A.M. Keen	Do.
20	— do —	2.7 km N of junction, Hwy 53 and Hwy 29, along Hwy 53	Dinoflagellates	Late Jurassic	W.R. Evitt	Do.
21	— do —	0.4 km upstream on Harbin Creek from junction of Harbin and Putah Creeks, 3.2 km N of Middletown	Pollen	Early Cretaceous (Aptian?).	— do —	Do.
22	— do —	2.1 km N of Harbin Springs-Big Canyon road junction	Pollen, dinoflagellates.	Late Cretaceous	— do —	Do.
23	— do —	0.16 km SW from NE cor. sec. 29 in Creek, T. 11 N., R. 7 W.	Dinoflagellates	Early Cretaceous (Berriasian and Valanginian).	— do —	Do.
24	— do —	0.16 km E from SW cor. sec. 17 T. 11 N., R. 7 W.	Pollen, dinoflagellates.	Early Cretaceous or Upper Jurassic.	— do —	Do.
25	— do —	0.08 km E, 1.05 km N, SW cor. sec. 27, T. 11 N., R. 8 W. on Harrington Flat Road	Foraminifers	Late Cretaceous (Campanian).	W. Sliter	Oral commun., 1976.
26	— do —	0.16 km E, 0.68 km S, NW cor. sec. 27, T. 12 N., R. 8 W.	Pollen, dinoflagellates.	Late Cretaceous	W.R. Evitt	Swe, 1968.

¹ Location data originally given in feet and miles, are converted to metric units in accordance with the system adopted by the U.S. Geological Survey.

and is traceable for more than 2 km along its strike. The chert, herein informally designated "The Geysers chert," depositionally overlies pillow basalt and is overlain by hydrothermally bleached and sheared graywacke. A Late Jurassic to Late Cretaceous age is assigned to this chert on the basis of the radiolarians in samples collected in 1974 by Pessagno and McLaughlin and subsequent resamplings in 1975 and 1976. A measured section of The Geysers chert is presented in table 3.

Two major zones of recrystallization in The Geysers chert that yielded no dateable radiolarians are subject to interpretation. A lower zone of recrystallization at 40.4–51.1 m separates the lower Tithonian from the upper Valanginian part of the chert in the measured section (table 3) and might conceivably represent in-place recrystallization of the missing upper Tithonian, Berriasian, and lower Valanginian. It is also possible

that part of the Lower Cretaceous section is cut out along a bedding-plane fault within the recrystallized zone because there is no evidence of erosion or reworking of the chert across this Tithonian to Valanginian break.

An upper zone of recrystallization between 63.9 and 65.9 m from the base separates the upper Valanginian from the lower Cenomanian part of the chert (table 3). This zone may represent a condensation of the missing Hauterivian, Aptian, and Albian Stages of the Lower Cretaceous. The presence in the overlying Cenomanian beds of numerous reworked Valanginian radiolarians, however, suggests the presence of an upper Valanginian to lower Cenomanian unconformity.

The Mesozoic absolute time scale is reliably correlated with the chronostratigraphic scale only in the Upper Cretaceous. Through radiometric dating of bentonites occurring in strata bearing ammonites, it

TABLE 3.—Measured section of The Geysers chert near The Geysers Resort, Sonoma County, Calif.
[Section measured by R. J. McLaughlin and H. N. Ohlin, September 1976.]

Measured interval (in meters)	Series	Stage	Radiolarian subzone	Lithology
Top of section 65.9 - 67.4±	Upper Cretaceous	Lower Cenomanian	10A	Contact with graywacke. White to gray, impure porcelaneous chert with reworked Valanginian radiolarians intersheared with hydrothermally bleached graywacke.
63.9 - 65.9	-----	Indeterminate (Unconformity?)	-----	Zone of recrystallization. Green to white chert, extensively recrystallized, partly covered by slope wash and faulted in region of fold hinge.
51.1 - 63.9	Lower Cretaceous	Upper Valanginian	5C	Blue-green, gray, and black chert, massive to bedded, with sporadic gray to gray-green porcelaneous shale partings to 96 mm thick. Displays sporadic differential recrystallization.
40.4 - 51.1	-----	Indeterminate	-----	Zone of recrystallization. Light-green to white chert, extensively recrystallized, and devoid of shale partings.
32.8 - 40.4	-----	-----	-----	Predominantly green-blue to white chert, in beds to 96 mm thick; blue-green shale partings to 36 mm thick.
20.7 - 32.8	Upper Jurassic	Lower Tithonian to upper Kimmeridgian.	1-2A	Predominantly green-blue to white chert with red mottling. Chert in beds to 96 mm thick; red shale partings to 24 mm thick.
0 - 20.7	-----	-----	-----	Red to blue-green chert, grading upward from red chert at base to mottled red and green chert; chert in beds as thick as 84 mm, with red shale partings to 24 mm thick.
Base of chert	-----	-----	-----	Contact with locally pillowed basaltic volcanic rocks.

has been possible to relate many Upper Cretaceous stages to the absolute time scale (Lanphere and Jones, 1977). Unfortunately, an integration of chronologic, chronostratigraphic, and biostratigraphic data is lacking for most of the Lower Cretaceous and Jurassic; only the following horizons can be accurately dated (from Lanphere and Jones, 1977):

1. Base of Cenomanian (Upper Cretaceous)—96 m.y. (five radiometric dates).
2. Base of the Hauterivian—134 m.y. (four radiometric dates).
3. Upper part of the Valanginian— 137 ± 5 m.y. (one radiometric date), and
4. The Jurassic-Cretaceous boundary is estimated, on a consensus of meager existing data, to be 138 ± 3 m.y.

These data suggest that the upper 16.3 m of The Geysers chert containing late Valanginian and early Cenomanian radiolarians, represents approximately 41 m.y. (see table 3). The implied hiatus in pelagic sedimentation between late Valanginian and early Cenomanian time appears to be 38 m.y. A substantial

amount of time is probably represented in the underlying 40.4 m of upper Kimmeridgian or lower Tithonian chert, but the durations of Jurassic stages are so poorly defined at present that speculations on this part of the time scale may be highly inaccurate. A crude estimate of pelagic sediment accumulation rates for the 12.8 m of upper Valanginian chert in this section can be made by assuming from these data that the upper Valanginian part of the chert represents the interval 137–134 m.y. ago (base of the Hauterivian Stage), a total of about 3 m.y. The rate of at least 12.8 m in 3 m.y. is equivalent to a minimum pelagic sediment accumulation rate of the order of 0.43 centimeter per 1000 years, disregarding the probable effects of post-depositional compaction and dewatering of the sediment.

From drilling in the modern oceans, rates of pelagic sedimentation have been determined for red clays and oozes composed of radiolarians, diatoms, and globigerinids. The rates range from 0.0 to 9.0 cm/1000 yr (Dietrich, 1963; Heath, 1974; Hays, 1971; Hays and Opdyke, 1967; Hamilton, 1967; von Huene and Kulm, 1971; Scholl and Creager, 1973; and Berger, 1974); the most common rates are 0.2–0.4 cm/1000 yr. The es-

estimated minimum sedimentation rate of 0.43 cm/1000 yr for the Valanginian part of The Geysers chert is consistent with these observed modern pelagic sedimentation rates.

Other pelagic Franciscan rocks

Franciscan rocks of early Cenomanian age are present at other places in the Coast Ranges, notably in melanges to the north and west of The Geysers-Clear Lake area. Discontinuous pods of pink to gray limestone cropping out in a melange north of Laytonville contain Cenomanian to Turonian and possibly Coniacian planktonic foraminifers (Gucwa, 1975; Wachs and Hein, 1975; Bailey and others, 1964). Another limestone of similar age, associated with locally pillowed basaltic flows and diabase, extends from an area west of Montara Mountain on the San Francisco peninsula southward to the vicinity of San Juan Bautista.

These limestone occurrences probably indicate areas of midocean carbonate deposition above the carbonate compensation depth and may thereby delineate the former presence of midocean topographic rises during Cenomanian and Turonian times. Rocks of Late Cretaceous and early Tertiary age in the Franciscan coastal belt (Evitt and Pierce, 1975) are in tectonic contact with older Franciscan rocks west of Laytonville.

CONSTRAINTS ON SUBDUCTION MODELS

The large time interval spanned by the 67.4 m-thick chert unit near The Geysers Resort places constraints on timing of subduction of Franciscan rocks in this area critical to the validity of currently disputed models of Franciscan subduction. It is clear from the biostratigraphic and structural data that the youngest Franciscan rocks beneath the Coast Range thrust in The Geysers area are of Late Cretaceous age and are, therefore, much younger than either the structurally overlying Coast Range ophiolite or the basal strata of the Great Valley sequence. These Late Cretaceous Franciscan rocks include, along with the dated cherts, sandstones metamorphosed to pumpellyite grade and locally to lawsonite grade (McLaughlin, 1975; McLaughlin and Stanley, 1976). Northeast of, and also within, The Geysers-Clear Lake area are metacherts, which are too highly metamorphosed to be dated paleontologically, associated with intact terranes of lawsonite and jadeite-grade metasandstone and metavolcanic rocks. These jadeite and lawsonite-bearing Franciscan rocks are thought to have undergone high-pressure metamorphism to blueschist in a subduction zone prior to Late Cretaceous time (Suppe and Armstrong, 1972; Lanphere and others, 1975; McLaughlin,

1975). For The Geysers area to have received pelagic sedimentation during the same time interval that active underthrusting and blueschist metamorphism occurred deep in an east-dipping subduction zone requires The Geysers to be situated far to the west-northwest or south-southwest of the subduction site. Alternatively, The Geysers area at that time may have been part of the upper plate of the Coast Range thrust, and the site of underthrusting might have been to the west-northwest or south-southwest. This reconstruction would require that subduction jump east of the The Geysers-Clear Lake area during post-early Cenomanian time.

Franciscan pelagic strata, including cherts and limestones, in the Coast Ranges are more than 95 percent by volume late Kimmeridgian to early Tithonian (subzone 1-2A) in age; the total volume of pelagic sediment in the Franciscan assemblage is proportionately very small. Early Cenomanian chert of the Franciscan assemblage, where examined in The Geysers-Clear Lake area, is associated with, or deposited at the top of, early Tithonian and late Valanginian cherts. Nowhere does the Cenomanian chert rest directly on basalt. If pelagic Franciscan strata were deposited on basaltic ocean crust that formed from sea-floor spreading throughout Late Jurassic to Late Cretaceous time, then a representative record of pelagic strata deposited directly upon basalt and spanning Late Jurassic to Late Cretaceous time would be expected. The chert data, however, suggest that east-directed sea-floor spreading was in fact extremely slow or inactive between late Valanginian and early Cenomanian time, a conclusion that is contradictory to previous studies indicating appreciable blueschist metamorphism and, by implication, subduction of other Franciscan strata during this interval (Suppe and Armstrong, 1972; Lanphere and others, 1975).

The notable absence of pelagic strata of post-Valanginian age except for the rare Upper Cretaceous limestones and cherts that are mostly in contact with older pelagic strata strongly suggests that if appreciable sea-floor spreading did occur during middle Cretaceous time, then such spreading was independent of the crust upon which Franciscan pelagic strata were deposited. Clearly, a model of Late Jurassic to Late Cretaceous west-stepping subduction is too simplistic to explain the time-space distribution of pelagic strata in the Franciscan assemblage.

Jones, Silberling, and Hillhouse (1978) have recently cast some doubt on tectonic models assuming that late Mesozoic sediments deposited along the western North American continental margin were subducted directly eastward. These workers present pale-

ontologic and paleomagnetic data indicating that a large allochthonous terrane of Triassic volcanic and sedimentary rocks, traced from Vancouver Island, British Columbia, to south-central Alaska, called Wrangellia, formed at low equatorial paleolatitudes. They suggest displacement of Wrangellia nearly 30° northward, implying large right-lateral motion and (or) oblique underthrusting between Wrangellia and the North American craton. By this model, suturing of Wrangellia to the craton would have occurred in eastern Oregon during Late Jurassic time (Jones and others, 1978). No paleomagnetic evidence for large-scale right-lateral motion between the upper plate Great Valley sequence and the lower plate Franciscan assemblage exists, but the possibility of such motion cannot be discounted in light of the data presented.

The relations shown indicate that Franciscan rocks in The Geysers–Clear Lake area could at no time have been in depositional contact with strata of the structurally overlying Great Valley sequence as suggested by Maxwell (1974). It is apparent that basal strata of the Great Valley sequence are significantly older than the youngest Franciscan rocks below the Coast Range ophiolite and that the Franciscan rocks were probably separated from Great Valley strata by many tens to hundreds of kilometers at the time of deposition.

CONCLUSIONS

We have demonstrated the age and structural relations of rock units above, below, and within the ophiolite sheet that regionally overlies the Franciscan assemblage in the northern California Coast Ranges. From these relations, the following conclusions are drawn:

The middle and upper part of the Coast Range ophiolite in The Geysers–Clear Lake region formed prior to and during early Tithonian time. The ophiolite underwent submarine erosion later in early Tithonian time, when as much as 1 km of the upper part of the ophiolite was locally stripped off. This erosion contributed coarse mafic debris to basal strata of the Great Valley sequence.

Radiolarian chert ages and structural relations in The Geysers–Clear Lake area clearly demonstrate that the Franciscan assemblage is younger than the structurally overlying Coast Range ophiolite and, in part, younger than basal strata of the Great Valley sequence that depositionally overlies the ophiolite. This relation necessitates a plate tectonic model for emplacement of the Franciscan beneath the Coast Range ophiolite. The available data do not support deposition of the Great Valley sequence on Franciscan rocks

in the Clear Lake region as suggested by Maxwell (1974). In fact, a model requiring large-scale original horizontal separation between pelagic sediments of the Franciscan assemblage and the Great Valley sequence seems mandatory. Pelagic sediments represented by The Geysers chert could not have been situated on a subducting oceanic plate near any active subduction zone during deposition because at least 41 m.y. elapsed before these sediments were thrust beneath ophiolite and the Great Valley sequence in post-early Cenomanian time. The chert data suggest that The Geysers area may have been part of the upper plate of the Coast Range thrust until post-early Cenomanian time.

The discovery of discrete chert units representing Late Jurassic to Late Cretaceous pelagic sedimentation in the Franciscan assemblage allows a correlation with coeval planktonic carbonate sedimentation in Franciscan terranes to the north and west of The Geysers–Clear Lake region. This correlation suggests the existence during Cenomanian time of significant submarine relief. Carbonate sedimentation occurred on submarine highs above the carbonate compensation depth. Pelagic deposition in The Geysers area occurred in deeper water below the carbonate compensation depth, perhaps along the flanks of or on top of, less elevated rises or on an abyssal plain.

REFERENCES CITED

- Bailey, E. H., Blake, M. C. Jr., and Jones, D. L., 1970, On-land Mesozoic oceanic crust in California Coast Ranges, in Geological Survey research, 1970: U.S. Geol. Survey Prof. Paper 700-C, p. C70–C81.
- Bailey, E. H., Irwin, W. P., and Jones, D. L., 1964, Franciscan and related rocks and their significance in the geology of western California: California Div. Mines and Geology, Bull. 183, 177 p.
- Berger, W. H., 1974, Deep sea sedimentation, in Burk, C. A., and Drake, C. L., eds., The geology of continental margins; New York, Springer-Verlag, p. 213–241.
- Berkland, J. O., Raymond, L. A., Cramer, J. C., Moores, E. M., and O'Day, M., 1972, What is Franciscan?: Am. Assoc. Petroleum Geologists Bull., v. 56, p. 2295–2302.
- Bezore, S. P., 1969, The Mount St. Helena ultramafic complex of the northern California Coast Ranges: Geol. Soc. of America Abs. with Programs, v. 1, no. 3, p. 5.
- Blake, M. C., Jr., and Irwin, W. P., and Coleman, R. G., 1967, Upsidedown metamorphic zonation, blueschist facies, along a regional thrust in California and Oregon, in Geological Survey research, 1967: U.S. Geol. Survey Prof. Paper 575-C, p. C1–C9.
- Blake, M. C., Jr., and Jones, D. L., 1974, Origin of Franciscan melanges in northern California: Soc. Econ. Paleontologists and Mineralogists, Spec. Pub. 19, p. 345–357.
- Blake, M. C., Jr., Jones, D. L., and Landis, C. A., 1974, Active continental margins; contrasts between California and New Zealand, in Burk, C. A., and Drake, C. L., eds., The geology of continental margins; New York, Springer Verlag, p. 853–872.

- Dickinson, W. R., 1970, Clastic sedimentary sequence deposited in shelf, slope, and trough settings between magmatic arcs and associated trenches: *Pacific Geology*, v. 3, p. 15-30.
- Dietrich, G., 1963, General oceanography, an introduction: New York, John Wiley & Sons, p. 19-24.
- Ernst, W. G., 1970, Tectonic contact between the Franciscan melange and the Great Valley sequence-crustal expression of a Late Mesozoic Benioff zone: *Jour. Geophys. Research*, v. 75, p. 886-902.
- Evitt, W. R., and Pierce, S. T., 1975, Early Tertiary ages from the coastal belt of the Franciscan Complex, northern California: *Geology*, v. 3, p. 433-437.
- Gucwa, P. R., 1975, Middle to Late Cretaceous sedimentary melange, Franciscan complex, northern California: *Geology*, v. 3, p. 105-108.
- Hamilton, E. L., 1967, Marine geology of abyssal plains in the Gulf of Alaska: *Jour. Geophys. Research*, v. 72, p. 4208-4210.
- Hays, J. D., 1971, Faunal extinctions and reversals of the earth's magnetic field: *Geol. Soc. America Bull.*, v. 82, p. 2433-2447.
- Hays, J. D., and Opdyke, N. D., 1967, Antarctic radiolaria, magnetic reversals, and climatic change: *Science*, v. 158, p. 1003-1004.
- Heath, G. R., 1974, Dissolved silica and deep sea sediments, in Hay, W. W., ed., *Geologic history of the oceans*: Soc. Econ. Paleontologists and Mineralogists, Spec. Pub. 20, p. 88.
- Hopson, C. A., Mattinson, J. M., and Pessagno, E. A., Jr., 1975, Record of Late Jurassic sea-floor spreading, California Coast Ranges: *Geol. Soc. America Abs. with Programs*, v. 7, no. 3, p. 326.
- Jones, D. L., Silberling, N. J., and Hillhouse, John, 1978, Wrangellia—A displaced continental block in northwestern North America: *Canadian Jour. Earth Sci.* (In press.)
- Lanphere, M. A., 1971, Age of the Mesozoic oceanic crust in the California Coast Ranges: *Geol. Soc. America Bull.*, v. 82, p. 3209-3212.
- Lanphere, M. A., Blake, M. C., Jr., and Irwin, W. P., 1975, Early Cretaceous metamorphic age of the South Fork Mountain Schist in the northern Coast Ranges of California: *Geol. Soc. America Abs. with Programs*, v. 7, no. 3, p. 340.
- Lanphere, M. A., and Jones, D. L., 1978, Cretaceous time scale from North America: *Am. Assoc. Petroleum Geologists*. (In press.)
- Ludwig, W. J., Nafe, J. E., and Drake, C. L., 1970, Seismic refraction, in Maxwell, A. E., ed., *The sea*: New York, Interscience, v. 4, pt. 1, p. 53-84.
- Maxwell, J. C., 1974, Anatomy of an orogen: *Geol. Soc. America Bull.*, v. 85, p. 1195-1204.
- McLaughlin, R. J., 1974, Preliminary geologic map of The Geysers steam field and vicinity, Sonoma County, California: U.S. Geol. Survey Open-File Rept. 74-238.
- 1975, Structure of Franciscan rocks in the central Mayacamas Mountains, Sonoma and Lake Counties, California: *Geol. Soc. America Abs. with Programs*, v. 7, no. 3, p. 345.
- 1976, Significance of age relationships above and below Upper Jurassic ophiolite in The Geysers-Clear Lake region, California: *Geol. Soc. America Abs. with Programs*, v. 8, no. 3, p. 394.
- McLaughlin, R. J., and Stanley, W. D., 1976, Pre-Tertiary geology and structural control of geothermal resources, The Geysers steam field, California: United Nations symposium on development and use of geothermal resources, 2d Proc., San Francisco, v. 1, p. 475-485.
- Pessagno, E. A., Jr., and Newport, R. L., 1972, A technique for extracting radiolaria from radiolarian cherts: *Micro-paleontology*, v. 18, no. 2, p. 231-234.
- 1977, Lower Cretaceous radiolarian biostratigraphy of the Great Valley sequence and Franciscan complex, California Coast Ranges: Cushman Found. for Foraminiferal Research, Spec. Pub. 15, 87 p.
- Platt, J. P., 1975, Metamorphic and deformational processes in the Franciscan complex, California—Some insights from the Catalina schist terrane: *Geol. Soc. America Bull.*, v. 86, p. 1337-1347.
- Saleeby, Jason, 1975, Breaking and mixing of Permian oceanic lithosphere-southwestern Sierra Nevada foothills, California: *Geol. Soc. America Abs. with Programs*, v. 7, no. 7, p. 1256.
- Scholl, D. W., and Creager, J. S., 1973, Geologic synthesis of Leg 19: Reports Deep Sea Drilling Project, v. 19, p. 900-902.
- Suppe, John, and Armstrong, R. L., 1972, Potassium-argon dating of Franciscan metamorphic rocks: *Am. Jour. Sci.*, v. 272, p. 217-233.
- Swe, Win, 1968, Stratigraphy and structure of Late Mesozoic rocks south and southeast of Clear Lake, California: Stanford Univ., Ph.D. thesis, 76 p.
- Swe, Win, and Dickinson, W. R., 1970, Sedimentation and thrusting of Late Mesozoic rocks in the Coast Ranges near Clear Lake, California: *Geol. Soc. American Bull.*, v. 81, p. 165-188.
- Van Eysinga, F. W. B., 1975, *Geological time table* (3d ed.): Elsevier Pub. Co.
- Van Hinte, J. E., 1976, A Jurassic time scale: *Am. Assoc. Petroleum Geologists Bull.*, v. 60, p. 489-497
- Von Huene, Roland, and Kulm, L. V., 1971, Tectonic summary of Leg 18: Initial Reports Deep Sea Drilling Project, v. 18, p. 966-969.
- Wachs, D., and Hein, J. R., 1975, Franciscan limestones and their environments of deposition: *Geology*, v. 3, p. 29-33.
- Wagner, D. L., 1975, Mesozoic geology of the Walter Springs area, Napa County, California: San Jose State Univ., San Jose, Calif., M.S. thesis, 68 p.

Pre-Tertiary Geology and Structural Control of Geothermal Resources, The Geysers Steam Field, California

ROBERT J. McLAUGHLIN

U.S. Geological Survey, Menlo Park, California 94025, USA

WILLIAM D. STANLEY

U.S. Geological Survey, Denver, Colorado 80225, USA

ABSTRACT

In the Geysers steam field of northern California, Upper Jurassic and Cretaceous rocks of the Franciscan assemblage form the core of a southeastward-plunging antiform that has been highly modified by late Tertiary and Quaternary faulting. These intensely deformed volcanic and sedimentary rocks are metamorphosed to assemblages containing pumpellyite, lawsonite, and jadeite, and exhibit textural reconstitution that generally increases in the direction of structurally higher rocks.

Comparison of the structure of these Franciscan rocks with microearthquake and resistivity data suggests that economically significant steam reservoirs are in part related to local fault-controlled structural traps. In an area of shallow steam production near Geysers Resort, the epicenters and foci of numerous microearthquakes and extensive hydrothermal alteration are associated with a zone of N 30°-35°W-trending faults that dip steeply to the northeast. The microearthquakes and hydrothermal alteration may be related to hot water- or steam-saturated rock in the fault zone. Structural control of steam resources is also indicated near Castle Rock Spring, approximately 4 miles southeast of Geysers Resort. A low resistivity anomaly over the Castle Rock Spring steam field is probably due to rock saturated with hot water. This presumed zone of water-saturated rock occupies an anticlinal warp between steeply dipping faults trending N 80°W in foliate metagraywacke, basaltic volcanic rocks, and serpentine. Steeply dipping faults trending N 50°W may bound the east side of the Castle Rock Spring steam reservoir.

INTRODUCTION

The Geysers steam field is located in the Mayacmas Mountains of northern California, about 110 km northwest of San Francisco. The field is a few kilometres south of Clear Lake basin, a center of major Quaternary volcanism, and a few kilometres northwest of Mount Saint Helena, the locus of late Tertiary volcanism (Fig. 1). The Geysers geothermal area is particularly significant since it is now the world's largest geothermal producer of electrical power (greater than 500 MW generating capacity by 1975), and it is also one of the few areas known to have vapor-dominated

hydrothermal systems (White, Muffler, and Truesdell, 1971). The next largest vapor-dominated hydrothermal system is in the Larderello and Monte Amiata areas, Italy.

The Geysers-Clear Lake area is one of several geothermal systems selected by the U.S. Geological Survey for detailed study. Detailed mapping of the pre-Tertiary rocks in the area was begun in 1973, and other geologic mapping and geochronologic studies of the Quaternary volcanic rocks by Carter B. Hearn and Julie Donnelly are also in progress. Similar work is also in progress in the Tertiary volcanic rocks to the southeast of The Geysers area, by K. F. Fox (Fig. 1). These mapping projects are providing the geologic data base to which geochemical, geophysical, and hydrologic studies will be applied for interpreting the mechanics of The Geysers geothermal system.

LATE MESOZOIC TECTONIC FRAMEWORK

Late Mesozoic rocks in The Geysers-Clear Lake area are assigned to two approximately coeval assemblages considered to have originally been deposited in widely separated basins to the east of a mid-ocean rift system. The late Mesozoic and early Tertiary Franciscan assemblage forms the basement complex of much of the California Coast Range, and is composed of a volcanic-sedimentary sequence, thought to represent a deep ocean trench or arc-trench gap deposit (Blake and Jones, 1974). The Great Valley sequence and the ophiolite complex present beneath its base are thought to represent rocks originally deposited and emplaced east of the Franciscan assemblage site of deposition. Deposition of Great Valley sequence strata presumably was upon continental granitic crust along the east side of the basin, but it overlapped onto ophiolite (oceanic crust) along the west margin of the basin.

The Franciscan assemblage has been highly tectonized and subjected to regional metamorphism related to abnormally high pressure and deep burial, resulting in the development of pumpellyite and lawsonite-bearing metamorphic mineral assemblages (Ernst, 1971; Blake, Irwin, and Coleman, 1967). In contrast to the Franciscan assemblage, the Great Valley sequence is only mildly deformed by folding and faulting, and metamorphism is confined to low-temperature zeolites attributable to deep burial (Dickinson, Ojkan-gas, and Stewart, 1969; Bailey and Jones, 1973). Present

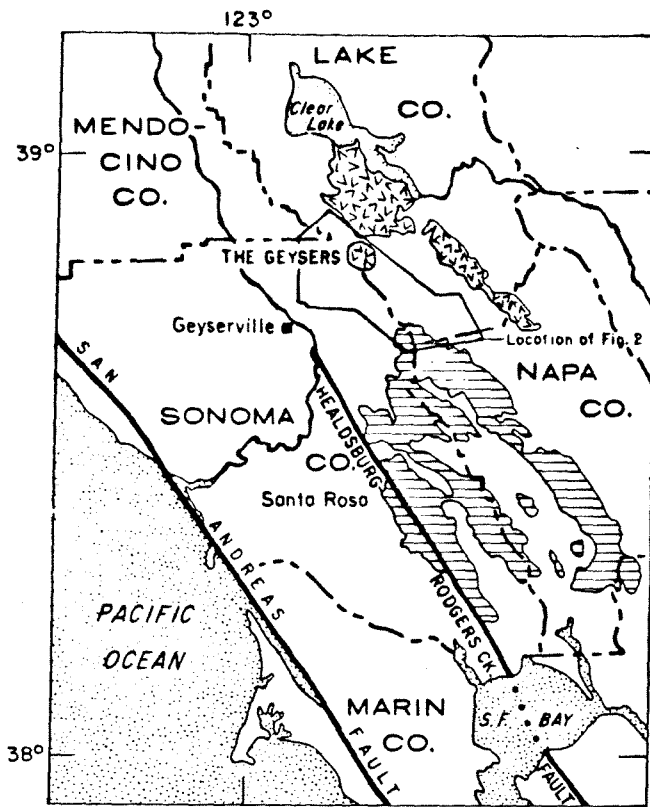


Figure 1. Location of The Geysers geothermal area and nearby late Tertiary and Quaternary volcanic rocks. The V pattern indicates location of Quaternary volcanic rocks; line pattern, late Tertiary volcanic rocks.

distribution and structural relations of the Great Valley sequence and the Franciscan assemblage indicate that the Great Valley sequence now overlies Franciscan rocks of equivalent age along a zone of regional thrust faulting, although in many areas this thrust relation is confused by later high-angle faults of probable Tertiary and Quaternary age. The regional thrust relation has been explained by many workers (Hamilton, 1969; Bailey, Blake, and Jones, 1970; Blake, Irwin, and Coleman, 1967) as a result of eastward subduction of the Franciscan assemblage beneath oceanic crustal rocks and Great Valley sequence strata deposited upon it. This subduction is thought to have begun during the mid-Cretaceous, presumably the result of convergence of an oceanic plate upon which Franciscan sediments were deposited, with the continental margin east of the Franciscan sediments. As this plate convergence progressed, the Franciscan deposits were subducted eastward beneath adjacent oceanic crustal rocks, eventually overriding the Great Valley sequence. Deformation and high-pressure metamorphism in the Franciscan assemblage are thought to have occurred during this period of subduction (Blake, Irwin, and Coleman, 1967). The process of subduction is thought to have ceased about 30 million years (m.y.) before present (Atwater, 1970), when convergent motion between the oceanic and continental plate boundaries changed to transform motion, initiating the San Andreas strike-slip system. Large scale strike-slip faulting has continued to the present day, obscuring the earlier thrust fault relations produced during the late Mesozoic and early Tertiary.

PRE-TERTIARY ROCK UNITS

Franciscan Assemblage

The Franciscan assemblage in The Geysers area is typical of Franciscan rocks over a large part of California. It consists largely of graywacke and minor shale, with shale being somewhat more abundant in the structurally higher, most deformed part of the assemblage (Fig. 2). The essential compositions of the graywackes vary widely with quartz 10-55%, total feldspar (plagioclase) 25-55%, and total lithics 20-55%. Nonautoclastic lithic fragments consist largely of chert and subequal amounts of mafic and silicic volcanic rocks (the ratio of chert to volcanic detritus varies between 1:1 and 5:1).

Altered intrusive and extrusive igneous rocks commonly referred to as greenstone, and consisting largely of pillow basalt, basaltic pillow breccia, basaltic tuff, and minor diabase and gabbro, are second in order of abundance in the Franciscan assemblage. These igneous rocks are now confined to the structurally higher parts of the assemblage and their contacts are in most instances tectonic, so that their original relation to the sedimentary rocks is largely undetermined. Radiolarian cherts associated with the graywacke and volcanic rocks and conglomerate are locally prominent constituents in structurally higher parts of the Franciscan assemblage.

The occurrence of blueschist metamorphic mineral assemblages in the Franciscan assemblage has been the object of many studies by others (Coleman and Lee, 1963; Blake, Irwin, and Coleman, 1967; Ernst, 1971; Coleman and Lanphere, 1971). In general, two modes of occurrence of blueschist are recognized in The Geysers area: (1) in schistose to gneissose tectonic inclusions from less than a meter up to several hundreds of meters long that are associated with other tectonic inclusions of eclogite or amphibolite along highly sheared zones and serpentinite contacts, and (2) in graywacke and interlayered volcanic rocks and chert that regionally have weak to highly developed metamorphic textural fabrics. These two modes of occurrence of blueschist minerals in the Franciscan assemblage were shown by Coleman and Lanphere (1971) and Lanphere, Blake, and Irwin (1975) to represent metamorphic events of different ages. The schistose and gneissose blueschist tectonic inclusions were shown to have been metamorphosed about 150 m.y. ago (Late Jurassic), whereas the rocks with regionally developed metamorphic textural fabrics were shown to have been metamorphosed 114-120 m.y. ago (Early Cretaceous) in northern California. Elsewhere in the Coast Ranges Franciscan rocks may have been subjected to even younger regional blueschist metamorphism.

Serpentinite is present along most faults and within highly sheared zones in the Franciscan assemblage (Fig. 2). A few serpentinite bodies are metamorphosed and contain the mineral assemblages antigorite \pm talc \pm actinolite \pm chlorite. Other partially to completely serpentinized peridotite bodies containing chrysotile and clinochrysotile are present either along steep dipping faults completely enclosed by Franciscan rocks or as klippen of the ophiolite below the base of the Great Valley sequence.

The Franciscan assemblage is known to range in age from Late Jurassic to early Tertiary (Eocene) (Blake and Jones, 1974). Within The Geysers area, however, fossil control is present only in the structurally higher parts of the

Franciscan assemblage, and strata in the structurally lower part of the section are of unknown age and separated by faults from the higher strata. Several dates have been obtained from radiolaria in cherts interlayered with volcanic and sedimentary rocks from the upper parts of the Franciscan assemblage in The Geysers area. These dates indicate a range in age of Late Jurassic (early Tithonian) to Early Cretaceous (late Hauterivian or early Barremian) (Emile A. Pessagno, written comm., 1973-74). One of these dates, obtained from a conglomerate clast of chert, yielded a Hauterivian or Barremian age, indicating that at least some of the structurally high clastic Franciscan rocks are younger than Hauterivian or Barremian.

Elsewhere in the Coast Ranges similar Franciscan rocks have been found to be no older than Tithonian (Blake and Jones, 1974), and therefore the Franciscan assemblage in The Geysers area is regarded to be Late Jurassic (early Tithonian) or younger. Franciscan sandstones of Tertiary age have been reported west of The Geysers area (Blake and Jones, 1974), but these rocks are arkosic in composition and generally contain significant (>3%) potassium feldspar (Bailey, Irwin, and Jones, 1964). Since the structurally low undated Franciscan rocks in The Geysers area are graywackes containing less than 1/2% potassium feldspar, and generally lithic to quartzose in composition, they are considered here to be no younger than Cretaceous.

Ophiolite complex. Ophiolite present below the base of the Great Valley sequence underlies Mount Saint Helena to the southeast, the prominent ridge between Geyser Peak and Black Mountain in the southwest part of the map area, and also outcrops for several kilometres along the north side of Cobb and Collayomi Valleys (Fig. 2). Ophiolite exposed at Geyser Peak consists of about 120 m of a basal sheared peridotite, above which is about 365 m of poorly exposed microgabbro and diabase, above which is an undetermined thickness of basalt pillows, tuff, pillow breccia, and diabase. The ophiolite of Mount Saint Helena is composed of about 600 m of peridotite in the lower part, above which is 520 m of gabbroic rock, above which is 300 m of diabase breccia (Bezore, 1969). Most of the peridotite and as much as 150 m of the overlying gabbro section present at Mount Saint Helena are missing from the ophiolite of Geyser Peak. Radiolaria from chert interlayered with the basaltic rocks of Black Mountain have been assigned a Late Jurassic (late Kimmeridgian and early Tithonian) age by Emile Pessagno (written comm., 1975), suggesting a Late Jurassic age for that part of the ophiolite.

Great Valley Sequence

Knoxville formation. A few small tectonically isolated patches of strata assignable to the Knoxville formation are present in the southwest and southeast parts of the map area in depositional contact with underlying ophiolite (Fig. 2).

Assignment of these isolated strata to the Knoxville formation is based on their age, lithologic similarity to the Knoxville elsewhere in the Coast Ranges, and upon the depositional contact relationship of these strata with underlying ophiolite. Considerable thicknesses of Knoxville strata are exposed to the north, in the Clear Lake area (Brice, 1953; Swe and Dickinson, 1970). The Knoxville formation in the map area is composed largely of dark

green to black mudstone and siltstone and less abundant fine-grained interbedded basaltic sandstone. Sporadic carbonate concretions in the mudstone exposed along The Geysers-Healdsburg road contain rare dinoflagellates of Early Cretaceous age (W. R. Evitt, written comm., 1973).

Although later faults now obscure the relation, mudstone interbedded with a sedimentary breccia composed largely of angular basalt and diabase detritus is locally present at the base of the Knoxville formation in depositional contact with underlying basaltic volcanic rocks of the ophiolite complex. This depositional relation can be observed along The Geysers-Healdsburg road near Black Mountain.

STRUCTURE OF PRE-TERTIARY ROCKS

Pre-Tertiary rocks in The Geysers area compose an extremely complex southeastward-plunging antiform, here referred to as the Mayacmas antiform. The Mayacmas antiform is a secondary flexure in the northward extension of the broader Diablo antiform (Bailey et al., 1964, Fig. 29), and its core is composed of deformed Franciscan rocks. The Franciscan core rocks are overlain to the northeast, southeast, and southwest by ophiolite and rocks of the Great Valley sequence. The distribution of these overlying rocks roughly outlines the southeastward plunge of the Mayacmas antiform. On the southwest this feature is flanked by a system of steeply dipping, northwest-trending strike-slip faults aligned with Alexander Valley—Geyser Peak and Little Sulphur Creek fault zones (Fig. 3).

Deformation of Franciscan rocks in the core of the Mayacmas antiform, as elsewhere in the Coast Ranges, largely predated the late Cenozoic regional warping and block faulting associated with formation of the Mayacmas and Diablo antiforms. The early deformation is thought to have occurred during eastward subduction and metamorphism of Franciscan rocks beneath the Great Valley sequence during the late Mesozoic and early Tertiary, or prior to about 30 million years ago (Atwater, 1970). Also present in the area, however, are prominent steeply dipping northwest- and east-west-trending fault sets that traverse the Mayacmas antiform and locally displace late Pliocene and Holocene deposits. Owing to the complexity of this faulting, it is difficult or impossible in some areas to distinguish faults produced during the late Mesozoic and early Tertiary from those produced during the late Tertiary and Quaternary. It is in fact probable that some of the more recent faulting in the area occurred along the older faults.

The dominant northwest structural grain in The Geysers region is due largely to the prevailing fault pattern (Fig. 3). This northwest-trending fault pattern consists of at least two components: (1) imbricate northeast- southeast- and southwest-dipping high- to low-angle thrust faults that separate tectonic slabs in the Franciscan assemblage, and (2) later, steeply dipping northwest-trending faults with vertical and strike-slip components overprinted upon the earlier thrust faults.

A prominent component of strike-slip movement on several of the later high-angle faults is inferred from several lines of evidence. Linear features on the surfaces of many of these steeply dipping faults indicate a strong lateral shear component, if it is assumed that these faults were not tilted from the horizontal or folded. Elsewhere, the distribution, structural dip, and compositions of the Geyser Peak and Mount Saint Helena ophiolite masses and associated overly-

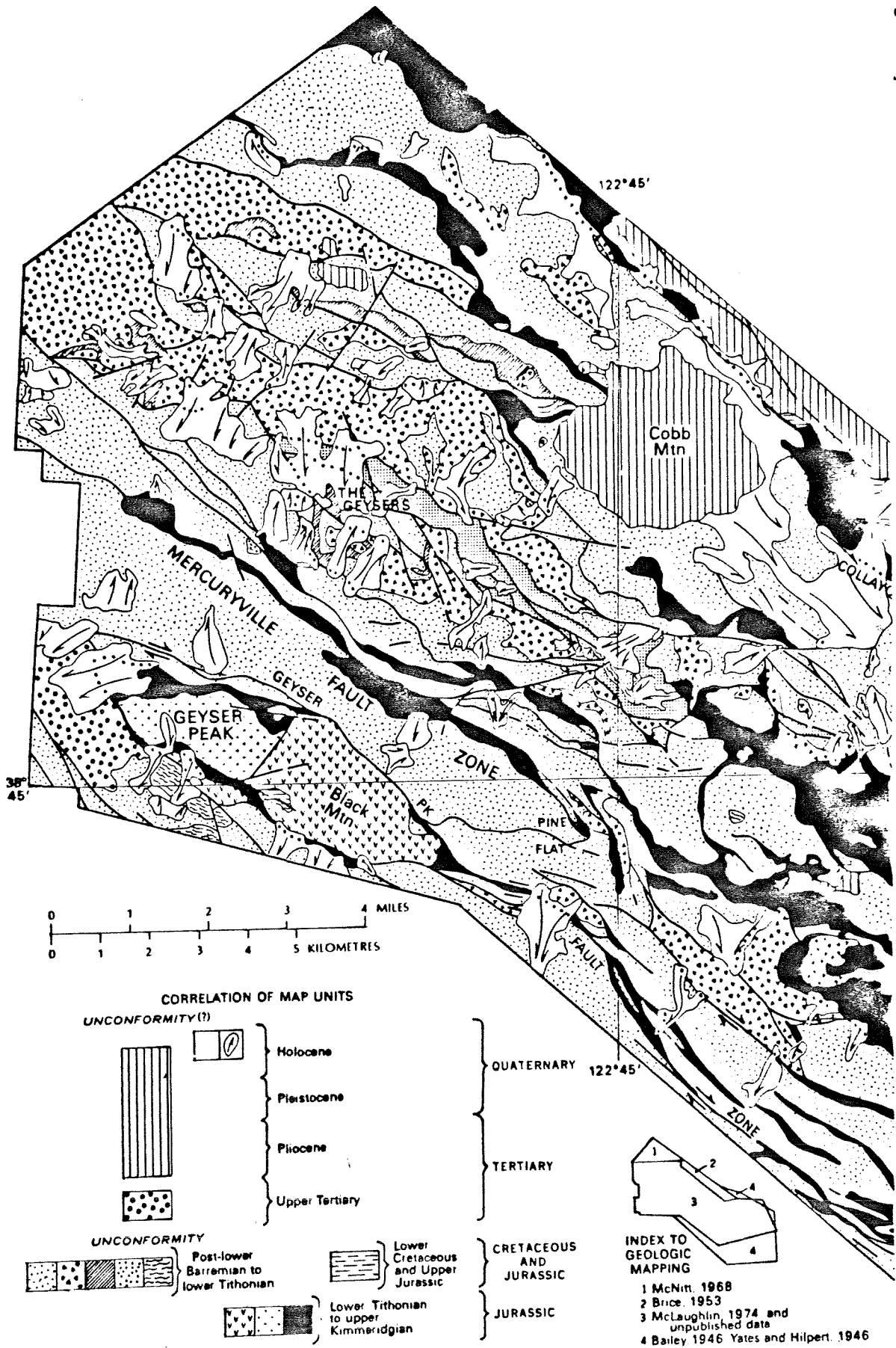


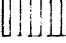
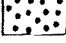



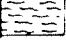
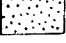
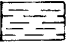
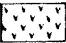
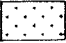



Figure 2. Generalized geologic map of the Geysers area, emphasizing the pre-Tertiary rocks.

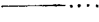

EXPLANATION

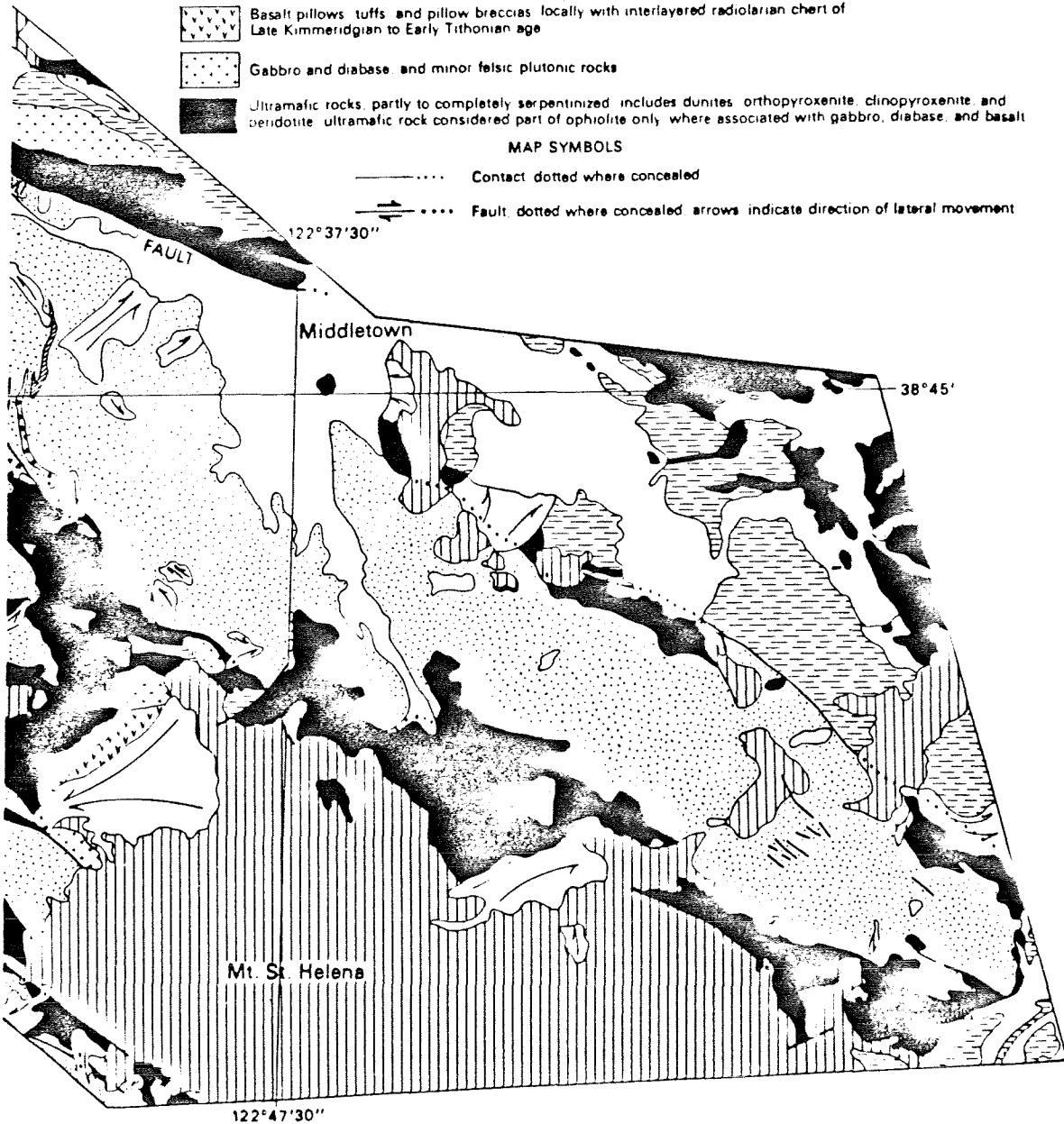
-  Landslide deposits (Quaternary)
-  Alluvium (Quaternary)
-  Volcanic rocks of Clear Lake (Quaternary) and Sonoma volcanics (Pliocene)
-  Nonmarine gravel (Upper Tertiary)
- FRANCISCAN ASSEMBLAGE (UPPER JURASSIC AND CRETACEOUS)**
-  Largely graywacke, shale, and conglomerate, in places pervasively sheared into melanges containing tectonic blocks of basaltic volcanic rock, chert, blueschist, amphibolite, or eclogite
-  Basaltic volcanic rocks, including pillow basalt, pillow breccia, diabase, and basaltic tuff
-  Chert, red, green, and white in color, locally containing abundant radiolaria
-  Prominent tectonic blocks of blueschist, amphibolite, and eclogite
-  Metamorphosed serpentine (antigorite ± talc ± actinolite ± chlorite mineral assemblage) exposed along Big Sulphur Creek

- GREAT VALLEY SEQUENCE (Upper Jurassic and Lower Cretaceous)**
-  Knoxville Formation, mudstone, siltstone, and fine-grained basaltic sandstone with minor carbonate concretions, sedimentary breccia composed largely of volcanic detritus locally present at base

- OPHIOLITE (Upper Jurassic)**
-  Basalt pillows, tuffs, and pillow breccias, locally with interlayered radiolarian chert of Late Kimmeridgian to Early Tithonian age
-  Gabbro and diabase, and minor felsic plutonic rocks
-  Ultramafic rocks, partly to completely serpentinized, includes dunites, orthopyroxenite, clinopyroxenite, and peridotite, ultramafic rock considered part of ophiolite only, where associated with gabbro, diabase, and basalt

MAP SYMBOLS

-  Contact, dotted where concealed
-  Fault, dotted where concealed, arrows indicate direction of lateral movement



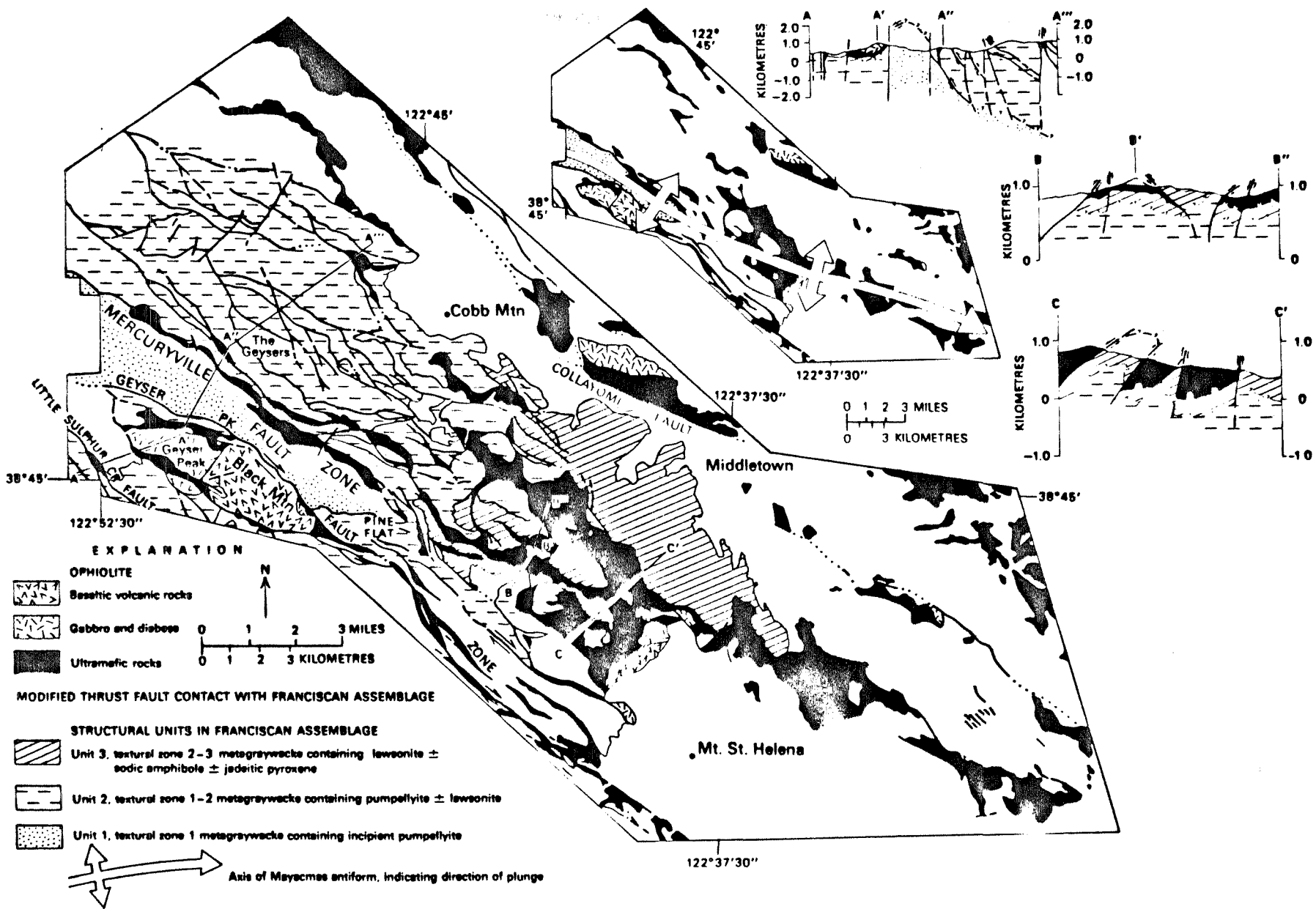


Figure 3. Map showing major structural units of the Franciscan assemblage in the Geysers steam field and vicinity, with respect to distribution of ophiolite and faults.

ing basal strata of the Great Valley sequence strongly suggest that a minimum right-lateral offset of 8-9 km has occurred along the Geyser Peak fault zone (Fig. 3).

Evidence for recent fault activity is also present in some areas. Southwest of Geyser Peak, along Little Sulphur Creek, the northwest-trending Little Sulphur Creek fault truncates late Tertiary nonmarine strata. Such physiographic features as sag ponds, linear trenches, and a right-laterally offset fence line (D. H. Radbruch, oral commun., 1974) along this fault suggest Holocene offsets. Elsewhere, near Geysers Resort (Fig. 4), Holocene alluvial terrace deposits are steeply tilted against a steep northwest-trending fault along Big Sulphur Creek. Associated with the faulting along Big Sulphur Creek are numerous microearthquakes (Hamilton and Muffler, 1972), further suggesting recent fault activity in that area.

Franciscan rocks in the core of the Mayacmas antiform are divided into three fault-bounded structural units (Fig. 3). The lowest, structural unit 1, is composed of strata of unknown age exposed along a N 40°W-trending belt between the steeply-dipping Mercuryville and Geyser Peak fault zones. Unit 1 is a relatively intact, flysch-like sequence of graywacke and minor interbedded concretionary black shale, compressed into tight southeast-trending folds. The graywacke of structural unit 1 is feebly reconstituted to textural zone 1 of Blake, Irwin, and Coleman (1967), and it contains the metamorphic mineral assemblage quartz (SiO₂) + albite (NaAlSi₃O₈) + phengite [K₂Al₄(Si₆Al₂)O₂₀(OH)₄] ± pumpellyite [Ca₄MgAl₅O(OH)₃(Si₂O₇)₂(SiO₄)₂ · 2H₂O].

Structural unit 2 overlies unit 1 north of the Mercuryville fault zone and south of the Geyser Peak fault zone. In the vicinity of Pine Flat, in the south part of the area, unit 1 terminates and is enclosed by unit 2. In contrast to the lower structural unit, unit 2 is highly tectonized, lithologically heterogeneous, and locally chaotic. Unit 2 is characterized as a broken formation of imbricate tectonic slabs up to several kilometres long. These slabs generally

are composed of relatively intact well-bedded graywacke, minor interbedded shale, conglomerate, and locally abundant basaltic volcanic rocks and chert. The larger intact slabs are separated by highly sheared shaly zones of tectonic melange containing smaller sheared masses of graywacke, conglomerate, basaltic volcanics, chert, locally abundant sporadic masses of foliate blueschist and eclogite, and prominent elongate serpentinite bodies. The rocks in structural unit 2 are feebly to moderately reconstituted, with the graywackes assigned to textural zones 1 to 2 of Blake, Irwin, and Coleman (1967). The metamorphic mineral assemblage recognized to date in graywackes of unit 2 includes quartz + albite + phengite ± pumpellyite ± lawsonite [CaAl₂Si₂O₇(OH)₂ · H₂O].

The highest structural unit mapped in the Franciscan, unit 3, overlies unit 2, wrapping over it to the northeast and southeast beneath the overthrust ophiolite complex at the base of the Great Valley sequence. Unit 3 appears to be terminated against the southeastward extension of the Geyser Peak and Mercuryville fault zones in the south part of the area. Lithologies present in tectonic unit 3 are identical to those in unit 2, except that all rocks in unit 3 are moderately to highly reconstituted texturally, with all the graywackes assigned to textural zones 2 to 3 of Blake, Irwin, and Coleman (1967). The metamorphic mineral assemblages quartz + phengite + lawsonite ± albite ± sodic amphibole [Na₂(Mg,Fe,Al)₃Si₈O₂₂(OH)₂] ± jadeitic pyroxene (NaAlSi₂O₆) has been recognized in graywackes of unit 3, with jadeitic pyroxene present only locally. Basaltic volcanic rocks and cherts interlayered with the graywackes may contain abundant sodic amphibole; the cherts may, in addition, contain stilpnomelane [K(Fe,Al)₁₀Si₁₂O₃₀(O,OH)₁₂].

RELATION OF STRUCTURE TO RESOURCES

Figure 5A illustrates the generalized structural model for a geothermal system indicated by Muffler and White (1972)

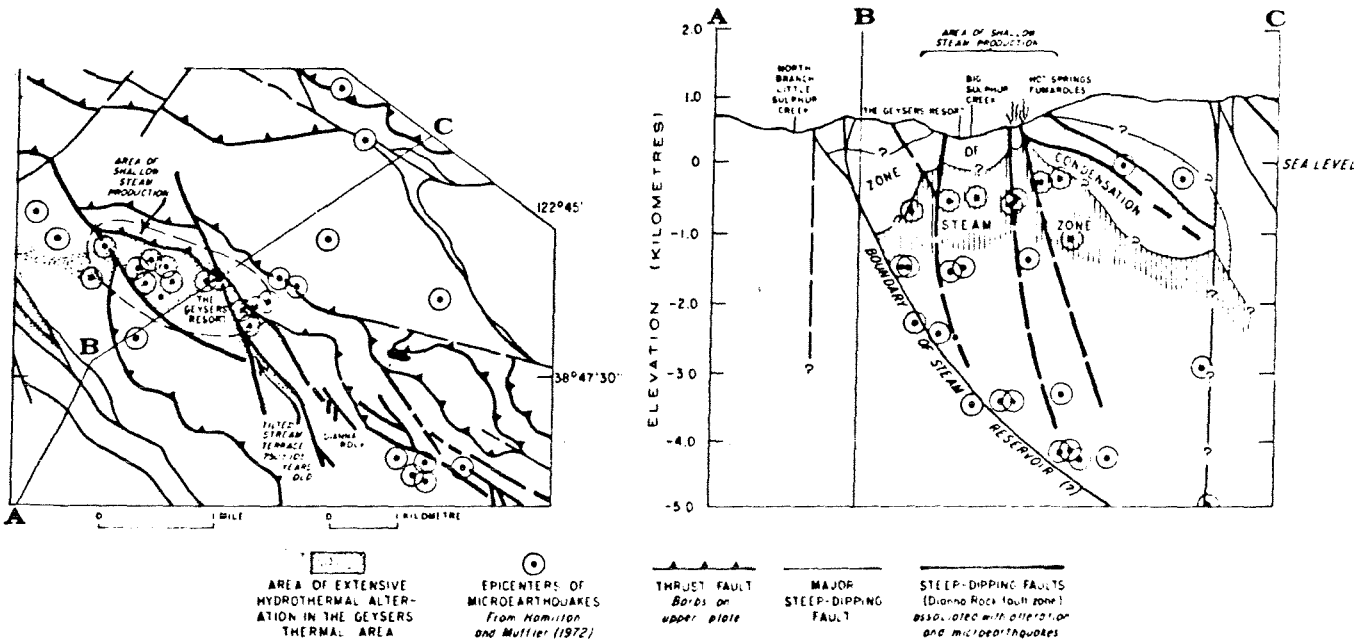


Figure 4. Map showing relation of hydrothermal alteration and microearthquakes to the Dianna Rock fault zone near Geysers Resort. Left: map view. Right: vertical cross section showing distribution of microearthquake hypocenters and inferred relation to steam reservoir.

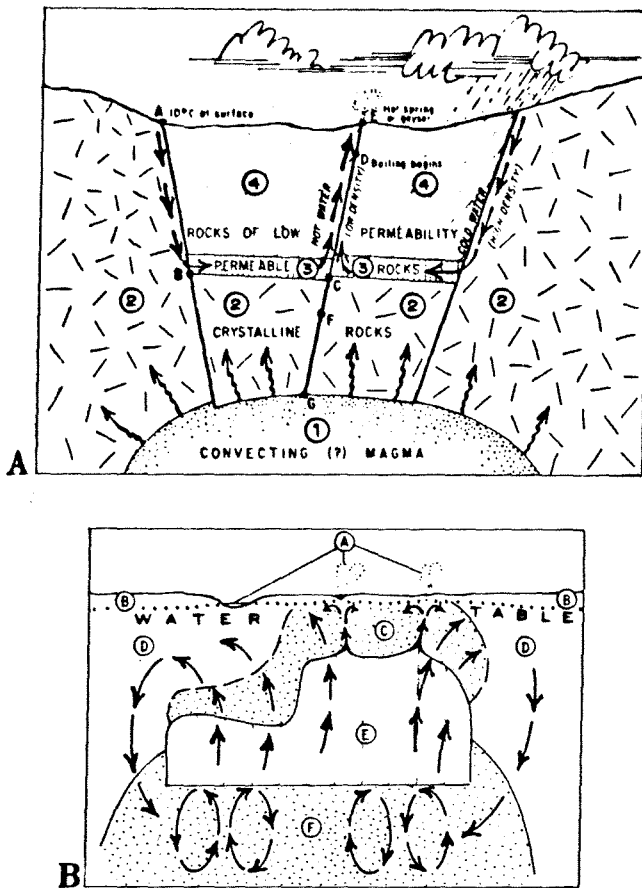


Figure 5. Idealized structural and dynamic models of a vapor-dominated geothermal system. A: Structural model; numbers correspond to references in text (from Muffler and White, 1972). B: Dynamic model (A) springs and fumaroles, (B) zone between ground surface and water table; (C) zone of steam condensation; (D) zone of convective and/or conductive heat flow; (E) zone of vapor-dominated reservoir; (F) deep zone of convective heat flow below a boiling water table (from White and others, 1971).

and Fig. 5B illustrates the generalized dynamic model of a vapor-dominated hydrothermal system as proposed by White, Muffler, and Truesdell in 1971. The essential structural components of a vapor-dominated geothermal system from these models appear to be: (1) a potent heat source within a few kilometres of the surface, overlain or enclosed by (2) thermally conductive crystalline rocks, overlain by (3) a reservoir rock that is overlain by (4) impermeable cap rocks that prevent excessive influx of water, or loss of steam and heat from the reservoir. In a vapor-dominated hydrothermal system the permeability of the reservoir rocks need not be high, so long as there can be sufficient convective circulation of steam and hot water in the zone of condensation above the steam reservoir (Fig. 5B). In The Geysers area this permeability in the reservoir rocks largely results from channelways produced by faults and fractures. At least some of these faults and fractures must have communication with the surface water table in order for there to be adequate, but not excessive, meteoric recharge to the system (White, Muffler, and Truesdell, 1971).

Available subsurface data indicate that steam production in The Geysers region is largely from fracture zones in

Franciscan graywacke. Since imbricate structure is characteristic of the Franciscan assemblage (Fig. 3) a model relating the structure to steam resources would be favored that provides for steam accumulation in graywacke at any of several structural levels. Steam production at The Geysers is largely from wells drilled to depths of 1.5-1.8 km (Hamilton and Muffler, 1972, p. 2084), but some producing wells as shallow as 150 m (McNitt, 1963) have been drilled near Geysers Resort. The reservoir rock for steam in the area of Geysers Resort may be provided in part by the thick slab of graywacke flysch of structural unit 1 that should be present at depth beneath this area (Fig. 3). However, slabs of fractured graywacke are also present in unit 2 rocks overlying unit 1, interlayered with relatively impermeable basaltic volcanic rock, sheared serpentinite, and melange. These structurally higher graywacke slabs may also provide the reservoirs for steam accumulation north and east of Geysers Resort.

Given the presence of suitable reservoir rocks at any of several structural levels, the structural conditions determining the presence of steam would appear to depend upon: (1) the presence of channelways such as faults, fractures, or bedding planes that allow percolation of meteoric water to some depth and provide an adequate but not excessive supply of water to the system, (2) the presence of structural traps for steam accumulation, and (3) a potent heat source.

Field relations and geophysical evidence in two areas illustrate the significance of local structure in controlling steam distribution. In the area of Geysers Resort a zone of N 30°-35°W-trending *en echelon* faults (Dianna Rock fault zone), along which numerous hot springs vent, crosses Big Sulphur Creek and extends into an area of extensive hydrothermal alteration and fumarolic activity (Fig. 4). Steeply tilted alluvial terrace deposits within the fault zone that contain carbonized wood with a radiocarbon age of 750 ± 105 years indicate that the fault zone is active. Recent activity along these faults is also indicated by the epicenters of numerous microearthquakes (Hamilton and Muffler, 1972) that are aligned along the Dianna Rock fault zone. First-motion fault plane solutions for the microearthquakes (Hamilton and Muffler, 1972, p. 2083-84) do not correspond directly to the mapped fault zone, but a plot of the microearthquake hypocenters projected horizontally onto a vertical cross section oriented roughly normal to the trend of epicenters (Fig. 4) suggests the presence of a boundary fault zone above which the microearthquakes occur. The boundary fault zone is inclined at about 55°-60° to the northeast.

Ward and Bjornsson (1971) showed that high frequencies of microearthquakes commonly are associated with geothermal areas, and they concluded that this activity results from the weakening and chemical alteration of rocks along faults and fracture zones owing to saturation by geothermal fluids.

By application of the findings of Ward and Bjornsson to The Geysers area, the Dianna Rock fault zone may be interpreted as a fracture zone lubricated by hot water. The fracture zone is interpreted to extend from the surface downward to a bounding fault inclined steeply to the northeast. The upper part of this fracture zone may correspond to a shallow zone of condensation above the steam reservoir (Fig. 4) since many steam wells near Geysers Resort were drilled to relatively shallow depths of between 50-360 m (McNitt, 1963, p. 14).

Further evidence of significant structural control of steam distribution in The Geysers region is present in the Castle

Rock Springs steam field, approximately 6.5 km southeast of Geysers Resort. The distribution of steam wells in this area indicates that a geothermal reservoir occupies the region of an anticlinal warp in eastward dipping foliate meta-graywacke and shale interlayered with minor basaltic volcanic rock and serpentinite (Fig. 6). Steep dipping N 80°W-trending faults approximately bound the north and south sides of this structural high, possibly providing conduits for recharge of the reservoir with meteoric water. The presence of a closed low resistivity anomaly (Stanley, Jackson, and Hearn, 1973) in this area reinforces the interpretation that conductive fluid is locally concentrated in the crest of this structural high (Fig. 6). This low resistivity anomaly within 2-3 km of the surface probably indicates a structurally high zone of hot water-saturated hydrothermally altered rocks above the steam reservoir, corresponding to the zone of condensation indicated by White, Muffler,

and Truesdell (1971) (Fig. 5B and Fig. 6). Leakage of geothermal water from the reservoir apparently occurs along several steeply dipping N 50°W-trending faults and fractures to the east of Castle Rock Springs, evidenced by the presence of Anderson hot spring and prominent zones of hydrothermal alteration along these faults. In addition to their acting as conduits for thermal leakage, some of these N 50°W-trending faults may also act as conduits for downward percolation of meteoric water for reservoir recharge and for upward migration and entrapment of steam at different structural horizons in the reservoir rocks, although there is no definite evidence to indicate that this occurs. The N 50°W-trending faults may also form the eastern structural boundary of the Castle Rock Springs steam reservoir.

In the two areas discussed, local structure appears to have considerable bearing on the local distribution of steam. It seems probable that such structures are also important

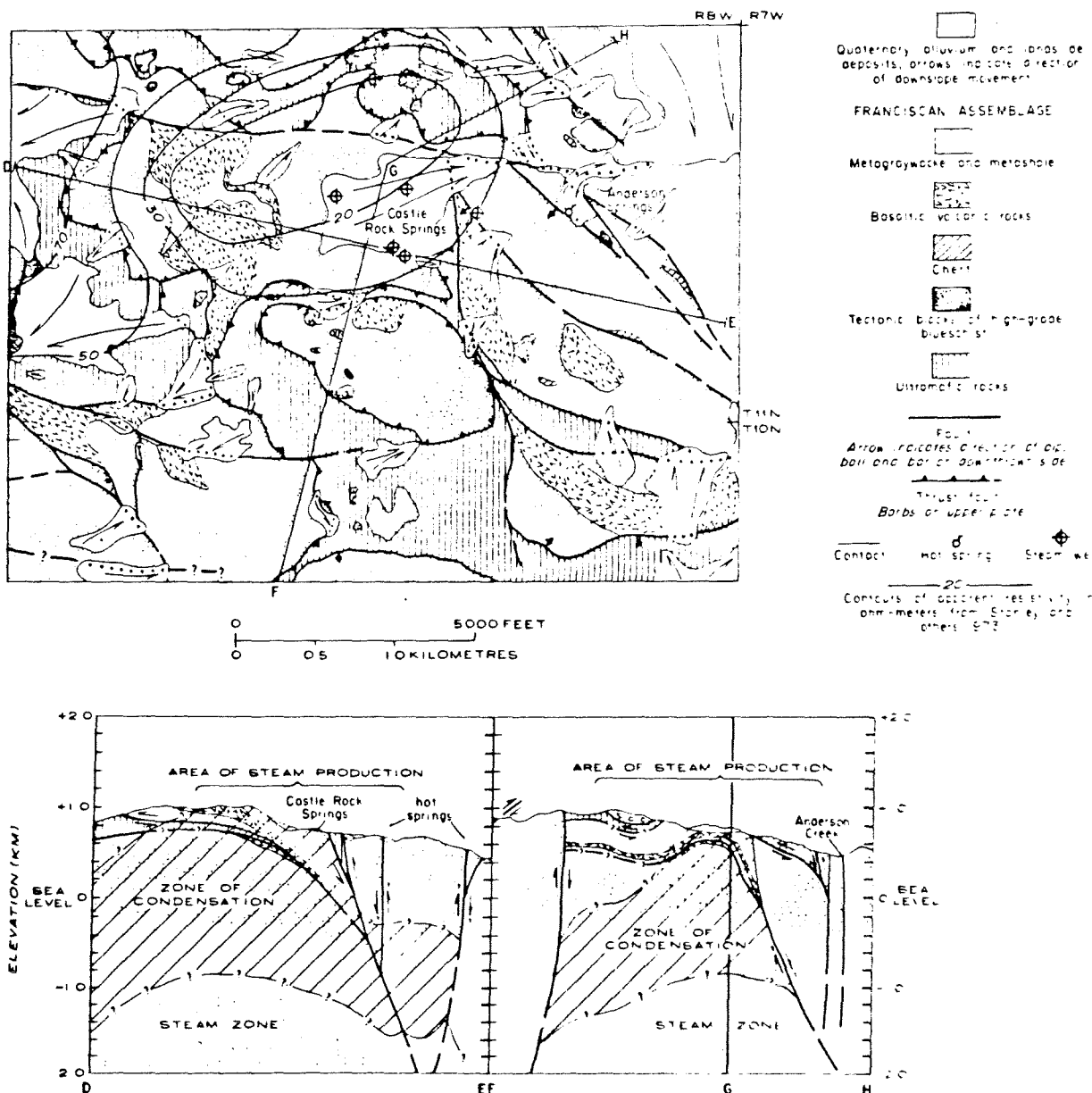


Figure 6. Geologic map and structural sections through the Castle Rock Springs steam field, showing inferred relation of structure and low resistivity anomaly to steam reservoir. Top: map view. Bottom left: structural section D-E. Bottom right: structural section F-G-H.

features of economically significant geothermal reservoirs elsewhere in The Geysers steam field, even though high heat flow and favorable reservoir rocks exist regionally over a vast area.

CONCLUSIONS

Detailed geologic mapping in The Geysers area of the Mayacmas Mountains indicates that the Franciscan assemblage is separable into three approximately stratiform structural units that form the core of a southeastward plunging antiform. A steeply dipping northwest-trending strike-slip fault zone bounds this antiform on the southwest. Textural reconstitution in Franciscan graywackes increases structurally upward, with the corresponding appearance of pumpellyite, lawsonite, and glaucophane, and/or jadeite, respectively, in structurally higher rocks. The Franciscan assemblage is overlain by a fragmented ophiolite complex in the Mount Saint Helena and Geyser Peak areas, and 8-9 km of right-lateral offset of the Mount Saint Helena and Geyser Peak ophiolite masses has occurred along the Geyser Peak fault zone. Elsewhere, the lower part of the ophiolite mass has been sheared into underlying Franciscan rocks along steeply dipping faults, possibly of middle-Tertiary or younger age.

Geothermal resources in The Geysers area tend to be concentrated within imbricated north-northeast- to southeast-dipping slabs of Franciscan graywacke. Critical parameters for economic concentrations of steam in the region appear to be: (1) the presence of channelways that allow percolation of meteoric water to some depth, providing an adequate but not excessive recharge of water to the system; (2) the presence of favorable local structural traps for steam accumulation in fault and fracture zones (such as in the Geysers Resort area) or in the crests of structural highs (such as in the Castle Rock Springs area); and (3) a potent heat source.

ACKNOWLEDGMENTS

Union Oil Co., Burmah Oil and Gas Co., Pacific Energy Corp., Shell Oil Co., and numerous private landowners have cooperated in providing access to their properties. The field work was accomplished with the assistance of D. H. Sorg in 1974, and H. N. Ohlin in 1975. Assignment of ages to radiolaria in cherts of the Franciscan assemblage and ophiolite was done by E. A. Pessagno, Jr., University of Texas at Dallas, and palynomorph studies were done by W. R. Evitt, Stanford University. The manuscript has benefited from reviews by Ken Crawford and Ivan Barnes, and from discussions and field observations with M. C. Blake, Jr., D. L. Jones, E. H. Bailey, and R. G. Coleman, whose previous work and experience with the Franciscan assemblage and Great Valley sequence provided most of the background upon which the geological research was based. The writers are indebted to all their colleagues at the U.S. Geological Survey involved in cooperative studies related to geothermal resources in The Geysers-Clear Lake area.

REFERENCES CITED

- Atwater, T., 1970, Implications of plate tectonics for the Cenozoic tectonic evolution of western America: *Geol. Soc. America Bull.*, v. 81, no. 12, p. 3513-3536.
- Bailey, E. H., 1946, Quicksilver deposits of the western Mayacmas District, Sonoma County, California: *Calif. Jour. Mines and Geology*, v. 42, no. 3, p. 199-230.
- Bailey, E. H., Blake, M. C., Jr., and Jones, D. L., 1970, On-land Mesozoic oceanic crust in California Coast Ranges: *U.S. Geol. Survey Prof. Paper 700-C*, p. C70-C81.
- Bailey, E. H., Irwin, W. P., and Jones, D. L., 1964, Franciscan and related rocks, and their significance in the geology of western California: *Calif. Div. Mines Bull.* 183, 177 p.
- Bailey, E. H., and Jones, D. L., 1973, Metamorphic facies indicated by vein minerals in basal beds of the Great Valley Sequence, northern California: *U.S. Geol. Survey Jour. Research*, v. 1, no. 4, p. 383-385.
- Bezore, S. P., 1969, The Mount Saint Helena ultramafic-mafic complex of the northern California Coast Ranges: *Geol. Soc. America, Abs. (65th Ann. Mtg., Cordilleran Sec.)*, p. 5.
- Blake, M. C., Jr., Irwin, W. P., and Coleman, R. G., 1967, Upside-down metamorphic zonation, blueschist facies, along a regional thrust in California and Oregon: *U.S. Geol. Survey Prof. Paper 575-C*, p. C1-C9.
- Blake, M. C., Jr., and Jones, D. L., 1974, Origin of Franciscan melanges in northern California: *Soc. Econ. Paleontologists and Mineralogists Spec. Pub.* 19, p. 345-357.
- Brice, J. C., 1953, Geology of Lower Lake quadrangle, California: *Calif. Div. Mines Bull.* 166, 72 pp.
- Coleman, R. G., and Lanphere, M. A., 1971, Distribution of age of high-grade blueschists, associated eclogites, and amphibolites from Oregon and California: *Geol. Soc. Amer. Bull.*, v. 82, no. 9, p. 2397-2412.
- Coleman, R. G., and Lee, D. E., 1963, Glaucophane-bearing metamorphic rocks of the Cazadero, California: *Jour. Petrology*, v. 4, p. 260-301.
- Dickinson, W. R., Ojakangas, R. W., and Stewart, R. J., 1969, Burial metamorphism of the Late Mesozoic Great Valley sequence, Cache Creek, California: *Geol. Soc. Amer. Bull.*, v. 80, no. 3, p. 519-526.
- Ernst, W. C., 1971, Do mineral parageneses reflect unusually high-pressure conditions of Franciscan metamorphism?: *Amer. Jour. Sci.*, v. 270, p. 81-108.
- Hamilton, R. M., and Muffler, L. J. P., 1972, Microearthquakes at The Geysers geothermal area, California: *Jour. Geophys. Research*, v. 77, no. 11, p. 2081-2086.
- Hamilton, W., 1969, Mesozoic California and the underflow of Pacific mantle: *Geol. Soc. Amer. Bull.*, v. 80, no. 12, p. 2909-2429.
- Lanphere, M. A., Blake, M. C., and Irwin, W. P., 1975, Early Cretaceous metamorphic age of the South Fork Mountain schist in the northern Coast Ranges of California: *Geol. Soc. America, Abs. (71st Ann. Mtg., Cordilleran Sec.)*, p. 840.
- McLaughlin, R. J., 1974, Preliminary geologic map of The Geysers steam field and vicinity, Sonoma County, Calif.: *U.S. Geol. Survey Open-file Map 74-238*.
- McNitt, J. R., 1963, Exploration and development of geothermal power in California: *Calif. Div. Mines and Geology Spec. Rept.* 75, 44 p.
- McNitt, J. R., 1968, Geology of the Kelseyville quadrangle, Sonoma, Lake, and Mendocino Counties, Calif.: *Calif. Div. Mines and Geology, Map sheet 8*.
- Muffler, L. J. P., and White, D. E., 1972, Geothermal energy: *The Science Teacher*, v. 39, no. 3, p. 1-4.
- Stanley, W. D., Jackson, D. B., and Hearn, C. B., Jr., 1973, Preliminary results of geoelectrical investigations near Clear Lake, California: *U.S. Geol. Survey Open-file Rept.*
- Swe, W., and Dickinson, W. R., 1970, Sedimentation and thrusting of late Mesozoic rocks in the Coast Ranges

- near Clear Lake, California: Geol. Soc. America Bull., v. 81, no. 1, p. 165-188.
- Ward, P. L., and Bjornsson, S., 1971, Microearthquakes, swarms, and the geothermal areas of Iceland: Jour. Geophys. Research, v. 76, no. 17, p. 3953-3982.
- White, D. E., Muffler, L. J. P., and Truesdell, A. H., 1971, Vapor dominated hydrothermal systems compared with hot water systems: Econ. Geology, v. 66, no. 1, p. 75-97.
- Yates, R. G., and Hilpert, L. S., 1946, Quicksilver deposits of eastern Mayacmas District, Lake and Napa Counties, Calif: Calif. Jour. Mines and Geology, v. 42, no. 3, p. 231-286.

Compressional and Shear Waves in Saturated Rock During Water-Steam Transition

HISAO ITO,¹ JOHN DEVILBISS, AND AMOS NUR

Rock Physics Project, Department of Geophysics, Stanford University, Stanford, California 94305

Compressional and shear wave velocities were measured in water-filled Berea sandstone as a function of pore pressure, with a constant confining pressure of 300 bars. The measurements were made at room temperature, 145°C, and 198°C. At 145°C, compressional velocity increased from vapor-saturated (low pore pressure) to liquid-saturated (high pore pressure) conditions, whereas shear wave velocity decreased. For compressional waves there was a velocity minimum and increased attenuation near the liquid-vapor transition. The results at 198°C show decreases of both compressional and shear velocities and a small velocity minimum for compressional velocity without marked attenuation. At both temperatures, V_p/V_s and Poisson's ratios increased from steam- to water-saturated rock. The results are compatible with the mechanical effects of mixing steam and water in the pore space near the phase transition and may be applicable to in situ geothermal field evaluation.

INTRODUCTION

Seismic methods are among the most important techniques used to explore for and evaluate geothermal reservoirs. These include microearthquake surveys for locating reservoirs, and physical property determinations, such as Poisson's ratio and seismic wave attenuation, for delineating the boundaries and state of reservoirs. The latter measurements are particularly interesting for the possible distinction between steam-bearing and hot water domains.

Hayakawa [1970] conducted a seismic reflection experiment at the Matsukawa geothermal area in Japan and obtained several strong reflections from the interface between cap rock and water reservoir. Denlinger and Kovach [1978] conducted a seismic reflection survey near the Geysers, California. They observed several strong reflections in situ which could be related to steam-producing fracture zones. Combs and Rotstein [1976] found extremely low values of V_p/V_s and Poisson's ratios in the Coso geothermal area. This suggests that the shallow subsurface rock is either undersaturated with respect to ground water or else contains steam in the pore spaces. They suggest on the basis of laboratory-observed Poisson's ratios at room temperatures [Nur and Simmons, 1969] that it may be possible to predict whether a geothermal system is vapor or hot water dominated. Recent results from the Geysers, California (H. M. Iyer, personal communications, 1979), suggest that seismic compressional waves may be strongly attenuated in the steam-bearing zone of the field.

The mechanisms by which steam influences Poisson's ratio σ and wave attenuation in hot rocks are not well established. The expectation that the compressional wave velocity V_p is low in relation to the shear velocity V_s with a corresponding low σ is based on laboratory measurements at room temperatures with air, not at geothermal reservoir conditions. The observed high attenuation for compressional waves has so far remained an empirical fact only, without adequate explanation or experimental verification. Experimental verification of the above effects at temperatures corresponding to geothermal reservoirs are clearly needed. At present, there are only few laboratory velocity measurements in rocks with water at ele-

vated temperatures [e.g., Spencer and Nur, 1976; Timur, 1977], and no data are available at all for steam-saturated rocks at these conditions.

This study fills in part of the data gap. Specifically, we report measured results of both compressional and shear velocities and wave amplitudes in porous rock at geothermal temperatures as the water in the pores is converted from liquid to vapor. Although the laboratory measurements are made over a frequency range which is 10^2 - 10^6 higher than typical in situ studies, the results should provide important physical insight into the effects of steam on wave propagation in porous rocks.

EXPERIMENTAL PROCEDURE

Measurements were made of the travel times and amplitudes of ultrasonic pulses in samples of Berea sandstone containing high-temperature pore water. In the experimental procedure, confining pressure and temperature are held constant, whereas the pore pressure is changed so that the pore fluid itself changes from liquid hot water to steam.

The samples are cylindrical in shape, 19 mm in diameter and 25 mm in length. The ends of the samples are ground parallel to within ± 0.05 mm. Samples are soaked in acetone to remove oil introduced during the grinding procedure and dried in a vacuum over (60°C, 760 mm Hg) for over 24 hours. They are then saturated with distilled, deionized water and sealed in a seamless annealed copper jacket (0.25-mm thickness).

The jacketed sample is placed under confining pressure and subjected to independently controlled pore pressure in an externally heated pressure vessel. The temperature, measured with a metal sheathed chromel/alumel thermocouple located adjacent to the copper jacket, is controlled to within $\pm 1^\circ\text{C}$ (using a Research Inc., 640 U Process Controller). The temperature is raised slower than $1^\circ\text{C}/\text{min}$ in order to avoid formation of new cracks [Richter and Simmons, 1974]. The pore water is controlled to about ± 0.1 bar through two capillary tubes, silver soldered into each end plug, at each end of the sample to ensure uniform pore pressure throughout the sample. A schematic diagram of the system is shown in Figure 1.

Ultrasonic compressional and shear wave velocities and amplitudes are measured using the conventional pulse transmission method, with a mercury delay line as a reference. In these experiments compressional and shear waves are generated using lead zirconate titanate (PZT) ceramic transducers (1 MHz)

¹On leave from Geological Survey of Japan, Takatsuku, Kawasaki, 213, Japan.

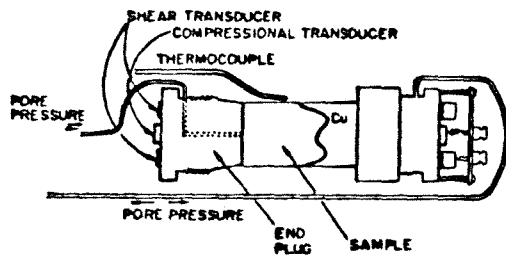


Fig. 1. Schematic diagram of the sample assembly.

which are glued with high-temperature conductive epoxy to short stainless steel plugs at each end of the sample. To generate clear shear waves we use a composite torsional transducer instead of the common shear plate transducer. A mode switch selects the compressional or shear transducer so that both velocities are measured under simultaneous conditions. Velocities in the sample are determined after the travel time through the end plugs is subtracted. The precision of the velocity measurements is better than 0.5%, and the accuracy is $\pm 3\%$.

Samples of Berea sandstone used were drilled perpendicular to the bedding plane. The porosity and grain density were measured to be 18.9% and 2.66 g/cm³, respectively. Several physical properties of Berea sandstone are summarized as follows:

grain density	2.66
total porosity	18.9%
	18.75%
crack porosity	0.25%
pore porosity	18.50%
water permeability	160 mdarcy

Grain density and the first value given for total porosity are from the present measurement, the second value given for total porosity, crack porosity, pore porosity, and water permeability are from *Zoback [1975]*.

DATA

Measurements in these experiments were made at the constant confining pressure of 300 bars and the temperature of 19°C, 145°C, and 189°C as a function of pore pressure. The pore pressure was changed from high pore pressure to low pore pressure (decreasing pore pressure cycle) and then increased again (increasing pore pressure cycle). At 19°C water pore pressure over the range from 0.0 to 7.0 bars produced almost no change in either V_p or V_s . In contrast, there are marked changes in the velocities, Poisson's ratios, and wave amplitudes with changing pore pressure at 145°C and 198°C. The results show in particular the following:

1. At 145°C there is a minimum in compressional velocity at a pore pressure of around 4 bars (Figure 2), which is very close to the water-vapor transition pressure of 4.2 bars at 145°C [*Keenan et al., 1969*]. Below this pore pressure the water is in the vapor phase, and above this pressure it is liquid. A minimum in shear wave velocity, in contrast, is not observed near the phase transition.

2. The compressional wave velocity in steam-filled rock is lower than that in water-filled rock. In contrast, the shear wave velocity is higher in steam-filled rock (Figure 2).

3. The Poisson's ratio and V_p/V_s ratio increase from steam saturation to water saturation (Figure 3).

4. There are marked changes in the wave amplitudes with pore pressure as shown in Figure 4, with a very sharp drop in the compressional wave amplitude at the water-vapor transition. This loss of amplitude is reproducible upon pore pressure cycling. In contrast, there is no minimum in the shear wave amplitude.

5. Both P and S amplitudes are greater when the pore fluid is vapor and smaller when it is hot water (Figure 4).

6. The time intervals from the first compressional arrival to the first, second, and third peaks were measured versus pore pressure (Figure 5). A maximum time interval, corresponding to a lower average wave frequency, was observed for the compressional wave but not for the shear wave near the water-steam transition. This suggests that the high-frequency components of the compressional wave are significantly more attenuated near the water-vapor transition.

At 198°C, with transition pressure of 14.9 bars, the behavior of wave velocities and amplitudes exhibits the following dependence on pore pressure: (1) there is a small maximum in compressional wave velocity (Figure 6) but little anomalous attenuation is observed (Figure 7); (2) both shear and compressional wave velocities decrease from steam-saturated (low pore pressure) to water-saturated (high pore pressure) rock (Figure 6); and (3) Poisson's ratio and V_p/V_s ratio increase from steam-saturated to water-saturated rock much like the 145°C data (Figure 3).

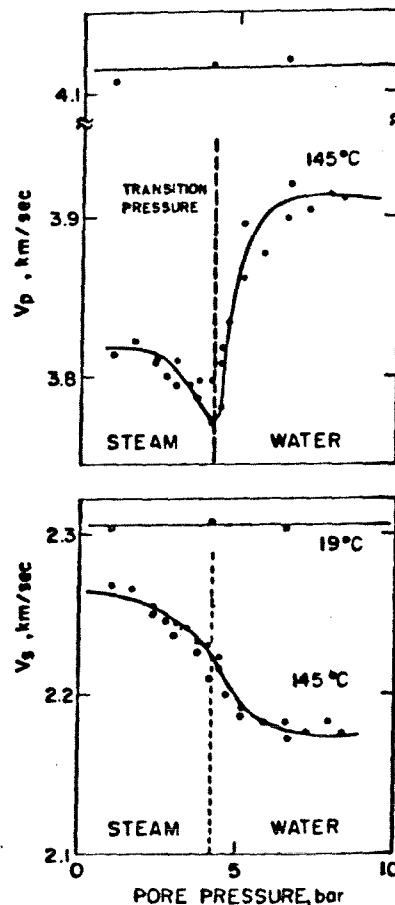


Fig. 2. Compressional V_p and shear wave velocity V_s versus pore pressure at 19°C and 145°C. Open circles show the data during decreasing pore pressure. The phase transformation pressure of 4.2 bars at 145°C is shown by the dashed line. The solid line is a free hand fit to the data.

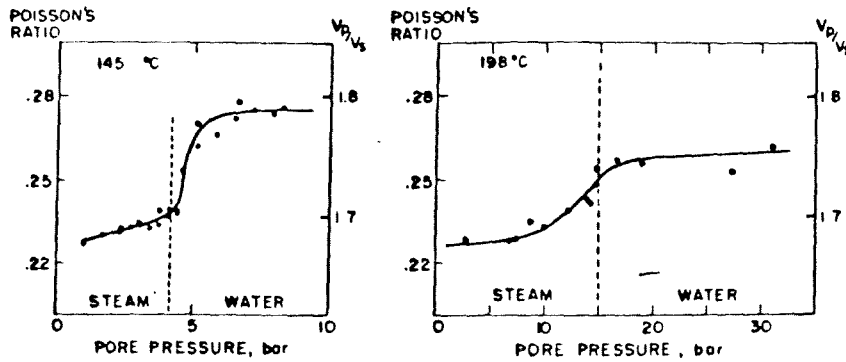


Fig. 3. Poisson's and V_p/V_s ratios versus pore pressure at 145°C and 198°C.

DISCUSSION

The simplest mechanism which seems capable of explaining the observations involves the combined effects of compressibility and density of a water and steam mixture, without direct interaction of the wave with the phase transformation process [Walsh, 1973]. Assuming that such a mixture is present in the rock near the phase transition for water, we can compute the bulk density and changes of bulk modulus of the rock as the fluid changes from steam to water. At low pore pressure where the rock is steam saturated, the bulk density is, ignoring the very small density of steam,

$$\rho_1 \approx \rho_m(1 - \phi) \tag{1}$$

where ρ_m is the mean grain density, ϕ is the porosity, and the bulk and shear moduli are K and μ , respectively. The velocities are

$$V_p = \left[\frac{K + (4/3)\mu}{\rho} \right]^{1/2} \quad V_s = \left[\frac{\mu}{\rho} \right]^{1/2} \tag{2}$$

At high pore pressure, where the rock is saturated with hot water, the density is

$$\rho_2 = \rho_m(1 - \phi) + \rho_f \phi \tag{3}$$

where ρ_f is the density of water at the given pressure and temperature conditions. The water-filled bulk K_2 and shear μ_2 moduli can be estimated from Gassman's relations, assuming that they apply [e.g., Spencer and Nur, 1976]:

$$\mu_2 = \mu_1 \quad K_2 = K_m \frac{K_1 + Q}{K_m + Q} \quad Q = \frac{K_1 K_m - K_1}{\alpha K_m - K_1} \tag{4}$$

where K_1 is the bulk modulus of the water, ϕ is the porosity, and K_m is the bulk modulus of the mineral grains. The shear

modulus is predicted to remain unchanged from steam to hot water, but the bulk density increases. Consequently, (2) predicts a lower V_s for water-saturated rock. For Berea sandstone, with $\phi = 0.19$, the predicted density decrease is $\Delta\rho/\rho \approx 0.09$, and hence $\Delta V_s/V_s \approx 0.04-0.05$, in agreement with the observed change of 0.04. The smooth and smeared out transition of V_s with pore pressure (Figure 2) suggests that the phase transformation does not occur at the same time throughout the rock. Instead, it may occur over a pore pressure interval, beginning at 1-2 bars below the transformation pressure at 145°C and ending 1-2 bars above. The shear velocity thus decreases smoothly with increasing density owing to decreasing amount of steam in the rock.

In contrast, the bulk modulus in water-saturated rock is higher than in a steam-saturated one, owing to the higher bulk modulus of the water compared with steam. Taking $K_1 \approx 1.7 \times 10^5$ bars from the data, $\phi = 0.19$, $K_f \approx 2 \times 10^4$ bars [Keenan et al. 1969], and $K_m \approx 3 \times 10^8$ bars [Simmons and Wang, 1971], we compute from (2) the water-saturated bulk modulus $K_2 \approx 2.6 \times 10^8$ bars. Compared with the measured value of $K_2 = 2.1 \times 10^8$, the agreement is reasonable.

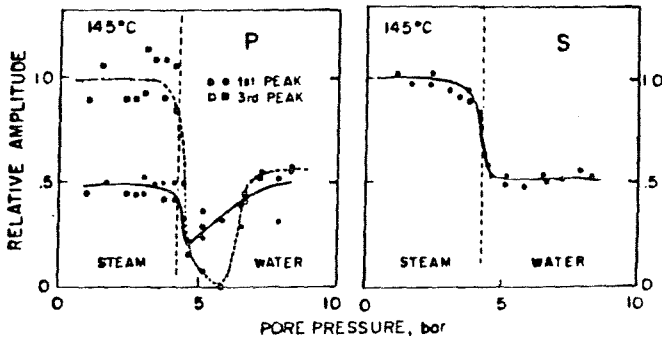


Fig. 4. Relative peak amplitudes of compressional P and shear S waves versus pore pressure at 145°C. Amplitudes at zero pore pressure are taken as unity.

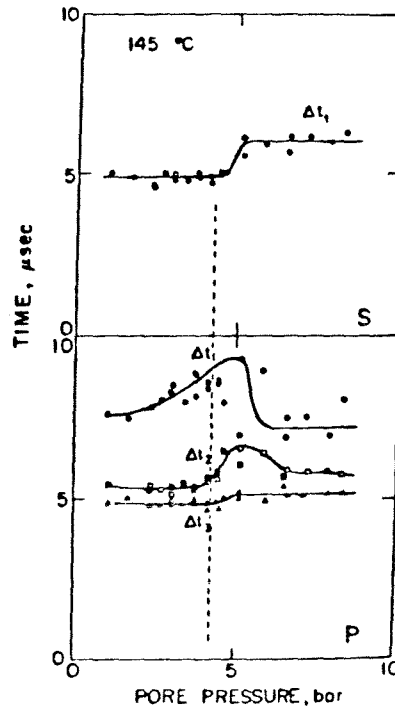


Fig. 5. Time intervals between the first arrival and the first (Δt_1), second (Δt_2), and third peaks (Δt_3) for compressional P and shear S waves at 145°C.

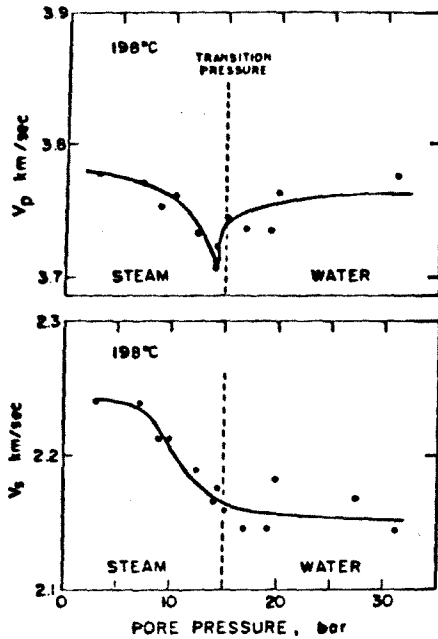


Fig. 6. Compressional and shear wave velocities versus pore pressure at 198°C. Phase transition pressure is shown by the dashed line.

We suggest that the minimum of the compressional velocity near the phase transformation may be due to the combined effect of increasing density as more and more steam transforms into water and the low fluid bulk modulus which remains low as long as any steam is present. To a first approximation the bulk modulus of the fluid phase K_f is given by the simple average

$$K_f^{-1} = \alpha K_{\text{steam}}^{-1} + (1 - \alpha) K_{\text{water}}^{-1} \quad (5)$$

where α is the fraction of steam in the pore space. Because $K_{\text{steam}} \ll K_{\text{water}}$, the value of K_f will remain low except when α is close to unity. Thus during the steam-water transition the bulk density is relatively high (close to the density of water-saturated rocks), whereas the fluid bulk modulus is low (close

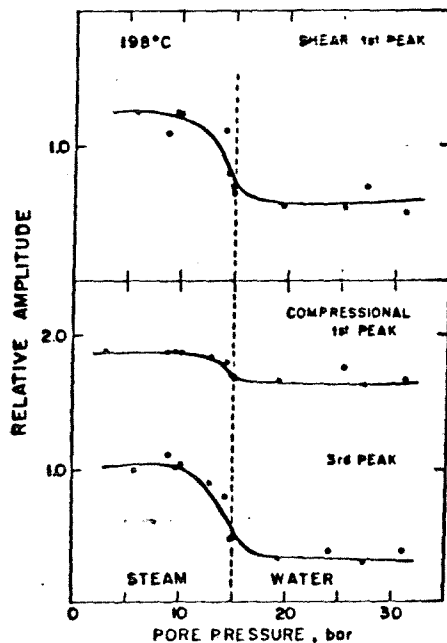


Fig. 7. Peak amplitude of compressional and shear waves versus pore pressure at 198°C.

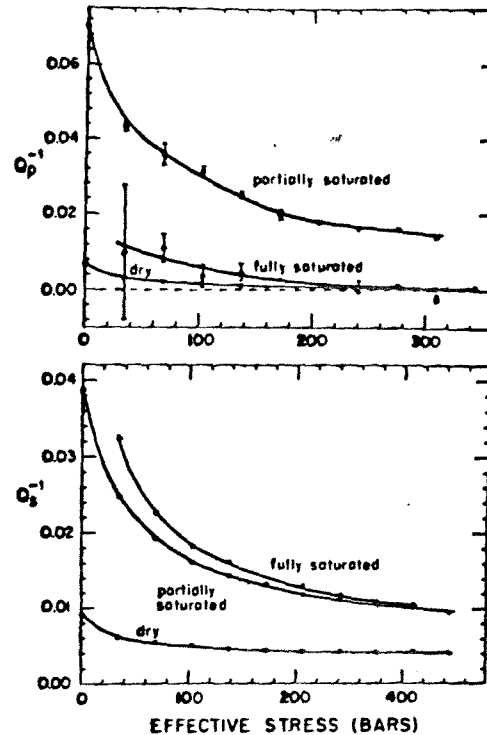


Fig. 8. Attenuation characteristics of dry, partly saturated, and fully saturated Massilon sandstone [from Winkler and Nur, 1979].

to that of steam). Taking again $\phi = 0.19$, we expect a density effect on V_p of up to 4%, comparable with the one observed for shear waves. As was seen in Figure 2, the lowest V_p value at the transition is about 2% lower than V_p with steam. Thus the observed effect is somewhat smaller than that calculated using the simplistic model. However, any increase in K_f above the steam value and decrease of density below the fully saturated value will tend to decrease the low velocity anomaly. We conclude therefore that the changes of V_p and V_s across the steam-water transition are consistent with the effects of simple mixing of hot water and steam during a sluggish phase transformation.

The role of the density in the mixed fluid phase is confirmed to some extent by the computed Poisson's ratio (Figure 3), which is independent of the density of the sample. We notice a simple increase from a low value in steam-saturated to a higher value in water-saturated rock, with monotonic change through the phase transformation. This is exactly the pattern expected from the changes in fluid compressibility.

We next show that the mixing mechanism explains also the observed attenuation characteristics, again without resort to a special interaction of the waves with the transformation mechanism. The nature of attenuation of seismic waves in rock saturated with steam, water, or a mixture of both may be inferred from experimental results at room temperature if it is assumed that the controlling factor is the compressibility of the fluid phase in the pores [Mavko and Nur, 1979; Kjartansson and Denlinger, 1977]. Recent measurement of Q_p^{-1} and Q_s^{-1} in fully saturated, partially saturated, and room dried sandstones [Winkler and Nur, 1979] revealed the following pattern, summarized in Figure 8. The values of Q_p^{-1} and Q_s^{-1} in room dry rocks are both relatively low, whereas fully saturated rocks show relatively large losses in shear but small losses in compression. In partially saturated rock, losses in compression are, in contrast, very large, much greater than in either the partly or fully saturated shear case. These qualitative results suggest

that in steam-saturated rock both Q_p^{-1} and Q_s^{-1} are expected to be relatively low; in the transition, Q_s^{-1} increases somewhat to its highest value in the water-saturated case. Q_p^{-1} , in contrast, should be very large in the transition region, with measurable decrease in the water-saturated state. This predicted behavior is consistent with the observed amplitude and frequency content data in this paper: (1) P and S amplitudes are relatively large in the steam-saturated rock; (2) the P amplitude is very low in the transition region and recovers in the water-saturated rock to about $\frac{1}{2}$ of the steam-saturated value; (3) the S amplitude gradually decreases in the transition region to a lower value in the water-saturated state; (4) the P frequency content is lowest in the transition.

The exact physical mechanism for the attenuation of seismic waves is not clear as yet: *Mavko and Nur* [1979] have proposed a local flow mechanism, which is particularly effective for compression in partially saturated rock and thus qualitatively consistent with observation. *Kjartansson and Denlinger* [1977] have proposed a thermal relaxation mechanism which is also fairly consistent with observations. Their mechanism predicts a rather strong dependence on temperature, which might help in explaining the differences between the behavior at 145°C and 198°C. Furthermore, the reasons for the smeared out nature of changes in velocities and amplitudes near the phase transformation are not clear. Aside from possible experimental causes which have not been identified, such smearing out may be caused by actual spreading of the transformation throughout the rock, with higher pressure required in narrower pores or microcracks. This effect may be specifically caused by localized anomalous capillary pressures in very thin cracks. *Kjartansson and Denlinger* [1977] have suggested also that thermal disequilibrium may be important, depending on wave length, temperature, and crack width. In their mechanism at least part of the attenuation in the transition region is caused by local heat flow between fluid and solid phases. The question is further complicated by the presence of clay minerals in the rock, which might influence the details of the transformation.

CONCLUSIONS

We have investigated ultrasonic wave propagation in Berea sandstone containing steam, water, and a mixture of vapor and liquid. The results show that V_p is abnormally low near the liquid-vapor phase transformation at 145°C and 4 bars pore pressure. The shear velocity does not have a minimum value during the transition. Poisson's ratio undergoes a marked increase upon transition from the steam-saturated to the water-saturated state. The amplitude of the P wave at 145°C also has a strong minimum near the phase transition, whereas the shear wave amplitude increases from liquid to vapor saturation.

All these results may be explained by the effects of a mixture of steam vapor and water in the pores at the transition conditions. For a few percent steam the density of the mixture is relatively high and similar to water, whereas the bulk modulus K is low and similar to steam. The shear velocity, which is insensitive to the bulk modulus of the fluid inclusions is therefore barely influenced, whereas the compressional velocity is sensitive to K and undergoes a measurable change. Further-

more, the increased attenuation of compressional waves near the liquid-vapor transition is probably due to localized fluid flow.

The results of this study suggest that in situ interfaces between steam- and hot water-saturated rock, if they exist, may be recognizable in detail by using high-resolution seismic methods. Furthermore, regions with both steam and hot water should exhibit anomalously low velocity and high attenuation of P waves but not of S waves. Poisson's ratio is, as expected, a good discriminator between steam and hot water in the pore space and may be a useful tool, as has been suggested in the past [e.g., *Combs and Rotstein*, 1976], on the basis of room temperature measurements. The data presented here demonstrate that the conclusion may actually be valid also at temperatures anticipated in geothermal areas.

Acknowledgments. We thank John Weeks and Peter Gordon, who helped in the design, construction, and initiation of various parts of this project. We are grateful to J. Spencer and Kate Hadley for their extensive and critical review of this manuscript. We are also indebted to J. Walls for the shear transducer design and extensive discussions. This study was supported by grant EY-76-S-03-0326 PA#45 from the Office of Basic Energy, the Department of Energy.

REFERENCES

- Combs, T., and Y. Rotstein, Microearthquake studies of the Coso geothermal area, China Lake, California, *Proc. 2nd U.N. Symp., Develop. Use Geothermal Res.*, 2, 909-916, 1976.
- Denlinger, R. P., and R. L. Kovach, Gravity and seismic observations in the Geysers geothermal area, Northern California (abstract), *Eos, Trans. AGU*, 59(12), 1200, 1978.
- Hayakawa, M., The study of underground structure and geophysical state in geothermal areas by seismic exploration, *Geothermics, Spec. Issue 2*, 2(1), 347-357, 1970.
- Keenan, J. H., F. G. Keyes, P. G. Hill, and J. G. Moore, *Steam Tables*, John Wiley, New York, 1969.
- Kjartansson, E., and R. P. Denlinger, Seismic wave attenuation due to thermal relaxation in porous media paper presented at 47th Meeting of SEG, Society of Exploration Geophysicists, Calgary, Canada, 1977.
- Mavko, G. M., and A. Nur, Wave attenuation in partially saturated rocks, *Geophysics*, 44(2), 161-178, 1979.
- Nur, A., and G. Simmons, The effect of saturation on velocity in low porosity rocks, *Earth Planet. Sci. Lett.*, 7, 183-193, 1969.
- Richter, D., and G. Simmons, Thermal expansion behavior of igneous rocks, *Inter. J. Rock Mech. Mining Sci. Geomech. Abstr.*, 11, 403-411, 1974.
- Simmons, G. S., and H. Wang, *Single Crystal Elastic Constants and Calculated Aggregate Properties: A handbook*, MIT Press, 370pp., Cambridge, Mass., 1971.
- Spencer, J., and A. Nur, The effects of pressure, temperature, and pore water on velocities in Westerly granite, *J. Geophys. Res.*, 81, 899-904, 1976.
- Timur, A., Temperature dependence of compressional and shear wave velocities in rocks, *Geophysics*, 42(5), 950-956, 1977.
- Walsh, J. B., Wave velocity and attenuation in rocks undergoing polymorphic transformations, *J. Geophys. Res.*, 78, 1253-1261, 1973.
- Winkler, K., and A. Nur, Pore fluids and seismic attenuation in rocks, *Geophys. Res. Lett.*, 6(1), 1-4, 1979.
- Zoback, M. D., High pressure deformation and fluid flow in sandstone, granite and granular materials, Ph.D. thesis, Stanford Univ., Stanford, Calif., 1975.

(Received September 19, 1978;
revised January 25, 1979;
accepted February 27, 1979.)

PORE FLUIDS AND SEISMIC ATTENUATION IN ROCKS

Kenneth Winkler and Amos Nur

Rock Physics Project

Geophysics Department,

Stanford University, Stanford, California 94305

Abstract. Seismic attenuation and velocities were measured in resonating bars of Massillon sandstone at various degrees of saturation. Whereas shear energy loss simply increases with degree of saturation, bulk compressional energy loss increases to ~95% saturation and then rapidly decreases as total saturation is achieved. This behavior is analogous to the behavior of shear and compressional velocities, but the effect on attenuation is larger by an order of magnitude. Our observations are in excellent agreement with the predictions of several models of energy loss involving partial or total saturation. Pore fluid attenuation mechanisms are expected to be dominant at least in the shallow crust.

Introduction

In recent years seismic attenuation has become of increasing interest to seismologists. This interest ranges from simultaneous inversion of velocity and attenuation data to obtain improved earth models [Randall, 1976], to the study of "bright spots" in hydrocarbon exploration [Sheriff, 1975]. To make full use of seismic data, it is necessary to interpret attenuation in terms of the physical properties of rocks. We need to know what mechanisms are responsible for loss of energy in seismic waves. Recently we have shown that the popular grain boundary friction mechanism is not important in the earth [Winkler *et al.*, 1979; Mavko, 1979]. In this paper we present evidence in support of another mechanism—fluid flow energy loss—which we believe to be dominant at least in the shallow crust.

The effect that pore fluids have on seismic velocities is well documented [Nur and Simmons, 1969; Elliot and Wiley, 1975; Domenico, 1976]. It is natural to suppose that pore fluids will also influence seismic attenuation, but very little experimental work has been done in this area. There is, however, no shortage of theoretical models of fluid loss mechanisms. Biot [1956] has considered inertial effects and macroscopic flow, but the resulting energy losses are probably insignificant below ultrasonic frequencies [White, 1965]. Viscous shear relaxation has also been shown to be a high frequency (or low viscosity) mechanism [Walsh, 1969; O'Connell and Budiansky, 1977] and is not important below ultrasonic frequencies for water saturated rocks. Inter crack "squeezing" flow [Mavko and Nur, 1975; O'Connell and Budiansky, 1977] may be important at low frequencies in fully saturated rock. White [1975] has presented a model for energy loss in macroscopically partially saturated rock that may be important in the earth, but is probably not important in the laboratory because of the small sample dimensions. A flow model based on partial saturation of individual cracks has been discussed by Mavko and Nur [1979], and a thermoelastic partial saturation mechanism has been presented by Kjartansson and Denlinger [1977]. Both models make similar predictions as to the relative size of shear and compressive energy losses, and either may explain the observations of Born [1941] and Gardner *et al.* [1964] that increasing fluid saturation causes increasing attenuation. Johnston and Toksöz [1977] have presented the first data on fully saturated rock, measured at ultrasonic frequencies. Although they concluded that fluid losses were negligible compared to frictional losses, other interpretations are possible.

Experimental Procedure

We have presented some experimental details in a previous paper [Winkler *et al.*, 1979] and will expand upon those here. However, a complete description of our experiments will be given in a forthcoming paper. We are using a bar resonance technique similar in principle to those used by Born [1941] and by Gardner *et al.* [1964]. Our samples are one meter long with a rectangular cross-section of 2.0 x 1.9 cm. Both torsional and extensional resonance modes are studied, with the fundamental resonance frequencies between 500–1700 Hz, depending on satu-

ration and stress conditions. Resonance frequencies are measured to 1 part in 10³ and converted to velocities using geometric corrections given by Spinner and Tefft [1961]. For the samples used in this study the conversions are $V_E = 2f_E$ and $V_S = 2.18 f_T$ where V_E and V_S are the extensional velocity and shear velocity, respectively, in m/sec and f_E and f_T are the corresponding resonance frequencies in Hz. P-wave velocity and Poisson's ratio are calculated from this data.

In this study the attenuation data was obtained by measuring the time constant of resonance decays using the relation $\tau = Q/\pi f$ where Q is the specific dissipation function. The same data could have been obtained from the half-width of resonance peaks, but we have used the peaks only to insure the purity of the resonance modes. Our system has been calibrated against an aluminum sample, and we estimate an absolute accuracy of 5–10% for our attenuation measurements. Relative precision is ~1%.

A unique feature of the experiments reported here is that pore pressure is controlled independently of confining pressure. The sample is jacketed with heat-shrink tubing with a light epoxy coating. Pore pressure is applied through capillary tubing connected to the sample at the support which is at the node of the fundamental resonance. The ability to control pore pressure is critical to the results presented here.

An additional feature involves our method of data analysis. Although we are measuring torsional (shear) and extensional (Young's modulus) attenuation, it is very useful to calculate P-wave attenuation (for use in seismology) and bulk compressional attenuation (for evaluation of mechanisms). To do this we have assumed that we can describe a solid using complex elastic moduli with small imaginary components and that the material is isotropic so that only two moduli are required. We use the correspondence principle [Fung, 1965] which lets us substitute complex moduli for their corresponding real moduli in the equations of linear elasticity. We also use the definition of attenuation (Q^{-1}) favored by O'Connell and Budiansky [1978], $Q^{-1} = \text{Im}(M)/\text{Re}(M)$, where M represents the complex modulus controlling a certain type of wave propagation. Straightforward algebra leads to the following results relating various measures of attenuation.

$$\frac{(1-\nu)(1-2\nu)}{Q_P} = \frac{1+\nu}{Q_E} - \frac{2\nu(2-\nu)}{Q_S} \quad (1)$$

$$\frac{1-2\nu}{Q_K} = \frac{3}{Q_E} - \frac{2(\nu+1)}{Q_S} \quad (2)$$

$$\frac{1+\nu}{Q_K} = \frac{3(1-\nu)}{Q_P} - \frac{2(1-2\nu)}{Q_S} \quad (3)$$

Q_S , Q_E , Q_P , Q_K represent the Q 's of shear waves, extensional waves, P-waves, and bulk compression, respectively. Poisson's ratio (ν) must be calculated from the velocities. It can also be shown that one of the following relations must be true.

$$Q_S > Q_E > Q_P > Q_K$$

$$\text{or} \quad Q_S = Q_E = Q_P = Q_K$$

$$\text{or} \quad Q_S < Q_E < Q_P < Q_K$$

The rock sample used in this study is Massillon sandstone. The porosity is 22% and the permeability is ~750 md. Anisotropy is less than 1% as measured by the velocities of ultrasonic P and S waves. The minimum Q measured in this study was ~20 and all data was taken at strains below those at which non-linear, frictional effects are observed [Winkler *et al.*, 1979]. Also, since we are relating Q 's taken at slightly different frequencies ($f_E \approx 1.5 f_T$) we must assume that Q is independent of fre-

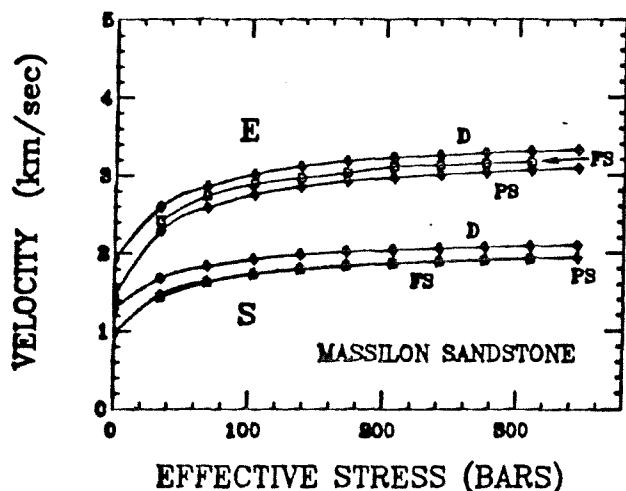


Fig. 1. Shear (S) and extensional (E) velocities in dry (D), partially (~95%) saturated (PS), and fully saturated (FS) Massilon sandstone. Pore fluid is water.

quency to use Eq. 1-3. We have verified this by measuring attenuation at several harmonics of the resonance frequency.

Observations

A series of three experiments was performed on a sample of Massilon sandstone. In the first experiment the sample was "room dry". After cycling confining pressure to eliminate hysteresis effects, attenuation and velocity data was taken vs. confining pressure. The rock was then evacuated to a pressure of 0.1 torr, then partially saturated with distilled water (pore pressure ~7 bars) and confining pressure was again varied. To achieve total saturation it was necessary to apply at least 15 bars pore pressure to the sample, so in the third experiment we held confining pressure constant at 345 bars and varied pore pressure. Because attenuation is a function of effective stress (in saturated rock), this procedure is equivalent to varying confining pressure in fully saturated rock. We do not have precise control over degree of saturation, but have estimated this from the velocities, as discussed below.

We will first discuss the velocity measurements because these help in understanding the attenuation data. Figure 1 shows the measured shear and extensional velocities and Figure 2 shows the shear velocities along with the computed P-wave velocities. Shear wave velocities decrease continuously as degree of saturation increases, whereas P-wave velocities decrease from dry to partial saturation, and sharply increase as total saturation is achieved. Similar results have previously been observed at

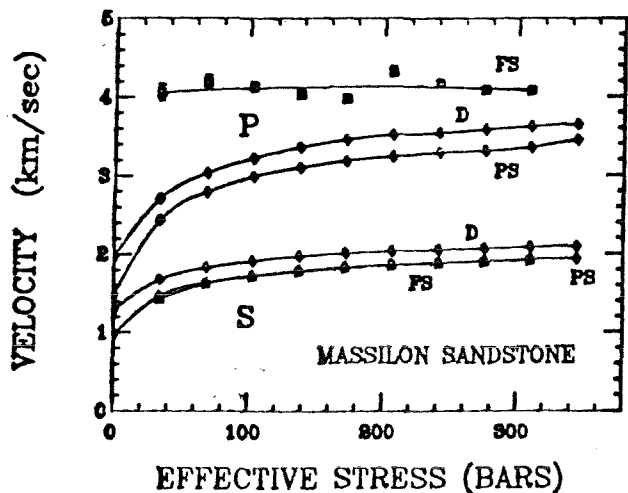


Fig. 2. Shear velocities (S) and computed P-wave velocities (P) in dry (D), partially saturated (PS), and fully saturated (FS) Massilon sandstone.

ultrasonic frequencies [Elliot and Wiley, 1975; Domenico, 1976], but this is the first such observation below 1 kHz. Note in Figure 2 that shear velocities are almost identical in partially and fully saturated rock. From this evidence and the well documented effect of pore fluids on shear velocity we have estimated that the rock is ~95% saturated when partially saturated. Note also in Figure 2 that the P-velocity in fully saturated rock is much larger than in partially saturated rock. This increase in P-velocity is our main evidence that we have in fact achieved total saturation. The transition from partial to total saturation can be achieved by increasing pore pressure from ~7 bars to ~15 bars. Presumably this either dissolves any gas remaining in the rock or forces water into a few remaining undersaturated pores.

The attenuation data obtained in these experiments is shown in Figures 3-6. Figures 3 and 4 show the observed shear and extensional attenuation. Figs. 5 and 6 show the computed P-wave and bulk compressional attenuation. Error bars on shear and extensional data are ~1% and are not shown, however, from the goodness of fit of the resonance decay to a decaying exponential, and these uncertainties were used in calculating the error bars in Figures 5 and 6. These relatively larger error bars result from uncertainties propagating through the calculations (Eq. 1 and 2), but they do not obscure the essential features of the data. Also, some of the calculated values of Q^{-1} are negative. Since negative values are physically impossible, these probably result from systematic errors in the data and should simply be interpreted as very small values of attenuation.

Figures 3-6 all show that attenuation decreases with increasing confining pressure. This feature is commonly observed [Birch and Bancroft, 1938; Gardner et al., 1964] and provides little insight into physical loss mechanisms. Presumably crack closure is responsible for this behavior, and all proposed mechanisms will show some pressure dependence.

Considerable insight into pore fluid attenuation mechanisms is obtained by comparing shear and bulk compressional attenuation (Figures 3 and 6) at various degrees of saturation. Shear attenuation is minimum in dry rock, is greater in partially saturated rock, and is maximum in fully saturated rock. However, while compressional loss is also minimum in dry rock and greater in partially saturated rock, the compressional loss is significantly reduced by total saturation. Also, in both dry and fully saturated rock, shear energy loss is greater than bulk energy loss. In partially saturated rock, however, shear energy loss is less than bulk loss. These results agree with those of Wyllie et al. [1962] and Gardner et al. [1964]. However, in neither of these studies was extensional attenuation measured in totally saturated rock and therefore they could not have observed the decrease in compressional energy loss. We are continuing these experiments with Berea sandstone, Sierra White granite, and porous Vycor glass. Although complete experiments have not yet been run, all data obtained thus far agrees with our observations on Massilon sandstone. In addition, qualitative attenuation measurements on P and S waves at ultrasonic frequencies [J. DeVilbiss, personal communication, 1978] show similar behavior as degree of saturation is varied.

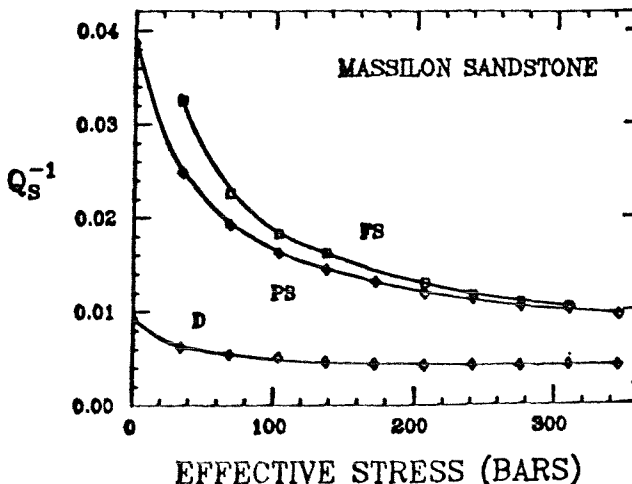


Fig. 3. Shear attenuation in dry (D), partially saturated (PS), and fully saturated (FS) Massilon sandstone.

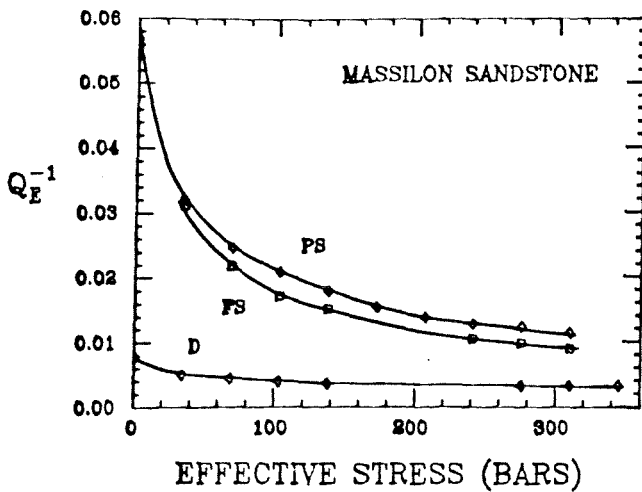


Fig. 4. Extensional attenuation in dry (D), partially saturated (PS), and fully saturated (FS) Massilon sandstone.

Discussion

Our observations can be explained remarkably well with several existing theories of pore fluid attenuation mechanisms. *Mavko and Nur* [1979] have discussed a model in which liquid droplets in a partially saturated crack flow in response to crack compression or dilation. *Kjartansson and Denlinger* [1977] have presented a model in which compression of the gaseous phase of the pore fluid causes adiabatic heating of the gas followed by an irreversible flow of heat into the rock and pore water. Both mechanisms predict that attenuation should increase with degree of saturation and then rapidly decrease at total saturation. They also predict that bulk compressional energy loss in partially saturated rock should be approximately twice as large as shear energy loss, and this is very close to what we have observed. To explain the observations on fully saturated rock, we use a mechanism proposed by *Mavko and Nur* [1975] and developed by *O'Connell and Budiansky* [1977]. This involves "squirting" flow between cracks as cracks at different orientations to the passing wave (or cracks of different aspect ratio) undergo differential compression. *O'Connell and Budiansky* [1977] have shown that this mechanism may cause significant shear attenuation over a broad frequency range, and that shear attenuation should be much larger than compressional attenuation. Again, this agrees with our observations.

Conclusions

The contrasting behavior of shear and bulk compressional attenuation is very clear from the accurate new data we have presented. As water

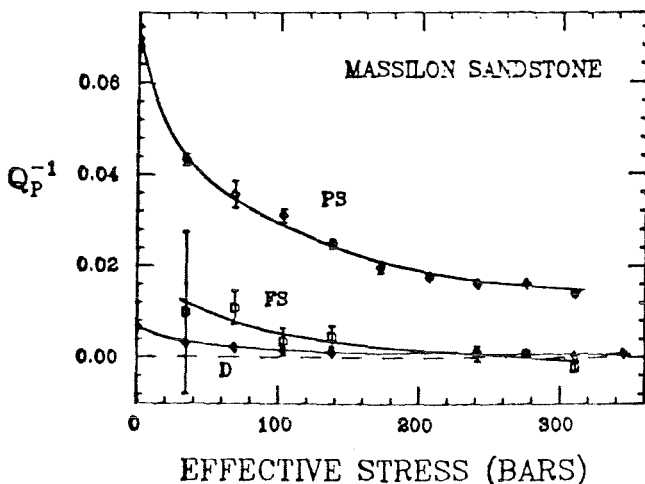


Fig. 5. Computed P-wave attenuation in dry (D), partially saturated (PS), and fully saturated (FS) Massilon sandstone.

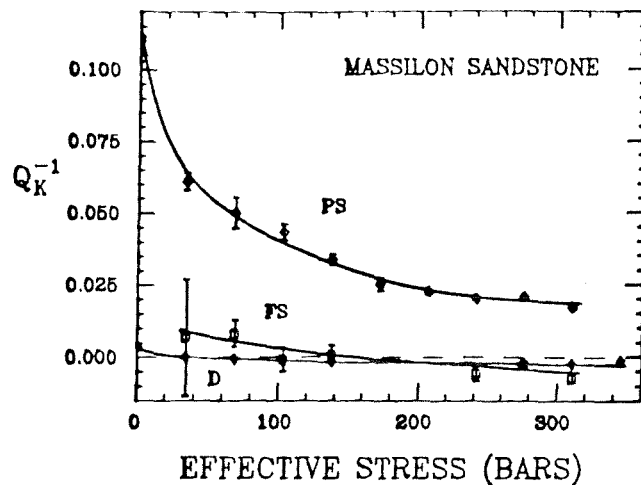


Fig. 6. Computed bulk compressional attenuation in dry (D), partially saturated (PS), and fully saturated (FS) Massilon sandstone.

is added to the pore space of rock, compressional energy loss is about twice as large as shear energy loss, and both increase with degree of saturation. The loss mechanism may be fluid flow [*Mavko and Nur*, 1979], thermoelastic [*Kjartansson and Denlinger*, 1977], or both. Shear attenuation continues to increase to 100% saturation. However, bulk attenuation reaches a maximum at approximately 95% saturation and then decreases with further saturation. At total saturation bulk loss is less than one third the shear loss. This minimization of bulk loss is predicted by both of the partial saturation mechanisms we have discussed as well as the total saturation mechanism developed by *O'Connell and Budiansky* [1977] involving flow between cracks.

The data also shows that in partially saturated rock (and for shear loss in fully saturated rock) pore fluid attenuation mechanisms clearly dominate over all mechanisms in dry rock. However, our samples were only "room dry" and so even here we may not have totally eliminated the fluid mechanisms. We do find, though, that in dry rock shear losses are greater than bulk losses, implying that the partial saturation mechanisms may not completely explain the behavior.

Although practical applications of these results must await further studies with different rocks and pore fluids, we may consider some potential uses. The results may enable us to better interpret the nature of gas related bright spots in reflection seismological surveys, as the attenuation due to the gas-liquid mix may be very significant. Attenuation in geothermal fields, particularly those with steam, may serve as a diagnostic tool due to the sensitivity to partial saturation.

There is, finally, an interesting speculation that can be made. The phenomenon of decreasing P-wave velocity with slight undersaturation of rock is the basis of the dilatancy-diffusion model of earthquake velocity precursors [*Nur*, 1972; *Anderson and Whitcomb*, 1975]. The great difficulty in detecting these anomalies [*Boore et al.*, 1975; *Allen and Helmsberger*, 1973] may have thrown doubt on the applicability of the model, but it may also simply reflect the small magnitude of the effect being sought. The maximum velocity change possible is on the order of 10-15% [Figure 2; *Winkler and Nur*, 1977] and if the dilatant zone is a small fraction of the seismic ray path, the net change in travel-time will not be resolvable. However, our results suggest that P-wave attenuation may be a much more sensitive indicator of undersaturation caused by dilatancy. Whereas P-wave velocity varies by ~15% (Figure 2), P-wave attenuation varies by a factor of five or more (Figure 5). Although attenuation is more difficult to measure than is velocity, the large size of this effect may make it easier to detect attenuation anomalies as evidence of stress accumulation in the crust.

Acknowledgments We are grateful to J. Walls for providing permeability measurements and to T. Jones for ultrasonic velocity measurements. This research was supported by a grant from the Earth Science Division, U.S. National Science Foundation.

References

- Allen, C.R., and D.V. Helmberger, Search for temporal changes in seismic velocities using large explosions in Southern California, in Proceedings of the Conference on Tectonic Problems of the San Andreas Fault System, *Stanford Univ. Publ. Geol. Sci.* 13, edited by R.L. Kovach and A. Nur, 436-445, 1973.
- Anderson, D.L. and J.J. Whitcomb, The dilatancy diffusion model of earthquake prediction, in Proceedings of the Conference on Tectonic Problems of the San Andreas Fault System, *Stanford Univ. Publ. Geol. Sci.* 13, edited by R.L. Kovach and A. Nur, 417-426, 1973.
- Biot, M.A., Theory of propagation of elastic waves in a fluid saturated, porous solid, I and II. *J. Acoust. Soc. Am.*, 28, 168-191, 1956.
- Birch, F. and D. Bancroft, Elasticity and internal friction in a long column of granite, *Bull. Seis. Soc. Am.*, 28, 243-254, 1938.
- Boore, D.M., A.G. Lindh, T.V. McEvilly, and W.W. Tolmachoff, A search for travel-time changes associated with the Parkfield, California earthquake of 1966, *Bull. Seis. Soc. Am.*, 65, 1407-1418, 1975.
- Born, W.T., The attenuation constant of earth materials, *Geophysics*, 6, 132-148, 1941.
- Domenico, N.S., Effect of brine-gas mixture on velocity in an unconsolidated sand reservoir, *Geophysics*, 41, 5, 882-894, 1976.
- Elliot, S.E. and B.F. Wiley, Compressional velocities of partially saturated unconsolidated sands, *Geophysics*, 40, 6, 949-954, 1975.
- Fung, Y.C., Foundations of solid mechanics, Prentice-Hall, 1965.
- Gardner, G.H.F., M.R.J. Wyllie, and D.M. Droschak, Effects of pressure and fluid saturation on the attenuation of elastic waves in sands, *J. Petrol. Tech.*, 16, 189-198, 1964.
- Johnston, D.H. and M.N. Toksoz, Attenuation of seismic waves in dry and saturated rocks, *Geophysics*, 42, 7, 1511, 1977.
- Kjartansson, E., and R. Denlinger, Seismic wave attenuation due to thermal relaxation in porous media, *Geophysics*, 42, 7, 1516, 1977.
- Mavko, G., Frictional attenuation: An inherent amplitude dependence, *J. Geophys. Res.*, in press, 1979.
- Mavko, G. and A. Nur, Melt squirt in the asthenosphere, *J. Geophys. Res.*, 80, 1444-1448, 1975.
- Mavko, G. and A. Nur, Wave attenuation in partially saturated rocks, *Geophysics*, in press, 1979.
- Nur, A., Dilatancy, pore fluids and premonitory variations in T_S/T_P travel times, *Bull. Seis. Soc. Am.*, 62, 1217-1222, 1972.
- Nur, A. and G. Simmons, The effect of saturation on velocity in low porosity rocks, *Earth. Plan. Sci. Lett.*, 7, 183-193, 1969.
- O'Connell, R.J. and B. Budiansky, Viscoelastic properties of fluid-saturated cracked solids, *J. Geophys. Res.*, 82, 36, 5719-5736, 1977.
- O'Connell, R.J. and B. Budiansky, Measures of dissipation in viscoelastic media, *Geophys. Res. Lett.*, 5, 1, 5-8, 1978.
- Randall, M.J., Attenuative dispersion and frequency shifts of the Earth's free oscillations, *Phys. Earth Planet. Int.*, 12, 1-4, 1976.
- Sheriff, R.E., Factors affecting seismic amplitudes, *Geophys. Pros.*, 23, 125-138, 1975.
- Spinner, S. and W.E. Tefft, A method for determining mechanical resonance frequencies and for calculating elastic moduli from these frequencies, *Proc. A.S.T.M.*, 61, 1221-1238, 1961.
- Walsh, J.B., New analysis of attenuation in partially melted rock, *J. Geophys. Res.*, 74, 4333-4337, 1969.
- White, J.E., Seismic waves: Radiation, Transmission and Attenuation, McGraw-Hill, 1965.
- White, J.E., Computed seismic speeds and attenuation in rocks with partial gas saturation, *Geophysics*, 40, 2, 224-232, 1975.
- Winkler, K. and A. Nur, Depth constraints on dilatancy induced velocity anomalies, *J. Phys. Earth*, 25, Suppl., 231-241, 1977.
- Winkler, K., A. Nur, and M. Gladwin, Friction and seismic attenuation in rocks, *Nature*, in press, 1979.
- Wyllie, M.R.J., G.H.F. Gardner, and A.R. Gregory, Studies of elastic wave propagation in porous media, *Geophysics*, 27, 569-589, 1962.

(Received October 24, 1978;
accepted December 4, 1978.)

ATTENUATION OF TELESEISMIC P-WAVES IN THE
GEYSERS-CLEAR LAKE REGION

By CHI YUE YOUNG and RONALD W. WARD
UNIVERSITY OF TEXAS AT DALLAS,
RICEARDSON, TEXAS 75080

ABSTRACT

During July and September 1976, the U. S. Geological Survey deployed 14 portable short-period seismographs along a line trending roughly northwest-southeast between Clear Lake and The Geysers to study travelttime delays of teleseismic P-waves associated with magma or partially molten zones beneath the geothermal system. The P-waves of 22 teleseismic events, suitable for attenuation analysis, were recorded by 13 seismographs. The events were digitized and spectrally analyzed using both periodogram and maximum entropy method (MEM). Seismograms exhibited both a significant drop in amplitude and waveform broadening.

The location and extent of the zones of high attenuation were qualitatively inferred from the power density spectra of the seismograms. The reduced spectral ratio technique was applied to determine the differential attenuation factor δt^* quantitatively, assuming that Q is independent of frequency. The maximum differential attenuation is about 0.3 second, which roughly corresponds to a 15 -km-thick zone with Q equal to 25 embedded in a high- Q medium. The lateral variation of δt^* was used to infer the Q structure in the frequency range 0.25 - 2.5 Hz assuming that the teleseismic wave propagating to each station

is identical when it enters the bottom of the crust-upper mantle model. A shallow zone of high attenuation extends from the Geysers steam field an undetermined distance toward the northeast and is 15 km wide. The zone of high attenuation deepens to the northwest between stations CL07 and CL08 and toward the southeast near station CL05. The thickest part is probably located beneath station CL06 or Mount Hannah and possibly station CL12, where the zone is very close to the surface. This anomaly extends southwest toward the Geysers steam field, which is associated with the vapor-dominated hydrothermal reservoirs inferred from other geophysical surveys.

INTRODUCTION

This study uses the lateral variation of power density spectra of P-waves observed across a geothermal system. The degree of attenuation of P-waves depends critically upon the physical state and thermal regime within the earth. The surface observations are then related to a quantitative model of the quality factor, Q . Studies of P-wave attenuation promise to constrain the geologic crustal structure beneath The Geysers, the site of the world's largest producer of commercial power.

Three mechanisms proposed for seismic attenuation are partial melting, grain boundary relaxation, and "high temperature internal friction background" (Jackson and Anderson, 1970). Each of these mechanisms depends on temperature. The degree of seismic attenuation reflects the thermal state of the medium and the extent of partial melting (Walsh, 1968, 1969). In the vapor-dominated porous medium that typifies the Geysers geothermal system, the coupling between fluid flow waves and seismic body waves in the zone of liquid-vapor mixture will affect the velocity and increase the attenuation of the seismic waves. Compressional or P-waves are the only ones affected by this mechanism (White, 1975).

The volcanic sequences of the area (fig. 1) range in age from 2.1 million years to 10,000 years (Donnelly and others, this volume). Changes in magma composition from basalt or andesite through dacite to rhyolite reflect a silicic differentiation process. Other detailed studies show that the Geysers-Clear Lake region is a structurally controlled geothermal resource area (McLaughlin, this volume). The Geysers steam reservoirs are related to the northwest-southeast trending faults dipping steeply northeast which control the structure

traps. A magma chamber beneath the Clear Lake volcanic field is also suggested as the heat source of the geothermal system (Isherwood, this volume).

Geophysical studies conducted in the Geysers-Clear Lake area include microearthquake surveys, gravity and magnetic surveys, seismic-reflection profiles, seismic refraction and teleseismic P-waves traveltimes delays. These investigations are detailed in other chapters in this volume as well as elsewhere (Iyer and others, 1979; and Majer and McEvilly, 1979). The gravity and magnetic studies have aided in determining the deep geologic structure, and the microearthquake studies have aided in mapping the active faults. The studies also suggest that the gravity, the P-wave traveltimes delays, and the electrical source of the geophysical anomalies could be a magma chamber or partially molten zone at shallow depth beneath the geothermal area.

If a magma chamber or partially molten zone does exist, it may or may not produce observable attenuation of seismic waves as they pass through the anomalous zone. For instance, in Yellowstone National Park a large magma chamber was inferred from the P-wave traveltimes residuals (Iyer, 1975) and yet the seismograms do not exhibit significant waveform broadening, one indication of seismic attenuation, but there is considerable (12 - 20 db) amplitude variation across the array. Using a spectral data analysis technique, such as the reduced spectral ratio method (Teng, 1968; Solomon, 1973), we have attempted to delineate the extent, size and possibly estimate the fraction of melt within the magma chamber at The Geysers. In applying this technique we assume that the effect of seismic attenuation dominates the spectrum of the seismogram compared to other medium effects such as crustal reverberation.

Acknowledgments. -- We thank H. M. Iyer, Craig Weaver, Tim Hitchcock, and Alan Walter of the U. S. Geological Survey in Menlo Park for helpful discussions, assistance in digitizing data, and providing computer programs to read the data at the North Texas Regional Computer Center in Dallas. Our thanks to Nancy Stetler and Charlotte Scott for typing the manuscript and Belle Koblentz for drafting the figures. This research was supported by the National Science Foundation (Research Applied to National Needs) Grant #AER75-23619 during the data acquisition and the U. S. Geological Survey, U. S. Department of Interior Grant #1408-0001-G-426, during the data analysis, interpretation, and preparation of the study.

DATA

During July 1976, and again from mid-August through the first week of September 1976, short-period vertical or three-component portable seismographs were deployed by the U. S. Geological Survey for a total of 42 days and operated at 14 stations along a northwest-southeast line in the Geysers-Clear Lake region (fig. 1). (One station produced no satisfactory data and has been excluded from the study.) The seismograms are used for the study

Figure 1 -- Near Here

of the teleseismic P-wave traveltimes (Iyer and others, 1979; Iyer and others, this volume) as well as the attenuation study.

The seismograms for a total of 22 events (table 1) were to have large enough

Table 1 -- Near Here

Figure 1. - Generalized geologic and structural map of the Geysers-Clear Lake area (modified from ~~Heam~~ and others, 1976) showing location of seismic array. Station CL14 produced no useful data and is not shown.

Table 1. - List of teleseismic events used in this study

Event No.	Date	Time	Lat N.	Long E.	Region	M	Depth (km)	Distance	Azimuth
		(G.m.t.)							(Degrees)
		H M S							
1	8-15-76	18:43:45.0	-25.129°	-179.699°	Figi	5.4	509	83.334	229.9°
2	8-16-76	12:28:32.4	51.918°	158.431°	Kamchatka	5.3	50	54.158	311.678°
3	8-16-76	14:06:45.9	32.753°	104.157°	Szechwan	6.1	16	93.792	316.572°
4	8-16-76	16:11:07.3	6.262°	124.023°	Philippines	6.4	33	103.831	270.041°
5	8-17-76	04:19:27.3	7.249°	122.939°	Philippines	6.2	22	103.948	271.540°
6	8-20-76	03:56:00.6	45.048°	149.781°	Kuril Is.	5.5	47	61.046	306.080°
7	8-20-76	06:54:11.3	-20.412°	-69.993°	N. Chile	5.6	81	77.080	130.200°
8	8-22-76	02:01:47.4	60.220°	-153.304°	Alaska	5.5	144	28.714	328.105°
9	8-22-76	21:09:41.9	-14.047°	170.939°	New Hebrides	5.7	31	81.434	244.110°
10	8-23-76	03:30:07.6	32.492°	104.181°	China	6.2	133	96.483	321.809°
11	8-24-76	21:26:12.2	-25.326°	-70.694°	Chile	5.6	8	80.440	133.859°
12	8-26-76	14:30:00.2	37.125°	-116.082°	Nevada Test Site	5.3	0	5.398	106.805°
13	8-28-76	02:30:09.2	52.597°	-175.343°	Aleutians	5.1	145	38.316	308.732°
14	8-28-76	02:56:57.5	49.969°	79.001°	E. Kazakh	5.8	0	89.155	346.322°
15	8-28-76	21:50:37.8	-10.669°	-78.189°	Peru	5.1	59	64.488	130.398°
16	8-30-76	08:37:54.8	1.099°	147.530°	Caroline Is.	5.8	53	89.291	270.725°
17	8-31-76	09:06:50.4	-30.099°	-178.114°	Kermadec Is.	5.4	55	86.193	225.642°
18	8-31-76	13:22:10.9	-28.290°	-176.633°	Kermadec Is.	5.5	51	83.976	225.803°
19	9-01-76	13:25:29.8	-20.414°	169.364°	New Hebrides	5.7	75	86.921	240.529°
20	9-02-76	10:20:25.9	13.259°	-89.989°	Guatemala	5.0	81	38.507	122.673°
21	9-04-76	11:54:20.0	-10.247°	161.094°	Solomon Is.	5.6	83	86.025	253.459°
22	9-09-76	09:27:45.2	77.828°	7.770°	Svalbard	5.2	5	59.526	10.747°

signal-to-noise ratio (S/N) for attenuation analysis and were selected for digitization at 100 samples per second. Most of the events arrived from three narrow ranges of azimuths: northwest, southeast, and southwest. The P-wave seismograms of various events exhibit significant amplitude variation across the array and a frequency shift to longer periods correlating with the amplitude decrease above the center of the array (fig. 2).

Figure 2 -- Near Here

The events recorded characteristically had emergent waveforms, possibly due to the heterogeneity of the crust and upper mantle beneath the geothermal area. In this region, the seismograms are usually accompanied by a high noise level, which severely contaminates some P-wave signals. These factors make the selection of a time window for the spectral analysis very difficult and introduced large uncertainties into amplitude spectra of the waves. In general, a time window less than 5 seconds is chosen and the power density spectrum is computed using both periodogram analysis (Blackman and Tukey, 1958) and Burg's Maximum Entropy Method (MEM) (Burg, 1967; Ulrych and Bishop, 1975). MEM generally gives a smoother spectrum than the periodogram analysis and is used in this study.

Figure 2. - Sample P-wave seismograms recorded by the Geysers-Clear Lake
vertical array for three events from different azimuths (see table 1).

MEASUREMENT OF DIFFERENTIAL ATTENUATION

Background

The effect of seismic attenuation can be observed qualitatively from the seismograms; however, the quantitative measurements of the attenuation factors are more useful for inferring important physical properties of the geothermal area. The observation of a teleseismic earthquake across a rather small area allows us to make certain simplifying assumptions as illustrated in figure 3. The P-wave entering the upper mantle beneath the geothermal area is approximately

Figure 3 — Near Here

plane with constant amplitude over the area. It propagates through the geothermal system and is recorded by seismographs on the surface. There is obvious lateral variation in amplitude, frequency content, and the coda duration of the waveform. To extract this information from the body wave signals, we can apply the technique of body wave equalization (Ben-Menahem and others, 1965), which has been used in different forms to study attenuation (Teng, 1968; Solomon and Toksüz, 1970; Ward and Toksüz, 1971; Solomon, 1972, 1973).

We can write the observed amplitude spectrum of a body wave as

$$\Lambda(f, \theta, \phi) = A_0(f, \theta, \phi) \Lambda_m(f) A_c(f) A_I(f) \quad (1)$$

where $A_0(f, \theta, \phi)$ is the source function which depends on frequency f and the propagation direction (θ, ϕ) . In general, A_0 includes the source time function, radiation pattern, and the finiteness effect due to the dynamics of rupture; Λ_m is the mantle transfer function, which includes geometrical spreading and

Figure 3. - Teleseismic P-wave incident beneath a model geothermal system showing variations in seismograph recordings on surface.

attenuation effects; A_c is the crustal transfer function for source and receiver, containing the effect of differential attenuation as well as reverberation and amplitude effects due to lateral velocity changes, and A_I is the instrumental transfer function, which is considered to be identical for all the stations used in this study.

As mentioned the aperture of the seismometer array is much smaller than the epicentral distances for the teleseismic events used in this study, and it can be assumed that the frequency-dependent source radiation pattern and the effects on the seismic waves of propagation through the mantle for a particular event are not functions of the particular coordinates. Therefore, the spectral ratio of A_0 and the spectral ratio of A_m may be considered independent of frequency. The spectral ratio R_{ij} for a given body wave recorded at two stations i and j from a single earthquake is obtained from

$$R_{ij}(f) = a_{ij} \frac{A_{c_i}(f)}{A_{c_j}(f)} \quad (2)$$

where a_{ij} contains the ratio of A_m , A_0 and A_I . This ratio is independent of frequency and a_{ij} will be treated as a constant. $A_c(f)$ is the crustal transfer function beneath the receiver and may be factored into three parts

$$A_c(f) = G \exp(-ft^*) \exp(-f \delta t^*) \quad (3)$$

where G represents a constant amplitude factor, t^* is a regional attenuation factor which will be assumed to be the same for all stations, and δt^* , called the differential attenuation factor, is the local effect and can be written as

$$\delta t^* = \pi \int \delta Q^{-1} v^{-1}(s) ds$$

$$= \pi f \delta Q^{-1} dt \quad (4)$$

where Q is the quality factor, v is velocity, and dt is the traveltime for the wave passing through the travel path ds . Substituting equation (3) into equation (2) gives

$$R_{ij}(f) = C_{ij} \exp \{-f (\delta t_{i}^{*} - \delta t_{j}^{*})\} \quad (5)$$

where C_{ij} is independent of frequency and is equal to $a_{ij}^{G_i/G_j}$. For convenience of calculation we assume that the δt^* for the reference station j is equal to zero. Taking the logarithm of both sides of equation (5) we get

$$\ln R_{ij} = \ln C_{ij} - f \delta t_{i}^{*} \quad (6)$$

Both C_{ij} and δt_{i}^{*} are assumed to be independent of frequency. Using a least-square error criterion, a straight line is fit to the spectral ratio versus frequency within a frequency band in which the signal-to-noise ratio is at least 6 db (typically 0.25 to 2.5 Hz). The negative of the slope of the straight line is equal to the estimated differential attenuation, δt_{i}^{*} . The power density spectra and spectral ratios for a typical event are illustrated in figure 4.

Figure 4 -- Near Here

Differential Attenuation

Q is the quality factor, which measures the anelasticity of a solid. Q^{-1} is a dimensionless parameter, indicating the fraction of the energy dissipated per cycle by a seismic wave, that is, a seismic wave loses $1/Q$ of its energy by

Figure 4. - Power density spectra (left) and spectral ratios from the Geysers-Clear Lake array for event No. 13. Smooth lines of power density spectra and broken lines of spectral ratios are computed using Maximum Entropy Method (MEM). Linear least-square error fit is shown for the spectral ratio short-dash line is fitted to the MEM spectral ratio.

anelastic loss for each wavelength it propagates. Partial melting, grain boundary relaxation, internal friction, and other mechanisms attenuate seismic waves. Each mechanism has a different dependence on frequency. Several mechanisms acting simultaneously may lead to a weaker dependence on frequency than is predicted for the individual mechanisms (Jackson and Anderson, 1970). In the present study, the spectral ratio is determined in a narrow frequency band (approximately 0.25 to 2.5 Hz) so that Q^{-1} in that band can be considered to be approximately independent of frequency.

The relation between the differential attenuation δt^* and the quality factor Q is expressed in equation (4). Assume a constant velocity of 6 km/s; then, a δt^* equal to 0.1 s for a station, a high seismic attenuation, could be produced by a 10-km-thick zone with a Q of 50, or a 5-km-thick zone with a Q of 25 embedded in a medium with infinite Q . The maximum individual δt^* observed across the Geysers-Clear Lake array is about 0.3 second.

The most important factor which affects the estimation of δt^* is the quality of the P-wave form. Many P-wave forms recorded in the Geysers-Clear Lake region are emergent, noisy, and exhibit interfering phases (fig. 2), which may be caused by the complexity of the local geology. Since δt^* according to equation (4) is integrated along the ray path, we can expect to see δt^* vary with the changes of epicentral distance and azimuth. This variation, which is caused by lateral changes of Q , may indicate the depth of the anomaly beneath the station.

The variation in the frequency content of the P-wave seismograms is documented by noting the frequency of the peak in the power density spectrum at each station for the events from the three primary azimuths, northwest, southwest, and southeast (fig. 5). The events from the southwest exhibit an average dominant frequency

Figure 5 -- Near Here

of 0.80 Hz at most stations. The events from this azimuth may be lower frequency. P-wave teleseisms arriving from the northwest and southeast exhibit greater variation in dominant frequency. For events from the northwest, stations CL01-04 have average dominant frequencies greater than 1.2 Hz. For events from the southeast the stations CL01 and CL05 have the highest dominant frequencies. Stations CL07 and CL13 are the lowest. This method of analysis is quite qualitative. However, it seems to indicate the presence of an attenuation anomaly between stations CL05 and CL09. The δt^* analysis will permit a more quantitative interpretation of the Q-structure.

In this study, we chose station CL02 as the reference station. Presumably it lies outside the region of the geothermal anomaly (fig. 1), and the attenuation of seismic waves recorded by this station is unaffected by the geothermal system. Station CL01 is located further away from the Clear Lake volcanic field (fig. 1) but did not record as many events well. The δt^* obtained for station CL01 is very small and shows no pronounced attenuation. This justifies the above assumptions that the reference station selected is unaffected by the geothermal system and also shows the stability of the spectral ratio technique applied in the study. The assumption that crustal reverberation effect can be neglected is supported by this data.

The δt^* calculated in this manner for each station and each of the twenty-two events listed in table 1. The events whose ray path pass too close to the core-mantle boundary are eliminated from the interpretation. Those events from azimuths other than the three primary azimuths are also eliminated leaving the thirteen events in table 2. The variation of δt^* with azimuth and distance for

Figure 5. - Dominant frequencies of P-waves studied are plotted along a northwest-southeast line. Lower frequency correlates with higher attenuation of seismic wave. Stations 11 and 13 are projected onto the line.

Table 2 -- Near Here

each station is plotted in figure 6. These data contain all the information needed by a generalized inversion algorithm to compute a detailed quantitative

Figure 6 -- Near Here

three-dimensional Q-model in a future study.

The δt^* calculated for several stations (CLO3, CLO4, CLO6, CL10, and CL12 in figure 6) are constant regardless of the change of epicentral distance or azimuth. Beneath these stations the observed attenuation anomaly must be shallow, and no lateral variation in attenuation can be inferred for the deeper part of the crust and upper mantle.

The δt^* data are independent of epicentral distance, within the resolution of the present data, but usually vary with azimuth. The values of δt^* were averaged for events from a given azimuth. The events were separated into three groups based on azimuth (northwest, southwest, and southeast).

A contour map of δt^* was drawn from the average δt^* values of table 2 (fig 7). Values from the nearest stations were used to produce a two-dimensional grid of values at equal increments, which have been contoured (chapter 6, Davis, 1973). The value of δt^* at a grid point is calculated from the five nearest data

Figure 7 -- Near Here

values. Each data value among the five nearest neighbors is weighted by the inverse distance from the station to the grid point. This contouring algorithm has been shown to produce small mean error though the rms error at a given control point may be larger than other schemes (Harbaugh and others, 1977).

Table 2. - List of the differential attenuation δt^* ,
in milliseconds, for each station
(station 2 is the reference station)

Event No. and Azimuth	STATION NO.											
	1	3	4	5	6	7	8	9	10	11	12	13
2NW	-17	139	75	68	---	---	-22	---	---	---	---	---
6NW	41	---	118	112	138	135	10	148	30	---	---	49?
8NW	-12	-59	114	184	124	165	83	---	114	181	182	229
9SW	25	129	114	128	---	---	18	131	36	-95?	87	---
12SE	8	15?	3?	-222?	-50?	---	61	54	104	-91?	-21?	33?
13NW	129?	208	201	205	156	312	87	66	201	---	273	223
14NW	37	-4?	174	60	106?	142	104	41	54	40	-11?	165
15SE	-282?	53	82	-124?	-205?	-6?	1?	25	-23?	41	---	---
17SW	15	84	120	---	---	40	41	230?	134	---	253	164
18SW	6	146	77	41	116	44	38	103	-78	---	194	63?
19SW	85	184	198	183	169	237	153	41	91	97	374?	174
20SE	-28	133	261	33	142	79	181	---	77	128	180	209
21SW	---	133	109	110	103	138	-45	164	64	64	180	---
SW	35	138	126	111	129	114	42	103	96	81	209	169
SE	-28	133	261	33	142	79	181	---	77	128	180	209
NW	4	174	127	142	139	204	50	107	115	130	227	226
Average	17	141	147	113	135	133	46	99	91	102	210	197

Figure 6. - Differential elevation for each station as a function of distance
and azimuth.

Figure 7. - Two-dimensional contoured surface fitted to averaged δt^* . Contour interval is .02 second. A, δt^* data for seismic waves from southwest. B, δt^* data from southeast. C, δt^* data from northwest. δt^* is assumed zero at the reference station, C1 02. The solid area has the maximum value of δt^* .

In figure 7A the observed δt^* is contoured for events to the southwest. These rays arrive perpendicular to the strike of the seismometer array, and this plot resembles refraction fan shooting. Low seismic attenuation is observed at station CL01. The geothermal system appears to be bounded on the southeast by the 90 ms contour. High attenuation occurs in a zone extending from The Geysers to the northeast. Three local areas exhibit high seismic attenuation, near stations CL03 and CL13, and a large area around station CL12 to the east-northeast of Mount Hannah. Regional high attenuation ($\delta t^* > 90$ ms) occurs in an area east of a line through Mount Konocti and station CL13.

Figure 7B shows seismic attenuation of events to the southeast. Attenuation with $\delta t^* > 90$ ms occurs over most of the map except for a low attenuation observed to the southeast. Local high-attenuation anomalies are associated with station CL03 and with CL12 as for events from the southwest. Another zone of high attenuation includes stations CL08 and CL13 and Mount Konocti.

The seismograms of teleseismic P-waves from the northwest (fig. 7C) show the highest attenuation. The southeast station, CL01, shows negligible attenuation as it did for events from other azimuths. High local attenuation is evident at stations CL03, CL13, and CL12, as it is for the other events, indicating a very shallow attenuation anomaly that is strongest at stations CL13 and CL12. The high-attenuation anomaly for events from the northwest lies south and east of Mount Konocti with the highest attenuation anomaly occurring near station CL12.

Q Structure

Partial melting in the crust or upper mantle produces a Q value for shear waves of less than 50 and correspondingly a Q less than 125 for P-waves (Solomon,

1972). Measurement of this Q can serve as evidence for the existence of a partially molten magma chamber or to map a liquid-vapor steam reservoir beneath a geothermal area. In order to obtain a preliminary simplified Q model from the δt^* data presented in the previous section the following assumptions are made:

1. At each station a simplified two-layer Q model is used. Q in the upper layer is 50, underlain by a half-space with infinite Q . The thickness of the layer will vary as δt^* varies from station to station. This model will give a preliminary estimate of the lateral distribution of the high attenuation zone. Any layer may be replaced by a thinner layer with lower Q value.

2. All the rays are assumed to be vertically incident from the bottom of the model, since the ray paths are incident within 20° of the vertical and there is no apparent variation of δt^* with epicentral distance. A cross section of the Q structure will be determined along a northwest-southeast trending line.

3. The velocity is assumed constant within the upper layer, so that the integration can be carried out easily. The simplified Q model of the Geysers-Clear Lake region is shown in Figure 8 as the thickness of the upper layer

Figure 8 -- Near Here

with $Q = 50$. The thickness of the low- Q layer is plotted for the average of the events from each of three azimuths and the average for all events.

Several stations, such as stations CL03, CL09, CL11, CL12, and CL13 exhibit little azimuthal variation of the thickness of the low- Q layer. The implication is that a zone of high attenuation lies immediately beneath the

Figure 8. - Simplified Q model for the Geysers-Clear Lake area showing thickness of a layer with Q equal to 50. Lines are for average $\delta t\%$. Stations CL11, CL12, and CL13 are projected onto abscissa but not connected to lines. Higher seismic wave attenuation has thicker low-Q layer.

station. The interpretation of the differential attenuation observations must consider the effect of the near-surface geology before confirming the thickness of the low-Q zone in figure 8. The near-surface local geology produces higher seismic attenuation than consolidated Cenozoic volcanic rocks, the Great Valley sequence, or the Franciscan assemblage. Station CL03 is situated on thick alluvial deposits. Station CL12 observes the highest differential attenuation of 0.3 second. Although it sits on thick young pyroclastic deposits, it is doubtful that the near-surface lithology accounts for all the attenuation. Alternative convincing explanations exist for the attenuation observed at stations CL11 and CL13.

The assumption that seismic waves are vertically incident from the bottom of the Q model may not be valid if the Q model varies with azimuth (see stations CL05, CL07, and CL08 in figures 7 and 8). This azimuthal variation will aid in estimating the depth of the low-Q zone. The low Q determined for stations CL06, CL11, CL12, and CL13 define a shallow high-attenuation zone stretching from stations CL13 to CL06 to CL12 (figure 7). This zone exhibits high attenuation independent of the azimuth of the events.

If the ray comes from the southeast (figure 7B) at a distance of 40° to station CL05, the angle of incidence is about 20° from vertical. A thin low Q layer for station CL05 is indicated for waves from the southeast. A thick low-Q zone is indicated for station CL05 for waves from the northwest at a distance of 40° (figure 7C). The eastern boundary of the low-Q region follows the contour for δt^* of 0.11 where it trends southwest-northeast and passes to the northwest of station CL05 (figure 7B). The zone of high attenuation must lie at some depth to the northeast of station CL05.

The results obtained for stations CLO7 and CLO8 are similar to station CLO5. We combine the interpretation for each station and postulate that a small low-Q zone (which is possibly elongated and connected to the zone around station CL13) is at a depth of about 8 km between stations CLO7 and CLO8. A narrow zone of high attenuation appears to dip from station CL13 toward Mount Konocti between stations CLO7 and CLO8. The low-Q zone is less than 4 km wide, which is the distance between stations CLO7 and CLO8. When seismic waves arrive from the southwest (almost vertical incidence), neither station CLO7 or CLO8 detects a zone of high attenuation.

A broad attenuation anomaly exists beneath Mount Hannah, centered at station CLO6 and bounded by station CLO5 and CLO8. The north east boundary of the anomaly can not be determined by this study because of insufficient data but it includes station CL12. The attenuation anomaly correlated with the teleseismic P-wave traveltime anomaly (Iyer and others, this volume). Isherwood (1975) identified a broad negative gravity anomaly centered beneath Mount Hannah, which he attributed to a magma chamber at a depth of 10 km.

Figure 9 -- Near Here

The present study suggests a shallower seismic attenuation anomaly trending southwest-northeast which may be produced by a magma chamber. The exact depth of this magma chamber will be determined in a future study from the attenuation data for these station locations using a generalized inversion of the data.

A consistent thick layer of low Q is obtained for stations CL11 and CL13, independent of azimuth. No gravitational anomalies with closed contours were found in this area. A buried magma chamber may not exist here. We prefer the interpretation that the region beneath stations CL11 and CL13 is capped by

Figure 9. - Bouguer gravity map of study area (after Isherwood, 1975). Contour interval is 5 mgal; dashed where data are incomplete.

impermeable rocks of the Franciscan assemblage that act as a conduit for vapor-dominated hydrothermal activity toward the southeast and the Geysers steam field (Isherwood, 1975; Goff and others, 1977).

Discussions and Conclusions

The small variation and small values of the differential attenuation factor δt^* for station CL01 suggest that the local geology of station CL01 is similar to that of the reference station CL02. Both stations are located outside the area affected by the geothermal system. The consistency of this result gave us confidence in applying the spectral ratio technique to study the seismic wave attenuation beneath a geothermal system. By carefully picking the correct P-phases recorded by each station, the errors in obtaining δt^* can be reduced to a minimum.

A broad low-Q zone is found beneath The Geysers and the Clear Lake area. This anomaly is bounded to the southeast by a southwest-northeast trend at station CL05, where there is a sharp decrease in the thickness of the low-Q layer, which appears to be buried at depth. The center of the shallow high-attenuation zone extends from station CL13 beneath Mount Hannah to station CL12. This may be the same source of the gravity low and positive teleseismic P-wave traveltimes delays found in that region, though the shape of the attenuation anomaly is different. The value of Q is low enough to indicate a partial melting zone or a magma chamber associated with the Geysers-Clear Lake geothermal area. The top of the low-Q zone is very close to the surface, as no significant variation in δt^* is observed for stations in this area with the changes of epicentral distances or azimuths.

A very shallow zone of high attenuation beneath station CL05 can not be explained. A low-resistivity zone (5-10 ohm/meters) is found by Stanley, Jackson, and Hearn (1973) at the same place, but the gravity studies by Isherwood (1975) did not detect this anomaly. The attenuation source must be very shallow and localized, though it probably is associated to some extent with the large anomaly extending beneath Mount Hannah. Another small low-Q zone is at a depth of approximately 8 km between stations CL07 and CL08. The width of this high attenuation zone is probably less than 4 km, as inferred from the small δt^* obtained for the waves from the southwest, incident almost vertically to these two stations. This result did not correlate with other geophysical evidence, but this low-Q zone may coincide with a contact between the Franciscan assemblage and Great Valley sequence in the bedrock beneath these two stations. Moderate to small attenuation of the seismic P-waves is observed at stations CL09 and CL10, and these two stations are probably not located above any magma chamber or partially molten zone directly related to The Geysers. Station CL08 is the northwestern boundary of the low-Q zone. At the surface, station CL08 is also located close to the northwest edge of the Cenozoic volcanic rocks. The source of attenuation of the seismic waves observed at stations CL09 and CL10 is probably related to the thick Cenozoic unconsolidated or weakly consolidated deposits.

The values of δt^* calculated for the waves from the southwest to stations CL11 and CL13 are smaller than those for the other two azimuths. The results suggest that the low-Q zone may not continue all the way across the Collayoni fault zone to become the thermal source driving the Geysers steam field. Instead, fracture zones act as channels directing the hydrothermal activity from the main heat source (the low-Q zone) toward the producing steam field.

The low-Q region determined in this study has a width about 15 km measured on a line trending northwest-southeast. The thickest part of the high-attenuation zone is probably located beneath station C506 or Mount Hannah and possibly beneath station CL12, where the tops of these anomalies are very close to the surface. The high-attenuation zone extends southwest toward the Geysers steam field. This attenuation anomaly is postulated to be associated with the vapor-dominated hydrothermal reservoirs to be consistent with other geophysical surveys. The northeastern boundary of the thermal source cannot be defined in this study.

REFERENCES CITED

- Ben-Menahem, A., Smith, S. W., and Teng, T. L., 1965, A procedure of source studies from spectrums of long period seismic bodywaves: Bull. Seism. Soc. Am., v. 55, p. 203-235.
- Blackman, R. B., and Tukey, J. W., 1958, The measurement of power spectra: Dover Publications, New York.
- Burg, J. P., 1967, Maximum entropy spectral analysis. Paper presented at the 17th Annual International Meeting, Soc. of Exploration Geophysicists, Oklahoma City, Oklahoma, October 31, 1967.
- Davis, John C., Statistics and Data Analysis in Geology, John Wiley & Sons, New York, 1973.
- Donnelly, J. M., B.C. Hearn, Jr., G. H. Curtis, and R. E. Drake, 1979, Geochronology and evolution of the Clear Lake Volcanics: U. S. Geol. Survey Prof. Paper, this issue.
- Goff, F. E., Donnelly, J. M., Thompson, J. M.; and Hearn, B. C., Jr., 1977, Geothermal prospecting in the Geysers-Clear Lake area, northern California: Geology, v. 5, p. 509-515.
- Harbaugh, John W., Doveton, J. H., and Davis, J. C., Probability Methods in Oil Exploration, John Wiley & Sons, New York, 1977.
- Hearn, B. C., Jr., 1976, Preliminary geologic map and cross section of the Clear Lake volcanic field, Lake County, California: U. S. Geol. Survey Open-File Map 76-751.
- Isherwood, W. F., 1975, Gravity and magnetic studies of the Geysers-Clear Lake region, California: Second UN Symposium on the Development and Use of Geothermal Resources, San Francisco, Proceedings, Lawrence Berkeley Lab., University of California, v. 2, p. 1065-1073.


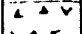
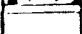


- Isherwood, W. F., 1979, Geophysical overview of The Geysers area: U. S. Geol. Survey Prof. Paper, this issue.
- Iyer, H. M., 1975, Anomalous delays of teleseismic P waves in Yellowstone National Park: *Nature*, v. 253, p. 425-427.
- Iyer, H. M., Oppenheimer, D. H., and Hitchcock, T., 1979, Abnormal P-wave delays in the Geysers-Clear Lake geothermal area, California: *Science*, v. 204, p. 495-497.
- Iyer, H. M., D. H. Oppenheimer, T. Hitchcock, J. N. Roloff, and J. M. Coakley, 1979, Large teleseismic P-wave delays in the Geysers-Clear Lake geothermal area, California: U. S. Geol. Survey Prof. Paper, this issue.
- Jackson, D. D., and Anderson, D. L., 1970, Physical mechanisms of seismic-wave attenuation: *Rev. of Geophysics and Space Physics*, v. 8, p. 1-63.
- Majer, E. L. and T. V. McEvilly, 1979, Seismological investigating at the Geysers geothermal field: *Geophysics*, v. 44, p. 246-269.
- McLaughlin, R. J., 1979, Tectonics of pre-Tertiary rocks and its relation to geothermal resources in The Geysers-Clear Lake area of northern California: U. S. Geol. Survey Prof. Paper, this issue.
- Stanley, W. D., Jackson, D. B., and Hearn, B. C., 1973, Preliminary results of geoelectrical investigations near Clear Lake, California: U. S. Geol. Survey Open-File Report, 20 p.
- Solomon, S. C., 1972, Seismic-wave attenuation and partial melting in the upper mantle of North America: *J. Geophys. Res.*, v. 77, p. 1483-1502.
- _____, 1973, Shear wave attenuation and melting beneath the mid-Atlantic ridge: *J. Geophys. Res.*, v. 78, p. 6044-6059.
- Solomon, S. C., and Toksöz, M. N., 1970, Lateral variation of attenuation of P- and S-waves beneath the United States: *Bull. Seism. Soc. Am.*, v. 60, p. 819-838.

- Teng, T. L., 1968, Attenuation of body waves and Q structure of the mantle:
J. Geophys. Res., v. 73, p. 2195-2208.
- Ulrych, T. J., and Bishop, T. N., 1975, Maximum entropy spectral analysis
and autoregressive decomposition: Rev. of Geophysics and Space Physics,
v. 13, p. 183-200.
- Walsh, J. B., 1968, Attenuation in partially melted material: J. Geophys. Res.,
v. 73, p. 2209-2216.
- _____, 1969, New analysis of attenuation in partially melted rock: J. Geophys.
Res., v. 74, p. 4333-4337.
- Ward, R. W., and Toksöz, M. N., 1970, Causes of regional variation of magnitudes:
Bull. Seism. Soc. Am., v. 61, p. 649-670.
- White, J. E., 1975, Computed seismic speeds and attenuation in rocks with partial
gas saturation: Geophysics, v. 40, p. 224-232.

ILLUSTRATIONS

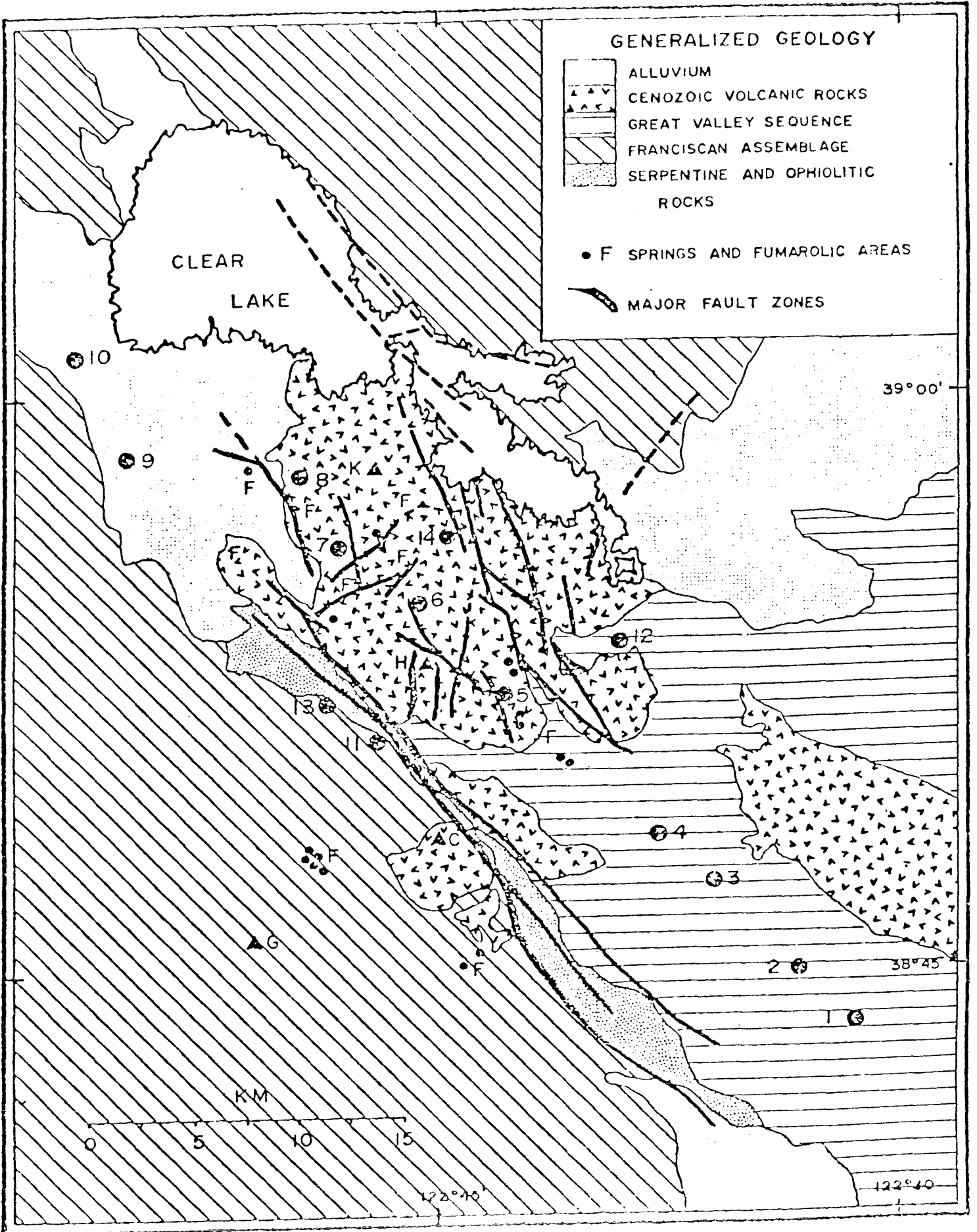
- Figure 1. Generalized geologic and structural map of the Geysers-Clear Lake area showing location of seismic array.
- Figure 2. Diagram showing sample P-wave seismograms recorded by the Geysers-Clear Lake array for three events.
- Figure 3. Diagram of teleseismic P-wave incident beneath a model geothermal system.
- Figure 4. Graphs showing power density spectra and spectral ratios from the Geysers-Clear Lake array for a typical event.
- Figure 5. Graph showing dominant frequencies of P-phases along northwest-southeast line.
- Figure 6. Graphs showing differential attenuation for each station as a function of distance and azimuth.
- Figure 7. Maps showing two-dimensional contoured surface fitted to averaged δt^* .
- Figure 8. Graph showing simplified Q model for the Geysers-Clear Lake KGRA.
- Figure 9. Bouguer gravity map of the Geysers-Clear Lake KGRA over area of seismic attenuation study.

GENERALIZED GEOLOGY

-  ALLUVIUM
-  CENOZOIC VOLCANIC ROCKS
-  GREAT VALLEY SEQUENCE
-  FRANCISCAN ASSEMBLAGE
-  SERPENTINE AND OPHIOLITIC ROCKS

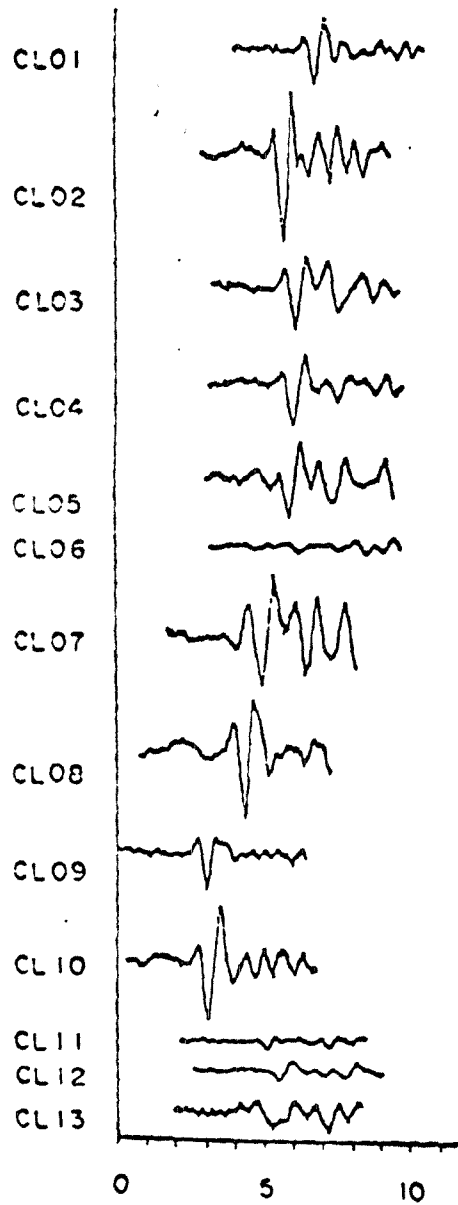
• F SPRINGS AND FUMAROLIC AREAS

 MAJOR FAULT ZONES

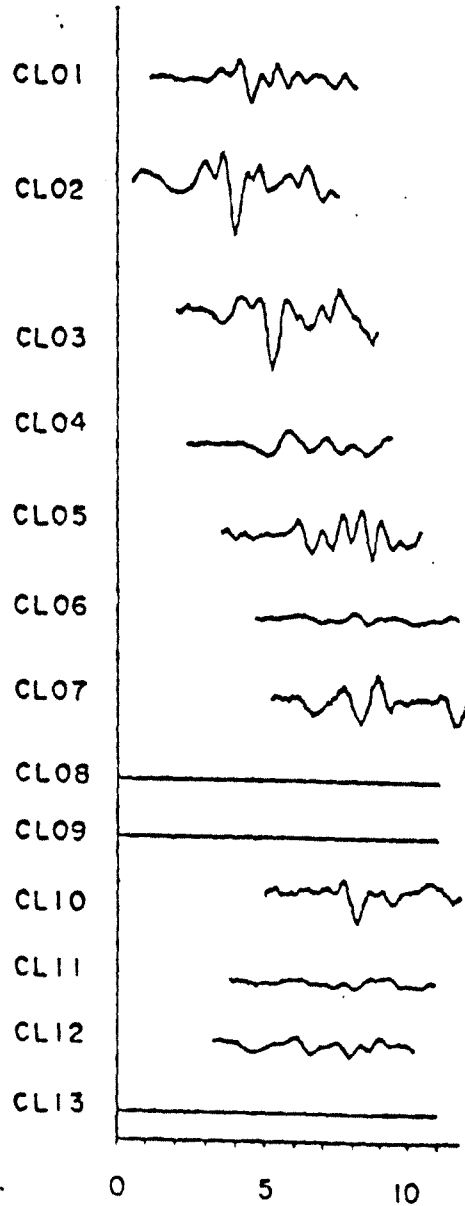


47.1

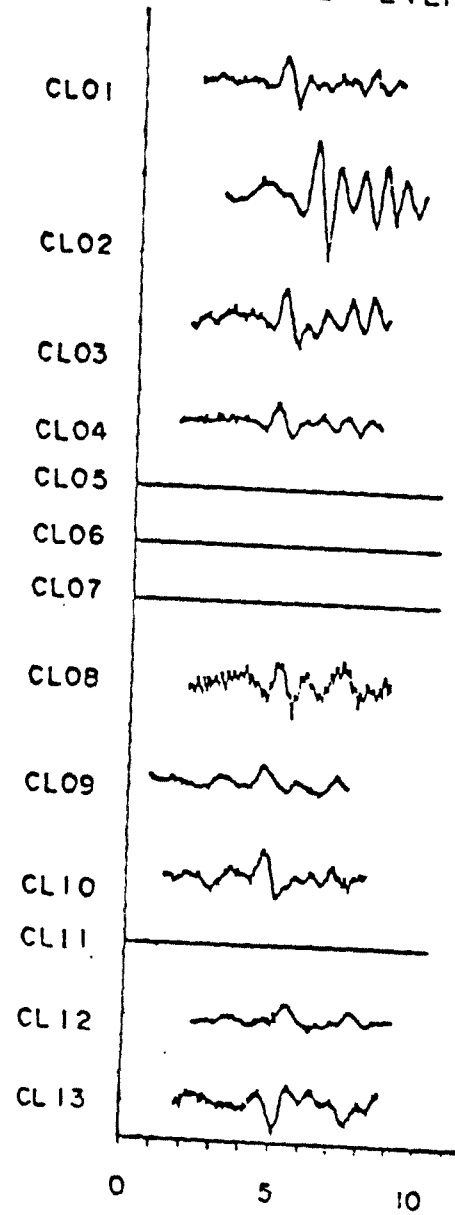
GEYSER EVENT 13



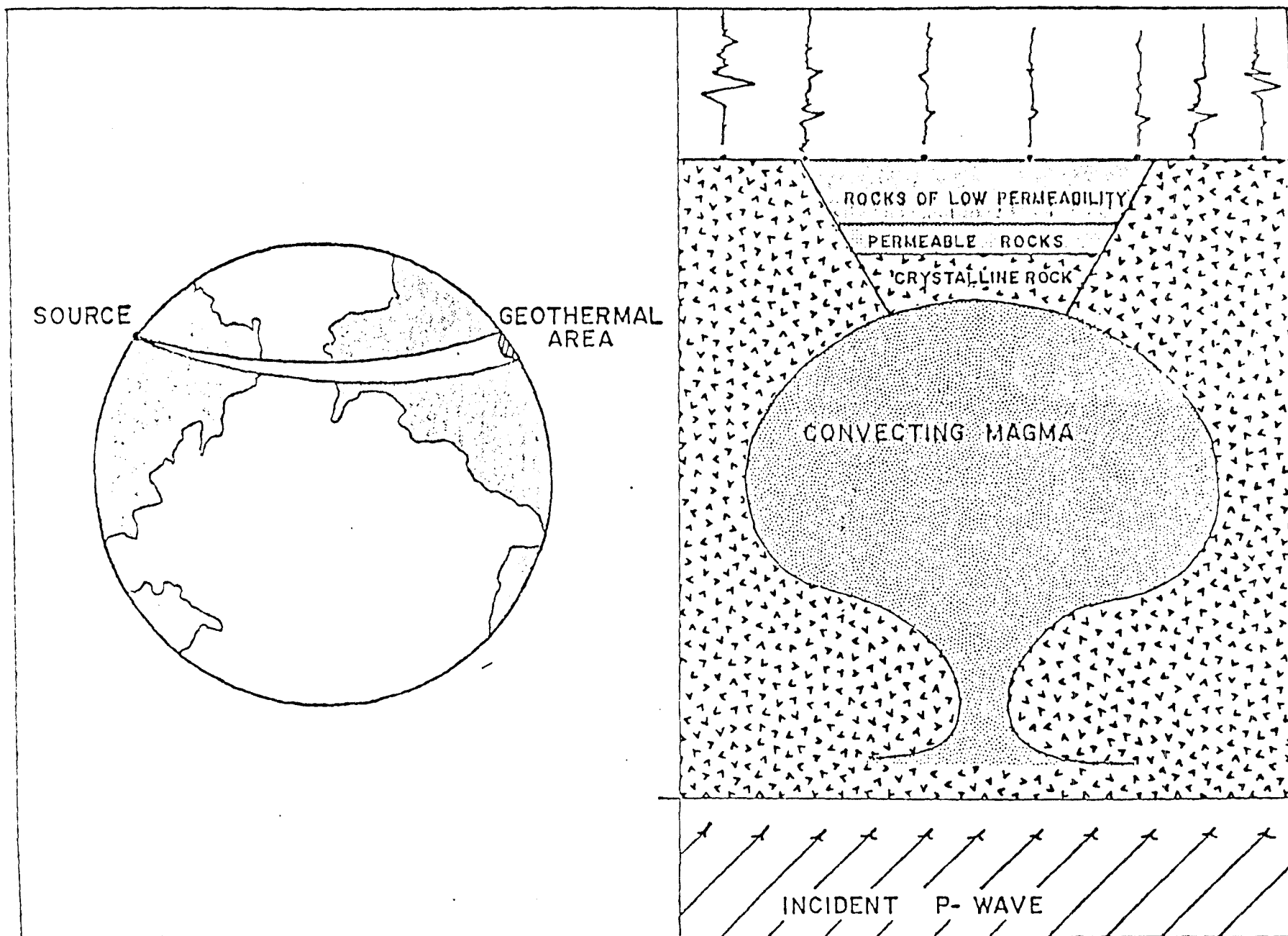
GEYSER EVENT 20

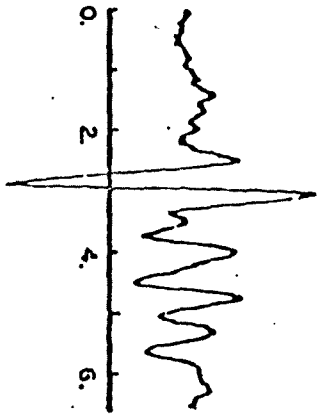


GEYSER EVENT 17

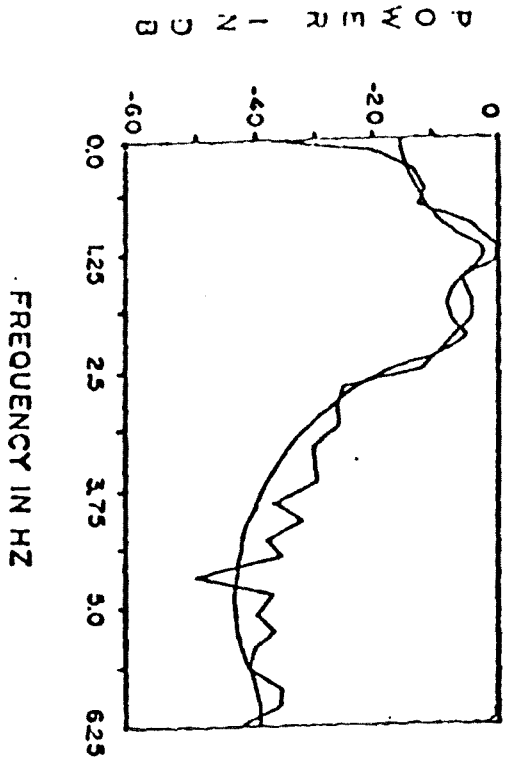


TELESEIMIC P-WAVES INCIDENT ON MODEL GEOTHERMAL SYSTEM





GEYSER EVENT 13

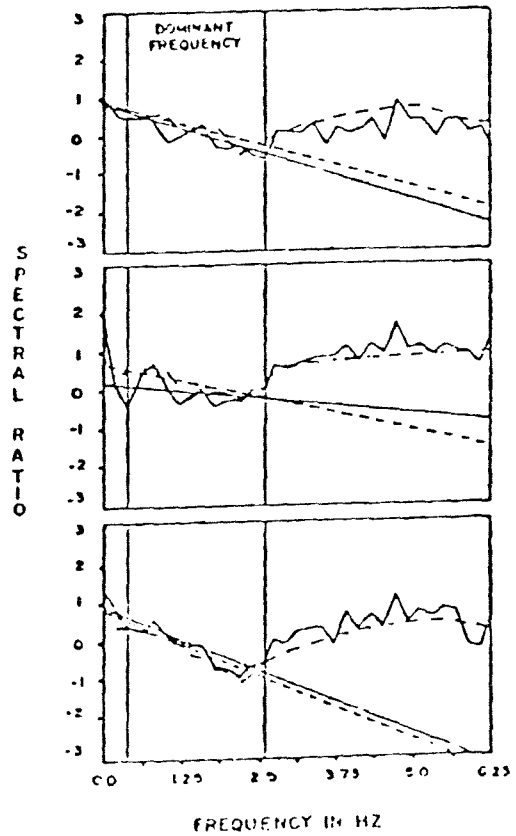
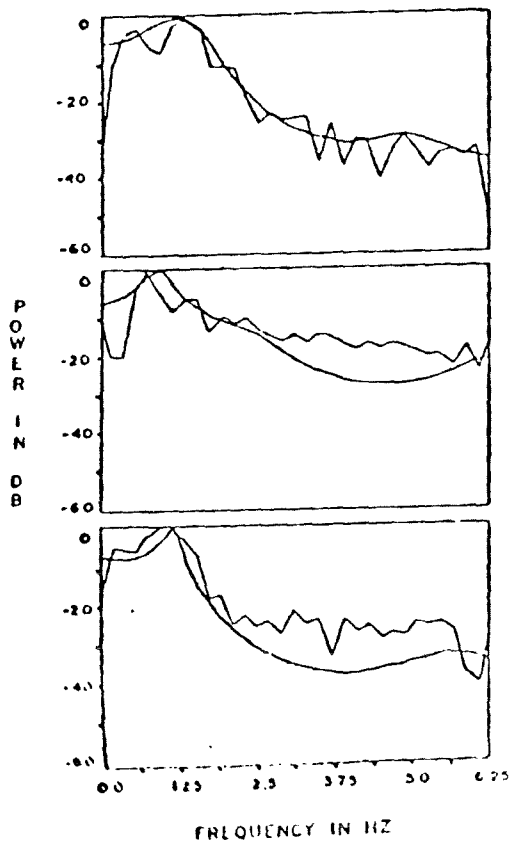
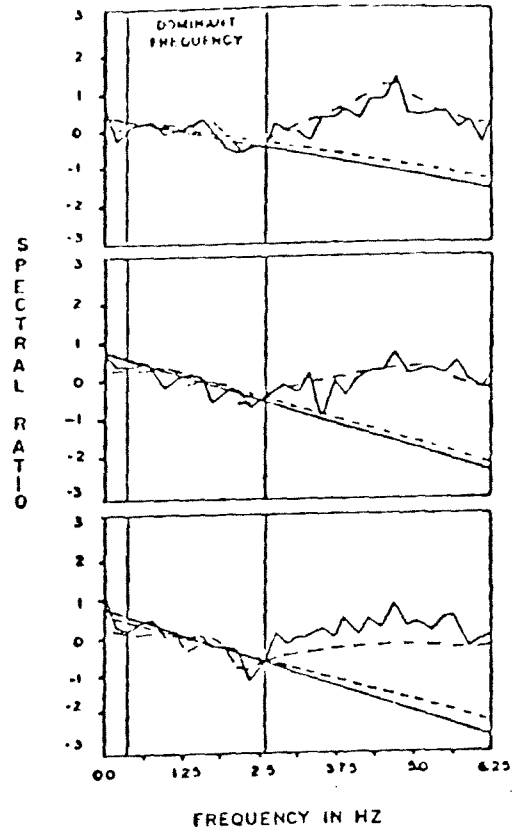
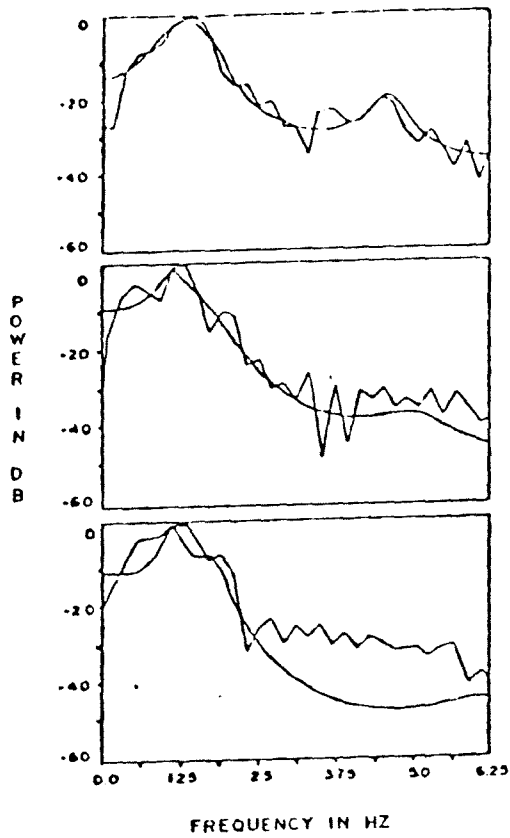


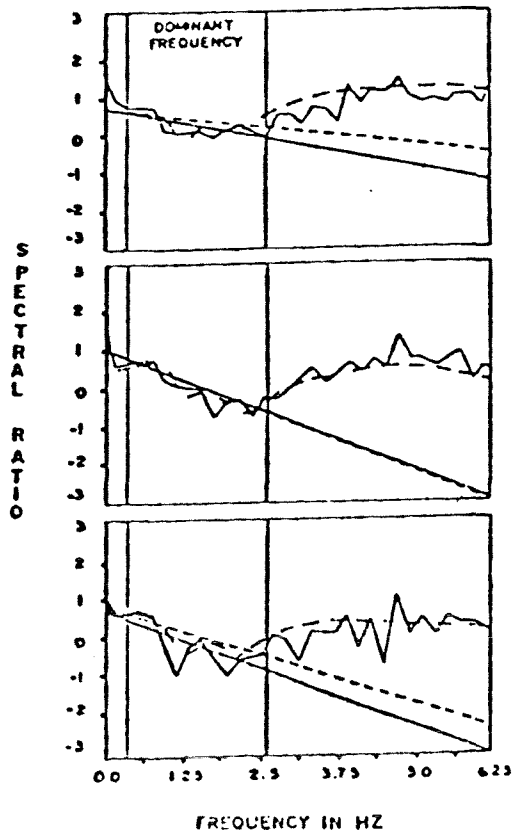
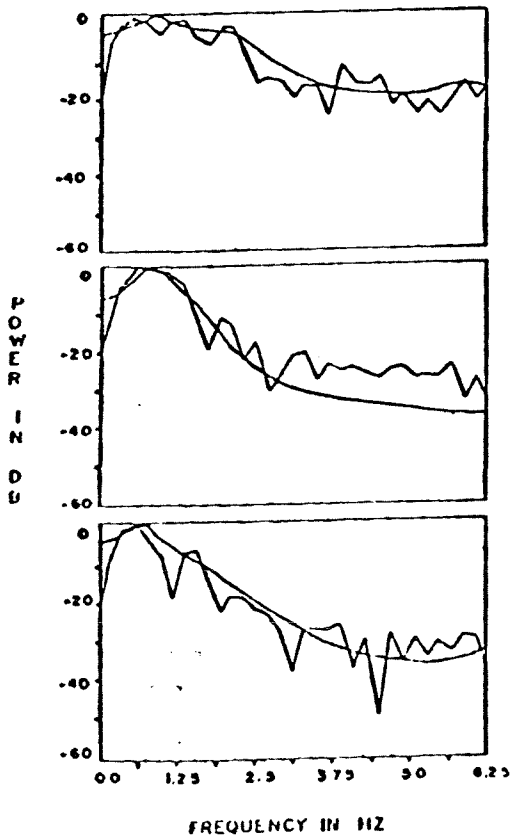
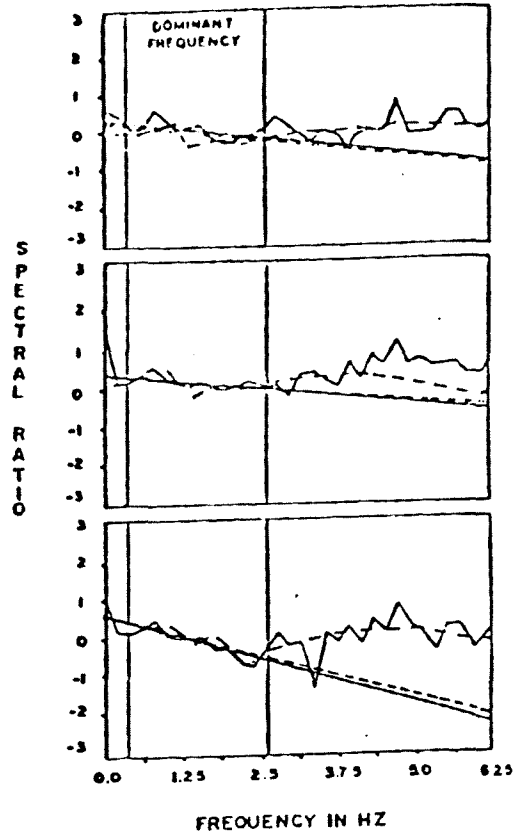
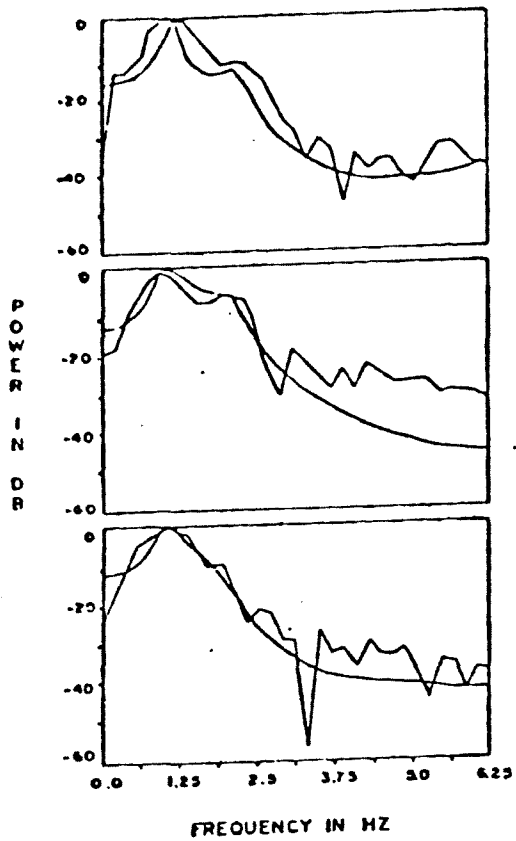
STATION 2

Fig. 1

Figure 1

Geology 101

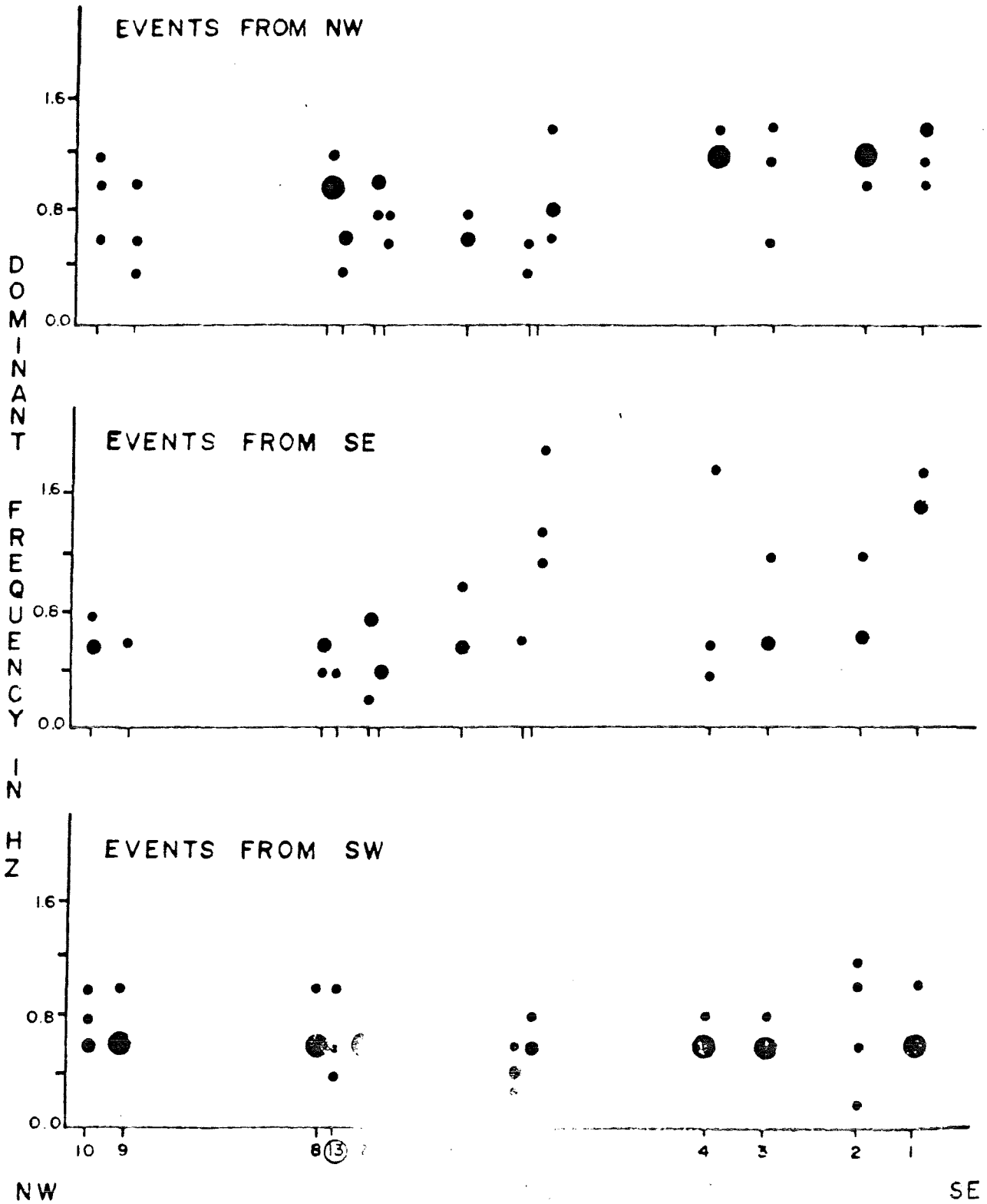




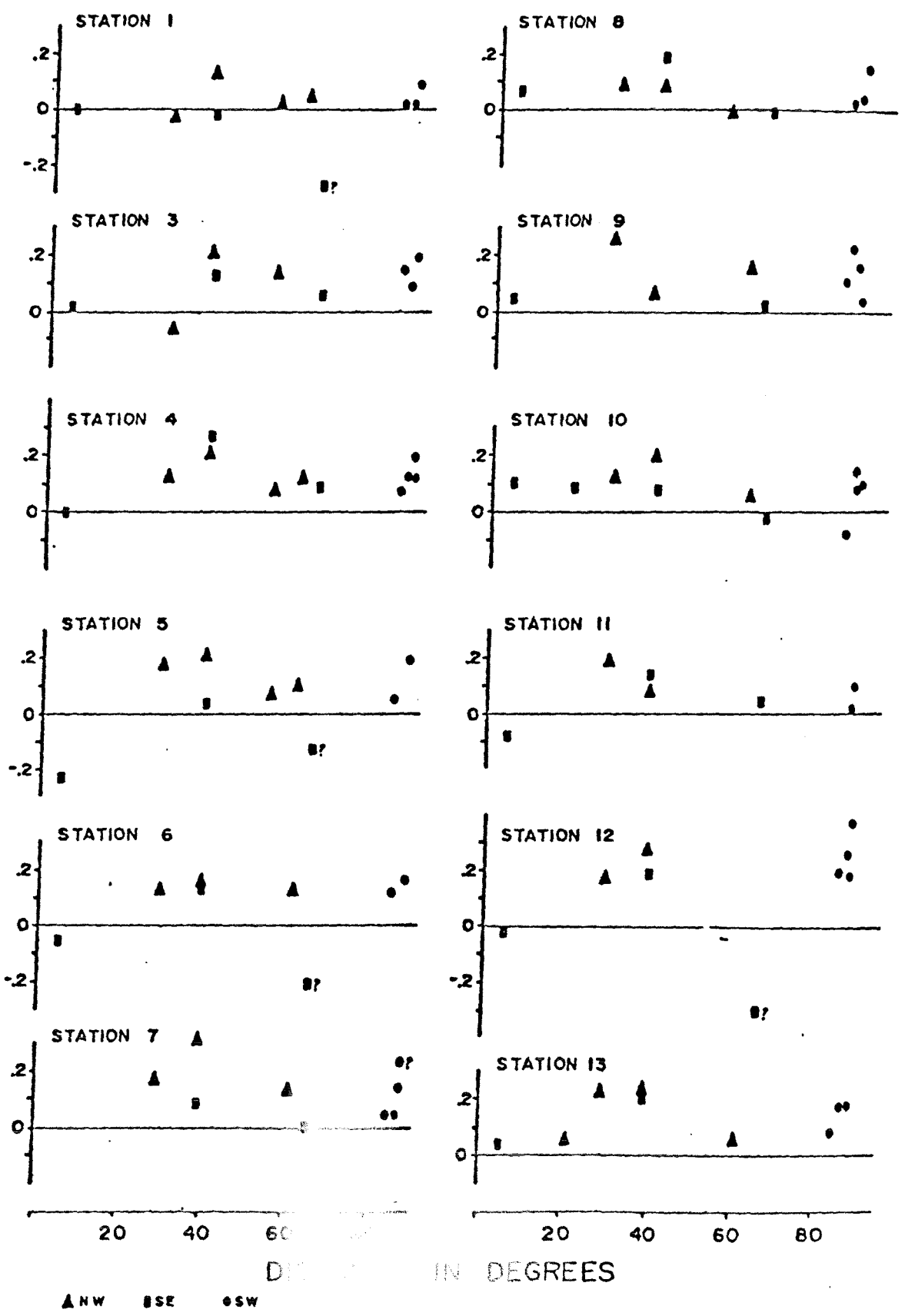
Handwritten signature or text at the bottom of the page.

SPECTRAL PEAK FREQUENCY

- 1 EVENT
- 2 EVENTS
- 3 EVENTS



DIFFERENTIAL ATTENUATION IN SECONDS



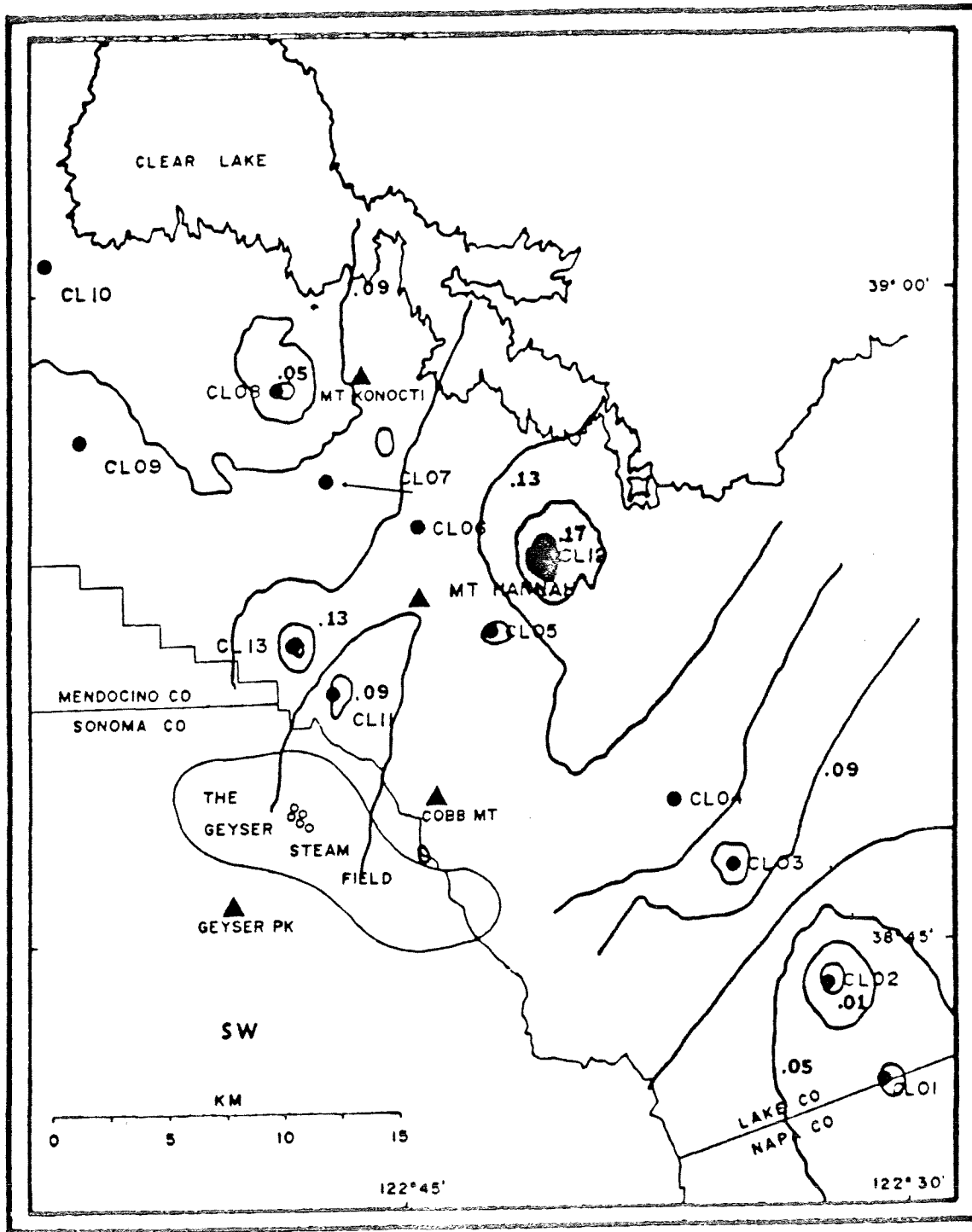


Figure 7A

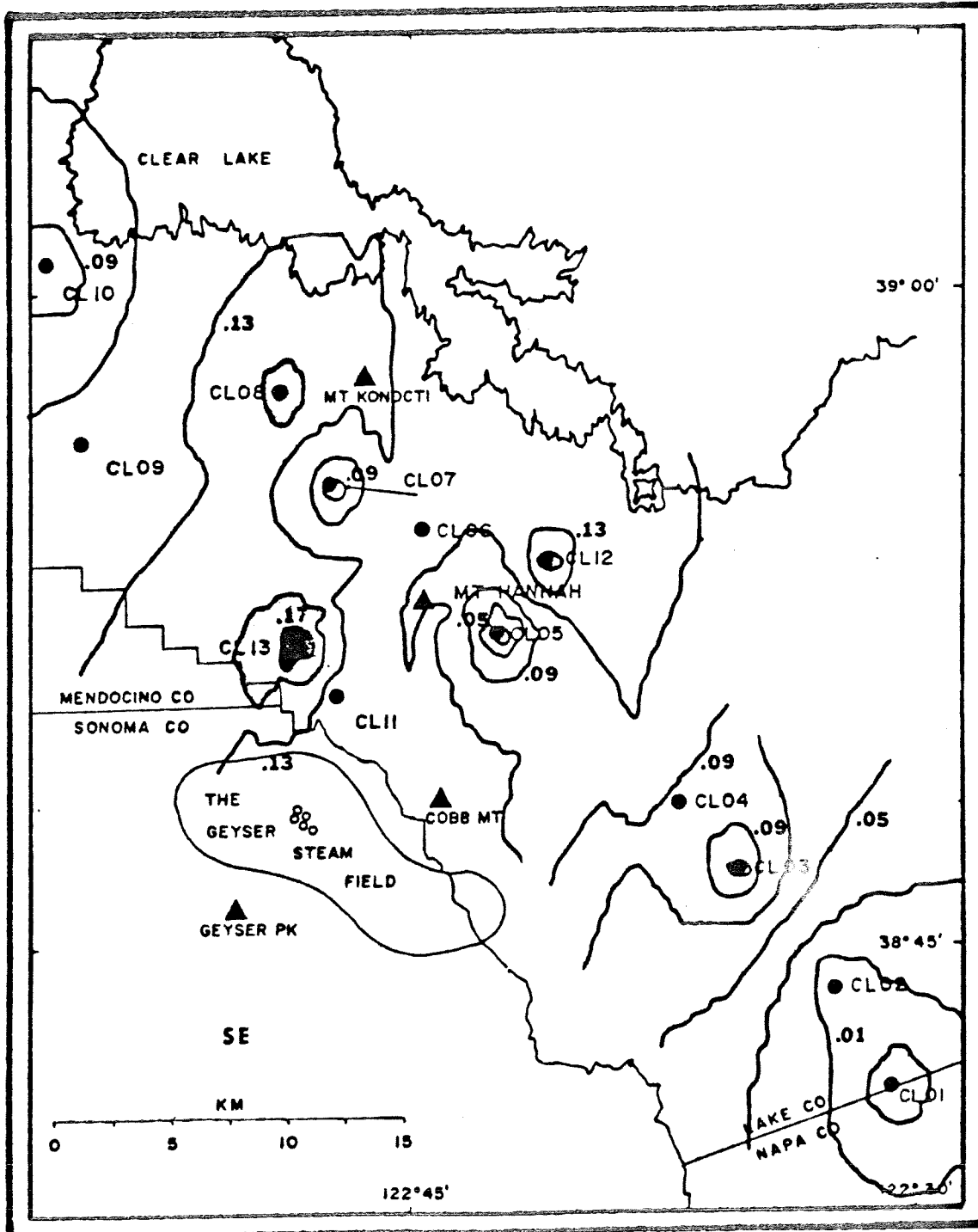
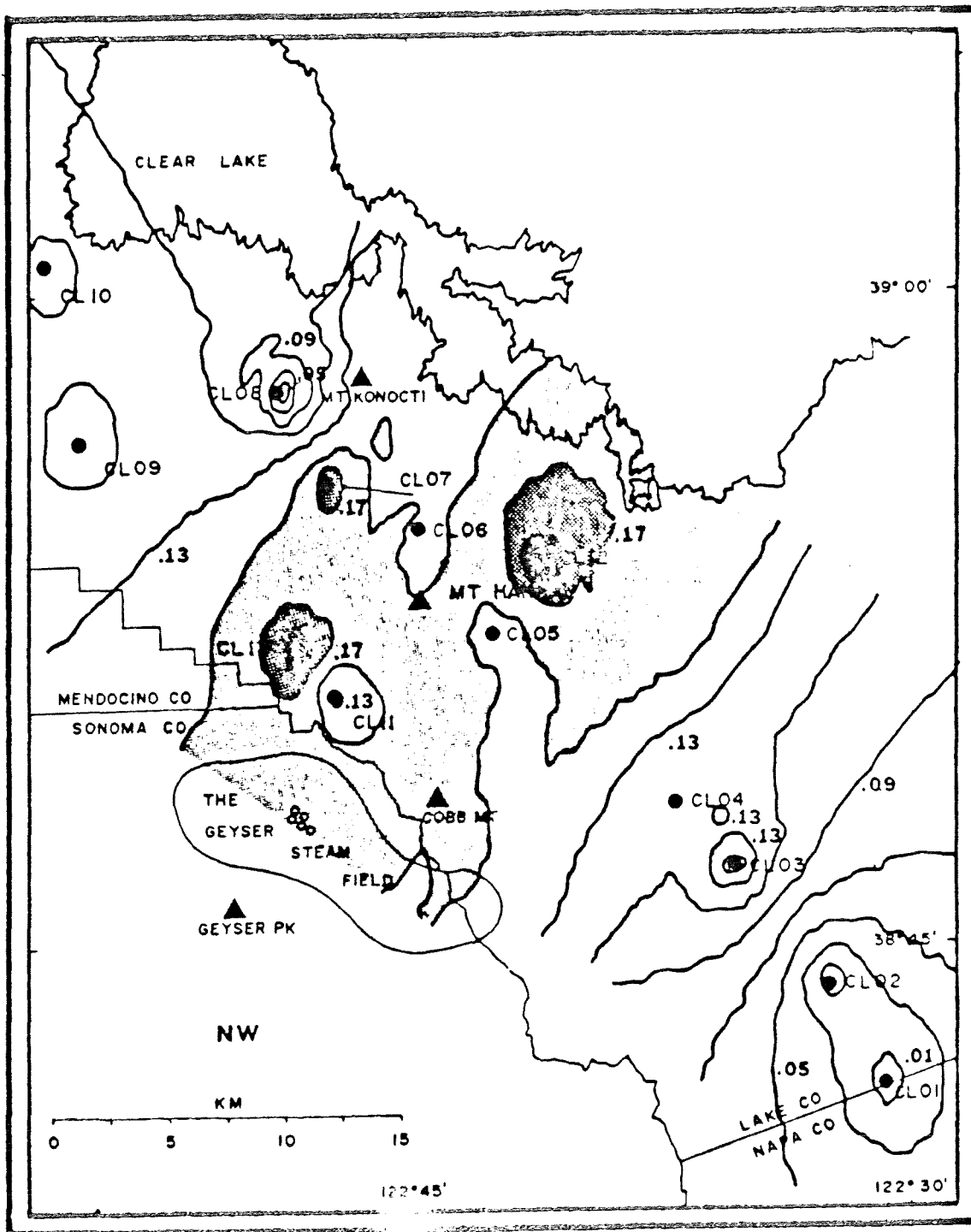


Figure 7B.



SIMPLIFIED Q MODELS
LOW Q LAYER THICKNESS

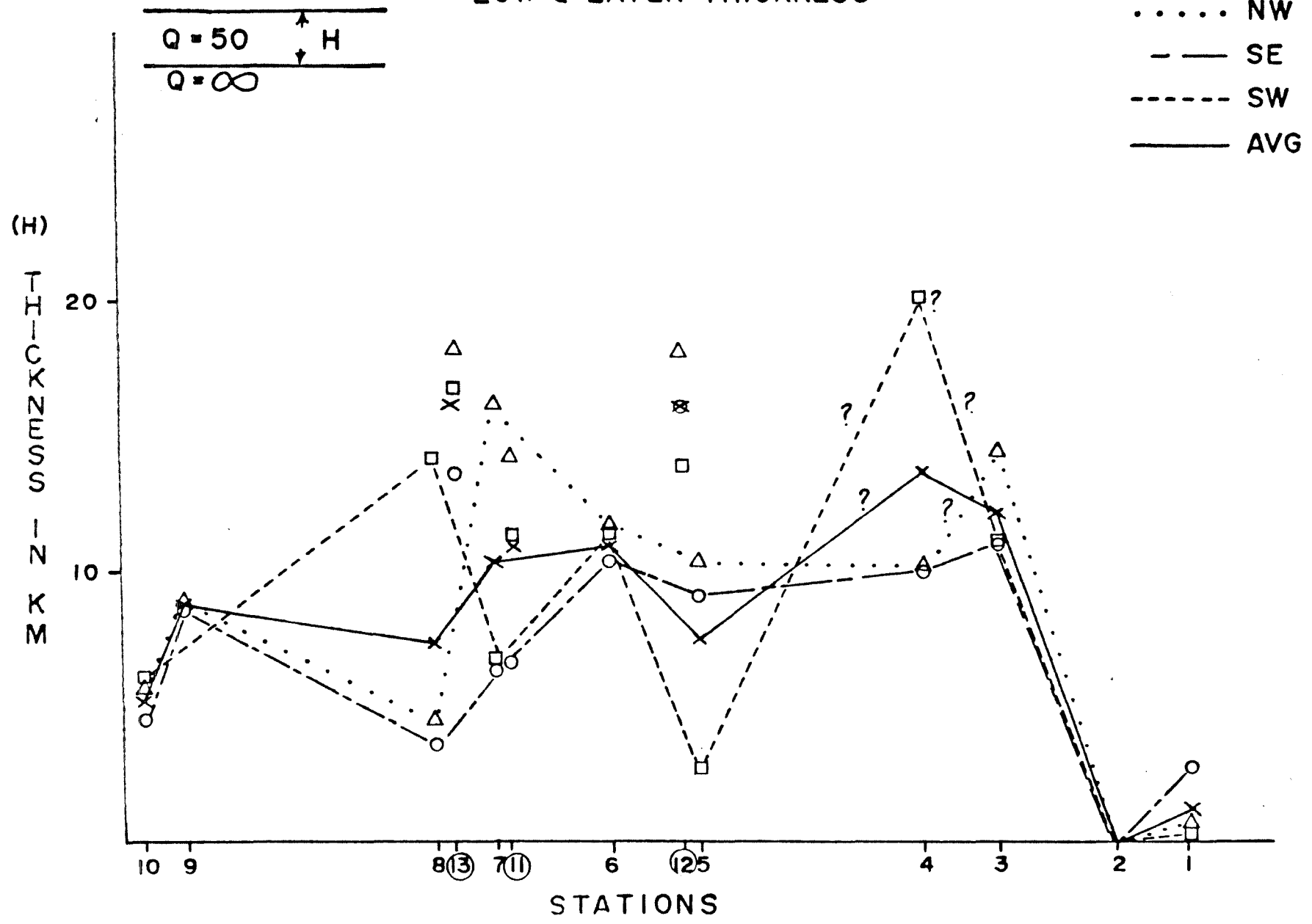


Figure 8.

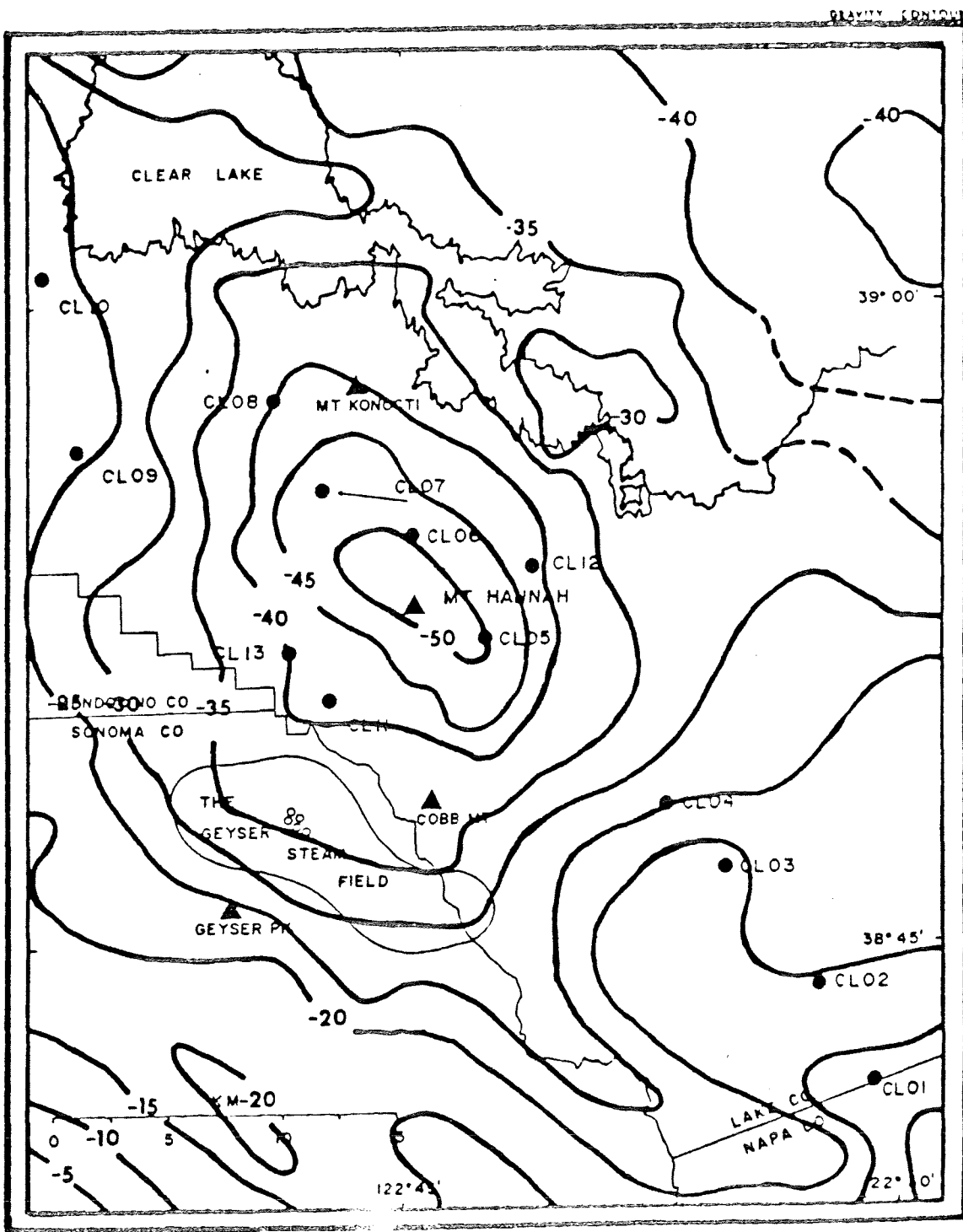


Figure 9.

2-D LINEAR INVERSION OF INACCURATE δt^* DATA

Ronald W. Ward

and

Chi-Yuh Young

Center for Energy Studies
University of Texas at Dallas
Richardson, Texas 75080

ABSTRACT

The two-dimensional generalized discrete linear inversion technique has been applied to inaccurate differential attenuation data of teleseismic P-waves to construct Q^{-1} models of geothermal systems. Four sources of δt^* errors are identified and modeled using synthetic data for 12 events and 11 stations. Various levels of random errors are added to synthetic data for 8 different assumed models, which are inverted to assess the effect of inaccuracies on the inferred Q structure. For signal to error ratios (S/E) above 5 the models are reproducible, between 5 and 1 a dramatic degradation of fidelity occurs and at 1 or below numerous low Q cells are identified as high Q and vice versa. Acquisition of more numerous better distributed data with lower error improves the quality of the inversion. An example from the Geysers-Clear Lake geothermal area with S/E of 4 is included to illustrate the use of this study in the interpretation of a zone of high attenuation lying in the middle crust southeast of Mt. Hannah.

INTRODUCTION

One class of theoretical geophysical problems involves predicting or computing the geophysical surface observations for an assumed earth model. For this class of forward problems the analytical relationship between the geophysical observation and the earth model parameters must be known, that is one can calculate theoretical values of observables corresponding to specific values of earth model parameters. After the solution of the forward problem is known, one can begin to address a second class of problems known as inverse problems. In the geophysical inverse problem, one seeks to estimate all values of earth model parameters, which produce a specific observation data set within a small tolerance, based on mathematical conditions such as minimizing the standard errors between the observed and theoretically calculated data.

General treatment of the geophysical inverse problem was presented in the lengthy discussion by Backus and Gilbert (1967, 1968, and 1970). They formalized the inversion of free oscillation data to obtain all possible earth structures consistent with these observations. Their earth model parameters are continuous spatial functions. The inversion requires the calculation of the Frechet derivative. Reparameterization and discretization of the linear or quasi-linear inverse problem were described by Wiggins (1972) and Jackson (1972) utilizing a method called spectral decomposition of the matrix (Penrose, 1955; Lanczos, 1961). Geophysical inverse theory has been applied to different geophysical problems with a variety of approaches, e.g., the stochastic seismic inverse (Der, et al., 1970; Franklin, 1970; and Jordan and Franklin, 1971), the Monte Carlo inverse of seismic traveltime data (Press, 1968; Wiggins, 1969), the non-linear of seismic traveltime data (McMechan and Wiggins, 1972; Jackson, 1973; and

Kennett, 1976), linear programming inversion of free oscillation and attenuation observations (Lee and Solomon, 1975), gravity data (Jupp and Vozoff, 1975; and Parker, 1975), and electromagnetic problems (Bailey, 1970; and Pelton, et al., 1978).

Recently, Aki and others (1976, 1977) used teleseismic P-wave travel-time residuals observed at a local array of seismographs, to calculate the three-dimensional perturbation of a velocity model. Both generalized inverse and stochastic inverse methods were applied to the data to successfully determine the existence of small-scale heterogeneities within the lithosphere. Later, Iyer (1978) applied their technique to the P-wave velocity anomaly beneath the Yellowstone geothermal system and inferred a zone of partial melting characterized by lower velocity than its surroundings extending to a depth of 250 km.

The present authors have applied the discrete linear inverse theory (Wiggins, 1972; Jackson, 1972) to infer an attenuation model for the earth beneath two geothermal systems (Young and Ward, 1979a and b) using the lateral variations of the power density spectra of teleseismic P-waves. These observations are corrupted by the two following types of errors; (1) errors due to departures of the earth from the theoretical attenuation model and the analysis procedures which assumes certain factors are predicted or removed and (2) errors in the estimation of the power density due to the short record length as well as the interfering waves, and ambient noise, corrupting the observation. The reduced spectral ratio technique (Teng, 1968; Ward and Toksoz, 1971; Solomon, 1970 and 1972; Ward and Young, 1975; Young and Ward, 1979a, b) expresses the observations as differential attenuation factors δt_{ij}^* of an event, i , observed at station, j . The objective of the present study is to determine the effect of these errors

on the interpreted Q-model. These results will provide a guide for interpreting field observations. The effect of errors will be studied by applying the inversion technique to synthetic observations for a large suite of known 2-D Q-models of different types. Synthetic data with different magnitudes of the signal to error ratio are inverted to measure the sensitivity of the inversion results to the size of the error. The δt^* data published for the Clear Lake volcano field in the paper by Young and Ward (1979a) is inverted to obtain a 2-D Q model.

THEORY OF DISCRETE LINEAR INVERSION

Most geophysical data can be described by an integral transform equation (Fredholm integral equation of the first kind).

$$e(x) = \int G(x,y) M(y) dy \quad (1)$$

where $M(y)$ is the unknown model parameter function, $e(x)$ is observations, and $G(x,y)$ is a kernel function derived from theory.

If the expression on the right hand side of equation (1) is a linear function of the model parameter $M(y)$ and $G(x,y)$ depends only on the difference in position, then it is correct for discretized model to approximate equation (1) in matrix notation as

$$\begin{matrix} A & X & = & Y \\ m \times n & n \times 1 & & m \times 1 \end{matrix} \quad (2)$$

where m spans the space of the geophysical observations, n spans the space of the unknown earth model parameters. The observational error and the variances of the unknown parameters can be treated as weighting factors and introduced on both sides of equation (2) (Wiggins, 1972). Equation (2) becomes

$$S^{-1} A W^{-1} X = S^{-1} Y$$

where S and W are diagonal matrices containing the weighting factor. The goal is to find a matrix H ($n \times m$) which can operate on equation (2) to give the optimal solution "X".

A $n \times n$ identity matrix, I , is defined as a matrix with all the diagonal elements equal to unity and the off-diagonal elements equal to zero. Then for any $n \times n$ matrix, B , $BI = IB = B$ must hold. H is called the inverse of B , if $HB = BH = I$. If B is orthogonal, then H is equal to the transpose of B

matrix, and a single inverse of A does not exist. However, there is still a possibility that a matrix H exists in a least square error sense and satisfies the criterion that HA or AH is close to I and the variance of X is minimum (Jackson, 1972).

The inverse matrix, H, of a square matrix B can be written in terms of the solution to the eigenvalue problem:

$$B V = V \Lambda \quad (3)$$

where Λ is a diagonal matrix containing the eigenvalues and V is the orthogonal matrix whose columns are the eigenvectors associated with the eigenvalues. Since V is orthogonal, multiplying equation (3) by V^T , factors the matrix B into three matrices, i.e. $B = V \Lambda V^T$, termed the spectral expansion of a matrix (Parker, 1977). If zero eigenvalues do not exist, the matrix H, the inverse of B is simply, equal to $V \Lambda^{-1} V^T$.

We can extend this idea to the generalized eigenvalue problem for a rectangular matrix as discussed by Lanczos (1961). Two sets of eigenvectors U and V may be found such that

$$A V = U \Lambda \quad (4a)$$

$$A^T U = V \Lambda \quad (4b)$$

or

$$A A^T U = U \Lambda^2 \quad (5a)$$

$$A^T A V = V \Lambda^2 \quad (5b)$$

where Λ is similar to that in equation (3) but contains the positive square root of the p non-zero eigenvalue of the matrix AA^T or $A^T A$ depending on whether the problem is underdetermined or overdetermined. Geophysically, U contains p data eigenvectors of length m associated with the observations. V contains p model eigenvectors of length n associated with the unknown earth

model parameters. The matrix A can be factored into the product of three matrices

$$\begin{matrix} A & = & U & \Lambda & V^T \\ m \times n & & m \times p & p \times p & p \times n \end{matrix} \quad (6)$$

and the inverse of A can be written as

$$H = V \Lambda^{-1} U^T \quad (7)$$

The existence and uniqueness of the matrix H for a linear system depends upon the rank p (p = the number of nonzero eigen values used) and the dimension m,n of the matrix A (Lanczos, 1961).

1. If $p=m=n$, (a well posed case), the solution is unique.
2. If $p=m>n$, (underdetermined case), the solution is not unique.
3. If $p=n<m$, (overdetermined case) the solution is unique provided the observations satisfy certain compatibility conditions.
4. If $p < \frac{m}{n}$, the solution is not unique and the observations will be constrained.

The geophysical inverse problems occur most often as case 2 - 4. However, the mathematical procedure to solve equation (2) for all cases is similar. The solution can be obtained in a least square error sense, by minimizing

$$\epsilon^2 = |AX-Y|^2$$

Both Wiggins (1972) and Jackson (1972) showed that "The natural inverse of a matrix" derived by Lanczos (1961) is essentially the same as the least square error solution, obtained using the spectral expansion technique.

The general solution X_g can be written as $X_g = H Y$. For statistically independent data, the variance of the model parameter, x_k , can be expressed as

$$\text{var}(x_k) = \sum_j H_{kj}^2 \text{var}(y_j) \text{ which is proportional to } \sum_j \left(\frac{v_{kj}}{\lambda_j} \right)^2 \quad (8)$$

For small nonzero eigenvalues λ_j , $\text{var}(x_k)$ becomes very large. It is necessary to set up a threshold to eliminate those eigenvalues which are too small. We will choose a threshold of 1% of the largest eigenvalue.

The underdetermined or overdetermined case can be considered separately.

1. From equation (2) and the expression for the general solution X_g , we have $X_g = HAX = HY$, where X represents the true solution. In this case $R = HA = VV^T$ is a measurement of the resolution for the underdetermined system (Backus and Gilbert, 1968; Jackson, 1972). The k -th unknown parameter is perfectly resolved, if the corresponding k -th row of the matrix is equal to a Kronecker delta function. R is thus called the resolution matrix.

2. Since $X_g = HY_{\text{obs}}$, then $AX_g = AHY_{\text{obs}} = Y_{\text{theoretical}}$. If the k -th row of $S = AH = UU^T$ is equal to a Kronecker delta function, then the k -th theoretical value is identical to the k -th observed value. The matrix shows the information contained in the observed data for the over-constrained systems (Wiggins, 1972), and is called the information density matrix.

If both R and S equals the identity matrix, then the solution is unique.

Jackson (1972) has shown that the approach, which gives the Lanczos solution, is optimal in a least square error sense, always exists, and minimizes $|X|^2$

$$r_k = \sum_{i=1}^m (H_{ki} A_{ij} - \delta_{kj})^2 \text{ for underdetermined case or,}$$

$$s_k = \sum_{j=1}^n (A_{ki} H_{ij} - \delta_{kj})^2 \text{ for overdetermined case.}$$

The above procedure gives a unique inverse matrix H after discarding the zero eigenvalues (or very small eigenvalues) and the eigenvectors associated with them. There are an infinite number of solutions which will have identical values of the least square error for an underdetermined system. These solutions all have identical components of the nonzero eigenvectors but different components of the zero eigenvectors. Any solution can be expressed as (also see Jackson, 1972).

$$X = V\alpha + V_0\alpha_0 \quad (9)$$

where $V\alpha$ is the solution obtained from the nonzero eigenvalues. Only α is fixed, and the columns of V_0 contain the eigenvectors associated with the zero eigenvalues, where α_0 is arbitrary. X in equation (9) satisfies the least square criteria for any α_0 , because $VV_0^T = 0$. The addition of $V_0\alpha_0$ into equation (9) does not change the square error $\epsilon^2 = |AX - Y|^2$.

The importance of the above result is that one can always choose α_0 to force the solution X toward a solution which is geophysically more meaningful. By introducing this idea into equation (9), Jackson shows that $\alpha_0 = V_0^T f$, and the final solution which best approximates the favored function, f , is given as:

$$X_f = X + V_0 V_0^T f \quad (10)$$

MEASUREMENT OF SEISMIC ATTENUATION AND INVERSION

Based on the results from theoretical and laboratory experiments, there are several possible mechanisms whose relative importance varies with the thermal regime, which can explain the observed seismic attenuation. Even small amounts of partial melting (Knopoff, 1964; Walsh, 1968, 1969; and Kjartansson, 1979) or partial saturation (White, 1975; Winkler and Nur, 1979) can enhance the attenuation of P-waves. Several attenuation mechanisms on a microscopic scale have been recognized such as grain boundary relaxation, internal friction (Jackson and Anderson, 1970), and more recently proposed dislocation bowing effect (Anderson and Minster, 1979). Although the relationship between seismic attenuation and temperature within a geothermal system is not well understood at present, the thermal state and concentration of partial melting are believed to contribute to high attenuation of seismic waves (Kjartansson, 1979). Mapping the lateral variation of seismic attenuation is an effective tool in locating and estimating the potential of a geothermal system.

The quantity that represents the amount of energy loss from a propagating wave, is the reciprocal of the quality factor, Q , of the medium through which the wave passes. Seismologists have tried to measure Q for different parts of the earth by using body waves and surface waves. The classical approach to this problem is to measure the absolute spatial decay rate of wave amplitudes in the time domain (Gutenberg, 1958). The problem with this approach is that it fails to account for such effects as the source mechanism, wave scattering and geometrical spreading. Anderson and Archambeau (1964) tried to avoid these difficulties by analyzing the amplitude of long period surface waves successively passing through a station. (1968) employed the spectral ratio technique applied to a large number of P-waves and obtained a detailed Q structure for

the deeper part of the mantle. This technique has been used in different forms to study attenuation phenomena and Q structure (Kanamori, 1967; Solomon and Toksöz, 1970; Ward and Toksöz, 1971; Solomon, 1972, 1973). More recently, Lee and Solomon (1975) inverted the surface wave phase velocity and attenuation data simultaneously to determine the shear wave velocity and Q-model with depth for the upper mantle.

Using reduced spectral ratio method, Young and Ward (1979a) made quantitative measurement of the attenuation of the teleseismic P-waves within a geothermal area. The details of the procedure to estimate δt^* were described in the paper published by Young and Ward (1979a). The quantity, δt^* , called the differential attenuation factor, represents the degree of the seismic attenuation. Larger positive values of δt^* represent higher seismic attenuation as observed at a station compared to a reference station with zero δt^* .

The relation between the quality factor, Q, and δt^* can be expressed as an integral formula (Teng, 1968)

$$\begin{aligned} \delta t^* &= \pi \int (\delta Q^{-1}) \frac{ds}{V} \\ &= \pi \int (\delta Q^{-1}) dT \end{aligned} \tag{11}$$

where V is velocity, dT is differential travelttime, and the integral is carried out along the ray path, ds. In equation 11, δt^* is the observed data we obtained from the spectral ratio method (Young and Ward, 1979a). δQ^{-1} is treated as unknown parameter. Assuming a spherically layered earth model, a ray tracing technique developed by Julian and Anderson (1968) is used to calculate dT. Further, we assume that the earth model is composed of discrete rectangular cells, with δQ^{-1} is constant (fig. 1). The

integral of equation 11 reduces to a summation, and the problem has been linearized.

$$\delta t_j^* = \pi \sum_{\text{ray}} (\delta Q^{-1})_i \Delta T_{ij} \quad (12)$$

where the summation is taken over the cells through which the ray passes and ΔT_{ij} is the travelttime to the jth station through the ith cell. Gathering n calculated δt^* values from P waves recorded at different stations for different events, equation 12 can be written in matrix form for m cells as

$$AX = \pi \begin{bmatrix} \Delta T_{11} & \dots & \Delta T_{m1} \\ \cdot & & \\ \cdot & & \\ \cdot & & \\ \Delta T_{1n} & & \Delta T_{mn} \end{bmatrix} \begin{bmatrix} \delta Q_1^{-1} \\ \cdot \\ \cdot \\ \cdot \\ \delta Q_m^{-1} \end{bmatrix} = \begin{bmatrix} \delta t^*_1 \\ \cdot \\ \cdot \\ \cdot \\ \delta t^*_n \end{bmatrix} = Y \quad (13)$$

The generalized linear inverse theory can be applied to equation 13 and solved for the unknown, δQ^{-1} . The standard deviations for the measurement of δt^* is used as weighting function of the observation. The thickness of the model layer can be used as weighting function of the unknown parameter.

SYNTHETIC Q^{-1} MODEL

The observation error of the measurement of δt^* from field seismograms can arise in the following ways:

1. Additional coherent waves in addition to the teleseismic P-wave signals give erroneous power spectra. Furthermore, there is background noise due to wind, weather, tides, etc., which is recorded by the seismometers, instrumentation noise and folding of the high frequency noise caused by the finite sampling rate of digitization.

2. The estimation of a true power density spectrum with a short time segment of a signal introduces estimation errors.

3. The complicated structure of the crust and upper mantle causes reverberation and scattering of a seismic wave, which is not adequately treated in the model.

4. For a particular teleseismic event, the seismic wave incident beneath the array may not be exactly the same for all stations in the array, due to the source radiation pattern, and slight differences in ray path through the crust at the source and the mantle.

The first two sources of errors can be considered as random noise. But the third and fourth sources of errors are strictly speaking biased by the earth's structure and source characteristic. These deterministic errors are so complicated that they can only be introduced into the synthetic data as simple random numbers. There is no loss of generality, since the primary interest is to determine the sensitivity of the inverted Q model to observation errors in the δt^* values. This sensitivity will be determined by performing a numerical inversion experiment on synthetic data.

Equation 12 gives the relation between the quality factor Q and the differential attenuation factor δt^* . In testing the inversion procedure, we choose the reference station to have infinite Q so that the inverted result can be compared with the original Q model directly. The crust beneath a geothermal system is divided into rectangular cells. The assumption that Q is independent of frequency and constant within each cell make equation 12 linear. The solution to the matrix equation given in equation 13 can be obtained using simple matrix algebra. In a well posed or overdetermined case, the inversion of error free synthetic data is expected to reproduce the original model. In the underdetermined cases, the solution is dependent on the sampling of the rays through the model. If a cell does not have a ray passing through it, then it is impossible to resolve the Q in that particular cell. The resolution matrix has a null vector for such a cell.

Synthetic δt^* data were calculated for 12 assumed teleseisms which were chosen arbitrarily to lie on either side of 2-D 3 layer Q model (Table 1). The epicentral distances of the events range from 40 to 81 degrees. A total of 132 synthetic δt^* values are obtained for 11 stations deployed on the earth's surface. Figure 2, shows an inversion of error free data which gives the original model of a low Q ($=100$) zone surrounded by cells with higher Q values ($=500$) used to generate the synthetic data. The measurement of δt^* from field seismograms is never error free. The sensitivity of the inverted Q model to observation errors in the δt^* values will now be investigated for several levels of error and sets of synthetic data for different Q models.

The different 2-D Q models used to generate synthetic δt^* values are shown in Figure 3. The models include both buried anomalies, shallow

Table 1: Synthetic Teleseismic Events

Event No.	Distance (in degrees)	
1	54.0	} Incident from left side of the model
2	51.0	
3	57.0	
4	60.3	
5	68.0	
6	61.6	
7	81.0	} Incident from right side of the model
8	79.0	
9	77.0	
10	40.5	
11	41.7	
12	39.3	

anomalies, broad anomalies, etc. for a total of 8 different models. Random errors are added to the synthetic δt^* and then inverted separately. A computer random number generator is used to generate the random errors. The size of the error is determined by the signal amplitude and the signal to error ratio. The signal amplitude is defined as the root mean square (rms) of the synthetic δt^* values. The signal to error ratio is defined as the ratio of the signal amplitude to the rms random errors, the rms error is equivalent to the standard deviation of a set of random numbers with zero mean. After the initial seed for the random number generator, the last random number saved from the previous run is the new seed for the next run to insure the errors are randomized.

The shape of the low Q zone in the synthetic model does not have a significant effect on the inversion result at higher signal to error ratio. This indicates that the synthetic teleseismic waves did sample each cell of the model uniformly. This is an important factor, which stabilizes the inversion procedure. However, when the signal to error ratio drops below 5, models with a broad low Q zone (such as model a, c, e, f and g in Figure 3) are resolved better than models with small isolated or narrow low Q zone (such as model b, d and f in Figure 3). This indicates that data sets with smaller signal to error ratio can not resolve the fine structure of the earth well.

Figure 4 shows the quantitative relationship between errors in the inverted Q model as a function of the signal to error ratio in the observed δt^* data. For each inversion of synthetic data the root mean square deviation of the inverted Q^{-1} values from the assumed Q^{-1} value in each cell is computed and plotted. Four different levels of error have been added to the synthetic δt^* observations for each of the eight models shown

in Figure 3. The reliability of the inverted model drops significantly as the signal to error drops below 2. An empirical curve has been fit to the data from this numerical inversion experiment and is plotted in Figure 4. The range of signal to error ratio in which most field δt^* observations is indicated in Figure 4. Field observations lie in a critical region. In general, it is difficult to determine the absolute Q value precisely. However, within this critical region of signal to error ratio, it is possible to separate low Q zones from high Q zones.

The dependence of the inverted Q model on the level of the error will be illustrated for a specific example in Figure 5. With random errors 5% of the signal (signal to error ratio equals to 20) added to the synthetic δt^* s, the inverted result produces a Q model which reproduces quite closely the original Q values (Figure 5a). The inverted Q model for data with signal to error ratio equal to 5 preserves the shape of the low Q zone but the Q values of the surrounding cells (High Q zone) deviate from their true values, and in some models negative Q begins to appear for high Q zone (not shown in Figure 5). However, the result is surprisingly good for such low signal to error ratio (Figure 5b). This indicates that a large number of data points stabilizes the inversion procedure for overdetermined cases. For a signal to error ratio of 2 the inverted model differs significantly from the true model. Non causal, negative Q values also occur in the inverted model. The high Q and low Q zones are still delineated except of that a few may be placed in the wrong group. When the signal to error ratio drops to 1, the number of cells placed in the incorrect category are more numerous and several additional negative Q values result. (Figure, 5c).

The information density matrix is defined in the previous section has been discussed by Wiggins (1972) and Jackson (1972). For a well posed case in which every item of data is required the information density matrix equals the identity matrix. For data containing errors, the closer a row of S is to the unit vector, the smaller the error component of the corresponding δt^* value. In editing the observed δt^* data, the degree of variation of each row of S from a unit vector is an indication of data contributing little information, which may be seriously in error. These data can then be eliminated prior to inversion.

2-D Q^{-1} MODEL FOR GEYSERS CLEAR LAKE, KGRA

The Geysers-Clear Lake Known Geothermal Resources Area (KGRA) is located about 110 km north of San Francisco in the Coast Range of California. Geological and geophysical studies suggest a magma chamber or partially molten zone exists beneath the Clear Lake Cenozoic volcanic field (Chapman, 1966, 1975; Hearn et al., 1975; Iyer et al., 1979). This anomalous zone could also cause high attenuation of teleseismic P-waves. Microearthquakes and explosive source refraction surveys across the production zone (Majer and McEvilly, 1979) identify a high Q layer (steam production zone) lying over a shallow low Q zone (depth below 2 km) which characterize the geothermal reservoir.

The differential attenuation factors, δt^* , were determined by Young and Ward (1979a) using the teleseismic P-waves recorded by 14 USGS portable stations. All the stations are deployed along a line trending roughly NW-SE between Clear Lake and the Geysers KGRA (Figure 6). The center of the array is close to Mount Hannah. The nearly linear distribution of the seismograph stations restricts the control on the inversion from the observed δt^* to a two-dimensional δQ^{-1} model. A total of 6 teleseismic events were used in this study, three with epicenters in the Aleutian Arc region, two with epicenters in South America (table 2). The standard deviation of the calculated differential attenuation factor is determined by the least square error of the straight line fit to the spectral ratio. This error level can be as high as the size of the δt^* value.

For these events, the signal to error ratio equals to 4. Reasons for this inaccuracy have been discussed in the previous section. The experience of the synthetic modelling indicates that it is possible to separate a low Q zone from a high Q zone from the inversion of such kinds of data, but

TABLE 2: List of the teleseismic events used in the inversion study

<u>Event #</u>	<u>Origin Time</u>	<u>Lat.</u>	<u>Long.</u>	<u>Epicenter</u>	<u>M_o</u>	<u>Depth</u>	<u>Δ</u>	<u>Azimuth</u>
1	8-16-76 122832.4	N51.918	E158.431	Kamchatka	5.3	50	54.16	311.68
2	8-20-76 035600.6	N45.048	E149.781	Kuril Is.	5.5	47	61.05	306.88
3	8-28-76 023009.2	N52.597	W175.343	Aleutians	5.1	145	38.32	308.73
4	8-24-76 212612.2	S25.366	W70.694	S. Chili	5.6	8	80.44	133.86
5	8-26-76 143000.2	N37.125	W116.082	NTS	5.3	0	5.40	106.81
6	9-02-76 102025.9	N13.259	W89.989	Guatemala	5.0	81	38.51	122.67

the exact values of Q are not well determined and may contain significant errors. Negative δQ^{-1} values for high Q zone are expected for such signal to error ratio. CL2 which lies to the southeast of the anomaly is used as a reference station. It was established previously (Young and Ward, 1979a) that seismic waves propagating to stations CL01 and CL02 experience negligible attenuation. The Q values in the model derived are based upon the assumption that station CL02 has infinite Q and hence it served as an upper bound on the true Q values. The δt^* observed for station CL11 and CL13 were not utilized in the inversion procedure. Both stations show high attenuation of seismic waves for teleseismic events occurring in different azimuths, indicating the existence of a shallow low Q region to the southwest of the ^(Callaymi) Callaymi fault zone as discussed elsewhere (Majer and McEvelly, 1979). The frequency range of the teleseismic P-waves and the near normal angle of incidence did not allow us to distinguish the relatively thin high Q layer mentioned by Majer and McEvelly.

Figure 7 shows a 3 layer Q model for the Geysers Clear Lake region. As noted earlier, the Q -values derived from the δQ^{-1} represent upper bounds on the true Q model. However, the relative change is preserved. The two-dimensional model is the cross section along the NW-SE line A-A' shown in Figure 6. The horizontal dimension of each cell is 8.25 km, with layer boundaries at the surface, 12, 20 and 33 km depth. The total dimension of the model is 50 km.

The near surface layer (0-12km) beneath the Clear Lake volcano field shows little attenuation except near the NW portion of the model south of Clear Lake. The intermediate layer between 12 and 20 km depth shows significant attenuation with Q values less than 50. The zone of maximum attenuation (Q less than 25) extends beneath Mt. Hannah approximately 12 km southeast. A zone of intermediate attenuation (Q less than 100) extends through

the crust beneath the Cenozoic volcanic field which may be the source supplying heat for the geothermal system.

The zone of high attenuation beneath Mt. Hannah is similar to that inferred from gravity data (Isherwood, 1979) and P-wave traveltime residuals (Iyer, et al., 1979). It extends somewhat further to the southwest than these studies predict.

CONCLUSIONS

Discretized Q^{-1} models for a geothermal system can be inferred by applying a generalized linear inversion technique to teleseismic P-wave differential attenuation data even in the presence of noise. The attenuation data is calculated using reduced spectral ratio method (Young and Ward, 1979a), assuming a reference station outside of the anomalous region observing infinite (or extremely high) Q ray paths. The inverted model is directly controlled by the quality and quantity of the differential attenuation data. Four causes of errors in δt^* obtained using the reduced spectral ratio technique from seismograms are discussed. Ambient noise or interfering coherent waves are one source of error. The estimation of the power density spectrum using a very short data segment contains an inherent error. The other sources of error occur due to the lack of knowledge of the earth structure near the receiver or the complexity of the source function. This lack of knowledge prevents accounting for these complexities in applying the reduced spectral ratio technique.

The effect of errors on the inversion is studied by inverting synthetic data with different levels of errors added. For a root mean square (rms) signal to rms error ratio of 20 the inverted Q values are essentially identical to the model used to generate the synthetic data (figure 5a). If the signal to error ratio drops to 5, the low and high Q zones can be identified, but the absolute values for Q^{-1} may vary by 10-25%. When the signal to error ratio drops to 1, it is still possible to identify low Q and high Q zones in a majority of the cases, but the Q values will be considerably in error. However, in the same level of signal to error ratio, if the number of coverage of the δt^* data is increased, the inverted Q^{-1} model will have values closer to the original model, which indicates simply that

the more reliable data observed, the better the inverted model. The values for a low Q zone tend to be better resolved than high Q zone for small signal to error ratio (Figure 5). Also, when signal to noise ratio is less than 5, the errors on high Q values may cause negative Q values. When the signal to error ratio is less than 1, the inverted results do not improve much regardless of the number of δt^* data involved.

Two-dimensional three layer Q^{-1} models of the crustal structure along a NW-SE trending line across the Clear Lake volcanic field is inferred from the δt^* observations of six teleseismic events. A low Q zone southeast of Mt. Hannah is found in the depth range between 12-20 km. This low Q zone could be related to the thermal regime in which temperatures are at least half the melting temperature enhancing grain boundary relaxation or thermally activated dislocation attenuation. Higher temperature mechanisms such as thermal climb or partial melting may be acting. The first and third layer are considered to be normal crustal structure, with the exception of the region south of the northeastern end of Clear Lake where it appears a low Q zone extends into the upper mantle. It is possible that the seismic rays did not sample the model thoroughly, so that small zones of low Q values can not be detected. A more detailed Q structure requires more good quality teleseismic events and denser distribution of seismograph stations.

REFERENCES

- Aki, K., A. Christofferson, and E. S. Huseby, (1976), "Three-dimensional seismic structure of the lithosphere under Montana LASA", Bull. Seism. Soc. Am., v. 66, p. 501-524.
- Aki, K., A. Christofferson, and E. S. Huseby, (1977), "Determination of the three-dimensional seismic structure of the lithosphere", J. Geophys. Res., v. 82, p. 277-296.
- Anderson, D. L. and C. B. Archambeau, (1964), "The anelasticity of the earth", J. Geophys. Res., v. 69, p. 2071-2084.
- Anderson, D. L., and J. B. Minster, (1979), "Seismic velocity, attenuation and rheology of the upper mantle", Abstracts for the Conference on Seismic Wave Attenuation, Stanford University Publication, Geological Sciences, Stanford University, California, V. XVII, p. 60-62.
- Backus, G. E. and J. F. Gilbert, (1967), "Numerical applications of a formalism for geophysical inverse problems", Geophys. J. R. Astr. Soc., v. 13, p. 247-276.
- Backus, G. E. and J. F. Gilbert, (1968), "The resolving power of gross earth data", Geophys. J. R. Astr. Soc., v. 16, p. 169-205.
- Backus, G. E. and J. F. Gilbert, (1970), "Uniqueness in the inversion of inaccurate gross earth data", Phil. Trans. R. Soc. Lond. . v. 266, p. 123-192.
- Bailey, R. C., (1970), "Inversion of the geomagnetic induction problem", Proc. R. Soc. London, v. 315, p. 185-194.
- Chapman, R. H., (1966), "Gravity map of Geysers area", California Div. Mines and Geology Mineral inf. Service, v. 19, p. 148-149.
- Chapman, R. H. (1975), "Geophysical study of the Clear Lake region, California," California Div. Mines and Geology, Special Report No. 116.

- Der, Z., R. Masse and M. Landisman, (1970), "Effects of observational errors on the resolution of surface waves at intermediate distances", J. Geophys. Res., v. 75, p. 3399-3409.
- Franklin, J. N., (1970), "Well posed stochastic extension of ill posed problems", J. Math. Anal. Appl., v. 31, p. 682-716.
- Grantmacher, F. R., (1960), The Theory of Matrices, v. 1 and 2, Chelsea Pub. Co., N. Y.
- Gutenberg, B., (1958), "Attenuation of seismic waves in the earth's mantle", Bull. Seism. Soc. Am., v. 48, p. 269-282.
- Hearn, B. C., Jr., J. M. Donnelly and F. E. Goff, (1975), "Geology and Geochronology of the Clear Lake Volcanics, California", 2nd UN Symposium on the Development and Use of Geothermal Resources, San Francisco, Proc., Lawrence Berkeley Lab., Univ. of California, p. 423-428.
- Isherwood, W. F., (1979), "Geophysical overview of the Geysers area", U.S. Geol. Survey Prof. Paper to be published.
- Iyer, H. M., D. H. Oppenheimer, and T. Hitchcock, (1979), "Abnormal P-wave delays in the Geysers-Clear Lake geothermal area, California", Science, v. 204, p. 495-497.
- Iyer, H. M., (1978), "Deep structure under Yellowstone National Park, USA: A continental hot spot", to be published in Tectonophysics.
- Jackson, D. D., (1972), "Interpretation of inaccurate, insufficient and inconsistent data", Geophys. J. R. Astr. Soc., v. 28, p. 97-109.
- Jackson, D. D., (1973), "Marginal solutions of quasi-linear inverse problems in geophysics: edgehog method", Geophys. J. R. Astr. Soc., v. 35, p. 121-136.

- Jordon, T. H. and J. N. Franklin, (1971), "Optimal solutions to a linear inverse problem in geophysics", Proc. Nat. Acad. Sci., v. 68, p. 291-293.
- Jupp, D. and K. Vozoff, (1975), "Stable iterative methods for the inversion of geophysical data", Geophys. J. R. Astr. Soc., v. 42, v. 42, p. 957-976.
- Kanamori, H., (1967), "Spectrum of short-period core phases in relation to the attenuation in mantle", J. Geophys. Res., v. 72, 2181-2186.
- Kennett, B. L. N., (1976), "A comparison of travel-time inversions", Geophys. J. R. Astr. Soc., v. 44, p. 517-536.
- Kjartansson, D., (1979), "Attenuation due to thermal relaxation in porous rocks", Abstracts for the Conference on Seismic Wave Attenuation, Stanford University Publication, Geological Sciences, Stanford University, California, VXVII, p. 68-69.
- Knopoff, L., (1964), "Q", Reviews of Geophysics, v. 2, p. 625-660.
- Lanczos, C., (1961), Linear differential operators, Chapter 3, D. Van Nostrand Co., London.
- Lee, W. B., and S. C. Solomon, (1975), "Inversion schemes for surface wave attenuation and Q in the crust and mantle", Geophys. J. R. Astr. Soc., v. 43, p. 47-71.
- Majer, E. L. and T. V. McEvelly, (1979), "Seismological investigations at the Geysers geothermal field", Geophysics, v.44, p. 246-269.

- McMechan, G. A. and R. A. Wiggins, (1972), "Depth limits in body wave inversions", Geophys. J. R. Astr. Soc., v. 36, p. 239-243.
- Parker, R. L., (1975), "The theory of ideal bodies for gravity interpretation", Geophys. J. R. Astr. Soc., v. 42, p. 315-334.
- Parker, R. L., (1977), "Understanding inverse theory", Ann. Rev. Earth Planet. Sci., v. 5, p. 35-64.
- Pelton, W. H., L. Rijo and C. M. Swift, Jr., (1978), "Inversion of two-dimensional resistivity and induced-polarization data", Geophysics, v. 43, p. 788-803.
- Penrose, R., (1955), "A generalized inverse for matrices", Proc. Camb. Phil. Soc., v. 51, p. 406-413.
- Press, F. (1968), "Earth models obtained by Monte Carlo inversion", J. Geophys. Res., v. 73, p. 5223-5234.
- Solomon, S. C., (1972), "Seismic-wave attenuation and partial melting in the upper mantle of North America", J. Geophys. Res., v. 77, p. 1483-1502.
- Solomon, S. C., and M. N. Toksoz, (1970), "Lateral variation of attenuation of P and S waves beneath the United States", Bull. Seism. Soc. Am., v. 60, p. 819-838.
- Teng, T. L., (1968), "Attenuation of body waves and Q structure of the mantle", J. Geophys. Res., v. 73, p. 2195-2208.

- Walsh, J. B., (1968), "Attenuation in partially melted material",
J. Geophys. Res., v. 73, p. 2209-2216.
- Walsh, J. B., (1969), "New analysis of attenuation in partially melted
rock", J. Geophys. Res., v. 74, p. 4333-4337.
- Ward, R. W., and M. N. Toksoz, (1971), "Cause of regional variation
of magnitudes", Bull. Seism. Soc. Am., v. 61, p.649-670.
- Ward, R. W. and C. Y. Young, (1975), "Mapping seismic attenuation anomaly
in the Coso Geothermal Area", AGU Trans., v. 56, p. 1021.
- White, J. E., (1975), "Computed seismic speeds and attenuation in rocks
with partial gas saturation", Geophysics, v. 40, p. 224-232.
- Wiggins, R. A., (1969), "Monte Carlo inversion of body wave observations,"
J. Geophys. Res., v. 74, 3171-3181.
- Wiggins, R. A., (1972), "The general linear inverse problem: Implication
of surface waves and free oscillations for earth structure",
Reviews of Geophysics and Space Physics, v. 10, p. 251-285.
- Winkler and A. Nur, (1979), "Pore fluids and seismic attenuation in rocks",
Geophys. Res. Letters, v. 6, p. 1-4.
- Young, C. Y. and R. W. Ward, (1979a), "Attenuation of teleseismic P-waves
in Geysers-Clear Lake Region, California", to be published in U. S.
Geol. Survey Prof. Paper.
- Young, C. Y. and R. W. Ward, (1979b), "Three-dimensional Q^{-1} model of
the Coso Hot Springs, Known Geothermal Resources Area", to be
published in J. Geophys. Res.

FIGURE CAPTIONS

- Figure 1. Relation between different attenuation factor, δt^* , and δQ^{-1} model. Seismic rays traced through the model are also plotted.
- Figure 2. Synthetic Q models with no errors add to the synthetic δt^* s.
- Figure 3. Different 2-D Q model used in the synthetic studies. Shaded areas have a low Q value of 100, other areas have a high Q value of 500.
- Figure 4. Relation between the signal to error ratio and the square errors of the inverted model.
- Figure 5. Synthetic Q models with different level of errors add to the synthetic δt^* . Signal to error ratio equal to a) 20, b) 5 and 3) 1, respectively.
- Figure 6. Geology of the Geysers-Clear Lake region. Station locations are shown in black dots. Two-dimensional Q model is constructed along line AA'. Solid triangles are mountains, K: Mount Konocit, H: Mount Hannah, C: Mount Cobb, and G: Geysers Peak.
- Figure 7. Two dimensional Q model for Geysers Clear Lake region along line AA' of figure 3, assuming infinite Q to station CL02.

Q^{-1} MODEL

$$\delta t_i^* = \pi \sum \Delta T_{ij} (Q_j^{-1})$$

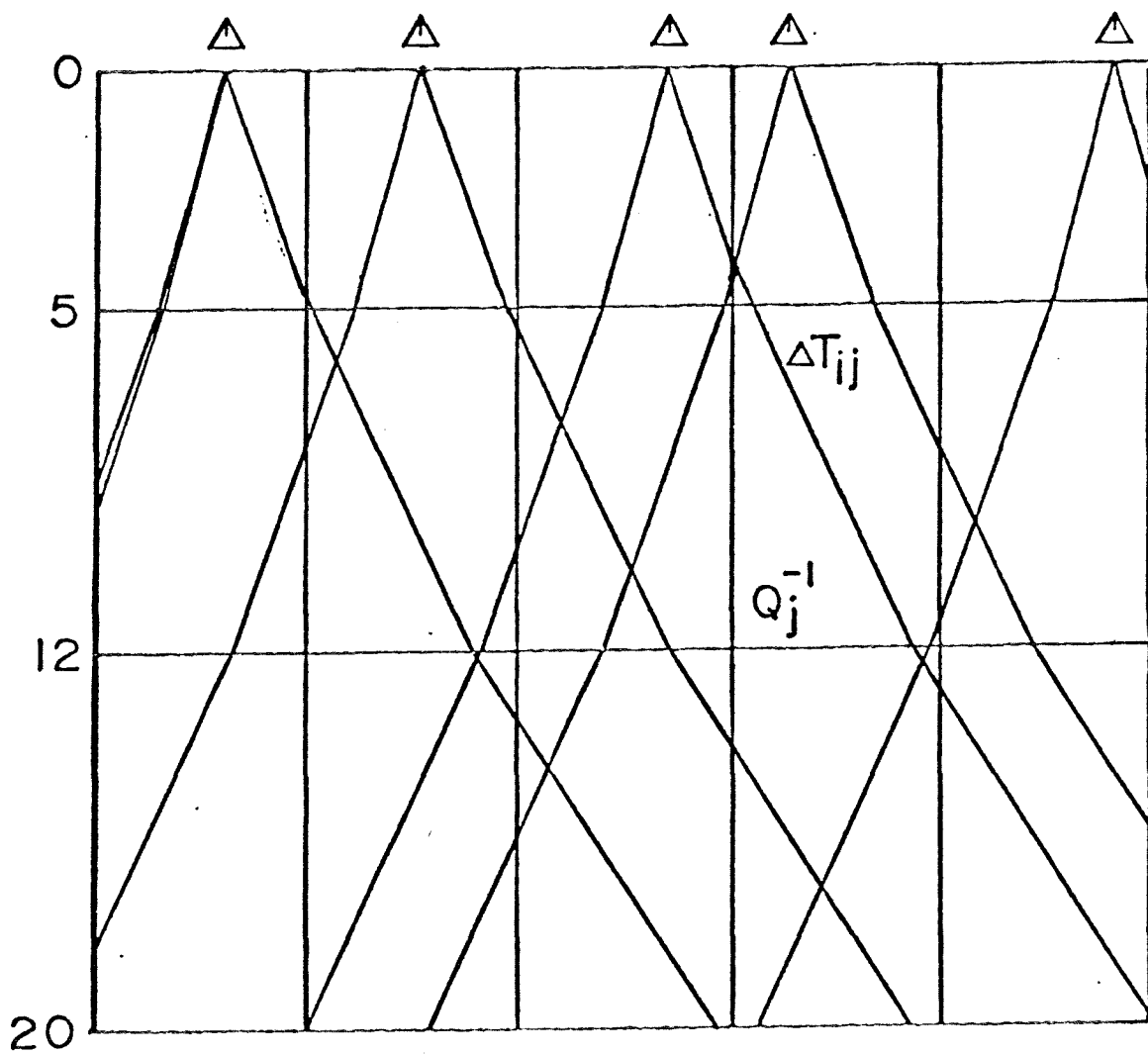


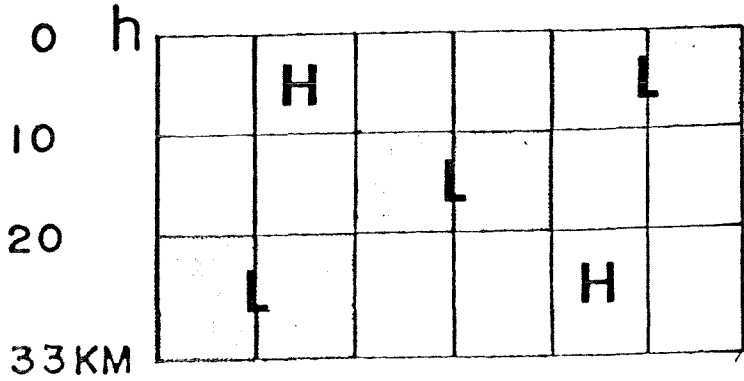
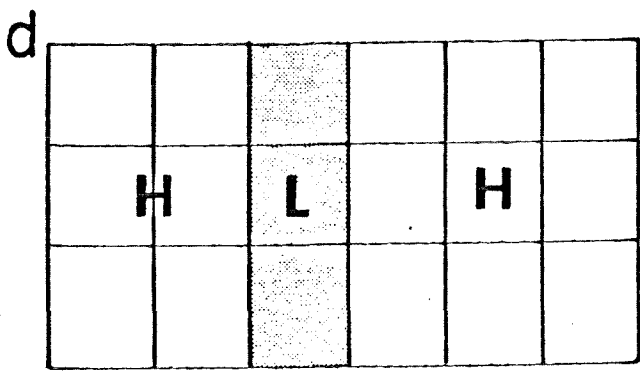
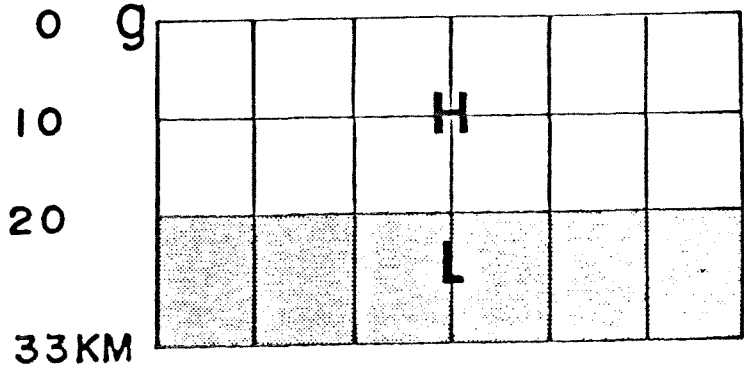
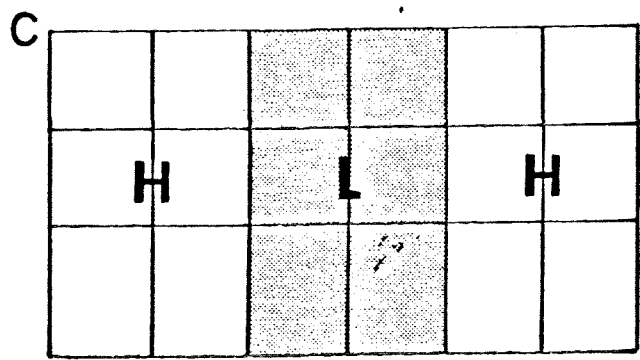
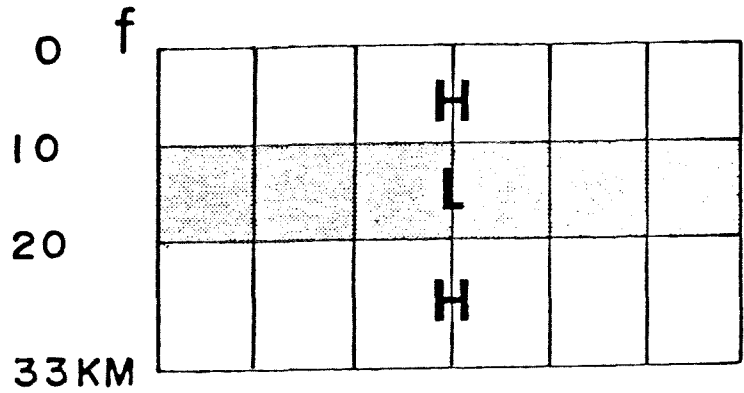
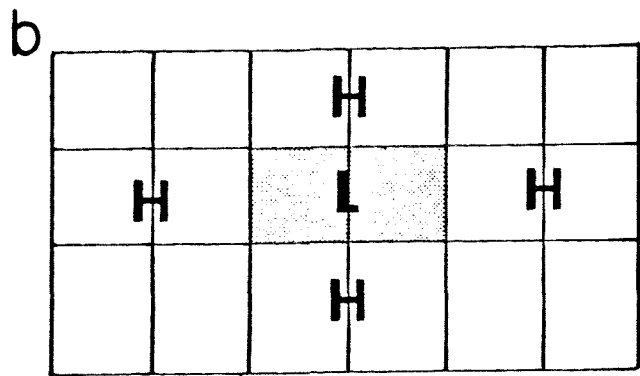
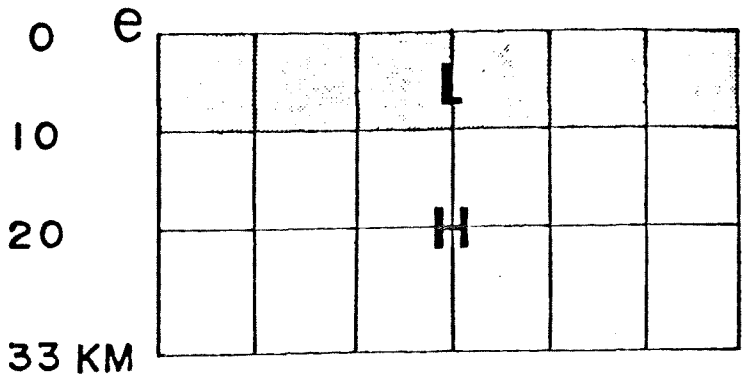
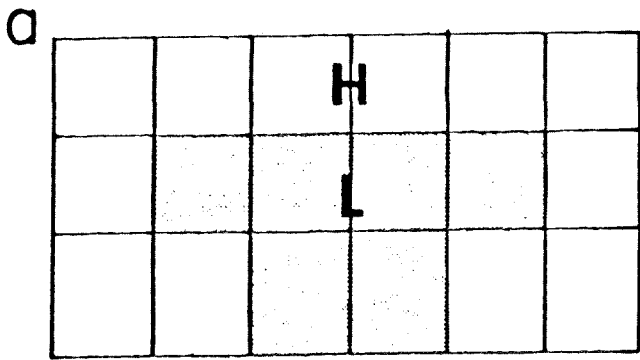
Figure 1

S/N = ∞

500	500	500	500	500	500	500
500	100	100	100	100	100	500
500	500	100	100	500	500	500

SYNTHETIC 2-D Q MODEL

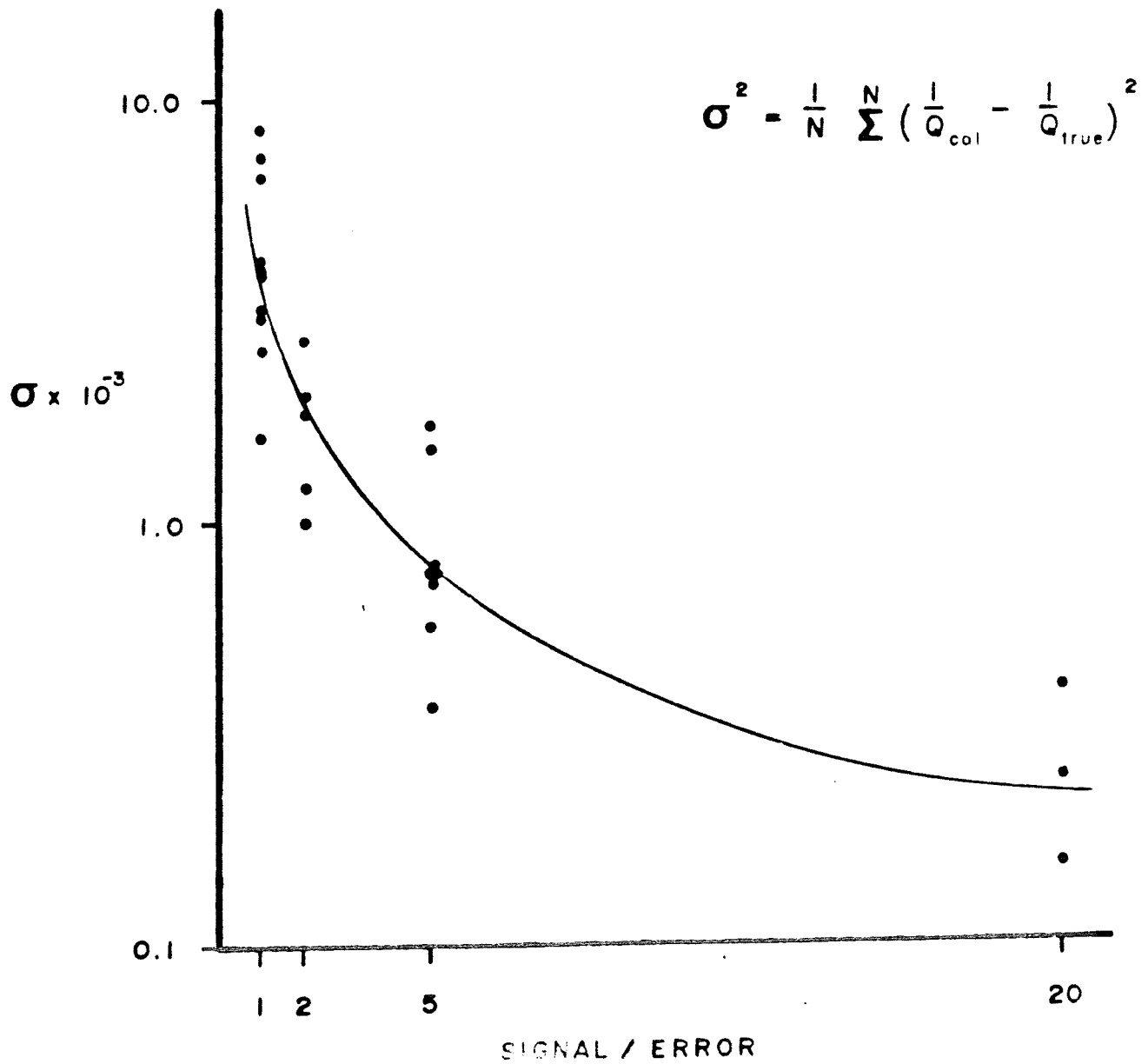
Figure 2



← 50 KM →

← 50 KM →

ERROR ANALYSIS



S/N = 20

539	488	521	486	473	507
541	100	99	101	101	530
494	484	98	100	491	490

SYNTHETIC 2-D Q MODEL

Figure 5a

S/N = 1.

469	828	890	- 682	- 168	- 108
482	117	105	60	34	40
206	337	68	124	- 403	- 117

SYNTHETIC 2-D Q MODEL

S/N = 5.

445	347	344	243	403	484
768	126	138	143	99	480
567	353	91	92	602	1449

Figure 5b

SYNTHETIC 2-D Q MODEL